Efficacy of Boron Neutron Capture Synovectomy in an Animal Model

by

Emanuela Binello

SB, Nuclear Engineering, 1995
Massachusetts Institute of Technology

SM, Nuclear Engineering, 1996
Massachusetts Institute of Technology

Submitted to the Department of Nuclear Engineering in partial fulfillment of the requirements for the degree of

DOCTOR OF PHILOSOPHY

at the

MASSACHUSETTS INSTITUTE OF TECHNOLOGY

June 1999

Author .....
April 30, 1999

Certified by .....
Jacquelyn C. Yanch
Associate Professor, Department of Nuclear Engineering
Thesis Supervisor

Certified by .....
Sonya Shortkroff
Research Associate, Harvard Medical School
Thesis Reader

Accepted by .....
Larry Lidsky
Professor, Department of Nuclear Engineering
Chairman, Department Committee on Graduate Students

Efficacy of Boron Neutron Capture Synovectomy in an Animal Model

by

Emanuela Binello

Submitted to the Department of Nuclear Engineering on April 30,1999 in partial fulfillment of the requirements for the degree of Doctor of Philosophy

Abstract

Boron Neutron Capture Synovectomy (BNCS) proposes to use the $^{10}B(n,\alpha)^{7}Li$ nuclear reaction to destroy inflamed synovium (a tissue lining articular joints) in Rheumatoid Arthritis patients. In a treatment, a boronated compound would be injected into the joint space and taken up by synovial cells. The joint would be irradiated with neutrons, inducing the boron neutron capture reaction with the potential of inducing cellular death in boron-loaded cells. The major goal of this thesis was to experimentally determine whether BNCS is effective in the ablation of arthritic synovium. This entailed neutron beam development and boron uptake characterization. Practical accelerator-based neutron sources were designed to deliver a target dose of 10,000 RBE-cGy to the synovium in under 30 minutes. The highest in vivo synovial boron uptake was achieved after intra-articular injection of 150,000 ppm of ^{10}B as $K_2B_{12}H_{12}$; an average synovial boron concentration of 19,000 ppm for 30 minutes post-injection was obtained. In vivo uptake results were consistent with results from in vitro and ex vivo studies. Animal irradiations were performed using the tandem electrostatic accelerator at MIT LABA and a newly constructed target and beamline assembly. Synovial target doses ranging from 1,400 to 140,000 RBE-cGy were delivered to the knee joints of antigen-induced-arthritic rabbits. Synovial necrosis was observed at doses approximately 10,000 RBE-cGy and above. The delivery of doses below 10,000 RBE-cGy resulted in decreased synovial inflammation in all cases except one where necrosis was also observed. Thus, BNCS was demonstrated to be an effective means for the experimental ablation of synovial tissue. Lastly, a boron compound screening method, based on in vivo prompt gamma neutron activation analysis, was evaluated experimentally and via simulation.

Thesis Supervisor: Jacquelyn C. Yanch
Title: Associate Professor, Department of Nuclear Engineering

Thesis Reader: Sonya Shortkroff
Title: Research Associate, Harvard Medical School

Acknowledgments

First and foremost, I would like to sincerely thank Professor Yanch for giving me the opportunity to work on BNCS. These last four years have been an incredible learning experience. I gratefully appreciate her encouraging me to participate in several conferences which were stimulating and imparted to me the excitement of being a member of a scientific community.

I would like to thank the other members of my thesis committee, Sonya Shortkroff and Professor Harling. Sonya, who was also my reader, provided invaluable expertise in the biological aspects of this work and Professor Harling provided insightful suggestions at critical stages.

Many others deserve acknowledgment. David Gierga, MIT LABA member, has been a reliable fellow researcher in BNCS. Other MIT LABA members, Susan White, Brandon Blackburn, Mark Sitek and Laura Murphy, made the laboratory an enjoyable environment. Kent Riley, of the MITR BNCT group, trained me on the PGNAA facility and was always willing to spare time for my PGNAA questions. Several technicians at the Brigham and Women's hospital (Cristina Viveiros, Gretchen Young, Xiu-Ying Zhang) and several MIT UROP students (Amy Ly, Michelle Ledesma, Cindy Chan) contributed in different ways. Drs. Ruth Shefer and Robert Klinkowstein, of Newton Scientific Incorporated, were the source of many interesting discussions and kept the accelerator running smoothly. MIT Reactor Operations and Radiation Protection were friendly and helpful. Professors Chen and Freidberg, as well as Dr. Bernard, agreed to serve on my defense committee.

And last, but not least, I would like to express deep gratitude to my family. Without their love, unfailing support, and constant encouragement, this thesis could not have been accomplished.

This work was supported by funds from the Lockheed Martin Idaho National Engineering and Environmental Laboratory (INEEL) and the United States Department of Energy (DOE).

This thesis is dedicated to my family.

Contents

List of figures

List of tables

1. Introduction

Rheumatoid Arthritis (RA) is a chronic systemic inflammatory disease which primarily targets the joints, rendering them swollen and painful. The incidence of RA is about 1% of the population. Women are affected three times more often than men and about 80% of patients develop RA between the ages of 35 and 50. Disease progression of RA is by no means uniform. After an onset which is typically insidious (55 to 70% of cases develop over the course of several weeks to months), patients may experience either an intermittent course of the disease, with potentially long periods of clinical remission not requiring continuous therapy, or a more progressive course of disease with endpoints of severe cartilage and bone destruction, implying a complete disabling of the joint.

There is no cure for RA. Treatment is aimed at reducing pain and inflammation, protecting joint structures, maintaining joint function and controlling systemic involvement. Thus, treatment is a palliative measure rather than curative. The first line of defense in treatment is the administration of non-steroidal anti-inflammatory drugs for the reduction of joint pain and swelling. When RA patients do not respond adequately to these, second-line drugs, also known as disease-modifying anti-rheumatic drugs, may be prescribed. If a patient fails to respond to the second-line drugs and corticosteroids, then immunosuppressive agents may be considered, although these drugs are not reported to have therapeutic benefits any greater than second-line drugs and certain agents may predispose patients to the development of neoplasms.

When one joint remains symptomatic despite the administration of second-line drugs, a surgical alternative may be proposed. Based on the prominent role of the synovium (lining articular joints) in causing persistent pain and swelling, physical removal of the inflamed synovium from the joint, i.e. synovectomy, may be recommended to alleviate painful symptoms. According to criteria established by the American Rheumatologic Association, synovectomy is indicated if synovial inflammation has been refractory to aggressive medical treatment for six months or longer.

Initially, synovectomy was effected via an open surgical procedure, although its popularity has declined in recent years due to the long recovery period and high morbidity associated with the operation. Surgical arthroscopic synovectomy is emerging as a synovectomy technique which is less invasive than open synovectomy, although it may still require rehabilitation and hospital stay. In Europe, Canada, Australia and New Zealand a non-inasive radiochemical synovectomy option, called radiation synovectomy, is also available. This therapeutic modality uses intra-articular injections of β-emitting radionuclides to ablate the synovium.

Boron Neutron Capture Synovectomy (BNCS) proposes to use the $^{10}B(n,\alpha)^{7}Li$ nuclear reaction to destroy rheumatoid synovium. In a treatment, a boronated compound would be injected into the

joint space where it would be taken up by the synovial cells. Then, the joint would be irradiated, inducing the boron neutron capture reaction which, in turn, has the potential of inducing cellular death in the boron-loaded cells via the dense local energy deposition of the lithium and α particles created by the capture reaction. The advantages of BNCS over open surgical synovectomy are that it is non-invasive and does not require either general anesthesia or prolonged hospitalization.The most significant advantage of BNCS over radiation synovectomy using β-emitters is that it does not require administration of radioactive substances. Given an appropriate neutron source, BNCS would be a simple technique involving an intra-articular injection of a boronated compound and subsequent neutron irradiation.

The goal of this thesis was to determine the efficacy of BNCS in an animal model. However, before being able to experimentally test the ability of BNCS to ablate arthritic synovium, several investigations had to be undertaken. This thesis describes these investigations in the following order. Chapter 2 presents information on RA, including disease characteristics, treatment options and animal models. Chapter 2 also details the physical principles behind using the boron neutron capture reaction to induce cellular death and tissue necrosis. In addition, chapter 2 presents the development of practical accelerator-based neutron sources. Then, chapter 3 describes uptake studies using various boronated compounds, as well as the measurement technique employed to quantify boron. Chapter 4 describes the full biological uptake characterization of $K_2B_{12}H_{12}$, which yielded results warranting its use in the experimental testing of the efficacy of BNCS. The efficacy study itself, performed with the tandem electrostatic accelerator in operation at MIT LABA and a newly constructed target and beamline assembly, is described in chapter 5. Investigations into the use of in vivo prompt gamma neutron activation analysis as a boron compound screening method is presented in chapter 6 and finally, the last chapter, chapter 7, presents a summary of relevant conclusions, as well as recommendations for future work.

2. Background

This chapter includes background information on rheumatoid arthritis and boron neutron capture synovectomy, as well as the design of practical accelerator-based neutron beams. Section 1 describes the rheumatoid arthritis disease, treatment options and the available animal models with an emphasis on the antigen-induced arthritis model used in this thesis. Section 2 describes the boron neutron capture reaction, the proposed boron neutron capture synovectomy treatment, and a comparison to the more traditional application of boron neutron capture therapy. Finally, section 3 presents results of simulation studies aimed at designing therapeutically useful accelerator-based neutron beams. This section concludes with a summary of further beam optimization, as well as construction of the moderator/reflector assembly used for the efficacy study reported in chapter 5.

2.1 Rheumatoid Arthritis

Rheumatoid Arthritis (RA) is a chronic systemic inflammatory disease which primarily targets the joints, rendering them swollen and painful. The incidence of RA is about 1% of the population. Women are affected three times more often than men, although this difference decreases with increasing age [Lipsky 1998]. Despite a relatively constant incidence in the world population, there are some exceptions, e.g. China with an incidence of about 0.3% and the Pima Indians in North America with an incidence of about 5% [Firestein 1997]. A trend toward a lower incidence in recent years compared to earlier studies was noted but this is confounded by several factors, including variations in the criteria of the American College of Rheumatology for classification of RA, differences in methods for case identification and population aging [Harris 1997]. About 80% of patients develop RA between the ages of 35 and 50 [Lipsky 1998].

The costs of RA represent a significant economic burden. Results of an incidence-based study of lifetime economic costs of RA have shown that the cost of RA is comparable to that of coronary heart disease and exceeded only by cancer and stroke [Stone 1984]. The dominant component of the lifetime cost of RA was indirect, or cost related to loss of work productivity due to the chronic and debilitating nature of RA (total cost was calculated as the sum of direct cost of medical care and indirect cost of work loss). An interesting implication is that although the incidence of RA is lower for younger individuals, their cost is higher since they have a longer life expectancy and the RA strikes them when they have the highest lifetime earning potential. It should be noted that the above study was based on lower marketplace earnings for women in comparison to men, so that attempts at converting this cost estimate based on 1977 dollars into present-day dollars should include a correction factor for the potentially higher marketplace earnings of women, since women are affected three times more often than men.

Cost varies with severity of disease, more severe cases incurring higher costs. Disease progression is by no means uniform in RA. After an onset which is typically insidious (i.e. 55 to 70% of cases develop over the course of weeks to months), patients may experience either an intermittent course of the disease, with potentially long periods of clinical remission not requiring continuous therapy, or a more progressive course with endpoints of severe cartilage and bone destruction that completely disable the joint [Harris 1997]. When symptoms return in cases of an intermittent course of RA (characteristic of about 20% of patients), they often involve previously unaffected joints [Rosenberg 1994]. Symptoms of RA typically affect smaller joints, such as those found in the hands and wrists, before larger joints, and extra-articular complications of RA may manifest themselves, especially in the eyes, lungs and heart [Rosenberg 1994].

The cause of RA is not known. Studies have indicated a genetic predisposition; for example, severe RA is found at about 4 times the expected rate in first-degree relatives of RA patients [Lipsky 1998]. One major factor is the product of the major histocompatibility gene called HLA-DR4, although in some populations the genetic connection with RA has been in gene products HLA-DR1 and Dw16. Thus, it is a particular amino acid sequence of the HLA-DR molecule which confers susceptibility to RA. In addition, some recent evidence has pointed to a genetic predisposition for the development of toxic reactions to drugs used to treat RA [Lipsky 1998].

Genetic factors, however, do not account for the incidence of RA and it is believed that there must also be environmental stimuli [Harris 1997]. Research aimed at determining the direct cause of RA has included consideration of bacteria and viruses, and bacterial heat shock proteins have also been implicated as potential exogenous agents. Study has been directed at potential endogenous or autoimmune causes, such as, for example, rheumatoid factor, which is an autoantibody. Although autoimmunity is unquestionably involved in the progression of the arthritic condition, a role in causation has not been definitively established. Currently, a hypothesis for the development of RA is that several environmental stimuli infect a genetically predisposed individual and, via some mechanism, inflammation is localized to joints and persists even in the absence of original stimuli because of autoimmunity [Firestein 1997]. The reason why the inflammatory response localizes to the joints is not understood.

Before considering the pathology of the rheumatoid joint, the anatomy and function of a normal joint are reviewed. Figure 2.1 shows a schematic of selected parts of a normal synovial joint. Each end of the two bones is covered by a thin layer of articular cartilage, a terminally differentiated tissue with poor capacity for repair once damaged [Walsh et al 1997]. Articular cartilage absorbs transmitted forces, protecting the bony ends, and contributes to joint stability. Other structures, not shown in the schematic, which contribute to joint strength and support include ligaments and tendons. The joint capsule is composed of a thick fibrous outer layer serving as a tough, albeit flexible, connection between the two bones and an inner layer covered by synovium, a specialized tissue which may be loosely collagenous (areolar synovium), more densely collagenous (fibrous synovium) or composed of mostly fat (adipose synovium) [Burkitt et al 1993]. The synovium, which can be divided into the subsynovium and synovial lining, lines all parts of the inside of the joint except over the articular cartilage and a small bare spot between the cartilage and synovial insertions into the subchondral bone [Harris 1997]. Highly vascularized, the subsynovium also contains an extensive lymphatic system. The surface of the synovium, the synovial lining, does not constitute a true membrane because there is no basement membrane separating it from the

subsynovium and the cells do not have typical cellular junctions. Two types of specialized cells form the synovial lining, generally 1 to 3 cells thick; type A cells, which have a macrophage-like appearance, and type B cells, which are more fibroblast-like. The principal functions of synovial cells, or synoviocytes, are the phagocytosis/endocytosis and the synthesis of various proteins, enzymes, glycoproteins, cytokines and glycosaminoglycans [Harris 1997]. Synoviocytes also synthesize hyaluronic acid, a major constituent of synovial fluid. In a normal joint, there is only a thin film of synovial fluid covering the synovium and cartilage surfaces. Synovial fluid serves to lubricate the movement of articular surfaces and enhance diffusion of nutrients into cartilage. A highly viscous filtrate of serum, synovial fluid can be thought of as a highly specialized and fluid form of synovial extracellular matrix, rather than a typical secretion [Burkitt et al 1993].

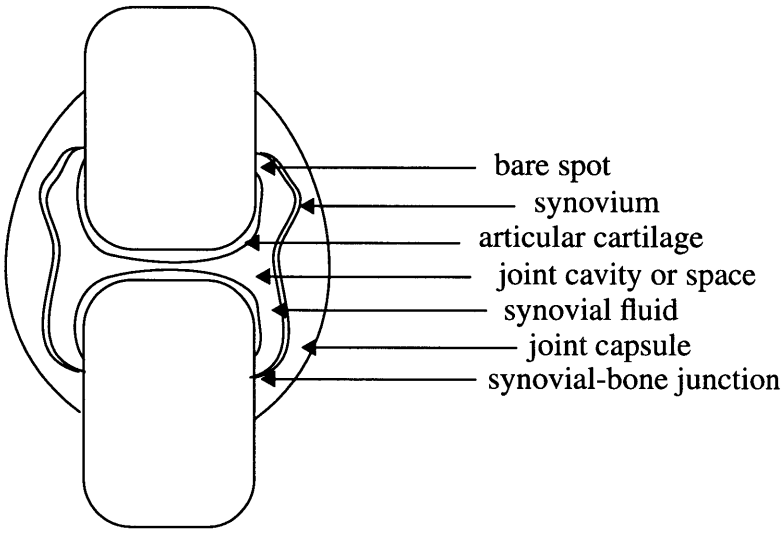

Figure 2.1: Schematic of selected anatomical parts of a normal synovial joint.

Having reviewed normal joint anatomy and structure, with particular emphasis on those structures significantly affected during the course of RA, attention is now turned to the pathologic changes in the knee joint resulting from RA.

2.1.1 Pathology

The progression of synovial pathology has been divided into 4 stages [Harris 1997]. In the first stage of RA, after the onset of synovitis, tissue becomes edematous, new capillaries begin to form and synoviocytes begin proliferating. In the next stage, synoviocytes continue to grow both in size and number, achieving a thickness of 10 to 12 cells (compared to the original of 1 to 3 cells). The volume of synovial fluid increases, as does the number of inflammatory cells, some concentrating near the proliferating capillaries. The synovium begins forming into a pannus (Latin for cloth), a vascular granulation tissue responsible for secreting enzymes which can seriously degrade both articular cartilage and bone. By stage 3, the rheumatoid pannus has achieved enough mass to invade the articular cartilage and bone at the synovial-bone junction. Articular cartilage and bone erosion begin. Finally, by stage 4, most of the cartilage has been lost from a particular joint and

bone erosion is underway. The pannus forms a bridge between the apposing bones, resulting in a fibrous ankylosis which eventually ossifies and causes complete loss of joint mobility, already limited in the early stages of RA by pain and swelling [Rosenberg 1994]. In addition to cartilage and bone erosion, several supportive structures in the joint, such as ligaments and tendons, may be affected and destroyed, consequently giving rise to joint deformations [Lipsky 1998]. Figure 2.2 shows a schematic of selected pathologic changes.

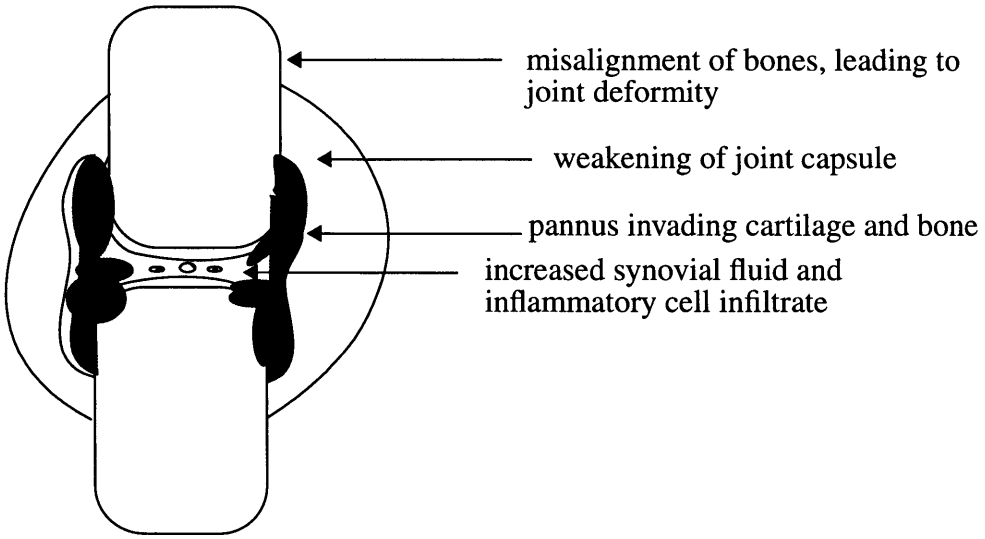

Figure 2.2: Schematic of selected pathological changes in an RA synovial joint.

Considerable study has been devoted to understanding the mechanism of cartilage destruction. Cartilage is destroyed by both mechanical and enzymatic processes. During the course of RA, proteoglycan, an important constituent of articular cartilage, is depleted and replaced by water, rendering it deformable and unable to rebound from compression [Firestein 1997]. Weakness of the cartilage is then exacerbated by the invading pannus; immunohistologic studies of the pannus-cartilage junction have shown elevated levels of collagenase and stromelysin, both members of the metalloprotease family of enzymes [Hasty et al 1990]. Since stromelysin is required for the full activation of collagenase, it may be regarded as more important for the destruction of cartilage in RA. In addition, stromelysin degrades proteoglycan core proteins, several types of collagen and other matrix components [Harris 1997]. Enzymes responsible for cartilage degradation are also found in the synovial fluid and can be derived from chondrocytes [Harris 1997]. The rate-limiting step in cartilage destruction is the enzymatic degradation of collagen, since loss of proteoglycans, which also contributes to the mechanical aspect of degradation, occurs relatively early in the inflammatory process [Firestein 1997].

2.1.2 Treatment options

There is no cure for RA. Treatment is aimed at reducing pain and inflammation, protecting joint structures, maintaining joint function and controlling systemic involvement [Lipsky 1998]. Thus, treatment is a palliative measure rather than curative. A cure can not be developed until the cause of RA has been determined.

Criteria have been established by the American College of Rheumatology for the diagnosis of RA [Arnett et al 1988]. Patients are said to have RA if they meet four of the following seven criteria: morning stiffness, arthritis of three or more joints, arthritis of hand joints, symmetric arthritis, rheumatoid nodules, serum rheumatoid factor or radiographic changes. The first four criteria must be present for at least 6 weeks. Despite the establishment of these specific criteria, there may be a long delay between the onset of symptoms and diagnosis of RA. One retrospective study of patients diagnosed with RA has reported a median time of 18 weeks for diagnosis following a medical encounter; the total median time, including the time between RA onset and a medical encounter, was 36 weeks [Chan et al 1994]. Delays of this kind may impact the degree to which therapeutic intervention affects disease management, depending on the patient's prognosis.

The type of recommended therapeutic intervention relies, in part, on the stage of the disease. A framework has been developed relating suggested management to disease stages [Harris 1997]. At a very early stage of RA, from days to several weeks following the onset of synovitis, when, in fact, a definitive diagnosis has not yet been made (although the patient begins to experience some symptoms such as morning stiffness, joint tenderness, pain and reduced grip strength), patient management focuses on physical therapy. Rest generally reduces joint inflammation; however, complete rest, or confinement to bed, is not recommended. Particular types of exercises can strengthen joint muscles and provide relief from symptoms without increasing inflammation. One important component of treatment at this stage is patient health education. Results from a study of patients subscribing to Stanford's Arthritis Self-Management Program suggest that patient health education has sustained health benefits while reducing costs [Lorig et al 1993].

From approximately six weeks to six months after onset, the disease progresses through stage 2, which may be characterized by clinical symptoms of continued joint swelling, morning stiffness, pain, fatigue, weakness and involvement of new joints. The severity of the symptoms depends on the aggressiveness of the disease. Synovial proliferation continues and a rheumatoid pannus begins to form. A definitive diagnosis of RA allows the initiation of a therapeutic drug regimen to manage the pain and inflammation.

In the next stage of the disease (3), from about six months to two years, as the rheumatoid pannus begins to invade cartilage and bone, clinical symptoms include loss of range of motion, decrease in dexterity and generalized weakness and debilitation. Treatment needs to be aggressive to delay irreversible damage to both cartilage and bone. Options at this stage include more aggressive drug therapy and potential participation of clinical trials of biological agents. It could be inferred that this includes clinical trials of new therapeutic modalities as well.

The final stage of the disease (4), ranging from two to over twenty-five years of active disease, is essentially an extension of stage three. Patients have likely developed joint deformity and have substantial loss of joint function. These symptoms are mainly a result of severe degradation of cartilage and bone. At this point, the emphasis of treatment is on surgical reconstruction.

The next subsections discuss treatment options in detail. The subsection on medical management describes available drug regimens, including mention of their side effects. Following this, there is a subsection on surgical management which includes a discussion of non-invasive radiochemical

alternatives, as well as examples of the development and experimental testing of new therapeutic modalities. Attention in these subsections is devoted solely to the knee, a relatively common joint to be involved in RA; the reported incidence of unilateral knee joint involvement is 30 to 35% [Fleming et al 1976].

Medical management

The first line of defense is administration of nonsteroidal anti-inflammatory agents or NSAIDs, for the reduction of joint pain and swelling. NSAIDs decrease inflammation by blocking the cyclooxygenase pathway and thereby stopping the production of prostaglandins, prostacyclin and thromboxanes. The most common and effective NSAID is aspirin [Lipsky 1998]. Side effects from aspirin may include gastrointestinal irritation, hematologic disturbance such as increased bleeding and potential renal side effects (rare if the patient has normal cardiovascular and renal function). Non-aspirin NSAIDs have no therapeutic advantages over common aspirin, although the incidence of gastrointestinal irritation is typically lower than aspirin [Lipsky 1998]. Due to the different chemical natures of these other NSAIDS, side effects vary significantly [Harris 1997].

When patients do not respond adequately to NSAIDs, second-line drugs are prescribed. These drugs are also called disease-modifying anti-rheumatic drugs, although that nomenclature may be misleading, since there is minimal evidence that the drugs slow down bone erosion [Lipsky 1998]. The most frequently used drug is methotrexate, an antimetabolite, whose major anti-inflammatory action is the enhancement of adenosine production [Harris 1997]. Clinical studies have shown long term significant improvement in all clinical disease variables as well as functional status [Weinblatt et al 1994]. Other second-line drugs include anti-malarial drugs, sulfasalazine, gold salts and D-penicillamine. Therapy with any of these results in clinical improvement. However, each drug is associated with considerable toxicity and requires careful monitoring. Interestingly, use of most second-line drugs was initiated on empirical, historical or serendipitous evidence rather than prospective design [Harris 1997].

Low doses of oral glucocorticoid treatment may be indicated as a bridge therapy when NSAIDs have been found insufficient to control the RA and second-line drugs have not begun having an effect [Harris 1997]. Glucocorticoids are also indicated for blunting toxic effects of second-line drugs, vessel inflammation, arthritis flares or systemic complications [Harris 1997]. Their anti-inflammatory action lies in their eventual inhibition of a protein (NF-κB) which moves into the nucleus and activates genes encoding for inflammatory molecules. Intra-articular injections of glucocorticoids may be used to control RA limited to several joints, prominent flares and tendon sheath inflammation. There are many potential side effects of glucocorticoids (corticosteroids in general) including osteoporosis and resultant fractures. There is a direct relationship between dose (daily and cumulative) and serious infections, gastrointestinal bleeds and/or ulcers [Harris 1997].

If a patient fails to respond to second-line drugs and corticosteroids, then immunosuppressive agents may be considered (azathioprine and cyclophosphamide). These drugs are not reported to have therapeutic benefits greater than second-line drugs and cyclophosphamide may predispose patients to the development of neoplasms [Lipsky 1998]. Considerable research is being done to investigate the feasibility of targeted immunotherapy and the development of new biological agents [Strand et al 1997].

Controversy exists over which second-line drug should be used first and when second-line therapy should begin, as well as when immunosuppressive agents are to be prescribed [Harris 1997]. There are different strategies: in the traditional pyramid approach, more potent drugs are used as the disease progresses; the saw-tooth strategy recommends using second-line drugs sequentially, switching drugs as soon as there is even a slight diminution of effect; finally, the combination therapy approach recommends planning a combination of second-line drugs, with the stance that the benefit is greater than the compounded risk of side effects [Harris 1997].

Surgical management

The most straightforward indication for surgical intervention exists when there is severe damage to articular cartilage and bone such that there is a substantial decrease in ambulatory function; essentially the only way to alleviate pain and restore function is via total joint replacement [Sculco 1998, Harris and Sledge 1990]. The principle of total knee replacement is to remove the damaged articular surfaces of the femur, tibia and patella and replace them with implants; a metal femoral component, a polyethylene tibial component and a polyethylene patellar component. All three components are fixed firmly into the bone with methylmethacrylate bone cement, which is necessary since fixation by bone ingrowth is not adequate in RA patients [Sculco 1998]. If the soft tissues (including the ligaments) surrounding the knee are deformed or asymmetric, "soft-tissue balancing" must be performed, i.e. the soft tissues are released from the bone and lengthened to make them symmetrical [Sculco 1998]. The reason behind the complete removal of cartilage lies in the clinical observation that remaining patellar cartilage may perpetuate synovial inflammation and increase susceptibility to flare-ups [Sledge and Ewald 1979]. When all cartilage has been excised, the synovium becomes quiescent [Harris and Sledge 1990].

Total knee replacements may have several complications. The worst potential complication is deep infection [Wilson et al 1990]. Fortunately occurring only in approximately 1% of the knee replacements [Sculco 1998, Harris and Sledge 1990], deep infection requires the removal of the prosthesis, a procedure associated with a prolonged period of morbidity [Anderson 1986]. Risk factors for the development of deep infection include the RA disease itself, obesity, steroid use and previous surgical intervention in the particular joint [Wilson et al 1990]. A more common complication is deep vein thrombosis [Sculco 1998], although it does not frequently give rise to clinically evident problems after knee replacement [Harris and Sledge 1990]. Other complications include delayed wound healing and formation of a haematoma [Sculco 1998].

Long-term results of total knee replacement are very good. One recent study evaluating 104 total knee replacements found good to excellent results in 81% after an average follow-up period of 12.7 years; the probability of the implant remaining functional in situ after 15 years was 91% [Rodriguez et al 1996]. For patients older than 60, total joint replacement lasts for the remainder of life in most cases [Windsor and Insall 1997]. Current data for younger patients is not complete enough for assess implant durability [Windsor and Insall 1997]. However, one study evaluating 44 knees in 28 patients ranging from 19 to 39 years for an average follow-up of 5 years found good and excellent results in 86% of the knees [Stuart and Rand 1988].

Concerns about total knee replacement revolve around the long-term durability of the implant; reimplantation of a new prosthesis is technically difficult and involves further removal of bone stock [Anderson 1996]. Besides problems with the patella (occurring in about 15% of patients), loosening of the tibial component is a common form of failure [Harris and Sledge 1990]. Results of revision surgery are not as good as results of the primary operation and the complete pain relief normally found after total knee replacement is not obtained as often [Windsor and Insall 1997].

A patient is discharged 4 to 6 days after unilateral knee replacement surgery [Sculco 1998]. Home physical therapy is instituted and most patients become weight bearing without external support within 6 to 8 weeks [Sculco 1998]. In 1990, the cost of the procedure ranged from $25,000 to $30,000 [Harris and Sledge 1990]. Although this is a considerable cost, it is believed that the functional improvement offered by total knee replacement is so great that the benefits outweigh the costs [Harris and Sledge 1990].

Despite the documented reliability and success of total knee replacement, it is advised that the surgery be considered very carefully in joints where the discomfort level is tolerable and factors, such as advanced age, increased risk and lack of patient motivation in following post-operative programs, are present [Sledge 1997]. Also, RA patients often have multiple joint involvement which adds to preoperative considerations; for example, patients with severe involvement in the wrist or hands may not be able to use crutches, necessary after knee surgery [Sledge 1997]. Total knee replacement is only indicated when there is severe pain deriving from cartilage destruction in the joint as evidenced by radiographic findings and when the joint has failed to respond to the most aggressive trial of anti-inflammatory agents [Anderson 1996]. It has been noted that surgery is elective since the ultimate outcome is independent of the timing of the operation; there are few exceptions that require surgery to be performed immediately [Anderson 1996].

There is another surgical option for patients who do not respond to anti-inflammatory drugs and continue to experience pain and swelling due to synovitis rather than significant damage to either articular cartilage or bone. This surgical option is called synovectomy, i.e. the removal of inflamed synovium from the joint. The reasoning behind it lies in the prominent role of the synovium in causing persistent pain, swelling and resultant decrease of joint function. As a consequence, removal of the synovium should decrease pain and swelling, leading to increased joint function. According to criteria of the American Rheumatologic Association, synovectomy is indicated if synovial inflammation has been refractory to aggressive medical treatment for six months or longer [Newman 1994, Whipple and Duval 1997]. Initially, synovectomy was effected via open surgical procedure, although at the present, it has been replaced by arthroscopic synovectomy. The following paragraphs discuss open surgical and arthroscopic synovectomy and present results of studies comparing the two procedures.

An early review of the literature and history of synovectomy stated that about 80% of patients improved after synovectomy [Geens 1969]. This statement, however, should be qualified by the small numbers of knees reported in the early literature, as well as relatively short follow-up times. A summary of subsequent studies, with larger sets of knees, longer follow-up times and controls, revealed controversy regarding the efficacy of synovectomy [Newman 1994]. Factors contributing to the controversy were identified as the lack of controls found in many studies and the nature of RA with its asymmetric pattern of involvement and variable nature [Newman 1994].

In order to ascertain the degree of controversy, the literature was examined with respect to the effect of synovectomy on three specific endpoints: pain, the recurrence of synovitis and evidence of joint destruction. Several confounding factors were encountered during this review. This included varying definitions with the respect to goals of synovectomy and consequent attribution of success, failure, benefit and improvement. This also included the presentation of clinical results, often grouping and averaging over patient subpopulations (for example, varying numbers of patients followed for varying amounts of time), potentially obscuring data and comparisons between studies.

Controversy over the efficacy of synovectomy with respect to decreasing pain essentially revolves around results of two controlled multicenter evaluations, one done by the US Arthritis Foundation Committee on the Evaluation of Synovectomy [AFC 1977, McEwen 1988] and the other by the Arthritis and Rheumatism Council and British Orthopedic Association [ARC 1976]. In the US study, pain was found to be less in synovectomized knees after 1 year. By the end of 3 years and 5 years, no statistically significant difference in pain was found between treated and control knees. The UK study found a significant decrease in pain in knees 1, 2 and 3 years after synovectomy. Both studies were controlled. However, the majority of controls in the US study were bilateral (i.e. patient with similarly involved knees had treatment on one knee and not the other) while in the UK study, only unilateral controls were used (i.e. only one of two patients with similar type of knee involvement was treated). The difference between the unilateral and bilateral controls was analyzed for one particular disease variable in the US study [McEwen 1988]. When both control sets were pooled, the difference in the disease variable was significant. However, when bilateral control knees were considered separately, statistical significance was lost. This may be suggestive of the cause for the difference between the two trials but no specific conclusion of this kind was drawn.

There are three very important things to note with regard to the US multicenter study. The first is that statistical significance is quite different from clinical significance [McEwen 1988]. Statistical significance is highly affected by variability of the data. On one hand, it is possible that a large difference in a disease variable could occur and not be significant because of large variability in the data. On the other hand, a small difference could be statistically significant due to consistency of the data but not clinically significant insofar as its magnitude. The second is that the US study did find improvement in pain at 1, 3 and 5 years in the majority of knees on which synovectomy had been performed when compared to pain before synovectomy. The reason why improvement was not found statistically significant is because improvement was also found in the control knees (although generally not quite as much as in the synovectomized knees). This could result from natural remission not uncharacteristic of RA progression; by the design of the trial, most knees were in a relatively early stage of RA. Improvement in control knees could also result from the increased rest, medication, physical therapy and/or other treatments on the control knees since by design of the trial both the control and synovectomized knees were treated in the same manner [McEwen 1988]. Thus, improvement in control knees could be an indirect result of synovectomy of the other knee. The last point also involves definition of efficacy and its impact on "success". In other words, qualifications may be appropriate, i.e. treatment can be considered successful if it can manage pain for x amount of time in about x% of knees.

Generally, the rest of the studies in the literature report improvement in pain after synovectomy. For example, one study, with an average follow-up time of about 3 years, found an improvement in pain in 73% of the patients [Ranawat et al 1972]. One study with an average follow-up of 7.5 years reported a satisfaction rate of 67% with respect to pain [Laurin et al 1974]. Finally, results of a study with even longer follow-up times (14 year average) still found decreased pain in 65% of the patients [Ishikawa et al 1986]. It was noted that generally improvement reaches a maximum plateau between six months and one year of synovectomy [Ranawat et al 1972]. Several authors report a gradual decrease of "good" results with increasing time (although this includes many variables), however, "success" rates remained high [Laurin et al 1964, Geens et al 1969, Ranawat et al 1972]. None of these studies included controls. Also, since the RA itself is so variable, it would be hard to accurately judge which knees could undergo remissions based on their initial presentation. Furthermore, the above studies include patients from a variety of different stages (in contrast to the multicenter evaluations where, by virtue of it being planned out as a single study the patient population was homogeneous).

Turning to the second endpoint, the data are variable with respect to the efficacy of synovectomy in controlling recurrence of synovitis. Recurrence in and of itself is not particularly surprising in light of reports that the regenerated synovium in synovectomized knees histologically resembles rheumatoid synovium [Goldie 1971, Patzakis et al 1973]. Comparison between synovial biopsies of original and regenerated synovium 1 to 3 years post-synovectomy from 26 patients showed minimal differences [Goldie 1971]. Abnormalities in the rheumatoid synovium have been found as early as 1 month after surgery [Patzakis et al 1973]. Histological appearance of rheumatoid synovium does not always result in a clinical recurrence of synovitis, although the frequency of histologic recurrence can serve as an upper limit of clinical recurrence. One study of 21 patients found that about 86% of biopsies from regenerated synovium 1 or more years after synovectomy were classified as rheumatoid; 67% of these had clinical recurrences [Patzakis et al 1973].

Table 2.1 shows conclusions/results as presented by a group of studies, which were selected on the basis of inclusion of detailed patient data. However, no meaningful conclusion can be drawn from the results as presented in table 2.1 because no adjustment was made for the variation in the time to recurrence. The studies were thoroughly reviewed and the frequency of recurrence, as determined by examination of the patient data, was divided into two sections, less than 2 years and greater than 2 years, and was based on the number of knee joints. Table 2.2 shows the results of this subdivision.

Table 2.1: Reported frequencies of synovitis recurrence in selected studies

Source		Follow-up (years)		Frequency		based on
Author	Year	Avg.	Range	%	fraction	
Geens et al	1969	1.9	0.6 - 4.0	46	13/28	knee
Patzakis et al	1973	2.6	0.1 - 10	67	14/21	patient
Ranawat et al	1972	2.8	1.0 - 8.0	13	8/60	knee
Verdeck & McBeath	1978	5.7	> 2.5	39	9/23	knee

Table 2.2: Subdivision of recurrence frequencies according to follow-up time

Source		Follow-up < 2 years		Follow-up > 2 years	
Author	Year	%	fraction	%	fraction
Geens et al	1969	27	4/15	69	9/13
Patzakis et al	1973	17	2/12	68	13/19
Ranawat et al	1972	30	8/27	0	0/33
Verdeck & McBeath	1978	NA		39	9/23

For follow-up times less than 2 years, results from the selected studies ranges from 17% to 30% (interestingly the study reporting 30% includes approximately twice as many knees joints as the other two). For follow-up times greater than 2 years, the recurrence frequency in the majority of studies tended to be greater, from 39% to 69%, although in one instance no recurrences were found. Unfortunately, one study with the largest numbers of knees (175) did not give a patient by patient description of results [Marmor 1973] and thus it was impossible to determine recurrence frequency as a function of follow-up time. Since 80% of the knees were evaluated for more than 2 years, it would be expected that the frequency of recurrence would be similar to that found at greater than 2 years; however, it was 5.7%, which is even less than the range found in the group with a follow-up time of less than 2 years.

The US controlled multicenter study found the frequency of recurrence in synovectomized knees to be 18% (23/130) during 3 years. The data were existent or detailed enough in only two of the above studies to allow the determination of recurrence in the same time frame. In Geens et al [1969] the frequency was 50% (2/4). More knees were followed for that length of time in the study by Patzakis et al [1973] and the frequency of recurrence was 33% (7/21). If data from Geens et al [1969] are not included, the frequencies of recurrences of Patzakis et al [1973] and the US multicenter study [AFC 1977] are close to the range of frequencies observed with follow-up times of less than 2 years. The US multicenter also examined recurrence in control knees, not done in any other of the selected studies, and found a recurrence frequency of 28% (34/120). Thus, the reduction in frequency in the synovectomized knees relative to control knees was 10% which was not deemed significant via statistical analysis.

The final endpoint examined in the literature was the effect of synovectomy on the progression of joint destruction as evidenced by radiological findings. The initial condition of the arthritic knee joint should play a role in the reported "successes", which, in accordance with often-stated goals, corresponds to the prevention of further radiological progression. Several studies, however, reporting the "failure" rate, did not specify the initial stage of the disease in patients.

In order to try to assess the effect of initial disease stage on cartilage thinning or joint destruction as based on the literature, subdivisions were made according to the initial disease stage. Table 2.3 shows the results. This time no detailed division was made on the basis of follow-up time and

knee contribution, since it seemed that radiographic stage would have a greater impact on results. The evaluation time for most of the studies was less than 5 years, except for the study by Ishikawa et al [1986] which extended from 10 to 23 years.

Table 2.3: Progression of joint destruction in selected studies divided by initial knee stage

Source		Stage I		Stage II		Stage III	
Author	Year	%	fraction	%	fraction	%	fraction
Geens et al	1969	0	0/1	60	3/5	90	17/19
Patzakis et al	1973	NA	NA	44	4/9	100	12/12
Ochi et al	1991	0	0/40	82	28/34	100	5/5
Ishikawa et al	1986	20	10/49	54	10/18	91	10/11

The study by Ochi et al [1991] is roughly in agreement with other studies in table 2.3. Although not included in the table, results are also given for a follow-up time of 1 year: stage I and III knees show the same results, while the stage II knees show a smaller percentage (47%) or fraction of knees (16/34) with evidence of progression of joint destruction [Ochi et al 1991]. This study also included bilateral controls: the reported progression in Stage II control knees at one and five years was 38% (13/34) and 77% (26/34), respectively. Control knees actually had a lower frequency of joint progression than the synovectomized knees as evidenced by radiological findings, although statistical analysis showed no significant difference. This corroborates results of the US study which also found no statistically significant difference between synovectomized and control knees in the progression of joint destruction, via observable cartilage thinning, at either three or five years after synovectomy [McEwen 1988]. A conclusion was drawn that the progression of joint destruction is affected more by the aggressiveness of the disease than by whether synovectomy was performed or not [AFC 1977, McEwen 1988]. An earlier study found no correlation between whether or not synovectomy was performed and the systemic deterioration due to progression of the disease; it was pointed out, however, that this did not necessarily cancel out potential benefits of synovectomy [Laurin 1974]. The compilation of data in table 2.3 seems to indicate that, when the knee joint is already at stage III before synovectomy (and already has prominent cartilage destruction), performing synovectomy will have no benefit in halting the further progression of degradation and most knees will continue to show progressive deterioration. When the knee joint is at stage II, this particular set of selected studies shows that about 70% of the knees (45/67) will have continued progression of joint destruction.

From the studies presented in table 2.3, it is clear that synovectomy should be performed when cartilage damage is not severe. Although there is general agreement on this [Newman 1994], some studies maintain that synovectomy performed in late stages of RA can result in temporary pain relief and functional improvement [Geens et al 1969, Verdeck and McBeath 1978]; one study has also suggested that synovectomy be regarded as a way of postponing total knee replacement [Jensen et al 1991].

The popularity of open surgical synovectomy has declined in recent years [Anderson 1986] and it is currently an uncommon surgical procedure [Clayton 1992]. Major drawbacks of open surgical synovectomy are a long recovery period and unpredictable "success" rates [Clayton 1992]; one study reported post-operative hospital stays of about 3 to 6 weeks [Ranawat et al 1972]. Despite these drawbacks, synovectomy does provide some pain relief and allows continued functioning of the patient's own joint components, while not precluding subsequent total knee replacement as necessary [Clayton 1992]. In theory all of the synovium should be removed, although in practice only about 80% is reachable in open surgical synovectomy [Laurin et al 1974]. An advantage of open surgery is that it allows the specific removal of synovium at the synovium-bone junctions which is critical [Clayton 1992].

Overcoming the obstacle of long morbidity associated with surgical synovectomy, arthroscopic synovectomy has gained popularity [Whipple and Duval 1997]. This suggests that it is not the principle of synovectomy (the physical removal of inflamed synovium) that has lost popularity but rather the unfavorable ratio of cost to benefit associated with open surgical synovectomy. In arthroscopic synovectomy, intra-articular areas are accessed via small incisions through which an arthroscopic sheath, shaver and inflow cannula are inserted into the knee. Intra-articular images are projected onto a television monitor [Whipple and Duval 1997].

Promising clinical studies have been reported [Smiley and Wasilewski 1990, Ogilvie-Harris and Basinski 1991, Ogilvie-Harris and Weisleder 1995]. The earliest of these studies reported that at two and four years, success rates (defined as little or no pain, no recurrent effusion, unchanged or improved ranges of motion, and little or no limitation of activity) were 90% and 57%, respectively [Smiley and Wasilewski 1990]. Synovectomy was performed via five to six portals, while the patient was under general or spinal anesthesia, and took approximately two hours on average to complete. Post-operative hospital stays ranged from six hours to eight days, with an average of 2.7 days; 20% of the procedures performed on an outpatient basis. No operative complications were reported. A subsequent study with follow-up periods of two and four years also found significant benefits with respect to pain, synovitis and joint function; success rates were 80% at four years post-synovectomy [Ogilvie-Harris and Basinski 1991, Ogilvie-Harris and Weisleder 1995]. The operating time was reported as 1 to 1.5 hours and patients were discharged on the day following the surgery, although they were already allowed to put weight on their operated knee joints on the day of the surgery [Ogilvie-Harris and Basinski 1991]. None of above studies used non-treated arthritic knees as controls.

Although most arthroscopic synovectomy procedures are still performed in a hospital setting, whether on an inpatient or outpatient basis, successful and cost-effective office-based arthroscopic synovectomies of the knee have been reported [Small et al 1994]. Performed on 106 knees under local anesthesia and light intravenous sedation, office-based arthroscopic synovectomy was found to have very few complications, less than 4%. Patients exited the operating table, walked back to the exam room, and were sent home on the same day, having been given an instruction booklet discussing wound care, showering and other pertinent information. Crutches were not usually necessary. Time for the procedure ranged from 30 to 45 minutes and constituted the basis for not permitting this procedure in patients younger than 16 years who "may not possess the emotional maturity to cooperate during a 30-to-45-min procedure under local anesthesia".

Two Japanese studies have been aimed at comparing arthroscopic and open surgical synovectomy [Shibata et al 1986, Matsui et al 1989]. In the first study, 10 open surgical synovectomies were compared with 14 arthroscopic synovectomies; three patients with bilateral involvement had open synovectomy on one knee and arthroscopic synovectomy on the other [Shibata et al 1986]. Results at one to two months after synovectomy showed no significant differences in the knees between arthroscopic and open surgical synovectomy, except for more complex post-operative management in open surgical synovectomy [Shibata et al 1986]. Results of a study in which 41 knees were synovectomized via arthroscopy and 26 knees via open surgery showed that clinical outcome was not dependent on the type of synovectomy performed; gradual deterioration of knee joint conditions was found in both groups [Matsui et al 1989]. Since clinical outcome is similar between the two synovectomy procedures, arthroscopic synovectomy is clearly superior to open surgical synovectomy insofar as it is less costly, less invasive and has less associated morbidity, in addition to the possibility of it being performed out of the hospital.

In Europe, Canada, Australia and New Zealand a noninasive radiochemical synovectomy option, called radiation synovectomy, exists. This therapeutic modality uses intra-articular injections of β-emitting radionuclides to ablate the synovial lining [Ansell et al 1963]. Several radionuclides have been tested, including, gold-198, yttrium-90 and dysprosium-165 [Shortkroff et al 1993]. Yttrium-90 colloids were deemed preferable to gold-198 ones because of the greater therapeutic effectiveness of the higher β energy, lower lymph node uptake and relatively good retention in the joints tested [Williams et al 1976]. In current European clinical practice, yttrium-90 colloids are most frequently and widely used, particularly for knees [Clunie and Ell 1995]. A randomized trial of radiation synovectomy and open surgical synovectomy showed comparable recurrence rates and similar results [Gumpel and Roles 1975].

Notwithstanding reported improvement rates of up to 60% after 1 year and 33% after 3 years [Oka 1975], the US Food and Drug Administration is reluctant to approve the routine use of this technique, the primary reason being concern over leakage and consequential radiation damage of the radioactive colloid [Shortkroff et al 1993, Davis and Chinol 1989]. A study measuring leakage rates of various yttrium preparations showed about 4% to 11% leakage at 24 hours, increasing to 15% and 25% at 5 days [Gumpel et al 1975]. Even the lower assumption of 5% to 10% leakage would result in a radiation absorbed dose of between 250 and 500 cGy to the liver and 5,000 to 10,000 cGy to regional lymph nodes [Dolphin 1973].

Attempts at reducing healthy tissue dose caused by leakage of the radioactive compound led to the development of a dysprosium-165 ferric hydroxide macroaggregate which accomplished this by the larger particle size and shorter physical half-life of dysprosium-165 [Hnatowich et al 1978]. Results of a clinical study of 111 patients with RA in the knee joints showed improvement in approximately 80% of the knees followed for two years post-operatively [Sledge et al 1987]. Leakage from the injected joint was minimal; the average leakage to liver, blood and inguinal lymph nodes, measured 24 hours after injection, was 0.64%, 0.03% and 0.24%, respectively [Sledge et al 1986]. A randomized multicenter double blind study found that dysprosium-165 and yttrium-90 were at least equally efficacious in effecting radiation synovectomy [Edmonds et al 1994]. One drawback of dysprosium-165 is that its short half-life requires the medical center to be located near a high-flux nuclear reactor. Despite promising results, radiation synovectomy is not an option for US patients.

Other modalities for synovectomy are being developed and investigated at an experimental level. Photodynamic synovectomy was performed in an animal RA model using a benzoporphyrin derivative as the photosensitizing compound; in this therapy, the photosensitizing compound is injected into the joint and, after some time, activated by light via intra-articular optical fibers [Trauner et al 1998]. Biodistribution studies showed compound accumulation primarily in the synovium and muscle, implying a relatively selective cellular kill. Tissue staining at two and four weeks post-treatment indicated synovial necrosis in the region of light activation in 50% of the knee joints at two weeks and 43% of the joints at four weeks, with no damage to other articular structures. Further work is being carried out to optimize the method of light delivery, since it may have a significant impact on the overall feasibility of photodynamic synovectomy.

Experimental laser synovectomy has also been tested [Raunest and Derra 1995]. In this study, two types of lasers, continuous and pulsed, were employed in combination with fibers 600 and 800 μm in diameter, respectively. Laser synovectomy was performed on a set of 14 rabbits; synovial necrosis, evident by histological analysis, was seen as early as four days after synovectomy and continued to be present until one to four weeks, depending on whether the laser was pulsed or continuous. Synovial regeneration occurred after one month in rabbit joints receiving pulsed laser synovectomy and was not seen for at least six months in the rabbits receiving continuous laser synovectomy. A set of control rabbits (14) received conventional open surgical synovectomy and showed histological evidence of synovial regeneration after one month.

Animal models are crucial for the development and testing of new therapeutic modalities, as well as continuing to answer questions about current ones. Examples include: anti-arthritic drugs [Hunneyball 1984], surgical synovectomy [Reichel and Weber 1986] and radiation synovectomy [Noble et al 1983, Zuckerman et al 1989]. The next section lists the animal models available for RA and discusses the model used in the following chapters.

2.1.3 Animal models

A multitude of experimental models in several types of animals exists and has been recently reviewed [Sokoloff 1984]. Classes of arthritis models include the following: infectious (viral, chlamydial, mycoplasma and postinfective), experimental immune (antigen-induced), systemic hypersensitization (via adjuvant, collagen, streptococcal cell wall, anti-bacterial sulfonamide), chemical (via lysosomal membrane destabilizers, charged macromolecules, polyrinoinosinate, zymosan, collagenase) and experimental rheumatoid factor inducement.

The Antigen-Induced Arthritis (AIA) rabbit model has been widely used in the literature for study relating to both the medical and surgical management of RA. The model has been shown to respond to drug treatment in a similar fashion to the clinical disease [Hunneyball 1984] and the size of the rabbit knee joint makes it attractive for testing of synovectomy treatment modalities [Reichel and Weber 1986, Zuckerman et al 1989, Trauner et al 1998]. The AIA rabbit was the model of choice for this thesis.

The first presentation of the AIA model used fibrin as the antigen [Dumonde and Glynn 1962]. Each rabbit was immunized by a set of intradermal injections of one type of fibrin with complete Freund's adjuvant. About one month later (following skin tests to check for fibrin reactivity) the fibrin suspension was injected intra-articularly. Rabbits were sacrificed at various time intervals post-injection to observe pathologic changes in their joints. Pathologic lesions found in the rabbit joint closely resembled the features found in human rheumatoid arthritis, i.e. hypertrophy and hyperplasia of the synovial lining cells, pannus formation with erosion of both articular cartilage and bone, chronic and persistent inflammation of the synovium with inflammatory cell infiltrate. No fibrous ankylosis was found which may have been due to the limited survival (16 weeks) time allowed to the rabbits. In view of the disease progression, these types of lesions may have arisen given more time. It was concluded that a chronic arthritic condition bearing a strong resemblance to human RA was induced following immunization via an intradermal injection of fibrin mixed in Freund's complete adjuvant and intra-articular injection of fibrin alone.

The sensitization step is essential in the production of a chronic arthritic reaction. Studies have shown that in the absence of sensitization, a chronic arthritic condition does not develop after an intra-articular challenge with antigen, or in other words, the production of chronic synovitis depends on the presence of systemic immunity to the appropriate foreign antigen [Jasin and Ziff 1969, Goldberg et al 1974]. This finding is independent of the antigen, whether bovine serum albumin (BSA) [Jasin and Ziff 1969], or autologous and homologous IgG [Goldberg et al 1974].

The severity of the arthritic response induced in the rabbits depends on the number and doses of intra-articular challenges with antigen. Results of a study done with BSA showed that multiple challenges produced severe cartilage and bone changes within three to ten weeks, whereas with a single challenge, although chronic synovitis was seen, there was no evidence of pannus invasion or cartilage and bone erosions within that time frame [Goldlust et al 1978]. Also, by increasing the frequency of intra-articular challenges, more severe changes were seen more rapidly.

The duration of the response has been shown to be affected by the type of Freund's adjuvant used [Henderson et al 1982]. Freund's complete adjuvant refers to a mixture which contains dead mycobacteria and thus stimulates the cell-mediated immunity. When the adjuvant is incomplete, it lacks the dead mycobacteria, and relies primarily on humoral immunity. Following sensitization with Freund's incomplete adjuvant, an arthus reaction (characterized by synoviocyte hypertrophy and hyperplasia, as well as influx of inflammatory cells) was seen within 3 days after challenge. Many inflammatory cells were found in the synovium between 5 and 11 days. However, after 14 days, the synovium returned to a normal appearance, differing, in this respect, from the use of complete adjuvant which has a more long-lasting or chronic reaction.

A protocol for AIA induction has been developed at the Orthopedic Research Laboratory of the Department of Orthopedic Surgery at the Brigham and Women's Hospital. It uses ovalbumin as the antigen [Consden et al 1971]. The booster immunization, performed three weeks after the first one, uses incomplete Freund's adjuvant, rather than complete. Antigen and adjuvant doses, as well as their timing, falls within standard procedures [Cooke 1988]. This protocol has been highly consistent in producing synovitis in rabbits. The type of rabbit chosen was the New Zealand white male rabbit, weighing 3 to 4 kg, and over 35 cm in length. The specific protocol used for the experiments to be presented later in this thesis is the following:

- first sensitization (after one week acclimatization)
  The sensitization solution is prepared by first dissolving 200 mg of ovalbumin in 10 ml of saline. This is then passed through a 0.45 μm filter and into a sterile glass syringe, which is attached to another sterile glass syringe containing 10 ml of Freund's complete adjuvant via a sterile stainless steel three-way stopcock. A thick, uniform emulsion is created by repeated injections between the two glass syringes. All manipulations are performed in a sterile hood. The emulsion is then transferred to a sterile glass vial which is sealed with a rubber stopper for transportation. Subcutaneous injections are given to each rabbit, delivering approximately 0.5 ml of the emulsion (four injections of 0.1 to 0.2 ml each). Twenty-five gauge, 5/8" needles are used with 1 ml disposable tuberculin syringes. A total of 5 mg of ovalbumin is administered subcutaneously.

- second sensitization (three weeks later)
  The procedure is the same as above except that Freund's incomplete adjuvant is used.

- arthritis induction (three weeks later)
  The induction solution is prepared by dissolving 200 mg of ovalbumin in 10 ml of saline. Again the solution is filtered through a 0.45 μm filter and placed into a sterile container for transportation. An anesthestic cocktail, consisting of 0.1 ml of xylazine (100 mg/ml) and 1 ml of ketamine (100 mg/ml), is administered intra-muscularly using a twenty-three gauge, 1" needle and a disposable 3 ml tuberculin syringe. The knee joint is shaved and caliper readings are taken. The shaved area is wiped down with both a povidone-iodine swabstick and alcohol swabs. Then 0.25 ml of the induction solution is injected intra-articularly using a twenty-seven gauge, 1/2" needle and 1 ml disposable tuberculin syringe. A total of 5 mg of ovalbumin is delivered intra-articularly. Several ranges of motion are performed on the joint in order to ease spreading of the ovalbumin to all parts of the joint. The rabbits are carefully monitored until they awake.

- pain management (from after induction to sacrifice)
  While rabbit is waking from the anesthesia required for the intra-articular injection, the first dose of a buprenorphine hydrochloride solution (0.3 mg/ml), a pain killer of opiate origin, is injected subcutaneously using a twenty-five gauge, 5/8" needle and 1 ml disposable tuberculin syringe. Injections are repeated every 12 hours until the time of sacrifice. The dose prescribed by veterinarians at the MIT animal facility is 0.2 ml, based on an average rabbit weight of 3.5 kg. Therefore, a total of 0.12 mg (0.4 ml) of buprenorphine is administered every day to each rabbit.

All the materials required for the above preparation are readily available from suppliers. The drugs used were the following: ovalbumin (A5378, Sigma Chemical Company, St. Louis, MO), Freund's complete and incomplete adjuvant (#0639-60-6 and 0639-60-7, respectively, DIFCO Laboratories, Detroit, MI), xylazine ("Anased Injectable", Lloyd Laboratories, Shenandoah, IA), ketamine ("Ketaset", Fort Dodge Animal Health, Fort Dodge, IA), buprenorphine ("Buprenex", Reckiett & Colman Pharmaceuticals Incorporated, Richmond, VA). Other materials, such as the disposable syringes and needles, alcohol swabs, iodine swabsticks, glass syringes, steel connector, flasks, calipers and shaver are standard.

2.2 Boron Neutron Capture Synovectomy

Boron Neutron Capture Synovectomy (BNCS) proposes to ablate rheumatoid synovium by using the boron neutron capture reaction, also written as $^{10}B(n,\alpha)^{7}Li$. This section describes the boron neutron capture reaction and its basis as a treatment modality. Then, the operating principles behind BNCS are detailed, as well as the advantages/disadvantages of this modality over other synovectomy options. Finally, BNCS is compared to the more traditional application of the boron neutron capture reaction and ramifications of the differences are discussed.

2.2.1 The $^{10}B(n,\alpha)^{7}Li$ reaction

The boron neutron capture reaction is based on the very high probability of ^{10}B (non-radioactive isotope of natural boron) capturing thermal neutrons. The thermal neutron capture cross section of ^{10}B is 3840 barns (1 barn=10^{-24} cm^2) and decreases with increasing neutron energy. When a ^{10}B nucleus captures a thermal neutron, a compound ^{11}B nucleus is formed. After about 10^{-12} second, the compound ^{11}B nucleus disintegrates into an alpha (α) particle and a ^{7}Li particle, which is excited 94% of the time and in the ground state 6% of the time. When the ^{7}Li particle goes into the excited state, the Q value of the reaction (or the energy released) is 2.31 MeV, with the $^{7}Li^*$ particle having 0.84 MeV and the α particle 1.47 MeV. The $^{7}Li^*$ nucleus promptly deexcites by emitting a photon with an energy of 0.48 MeV. When ^{7}Li is in the ground state, the Q value of the reaction is 2.79 MeV, divided into 1.01 MeV and 1.78 MeV between the ^{7}Li and α particle, respectively. Figure 2.3 schematically illustrates the possible events following the capture of a thermal neutron by ^{10}B. The average energy released, or average Q value, weighted by the event probabilities, is 2.34 MeV, with 0.85 MeV carried by the ^{7}Li particle and 1.49 MeV carried by the α particle.

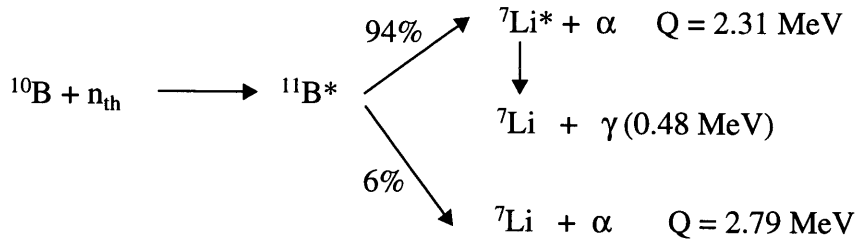

Figure 2.3: Sequence of events following the capture of a thermal neutron by a ^{10}B nucleus.

Both the ^{7}Li and α are heavy charged particles giving rise to closely spaced ionizations. They have a high linear energy transfer (LET) of around 200 keV/μm. On average, the ranges of the ^{7}Li and α particles are 5 and 9 μm, respectively. The ranges are a little smaller if looking only at the reaction which occurs 94% of the time, i. e. 4 and 7 μm for the ^{7}Li and α, respectively. Assuming that the diameter of a cell is 10 μm, then, if ^{10}B inside a cell captures a thermal neutron, all of the

energy released in the reaction is deposited within that cell (the 0.48 MeV photon emitted by $^{7}Li^{*}$ does not contribute to the local deposition of energy since it has a low linear energy transfer). The high ionization density of both the α and ^{7}Li particles has the potential to cause complex damage to DNA in association with adjacent structures, damaging the cells with little or no possibility of subsequent repair [Goodhead 1989]. Herein lies the basis of the use of the boron neutron capture reaction for therapy: by delivering ^{10}B to selected cells, their death can be induced by irradiation with thermal neutrons.

It is desirable to have as large a number of ^{10}B nuclei as possible, since it would lower the number of thermal neutrons required and thereby minimize the energy deposited by the interaction of thermal neutrons with nuclei present in surrounding tissue. The two most important interactions are the capture of thermal neutrons by hydrogen and nitrogen. Capture of a thermal neutron by hydrogen, written as $^{1}H(n,\gamma)^{2}H$, produces a deuteron and a 2.22 MeV photon. The photon has a low LET and does not deposit its energy locally, thereby contributing to the deposition of energy over a large volume of tissue. Capture of a thermal neutron by nitrogen, written as $^{14}N(n,p)^{14}C$, creates an recoil proton with 0.584 MeV and a carbon nucleus with 0.042 MeV, for a total Q value of 0.626 MeV. The energy deposition for this reaction is relatively local, its products traveling less than 1 mm in tissue.

It must be emphasized that it is the combination of low-energy neutrons with ^{10}B nuclei that results in the specific destruction of cells. The ^{10}B nucleus needs to be activated (via irradiation with low-energy neutrons) to cause the magnitude of energy deposition necessary for cell death. Alone, it has no significant deleterious effects. Natural boron, made of 20% ^{10}B and 80% ^{11}B, is an ubiquitous element in rocks, soil and water [Woods 1994]. A recent review of the literature on the boron content of foods reports that vegetables are rich in boron with an average content of 13 µg/g [Nielsen 1986]. Daily intake of boron by humans can vary widely depending on proportions of various foods in their diets [WHO 1996]. Although most of the studies have been performed in animals, two studies have reported an effect of boron depletion in humans, suggesting a possible role of boron in preventing calcium loss and bone demineralization [Nielsen et al 1988, Nielsen et al 1990]. Hypothesized mechanisms include an effect of boron on parathormone activity, thereby influencing metabolism of calcium, phosphorous, magnesium and cholecalciferol [Nielsen 1986]. A double-blind clinical pilot study found that 50% of patients with confirmed osteoarthritis who took a boron supplement improved, compared to 10% receiving a placebo [Travers et al 1990].

2.2.2 Proposed BNCS treatment

BNCS proposes to use the $^{10}B(n,\alpha)^{7}Li$ reaction to destroy rheumatoid synovium. In a treatment, a boronated compound would be injected into the joint space/cavity where it would diffuse to the synovial lining and be taken up by the synoviocytes. Then, the joint would be irradiated, inducing the boron neutron capture reaction which, in turn, would induce cell death via the dense energy deposition of its products as described previously. Figure 2.4 shows a schematic of the proposed two-step treatment. One attractive feature of such a binary treatment modality is that each of the components can be manipulated independently. As will be detailed in the following paragraphs, BNCS has several advantages over existing modes of synovectomy.

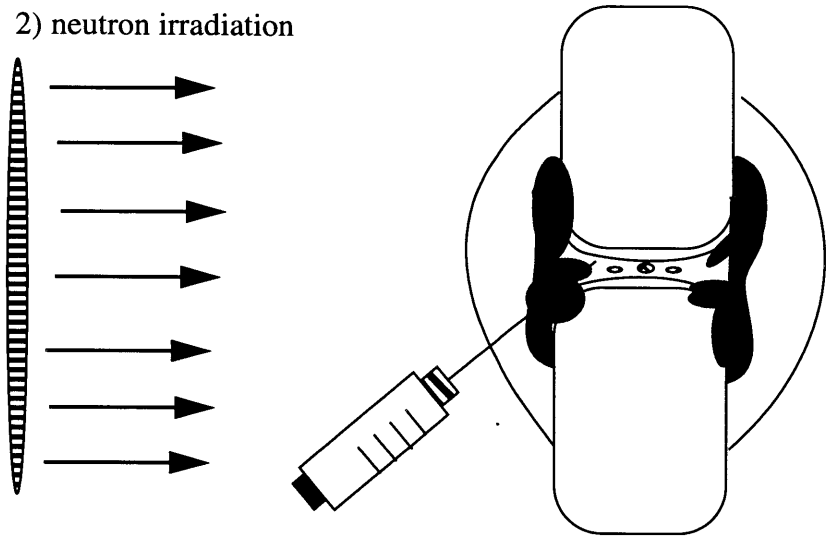

Figure 2.4: Schematic of Boron Neutron Capture Synovectomy (BNCS), a novel treatment for RA.

The advantages of BNCS over open surgical synovectomy are clear in that it is non-invasive and does not require general anesthesia (particularly important since populations are getting older, on average, and are more likely to have concomitant heart complications) or hospitalization (which dramatically increases cost). In addition, BNCS is technically easier to accomplish. Furthermore, given an appropriate boron compound and neutron source, synovectomy via the boron neutron capture reaction could be achieved in significantly less time; treatment times as low as several minutes are theoretically possible. The cost of carrying out BNCS (after an initial investment for the neutron source) would be limited to the acquisition of the boron compound and the time of the personnel. These factors point to BNCS as a potentially cost-effective synovectomy option.

Recent advances in arthroscopic synovectomy have enabled it to be performed as an office-based procedure, thereby overcoming some of the disadvantages of open surgical synovectomy such as the administration of general anesthesia and long hospitalization periods [Small et al 1994]. Reported times for the procedure range from 30 to 45 minutes [Small et al 1994]. BNCS could be effected in comparable times, with potential for even lower therapy times.

The most significant advantage of BNCS over radiation synovectomy is that it does not require administration of radioactive substances. Radiation synovectomy is technically as easy as BNCS (also only requiring an intra-articular injection) and also does not necessitate general anesthesia or hospitalization. However, it uses radioactive colloids which may leak outside of the joint and deliver radiation dose to other parts of the body. It is primarily because of this concern that the US Food and Drug Administration has been reticent to approve radiation synovectomy for routine use in the US [Shortkroff et al 1993]. In BNCS, compound leakage is not a problem since the boron must be activated in order to cause damage and activation is easily controlled by beam size.

In the US, after the decline of popularity of open surgical synovectomy and before the emergence of arthroscopic synovectomy, the tendency has been to prolong the administration of second-line drugs and cytotoxic drugs, despite accumulating evidence of the lack of joint response, until the point where total knee replacement is clearly indicated. BNCS could have an advantage over this type of management in that it could avoid the unpleasant side effects typically encountered with second-line and cytotoxic drugs, without precluding eventual total knee replacement.

2.2.3 Comparison to Boron Neutron Capture Therapy

The traditional application of the boron neutron capture reaction for treatment, or boron neutron capture therapy (BNCT), has been directed at the brain tumor, glioblastoma multiforme, although melanoma tumors, both cutaneous and intracranial have also been included [Barth et al 1992]. There are currently three clinical trials worldwide using epithermal neutron beams. Two are in the US, one at Harvard-MIT in Boston, Massachusetts [Busse et al 1998] and the other at Brookhaven National Laboratory in Upton, New York [Diaz et al 1998]. The third is in Europe, at the High Flux Reactor in Petten, The Netherlands [Sauerwein et al 1998]. Japan has a history of performing BNCT [Kanda 1997] and continues to perform treatments for both glioblastoma [Nakagawa and Kageji 1998] and melanoma tumors [Mishima 1998], using both thermal and epithermal beams. The boron compound used in the US is borono-phenylalanine while the European study uses $Na_2B_{12}H_{12}$. Treatments in Japan have used both compounds. In a treatment, patients are given the boron compound either orally or intra-vascularly. After some time, to allow the boron compound to accumulate in the tumor site, irradiation regimens are begun. The epithermal beams typically have an average energy of 2 keV (range from 4 to 40 keV), enabling penetration up to 7 cm below the skin surface [Yanch et al 1992, Wheeler et al 1990, Clement et al 1990].

Although based on the same physical principle, the different nature and depth of the target tissue in BNCS leads to significant differences in therapy parameters with respect to both the delivery of the boron compound and the design of an appropriate source of neutrons. The method of boron compound delivery to the target tissue differs between BNCT and BNCS. In BNCT, the boron labelled compound is administered intra-vascularly or orally and must reach the tumor via the body's metabolic pathways. In BNCS, the boron compound is delivered by a local intra-articular injection, making it more likely that high boron concentrations be achieved in target tissue. Higher boron concentrations imply shorter therapy times and a decrease in background dose, which is particularly important for BNCS patients, since they are otherwise healthy individuals (in contrast with terminal BNCT patients). The target tissue in BNCS is rheumatoid synovium, which typically lies 1.3 to 1.5 cm. below the surface of the skin. This is in contrast with tumors treated via BNCT which may extend up to 7 cm below the surface of the skin. Therefore, it could be expected that a less penetrating neutron beam is required for BNCS compared to BNCT.

The following section presents the design of accelerator-based neutron sources appropriate for BNCS, including determination of the therapeutically useful neutron energy range, selection of moderator/ reflector materials and consideration of various light ion reactions. It ends with a description of further neutron beam optimization and the construction of a moderator/reflector assembly [Gierga et al 1999].

2.3 Accelerator-based neutron beams

BNCS could be performed using either a reactor-based or an accelerator-based neutron source. However, the advantage of a compact accelerator-based source is that it could be installed in a hospital environment or medical center and thus be readily available for clinical treatment. In fact, there has been an increasing amount of interest in accelerator-based neutron sources for BNCT [Beynon et al 1997, Chu et al 1997, Klinkowstein et al 1997, Nigg et al 1997, Teichman and Crawford 1997]. A high current tandem electrostatic accelerator has been designed and installed at the Massachusetts Institute of Technology Laboratory for Accelerator Beam Applications (MIT LABA) by Newton Scientific Incorporated, Cambridge, Massachusetts. This tandem electrostatic accelerator can deliver multi-milliampere proton or deuteron beams up to 4.1 MeV in energy [Klinkowstein et al 1997].

This section presents the design of accelerator-based neutron beams for BNCS. The first step in the process was to determine the therapeutically useful neutron beam energy range. This was done by developing a knee joint phantom and studying, via simulation, the dosimetric properties of ideal (monoenergetic and photon-free) neutron beams ranging from 0.025 eV to 100 keV in energy. The beams were modeled as isotropic in order to approximate the angular characteristics of a beam following moderation by a large mass of low-Z material. Results of this section (2.3.1) are applicable to the development of both reactor-based and accelerator-based neutron sources, provided that the beams are approximately isotropic in direction when they interact with the patient.

Then, attention was turned to the design of a moderator/reflector assembly (2.3.2) for the MIT LABA accelerator which would be able to moderate the energetic neutrons emerging from the accelerator down to the therapeutically useful neutron energy range. Initial studies were based on the two most studied reactions for accelerator-based BNCT, $^{7}Li(p,n)^{7}Be$ and $^{9}Be(p,n)^{9}B$. Materials were chosen for the moderator/reflector assembly and in-air dosimetry simulations were run to determine the dose and flux dependence on assembly dimensions (moderator length and diameter, as well as reflector thickness and length). In-phantom dosimetry simulations were carried out to quantify the effects on therapy parameters and examined the sensitivity of therapy parameters to varying synovial ^{10}B concentrations for two potentially useful beams. Then, in 2.3.3, results of an investigation into several other neutron producing reactions is presented.

Further neutron beam optimization studies by other members of MIT LABA [Gierga et al 1999], as well as developments in target cooling [Blackburn et al 1998], led to the construction and installation of a target and moderator/reflector assembly for the MIT LABA tandem electrostatic accelerator. The last subsection (2.3.4) summarizes their work, with emphasis on the specific aspects of their work, e.g. improvements in therapeutic ratios by the addition of rear and side reflectors, pertinent to the animal irradiation experiments to be described in chapter 5.

2.3.1 Determination of optimal neutron beam energy range

The calculational tool used for the beam design was the Monte Carlo for N-particle transport code (MCNP), version 4B [Briesmeister 1986], installed on Sun Sparc Stations at the Whitaker College Biomedical Imaging and Computational Laboratory at MIT. Advantages of this code include use of point-wise continuous energy cross-section data from a number of sources, three-dimensional freedom in designing configuration of materials and a sophisticated built-in geometry package to aid in debugging.

Method

The geometry used for the ideal beam studies is shown in figure 2.5. The knee phantom consists of a series of concentric cylinders representing the different tissue layers found in the arthritic joint. The tissue thicknesses of the knee joint phantom were estimated from Magnetic Resonance images of human arthritic knees to be as follows: 1 cm for the skin and overlying tissue, 0.3 cm for the subsynovium, 0.15 cm for the synovium, 0.2 cm for the joint fluid space, 0.2 cm for the articular cartilage and 5 cm for the bone. The total diameter of the knee phantom is 8.70 cm. A 10 cm diameter isotropic neutron beam was placed 1.65 cm away from the phantom surface. Particle fluences were tallied in a cross-section of a cylinder, with width of 2.5 cm and height of 6 cm, in the plane perpendicular to the beam.

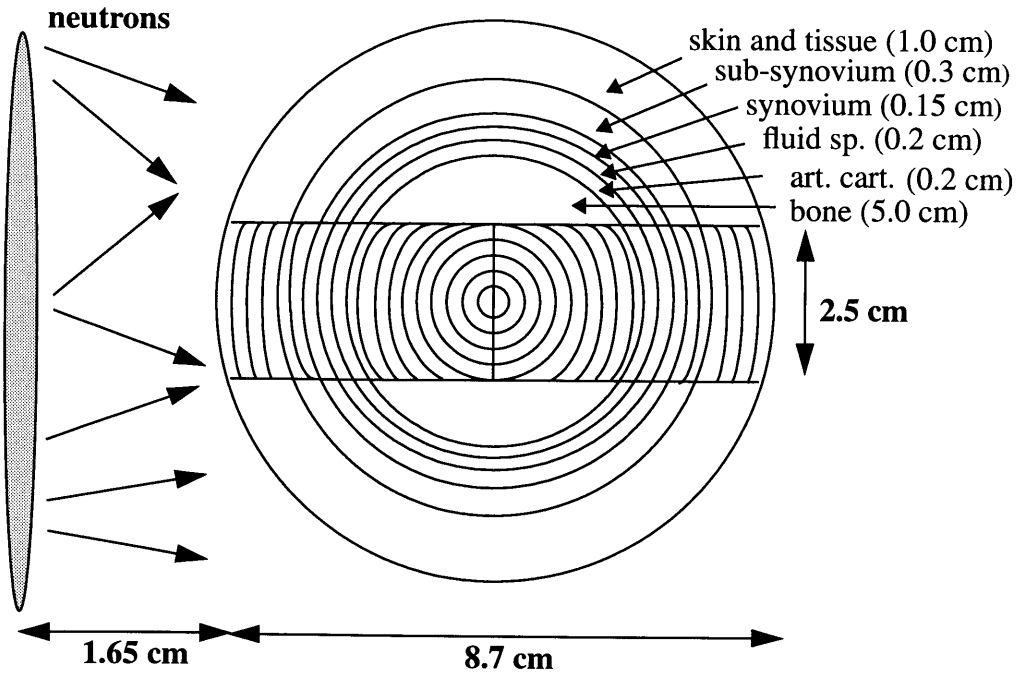

Figure 2.5: Geometry of the MCNP cylindrical human knee joint phantom with an ideal neutron source.

Simulated beam energies ranged from 0.025 eV to 100 keV and the neutron source was assumed to emit 3.60×10^{12} n/s. The particle fluence was determined as a function of depth for all beam components: thermal neutrons (neutrons with a maximum cutoff energy of 0.36 eV), nonthermal neutrons (neutrons with energies above 0.36 eV) and induced gammas (including the 478 keV prompt gamma ray emitted from the boron neutron capture reaction). Neutron and photon dose rates were obtained by modifying the neutron and photon fluxes by fluence-to-kerma conversion factors [Caswell et al 1982, Zamenhof et al 1975]. To estimate the $^{10}B(n,\alpha)^{7}Li$ contribution to dose to the synovium, the thermal neutron flux was modified by ^{10}B fluence-to-kerma conversion factors [Zamenhof et al 1975] and multiplied by ^{10}B concentration. It must be noted that ^{10}B in the form of $K_2B_{12}H_{12}$ was explicitly modeled in order to accurately simulate neutron flux depression and photon production from the boron neutron capture reaction. The boron dose contribution to other tissues was calculated in the same way. No weighting was applied to account for the relative biological effectiveness (RBE) of the different types of radiation.

Determination of a therapeutically useful beam energy was based on the examination of the ratio of synovium dose to each of two healthy tissues: skin and bone surface. It has been empirically determined in clinical trials of radiation synovectomy using β-emitting radionuclides that a dose of 10,000 cGy is required for clinical success [Deutsch et al 1973]. This, combined with the observation that at 800 cGy mild and reversible skin reddening occurs [Nias 1990] led to the determination of a highly conservative minimum synovium/skin therapeutic ratio of 12. Bone has been identified as a tissue to be protected as much as possible during radiotherapy procedures involving bone [ICRP30 1975]. No dose limits were set since potential carcinogenic effects to the bone are stochastic. All therapeutic ratios are calculated with the "front" half of the knee phantom only, that is, the total dose to the front layer of the synovium (calculated by summing the dose components in each tally volume) was divided by the total dose to the front layer of skin or bone, depending on the therapeutic ratio being calculated.

Several scenarios of boron distribution in the synovium and bone were simulated, as summarized in Table 2.4. Boron concentration was not varied in the skin, since it is unlikely that intra-articular injections of a boronated compound would lead to accumulation in the skin. Concentration in the skin was kept at 1 ppm, which is conservative considering reports of an average of 0.1 ppm in the skin of healthy [Forbes et al 1954] and arthritic [Havercroft and Ward 1991] individuals.

Table 2.4: Distributions of boron concentrations in the phantom for ideal beam studies

comb#	skin (ppm)	synovium (ppm)	bone surface (ppm)
0	1	1,000	1
1	1	100	10
2	1	1,000	100
3	1	10,000	100

The most ideal case, with ^{10}B in the synovium only and all other tissues contain 1 ppm of ^{10}B, is represented by combination#0. In combinations #1 and #2, the synovium/bone uptake ratio was maintained at 10, while the magnitude of concentrations in both of the tissues was increased by a factor of 10. Finally, in combination #3, the synovium/bone surface ratio was increased to 100 by keeping the bone surface concentration at 100 ppm and increasing synovial concentration to 10,000 ppm.

The most extensive number of simulations was performed for combination#0, 21 energies (0.025, 0.1, 1, 5, 10, 25, 50, 75, 100, 125, 250, 500, 750 eV and 1, 2, 3, 5, 7, 10, 50, 100 keV), while for each of the following combinations, 10 energies were simulated (0.025, 0.1, 1, 10, 100 eV and 1, 10, 100 keV). For each simulation, 160 million particle histories were run and statistical errors (representing one standard deviation from the mean) were as follow: gamma flux $\leq 5\%$ between 0.02 eV and 10 keV and $< 13\%$ between 10 keV and 100 keV; total neutron (including thermal and nonthermal) flux $\leq 2\%$ at all energies; boron $\leq 5\%$ at all energies. This corresponds to an error in the therapeutic dose ratios of: $\leq 6\%$ between neutron energies of 0.025 eV and 10 keV, and $< 14\%$ between neutron energies of 10 keV and 100 keV.

Results and discussion

Individual dose components were plotted as a function of depth in the joint model for each energy of each boron uptake combination. A full set of plots is included in Appendix A. Figure 2.6 shows sample dose profile for combination #2; four peaks appear in the plot since boron was added to the synovium and bone surface, which extend from the "front" to the "back" of the phantom.

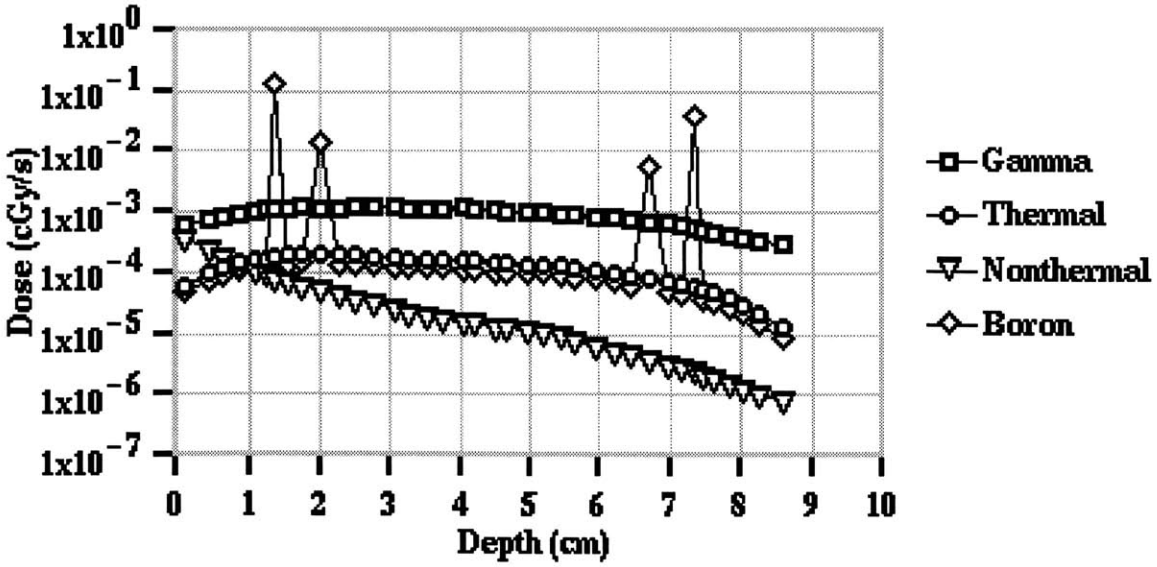

Figure 2.6: Sample dose depth profile in the MCNP knee joint phantom with 1,000 ppm of ^{10}B in the synovium and 100 ppm in the bone surface at an ideal neutron energy of 1 keV.

The large number of energies tested for combination #0 allows for a relatively precise estimate of the rise in nonthermal neutron dose rate in the skin. By 125 eV, the nonthermal component is about equal to the thermal neutron and by 2 keV, the nonthermal neutron dose rate equals the gamma dose rate in the skin. The energy at which the nonthermal neutron dose rate to the skin approaches the boron dose rates to the synovium and bone surface depends on the amount of boron. For example, in combination #0, with 1,000 ppm in the synovium and 1 ppm of boron in all other tissues, the nonthermal neutron dose rate in the skin is lower than the synovial boron dose rate (by about a factor of 2) even at 100 keV. This is also true in combination#2 where it is observed that the nonthermal neutron dose rate in the skin exceeds the bone surface boron dose rate by almost a factor of 3.

Figure 2.7 shows plots of the (a) synovium/skin and (b) synovium/bone surface dose ratio versus ideal neutron beam energy. The curves in figure 2.7 (a) show that the synovium/skin dose ratio follows the same trend for all combinations of boron concentrations. It increases after 0.025 eV, reaching a broad plateau between about 1 eV and 1 keV; after 1 keV, the curve drops (the decrease begins just after 100 eV). At 5 keV, the synovium to skin dose ratio is the same as at 0.025 eV.

There is no difference between combinations #0 and #2. This makes sense in that the bone surface lies behind the synovium and perturbations of bone concentration should not affect the dose ratio of synovium to skin, which is the first tissue encountered by the beam. Considering the goal of a synovium/skin ratio greater than or equal to 12, combinations #0 and #2 are both acceptable from thermal energies until just over 10 keV, while combination#1 is only acceptable from about 1 eV to 1 keV. Finally, in combination#3, the synovium/skin ratio is above 12 at all energies except for 100 keV, at which energy it is 12, rendering the potentially acceptable therapeutic range from thermal energies to 100 keV.

A comparison of combinations #1 and #2 shows a proportional increase in therapeutic ratio with synovial boron concentration. For example, at 0.025 eV, the synovium/skin uptake ratio is increased by a factor of 10 (synovium from 100 to 1,000 ppm) and the therapeutic ratio also increases by a factor of 10 (from 5 to 50). This trend is roughly constant throughout the most of the energy range tested. The therapeutic ratio for combination #1 (about 5) is not the same as the uptake ratio (100) because of the high gamma contribution at the surface of the skin with respect to the boron dose at the synovium and the decrease in the thermal neutron flux between the skin and synovium. The rise in the therapeutic ratio is linear with increase in synovial concentration from 100 ppm to 1,000 ppm because the dose rates in the skin are the same and similar behavior in thermal neutron flux is seen between the skin and synovium, such that the only change is the increase in boron concentration. When synovium concentration is increased by another factor of 10 (combination#3), the increase in the therapeutic dose ratio is not proportional. At 0.025 eV, the increase is by a factor of 4 (from 50 to 200). This is a result of flux depression from the large amount of boron in the synovium (10,000 ppm). The flux depression accounts for a 60% decrease in neutron dose rate at synovium (it is about 15% of skin level, instead of 50% as in the previous example) leading to a correspondingly lower therapeutic ratio. Instead of seeing a therapeutic ratio of 500 (linear), the ratio is 200 (=500-(0.6*500)). The difference between combinations#2 and #3 remains the same, within statistics, throughout most of the energy range tested.

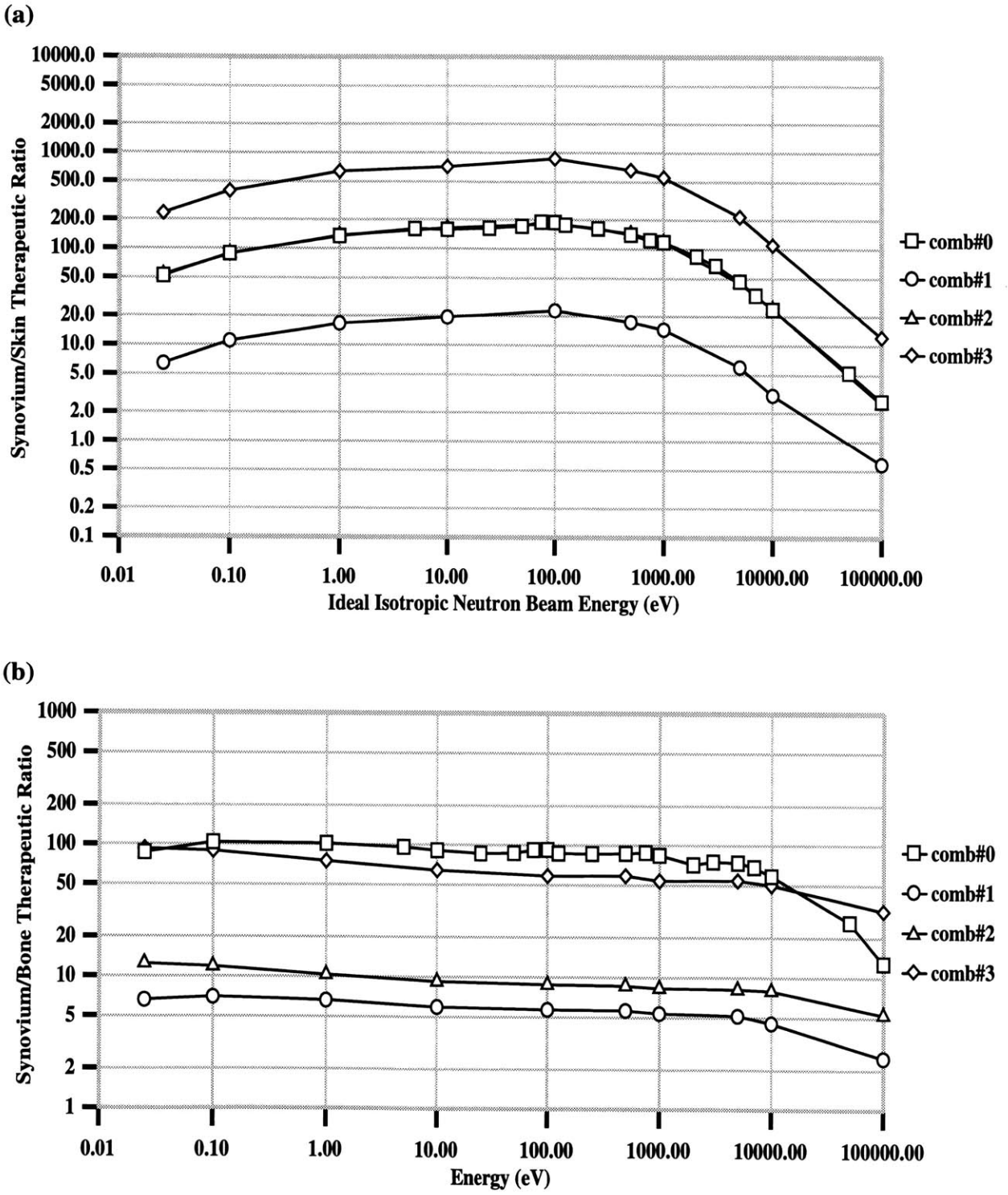

Figure 2.7: Dependence of (a) synovium/skin and (b) synovium/bone surface therapeutic dose ratios on ideal neutron beam energy.

Figure 2.7(b) shows the synovium to bone surface ratio as a function of neutron energy. In all combinations of uptake, the ratio decreases slowly throughout most of the energy range tested, with sharper decreases seen at energies above 10 keV. Since the boron concentration of both the synovium and bone surface is altered, the effect of both the ratio and the magnitude of the boron tissue concentrations can be examined. A comparison of the results of combinations #1 and #2 allows the investigation of the effect of the uptake ratio on the range of neutron energies yielding optimal synovium/bone dose ratios. The synovium/bone uptake ratio in combinations #1 and #2 is 10. However, the magnitude of the concentrations used to calculate the uptake ratio is different; in combination #1, the synovium has 100 ppm and the bone 10 ppm, while in combination #2, the synovium has 1000 ppm and the bone 100 ppm. Although the uptake ratio is the same in both combinations #1 and #2, the therapeutic ratio is not. At 0.025 eV, the ratio for combination#1 is about 5 while for combination#2 it is about 10 and thus equal to the uptake ratio. In combination #1, the therapeutic ratio is lower than the uptake ratio because of the high gamma contribution with respect to the other dose components. As the dose rate from boron increases, combination #2 (1,000 ppm), the boron dose component dominates over the gamma dose and thus the therapeutic dose ratio becomes primarily determined by the boron concentrations, or the uptake ratio. This is why at high neutron energies sharp decreases are seen in therapeutic dose ratio; the nonthermal neutron dose rate begins to dominate over the boron dose rate. The synovium/bone therapeutic dose ratios for combinations #1 and #2 exhibit similar decreases as neutron energy is increased; the ratio are the same between the energies of 0.025 to 1 eV and between 10 eV and 10 keV (all within MCNP statistical fluctuation of 6%). In combination #1, the average ratio decreases from 6.7 to 5.4, while in combination #2, the ratio decreases from 12 to 8.9. At 100 keV there is a sharper drop to 2.6 and 5.3, respectively.

Comparison between combinations #2 and #3 allows the investigation of the effect of uptake ratio on range of energies required for optimal therapeutic dose ratios. In these two combinations, the magnitude of the bone concentration is constant at 100 ppm, while the synovial uptake varies from 1,000 and 10,000 ppm, yielding uptake ratios of 10 and 100, respectively for combinations #2 and #3. At 0.0025 eV, the synovium/bone uptake ratio in combinations #2 and #3 are roughly the same as the therapeutic ratios and this trend is observed throughout most of the range tested. This is expected based on the reasoning in the previous comparison; the boron concentration of the synovium in both combinations is such that it is the dominant dose component. The average ratio is 86 between 0.025 and 1 eV and decreases to 57 between 10 eV and 10 keV. At 100 keV, the ratio has dropped by 44% to 32.

Comparison between combinations #0 and #2 also allows investigation of the effect of the uptake ratio, but this time the synovial concentration is constant, and the bone concentration changes from 1 ppm to 100 ppm, yielding ratios of 1,000 and 10, respectively. Based on the difference of uptake ratios, a 100-fold difference between the therapeutic ratios should be observed. However, a comparison between the combinations shows that the synovium/bone surface ratio only increases by a factor of 10. This occurs because the gamma dose rate at the bone surface in combination#1 is one order of magnitude higher than the boron dose rate, again supporting the hypothesis that linearity in the therapeutic ratio may only occur when the boron dose rate at the synovium is the primary dose component. The average synovium/bone therapeutic ratio between 0.025 and 1 keV is 94. By 10 keV, the ratio is 59 and then decreases sharply to 13 at 100 keV.

Conclusions

The general principle in the determination of a therapeutically useful neutron energy range is to keep both therapeutic dose ratios, synovium/skin and synovium/bone surface, high. Considering the shape of the synovium/skin curve, a plateau is seen from 1 eV to 1 keV. The synovium/bone surface ratio is higher at thermal energies, thereby enlarging the range to include thermal energies. However, the synovium/skin ratio at thermal energies is the same as at 5 keV, therefore making the therapeutically useful neutron energy range from 0.025 eV to 5 keV.

The desired therapeutic neutron energy range can be affected by varying boron concentration in the synovium, skin and bone surface. The uptake ratio modeled in the synovium and bone surface correspond closely to the therapeutic dose ratio if the dose rate due to boron is the primary dose component in the tissues. This is particularly important at low boron concentrations where the gamma dose may be larger and at high neutron energies where the nonthermal neutron dose becomes more prominent. For example, a synovium/bone uptake ratio of 10 (100/10) corresponds to a therapeutic dose ratio of 5, while with an uptake ratio of 1000/100, the therapeutic dose ratio is approximately the same as the uptake ratio, i.e. 10. However, changing the boron concentrations in synovium and bone does not affect the general trend observed in synovium/bone curves, i.e. higher ratio between 0.025 eV and 1eV, with a 20 to 30% decrease between 1eV and 1 keV, and a sharper decrease after 10 keV. No minimum number was set for the synovium/bone ratio since the goal was to keep the ratio as high as possible.

The synovium/skin, on the other hand, has a minimum design goal of 12, although it should be stressed that this is very conservative (based on development of mild, reversible, skin reddening) at 800 RBE-cGy and the expected therapeutic synovial dose of 10,000 RBE-cGy). The skin was always modeled with 1 ppm of boron, which implies that the effect of both uptake ratio and boron concentration magnitudes, are the same. A synovial boron concentration of 100 ppm (ratio 100) limits the acceptable neutron energy range from 1 eV to 1 keV (ratios ranged from 15 to 23). When the synovial boron concentration is increased to 1,000 ppm (ratio 1000), then the useful neutron energy range becomes larger, ranging from 0.025 eV to 10 keV (the ratio exceeded 45 between 0.025 eV and 5 keV, and was 24 at 10 keV). Finally, as the synovial boron concentration is further increased, the therapeutic dose ratios allows for even greater latitude in neutron beam energy requirements, with the entire range tested, from 0.025 eV to 100 keV, yielding acceptable therapeutic dose ratios.

2.3.2 Design of moderator/reflector assembly

Initial moderator/reflector design studies were based on two of the most studied reactions for accelerator-based BNCT, the $^{7}Li(p,n)^{7}Be$ and $^{9}Be(p,n)^{9}B$ reactions. The yield of 2.5 MeV protons impinging on a lithium target is 8.9×10^{11} n/s/mA, with a maximum neutron energy at 0^{o} of 780 keV [Liskien and Paulson 1975]. Lithium targets are attractive due to the high neutron yields from relatively low proton beam power and low neutron energy. Disadvantages of lithium targets are the low melting point and thermal conductivity which make target cooling a challenge. Beryllium targets have a higher melting point and better thermal conductivity. An incident proton energy of

4.0 MeV results in a yield of 5.25×10^{11} n/s/mA with the maximum neutron energy at 2.2 MeV [Howard et al 1996]. A disadvantage of beryllium is that higher proton energies are needed and higher neutron energies are generated, for comparable or smaller yield relative to ^{7}Li.

The maximum neutron energies from the above two reactions (0.8 and 2.2 MeV, respectively) are significantly higher than the design goal of the therapeutic neutron energy range and thus intense moderation of source neutrons is required. A neutron reflector is important in order to improve the yield of therapy neutrons at the irradiation position by scattering non-therapy neutrons back into the moderator and thereby giving them another chance to become therapy neutrons. Shielding issues were not considered.

Materials for the moderator/reflector assembly were chosen by judicious application of extensive studies of moderator/reflector materials for BNCT [Yanch et al 1992]. An optimal moderator should have a large scattering cross section and a low-Z. Furthermore, nonthermal neutron contamination and production of capture gammas should be kept to a minimum. Previous studies, involving a detailed investigation of alumina, beryllium oxide, titanium deuteride, light water and heavy water, showed that alumina, titanium deuteride and light water produced a significant number of energetic capture gammas, excluding them as desirable materials [Yanch et al 1992]. The other two, heavy water and beryllium oxide, were found to be somewhat similar in their moderating abilities [Yanch et al 1992]. Heavy water was chosen as the moderator since it is less toxic and expensive than beryllium oxide, as well as more readily available.

An optimal reflector should be found among heavy isotopes which can scatter back the neutrons, thereby increasing the yield, without creating excess gamma rays. Investigation of the reflectivity of several materials, namely lead, bismuth, graphite and alumina, showed that lead, graphite and alumina were all similar in reflectivity, whereas bismuth was less reflecting [Yanch et al 1992]. Studies also showed that graphite was cleanest in terms of gamma production [Yanch et al 1992]. For BNCT beam design, graphite was dismissed because it was considered to be too moderating based on the determination that energies ranging from 4 eV to 40 keV were therapeutically useful [Yanch et al 1991]. However, BNCS requires a lower range of therapeutic neutron energies and, as a consequence, the additional moderating ability of graphite is desirable. This, in addition to the low production of contaminating gammas, led to the choice of graphite as reflector material.

Dosimetry was then simulated both in-air and in-phantom. The moderator and reflector geometry consisted of two concentric cylinders. Previous work showed that cylindrical geometry is optimal for a reflector assembly, as compared to a conical or a paraboidal shape [Zhou 1990]. Accelerator target dimensions were 5 cm in diameter and 1 cm in thickness. The target was placed about 1 cm into the moderator since it was found that this results in greater yield of neutrons [Zhou 1990]. For in-air dosimetry calculations, particle flux of all components (thermal, nonthermal and gamma) was tallied across the surface of the moderator end, while for in-phantom dosimetry calculations, particle flux was tallied in the joint phantom described in section 2.3.1. Dose rates were obtained via fluence-to-kerma conversion factors [Caswell et al 1982, Zamenhof et al 1975]. The dose per starting neutron was multiplied by assumed yields of 8.9×10^{11} n/s/mA and 5.25×10^{11} n/s/mA for 2.5 MeV ^{7}Li(p,n)^{7}Be and 4.0 MeV ^{9}Be(p,n)^{9}B reactions, respectively, to obtain dose rates per unit particle current.

In-air dosimetry

In-air dosimetry simulations investigated the dependence of flux and dose on the diameter and length of the moderator/reflector assembly. The MCNP geometry is shown below in figure 2.8. A lithium target was initially modeled and if the parameter was found to vary, a beryllium target was also modeled. Only one parameter was varied at a time. First, moderator diameter was varied from 10 to 24 cm, in increments of 1 cm between 10 cm and 15 cm, and then at diameters of 18 cm and 24 cm. Then, reflector thickness was varied from 5 cm to 24 cm, in increments of 5 cm from 10 to 15 cm, and then in increments of 3 cm from 15 to 24 cm. Turning to assembly length, the length of the part of the reflector behind the moderator was changed from 5 to 15 cm. Finally, moderator length was varied from 20 to 60 cm, in increments of 5 cm.

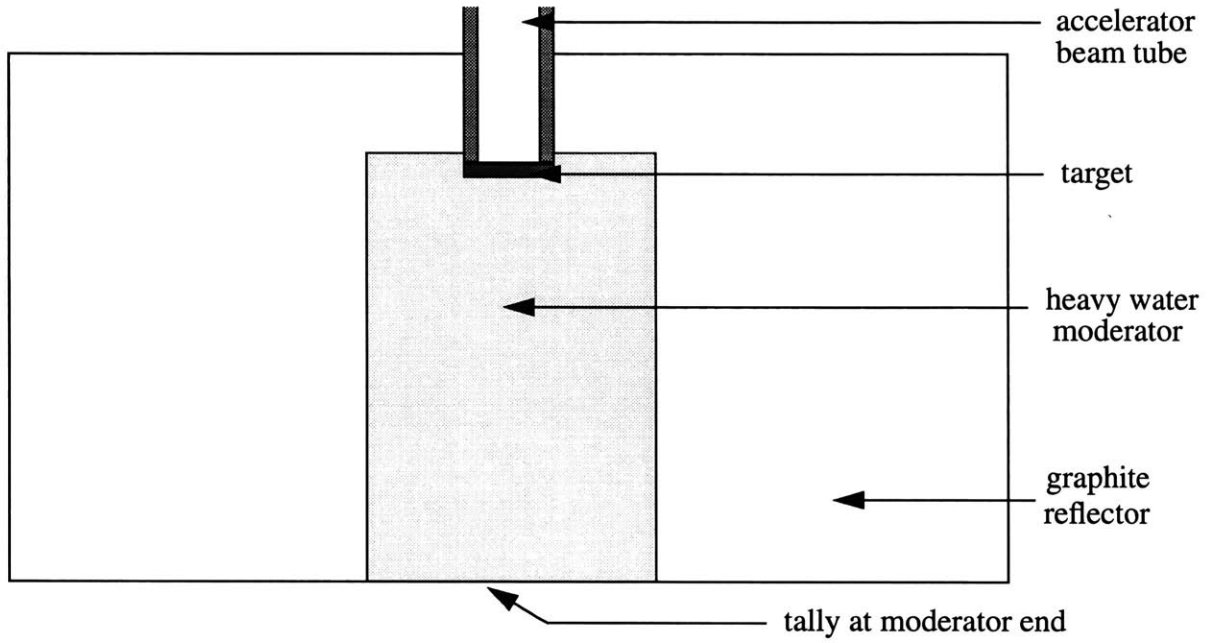

Figure 2.8: MCNP geometry of moderator/reflector assembly for in-air dosimetry.

The effect of variation in moderator diameter on flux and dose at the moderator exit surface is shown in figure 2.9 (other parameters were: reflector thickness 15 cm, moderator length 45 cm, reflector length 50 cm). The range of moderator diameters to be tested was chosen on the basis of being slightly bigger than the joint phantom (10 cm) without being so large (greater than 24 cm) that the moderator would begin to encroach upon the junction of the lower abdomen and thigh. As can be seen in figure 2.9, varying moderator diameter did not have a significant effect on the gamma or thermal neutron flux. Both the nonthermal flux and dose decreased, since additional heavy water moderation in the radial direction scattered more neutrons back into the beam which then became thermalized. An increase in diameter beyond 15 cm did not lead to further decrease in nonthermal neutron dose (within statistical error). The moderator diameter was set at 15 cm, since this was considered large enough to accommodate variations in human knee sizes and increases in diameter did not lead to increases in particle flux.

(a)

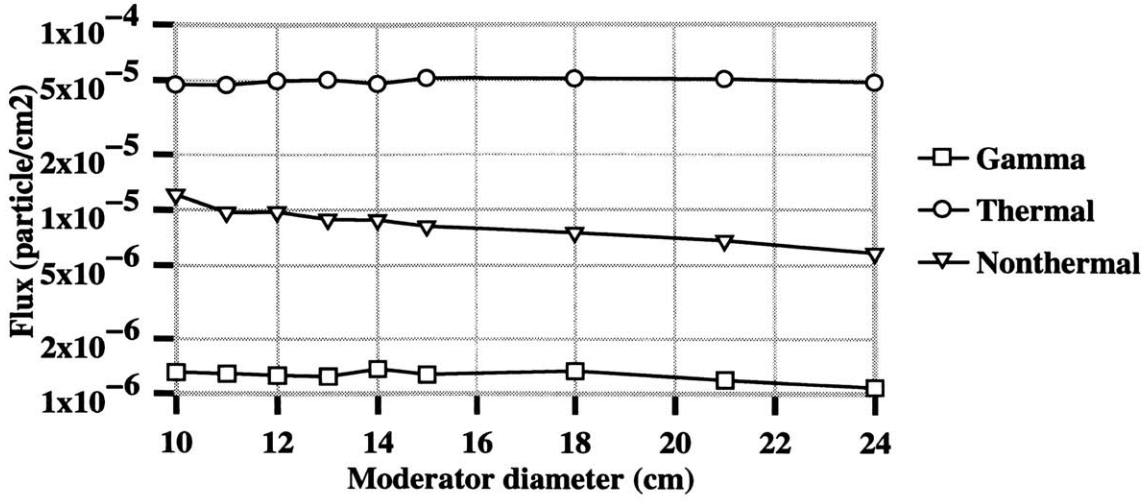

(b)

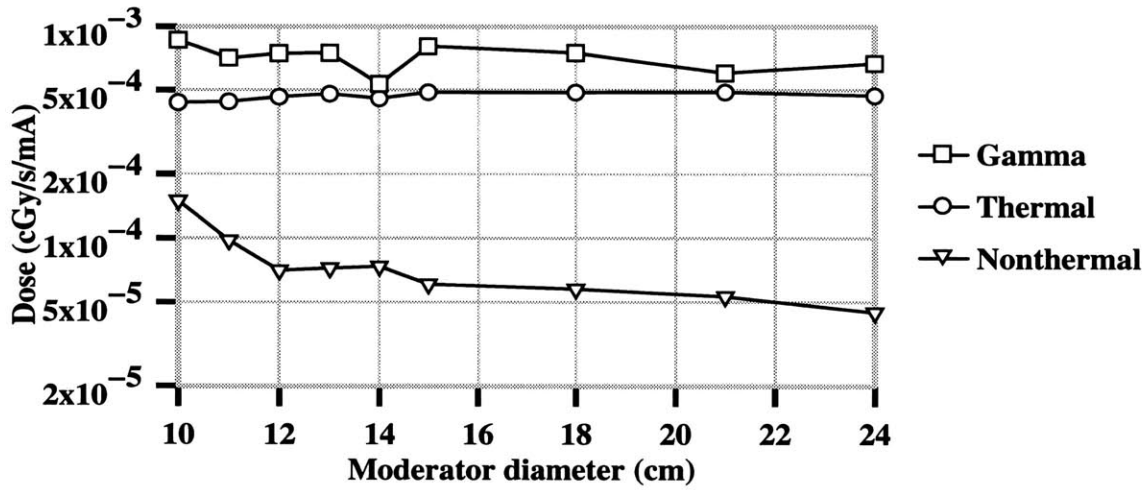

Figure 2.9: Effect of varying moderator diameter on the (a) flux and (b) dose at moderator end. Other assembly dimensions: moderator length 45 cm, reflector thickness 15 cm, reflector length 50 cm. Simulations performed using the 2.5 MeV protons on a lithium target.

Simulations then examined the effect of varying reflector thickness and length on the flux and dose at the moderator end. Results corroborated an earlier study which found no significant increases in flux or dose beyond 18 cm [Yanch et al 1992]. Simulations examined the effect of increasing reflector length from 40 cm to 50 cm, corresponding to an increase in the length of the area behind the moderator from 5 to 15 cm, respectively. An overall increase in total flux and dose was observed, as expected, since additional reflector caused more neutrons to be scattered back into the moderator. The larger increase in dose was due to gammas since neutrons emanating in the backward direction from the target are more thermal, resulting in greater absorption. It was thus decided to keep the reflector length behind the moderator at 5 cm.

Finally, moderator length was varied. As shown in figure 2.10, the change in moderator length had a significant effect on both flux and dose. The nonthermal neutron flux was dominant until about

27 cm of heavy water. With respect to dose rate, about 35 cm of heavy water were required to reach the point where the nonthermal dose rate was equal to the dose rates of other components.

(a)

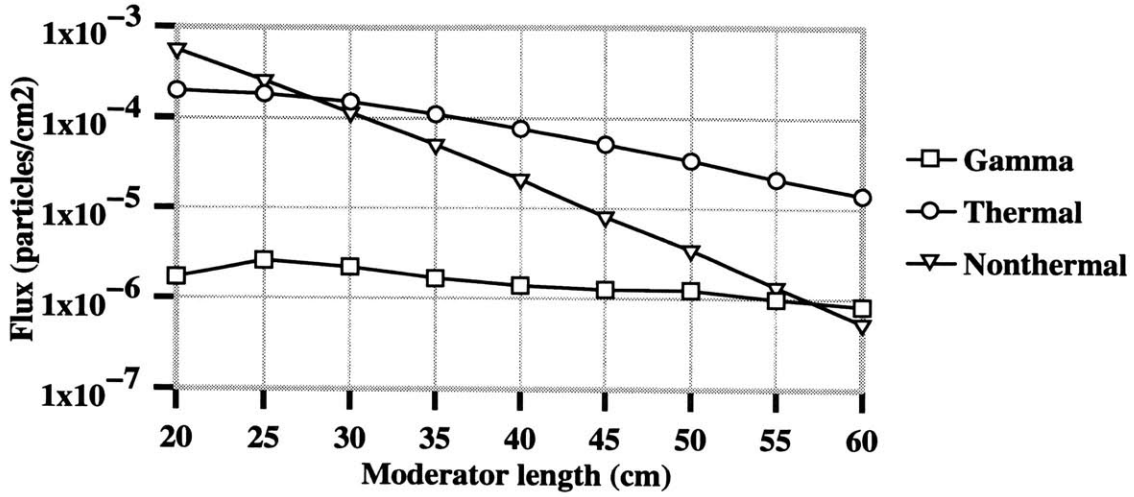

(b)

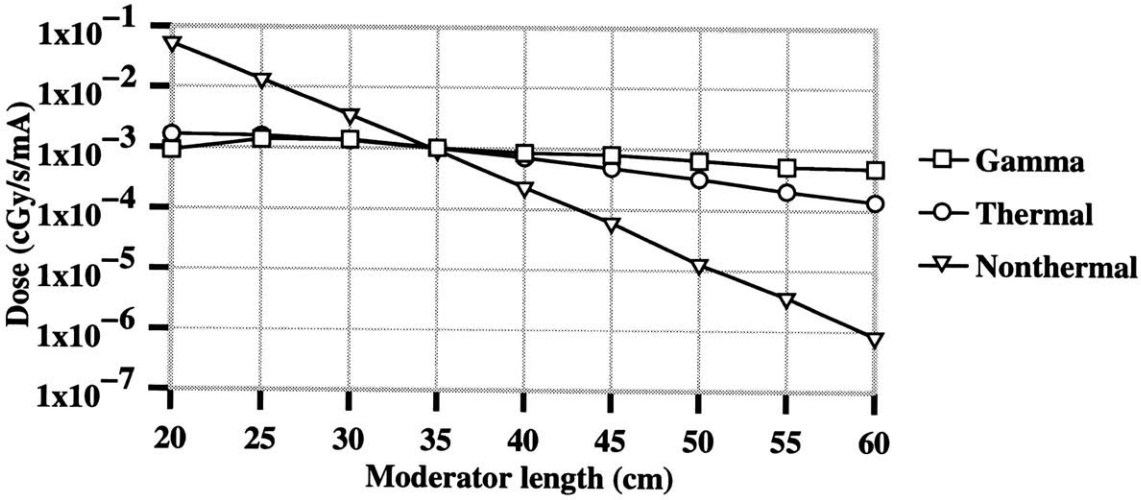

Figure 2.10: Effect of varying moderator length on (a) flux and (b) dose at moderator end from 2.5 MeV protons on lithium target. Other assembly dimensions: moderator diameter 15 cm, reflector thickness 18 cm, reflector length 5 cm greater than moderator length.

Because of these significant results, the same simulations were run with the 4.0 MeV protons on a beryllium target and results are shown in figure 2.11. Both the flux and dose rates are lower than when the lithium target was used, due to the lower yield of the $^{9}Be(p,n)^{9}B$ reaction compared to the $^{7}Li(p,n)^{7}Be$. Also more heavy water moderation is required for the nonthermal neutrons to reach an equivalence point with other components. The nonthermal flux component is dominant until 30 cm of moderator, compared to 27 cm required with lithium. In order for the nonthermal neutron dose rate to be equal to the other dose components, 40 cm of moderating material are required (compared to 35 cm required for lithium). The difference is due to the harder neutron spectrum from the beryllium.

(a)

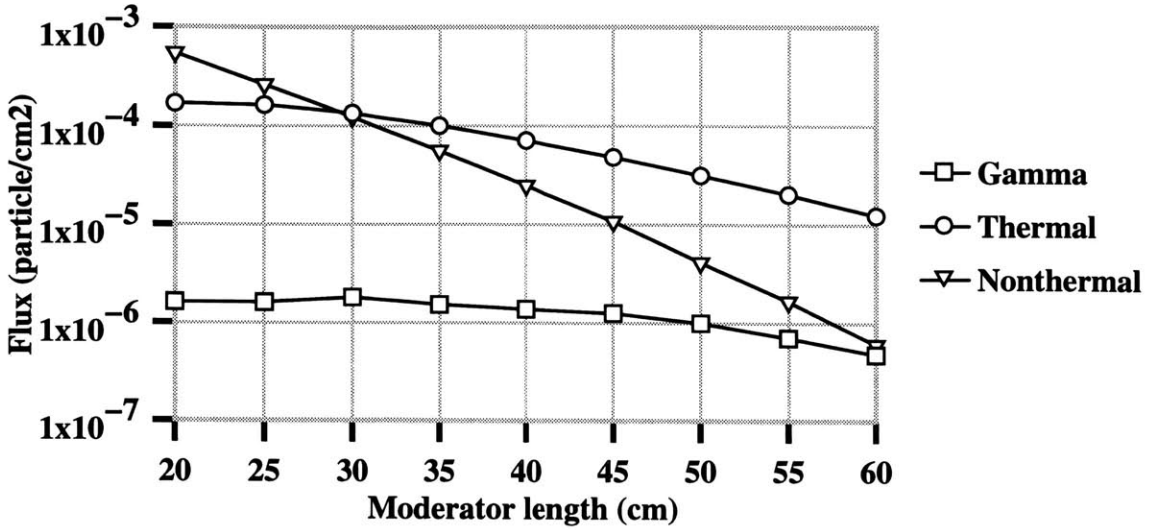

(b)

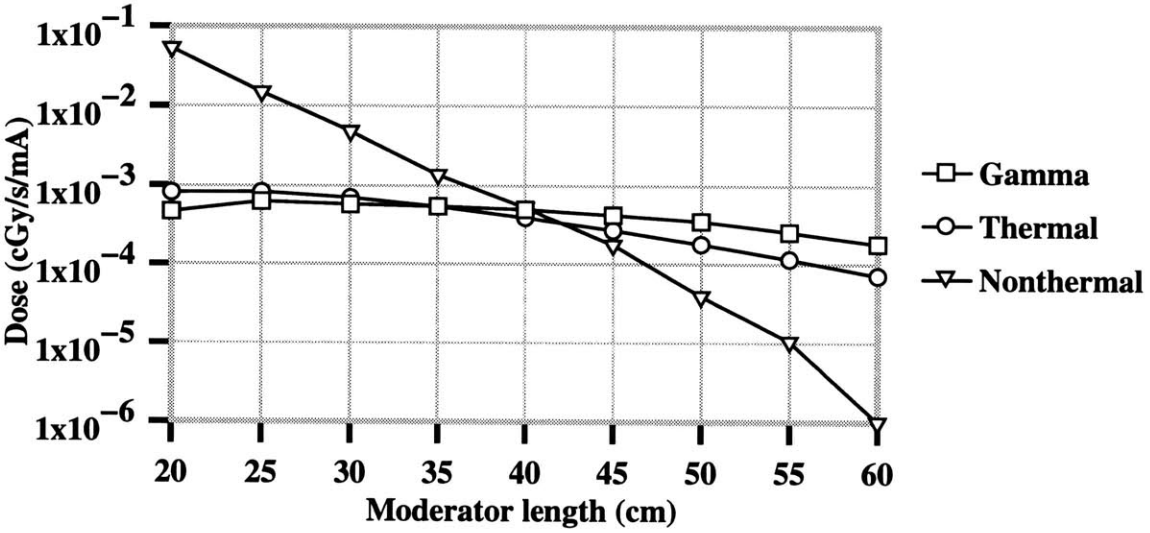

Figure 2.11: Effect of varying moderator length on (a) flux and (b) dose at moderator end from 4.0 MeV protons on a beryllium target. Other assembly dimensions: moderator diameter 15 cm, reflector thickness 18 cm, reflector length 5 cm greater than moderator length.

It should be noted that the thermal neutron and photon doses cannot be avoided in that thermal neutrons are needed to induce the $^{10}B(n,\alpha)^{7}Li$ reaction and photons are created by the neutron capture reactions in both hydrogen and ^{10}B. Therefore, it may not be necessary to decrease the nonthermal component further, since it would also have the negative effect of reducing dose rate (this holds true if increasing moderator length is the parameter modified). In order to accurately evaluate this (as well as other effects to be described later) dosimetry simulations were run in a tissue-equivalent phantom.

In-phantom dosimetry

The MCNP geometry used for in-phantom dosimetry simulations is shown in figure 2.12. The effect of three moderator lengths was examined in the same joint phantom developed for the ideal beam studies. The lengths chosen were 20 cm (dominant nonthermal dose), 35 cm (approximate equivalence of nonthermal with other dose components) and 50 cm (thermal and photon doses dominant). Moderator diameter was fixed at 15 cm. Reflector thickness was fixed at 18 cm and the length of the reflector section behind the moderator at 5 cm. Both lithium and beryllium targets were modeled at each length and an ideal boron distribution of ^{10}B was assumed, i.e. 1,000 ppm ^{10}B in the synovium and 1 ppm ^{10}B in all other tissues (concentrations were modeled explicitly). The beams were evaluated in terms of three therapy parameters: synovium to skin ratio, synovium to bone surface ratio and therapy time. Therapeutic ratios were calculated as in the ideal beam studies, except for application of the following RBE values: 4.0 for the ^{10}B reaction products, 3.8 for neutrons and 1.0 for photons [Harling et al 1994]. Therapy time was calculated by dividing 10,000 RBE-cGy, dose delivered in clinical trials of radiation synovectomy using β-emitters [Deutsch et al 1993], by the total RBE-weighted dose rate to the synovial lining in the front half of the phantom (the posterior synovium receives 10% to 20% of the dose delivered to the anterior synovium and if one were to take into account delivery of a therapeutic dose to the posterior layer, therapy times may be 70% to 80% higher).

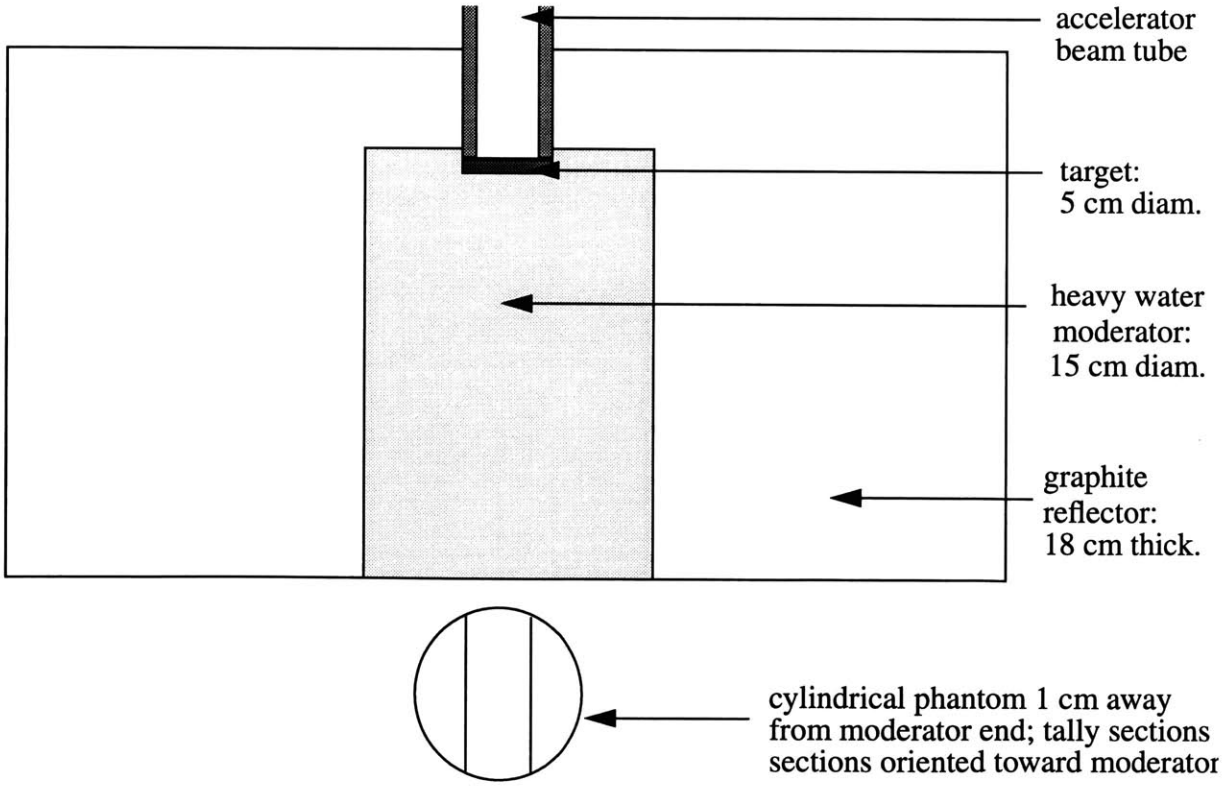

Figure 2.12: MCNP geometry of moderator/reflector assembly for in-phantom dosimetry.

The sensitivity of the therapy parameters to the concentration of ^{10}B in the synovium was also examined at a given moderator length. The moderator length simulated for the lithium source spectrum was 20 cm based on the short therapy time and acceptable therapeutic dose ratios. With the beryllium source spectrum, 5 cm of moderator were added for a total moderator length of 25 cm. Synovial ^{10}B concentration was varied from 100 ppm to 20,000 ppm (based on in vivo uptake studies to be presented in chapter 4). Results are given in units of min-mA.

Figures 2.13, 2.14 and 2.15 show the dose rates of various components per depth in the knee joint phantom at moderator lengths of 20, 35 and 50 cm, respectively. Each figure shows both lithium and beryllium targets, labelled (a) and (b), respectively. At a D_2O moderator length of 20 cm, the nonthermal dose dominates over the other components at the surface of the phantom, as expected from the in air dosimetry results. A larger difference is seen with the beryllium target, figure 2.13(b), than the lithium one, figure 2.13(a), due the harder neutron spectrum from the beryllium target. This affects the depth at which the nonthermal neutron dose becomes equal to the gamma dose (which is always higher than the thermal neutron dose); with a lithium target this occurs within 1 cm of tissue, while with a beryllium target it takes approximately 2 cm of tissue. When the moderator length is increased to 35 cm, the nonthermal dose component throughout the length of the phantom is below the other dose components with a lithium target, figure 2.14(a), and equal to the others with the beryllium target, figure 2.14(b). At a moderator length of 50 cm, the beam emerging from the lithium target, figure 2.15(a), is dominantly thermal in its energy deposition at the surface and throughout the phantom, with the nonthermal dose contribution smaller than the thermal by about two orders of magnitude. With the beryllium target, figure 2.15(b), the dose due to nonthermal neutrons is about one order of magnitude smaller than that due to thermal neutrons.

The effect of the different moderator lengths on the three therapy parameters specified previously (ratio of synovium to skin dose, ratio of synovium to bone surface dose and therapy time) was quantified and is shown in table 2.5. Statistical errors in the therapeutic ratios for moderator lengths of 20, 35 and 50 cm were $\leq$ 6%, 3% and 6%, respectively (note: statistical error with the lithium target at 50 cm was less than 4%). Statistical error in therapy time ranged from 2% to 5%.

Table 2.5: Effect of moderator length on RBE-weighted in-phantom therapy parameters

D_2O length (cm)	Target material	Synovium/skin	Synovium/ bone surface	Therapy time (min-mA)
20	Lithium	73	122	8
	Beryllium	43	72	15
35	Lithium	173	223	27
	Beryllium	146	193	48
50	Lithium	157	229	105
	Beryllium	156	224	184

(a)

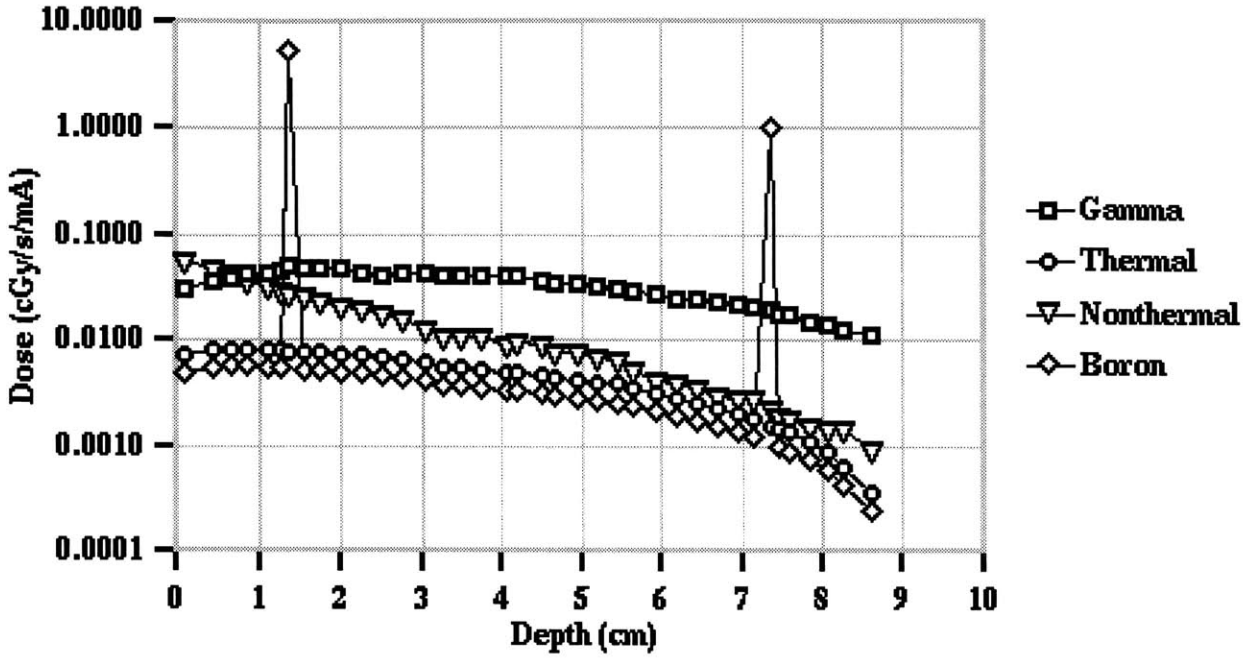

(b)

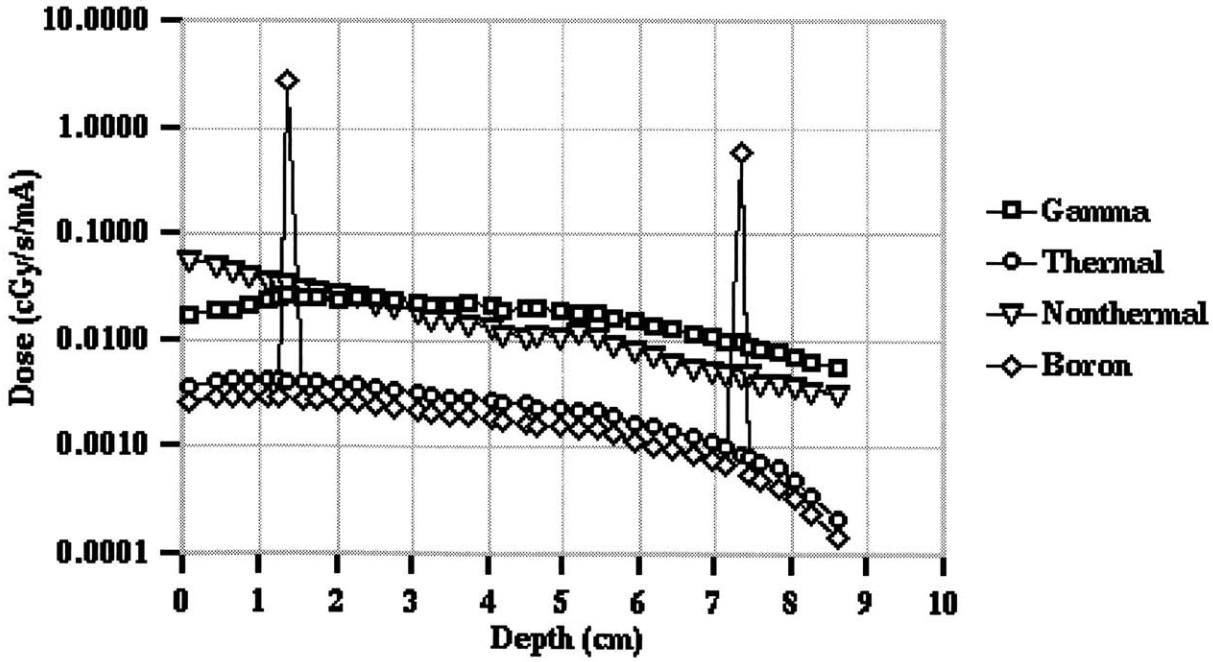

Figure 2.13: Dose profiles in the MCNP knee phantom, with a moderator length of 20 cm, using the (a) 2.5 MeV ^{7}Li(p,n) and (b) 4.0 MeV ^{9}Be(p,n) source spectra. Other assembly dimensions: moderator diameter 15 cm, reflector thickness 18 cm, reflector length 25 cm.

(a)

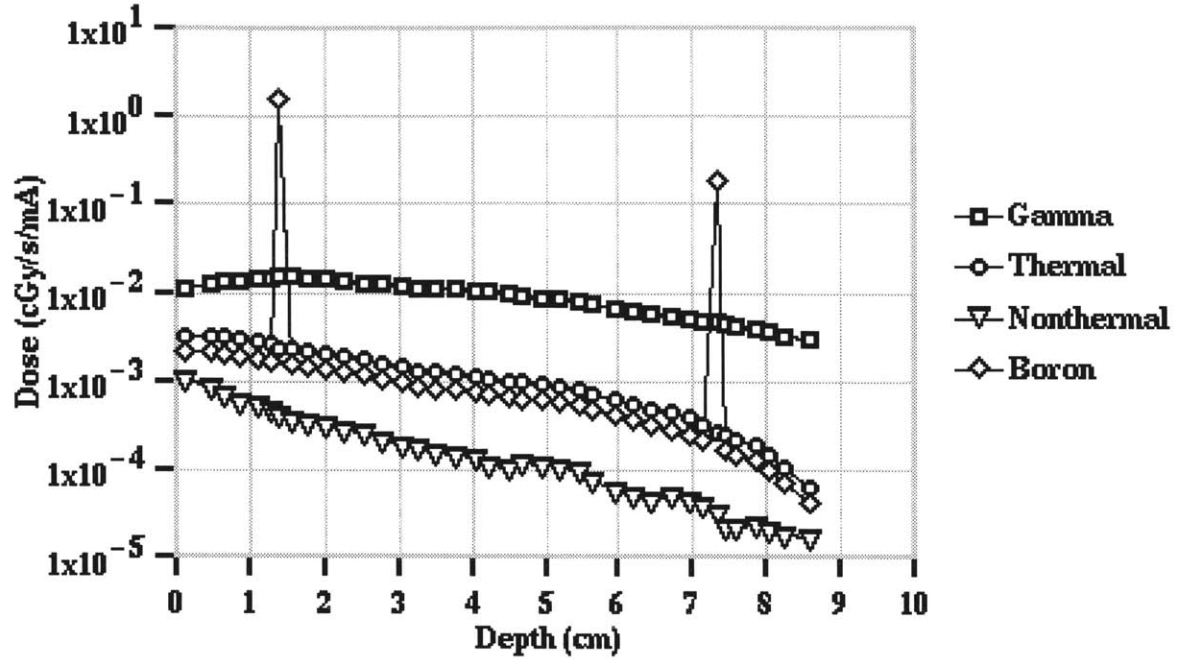

(b)

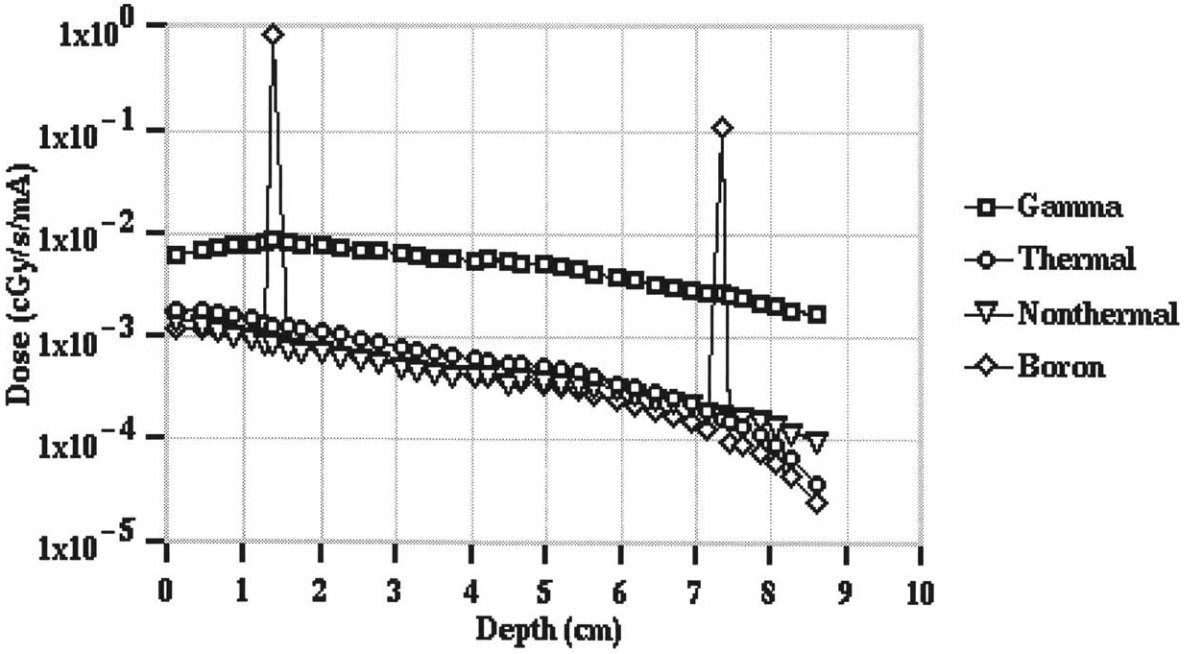

Figure 2.14: Dose profiles in the MCNP knee phantom, with a moderator length of 35 cm, using the (a) 2.5 MeV ^{7}Li(p,n) and (b) 4.0 MeV ^{9}Be(p,n) source spectra. Other assembly dimensions: moderator diameter 15 cm, reflector thickness 18 cm, reflector length 40 cm.

(a)

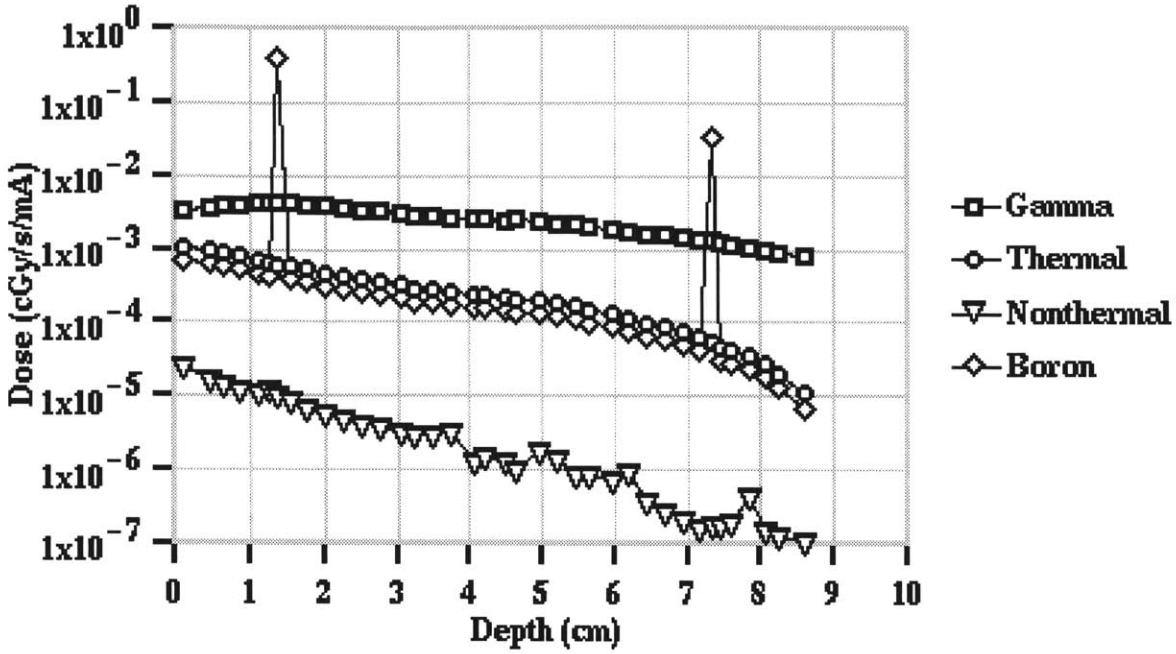

(b)

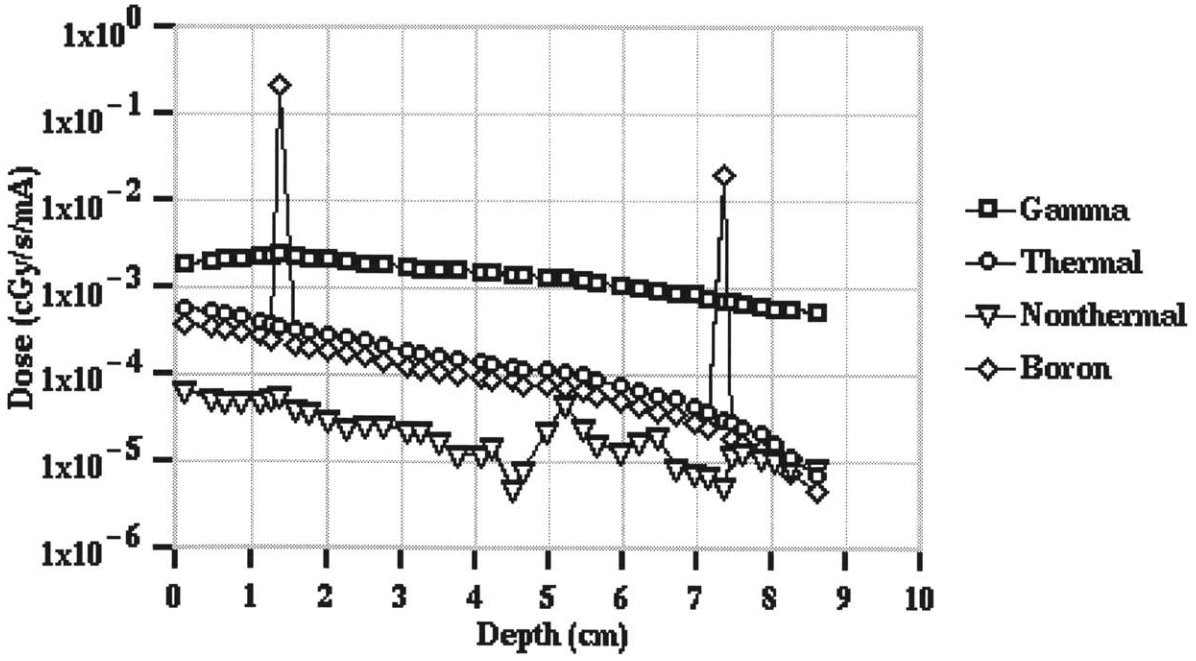

Figure 2.15: Dose profiles in the MCNP knee phantom, with a moderator length of 50 cm, using the (a) 2.5 MeV ^{7}Li(p,n) and (b) 4.0 MeV ^{9}Be(p,n) source spectra. Other assembly dimensions: moderator diameter 15 cm, reflector thickness 18 cm, reflector length 55 cm.

All beams meet the design goal of a minimum synovium to skin ratio of 12 and also have high synovium to bone surface ratios. Beams with 20 and 35 cm of moderator have therapy times of less than one hour (ranging from 8 to 50 minutes) based on 1 mA of particle current, while beams with moderator lengths of 50 cm have therapy times of about 2 to 3 hours. In order to have a better understanding of the trends and magnitudes, data from table 2.2 were plotted in figure 2.16.

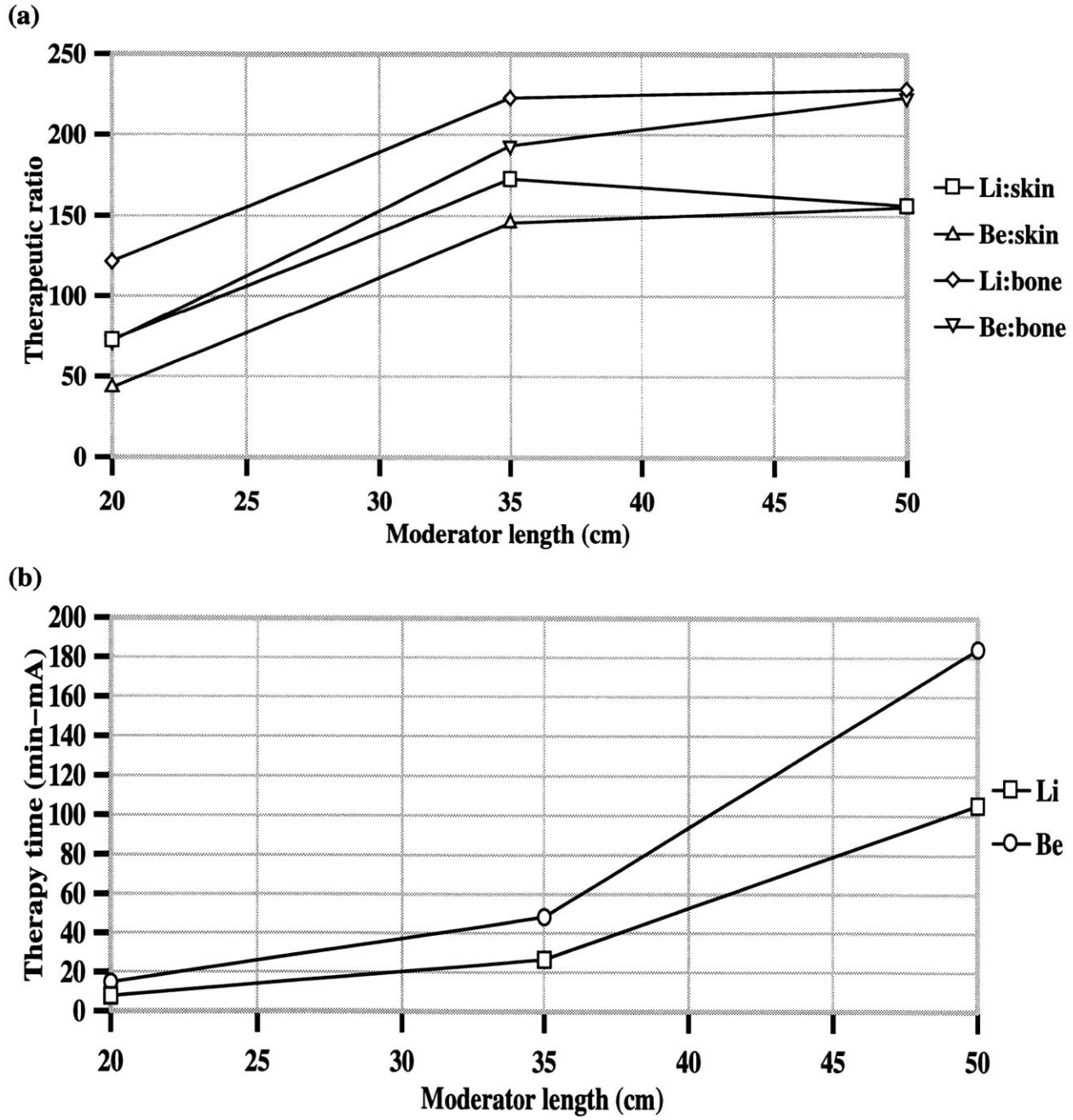

Figure 2.16: Therapy parameters, (a) dose ratios and (b) therapy time, calculated in the MCNP knee phantom at different moderator lengths using the 2.5 MeV ^{7}Li(p,n) and 4.0 MeV ^{9}Be(p,n) source spectra.

As shown in figure 2.16, there is no improvement in therapeutic dose ratios, using either the Li(p,n) or Be(p,n) source, following moderation with more than 35 cm of heavy water. The ratio of synovium to skin with 50 cm of moderation is more than one standard deviation smaller than with 35 cm using the Li(p,n) reaction. This is a result of the dominating thermal component of the dose rate, as shown in figure 2.15(a). Results from the ideal beam study, figure 2.7(a), show a decrease in the synovium to skin dose ratio at thermal energies compared to nonthermal energies. This suggests that a near maximum synovium to skin ratio may be observed following about 35 cm of heavy water moderation using the Li(p,n) source. The synovium to skin ratio remains the same (within statistical fluctuation) with the Be(p,n) neutron source. This could be a result of the spectral differences; Be(p,n) has a harder spectrum and, as shown in figure 2.11, requires more moderation to achieve the same level of thermalization compared to Li(p.n). The ideal beam study shows no significant differences in the ratio of synovium/skin dose between energies of 1 eV and 1 keV. It is also interesting to note that the synovium to skin ratio achieved at 20 cm with Li(p,n) is equivalent to that obtained with a moderator length of 25 cm with the Be(p,n) reaction. This is a further corroboration of the behavior seen in figures 2.10(b) and 2.11(b).

The ratio of synovium/bone ratio does not change between 35 and 50 cm of moderation with the Li(p,n) reaction while it increases with Be(p,n). Furthermore, the ratio is higher with Li(p,n) than Be(p,n). This behavior may be explained on the basis of spectral differences between the reactions and results of the ideal beam studies. The Li(p,n) reaction has a softer neutron spectrum and results from the ideal beam study show that the synovium/bone ratio is higher at thermal energies. So, it would be expected that the synovium/bone ratio to be higher for the Li(p,n) reaction than for the Be(p,n) and not change, since the neutrons are mostly thermal in energy.

Figure 2.16(b) shows that therapy time increases when moderator length is increased. This is expected because additional moderator material decreases the neutron flux and dose rate so that a longer time is required for the delivery of equivalent dose. Since the boron dose rate is calculated via convolution of the thermal neutron flux by ^{10}B fluence-to-kerma conversion factors [Zamenhof et al 1975] and multiplication by the ^{10}B concentration, the boron dose rate decreases with decreasing thermal neutron dose rate and thus shorter moderator lengths lead to shorter therapy times. A higher yield is also part of the reason behind the shorter therapy time with the Li(p,n) reaction rather than the Be(p,n) reaction at the same moderator length. Therapy time dramatically worsens as the moderator length is increased from 35 and 50 cm. This, combined with the lack of significant improvement in therapeutic ratios, renders moderator lengths beyond 35 cm, with the Li(p,n) and Be(p,n) neutron source spectra, suboptimal for BNCS.

The above simulations assumed a synovium ^{10}B concentration of 1,000 ppm. However, in BNCS, a larger range of uptake is achievable (as will be shown in Chapter 4). This affects both therapy time and therapeutic dose ratios, since longer times result in increased exposure of healthy tissues. Figure 2.17 shows the effect of varying synovial ^{10}B concentration, from 100 ppm to 20,000 ppm on therapeutic parameters: (a) synovium/skin and synovium/bone surface ratios and (b) therapy time. Moderator length was fixed at 20 cm for the lithium target, which had the shortest therapy times with acceptable dose ratios. For the beryllium target, an additional 5 cm of moderator were added for a total of 25 cm. Other dimensions of the moderator/reflector assembly were kept the same as the previous simulations.

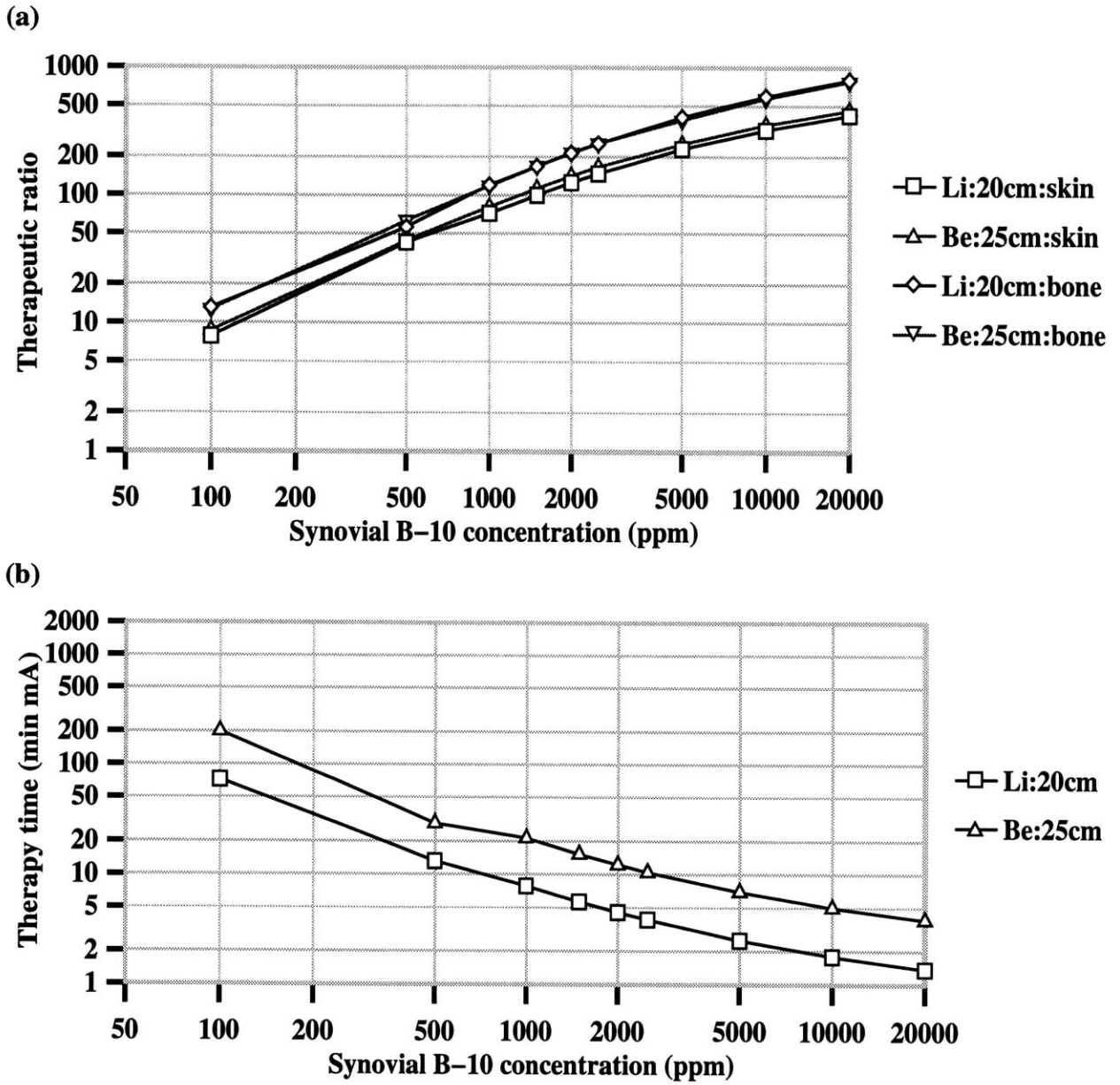

Figure 2.17: Sensitivity of therapy parameters, (a) dose ratios and (b) therapy time, to varying synovial ^{10}B concentration in the MCNP knee phantom for two beams.

As expected from both in-air and in-phantom dosimetry simulations, a 5 cm offset in moderator length rendered the therapeutic dose ratios, figure 2.17(a), essentially the same between Li(p,n) and Be(p,n) reactions. About 200 ppm are needed to meet the design goal of a minimum ratio of 12 and the maximum concentration, 20,000 ppm, leads to a synovium to skin dose ratio of 500. The synovium/skin dose ratio increases in a roughly linear fashion between 100 ppm and 1,000 ppm, after which the ratio continues to rise with a smaller slope. This behavior is a result of flux depression; the neutron flux is lowered due to the large amount of boron present (which captures thermal neutrons). The synovium to bone surface dose ratio also increases as the synovial boron concentration is increased. The increase is roughly linear over a larger range, until about 5,000 ppm, after which, the ratio continues to increase at approximately half of the rate. The reason why

the synovium/bone ratio is linear over a larger range compared to the synovium/skin ratio is due to its location with respect to the synovium, i.e. behind the synovium rather than in front as the skin, which makes the effect of flux depression smaller.

Therapy time, figure 2.17(c), decreases with increasing synovial ^{10}B concentration, as expected. For BNCS to be competitive with the emerging synovectomy techniques such as office-based arthroscopic synovectomy [Small et al 1994], therapy time should be approximately 30 minutes. With this cutoff, synovial ^{10}B concentrations of about 300 and 500 ppm are required with lithium and beryllium, respectively. At these concentrations the synovium/skin dose ratio design criterion (minimum of 12) is met and synovium to bone surface ratios range from 30 to 50. This implies that the bone surface may receive between 200 and 300 cGy. Although no design goals have been set for the synovium to bone surface ratio, except that it be maximized, it should be noted that the lowest reported case of femur head bone necrosis and/or fracture of the femur, with fractionated conventional radiation therapy treatments using high energy x-rays, has been at 2,000 cGy [Emami et al 1991], which would correspond to a synovium/bone surface dose ratio of 5. Clinical experience has shown that a dose of 5,200 cGy leads to a 5% incidence of bone necrosis and/or femur fracture within 5 years [Emami et al 1991].

With a synovial ^{10}B concentration of 1,000 ppm, the synovium to skin ratios are well above the design criteria, around 70 to 80, and the synovium to bone ratios are around 120, implying a total dose to bone of 83 cGy. Therapy can be completed in 20 minutes or less, with either target. Higher concentrations, such as 5,000 ppm, allow therapy times of less than 10 minutes with therapeutic dose ratios of over 200. Further increases in concentration do not yield increases as dramatic as those observed between 300 ppm and 5,000 ppm for a lithium target and between 500 ppm and 5,000 ppm with a beryllium target. An implication of figure 2.17 is that the minimum synovial uptake of a boronated compound for BNCS is 300 ppm with a lithium target, or 500 ppm with a beryllium target in order to meet design criteria.

In conclusion, this section has shown via Monte Carlo simulation studies that accelerator-based neutron beams for BNCS can be designed to result in high therapeutic ratios and low therapy times. The materials of choice, with either a lithium or beryllium target, is D_2O for the moderator and graphite for the reflector. In-air dosimetry allowed the determination of optimal moderator diameter and reflector dimensions, as well as determination of a preliminary range of moderator lengths. The effect of moderator length was examined in the joint phantom (with both lithium and beryllium targets) and quantified via the calculation of therapy parameters, i.e. synovium to skin dose ratio, synovium to bone surface dose ratio and therapy time. The most dramatic increase in therapeutic dose ratios was observed when the moderator length was increased from 20 to 35 cm, with much smaller improvements from 35 to 50 cm. However, assuming 1,000 ppm of ^{10}B in the synovium, the shortest moderator length modeled, 20 cm, gave the shortest therapy times and highly acceptable therapeutic dose ratios. The effect of synovial ^{10}B concentration on therapy parameters was examined for moderator lengths of 20 cm with a lithium target and 25 cm with a beryllium target. Synovial ^{10}B concentrations of 300 ppm with a lithium target and 500 ppm with a beryllium target yield acceptable therapeutic parameters, including therapy times less than 30 minutes, a criterion that makes BNCS competitive with other emerging synovectomy techniques such as office-based arthroscopic synovectomy [Small et al 1994].

The above simulation study only examined the Li(p,n) and Be(p,n) nuclear reactions. However, each has disadvantages, including serious target cooling challenges with the Li(p,n) reaction and high proton energy requirements for the Be(p,n) reaction. Thus, several other light ion reactions were investigated for BNCS. The next section presents results of this investigation.

2.3.3 Investigation of light ion candidate nuclear reactions

The neutron producing candidate nuclear reactions considered are shown in table 2.6. The Li(p,n) and Be(p,n) reactions are included for comparison. These nuclear reactions can be accessed using low-energy accelerators, commercial neutron generators or biomedical cyclotrons.

Table 2.6: Light ion nuclear reactions investigated for BNCS

Reaction	Ion Energy (MeV)	Max. Neutron Energy (MeV)
$^{7}Li(p,n)^{7}Be$	2.5	0.8
$^{9}Be(p,n)^{9}B$	4.0	2.1
$^{9}Be(d,n)^{10}B$	2.6 - 7.0	7 - 11
$t(d,n)^{4}He$	0.25	14
$d(d,n)^{3}He$	0.25	2.5

Full neutron energy and angular information were input into MCNP for the Li(p,n) and Be(p,n) reactions, with yields of $8.96x10^{11}$ n/s and $5.25x10^{11}$ n/s, respectively and assuming 1 mA of beam current [Liskien and Paulson 1975, Howard et al 1997]. Since neutron energy and angular information were not available for the Be(d,n) reaction, the 0° neutron yields and energies were used and the distribution was assumed to be isotropic; total neutron yield, based on 1 mA, was $1x10^{12}$ n/s [Meadows 1991]. Neutron fluxes of the d(d,n) and t(d,n) reactions were assumed to be $4x10^{9}$ n/sec and $4x10^{11}$ n/sec, based on fluxes obtainable from commercial generators for 1 mA of current [Sodern 1996].

MCNP simulations were performed in a tissue-equivalent phantom using the geometry shown in figure 2.9. A ^{10}B concentration of 1,000 ppm was explicitly modeled in the synovium to account for effects of flux depression and induced photons. All other tissues were modeled with 1 ppm ^{10}B. Therapy parameters, i.e. synovium to skin dose ratio, synovium to bone surface dose ratio and therapy time, were calculated as in previous sections, using RBE weighting (again, 4.0 for the boron neutron capture reaction products, 3.8 for all neutrons and 1.0 for photons). The therapeutic ratios and total time (in min-mA) to deliver 10,000 RBE-cGy to the synovium for five neutron producing reactions and varying moderator lengths are shown in Table 2.7.

Table 2.7: RBE-weighted in-phantom therapy parameters of various light ion reactions

Reaction	Ion energy (MeV)	Moderator length (cm)	Synovium/ skin	Synovium/ bone surface	Therapy time (min-mA)
$^{7}Li(p,n)^{7}Be$	2.5 MeV	20	73	122	8
		35	172	223	27
		50	157	229	105
$^{9}Be(p,n)^{9}B$	4.0 MeV	20	43	72	15
		30	117	164	31
		50	153	221	179
$^{9}Be(d,n)^{10}B$	2.6 MeV	20	28	43	8
		30	70	95	17
		50	104	168	100
	7.0 MeV	50	43	61	7
$d(d,n)^{3}He$	0.23 MeV	20	15	22	2,316
		30	46	65	4,540
$t(d,n)^{4}He$	0.23 MeV	30	5	6	59
		50	10	11	259

The first three reactions listed in Table 2.4 produce favorable therapeutic parameters over the range of moderator lengths investigated. For the 20 cm moderator length, synovium to skin ratios exceed the minimum value of 12 by a factor of two or more and therapy times range from 8 to 15 minutes per milliampere of ion current. Proton and deuteron accelerators that operate at the required energies and currents between 0.2 - 1 mA have been developed and the development of multimilliampere systems is underway [Klinkowstein et al 1997]. The d(d,n) and t(d,n) reactions do not appear to be suitable for therapy due to excessively long therapy times and poor therapeutic ratios, respectively. There would need to be a hundred-fold increase in synovial ^{10}B concentration, i.e. 100,000 ppm, in order for the d(d,n) reaction, with 20 cm of moderation, to have a therapy time around 20 minutes. The t(d,n) reaction, with 30 cm of moderation, could be competitive with the Be(d,n) reaction if the synovial ^{10}B concentration were significantly higher.

While the Li(p,n) reaction gives the highest therapeutic ratios, the Be(p,n) and Be(d,n) reactions have the advantage that a beryllium target is more favorable in terms of thermal, mechanical and chemical properties than lithium. Use of the Be(d,n) reaction, with Ed=2.6 MeV, has the further advantage that a relatively low accelerator beam energy is required. Therapy parameters for both the 4.0 MeV Be(p,n) and 2.6 MeV Be(d,n) reactions have been plotted as a function of moderator length in figure 2.18. Additional points for the 4.0 MeV Be(p,n) have been included as available from previous sections.

(a)

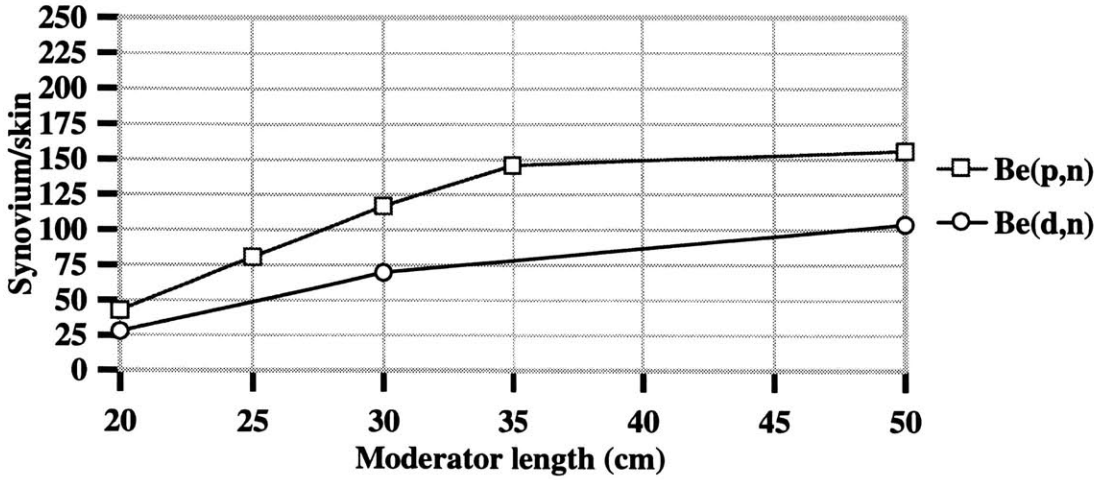

(b)

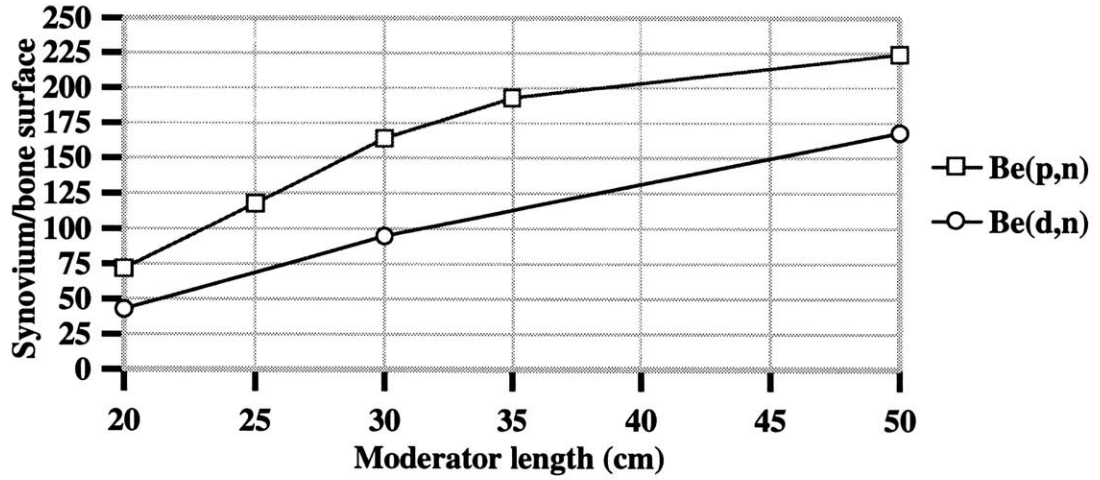

(c)

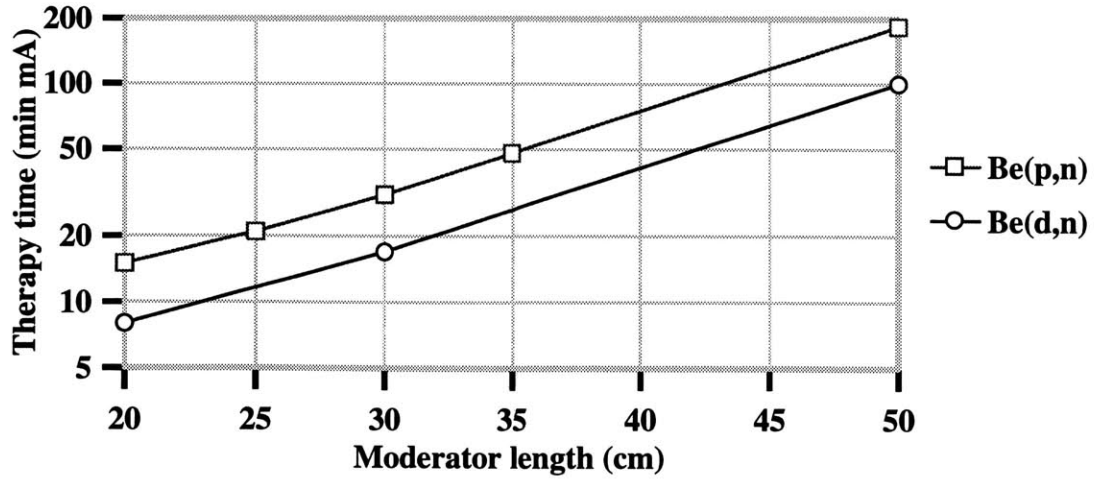

Figure 2.18: Comparison of the 4.0 MeV ^{9}Be(p,n) and 2.6 MeV ^{9}Be(d,n) reactions with respect to (a) and (b) therapeutic ratios, and (c) therapy time, as a function of moderator length

Although the therapeutic dose ratios, figure 2.18(a) and (b), are 1.5 to 1.7 times higher with the Be(p,n) reaction than the Be(d,n) reaction at each of the moderator lengths tested, therapy time, figure 2.18(c), is always more favorable for the Be(d,n) reaction. However, comparing results between the Be(p,n) reaction with 20 cm of moderator and the Be(d,n) with 30 cm of moderator shows that higher therapeutic ratios with comparable therapy times (17 min vs. 15 min) can be achieved with the Be(d,n) reaction at the expense of an additional 10 cm of moderating material.

In conclusion, therapeutically useful accelerator-based neutron beams for BNCS can be produced via the ^{7}Li(p,n), the ^{9}Be(p,n) or the ^{9}Be(d,n) reactions. Monte-Carlo simulations of coaxial D_2O moderator and graphite reflector configurations predict high synovium to skin and synovium to bone dose ratios and acceptable therapy times for these reactions. Neutron beams based on the d(d,n) or t(d,n) reactions are not suitable for BNCS due to very low dose rates (the d-d reaction) or very poor therapeutic ratios (the d-t reaction).

The next section describe further neutron beam optimization studies [Gierga et al 1999] and target cooling development [Blackburn et al 1998] performed by other members of MIT LABA, leading to the construction of the target and moderator/reflector assembly used for the animal irradiations to be presented in chapter 5.

2.3.4 Further optimization and construction of moderator/reflector assembly

Further neutron beam optimization by other members of MIT LABA has included investigations of parallel-opposed irradiations, additional reflectors, thermal neutron filters, shielding and whole body dose resulting from a typical knee treatment [Gierga et al 1999]. The two aspects of their work which will be summarized here are the improvements with parallel-opposed irradiations and additional reflectors.

MCNP simulation studies showed that, with the same moderator/reflector configurations, parallel-opposed beams provide a significant improvement over single beam irradiation in all therapy parameters [Gierga et al 1999]. To examine the effect of parallel-opposed beam irradiations, the previously described knee joint phantom was divided into eight sections. Therapy parameters were weighted with the same RBE values previously listed and were reported as follows: skin dose (instead of synovium to skin ratio), corresponding to the section with the highest dose; the synovium to bone dose ratio, corresponding to section with the lowest ratio; and therapy time, corresponding to the time for the synovium section with the lowest dose rate to receive 10,000 RBE-cGy. The benefit of parallel-opposed irradiations was shown for a number of reactions at different moderator lengths. However, only one characteristic example will be reported here, i.e. the Be(p,n) reaction with a proton energy of 4.0 MeV and a moderator length of 15 cm (moderator diameter was 9 cm and reflector thickness 18 cm). Under these conditions, a single beam yielded a skin dose of 592 RBE-cGy, a synovium to bone ratio of 65 and a therapy time of 12 min-mA. Parallel-opposed irradiation yielded a skin dose of 203 RBE-cGy, a synovium to bone ratio of 73 and a therapy time of 7 min-mA. The largest improvements were in skin dose (factor of 3) and therapy time (factor of 2).

Improvement was also found by the addition of rear and side reflectors, enabling a more efficient use of the beam since neutrons are redirected toward the phantom instead of simply exiting [Gierga et al 1999]. When rear and side reflectors are used, the phantom is essentially surrounded by reflecting material except for the side facing the neutron beam. Investigation of materials as back reflectors (including lead, beryllium and graphite) indicated that lead was inferior, while beryllium and graphite were comparable. Since graphite is relatively inexpensive and easier to work with, graphite was the material of choice. Comparison of heavy water and graphite as side reflector materials showed no statistical advantage in using heavy water, hence graphite was also chosen as the side reflector. The dimensions of the rear and side reflectors were systematically varied in order to find the optimal geometry for treatment of a knee joint. Optimal dimensions were found to be as follows: for the back reflector, width and height of 45.2 cm and thickness of 10 cm; for the side reflector, width and height of 30 cm and thickness of 8.7 cm. A comparison was made of human knee joint parameters for a parallel-opposed irradiation using the Be(p,n) reaction with and without the additional reflectors. When no additional reflectors were present, skin dose was 355 RBE-cGy, the synovium/bone ratio 49 and therapy time 16.2 min-mA. When the rear and side reflectors were added, skin dose decreased to 203 RBE-cGy, the synovium/bone ratio increased to 73 and therapy time decreased to 7.3 min-mA.

Since beryllium-based nuclear reactions such as the Be(p,n) and Be(d,n) have been shown to be feasible for BNCS, as well as BNCT, development of a beryllium target was undertaken at MIT LABA [Blackburn et al 1998]. It has been estimated that for BNCT currents of 2.5 to 4.0 mA will be needed for reasonable therapy times using beryllium targets [Shefer et al 1994]. This means that from 8 to 16 kW of power must be removed from the target and heat flux levels can reach 10 to 20 MW/m^2 [Blackburn et al 1998]. A beryllium target was designed which used a submerged jet impingement cooling method and experimental testing on a prototype revealed that 30 kW of power, with local heat fluences of 60 MW/m^2, could be removed, thus showing that it can amply meet power and heat flux requirements [Blackburn et al 1998].

Neutron beam optimization, as well as the development of an beryllium target capable of handling the required heating loads, led to the construction of a target/moderator/reflector assembly, i.e. a full beamline. The target itself consists of a beryllium tube 4 cm long and 3.2 cm in diameter which seals to an aluminum tube. It is electrically insulated from the aluminum tube by O-rings and a thin teflon ring. The aluminum tube is surrounded by two concentric coolant tubes which provide the structure for the submerged jet impingement method. Current and temperature on the target are measured by a thermocouple which has been attached to the center of the target on the coolant side. The target assembly is movable along the central axis of the moderator/reflector assembly, thereby allowing the distance between the target and moderator end to vary from 0 to 23 cm. The moderator is 9 cm in diameter and 23 cm in length. It is surrounded on three sides by an 18 cm thick graphite reflector whose inner surface is coated with resin in order to make it impervious to the heavy water.

In summary, this chapter has provided background information on RA and other synovectomy procedures. The principles behind BNCS were detailed and compared to BNCT. Finally, the development of accelerator-based neutron sources was described. The next chapter discusses the evaluation of several boron-containing compounds as a step towards the animal irradiations to be discussed in chapter 5.

3. Uptake of several boron-containing compounds

Determination of boron uptake by tissue is of primary importance for the determination of the required neutron beam parameters to deliver a specific therapeutic dose. This chapter presents results of uptake studies using several boron-containing compounds. The first section (3.1) describes materials and methods, including the measurement method for determination of ^{10}B concentration in hydrogenous samples, the preparation of the boronated compounds used for the uptake studies and experimental parameters. This section also includes a discussion of other boron compounds which were considered but not evaluated for various reasons. Results of the uptake studies are presented in section 3.2, divided according to the boron-containing compound. Then, conclusions are drawn in section 3.3.

3.1 Materials and methods

3.1.1 Prompt gamma neutron activation analysis

The ^{10}B concentration in tissue was measured via prompt gamma neutron activation analysis (PGNAA), a technique where sample irradiation and spectroscopic analysis occur simultaneously. Analysis of ^{10}B by PGNAA depends on the detection of the 478 keV gamma-ray emitted from the excited state of ^{7}Li, created when ^{10}B captures a thermal neutron (see section 2.2). The PGNAA Facility at the MIT Research Reactor uses a focused diffracted neutron beam with a flux at the sample position of $1x10^{7}$ n/cm^{2}s [Riley and Harling 1998].

In this facility [Riley and Harling 1998], a well moderated beam of thermal neutrons emerging from the reactor's heavy water reflector passes through two 15 cm sections of sapphire single crystal, which serve to transmit the maximum amount of neutrons with 0.0143 eV of energy, while reducing contamination by fast neutrons (higher than 0.5 eV) and photons. The neutrons are incident on a multilayered set of graphite single crystals which focus the diffracted beam in the vertical direction while sampling thermal neutron energies within 10% of 0.0143 eV. The focused diffracted beam is collimated by tapered ^{6}Li collimators before reaching the sample position, which is surrounded by shielding composed of 1 cm of $^{6}Li_2CO_3$ powder housed within sheets of teflon. A High Purity Germanium detector (Canberra Industries, Malden, CT) positioned at 90° from the sample, is surrounded coaxially by the same type of lithium powder although housed in a thin walled aluminum cylinder rather than teflon. The end of the detector facing the sample is shielded by a 0.7 cm thick disk of solid $^{6}Li_2CO_3$. Samples can be inserted and removed while the beam is on. Spectral data are displayed on a personal-computer-based multichannel analyzer,

which is connected to the various electronic components (i.e. preamplifier, amplifier) required for conversion of the detector pulses. The PGNAA facility can analyze relatively large samples (about 0.5 ml) with a few ppm (μg/g) of ^{10}B to within 10% statistical uncertainty in a few minutes. Smaller samples (to 0.02 ml) can be measured to the same statistical uncertainty with longer counting times.

For each sample, the count rate of gamma-rays coming from both the hydrogen capture reaction (2.2 MeV) and the boron neutron capture reaction (478 keV) was determined by measuring the area under the appropriate gamma peak and dividing by irradiation time. The background counts for the gamma-rays resulting from the hydrogen capture reaction were measured by counting an empty teflon vial while the background rate for the gamma-rays resulting from the boron neutron capture reaction was measured by counting a sample of deionized water, under the assumption that the boron content of deionized water and soft tissue were similar. Since tissue samples varied greatly in size, boron backgrounds of similar sizes were prepared and then subtracted from the respective tissue samples. It should be noted that tissue samples whose hydrogen count rate was less than twice the count rate of the hydrogen background were excluded.

The count rates for the boron and hydrogen neutron capture reactions were obtained to calculate the $^{10}B/^{1}H$ ratio (B/H ratio) which was then used to calculate the ^{10}B concentration. Using this ratio reduces effects of inconsistent sample positioning in the beam and variations in the thermal neutron flux during measurement. A calibration curve, relating B/H ratio to boron concentration (ppm), was constructed each time PGNAA was performed. The dependence of the slope of the calibration curve on the volume of the standard was tested with three standard weights: 0.05, 0.10 and 0.15 ml. The slope of the calibration curve was found to be within 5%. The 0.05 ml weight of standards do not cover the entire bottom of the teflon vial and special attention was devoted to making sure that the drop was always oriented toward the detector. This was also done for small tissue samples in order to further decrease the effects of inconsistent sample positioning.

Since the boric acid standards used for calibration only went up to 1500 ppm ^{10}B in concentration, and given the high concentrations of boron that were measured in tissue samples, the linearity of the PGNAA facility at higher concentrations was tested. This was done by preparing 6 samples of a ^{10}B enriched boron compound ($K_2B_{12}H_{12}$) such that ^{10}B concentrations ranged from 75 ppm to 37,500 ppm ^{10}B (i.e. 75, 150, 750, 3640, 7500 and 37500 ppm). The measured B/H ratio was a linear function of ^{10}B concentration up to 37,500 ppm and the slope was within 10% of the slope measured with low concentration boric acid standards. Therefore, PGNAA was deemed a reliable measurement technique at high, as well as low, concentrations. The next subsections (i) and (ii) will describe the details behind the preparation of the boric acid standards and the data analysis.

(i) Preparation of boric acid standards for calibration

The preparation of boric acid standards was divided in two parts; the preparation of the mother solution (1500 ppm ^{10}B) and preparation of daughter solutions (750, 300, 150 and 30 ppm ^{10}B). The mother solution was prepared by scaling the relationship found in previous work that a boric acid standard of 100 ppm ^{10}B is prepared by dissolving 3.104165 g of boric acid in a 1000 ml solution composed of one third saline and two thirds deionized water [Chabeuf 1993]. The first

step was to prepare the salt solution; 50 ml of saline and 100 ml of deionized water were mixed together. Then, 4.6562 ±0.001 g of boric acid (Boric Acid 951 from the National Institute of Standards and Technology, Gatherburg, MD 20899) was weighed out in a light plastic boat and dissolved in 100 ml of the mixture solution.

The daughter solutions were prepared using the following formula:

$$K_1 V_1 = K_2 V_2 \qquad \text{(Eq. 3.1)}$$

where K_1 is the original concentration (ppm), V_1 is the unknown volume (ml), K_2 is the desired concentration (ppm) and V_2 is the desired volume (ml). For example: in order to obtain 10 ml of 750 ppm solution out of the 1500 ppm mother solution, the above equation becomes

$$1500 \cdot V_1 = 750 \cdot 10$$

which can be solved to yield

$$V_1 = 5ml$$

This means that 5 ml of the 1500 ppm solution must be added to the salt solution, yielding 10 ml of the 750 ppm standard. The following table, 3.1, summarizes the preparations.

Table 3.1: Preparation of PGNAA standards below 1500 ppm ^{10}B

Concentration (ppm)	The 1500 ppm Standard (ml)	Salt solution (ml)
750	5.0	5.0
300	2.0	8.0
150	1.0	9.0
30	0.2	9.8

(ii) Data analysis

The B/H ratio was determined for all samples using the following equation

$$\frac{B_t}{H_t} = \frac{B_n - B_0}{H_n - H_0} \qquad \text{(Eq. 3.2)}$$

where B_n is the count rate of the gamma-rays from the boron neutron capture reaction, B_0 is the associated background count, H_n is the count rate of the gamma-rays from the hydrogen capture reaction and H_0 is its background.

The calculation of error was performed in several steps. The first step was to determine the error in the count rates for each peak in each sample, i.e. the individual errors in B_n, B_0, H_n, H_0. This was done using the error calculation formula for "Multiplication or Division by a Constant" [Knoll 1989]. Then the error in B_t and H_t, or net boron and hydrogen count rates for each sample was determined by directly applying the formula for the error in "Sums or Differences of Counts" [Knoll 1989]. The third and last step was to determine the error in the B/H ratio given knowledge of the error in both the net boron and hydrogen count rates. This was calculated by applying the

error propagation formula for "Multiplication or Division of Counts" [Knoll 1989], i.e.

$$\left(\frac{\Delta(B/H)}{B/H}\right)^2 = \left(\left(\frac{\Delta B_t}{B_t}\right)^2 + \left(\frac{\Delta H_t}{H_t}\right)^2\right) \quad \text{(Eq. 3.3)}$$

This equation can be solved to yield the percent error in the B/H ratio.

A calibration curve was constructed by plotting the B/H ratio of the standards versus their ^{10}B concentration. The data were linearly fit with the origin of the line forced through (0,0). The error in the slope was given as part of the line fit done with Macintosh Kaleidagraph.

The next step in analysis of the data was to determine the ^{10}B concentration for the samples using the calibration curve. The B/H ratio of each sample was divided by the slope of the calibration curve since the slope was the increase in B/H ratio over the increase in concentration. Again, error was calculated by applying standard error propagation formula [Knoll 1989], i.e.

$$\left(\frac{\Delta C}{C}\right)^2 = \left(\left(\frac{\Delta(B/H)}{B/H}\right)^2 + \left(\frac{\Delta m}{m}\right)^2\right) \quad \text{(Eq. 3.4)}$$

where ΔC is the error in concentration, C is the concentration, Δm is the error in the slope of the calibration curve and m is the slope of the calibration curve.

In cases where there was too little ^{10}B and the sample was too small for statistical uncertainty of less than 20% to be reached within one hour (except for backgrounds), the following relationship was used [Riley 1997] to determine the lowest detectable concentration (LDC):

$$LDC = \left(3.29 \cdot \left(\frac{\sqrt{B}}{S\sqrt{T}}\right)\right) \cdot \frac{1}{W} \quad \text{(Eq. 3.5)}$$

where B is the background count rate which is equal to 100 cps, S is the sensitivity of the facility and equals 18 cps/μg, T is the count time in seconds and W is the weight of the sample in grams. Therefore, the unit of LDC is units of μg/g or ppm.

3.1.2 Compound preparation

Several compounds were considered for uptake evaluation. The ^{10}B concentration of the boron compounds was first tested and, if adequate, uptake evaluation was performed. The compounds described in this subsection are the (i) boron particulate and (ii) ferric hydroxide macroaggregate for which uptake evaluation was performed. The last subsection (iii) will describe compounds considered but not evaluated.

(i) Boron Particulate

The boron particulate is 99.9% boron metal, 94% enriched in ^{10}B. The particles are spherical and have a wide distribution of sizes, ranging from 5 to 40 μm, with the diameter of the average sized particle estimated at 15 μm [Johnson 1994]. Preparation of a solution of this compound is very straightforward and just involves the suspension of different quantities of the particulate in saline.

The concentrations used were 0.10 mg/ml, 0.50 mg/ml and 1 mg/ml, or, in units of ppm (μg/g), 100, 500 and 1000 ppm of boron (or 94, 470 and 940 ppm of ^{10}B ppm, based on enrichment).

(ii) Ferric hydroxide macroaggregate

Preparation of this compound required a substantial amount of development work. The idea of using a ferric hydroxide macroaggregate was derived from its use in the delivery of β-emitters to the synovium for radiation synovectomy. The size of the macroaggregate particles is about 100 times larger than the other colloids used in radiation synovectomy but it is smaller than the boron particulate. This larger size was hence expected to have a reduced leakage rate and indeed leakage from the injected joint was minimal, ranging from 0.03% to 0.24% [Sledge et al 1986]. In order to use a ferric hydroxide macroaggregate for BNCS, a boron compound had to be incorporated into the macroaggregate. Determination of an adequate compound, as well as concentrations of the reaction components, was carried. out. The first compound used to incorporate boron into the macroaggregate was boric acid, H_3BO_3 (same as used for boric acid standards).

Steps performed in preparation of the boric acid ferric hydroxide macroaggregate (BA-FHMA) were similar to those for ^{165}Dy [Hnatowich et al 1978]. The protocol is summarized below:

Step 1: mixed 2.0 ml of saline + 0.5 ml of Fe^{2+} ($FeCl_2$ 10 mg/ml) + varying H_3B0_3

These were mixed in a 10 ml vacutainer tube, using 10 ml tuberculin syringes and eighteen gauge, 3 1/2" needles. The saline, serving as solvent, was sterile.

Step 2: added 1 ml of 0.1 M NaOH to precipitate Fe^{2+}, inducing the reaction

$Fe^{2+} + 2OH^- \text{---> } Fe(OH)_2 \text{---> } Fe(OH)_3$ {since exposed to O_2}

The $Fe(OH)_2$ is light green while $Fe(OH)_3$ is a reddish brown gelatinous precipitate. During the precipitation, either the BO_3^{3-} or the $B(OH)_4^-$ ion should be trapped within the molecular structure of the $Fe(OH)_3$, forming a macroaggregate. Since in aqueous solution H_3BO_3 dissociates into $B(OH)_4^-$, this is more likely to be trapped in the macroaggregate than BO_3^{3-}. Extra Fe^{2+} (0.1 ml) was added to the last three tubes (table 3.2) in order to form the precipitate.

Step 3: washed twice with polyvinylpyrrolidone (PVP) in order to remove the colloidal-sized particles (fines). To the precipitate, 1 ml of dilute PVP (7.5 mg/ml) was added and the tubes were centrifuged at 1500 ppm for 5 minutes. The supernatant was removed (first supernatant) and 5 ml of concentrated PVP (16 mg/ml) were added. The tubes were once again centrifuged at 1500 rpm for 5 minutes and the supernatant once again removed (second supernatant).

Table 3.2 summarizes the results. The column listed "Ideal Concentration (ppm)" was determined by dividing the amount of ^{10}B (μg) placed in the sample by the sample's final weight (in ml). Hence, this division (μg/g) should yield the ideal boron concentration if all of the boric acid were trapped within the macroaggregate. All boron concentrations are expressed in terms of ^{10}B. The ^{10}B boric acid samples were prepared by scaling the relation that 3.104165 g in 1000 ml is equal to 100 ppm [Chabeuf 1993], as described in section 3.1.1.

Table 3.2: Results of BA-FHMA

#	Preparation	Amount of ^{10}B (μg)	Weight. (ml)	Ideal ppm [^{10}B]	Measured ppm [^{10}B]
1	1 ml of 100 ppm	100	0.20	500	0.3± 17%
2	1 ml of 150 ppm	150	0.35	430	2.6± 14%
3	0.4 ml of 750 ppm	300	0.30	1000	3.8± 14%
4	0.8 ml of 750 ppm	600	0.30	2000	11.2± 13%
5	0.7 ml of 1500 ppm	1000	0.30	3333	15.0± 14%
6	1.0 ml of 1500 ppm	1500	0.30	5000	12.5± 14%

Although the measured concentration increased with increasing concentration, little of the boric acid was trapped in the macroaggregate, less than 1% of the ideal concentration. This contrasts the finding with dysprosium, where recovery rates of about 96% are seen [Shortkroff et al 1993]. However, a larger concentration of dysprosium was used. It was decided to increase the boron concentration of boric acid to its maximum (saturation) and to save the supernatant in step 3 to see if it contained significant amounts of boron.

A saturated solution of 0.276 g of boric acid per ml of saline was prepared and 1 ml was used for the procedure. Results are shown in table 3.3. The concentration of the BA-FHMA precipitate did increase, by about a factor of 15, and still remained at about 1% of the ideal concentration. The first supernatant had a higher boron concentration than the precipitate, indicating that much of the boric acid was not firmly retained in the macroaggregate initially and was washed away. However, the second supernatant had little boron compared to the first one (about 1%) or compared to the precipitate (2%), indicating that more leakage of the boric acid was not likely with further washes. If the boric acid were enriched in ^{10}B, then the boron concentration would be 1015 ppm. When injected into a rabbit joint, the "effective" concentration of a boronated compound is diminished by a factor of 5 (0.25 ml of compound is injected into about 1 ml of synovial fluid), therefore higher boron concentrations are required. Since the boron concentration of boric acid was poorly incorporated into the FHMA, attention was turned to another boron containing compound that would produce a higher yield of boron into the macroaggregate.

Table 3.3: Highest BA-FHMA result

Preparation	Sample	Weight (ml)	Measured [^{10}B] (ppm)
1 ml of 8,900 ppm	precip	0.2	203± 12%
	1st spnt.	0.1	314± 12%
	2nd spnt.	0.1	4± 13%

The next compound considered for incorporation into the macroaggregate was $K_2B_{12}H_{12}$ (KBH), the potassium salt form of a well studied polyhedral borane ion [Cotton and Wilkinson 1985]. A similar protocol was followed, except that higher amounts of iron and NaOH were used (1 and 1.5 ml, respectively). With the KBH compound, the ion that coprecipitated with the macroaggregate is $B_{12}H_{12}^{2-}$. Various ^{10}B concentrations of KBH were prepared. The amount of ^{10}B (μg) added was calculated in the following manner. First the compound concentration was determined by dividing the amount of KBH dissolved by the volume of the water. Compound concentration is not the same as boron concentration because boron is just one of the compound's constituents. Taking into account that KBH was unenriched (20% ^{10}B and 80% ^{11}B), the ^{10}B concentration of the KBH compound was determined to be about 11% by weight. Since 1 ml was used in the experiment, the total amount of ^{10}B in the compound was calculated to be the ^{10}B concentration divided by the volume used. Experimental results are summarized in table 3.4.

As can be seen in the table, the concentrations in the first supernatants were about 3 to 10 times higher than those seen in the precipitates. The second supernatants had concentrations between 4 and 10 ppm, which is about 4 to 40% of the concentration found in the precipitates. However, when compared to the first supernatants, the concentration of the second supernatant was quite low (from 3 to 5%), indicating that most of the compound was washed away in the first step. None of the concentrations found in the precipitates would be acceptable for in vivo evaluation since several hundred ppm of boron are required in the synovium, as discussed in 2.3; the concentration of the boron compound to be injected needs to be higher than the concentration required in the synovium.

Table 3.4: Initial results of KBH-FHMA

Preparation	Sample	Weight (ml)	Amount of ^{10}B (μg)	Ideal [^{10}B] (ppm)	Measured [^{10}B] (ppm)
1 ml of 3 mg/ml	precip.	0.20	330	1650	38 ± 8%
	1st spnt.	0.10			151 ± 8%
	2nd spnt.	0.10			4 ±10%
1 ml of 6 mg/ml	precip.	0.40	660	1650	26 ± 8%
	1st spnt.	0.10			142 ± 8%
	2nd spnt.	0.10			6 ±10%
1 ml of 12 mg/ml	precip.	0.25	1320	5280	23 ± 8%
	1st spnt.	0.10			220 ± 8%
	2nd spnt.	0.10			10 ±10%
1 ml of 20 mg/ml	precip.	0.20	2640	13200	99 ± 8%
	1st spnt.	0.10			328 ± 8%
	2nd spnt.	0.10			10 ± 9%

The KBH solutions used in the preparation of the macroaggregate were relatively low in boron concentration. Therefore, the KBH concentration used in the preparation of the KBH-FHMA was increased, as well as the concentration of the ferric ion to ensure that incorporation of KBH into the macroaggregate would not be limited by the number of ferric ions available. Table 3.5 shows the preparations of KBH and their ^{10}B content as measured via PGNAA (the highest was difficult to dissolve and heat had to be applied).

Table 3.5: Preparation of higher KBH concentrations for KBH-FHMA

Preparation	Weight (ml)	Measured [^{10}B] (ppm)
200 mg/2 ml	0.05	19562 ± 8%
1000 mg/3 ml	0.05	37569 ± 9%
2000 mg/5 ml	0.05	38259 ± 8%

Table 3.5 shows that the measured ^{10}B concentrations for the 1000mg/3ml and 2000mg/5ml are essentially the same, at 38,000 ppm, indicating that 1000mg/3ml or 330 mg/ml is approximately the saturation point for KBH. The first two KBH preparations were used with both the standard ferric ion concentration (10mg/ml) and a more concentrated solution (500 mg/ml). For the last preparation, only the more concentrated solution of ferric ion was used, since it was expected that with that much boron compound, more ferric ion would be necessary. In addition to more ferric ion, the amount of NaOH added was increased accordingly from 1.0 ml to 1.5 ml. Results of these modifications are shown in table 3.6.

Table 3.6: Optimized results of KBH-FHMA

Preparation	Sample	Wt (g)	[^{10}B] (ppm*) (Fe^{2+}=10 mg/ml)	[^{10}B] (ppm*) (Fe^{2+}=500 mg/ml)
1.0 ml of 200mg/ 2ml	precip.	0.15	279 ± 8%	811 ± 5%
	1st spnt.	0.10	1381 ± 8%	1456 ± 6%
	2nd spnt	0.10	156 ± 8%	131 ± 6%
1.5 ml of 1000mg/3ml	precip.	0.15	1142 ± 8%	3260 ± 6%
	1st spnt.	0.10	7150 ± 9%	6200 ± 7%
	2nd spnt.	0.10	1411 ± 8%	623 ± 6%
2.5 ml of 2000mg/5ml	precip.	0.15	NA	4728 ± 7%
	1st spnt.	0.10	NA	12550 ± 8%
	2nd spnt.	0.10	NA	1124 ± 7%

*percent errors refer to the PGNAA counting errors

Results from table 3.6 indicate that increasing the ferric ion concentration increased the amount of KBH in the precipitate by about a factor of 3. As before, the concentration of the first supernatant was higher than the concentration in the precipitate, indicating that much of the KBH was washed away. Looking at the column with the high ferric ion concentration, the boron concentration of the second supernatant was around 10% that of the first supernatant and from 16% to 24% that of the precipitate (with an average of 20%). The highest preparation of KBH, with the high ferric ion concentration, resulted in a KBH-FHMA with a ^{10}B concentration of 4,700 ppm, which was deemed sufficiently high to warrant evaluation in vivo.

The question then arose of whether the relatively large size of the KBH-FHMA would affect the energy deposition of the alpha and lithium particles (from the boron neutron capture reaction) in light of their short ranges. To address this issue, simulations were performed with a calculational tool called TRIM [Ziegler et al 1996]. The ferric hydroxide molecule was modeled as the medium through which the lithium and alpha particles had to travel. The density was modeled as 2.76 g/cc (as calculated based on data from the CRC Handbook of Chemistry and Physics and TRIM). The simulations showed that the projected range of a 1.50 MeV alpha particle in the macroaggregate was 4.42 μm (while that of the 0.850 MeV lithium particle was 2.28 μm) which implied that the size of the KBH-FHMA should be smaller than 4.4 μm in order to allow the particles to leave the macroaggregate and deposit their energy directly into the cell. It was assumed that KBH would remain in the ferric hydroxide macroaggregate.

It therefore became necessary to at least roughly determine the distribution of particle size and concentration. To try to increase the number of particles at a reduced particle size, sonication was tested and a comparison made between not sonicated and sonicated samples. The KBH-FHMA was prepared with the high concentrations of KBH and ferric ion solution. The original precipitate was washed once with 5 ml of concentrated PVP and then resuspended in 4 ml of saline, totalling 5.5 ml in volume which was used to compose four sets (2 each for not sonicated and sonicated). Sonication was done for 1 minute. For each of the four sets, serial filtration was performed with filter sizes of 8, 5, 3, 2 and 1 μm.

The data are shown in table 3.7. Results for the not sonicated and sonicated sets were averaged over the two samples unless otherwise noted at each filter size. As can be noted from the table, there is large variability between the two samples. This variability was introduced in the filtration step because different amounts of saline were required to push the KBH-FHMA solution through the filters and keep as many of the particles as possible. However, since the PGNAA measurement normalizes to hydrogen background, this greatly affected the measurement.

The supernatant of most interest was the one after 5 μm, based on the TRIM results showing that the average particle range of the 1.5 MeV alpha particle was 4.42 μm. It was considered better to have particles 0.58 μm greater than the desired range, rather than to eliminate potentially useful particles by using the supernatant after the 3 μm filter (4 μm filter was not available). Comparison between the supernatants after the 5 μm filter of the not sonicated and sonicated samples in table 3.7 revealed that the ^{10}B concentration was greater in the not sonicated set of samples and led to the conclusion that there was no advantage to sonication.

Table 3.7: Results of sonication experiment with KBH-FHMA

	Not sonicated		Sonicated	
	ave. [^{10}B]* (ppm)	high/low (ppm)	ave. [^{10}B] * ppm	high/low (ppm)
spnt after 8 μm filter	1768	1848/1688	1376	1510/1241
spnt after 5 μm filter**	1503	NA	915	NA
spnt after 3 μm filter	934	1065/802	682	NA
spnt after 2 μm filter	564	581/547	486	NA
spnt after 1 μm filter	389	485/293	337	NA

* PGNAA counting error ranged from 4% to 13%, with an average of 7%

** a spillage occurred with the sonicated 5 μm filter such that there was only one sample available in the sonicated set after that size. Also, in the not sonicated set, only one 5 μm was retrieved.

Thus, the macroaggregate compound, KBH-FHMA, was prepared for uptake evaluation. On the morning of the uptake experiment, the macroaggregate was prepared by adding 3 ml of a KBH solution made from 350 mg/ml to 1.5 ml of $FeCl_2$ at high concentration (500 mg/ml). Then 1.5 ml of 0.1M NaOH was added. An aliquot of the original precipitate was taken for measurement via PGNAA. The original precipitate was washed twice with PVP. Then 3 ml of saline were added and the vacutainer tube was shaken well. The solution was passed through a 5 μm filter, in two parts of 1.5 ml each. An aliquot was taken for PGNAA analysis and the rest was taken for the uptake study. To ascertain the stability of the KBH-FHMA, an aliquot of the solution remaining after the uptake experiment was taken 24 hours after the uptake study and its boron concentration measured via PGNAA. The results of the PGNAA measurements are shown in table 3.8. As can be seen from the table, the original precipitate had over 5,000 ppm ^{10}B taken up. The aliquots taken immediately after preparation and 24 hours later both had 2,300 ppm ^{10}B within 1%. Thus, a KBH-FHMA preparation was achieved with high boron concentration and particle sizes less than 5 μm. If the KBH were 100% enriched in ^{10}B, the ^{10}B concentration of the KBH-FHMA (2,320 ppm) would scale to 11,600 ppm of boron. This was the preparation of boron compound injected intra-articularly in the in vivo uptake evaluation whose parameters and results are detailed in sections 3.1.3 and 3.2.2, respectively. Further work with this particle could include the development of a method for testing how long the KBH remains incorporated into the FHMA.

Table 3.8: Preparation of KBH-FHMA for the uptake study

Compound	Weight (g)	^{10}B concentration (ppm ±%)
original precipitate	0.01	5,096 ± 13%
spnt after 5 μm filter	0.09	2,320 ± 11%

(iii) Other compounds

Several other compounds were considered, though not evaluated. The first of these was boronated magnetic microparticles. The idea would be to inject the boronated magnetic microparticles into the knee joint and keep them localized to the joint by using appropriately designed magnetic fields and field gradients. This, in theory, would provide a more uniform distribution of the particles throughout the joint space. The microparticles would then be taken up by the synoviocytes via phagocytosis and, as before, the joint would be irradiated by neutrons with the potential to induce cellular kill by the boron neutron capture reaction. Microparticles, in general, have emerged as an important tool in the study of cellular phagocytosis and the identification of factors influencing the process [Fernandez-Repollet and Schwartz 1988]. Several biomedical applications have been suggested for magnetic microparticles [Strand et al 1988]. For example, one study has examined the efficacy of magnetic microparticles in the in vitro depletion of T cells from the bone marrow for reducing the incidence and severity of bone marrow transplant rejection [Platsoucas et al 1988]. Another study investigated the use of magnetic microparticles to deliver site specific drugs in a rat model [Widder et al 1978]. Results showed that magnetic albumin microparticles, with the chemotherapeutic agent entrapped inside the albumin matrix, could be concentrated at a specific predetermined site in vivo by application of a magnetic field about 0.8 T in strength [Widder et al 1978]. The magnetic field strength required to accumulate the particles, (0.8T) is about half of the strength routinely used in clinical MRI studies (1.5T) and has not been shown to have deleterious effects on humans.

Boronated magnetic microparticles for BNCS were prepared from a mixture of ferric chloride ($FeCl_3$), ferrous sulfate ($FeSO_4$) and lithium tetraborate ($Li_2B_4O_7$) [Shapiro 1997]. The quantities of these components were varied to maximize the magnetic properties of the particles as well as the amount of boron incorporated into the magnetite. The ability of external permanent magnets to stop and attract the particles was also tested with various magnet configurations. Results showed that the microparticles had 7,400 μg of boron per g of magnetite and 7 ppm of boron in solution made from 3 mg/ml of particles/saline [Shapiro 1997]. Magnet strengths of 0.8T were successful in attracting and controlling the magnetic particles in water fluid velocities of about 750 ml/min, a value approximating the rate of human blood flow [Shapiro 1997].

Measurement of this preparation with PGNAA gave a ^{10}B concentration of about 2 ppm which implied a natural boron concentration of 6 ppm, confirming the 7 ppm of boron within statistical uncertainty. Requests for a more concentrated solution led to the preparation of two solutions with particle concentrations of 23 and 36 mg/ml of saline. The latter of these preparations represented the maximum solubility of the magnetic microparticles in saline; it was very viscous and difficult to draw up with a pipette. PGNAA measurements of the solutions revealed that 18 and 32 ppm of ^{10}B, respectively, were present. In terms of natural boron, or if the particles were made with enriched lithium tetraborate, this would correspond to concentrations of 90 and 160 ppm. These concentrations were considered too low to warrant continuing to uptake studies.

The next type of compound considered was a boronated liposome. A liposome is made of many lipids (primary constituents of cell membranes) connected together which can entrap compounds and serve as a biodegradable pharmacological carrier. Arthritic synovium is actively phagocytic which is favorable for a liposomal delivery of compounds. The idea of using liposomes to deliver

drugs consists of the liposome associating with the synovium and being taken up by either fusion with the cell membrane or endocytosis and ultimately ending up in a secondary lysosome in the cell where it would be degraded and its contents (the drug) would be released. Liposomes have been used to encapsulate various drugs for RA, including methotrexate [Foong and Green 1993], lidocaine [Hou and Yu 1997] and corticosteroids [Shaw and Dingle 1980, Bonanomi et al 1987]. The use of liposomes has also been investigated for radiation synovectomy, with both yttrium-90 [Utkhede et al 1994] and dysprosium-165 [Zalutsky et al 1988], and should be pursued for BNCS.

Very brief consideration was given to boronating gold salts, which are already used as a form of treatment for RA [Gordon 1993]. However, severe problems exist with this. One of the postulated mechanisms of gold is the inhibition of macrophage activity, which would result in a decrease in phagocytic activity and therefore a reduction in the potential uptake of the boronated gold salt. Furthermore, it would be difficult to distinguish between the effects of gold and boron neutron capture synovectomy in the production of a potentially beneficial results. Finally, gold has several toxic side effects. Therefore, the idea of boronating gold salts was discarded.

3.1.3 Uptake study parameters

Uptake was measured in vivo using an AIA rabbit model (described in 2.3). On the third day after arthritis induction, 0.25 ml of the boron compound was injected intra-articularly. After varying times, the rabbits were sacrificed and the synovium was excised, as well as several other of the joint tissues. Tissues were kept frozen at -70° C, until analysis of ^{10}B content could be performed.

With the boron particulate, the time between injection and sacrifice was kept constant at 1 hour, while the boron concentration was increased from 100 ppm to 1,000 ppm. Time was not varied on the basis of previous ex vivo uptake studies which found that most of the synovial uptake occurred within 1 hour [Johnson 1994]. In the study with the KBH ferric hydroxide macroaggregate, the concentration of the compound was kept constant and the time between injection and sacrifice was varied from 4 to 24 hours, based on leakage rates found with dysprosium [Sledge et al 1986]. Concentration was not varied.

3.2 Results and discussion

The results of the uptake studies of the two compounds considered for use in BNCS are presented in this section according to boron compound. The boron particulate is discussed first (3.2.1) and is followed by the KBH ferric hydroxide macroaggregate (3.2.2).

3.2.1 Boron particulate

Table 3.9 presents results of in vivo uptake of boron particulate as a function of the concentration of the particulate, for a fixed time between intra-articular injection and rabbit sacrifice. For all concentrations, except 1 mg/ml, three rabbits were sacrificed (n=3). In the 1 mg/ml set, two of the rabbits were misinjected; upon dissection, a large coagulate of boron particulate was noticed in the muscle below the knee joint. Two samples of the muscle revealed concentrations of 200 and

500 ppm (± 10%). In the 1 mg/ml rabbit that was properly injected, a large coagulate was found in the synovial fluid. It was taken out of the synovial fluid and its concentration was measured to be 2,700 ± 10%ppm. To eliminate coagulation, 1% hyaluronate was added to the saline for the 0.5 and 0.1 mg/ml concentrations. Counting error for the samples shown in table 3.9 ranged from 10% to 20%, with an average of 11%.

Table 3.9: Synovial uptake of boron particulate

Concentration of particulate	Synovium	Range of uptake (ppm)	Average uptake (ppm)
0.1 mg/ml	anterior	1 - 3	2.3
(n=3)	posterior	1 - 6	3.3
0.5 mg/ml	anterior	3 - 20	16
(n=3)	posterior	1 - 190	67
1.0 mg/ml	anterior	248	NA
(n=1)	posterior	34	NA

As can be seen from table 3.9, average uptake by the synovium (both anterior and posterior) was very low with the 0.1 mg/ml preparation. Uptake using the 0.5 mg/ml particulate concentration was more than 5 times that found with the 0.1 mg/ml concentration; however, the range was quite large, especially in the posterior synovium (1 to 190), implying that the boron particulate was not well distributed throughout the joint.

Tables 3.10 and 3.11 show the distribution of the particulate in other parts of the joint obtained using the 0.1 mg/ml and 0.5 mg/ml preparations. Since only one animal was successfully injected with the 1.0 mg/ml preparation, results ware presented in the following paragraph. Counting error for samples (except cartilage, addressed as footnotes) in table 3.10 ranged from 10% to 21%, with an average of 16%, while counting error for samples in table 3.11 ranged from 9% to 27%, with average of 14%, respectively.

In the one rabbit which was properly injected with the 1 mg/ml particulate suspension, patellar uptake was 4 ppm, while cartilage uptake was 44 ppm and ligament uptake was higher at 96 ppm. The tendon was not taken, but the meniscus was taken and it had 36 ppm of ^{10}B. Synovial fluid had 381 ppm of boron. Two other body fluids, blood and urine, had ^{10}B concentrations of 0.3 and 1.4 ppm, respectively. It should be noted that muscle and fat tissue have been reported as having a natural boron concentration of 0. 1 ppm, while blood has found to have 0.2 ppm of natural boron [Forbes et al 1954].

Synovial uptake at the highest preparation, 1 mg/ml, is about an order of magnitude lower than the values found in ex vivo experiments also after 1 hour incubation with boron particulate [Johnson 1994]. Granted that there is only one animal and it could represent an extreme end of a range, but still, the uptake is significantly lower. The low uptake makes sense in light of the coagulate that was found in the synovial fluid. Only the boron particles that were separate from the coagulate were taken up by the synovium, and other tissues in the joint. Perhaps the boron particulate could

be coated with something to prevent its coagulation and ensure a more homogeneous spreading throughout the joint.

Table 3.10: Uptake of 0.1 mg/ml boron particulate by other constituents of the joint

Joint part	Range of uptake (ppm)	Average uptake (ppm)
patella	0.02 - 1	0.6
tendon	0.40 - 4	1.8
ligament	2 - 41	16
cartilage*	0.04 - 55	19
fluid	17 - 116	52

*for 2 of the 3 samples, the lowest detectable concentration, rather than actual concentration, was determined, i.e. the samples had less than 0.04 and 0.91 ppm. The third sample had a concentration of 55 ± 26% ppm. In order to obtain an average, the lowest detectable concentration (LDC) was used, therefore serving as a conservative estimate.

Table 3.11: Uptake of 0.5 mg/ml boron particulate by other constituents of the joint

Joint part	Range of uptake (ppm)	Average uptake (ppm)
patella	1 - 3	2
tendon	1 - 2	2
ligament	1 - 7	4
cartilage*	3 - 23	12
fluid	14 - 64	37

*for 1 of the 3 samples, the LDC rather than actual concentration was determined to be less than 9 ppm. The other 2 samples had concentrations of 3 ± 13% ppm and 23 ± 34% ppm. In order to obtain an average, the LDC was used again, thereby serving as a conservative estimate.

Of the other joint constituents, the highest boron concentration was found in the synovial fluid. There was no correlation between injection concentration and boron concentration, although, only one datum exists at the highest concentration. The value for blood at the 1 mg/ml concentration is about one order of magnitude lower than the average value of 3 ppm found with the 0.1 and 0.5 mg/ml boron preparations. However, since there is only one datum at 1 mg/ml it is difficult to make a comparison. The cartilage and ligaments generally had higher uptake, with values of 44 and 96 ppm, respectively, found with the 1 mg/ml particulate preparation. This could be explained by the following observations: cartilage is in direct contact with synovial fluid at the articulating surfaces; several areas of ligament are covered by synovium which would affect the measurement (since PGNAA averages over the whole tissue) and the small size of the ligament may make the concentration even higher because PGNAA is normalized to the hydrogen content of a sample. An example of this last point follows. Assuming that a ligament sample had a weight of 0.03 g

and a boron concentration of 5 ppm, if there were 0.01 g of synovium with a boron concentration of 250 ppm in the ligament sample, then the measured boron concentration of the ligament sample would be 170 ppm.

3.2.2 Ferric Hydroxide Macroaggregate

Table 3.12 shows the uptake obtained in vivo as a function of time after an intra-articular injection of the KBH-FHMA preparation described in section 3.1.2. Three rabbits were sacrificed at each time point (n=3). Results in table 3.12 have been scaled to 100% enrichment in ^{10}B. Counting error ranged from11% to 16%, with an average of 14% for the samples in table 3.12.

Table 3.12: Synovial uptake of KBH-FHMA

Time (hours)	Synovium	Range of uptake (ppm)	Average uptake (ppm)
4	anterior	20 - 75	40
	posterior	30 - 50	40
24	anterior	10 - 45	30
	posterior	25 - 225	100

Synovial uptake of KBH-FHMA after 4 hours did not differ between the anterior and posterior parts of the synovium, averaging at 40 ppm. The range was about twice as large for the anterior as opposed to the posterior synovium. The boron compound seems to have distributed in a relatively homogeneous manner throughout the synovium at 4 hours post-injection. The synovial boron concentration at 24 hours post-injection did not change significantly, though the average posterior concentration was a factor of two higher which is due to the 225 ppm point laying far from the other two points (at 25 and 30 ppm). The relatively small change in synovial uptake (barring the 225 ppm point in the posterior synovium) is consistent based on two other findings as follows. Leakage rates with the dysprosium-based ferric hydroxide macroaggregate in an AIA rabbit model were less than 1% after 24 hours [Sledge et al 1977]. This may imply that the available boron concentration, in the form of the KBH-FHMA, to the synoviocytes should remain relatively constant for 24 hours. The postulated uptake mechanism of the FHMA is via phagocytosis. Ex vivo uptake studies with a boron metal particulate, which also taken up by phagocytosis, showed that the bulk of the uptake occurred within 1 hour when compared to 24 hours, although there was some increase at 24 hours [Johnson 1994]. This may imply that the bulk of synovial uptake occurs within the first hour, which in turn may imply that no large difference should be seen between uptake at 4 and 24 hours.

Although the synovial uptake of ferric hydroxide macroaggregate has not been studied per se (for radiation synovectomy, the purpose of the FHMA is to keep the dysprosium in the joint cavity so that a β particle, which has a range on the order of millimeters, can travel and deposit its energy into the synovium; actual phagocytosis by the synovium is not necessarily a goal), uptake of iron by synoviocytes has been documented with iron in the form of iron dextrate [Ball et al 1964]. Uptake was measured in normal rabbits and great inhomogeneity in terms of absorptive capacity

was exhibited, with about half of the cells taking up the iron; the inflammatory response induced by the synovial uptake of iron was transient, presenting no unusual features [Ball et al 1964].

The next tables, 3.13 and 3.14, show the boron uptake in other constituents of the joint, namely the patella, tendon, ligament, cartilage, meniscus and synovial fluid. Average counting error for the samples in tables 3.13 and 3.14 (not including patella and tendon samples) were 15% (range: 13% to 17%) and 13% (range: 13% to 17%), respectively.

Table 3.13: Uptake of KBH-FHMA at 4 hours by other constituents of the joint

Joint part	Range of uptake (ppm)	Average uptake (ppm)
patella*	<1, 2	<2
tendon**	<2 - 30	11
ligament	5 - 150	80
cartilage	5 - 30	15
meniscus	45, 80	65
fluid	95-140	115

*only two samples obtained, one with <1 ppm and the other with <2 ppm
**two samples had <2 ppm while the third had 30 ± 15% ppm; the average was calculated by assuming that two tendons had 2 ppm and the third had 30 ppm.

Table 3.14: Uptake of KBH-FHMA at 24 hours by other constituents of the joint

Joint part	Range of uptake (ppm)	Average uptake (ppm)
patella*	<1 - 2	<2
tendon**	<2	NA
ligament	85 - 255	150
cartilage	30 - 115	65
meniscus	5 - 40	25
fluid	90, 225	175

*of three samples, two samples had <2 ppm, while one had <1ppm
**only one tendon sample was dissected, therefore no average is given

Comparison of the average synovial uptakes after 4 hours to the average boron concentrations in the other constituents of the joint at the same time point shows that the ligament, meniscus and synovial fluid have higher boron concentrations. After 24 hours, average boron concentrations in the cartilage, ligament and synovial fluid are higher than either anterior or posterior synovium. At all times, there is large variability in the data, making it difficult to distinguish trends in boron concentrations with increasing time.

Table 3.15 shows the boron concentration in the blood and urine at 4 and 24 hours post-injection of the macroaggregate (counting error ranged from 10% to 20% and averaged 13%). There is no difference with time for either blood or urine. The elevated boron concentration in the blood may indicate that the KBH has escaped from the macroaggregate, since work in the literature has shown that leakage rates of the macroaggregate from the joint are minimal [Noble et al 1983]. Assuming a urine volume of about 20 ml, 75 ppm (the average at 24 hours) equals 1500 μg of boron. Given that the total amount of boron injected into the joint was 2900 μg (0.25ml*11,600 ppm), the boron concentration in the urine at 24 hours could represent as much as 52% of the total boron injected. It should be noted that there is no chemical bonding involved in the formation of the KBH-FHMA but rather the macroaggregate is achieved by a physical co-precipitation.

Table 3.15: Boron concentration in body fluids after injection of KBH-FHMA

Time (hours)	Body fluid	Range of uptake (ppm)	Average uptake (ppm)
4	blood	5 - 40	15
	urine	45 - 105	70
24	blood	20 - 30	25
	urine	45 - 125	75

3.3 Conclusions

The in vivo uptake of several boron-containing compounds was evaluated and none of these resulted in uptake characteristics which warranted their use in animal irradiation studies. Further compound development work is required in order for the boron compounds tested in this chapter, to produce more favorable characteristics. Further investigation of the other boron compounds under consideration is necessary before their potential for uptake evaluation can be determined.

4. Uptake of $K_2B_{12}H_{12}$

This chapter is devoted solely to the uptake of $K_2B_{12}H_{12}$. When in solution, $K_2B_{12}H_{12}$ dissociates into $2K^+$ and $B_{12}H_{12}^{2-}$. The original isolation of the $B_{12}H_{12}^{2-}$ ion [Pitochelli and Hawthorne 1960] suggested an icosahedral arrangement. The structure was confirmed by an X-ray diffraction study of $K_2B_{12}H_{12}$ [Wunderlich and Lipscomb 1960] which found that the symmetric structure of $B_{12}H_{12}^{2-}$ in $K_2B_{12}H_{12}$ is slightly distorted by steric interactions between the K^+ and $B_{12}H_{12}^{2-}$ ions. There are 6 boron-boron distances of 1.755 A and 24 of 1.780 A, and these deviations from the mean distance of 1.77 A for a regular icosahedron suggested that when the $B_{12}H_{12}^{2-}$ ion is alone (i.e. missing K^+), it has full icosahedral geometry [Wunderlich and Lipscomb 1960, Lipscomb 1963]. The volume of $B_{12}H_{12}^{2-}$ is equivalent to that of a benzene molecule spinning on a twofold axis [Muetterties and Knoth 1968]. A schematic of the structure of $B_{12}H_{12}^{2-}$ is shown in figure 4.1.

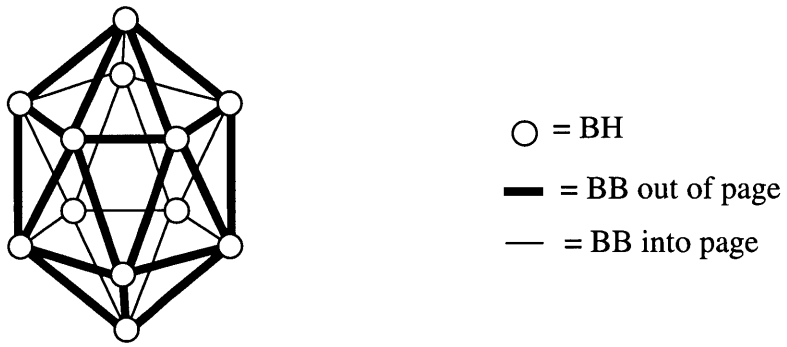

Figure 4.1: Schematic of the structure of $B_{12}H_{12}^{2-}$, which, along with $2K^+$, constitute $K_2B_{12}H_{12}$.

The $B_{12}H_{12}^{2-}$ ion is the most symmetric of all the polyhedral borane ions and has the maximum resonance stabilization, leading to an overall high level of stability [Muetterties and Knoth 1968]. This stability is reflected in both pyrolytic and hydrolytic aspects. With a cesium salt, $B_{12}H_{12}^{2-}$ has been heated to about 800° in an evacuated sealed tube without showing any signs of significant decomposition [Muetterties et al 1964]. It is also thermally stable in air, which implies that it is very resistant to oxidation. The $B_{12}H_{12}^{2-}$ ion is not attacked by NaOH, a strong base, at elevated temperatures and it has been found to be stable in hydrochloric acid (3N) at a temperature of 95° [Muetterties et al 1964]. It does show reactivity in strong acidic solutions and exchanges its hydrogens with the surrounding water; however, this does not lead to an effective change in its structure [Muetterties and Knoth 1968].

Most of the salts of $B_{12}H_{12}^{2-}$, except for the silver salts, have a wide range of solubilities in water and other solvents [Muetterties and Knoth 1968]. Like the other polyhedral borane ions, $B_{12}H_{12}^{2-}$ is susceptible to attack by strong electrophiles for substitution reactions involving exopolyhedral ligands; the $B_{12}H_{11}SH^{2-}$ ion is prepared by reacting the conjugate acid of $B_{12}H_{12}^{2-}$ with hydrogen sulfide and a boron compound, $B_{10}Cl_8(SH)_2^{2-}$ [Knoth et al 1964]. The sodium salt form of $B_{12}H_{11}SH^{2-}$, or $Na_2B_{12}H_{11}SH$, is currently being used for BNCT clinical trials in Europe and Japan.

Initial preparations of the $B_{12}H_{12}^{2-}$ ion were very low in yield [Pitochelli and Hawthorne 1960]. However, further developments led to the synthesis of $B_{12}H_{12}^{2-}$ from borax, the principal boron ore via an intermediate diborane [Miller et al 1964]. Currently, $K_2B_{12}H_{12}$ (KBH) is commercially available; the boron may be unenriched (Strem Chemicals, Newburyport, MA) or enriched (Boron Biologicals, Rayleigh, NC). The first section in this chapter (4.1) describes the materials and methods used to investigate uptake and the next section (4.2) presents and discusses the results of this investigation. Conclusions are drawn at the end of this chapter (4.3).

4.1 Materials and methods

Uptake of KBH has been characterized on three levels; in cells, tissue and animals. This section details the materials and methods employed to analyze uptake at all of these three levels. First, the in vitro experimental methods are described (4.1.1), followed by the ex vivo methods (4.1.2) and in vivo methods (4.1.3).

4.1.1 In vitro boron uptake

Characterization of in vitro uptake required some development work. A preliminary experiment was performed with synovial cells explanted from human RA tissue. However, due to the limited availability of synovium, it became necessary to use a human cell line for experimentation. Since the majority of the cells found in human RA synovial tissue are macrophages, experiments were performed with the THP1 cells, which constitute a well characterized human monocytic cell line [Tsuchiya et al 1980].

An ampule of the THP1 cell line (American Tissue Culture Collection, Rockville, MD) was thawed by direct placement into a water bath heated to 37° C. The ampule was rapidly agitated for 40 to 60 seconds and, as soon as the cells had minimally defrosted, a drop of medium was applied. After a minute, another drop of medium was applied and this was repeated until the ampule was full. Contents of the ampule were transferred to a microcentrifuge tube and the cells were washed to remove dimethysulfoxide (used to preserve the frozen cells) by centrifugation for 10 minutes at 1400 rpm and aspiration of the supernatant. The THP1 cells were resuspended in culture medium and transferred to T150 flasks with vented caps (0.22 μm filter).

The culture medium used to maintain the THP1 cell line was RPMI 1640 (Gibco BRL, Rockville, MD). To each 500 ml bottle of RPMI 1640 medium, 10 ml of 100x antibiotic-antimycotic (Gibco

BRL, Rockville, MD) and 50 ml of certified Australian fetal bovine serum (Hyclone Laboratories, Logan, UT) were added. In order to prevent the differentiation of the monocytes to macrophages, 2-mercaptoethanol (Sigma Chemical Company, St. Louis, MO) was added to the culture medium in the following manner: first, 19.5 μl of 2-mercaptoethanol were mixed with 5 ml of incomplete RPMI 1640 medium, then the solution was filtered with a 0.22 μm filter and finally 0.5 ml of this solution was added to the culture medium. To change medium, cells were transferred to 50 ml centrifuge tubes and centrifuged for 10 minutes at 1400 rpm. The supernatant was removed and replaced with new medium. The cells were then transferred to T150 culture flasks. Medium was replaced with fresh medium 3 times per week. During the first week after thawing, cell growth was sluggish and the doubling rate of about 60 to 70 hours [Tsuchiya et al 1980] was not observed; however, after about one week, the cells were growing healthily and quickly. Therefore, no experiments were performed with the monocytes during the first week post-thawing.

Once the cell lines were established, several preliminary experiments were performed and some major problems were encountered. The first was in the washing step. Although the mechanism of KBH uptake is not precisely known, it is likely based on diffusion and therefore may be affected by washing, i.e. the measurement of cellular uptake may be perturbed. Another major problem was that in all experiments phosphate buffered saline (PBS) was added to the microcentrifuge tubes at the end of the experiment in order to transfer the cell pellet to the teflon vials required for measurement via PGNAA. However, PGNAA measures the boron concentration of the entire solution in the teflon vial which contains PBS as well as the cell pellet. Hence, measurement yielded the boron concentration (ppm) of the solution and NOT just of the cell pellet. A further problem was that incubation in microcentrifuge tubes led to the unequal access of the cells to the boronated medium, since cells settled at the bottom of the tubes during incubation.

It should be noted that, unlike other cell uptake studies [Fairchild et al 1990, Nguyen et al 1993, Capala et al 1996], in this study no effort was directed toward determining whether the boron was intracellular. The goal of these experiments was to measure the concentration of boron inside and on the surface of the cell; and it is this association which will be called cellular "uptake". It should be stressed that this study was a preliminary attempt at the development of a method to determine cellular uptake by non-adhering monocytic cells representing synovial cells.

A protocol was developed to eliminate the problems encountered in the preliminary experiments described above. In this protocol, cells were incubated with boronated medium in cell wells and transferred to microcentrifuge tubes, which were centrifuged at a high number of revolutions per minute (e.g. 1600 rpm). Then, the supernatant was drawn off with glass pasteur pipettes to the point of also drawing up some cells, and leaving behind as little solution as possible. The wash step was eliminated and the sample considered ready for PGNAA.

The microcentrifuge tube with the cell pellet and the empty teflon vial were weighed. PBS was added to the microcentrifuge tube and the pellet was resuspended (the exact amount of PBS added does not matter since it is corrected by the scaling ratio as described below; 0.2 ml was found to be adequate for resuspension). The solution (with both PBS and the resuspended pellet) was then transferred from the microcentrifuge tube to the teflon vial. Both the teflon vial and the empty microcentrifuge tube were weighed to obtain weights of the solution and cell pellet, respectively. By weighing the microcentrifuge tube after the cell pellet has been removed, the weight of the

cells left behind was taken into account. The weight of the solution was divided by the weight of the pellet to obtain the scaling ratio. The ^{10}B concentration of the solution, measured by PGNAA, was multiplied by the scaling ratio to determine the ^{10}B concentration in cells, or cellular uptake. This is described by: [μg of ^{10}B/g of solution]*[g of solution/g of pellet] = μg/g of pellet. Scaling the measured boron concentration by the ratio is allowed from the point of view of PGNAA because the sample is homogeneous. All PGNAA counting errors were kept below 10%.

In order to test the sensitivity of this method to cell incubation concentration (i.e. the number of cells per ml of the boronated incubation medium) and the number of cells in the cell pellet, cell incubation concentration was varied from $1x10^6$ to $7x10^7$ cells/ml and incubation volume was kept a1 1 ml. Results are shown in figure 4.2. The average uptake is approximately the same at $1x10^6$ and $5x10^6$ (3,600 and 3,500 ppm, respectively), decreases at $1x10^7$ (2,900 ppm), and is the same at $3x10^7$ and $7x10^7$ (2,300 ppm). Statistical analysis via the Student's t-test revealed that there was a significant difference ($p<0.05$) between the uptake of $1x10^6$ and both $3x10^7$ and $7x10^7$, as well as $5x10^6$ and both $3x10^7$ and $7x10^7$. The data have a slope of $-1.81x10^{-5}$ ppm/cell with an R^2 of 0.29.

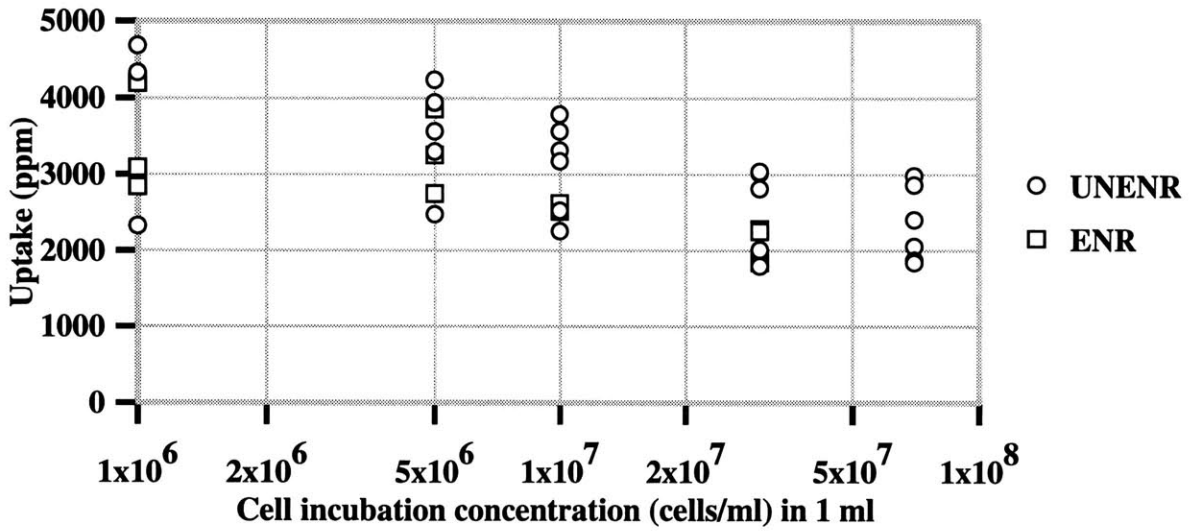

Figure 4.2: Cell uptake as a function of cell incubation concentration. However, since all the incubations were done in 1 ml, this also represents cell uptake as a function of pellet size.

The variability in the data decreases with increasing cell incubation concentration and pellet size, from being almost 3,000 ppm at $1x10^6$ to being over 1,000 ppm at $7x10^7$, which may be indicative of the sensitivity of the method to low cell incubation concentrations and low pellet sizes. Since the incubation volume was kept constant at 1 ml, the size of the pellet also varied. Therefore, two parameters were varied simultaneously in figure 4.2. To separate the effects of cell incubation concentration and pellet size, two experiments were designed as summarized in table 4.1. In order to test the effect of cell incubation concentration alone, pellet size was kept at $6x10^7$ cells while the cell incubation concentration was varied. In order to test the effect of pellet size alone, the cell incubation concentration was kept at $1x10^6$ cells/ml and the incubation volume was varied. The incubation time was kept at 1 hour and boron concentration at 5,000 ppm.

Table 4.1: Testing effect of cell incubation concentration and pellet size separately

Variation in cell concentration	
pellet size constant @60 million	
1 ml	60 million/ml
2 ml	30 million/ml
4 ml	15 million/ml
6 ml	10 million/ml
12 ml	5 million/ml

Variation in pellet size	
cell conc constant @1million/ml	
1 ml	1 million cells
5 ml	5 million cells
10 ml	10 million cells
30 ml	30 million cells

The incubations with 1 ml of boronated fluid and cells were carried out in 12-well plates, while incubations with 2 to 5 ml of fluid and cells were carried out in 6-well plates. For larger volumes, 6 to 12 ml, incubation was performed in T75 tissue culture flasks. The 30 ml incubation was done in a T150 tissue culture flask. After incubation, contents of the 6-well and 12-well plates were transferred to 15 ml centrifuge and microcentrifuge tubes, respectively. Contents of T75 and T150 flasks were transferred to 15 and 50 ml centrifuge tubes, respectively. Centrifugation lasted approximately 10 minutes at 1400 rpm. When the 15 and 50 ml centrifuge tubes were used, the supernatant was removed, except for about 1 ml. Cells were resuspended and then transferred to microcentrifuge tubes and centrifuged for another 10 minutes at 1600 rpm. This was done in order to obtain a tighter cell pellet which, in turn, allows more of the supernatant to be drawn off and less of the cells to be removed. An experiment in which this second transfer was not performed did not yield usable cell pellets.

The results of the experiments separating the effects of cell incubation concentration and pellet size are shown in figures 4.3 and 4.4, respectively.

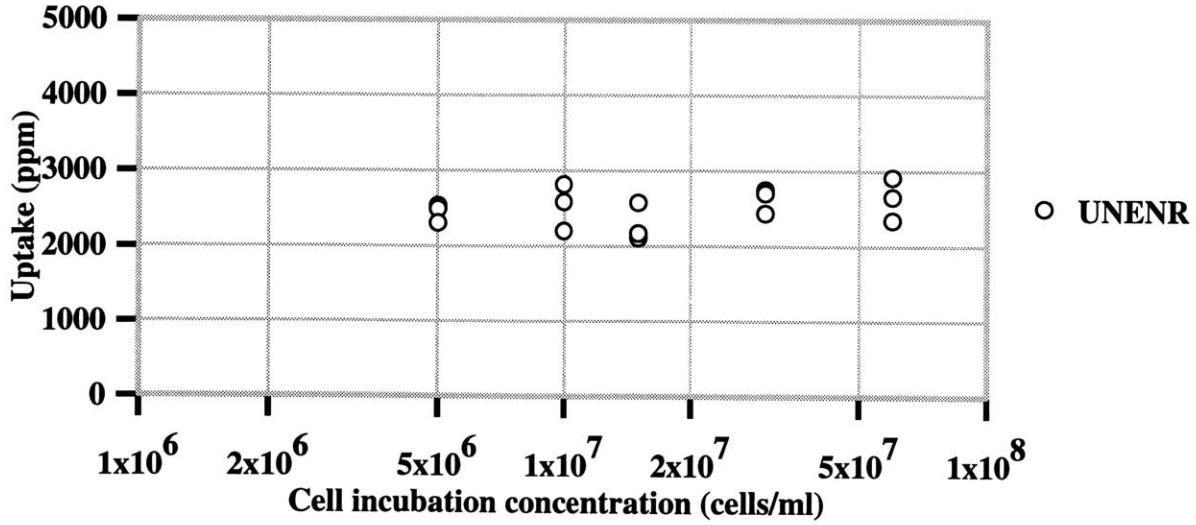

Figure 4.3: Cell uptake as a function of cell incubation concentration (constant pellet size).

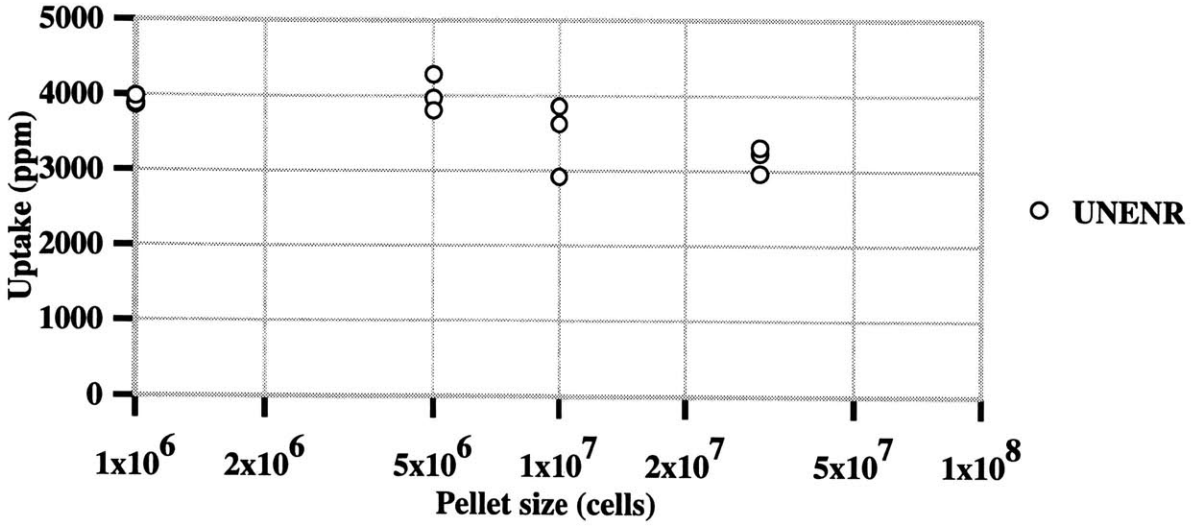

Figure 4.4: Cell uptake as a function of pellet size (constant cell incubation concentration).

Results shown in figure 4.3 indicate that, for a constant and large pellet size ($6x10^7$ cells), uptake does not vary significantly as a function of cell incubation concentration during the course of 1 hour and over the range tested. The slope of the data is $4.2x10^{-6}$ (R^2=0.13), with an error of 75%.

Cell uptake as a function of pellet size is shown in figure 4.4. The data as a whole have a slope of $2.78x10^{-5}$ ppm/cell with R^2 of 0.55. Statistical analysis via the Students t-test showed a significant ($p<0.05$) difference between the average uptake at $1x10^6$ cells (3,900 ppm) and $3x10^7$ cells (3,200 ppm). The higher uptake observed with smaller pellet sizes could be attributed to the supernatant residue. When the cell pellet is small, it is difficult to completely remove the supernatant, since it requires taking up cells as well (if there are not many cells, one cannot be as aggressive in taking up the supernatant in order to preserve the cells) and a drop of supernatant is likely to remain behind. Since the pellet size is small, even a drop of supernatant will have an effect on the B/H ratio. In order to diminish the effect of supernatant residue on experimental results, all further experiments were performed with a cell pellet size of $3x10^7$ cells. For practical ease, incubation volume was kept at 1 ml, which implies that the cell incubation concentration was $3x10^7$ cells/ml.

Cell experiments were carried out to investigate uptake as a function of boron concentration and time. Since the in vitro system does not take into account factors found in vivo such as circulatory and lymphatic flow, compound washout studies were performed as a first approximation. For all experiments, three samples (n=3) were obtained per point. The boronated medium was prepared by dissolving KBH directly into the medium. The given boron concentrations are scaled to 100% enrichment in ^{10}B in the case of the unenriched KBH compound. Experimental conditions are detailed below.

(i) Uptake as a function of boron concentration
Boron concentration was increased from 500 to 5,000 ppm. Incubation time was kept at 1 hour.

(ii) Uptake as a function of time
Time was increased from 5 to 80 minutes. The boron incubation concentration was 5,000 ppm.

(iii) Compound washout
Cells were incubated in 1 ml of boronated medium for 1 hour and then reincubated in boron-free medium for incubation times ranging from 15 to 120 minutes. The boron concentration of the original incubation medium with unenriched KBH was 6,500 ppm (within 10%), while that of the incubation medium using enriched KBH was 5,000 ppm (within 10%).

It should also be noted that this cellular uptake method is sensitive to weighing errors, potentially resulting in large variability. The potential error in the measurement of the weight of the cell pellet (which affects the calculated cellular uptake by affecting the scaling ratio) may be as high as 25%, determined by examination of the uncertainty in the weight of the smallest cell pellet.

In order to estimate the variability in cellular uptake, data was compiled from several experiments where cell samples (cell incubation concentration of $3x10^7$ cells/ml and incubation volume of 1 ml) were incubated in 5,000 ppm of boronated medium for 1 hour. The standard deviation in uptake was approximately 30%. Propagation of this variability with the maximum potential PGNAA counting and weighing error leads to a total potential error/variability of 40%.

4.1.2 Ex vivo boron uptake

Samples of human RA synovium and cartilage were obtained from the operating room of the Brigham and Womens Hospital, Boston MA. The tissue, excised from RA patients undergoing total knee replacements, was minced and incubated in cell well plates with boronated medium of varying KBH concentrations for varying times. After incubation in boronated medium, samples were thoroughly rinsed in saline and uptake was quantified via PGNAA. All counting errors for synovium and cartilage samples were below 10% and 14%, respectively. Boron concentrations were scaled to 100% ^{10}B enrichment in the case of unenriched KBH.

It may be reasonable for uptake to be affected by the size or weight of the tissue. When sample size is large, it may take longer for the compound to penetrate through the entire tissue and achieve the same concentration which is achieved more quickly with smaller size samples. Thus, for a constant incubation time, the boron concentration of larger samples may be lower. The effect of tissue weight on measured tissue uptake was examined by a compilation of data from several experiments and results are shown in figure 4.5 (it should be noted that only samples whose hydrogen counts were twice as large as background were included).

A linefit through the data in figure 4.5 resulted in the equation y=2194-1588x with an R^2 value of 0.47. Although there is large scatter, a trend towards lower uptake with increasing tissue weight is suggested. If weights above 0.25 g are excluded, then the decrease in slope is within PGNAA counting error (10%) and the R^2 value is 0.04, indicating an almost complete lack of correlation. Comparisons between tissue and cell uptake only includes tissue weights between 0.08 g and 0.25g.

In order to estimate the variability in the tissue (and avoid potential size-dependent effects), the standard deviation was calculated using 19 samples ranging from 0.08 to 0.25 g. The standard deviation was 25% of the mean. Reasons for the variability include variable amounts of fat and connective tissue in the synovium samples, variable synovial cell density/hyperplasia, variable states of inflammation. Propagation of this variability with PGNAA counting error, yields a total potential error/variability of 30%.

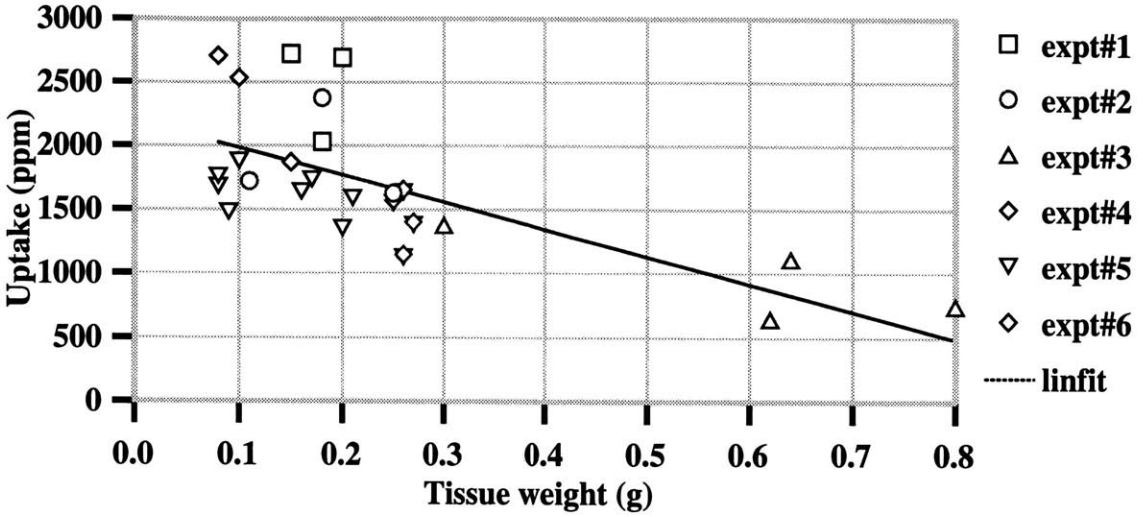

Figure 4.5: Tissue uptake as a function of tissue weight.

Experimental conditions parallel those of the in vitro studies (4.1.1) and are as follows:

(i) Uptake as a function of boron concentration
Samples of human excised RA synovium, ranging from 0.1 to 0.2 g in size, were incubated in boron concentrations varying from 500 to 5000 ppm (within 10%) for 1 hour. Three samples were obtained per concentration (n=3). This experiment was repeated with a 2 hour incubation time.

The uptake of cartilage from RA patients undergoing total knee replacement was investigated as a function of incubation concentration, ranging from 500 to 5000 ppm (within 10%). Incubation times were 1 and 24 hours and sample sizes (n=3) ranged from 0.02 to 0.05 g.

(ii) Uptake as a function of incubation time
Samples of human RA synovium, ranging from 0.11 to 0.25 g in size, were incubated for times ranging from 15 minutes to 1 hour, in boronated medium containing 5,000 ppm of boron (within 10%) with a sample size of three (n=3).

(iii) Compound washout
Samples of human RA synovium (0.08 to 0.20 g; n=3) were incubated in boronated medium with a concentration of 5,000 ppm of boron for 1 hour, rinsed thoroughly and reincubated in boron-free medium for 30, 60 and 120 minutes. Boron incubation concentration was then increased to 30,000 ppm and the initial incubation time was 1 hour, followed by reincubation times ranging from 1 to 24 hours. The sample sizes were 0.3 to 0.5 g. Since the deadtime of the detector was too high, samples were redissected into smaller pieces. At the 0 minute reincubation time, samples sizes

were 0.02 to 0.05 g (n=21). At the 1, 4 and 24 hour times, ranges of sample sizes were 0.03 to 0.08 g (n=20), 0.05 to 0.10 g (n=16) and 0.05 to 0.13 g (n=12), respectively. Several samples (n=12) were used for a double washout, i.e. samples were first incubated in boronated medium at 5,000 ppm for 1 hour, reincubated in boron-free medium for 1 hour and reincubated again in boron-free medium, for 24 hours. Samples ranged from 0.05 to 0.09 g.

4.1.3 In vivo boron uptake

The AIA rabbit model described in 2.1 was used and on the third day after the arthritis induction, 0.25 ml of KBH (dissolved in sterile saline) was injected intra-articularly into the arthritic knee joints of anesthetized rabbits. The knees were subjected to several (2 to 4) ranges-of-motion to ensure adequate distribution of the boron compound throughout as much of the synovial joint space as possible. Two boron concentrations were tested for in vivo uptake (i) 5,000 ppm and (ii) 150,000 ppm. At each concentration, uptake was tested as a function of time. For the 5,000 ppm concentration, time varied from 0.25 to 24 hours (n=3 to n=4), while for the 150,000 ppm boron concentration, time was varied from 5 to 60 minutes (n=3 to n=6). After the designated time, the rabbits were sacrificed and their knee joints dissected typically within 5 minutes. The first incision was made across the subpatellar tendon. Then, two incisions were made on both sides of the patella and the flap with the patella and tendon was lifted. Synovial fluid was obtained with a syringe as it began flowing out of the joint. The synovium, patella, tendon, ligament and menisci were dissected. Cartilage was scraped off the femur and bone chips were taken from the tibia (near the junction between the bone and synovium). Dissections were performed using standard surgical knife handles and disposable blades. A full biopsy was performed on the rabbits injected with 5,000 ppm of boron and whose joints were dissected after 4 hours. Blood and urine samples were obtained from these rabbits, as well as from the rabbits sacrificed after 30 minutes. Samples were frozen at -70° until uptake could be quantified via PGNAA.

Potential error and variability in the uptake of both synovium and other joint constituents are large and inextricably linked. Reasons for variability in synovial uptake include variation in synovial cell density/hyperplasia, vascular density and permeability, fat and connective tissue content in the synovium as a whole, as well as the dissected sample. In order to provide an estimate of the maximum potential error/variability, the standard deviation was calculated for samples dissected at three time points (5, 15, and 30 minutes) following an intra-articular injection of 150,000 ppm. The maximum standard deviation was 50%.

Reasons for variability in other joint constituents include variation in synovial "contamination" (the synovium lines the entire joint and it is difficult to completely clear other joint constituents of synovial residue), evaporation/drying during dissection and PGNAA, as well as freeze-drying since in some instances, several weeks elapsed between dissection and PGNAA (this particularly affects low-weight samples such as cartilage and ligaments, potential rendering the measured uptake artificially high). The potential error/variability present for the other joint constituents was estimated in the same manner described above for synovium. The maximum standard deviation observed for patellar, meniscal and cartilage uptake was 60%. For tendon samples, the maximum standard deviation was 70%, while for ligament samples, the maximum standard deviation was 80%.

4.2 Results and discussion

This section presents the results of the uptake experiments. As in the methods section, the in vitro results are first discussed (4.2.1), followed by the ex vivo (4.2.2) and the in vivo (4.2.3) results.

4.2.1 In vitro boron uptake

This subsection presents results of the investigation of in vitro, or cellular, uptake as a function of (i) boron incubation concentration and (ii) incubation time and (iii) compound washout in cells upon reincubation in boron-free medium.

(i) Uptake as a function of boron incubation concentration

Although the mechanism of uptake is not precisely known, based on the small size and structure of $B_{12}H_{12}^{2-}$, it is likely that KBH is taken up via diffusion or pinocytosis rather than phagocytosis. Incubation of cells in well plates leads to equal access of the cells to boron; they are completely surrounded by boronated medium. This has two implications. The first is that if uptake is not seen in vitro, then it is unlikely for uptake to be seen ex vivo or in vivo, unless by the extracellular matrix (which is not as desirable as cellular uptake for cellular kill based on the boron neutron capture reaction). The second implication is that cellular uptake may represent an upper limit to the uptake seen ex vivo, since the cells in the tissue may not have as complete and ready access to the boronated medium and the extra hydrogen mass of the matrix may affect the B/H ratio.

Figure 4.6 shows that cellular uptake increases with increasing boron incubation concentration. Average uptake ranged from 55 to 60% of the concentration of the original boron incubation medium. The linearity of the increase was tested by fitting a line through the points and excellent agreement was found between the calculated average (not plotted) and line fit (with an equation of y=-2.9 +0.57x), indicating that uptake is linear function of boron incubation concentration.

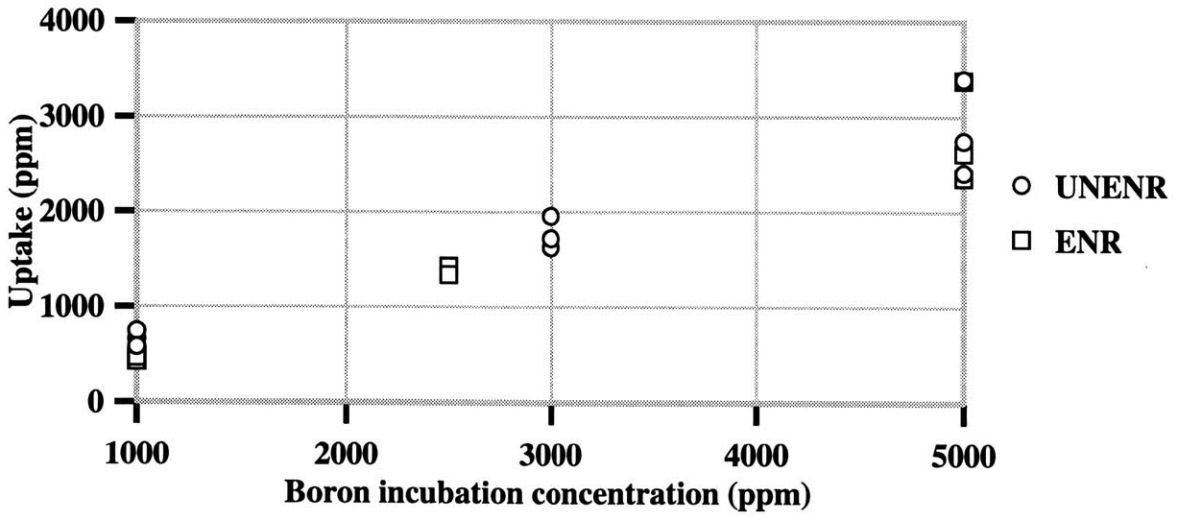

Figure 4.6: Cell uptake as a function of boron incubation concentration.

(ii) Uptake as a function of time

It was expected that cell uptake would occur very rapidly since all of the cells are equally exposed to the boronated medium and that, as a consequence, there should not be much difference in uptake as a function of time. Figure 4.7 shows that the value of the measured boron concentration of the cells oscillated around the average value reached at 5 minutes. There was no statistically significant difference in uptake as a function of incubation time.

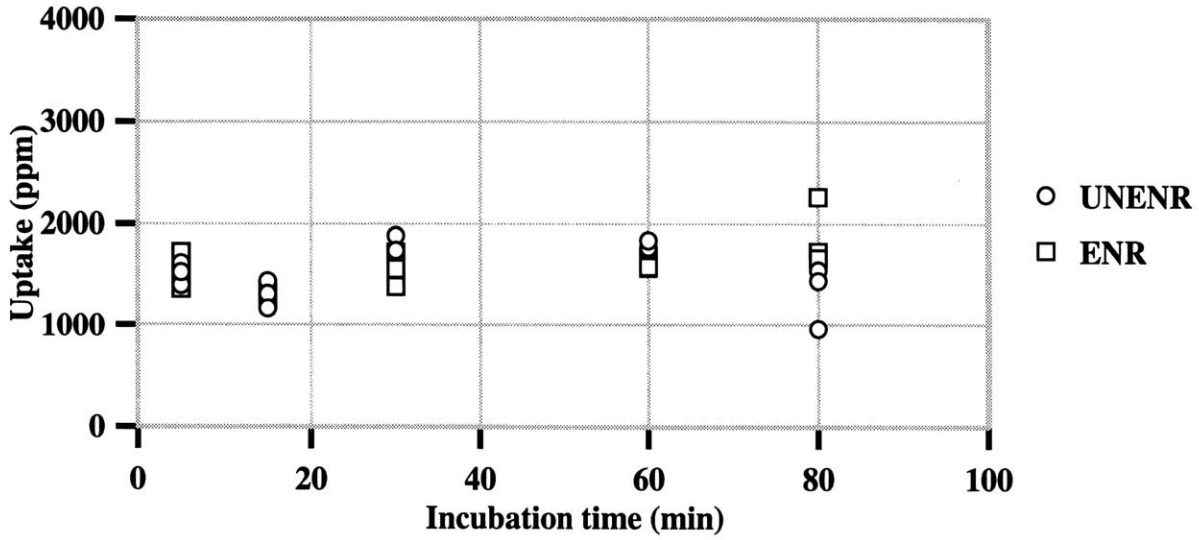

Figure 4.7: Cell uptake as a function of incubation time.

The results at 60 minutes shown in figure 4.7 may be compared to those at the 5,000 ppm boron incubation concentration shown in figure 4.6 (since the uptake as a function of time experiment was also done with 5,000 ppm boron incubation concentration and the uptake as a function of boron incubation concentration experiment had a 1 hour incubation time). Uptake in figure 4.7 ranges from 1,600 ppm to 1,800 ppm with an average of 1,700 ppm, while in figure 4.6, it ranges from 2,400 to 3,400 ppm with an average of 2,800 ppm. The average values are within 40% of each other, which is within the potential error/variability as estimated in the in vitro boron uptake methods section (4.1.1)

(iii) Compound washout

Figure 4.8 shows that the average boron concentration in cells upon reincubation for varying times (between 15 and 120 minutes) in boron-free medium does not change significantly over the range of reincubation times tested. Based on the previous reasoning which argued that compounds whose uptake was based on diffusion have a very rapid uptake, it was expected that the efflux should be rapid as well and that further changes in time should not have a large impact on uptake. The average boron concentration found at the various reincubation times reveals that about 15% of the boron concentration with no reincubation (2,400 ppm is the average concentration of all samples incubated in 5,000 ppm for 1 hour), is observed upon reincubation. This should be a lower limit, since all the cells are equally exposed to the boron-free medium and there is no extra cellular matrix to affect the B/H ratio.

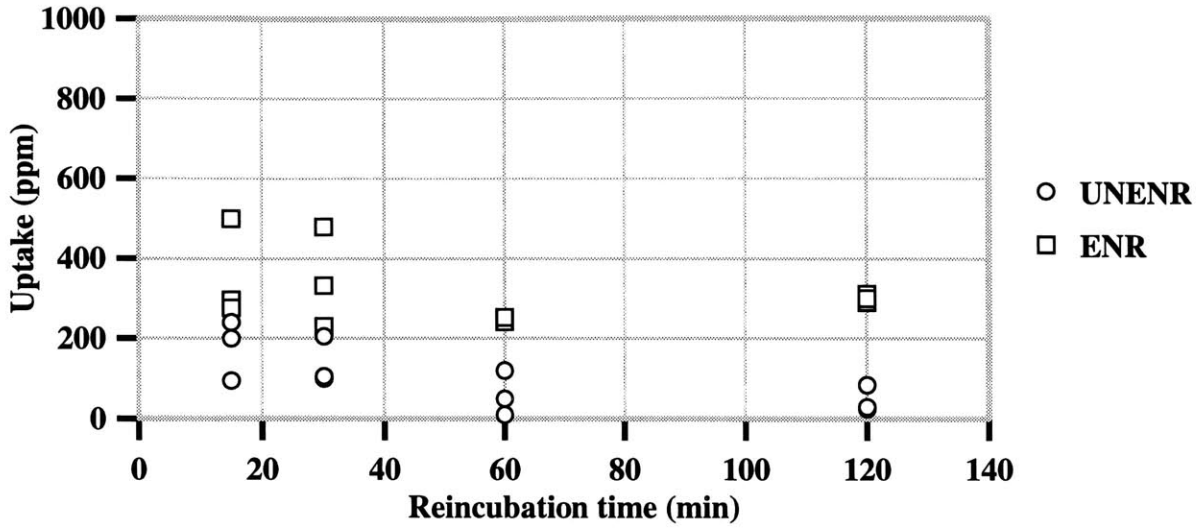

Figure 4.8: Compound washout from cells upon reincubation in boron-free medium.

A significant difference exists between the enriched and unenriched KBH compounds at 60 and 120 minutes. This could be due to the higher salt concentration of the unenriched compound. If the increased concentration were near an isotonic threshold, the cell membrane may have become somewhat fragile during the initial incubation and thus, upon resuspension in boron-free medium at the longer reincubation times, the cell membrane may have broken down and dispersed the cell contents into the supernatant. Average boron concentrations in the supernatants at the longer times were somewhat higher than cellular boron concentrations (75 ppm vs. 55 ppm). At shorter times, cell boron concentrations were higher than the supernatants. With enriched KBH, cell boron concentrations remained significantly higher than supernatant boron concentrations at all times (330 vs. 70 ppm). The magnitude of boron concentrations in the pellet was greater with enriched rather than unenriched KBH (330 vs. 75 ppm) which may lend support to the hypothesis that some cells may have lysed in the unenriched case.

4.2.2 Ex vivo boron uptake

This subsection presents results of ex vivo, or tissue, uptake studies. The pattern of presentation follows that of the in vitro studies (4.2.1), i.e. first results of uptake studies as a function of (i) boron incubation concentration and (ii) incubation time are presented followed by (iii) results of compound washout studies. Direct comparisons are made between cell and tissue uptake studies.

(i) Uptake as a function of boron incubation concentration

Figure 4.9 shows that tissue uptake increases with increasing boron incubation concentration. At 500 ppm, the range is from 160 to 225 ppm, with an average of about 200 ppm. At the second boron incubation concentration (2,500 ppm), the average of three points is 1,600 ppm and at 5,000 ppm boron incubation concentration, the average uptake is 2,500 ppm. A linear curve was

fit to the data in figure 4.9 (y=0.5+92x) and there was excellent agreement between the average values and the curve fit. Sample weights, ranged from 0.1 to 0.2 g, and thus were within the range where no correlation was found between tissue uptake and weight.

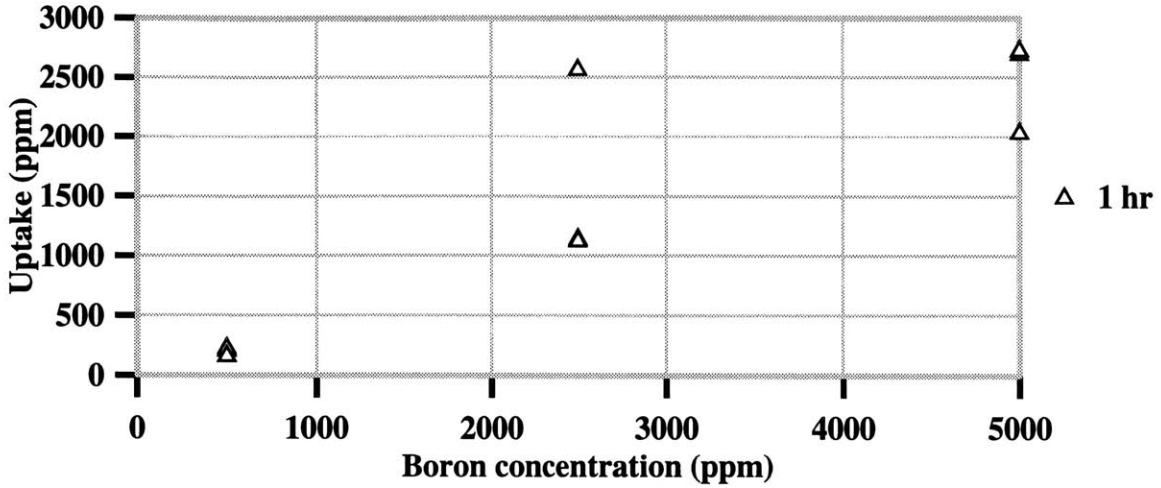

Figure 4.9: Tissue uptake as a function of boron concentration.

A comparison of uptake as a function of boron incubation concentration between cells (figure 4.6) and tissue (figure 4.9) is shown in figure 4.10. The increase in tissue uptake follows a trend similar to that of the cells, in both magnitude and slope of the response to increasing boron concentration. This may indicate that, at least as far as the level of boron uptake, cell studies may be predictive of the behavior of KBH uptake in tissue.

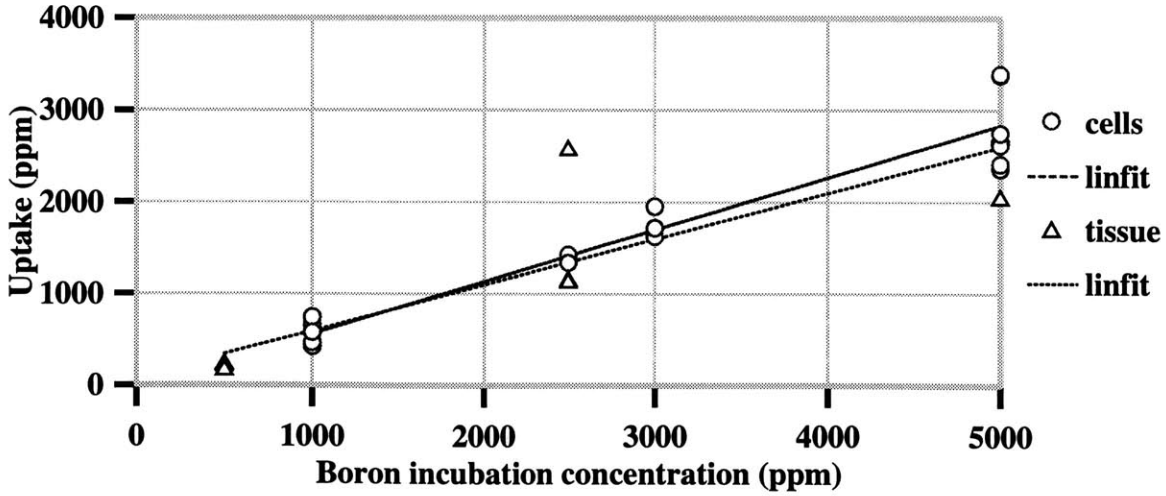

Figure 4.10: Comparison of cell and tissue uptake as a function of boron concentration.

Figure 4.11 shows uptake as a function of boron incubation concentration when incubation time is increased to 2 hours. As expected, there is a linear increase in synovial uptake with increasing boron concentration.

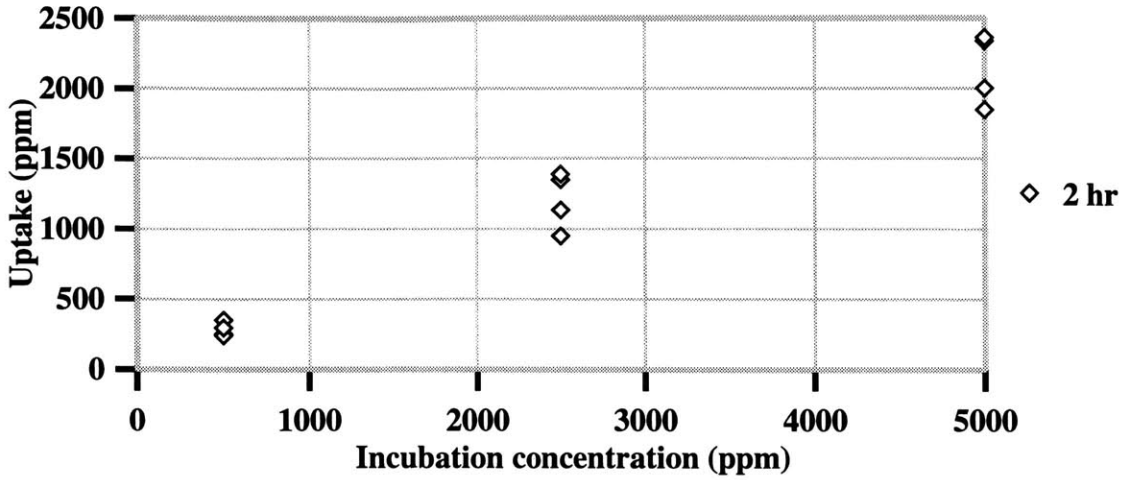

Figure 4.11: Tissue uptake as a function of boron concentration (2 hour incubation time).

The uptake of RA cartilage was examined as a function of boron incubation concentration at two different times (figure 4.12). Average uptake for the 1 hour incubation increased tenfold, from 20 ppm to 200 ppm, as the boron incubation concentration was increased tenfold, from 500 to 5000 ppm. Cartilage uptake was roughly 10% of the uptake seen in the synovium. This may be partially due to the relative acellularity of cartilage compared to the synovium; uptake may be mostly extracellular and be washed off in the rinsing step. At 24 hours, the average uptake following an incubation in 500 ppm of medium was 10 ppm. When the boron incubation was increased tenfold to 5,000 ppm, the average concentration was 140 ppm, over a factor of ten higher. Comparison of the average uptake at both 500 and 5,000 ppm for the different time points shows that the average uptake is smaller at 24 hours, although the data overlap and statistical significance (calculated via the Student's t-test) is not achieved. The low cartilage uptake, despite the small sample weight (0.02 to 0.05 g), is noteworthy, since, as previously discussed, when a sample is small in size, the boron may easily and rapidly diffuse throughout the entire tissue.

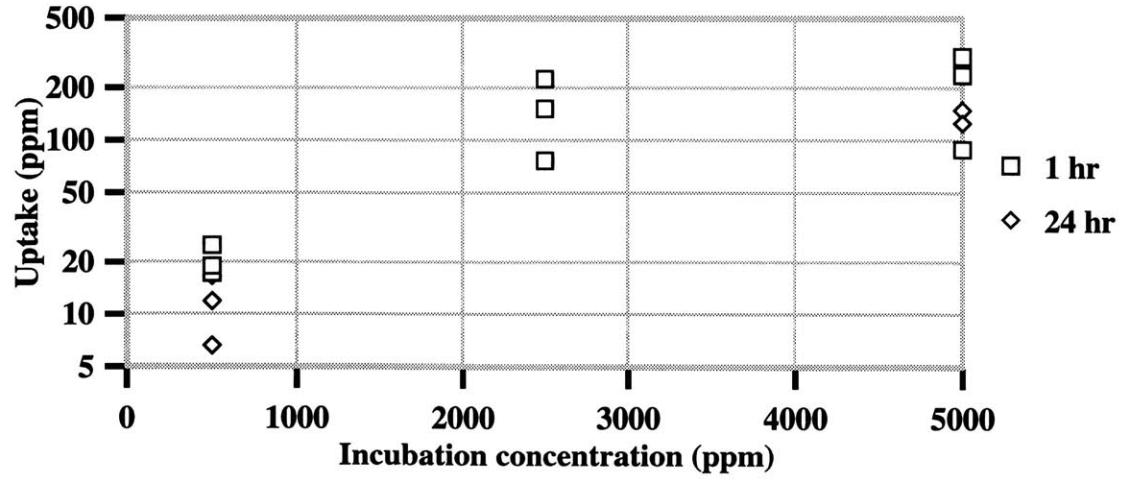

Figure 4.12: Cartilage uptake as a function of boron incubation concentration.

(ii) Uptake as a function of incubation time

Figure 4.13 shows that the increase in tissue uptake starts to level after an incubation time of 30 minutes; the average uptake increases only about 25% (from about 1500 to 1900 ppm) while between 15 and 30 minutes average uptake increases by a factor of 1.5. This may be explained by diffusion of the boron compound throughout the tissue. At 15 minutes, KBH has only diffused through part of the tissue and by 30 minutes, it has pervaded through most of the tissue, with only a few regions left untouched, such that an increase in time cannot increase the concentration much more. Accordingly, incubation times shorter than 15 minutes would be expected to result in lower uptake since the tissue sample would just begin to be perfused.

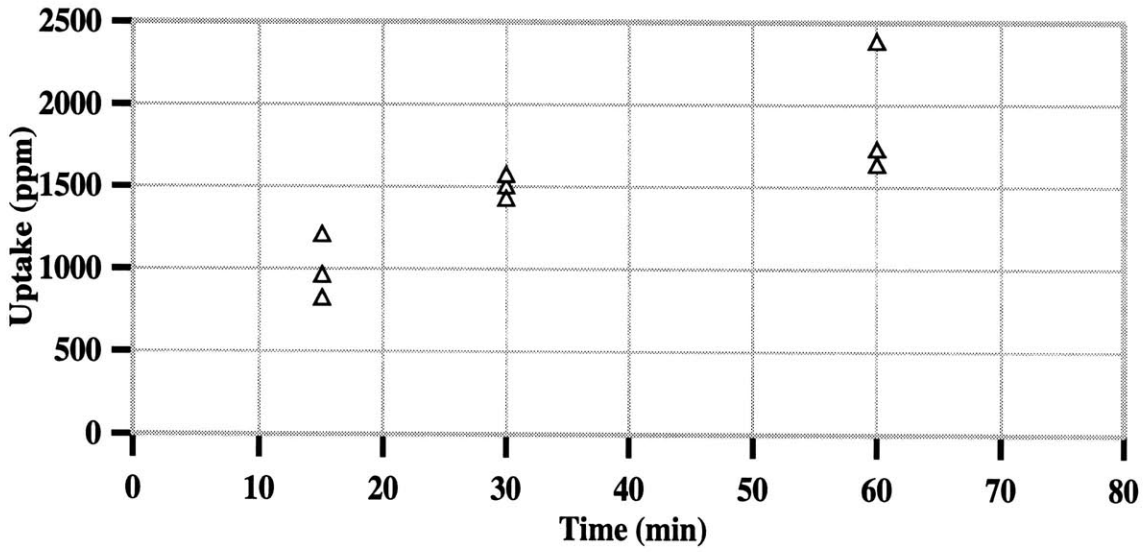

Figure 4.13: Tissue uptake as a function of incubation time.

Some corroboration of this hypothesis can be seen in figure 4.14 which compares tissue and cell uptake as a function of incubation time. At 15 minutes, average tissue uptake is lower than cell uptake, while at 30 and 60 minutes, it lies in the range of cell uptake. This makes sense in light of the rapid diffusion into the cells in vitro. It takes more time for all the cells in the tissue to become exposed to the boron.

There are not enough tissue samples in figure 4.14 to achieve statistical significance between the cells and tissue at the 15 minute time point. However, a trend is suggested. Based on this model of uptake, it would be expected that the difference between cell and tissue uptake would be more pronounced if tissue samples were incubated for 5 minutes (i.e. it would be expected that tissue uptake would be substantially lower than cell uptake). It would also be expected that for larger samples of human synovium, it would take longer for an equivalent concentration to be achieved, since it would take longer for the KBH to diffuse the entire tissue sample. In fact, this has already been examined and results were shown in figure 4.5 where despite the large scatter, a trend of decreasing uptake with increasing sample weight beyond 0.25 g was clearly evident.

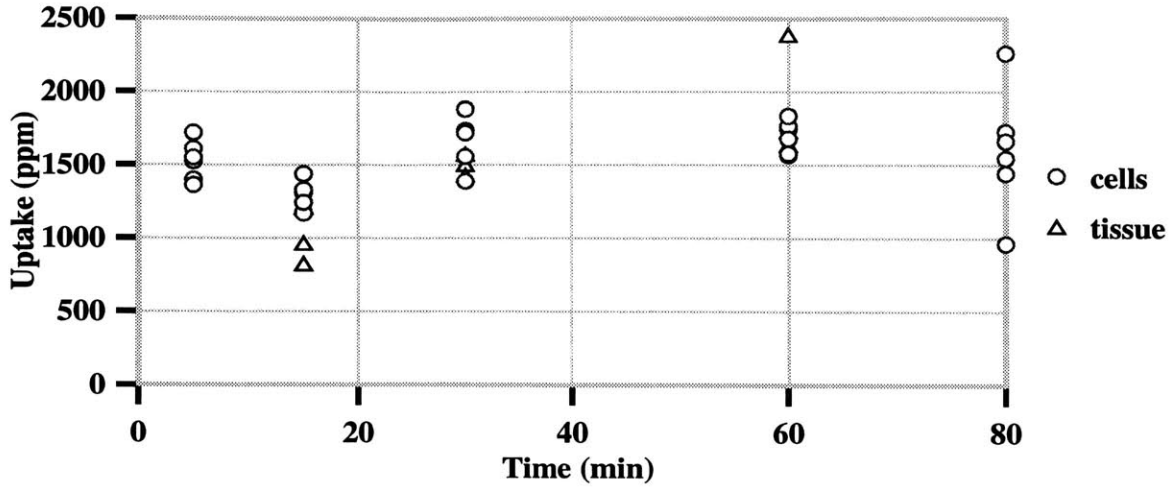

Figure 4.14: Comparison of cell and tissue uptake as a function of incubation time.

(iii) Compound washout

Figure 4.15 shows that on average, 25%, 20% and 18% of the boron incubation concentration was retained, upon reincubation for 30, 60 and 120 minutes, in boron-free medium. This is consistent with figure 4.13, where the bulk of the boron movement (in the opposite direction) occurs within 30 minutes; as time is increased, the boron that is in the innermost part of the tissue sample would continue to leak out at a slower rate since it must travel through the outermost tissue. Statistical analysis did not show the decrease at different reincubation times to be significant.

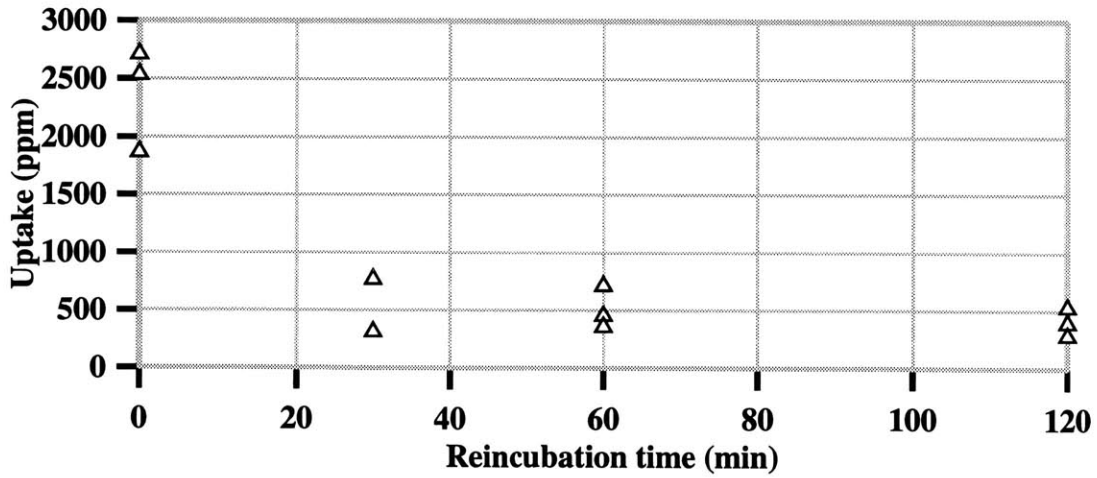

Figure 4.15: Compound washout from tissue.

A comparison between cellular and tissue washout is shown in figure 4.16. There is agreement between the two types of uptake studies, although the washout occurs to a greater extent with cells. This is expected since in the in vitro system, all cells are equally exposed to the boron-free medium.

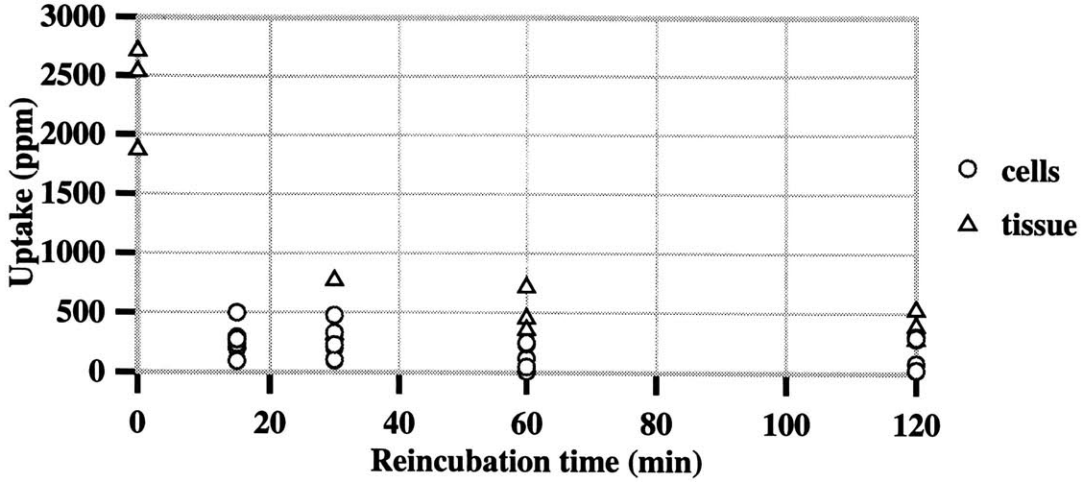

Figure 4.16: Comparison of compound washout from cells and tissue.

When the washout experiment was repeated at 30,000 ppm of boron, with 1 hour incubation time and varying reincubation times, as shown in figure 4.17, the boron concentration seen after 1 hour of reincubation time averages 40% of the concentration seen with no reincubation, a factor of two higher than the relative boron concentration after incubation with 5,000 ppm (20%). This is most likely due to the absolute amount of boron present; it may take longer for 30 mg of boron to seep out from tissues than 5 mg (1 ml incubation volume). The boron concentration remains higher, even after 4 hours of reincubation in boron-free medium, with an average concentration around 30% of that seen with no reincubation. It is expected that uptake would continue to gradually decrease as reincubation time is increased. There is no statistically significant difference in boron concentration over the reincubation times shown in figure 4.17. Using the average concentrations at 0 and 1 hour: for the 5,000 ppm incubation concentration, the boron concentration decreased by 1,861 ppm in 1 hour; for the 30,000 ppm concentration, the boron concentration decreased by 14,600 ppm in 1 hour

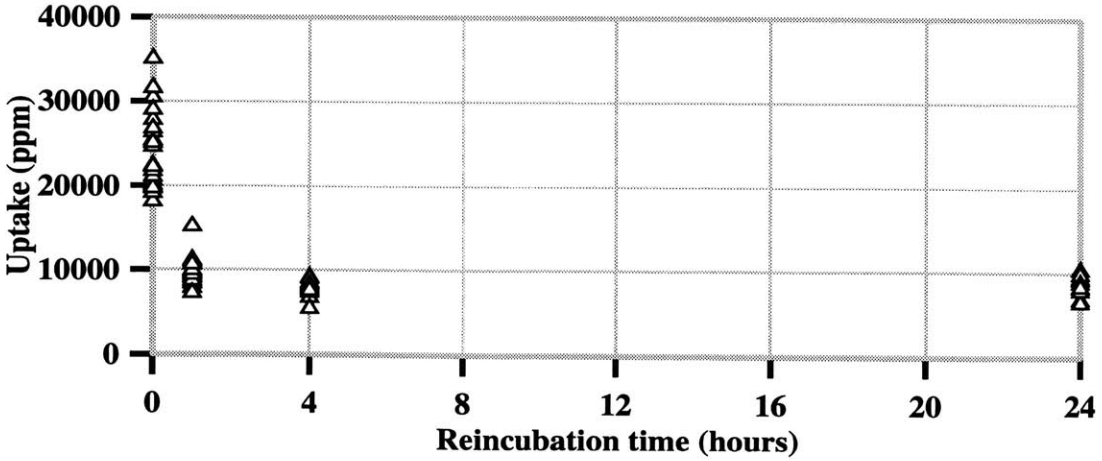

Figure 4.17: Compound washout from tissue (30,000 ppm boronated medium).

Tissue samples from the double washout experiment, where samples were incubated in 30,000 ppm of boronated medium and then reincubated twice in boron-free medium, had an average boron concentration of 3,500 ppm, or about 40% of the concentration found after the first washout (which, in turn, was about 40% compared to samples with no reincubation). This is consistent with results shown in figure 4.17.

4.2.3 In vivo boron uptake

The following subsection will present results of in vivo uptake following intra-articular injections of 0.25 ml of two KBH concentrations into the arthritic knee joints of anesthetized rabbits. The solutions were prepared by directly dissolving KBH in saline to yield boron concentrations of (i) 5,000 ppm and (ii) 150,000 ppm.

(i) Injection concentration 5,000 ppm

The knee joints of several rabbits were used for each time point, i.e. 4 joints at 0.25 and 1 hour, and 3 joints at 0.50, 4 and 24 hours. Table 4.2 shows the results of in vivo uptake by the synovium following a 0.25 ml injection of 5,000 ppm of boron (i.e. a total of 1.25 mg of boron were injected). Average synovial sample weight from each set of rabbits ranged from 0.10 to 0.26 g. Counting error (except for 24 hours samples) ranged from 9% to 14%, with an average of 11%.

Table 4.2: In vivo synovial uptake (5,000 ppm injection concentration)

Time (hr)	Range (ppm)	Mean (ppm)
0.25	265 - 950	490
0.50	35 - 190	130
1.00	30 - 50	40
4.00	5 - 10	7
24.0*	< 1	---

*Due to the low boron concentrations, counting was stopped after 60 minutes and the lowest detectable concentration (LDC) was calculated for inclusion in the table.

There is a significant decrease in average synovial uptake with time. At the 15 minute time point, the average synovial concentration is about 10% of the initial injection concentration. However, if one considers that there is about 1 ml of fluid already present in the rabbit joint before injection of the 0.25 ml of 5000 ppm of boron, then the effective concentration of the compound is lower by a factor of five, i.e. 1000 ppm, and the concentration observed at 15 minute represents about 50% of the original boron concentration available. This is consistent with in vitro and ex vivo studies which found 20% to 60% of the boron concentration in samples after incubation in 5,000 ppm boronated medium.

A difference between the in vivo and ex vivo studies is the temporal behavior of uptake; ex vivo, a longer incubation results in higher uptake while it results in lower uptake in vivo. However, the ex vivo system does not take into account many factors which are found in vivo such as circulatory and lymphatic flow. Washout studies were performed to provide a first approximation of in vivo uptake. The tissue following reincubation times ranging from 0.50 to 2.0 hours, exhibited average boron concentrations in tissue ranging from 18 to 25% of the boron concentration found with no reincubation, as shown in figure 4.14. This implied that in vivo boron may leave the joint quickly (since the surrounding areas in the joint are also initially boron-free); as shown in table 4.2, the average synovial uptake in vivo after 30 minutes was 30% that at 15 minutes. Then, after another 30 minutes (total of 1 hour), boron concentration again decreased to about 30% of the previous value (similar to a double washout) and by 4 and 24 hours, the injected boron had essentially cleared from the joint, with less than 10 ppm found in any synovium sample.

As can be noticed from table 4.2, there is large variability in the data of synovial uptake. This is an inherent property of this type of experiment and will also be seen in the uptake of the other joint tissues. Dissection of the synovium and separation of the synovium from the other joint tissues is challenging. Also, the degree of arthritic response in the knee joints of the rabbits may vary, resulting in varying amounts of arthritic synovium available.

One study in the literature has examined the clearance of 0.2 ml of a radioactively labelled sodium iodide solution following intra-articular injection into the knee joints of non-arthritic New Zealand white rabbits and found that half the solution was cleared from the knee joint within 0.20 hours, or 12 minutes [Kellaway and Chawla 1982]. Although generally, synovial permeability is increased in arthritic joints, the effect may be size dependent. One study has found that arthritic synovium is less permeable to small molecules (such as tritiated water, urea, rate and glucose) than normal joint synovium, while it is more permeable to large molecules such as proteins [Simkin and Pizzorno 1979]. The reasoning given for this finding is that smaller molecules which diffuse through the synovial tissue to the capillaries will take longer in an arthritic joint due to the increased length of tissue that the molecules must traverse, whereas larger molecules, for which the bottleneck time is traversing capillary epithelial junctions, will enter the capillaries more quickly in an arthritic joint than a normal joint due to the increased capillary leakiness in the arthritic joint [Simkin and Pizzorno 1979]. The molecular weight of urate is 167 g/mole and thus relatively close to sodium iodide and the $B_{12}H_{12}^{2-}$ ion, 150 and 144 g/mole, respectively. This may suggest that the radioactively sodium iodide solution may clear more slowly in an arthritic joint.

Table 4.3 shows the uptake of boron by other joint tissues in order of their dissection (no cartilage samples are included because the majority of samples did not have hydrogen count rates twice as high as background). At 15 and 30 minutes, the average boron concentrations in these joint tissues are lower than the synovial boron concentrations. At 1 and 4 hours, since the concentration in the synovium is so low, several joint tissues have boron concentrations higher than the synovium. By 24 hours, there is essentially no boron remaining in the joint. PGNAA counting error (except for the 24 hour samples) ranged from 9% to 22%, with an average of 15%. The 24 hour samples were counted for limited amounts of time and the lowest detectable concentration (LDC), described in 3.1.1, was calculated.

Table 4.3: In vivo uptake by other joint tissues (5,000 ppm injection concentration)

Time (hr)	Range and (mean) are in units of ppm				
	Patella	Tendon	Ligament	Menisci	Bone chips
0.25	5 - 15 (13)	1 - 95 (44)	135 - 425 (282)	130-230 (181)	20 - 95 (44)
0.50	5 - 25 (18)	5 - 90 (33)	20 - 115 (58)	NA	NA
1	5 - 15 (10)	5 - 40 (19)	75 - 485 (294)	95 - 170 (125)	15 - 50 (30)
4	5 - 15 (8)	5 - 5 (5)	10 - 140 (55)	10 - 55 (30)	10-25 (18)
24*	< 2	< 3	< 5	< 2	< 16

*The boron concentrations listed in the table represent the lowest detectable concentration (LDC).

The patella is an oval shaped piece of bone (0.4 to 0.5 g on average) that is encapsulated within the tendon. Surrounded by synovium, its surface has a layer of cartilage. During the dissections, synovium is cleared from the patella as much as possible. Average patellar boron concentration at 15 minutes is about 3% of the average synovial concentration at the same time point and remains approximately the same through 4 hours, before decreasing to less than 2 ppm at 24 hours.

Tendons and ligaments do not have many structural and/or anatomical differences between them (ligaments insert into bones on both ends and sometimes have higher elastin/collagen ratios). However, over the first hour, ligaments have average boron concentrations about 2 to 15 times higher than tendons. Ligaments are low weight samples (average 0.04 to 0.07 g) compared to the tendon (average 0.2 to 0.4 g) and are covered by synovium in some areas. In samples with little hydrogen (or low weight), even a small amount of boron may significantly affect the B/H ratio used to determine boron concentrations. This may be the reason for the high measured value of ligament boron uptake, as compared to the tendon.

Menisci are two wedges, roughly shaped like a C, essentially made of cartilage (albeit a tougher and more fibrous type than exists on the articulating surfaces). They lay in the space between the femur and tibia and act in distributing loads, as well as dispersing synovial fluid, across cartilage surfaces. Average meniscal uptake at 15 minutes is 37% that of the synovium at the same time. This implies that if 10,000 cGy were to be delivered to the synovium, then 3,700 cGy may be delivered to the cartilage. It should be noted that one study delivered an intra-operative x-ray dose of 5,000 cGy directly to the cartilage of AIA rabbits and found no degenerative changes to the cartilage over a 15 month period of observation [Takahashi et al 1992]. Meniscal uptake is indeed higher than synovial uptake at later times. However, since the synovial uptake is too low to be therapeutically useful at those later times, the higher uptake of the meniscus, when compared to the synovium, does not become a significant issue.

Bone chips (0.1 to 0.2 g) were taken from the femur and had about three times as much boron as the patella between 0.25 and 4 hours. This is significantly higher than bone boron concentration reported in the literature from bones of RA patients [Havercroft and Ward 1991]. It is possible that boron came into contact with bone at the junction between synovium and bone and some of the boron proceeded down the bone. It is also possible that boron spread to the bone during the dissection (bone chips were always taken last). The concentration at 15 minutes is about 10% that of synovium, implying that the bone may get about 1,000 cGy of dose, based upon a 10,000 cGy target dose from clinical trials using β-emitters [Deutsch et al 1993]. The lowest reported case of femur head bone necrosis and/or fracture of the femur in humans following radiation therapy treatments with high-energy photons has been found at 2,000 cGy, a factor of two higher than the potential bone dose [Emami et al 1991]. The average dose reported to cause damage to the femur is 5,900 cGy [Emami et al 1991].

The non-injected and non-arthritic knees of two rabbits (from the 0.25 and 1 hour post-injection) were dissected and the boron concentration of the tissues measured. Synovial concentration of boron was less than 1 ppm in both of the knees. The concentration of boron in other joint tissues is summarized in Table 4.4. All PGNAA counting errors were kept below 14%, unless otherwise noted. No synovial fluid was available (the amount in non-arthritic rabbits is very small).

Table 4.4: Boron concentration in joint tissues of two representative non-injected knees

Time (hr)	Patella (ppm)	Tendon (ppm)	Ligament (ppm)	Menisci (ppm)	Bone chips (ppm)
0.25*	< 1	< 1	< 2	< 2	< 2
1.00	5	2	45	10	30

*The boron concentrations listed in the table represent the lowest detectable concentration (LDC).

Although no literature is readily available on the boron content of the various structures in normal rabbit joints, it was expected that it should be on the order of a few ppm based on human data [Forbes et al 1954]. At 15 minutes, this was found to be true, with less than 2 ppm found in any part of measured tissues of the joint. However, at 1 hour post-injection, there were tens of ppm in the ligaments, menisci and bone chips. This may be explained by circulation and accumulation of boron in the other joint after 1 hour. It should be noted, however, that the non-injected joint is also not irradiated. If adequate shielding is placed around the non-injected joint, it should not receive a significant neutron dose which implies that the boron neutron capture reaction will not be induced to a significant degree. It must be stressed that it is the combination of the boron with the neutrons that potentially induces cellular kill based on the boron neutron capture reaction.

Table 4.5 shows the boron concentrations measured in various body fluids extracted from the AIA rabbit, such as synovial fluid (from the injected joint), blood and urine. Samples of synovial fluid were collected first, immediately upon the opening of the joint. Blood was taken at the time of sacrifice at all times. Urine was only collected at the 0.5 and 4 hour times and was the last fluid to be extracted, after the completion of the dissection. All PGNAA counting errors were kept below 15% unless otherwise noted.

Table 4.5: Boron concentration in several body fluids (injection concentration 5,000 ppm)

Time (hr)	Range and (mean) are in units of ppm		
	Synovial fluid	Blood	Urine
0.25	30 - 245 (129)	1 - 10 (3)	NA
0.50	150 - 280 (208)	5 - 5 (5)	5 - 35 (18)
1	NA	1 - 5 (3)	NA
4	10,15 (13)	1 - 5 (4)	45 - 55 (50)
24*	< 11	< 5	NA

*The boron concentrations listed in the table represent the LDC.

There is a high boron concentration in the synovial fluid at 0.25 and 0.5 hours, decreasing by an order of magnitude by 4 and 24 hours. At 0.25 hours, the average boron concentration is higher in the synovium than the fluid (although the spread is quite large in both). This would be expected since the boron should be leaving the synovial fluid and be taken up by the synovium. However, according to this reasoning, by 0.50 hours, the boron concentration of the synovial fluid should have continued to decrease, but instead it is higher than the synovium. Samples of synovial fluid were relatively large (0.1 to 0.2 g) and hence the reasoning previously applied to ligament uptake cannot be applied here. One potential explanation is that boron may have accumulated in a pocket in the joint, which may have been disturbed upon dissection. The average amount of boron in the synovial fluid based on the recovered volumes was around 30 μg. By 4 and 24 hours there was only around 10 ppm left in the synovial fluid, which is comparable to the boron concentration of the synovium at equivalent times. Insofar as neutron irradiations, boron in the synovial fluid is not a great cause for concern since it primarily includes inflammatory cells and molecules which aid in promoting inflammation. Accumulation of boron in the synovial fluid may lead to a sparing of the articular cartilage and menisci due to flux depression of the incoming neutrons.

The boron concentration in blood remains fairly constant throughout 24 hours. Once the boron compound is in the vicinity of blood capillaries, the boron could easily diffuse into the capillaries (i.e. from the interstitial to intravascular space) since the $B_{12}H_{12}^{2-}$ ion is relatively small. Then, equilibration could take place relatively quickly since blood flow in the rabbit is about 150 ml/min [Hexeberg et al 1995], which is high considering that the total blood volume in a rabbit is about 200 ml, calculated using 3.5 kg weight (representative of the New Zealand white rabbits used in this study) and 56 ml/kg as a middle range value of reported cardiac volumes [Armin et al 1952]. An accurate estimation of the time needed for equilibration would depend on the percentage of cardiac volume which reaches the lower extremities in a rabbit, as well as precise readings of heart rate, which is reported to range from 306 to 333 bpm [Mott 1965].

Boron concentration in the blood would be expected to decrease when the substance has been completely filtered and cleared by the kidneys. The blood data acquired at 24 hours does not allow any conclusions to be drawn since counting was not continued to achieve a value for the samples but rather just the lowest detectable concentration given a particular counting time. Furthermore, blood was not acquired from non-injected rabbits in order to ensure that the boron concentrations seen are truly a result of an injection of boron and are significantly above background. Although the rabbits were not placed on boron-rich diets, measurement of the boron concentration levels in rabbit blood would confirm the assumption.

The boron concentration in the urine at both 0.5 and 4 hours is significantly high. Assuming that the volume of urine in the bladder was 20 ml and using average urine boron concentrations of 18 and 50 ppm at 0.5 and 4 hours, respectively, this could represent about 30% and 80% of the total amount of injected boron (1.25 mg). Therefore, by 4 hours, the bulk of the injected amount could excreted in the urine, given the measurements performed. No samples of urine were obtained at 1 hour and the bulk of the boron compound may have already been excreted in the urine as early as 1 hour after injection.

Based on the average values of blood and urine concentration at 4 hours, as well as an average value of urine flow, one may obtain a preliminary estimate of renal clearance of KBH. The urine volume from a 24 hour collection is 130 ml/kg on average [Kozma et al 1974]. For a 3.5 kg rabbit, this yields an average urine flow of 0.32 ml/min. Assuming that blood and plasma concentrations of boron are the same (5 ppm) and using a boron concentration of 50 ppm in the urine, calculation of clearance yields 3.2 ml/min. This can be compared to the clearance of creatinine, a substance which is neither secreted nor absorbed by the kidneys and has a relatively similar molecular weight (192 g/mole) to $B_{12}H_{12}^{2-}$. The average renal clerance of creatinine for a 3.5 kg rabbit is 11.2 ml/min [Kozma et al 1974]. It is expected for the renal clearance of $B_{12}H_{12}^{2-}$ to be lower since it has negative charges and, as studies with dextrans have shown, negatively charged molecules are filtered less well than neutral or positively charged molecules [Valtin and Schafer 1995]. In humans, creatinine clearance is slightly higher than the glomerular filtration rate as measured by inulin (since tubules themselves secrete small amounts of creatinine). However, in rabbits, inulin clearance is higher than creatinine (inulin clearance was not provided for comparison since its molecular weight is an order of magnitude greater than $B_{12}H_{12}^{2-}$). A precise determination could be obtained by a direct measurement, i.e. emptying the bladder, injecting the compound, and then collecting both plasma and urine at a series of later times. Regardless of the precise value, it can be deduced that the $B_{12}H_{12}^{2-}$ ion is rapidly filtered once it reaches the kidneys, implying that the bottleneck of time for excretion is the time that the boron compound takes to reach the kidneys.

Results of the biopsies were performed on the 4 hour rabbits are shown in table 4.6. All of the organs dissected had less than 5 ppm. Although there is no readily available data in the literature on the boron concentration of rabbit organs, boron concentrations on the order of those found in human organs, i.e. less than 1 ppm, may be expected [Forbes et al 1954]. The values in table 4.6 are slightly higher than those found in normal human organs. Again, it should be noticed that these areas are not irradiated and therefore should not receive radiation dose via the boron neutron capture reaction.

Table 4.6: Biopsy results for 4 hour rabbits (5,000 ppm injection concentration)

	Range (ppm)	Mean (ppm)
Lung	1 - 4	3
Kidney	3 - 5	4
Spleen	3 - 5	4
Rt. Inguinal	2 - 3	3

Overall, by 15 minutes post-injection, an intra-articular injection of 1.25 mg of boron in the form of KBH dissolved in saline yielded synovial boron concentrations, which were, according to the beam design criteria developed in section 2.3.3, therapeutically useful. This requirement was developed for humans and the retention of the boron compound in a human joint could be longer. Furthermore, even if clearance time were not longer, the moderator length used to develop the 300 ppm criterion could be made somewhat shorter, which could allow therapy time to be within the 15 minute window of high uptake, while maintaining the minimum therapeutic ratios of synovium to skin and synovium to bone dose. Higher boron concentrations, however, would allow greater latitude in neutron beam requirements and shorter therapy times.

(ii) Injection concentration 150,000 ppm

The boron concentration of the injected solution was increased to 150,000 ppm, corresponding to an injection of 37.5 mg of boron in saline. Dissection times post-injection were varied from 5 to 60 minutes over two sets of rabbits (7/98 and 11/98). Six rabbits were sacrificed at each of the 5, 15 and 30 minute times while three rabbits were sacrificed at 60 minutes. Since the boron synovial concentration resulted in detector deadtimes unacceptably high, several synovium samples had to be redissected. Results of the synovial uptake in vivo are shown in figure 4.18.

The data in figure 4.18 show a large error/variability in uptake at each time point. As was stated in the methods section, the maximum standard deviation present at 5, 15 and 30 minutes was 50% of the mean. Although this is quite large, it is not uncharacteristic of the standard deviations found in the literature. For example, one study examined the clearance of iodine and radioactively labelled human serum albumin from the knee joints of eleven RA patients and nine osteoarthritis patients after intra-articular injections [Wallis et al 1985]. Iodine clearance in the group of eleven RA patients ranged from 0.95 to 3.22 ml/min, with an average of 1.92 ml/min. The standard deviation, calculated from the detailed patient data, was 49% of the mean. This is similar to the standard deviation calculated from data in figure 4.18 and although it is based on human joints and thus not directly applicable to rabbit joints, it suggests that the large error/variability, as estimated from the standard deviation, may be an inherent characteristic of experiments examining the clearance of substances from an arthritic joint.

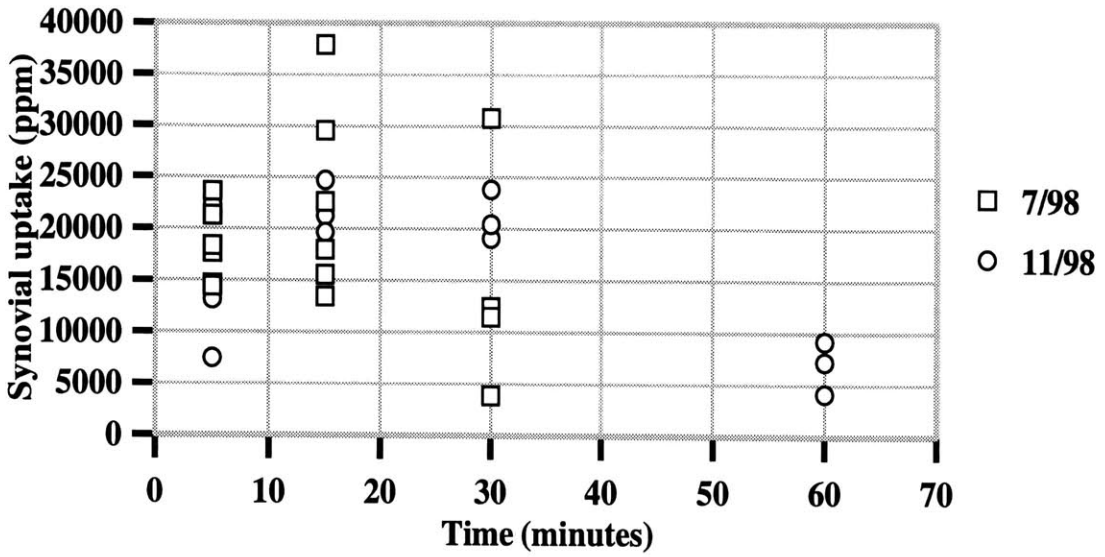

Figure 4.18: In vivo synovial uptake as a function of time (150,000 ppm injection concentration).

As can be seen from figure 4.18, synovial uptake is very high. The difference in uptake over the first 30 minutes is not statistically significant and the time-averaged uptake is 19,000 ppm. At 60 minutes, average synovial concentration significantly decreased to about 7,000 ppm, or 37% of the concentration found between 5 and 30 minutes. If the existing synovial fluid is taken into account, the original injection concentration is diluted by a factor of 5 which makes the average uptake over 30 minutes about 60% of the boron injection concentration, similar to the percent found with the previous boron injection concentration of 5,000 ppm. The average synovial boron concentration at 15 minutes roughly scales with injection concentration.

There is a substantial difference in synovial uptake as a function of time between the injection concentrations of 5,000 and 150,000 ppm. Whereas synovial concentration between 15 and 30 minutes significantly decreased with an injection concentration of 5,000, concentrations remained about the same between 15 and 30 minutes with an injection concentration of 150,000 ppm. This is most likely due to the increased amount of boron injected (1.25 mg vs. 37.5 mg) This concept was illustrated in the tissue washout studies. With an original boron incubation concentration of 30,000 ppm, synovial concentration after 1 hour reincubation in boron-free medium was about 40% of the concentration found in tissues with no reincubation (figure 4.17). When the boron incubation concentration was 5,000 ppm, synovial concentration was about 20% of that found with no reincubation (figure 4.15). Therefore a proportionally greater amount of boron was retained by tissue when incubated in a higher boron incubation concentration. This could also be expressed in terms of time; it takes a longer reincubation time for the tissues originally incubated with the 30,000 ppm to reach 20%.

Figures 4.19, 4.20, 4.21, 4.22 and 4.23 show the boron uptake of the other joint tissues. The upper limit of the y-axis in each of the following plots has been set at 20,000 ppm to give a comparison to synovial uptake which averaged 19,000 ppm between 5 and 30 minutes after injection.

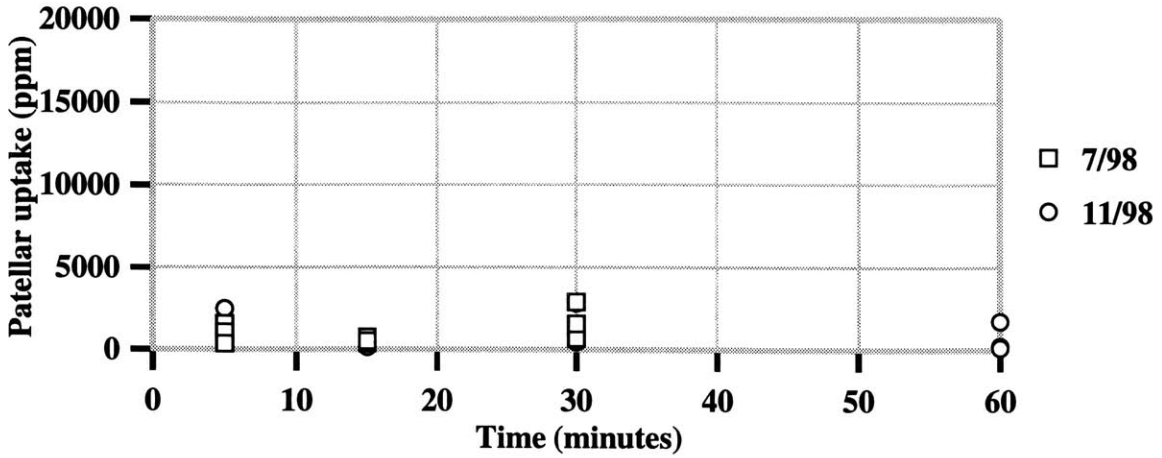

Figure 4.19: In vivo patellar uptake as a function of time (150,000 ppm injection concentration).

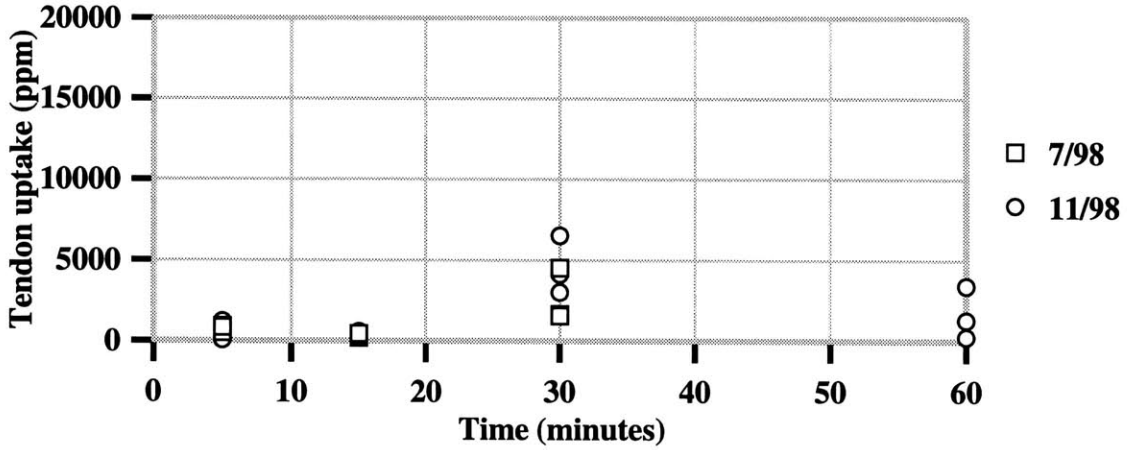

Figure 4.20: In vivo tendon uptake as a function of time (150,000 ppm injection concentration).

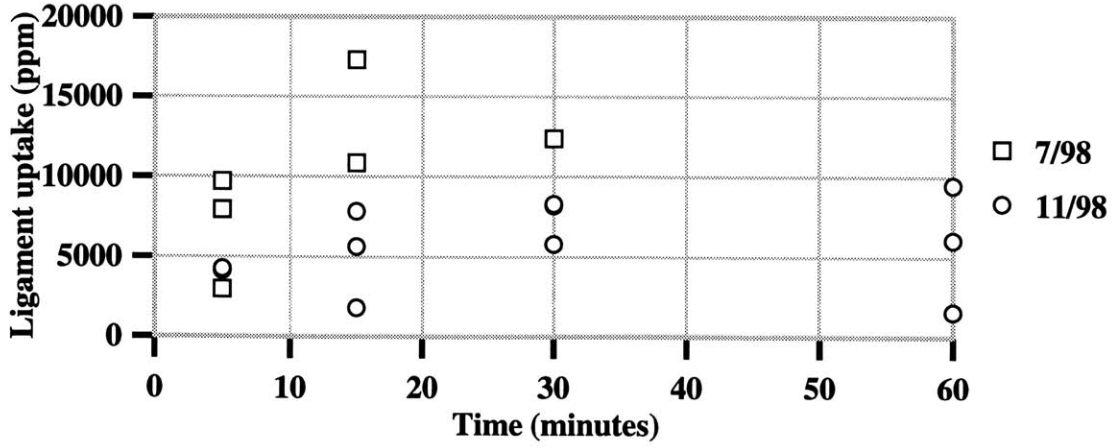

Figure 4.21: In vivo ligament uptake as a function of time (150,000 ppm injection concentration).

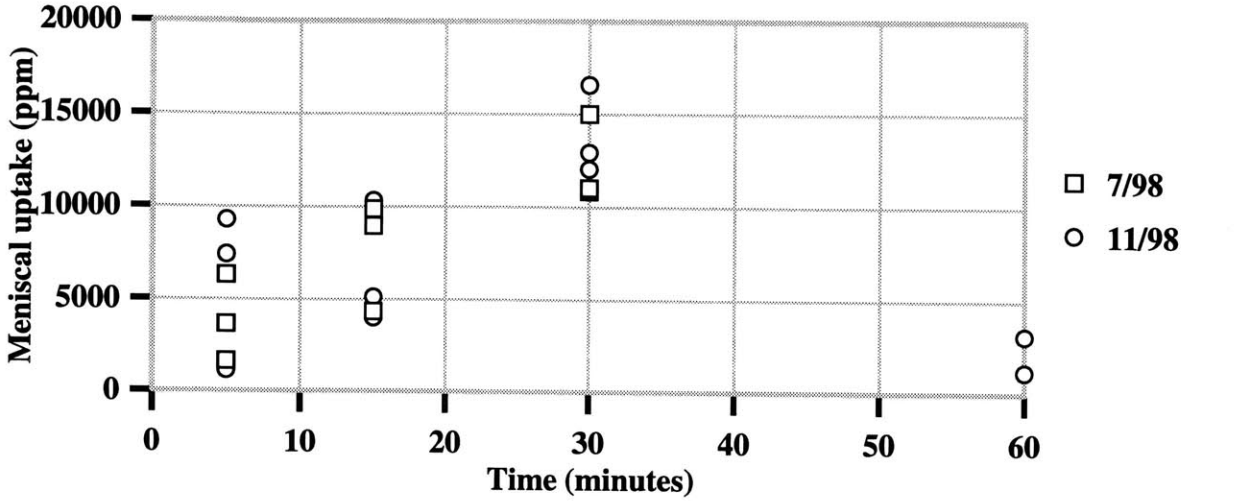

Figure 4.22: In vivo meniscal uptake as a function of time (150,000 ppm injection concentration).

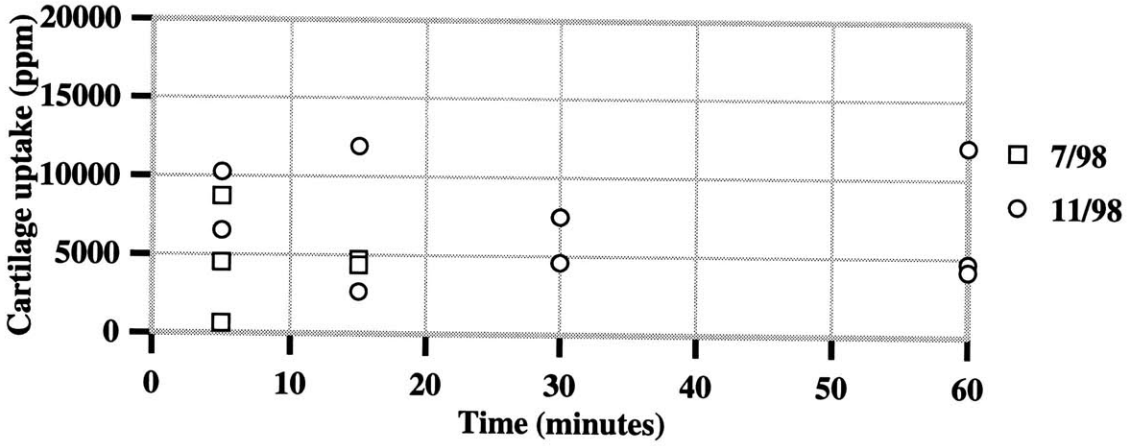

Figure 4.23: In vivo cartilage uptake as a function of time (150,000 ppm injection concentration).

As can be seen in figure 4.19, there was no significant difference in patellar uptake over the course of 60 minutes (the time averaged uptake over 30 minutes was 1,200 ppm). Tendon uptake, shown in figure 4.20, significantly increased between 5 and 30 minutes and then decreased at 60 minutes, although the difference between uptake at 30 and 60 minutes was not significant. Ligament uptake, shown in figure 4.21, was high and had a wide range (the time averaged uptake over 30 minutes was about 8,400 ppm). Meniscal uptake, shown in figure 4.22, significantly increased between 15 and 30 minutes, from an average of 7,100 to 13,100 ppm and decreased at 60 minutes. Finally, cartilage uptake (also low-weight) did not change significantly over the times tested and, as shown in figure 4.23, the time-averaged uptake value was around 6,400 ppm.

Figure 4.24 takes the ratio of the average synovial uptake to average healthy tissue uptake at each time post-injection. To have an idea of average dose to the healthy tissue based upon the delivery of 10,000 cGy to the synovium, the average uptake ratio was used to calculate average dose shown in figure 4.25.

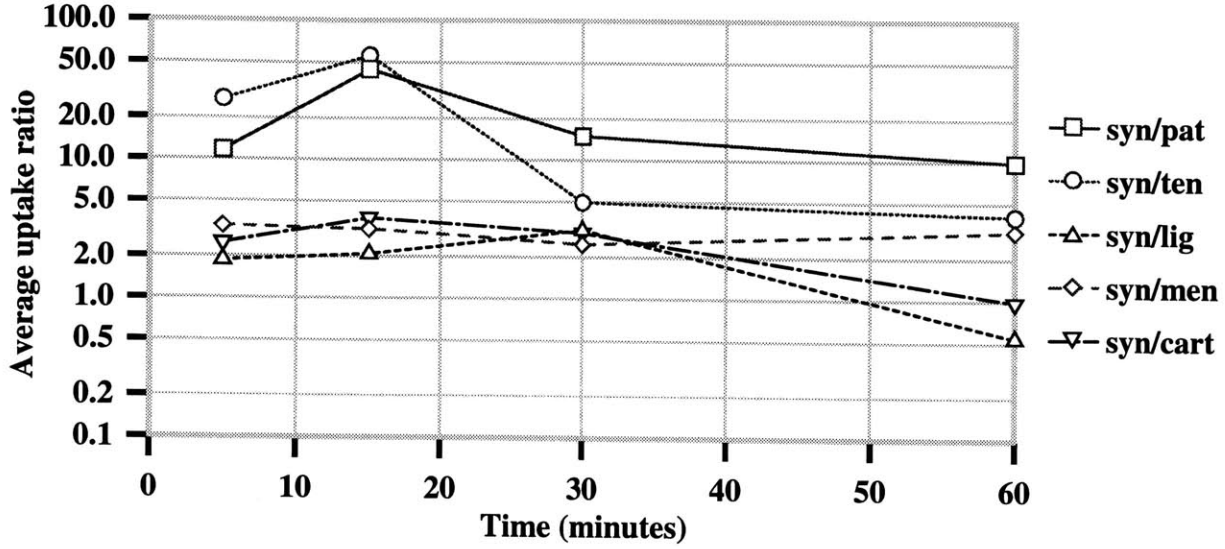

Figure 4.24: Average uptake ratios of synovium to other joint tissues.

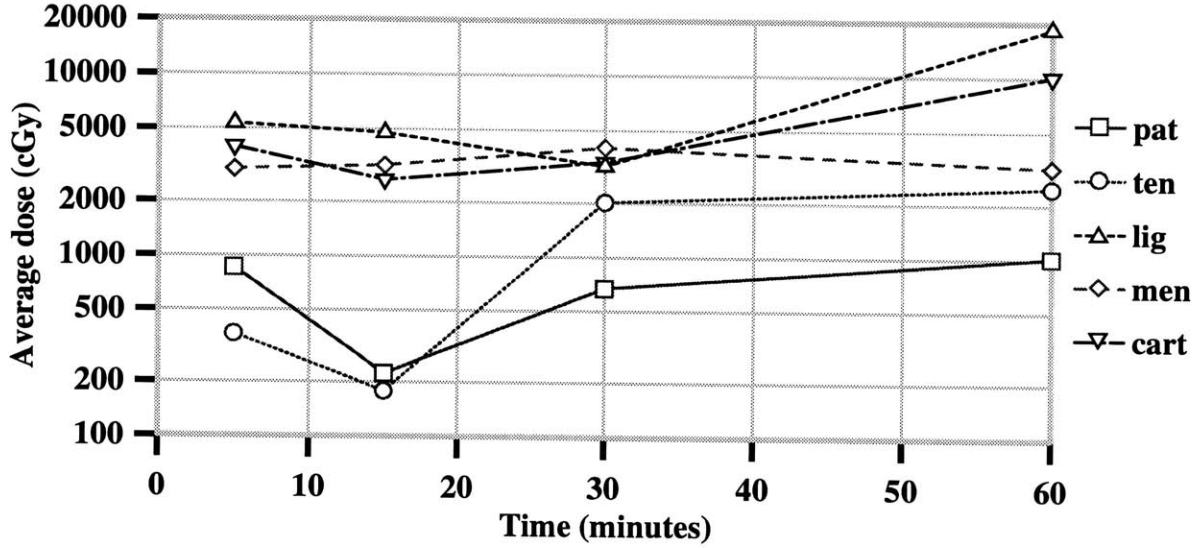

Figure 4.25: Average dose to joint tissues based on the delivery of 10,000 cGy to the synovium and uptake ratios in figure 4.24.

It should be noted that the range of the uptake ratio in figure 4.24 is large due to the large variation in uptake shown in figures 4.19 through 4.23. The average dose plotted in figure 4.25 does not take into account flux depression, which, with 19,000 ppm in the synovium, may be significant.

Based on figure 4.25, the highest average dose delivered to the patella (about 1,000 cGy) would be at 5 and 60 minutes post-injection. This is approximately a factor of 2 below the lowest dose that has been reported to cause necrosis in the head of the femoral bone in clinical treatments using high energy photons [Emami et al 1991]. Although no data specifically dealt with the tolerance of the patella, bone in the patella should be similar enough in structure to femoral bone for this result to be applicable.

Although tendon and ligament are quite similar in anatomy, the measured boron concentration in the ligament is several times higher than the tendon at all the times tested after injection of the boron compound. Ligament average dose is around 5,000 cGy (with slight drops) between 5 and 30 minutes and then increases to 20,000 cGy by 60 minutes. However, as discussed in chapter 3, ligament uptake may be artificially high.

Studies have been performed looking at the effects of gamma irradiation on the mechanical and material properties of bone-patellar tendon allografts [Gibbons et al 1991, Salehpour et al 1995]. Since the purpose of the irradiation was sterilization, high gamma ray doses were employed, from 20,000 and 30,000 cGy [Gibbons et al 1991] to 40,000 and 80,000 cGy [Salehpour et al 1995]. At a gamma dose of 20,000 cGy, no significant difference was found in the mechanical and material properties when compared to controls; weakening of the tendon in terms of mechanical stress and strain was found with 30,000 cGy of irradiation dose [Gibbons et al 1991]. Higher doses resulted in further weakening of the tendon [Salehpour et al 1995]. Clinical studies on muscular tissue involved in radiotherapy using high energy-photons, found that a dose of about 5,000 cGy has an chance of about 1% of resulting in muscle inflammation within 5 years [Emami et al 1991]. Thus, 5,000 cGy may serve as a rough guideline for an upper dose limit to tendons and ligaments. As shown in figure 4.25, on average, this level of dose is not reached. Extra consideration may be required for patients with RA, however, since they may already be subject to a general weakening of connective tissues, such as tendons and ligaments, which may affect tolerance to radiation.

The two cartilaginous tissues, articular cartilage and menisci, have similar average uptake ratios between 5 and 30 minutes, as shown in figure 4.24, and result in average doses between 2,000 and 5,000 cGy, as shown in figure 4.25. Intra-operative doses of 50,000 cGy via delivery of x-rays have been shown to result in no obvious or significant damage to articular cartilage in the knee joints of rabbits [Takahashi et al 1992]. Intra-operative dose was not increased in this particular study [Takahashi et al 1992] to examine the effects of increased dose or to determine at which point, significant cartilage necrosis would occur. Clinical studies using high energy gamma rays have concentrated their attention on the cartilage in the larynx and have found that an average dose of 7,000 cGy results in cartilage necrosis in 5% of the patients within 5 years [Emami et al 1991]. According to figure 4.25, the average cartilage dose remains below 5,000 cGy at early times between 5 and 30 minutes, rising above 7,000 cGy after 50 minutes of irradiation, which is longer than the target therapy time of 30 minutes. Average meniscal dose remains below 5,000 cGy at all times tested. In order to accurately determine the dose at which cartilage begins to show negative effects, such as necrosis, in the context of dose primarily from the boron neutron capture reaction, experimentation with this specific goal is necessary.

After 30 minutes, the average uptake ratios of meniscus and cartilage diverge, with the cartilage ratio decreasing and the meniscal ratio remaining approximately the same (figure 4.24). The decrease in the cartilage ratio is due to the decreasing synovial concentration, since cartilage uptake remains roughly constant between 30 and 60 minutes (figure 4.23), due, in part, to the lower degree of vascularization in the cartilage. The ratio of synovial to meniscal uptake remains approximately the same between 30 and 60 minutes because both synovial and meniscal uptake decrease proportionally as boron is being cleared from the joint. Although menisci are essentially made of cartilage and as such are relatively avascular with abundant extracellular matrix, the outer

one third of a meniscus has high enough blood perfusion to allow wound healing and matrix remodelling [Arnoczky and Warren 1983]. This may contribute to the egress of boron from the menisci by 1 hour, particularly if the majority of the uptake was in the outer one third.

Although it would be clearly negative to induce meniscal weakening due to BNCS, it should be noted that meniscectomy, or removal of the meniscus, was often performed at the same time as synovectomy [Ranawat et al 1972, Marmor 1973], motivated by inflammation of the parameniscal synovium and increased ease of synovium removal [Newman 1994]. Other synovectomy studies, however, indicated meniscectomy only if the menisci were severely damaged [Laurin et al 1974, Ishikawa et al 1986] and current indication for treatment of meniscal tears advocates as little removal as possible for effective symptom relief [Boland and Deland 1994], particularly in view of studies finding a higher incidence in degenerative changes (osteoarthritic) in the joints of some patients following meniscectomy [Neyeret et al 1994, Rangger et al 1995, Roos et al 1998]. On the other hand, various other studies have found no significant difference between outcomes of partial or total meniscectomies [Hede et al 1992, McGinty et al 1977, Tapper and Hoover 1969]. It should be noted that the majority of the patients included in the above studies did not have RA and were often athletic individuals. Different considerations may arise with RA patients. In some RA patients (particularly those afflicted with a severe course of the RA disease), the issue may be mute, however, since, as a result of disease progression, they may develop osteoarthritic changes and be candidates for total knee replacements (in which case the presence of the meniscus is not relevant to the outcome of the replacement operation).

Figure 4.26 shows the boron concentration in synovial fluid as a function of time. Although there were six rabbits sacrificed at each of the times, synovial fluid could not be obtained from all the rabbits. This was due to technical difficulties; when the joint is opened, synovial fluid often spills over before it can be taken up with a syringe.

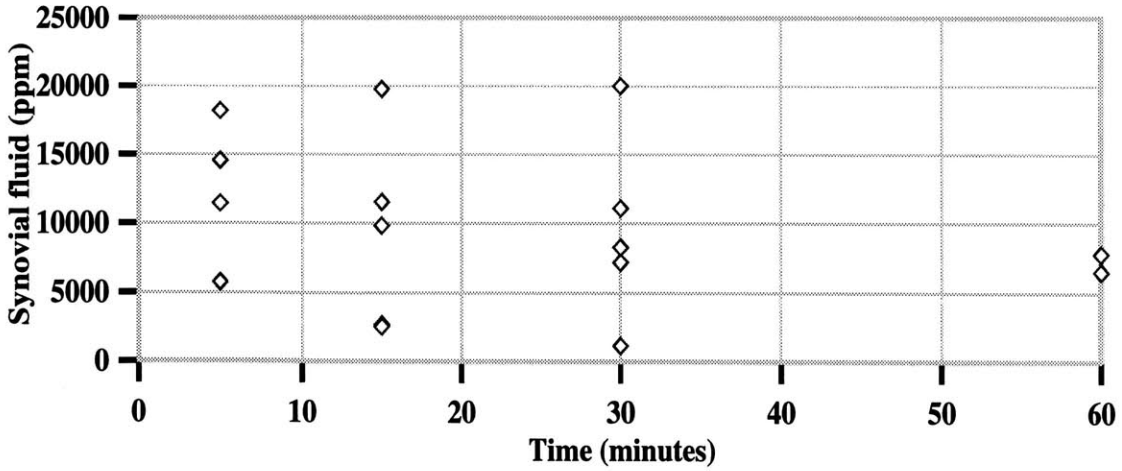

Figure 4.26: In vivo synovial fluid uptake (150,000 ppm injection concentration).

The average synovial concentration is about 12,500 at 5 minutes, 9,600 ppm at 15 minutes and 10,200 ppm at 30 minutes, for an average of 10,800 ppm over 30 minutes. At 60 minutes, the average concentration is about 7,200 ppm. The amount of fluid recovered varied greatly and it is

not possible to draw any conclusions about the total amount of boron in the synovial fluid. The large variability in the boron concentration of the fluid samples is also a result of the difficulty in acquisition of the fluid (sometimes mixed with the blood flowing out of the joint).

The possibility that large synovial fluid boron concentrations may aid in the sparing of cartilage dose was tested with ideal beams of different energies and the MCNP model of a human joint shown in figure 2.14. Three combinations of synovial, cartilage and synovial fluid concentrations of boron were tested as summarized in table 4.7.

Table 4.7: Ideal beams with boron in synovium, synovial fluid and cartilage.

Set	synovium	syn. fluid	cartilage
A	10,000 ppm	10,000 ppm	5,000 ppm
B	20,000 ppm	20,000 ppm	10,000 ppm
C	20,000 ppm	1 ppm	10,000 ppm

The first set, A, was designed to investigate the dose ratio with a pessimistic synovium to cartilage uptake ratio of 2. The second set, B, kept the same uptake ratio, while increasing the magnitude of the boron concentrations. Finally, the third set, C, looked at the effect of boron in synovial fluid. Five isotropic ideal beam energies were tested: 0.025, 10, 100 eV and 1, 100 keV. Results of these simulations are shown in figure 4.27 (individual depth dose profiles for each of these simulations are included in Appendix B).

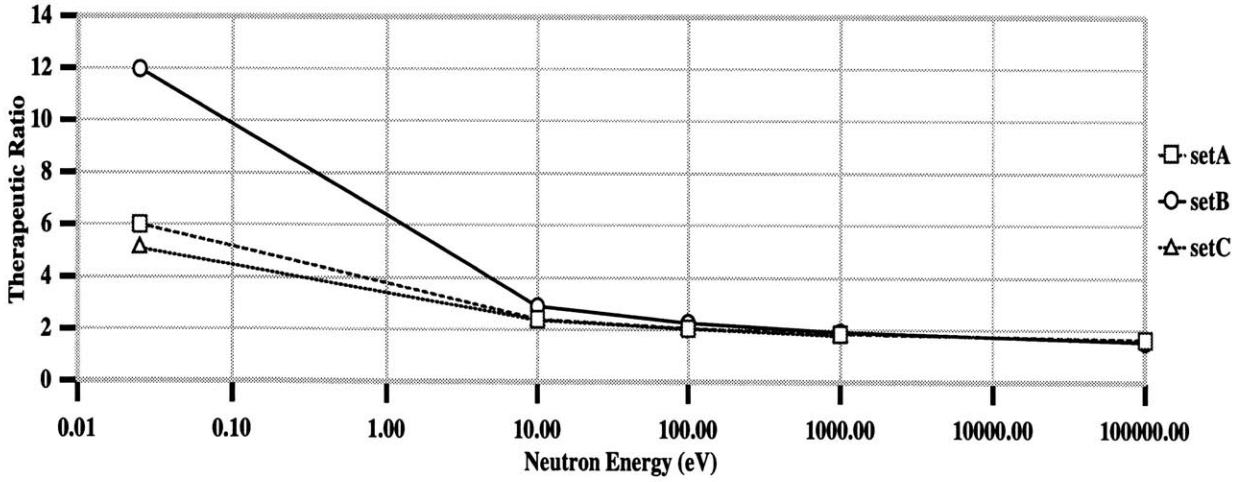

Figure 4.27: Synovium to cartilage therapeutic ratio versus ideal neutron beam energy.

At thermal energies, the therapeutic ratio for set B is twice as large as that for set A, although sets A and B have the same synovium/cartilage boron concentration ratio. This is primarily due to flux depression; in set A, the neutron dose rate decreases by a factor of 3 at the cartilage, whereas in set B, the neutron dose rate decreases by a factor of 6. Comparing sets B and C shows the effect of not having boron in the synovial fluid. The therapeutic ratio is 2.4 times lower which indicates

that at thermal energies having boron in the fluid is beneficial and actually spares the cartilage. Again, the primary mechanism by which this occurs is increased flux depression. In set C, the neutron dose rate only decreases by a factor of 2.5 and combining this with a factor of 2 difference in boron concentration leads to an overall factor of 5. The difference between uptake ratio and therapeutic ratio decreases as the neutron beam energy is increased, such that by 100 eV, the uptake and therapeutic ratios are approximately equal and remains so until 100 keV (the decrease in therapeutic ratio seen at 100 keV compared to 1 keV is within statistical errors). This is due to the increasing dominance of nonthermal neutron flux over thermal neutron flux, which incurred the flux depression leading to a higher therapy ratio with respect to uptake ratio.

This finding was tested in rabbit and human knee joint phantoms with the uptake ratios of Set B and the 1.5 MeV Be(d,n) reaction [Gierga 1999]. A synovium/cartilage uptake ratio of 2 (with boron also in the synovial fluid) led to a therapeutic dose ratio of 2.3 in the rabbit phantom and 3.1 in the human knee phantom, representing an increase of 13% and 35%, respectively. The increase was larger in the human knee joint phantom as a result of the larger amount of total boron in the synovial fluid (due to the higher volume of fluid found in the human knee joint compared to the rabbit joint).

4.3 Conclusions

The uptake of $K_2B_{12}H_{12}$ has been characterized in vitro (monocytic cell line), ex vivo (human excised RA synovial tissue) and in vivo (AIA rabbit model). A method for measurement of boron uptake by non-adhering monocytic cells was developed and results obtained were consistent with results of tissue uptake studies. Good agreement between cells and tissues was found in boron uptake as a function of boron incubation concentration. The boron uptake levels achieved in the tissue lay within the range of those achieved in cells between 15 and 60 minutes, while at times less than 15 minutes, tissue uptake was lower. This was expected, since in tissue the compound necessitates more time to diffuse through the entire tissue, while in vitro, the compound is equally accessible to all cells. Studies of compound washout showed agreement, although the washout occurred to a greater extent in cells, which, again, was expected since all cells are equally exposed to the boron-free medium.

Measured uptake in tissue samples was affected by tissue weight and this was hypothesized to be a result of diffusion of the compound through the tissue. Measured uptake in cell samples was also affected by weight (the size of the pellet) and this was attributed to technical limitations in the complete aspiration of the supernatant. The results of cellular uptake may serve as an indication of whether the uptake achieved ex vivo is at least partly due to cell uptake rather than the entrapment of boron in the extracellular matrix of tissue. Furthermore, measurement in an in vitro system should represent the maximum achievable boron concentration in tissue, since in the cell culture system there is no extracellular matrix to hinder access to the boronated medium or to "dilute" the measurement of the boron concentration calculated via the B/H ratio.

Synovial concentrations in vivo, obtained by dissection of arthritic rabbit knee joints following intra-articular injection of 0.25 ml of varying boron concentrations in the form of KBH, were roughly consistent with predictions from tissue uptake studies. While the relative synovial boron

concentrations after 15 minutes were similar for the two concentrations used (implying a roughly linear increase in uptake with increasing concentration), the boron concentration in the synovium after 30 minutes differed, possibly due to the absolute magnitude of boron injected (1.25 and 37.5 mg with 5,000 and 150,000 ppm of boron, respectively). Whereas with an injection concentration of 5,000 ppm, only an average of 27% was present at 30 minutes relative to 15 minutes, when the injection concentration was 150,000 ppm, the average synovial boron concentration at 30 minutes was approximately the same as the concentration at 15 minutes. In other words, it takes longer for the boron to be cleared from the synovium when the injection concentration is 150,000 ppm. Renal clearance of the compound is rapid based on a preliminary estimate and a large part of the injected boron was recovered in the urine. The boron concentration in the other tissues of the joint were such that the ratio of synovium to healthy tissue uptake ranged from 2 to 30 over 30 minutes after injection. Implications of the uptake ratios were discussed in terms of the potential dose delivered to other tissues of the joint. Overall, uptake following an intra-articular injection of 0.25 ml of 150,000 ppm of boron (in the form of the KBH compound) resulted in an average synovial boron concentration of 19,000 ppm over 30 minutes post-injection. This was more than adequate to warrant continuation to animal irradiation studies, where a BNCS treatment would be carried out and the effects on both the synovium and other joint tissues could be examined.

The effect of synovial fluid boron concentration on cartilage dose was examined via a set of MCNP simulations of isotropic ideal beams and the phantom used throughout chapter 2. Results showed that high levels of boron in the fluid spare cartilage, particularly around thermal neutron energies due to flux depression. This sparing effect disappears as neutron energies reach about 10 to 100 eV and the therapeutic dose ratio approximates the uptake ratio.

Although this compound was found to yield high synovial uptake in rabbits, which bodes well for eventual success of BNCS, work needs to be performed to understand the pharmacokinetics of the compound in humans and determine potential toxic side effects. The sodium salt of $B_{12}H_{12}^{2-}$ has been found to have a low order of acute toxicity in rats [Muetterties et al 1964]. The oral toxicity to rats was roughly comparable to sodium chloride, based on findings of approximately acute lethal toxicity at ion concentrations greater than 7.5 g/kg in rats [Muetterties et al 1964]. Since salts typically dissociate from the ion, and salt imbalances are easily taken care of by kidneys, the toxicity may be referring to the ion itself. In this study, the ion concentration for an average rabbit body mass of 3.5 kg, was 10.7 mg/kg and no obvious adverse effects were noted in the rabbits. Even if the same boron concentration of 150,000 ppm were to be injected intra-articularly in humans, the ion concentration would be 4.3 mg/kg, based on an injection volume of 2 ml (typical volume in radiation synovectomy with Dy-165 [Shortkroff 1998]) and an average human weight of 70 kg. One drawback to the potassium salt form is that potassium balance is often delicate. However, the concentration of potassium which would be injected, with an injection volume of 2 ml and average human weight of 70 kg, would not be very high at 2.32 mg/kg.

However, before these issues can be considered in more depth, the efficacy of BNCS in an animal model must be determined. The next chapter will present results of rabbit irradiations. In these studies, AIA rabbits received an intra-articular injection of 0.25 ml of 150,00 ppm of boron in the form of enriched KBH and their joints were irradiated with the tandem electrostatic accelerator currently in operation at MIT LABA, using the 1.5 MeV Be(d,n) reaction as the neutron source, and thereby effecting a BNCS treatment.

5. Animal irradiations using $K_2B_{12}H_{12}$

The primary goal of this experiment was to determine whether synovium can be ablated via BNCS. Using KBH as the boron compound, the efficacy of BNCS was tested on the AIA rabbit model with the tandem accelerator in operation at MIT LABA. The effect of BNCS on cartilage was also examined as part of the efficacy question. Throughout this thesis, 10,000 cGy has been quoted as the target dose required for clinical success, based on radiation synovectomy trials using β-emitters such as yttrium-90 and dysprosium-165 [Deutsch et al 1993, Sledge et al 1986]. However, clinical benefit with a β dose of 6,000 cGy has been reported [Bridgman et al 1973]. No detailed dose study is readily available in the literature. In addition, since BNCS uses α rather than β particles to effect synovectomy, target dose requirements may differ. Therefore, a dose escalation study was performed. This chapter describes the methods (5.1), the results (5.2) and the conclusions (5.3) of this investigation.

5.1 Materials and methods

Three days after intra-articular challenge with ovalbumin, as described in Chapter 2.3, New Zealand white male AIA rabbits were anesthetized and injected intra-articularly with 0.25 ml of a KBH/saline sterile solution containing 150,000 ppm of ^{10}B (enriched boron). Each rabbit was placed on a polyethylene stand which covered a solid block of graphite serving as a back reflector. Two small rectangular graphite blocks, side reflectors, were attached with velcro to the back reflector and were adjusted to be at the same level as the rabbit knee, since it has been shown that graphite reflectors improve treatment time and therapy parameters [Gierga et al 1999]. Figure 5.1 shows a schematic of the reflector arrangement. Plastic bags filled with graphite powder were taped to the graphite back and side reflectors to surround the joint on three sides. After the rabbit was on the stand, the knee joint was positioned between the bags of graphite powder. The stand (and reflectors) was then carefully positioned against the plexiglass window at the moderator end such that the rabbit joint was in the center. Figure 5.2 shows the rabbit ready for irradiation

Neutron irradiation was performed using the tandem electrostatic accelerator at MIT LABA [Klinkowstein et al 1997] and the target/moderator/reflector assembly described in Chapter 2.3. The $^9Be(d,n)^{10}B$ reaction was used as the neutron source with an incident deuteron energy of 1.5 MeV. The adjustable target was placed 8 cm from the end of the moderator/reflector assembly. Three rabbits were irradiated at each of the target doses, ranging from 1,400 to 140,000 RBE-cGy. Details on doses and irradiation parameters are given in section 5.1.1. A camera was placed inside the radiation vault and connected to a television monitor in the control room to monitor the rabbit during irradiation.

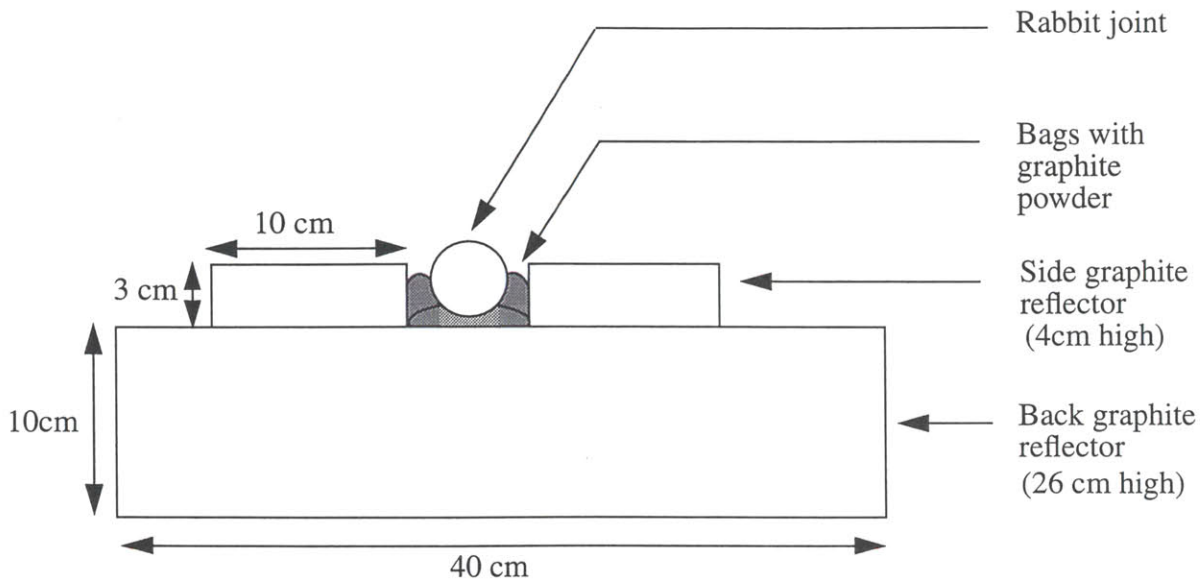

Figure 5.1: Schematic of the arrangement of graphite reflectors, viewed from the top.

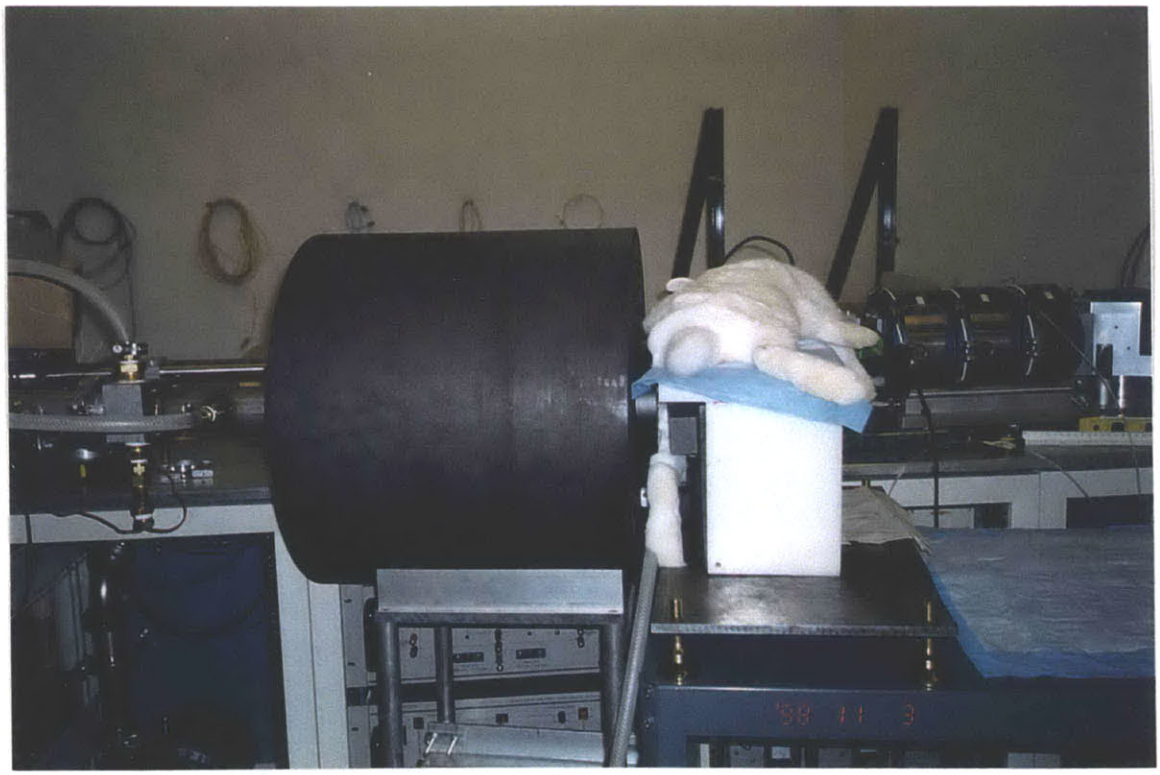

Figure 5.2: Photograph on rabbit of stand (with its knee joint between the moderator end and graphite reflectors) ready for irradiation to begin.

Several control experiments were performed, including injection of the rabbit knees with the boron compound without neutron irradiation and neutron irradiation without the injection of the boron compound. Also, non-treated arthritic joints were taken for comparison to treated knees and confirmation of the production of AIA in the joint, as indicated by gross observation of an increase in both joint diameter and temperature.

Of the three rabbits irradiated at each dose, the whole joint was taken from two of the rabbits, while synovial tissue only was dissected from the other rabbit. Analysis of whole joints (as well as synovial tissue only specimens) was carried out via histologic evaluation after haematoxylin and eosin staining. Haematoxylin is a basic dye which stains acidic structures a purplish blue; nuclei have a strong affinity for the dye due to their high DNA and RNA content. Eosin is an acidic dye which stains basic structures red or pink; most cytoplasmic proteins are basic attracting the eosin dye. Staining, as well as the preparation of the tissue (hard and soft), was carried out by personnel of the Department of Orthopedic Surgery at the Brigham and Womens' Hospital, Boston, MA. A brief description of the procedure follows.

Upon dissection, the whole joints (as well as synovial tissue alone) were fixed in 10% phosphate buffered formalin for several days. The whole knees then had to be decalcified before embedment in paraffin (Paraplast, VWR Scientific, Boston, MA). To allow the decalcification solution, 10% formic acid in a sodium citrate buffer (Mallinckrodt, Paris, KY), to penetrate the entire specimen more quickly. the whole knees were cut into several 1 cm sections. The 1 cm sections were cut in the plane perpendicular to the shaft of the femur around the level of the patella. Decalcification required six to eight weeks. Tissue was then dehydrated with ethanol and cleared with Histoclear and chloroform to make it ready for embedment in paraffin. The embedded sections were cut into 7 μm thick slices and placed on glass slides for staining. After sections were deparaffinized and rehydrated, they were stained with Harris' haematoxylin and eosin following a standard staining protocol. The slides were then dehydrated, cleared with xylene and coverslipped with Permount.

One issue that arose was how long to wait after the irradiations to sacrifice the rabbit and obtain the tissue; the time needed to be long enough for necrosis to be significant at a histological level without substantial cell infiltration to accommodate the debris. Further discussion of this issue and its resolution is presented in section 5.1.2.

5.1.1 Irradiation parameters

Calculation of irradiation time via MCNP required input of the yield of the $^{9}Be(d,n)$ reaction with an impinging deuteron energy of 1.5 MeV. A curve showing the yield of the $^{9}Be(d,n)$ reaction with a deuteron energy of 1. 4 MeV has been reported in the literature [Whittlestone 1976]. The yield, integrated over angle, has been read from this curve and extrapolated to a deuteron energy of 1.5 MeV, resulting in a value of 3.6×10^{16} n/min/mA [Song 1998]. At the time of the neutron irradiations, no information on the angular distribution of the yield was available and therefore, an isotropic source was assumed.

Experimental validation of in-phantom dose rates predicted by MCNP simulations was carried out by MIT LABA members [Gierga et al 1999]. This was done via mixed-field dosimetry, a method

that has been used extensively to characterize both reactor and accelerator beams for BNCT [Rogus et al 1994, White 1998]. The adjustable beryllium target was placed 8 cm from the end of the moderator/reflector assembly and measurements were made in a brain phantom, on loan from the BNCT group at the MIT reactor [Harling et al 1995]. Measurements were then compared to simulations at depths of 1 and 3 cm [Gierga et al 1999]; results are reproduced in table 5.1.

Table 5.1: Comparison of dose rate measurement and simulation [Gierga et al 1999]

	Thermal neutron (cGy/min/mA)		Fast neutron (cGy/min/mA)	
Model	1 cm	3 cm	1 cm	3 cm
Experiment	0.63±0.04	0.53±0.03	33±5	14±2
Simulation - no scaling	0.83±0.02	0.77±0.02	53±2	31±1
Simulation - scaled	0.63±0.01	0.58±0.01	40±1	24±1

Based on the strong dependence of synovial boron dose, which accounts for 95% of the synovial total dose, on the thermal neutron dose, results were scaled by 0.76 such that at 1 cm, the dose rates due to thermal neutrons were the same in both simulation and experiment [Gierga et al 1999]. With the scaling factor, the thermal neutron dose rate at 3 cm agreed between measurement and simulation, ensuring that the best estimate of therapy time was found for the simulations using the 1.5 MeV Be(d,n) reaction [Gierga et al 1999]. The scaled yield is 2.7×10^{13} n/min/mA.

Simulations were performed [Gierga 1998] with the rabbit joint phantom (scaled from the human knee joint phantom) to first determine the therapy time to deliver 10,000 RBE-cGy, assuming 19,000 ppm of boron in the synovium which is achievable as shown in the uptake results of figure 4.18. The same RBE values used in chapter 2.3 were applied, namely 1.0 for photons, 4.0 for neutrons and 3.8 for the products of the boron neutron capture reaction (therefore, physical doses are approximately a factor of 4 lower). Therapy time, based on a synovial boron concentration of 19,000 ppm and a target dose of 10,000 RBE-cGy (as well as the scaling factor from table 5.1), was 0.84 min-mA. Irradiation time was maintained at 20 to 25 minutes post-injection (since the average synovial boron concentration was found to be approximately constant during this interval, as seen in figure 4.18) and an integrated charge of 0.0504 C was delivered. The delivery of 10,000 RBE-cGy to the synovium resulted in a maximum skin dose of 223 RBE-cGy and a minimum synovium/bone ratio of 68, both of which are well within criteria as established in neutron beam design (chapter 2.3). Therapy parameters for doses other than 10,000 RBE-cGy can be scaled (assuming a synovial boron concentration of 19,000 ppm). Table 5.2 lists the synovial target doses delivered in the present study.

The two highest target doses required more than one irradiation interval. More specifically, the target dose of 140,000 RBE-cGy required three irradiation intervals, i.e. the knee was injected, irradiated for 20 to 25 minutes (interval #1), reinjected, irradiated for another 20 to 25 minutes (interval #2), again reinjected and irradiated for 20 to 25 minutes (interval #3). The target dose of

68,000 RBE-cGy required 2 irradiation intervals. It should be noted that the calculation of these two doses was based on a synovial boron concentration of 19,000 ppm for the first irradiation interval and 25,900 for the next intervals based on the assumption of a baseline synovial boron concentration value of 6,900 ppm between 30 and 60 minutes (since figure 4.18 shows that at 60 minutes the average synovial boron concentration is 6,900 ppm) in addition to the concentration achievable in the synovium upon injection. Assuming 25,900 ppm of boron in the synovium, the therapy time to deliver 10,000 RBE-cGy to the synovium is 0.7 min-mA. Therefore, target doses were calculated by assuming a therapy time of 0.84 min-mA for the first irradiation interval and 0.70 min-mA for the other irradiation intervals and then scaling.

Table 5.2: Irradiation parameters for efficacy study

Set (n=12/set) (n=3/dose)	Target dose (RBE-cGy)	Current (within 5%) (μA)	Integrated charge (C)	Irradiation intervals (#)
A (7/98)	140,000	135	0.6210	3
	68,000	100	0.3105	2
	12,000	41	0.0621	1
	6,200*	26	0.0311	1
B (11/98)	13,000	44	0.0655	1
	6,500	22	0.0327	1
	3,600	12	0.0182	1
	1,400	5	0.0072	1

*one of the three rabbits received a dose of 5,000 rather than 6,200 RBE-cGy with an approximate current of 20 μA; total integrated charge delivered was 0.0250C.

Doses around and less than 10,000 RBE-cGy were calculated in one interval only, i.e. for 20 to 25 minutes, and thus were based on an average synovial uptake of 19,000 ppm during the interval. It should be noted that the linear scaling of therapy parameters is restricted by concentration. The inability to scale therapy parameters with synovial boron concentration is due to flux depression, an important effect at high boron concentrations. The error incurred in linear scaling has been quantified by a comparison between therapy time with 19,000 ppm of boron explicitly modeled in the synovium and scaling of therapy time from 1,000 ppm; the difference was 60% [Gierga 1999]. The relationship between therapy time to deliver 10,000 RBE-cGy to the synovium and synovial concentration of boron, at a heavy water moderator length of 8 cm, has been calculated with MCNP using a rabbit joint model [Gierga 1999] and results are reproduced in figure 5.3. Therapy parameters for a rabbit synovial boron concentration of 1,000 ppm are a maximum skin dose of 2,180 RBE-cGy and a minimum synovium to bone dose ratio of 6.7. This is a factor of ten lower than would have been expected, scaling down from the values achieved with 19,000 ppm, again showing the effect of flux depression and the inability to linearly scale with boron concentration.

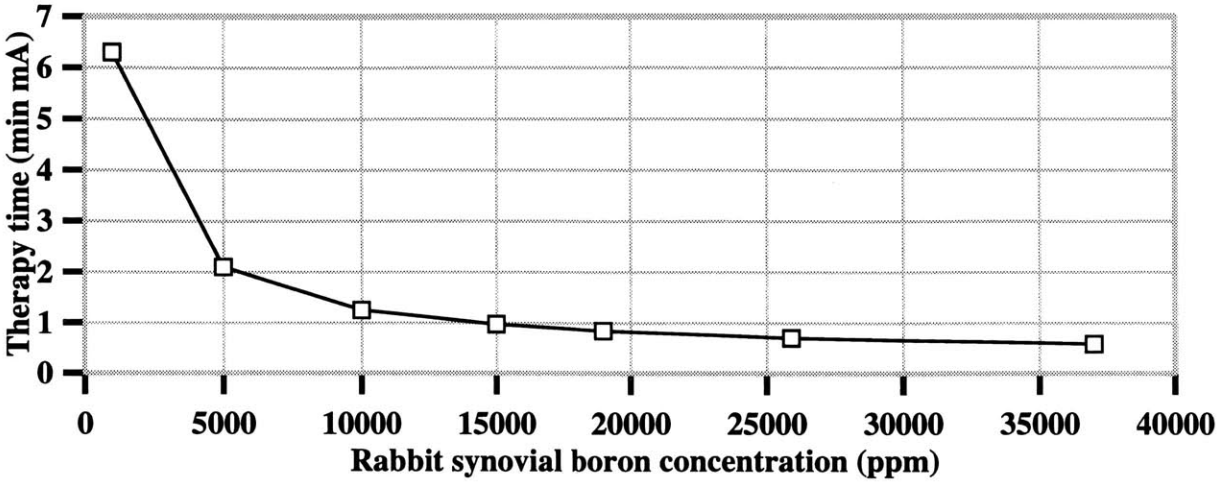

Figure 5.3: Time to deliver 10,000 RBE-cGy to all areas of the synovium versus rabbit synovial boron concentration [Gierga 1999].

The target doses in table 5.2 are based on an average synovial uptake of 19,000 ppm observed over 30 minutes post-injection as shown in figure 4.18. However, there is significant variation in uptake; the lowest and highest values of uptake being 3,900 and 37,000, respectively. Using the results of figure 5.3, the therapy time to deliver 10,000 RBE-cGy is 3.1 and 0.58 min-mA for the low and high values, respectively. When more than one irradiation interval is required, the low and high end of the values at 60 minutes (4,200 and 9,200 ppm) is added for calculation of the therapy time. The variation in dose based on uptake for all of the target doses in table 5.2 and ranges from 27% to 39%. An estimate of the potential error due to the uncertainty in the neutron yield assumed for the ^{9}Be(d,n) reaction deriving from the scaling factor, is 24%. Propagation of the error resulting from biological uptake with that from neutron yield uncertainty yields a range of error from 36% to 46%.

The joint serving as a control for effects of neutron irradiation was irradiated for 70 minutes at an accelerator current of 130 μA. It received the neutron dose delivered to the animal receiving the highest dose to the synovium, 140,000 RBE-cGy and it therefore represents a worst case scenario.

5.1.2 Optimal time after irradiation for observation of necrosis

The purpose of the experiment described here was to determine the time required to observe necrosis histologically without significant infiltration of inflammatory cells to accommodate the debris, which would make it difficult to distinguish between the changes caused by the induced arthritis and those caused by irradiation. Thus, arthritis was unilaterally induced in two rabbits. In order to ensure that necrosis should be achieved, a target dose of 140,000 RBE-cGy, was delivered to the synovium via three injections of 0.25 ml of 150,000 ppm, one for each irradiation interval of 25 minutes, at 135 μA using the 1.5 MeV ^{9}Be(d,n) reaction. Rabbits were then sacrificed and synovial tissue was dissected at 4 and 72 hours after irradiation.

Figure 5.4 shows histological sections of tissue 4 hours after irradiation. The top part of the figure, 5.4(a), shows an elongated blood vessel, with an increased endothelial permeability, from which neutrophils are migrating into the surrounding tissue in response to the tissue damage caused by irradiation. This is a typical phenomenon in the development of an acute inflammatory exudate [Burkitt et al 1996]. Increased vascular permeability also allows leakage of fluid into surrounding tissue, accounting for the edematous appearance of the matrix. Fibrinogen protein (staining pink), to be later converted to fibrin, is also leaking into the tissue from the blood vessel as part of the acute inflammatory response.

Figure 5.4(b) shows a synovial villus 4 hours after treatment via boron neutron capture. There is scattered evidence of eosinophilic debris (spots of bright pink stain) and pyknotic nuclei (small spots of intense purple stain). These two features are an indication of necrosis. The eosinophilia is due to a degeneration of structural proteins while the pyknosis is due to a condensation of nuclear material including chromatin clumping, possibly in response to a reduced pH from anaerobic and terminal metabolism [Burkitt et al 1996]. A few cells may be exhibiting cloudy swelling, such that the cytoplasm of the cells stains more faintly [Burkitt et al 1996]. Several cells appear healthy.

Figure 5.5 shows histological sections of tissue at 72 hours post-irradiation. In figure 5.5(a), both the synovium and subsynovium have a marked appearance of pyknotic nuclei and karyorrhectic fragments which are pieces of nuclear material occurring from further degeneration of pyknotic nuclei thar break into many fragments. When karyolysis, or the breakdown of nuclear material, is complete, all of the nuclear material is lost and dead cells become anucleate, homogeneous, eosinophilic masses [Burkitt et al 1996]. This is clearly seen in figure 5.5(b), where the synovium and subsynovium show a dramatic loss of cells and a thickened fibrous lining. One cell in the lower left corner has a pyknotic nucleus and intensely staining eosinophilic cytoplasm. Several cells are showing advanced stages of cell swelling. The few healthy cells existent in this area are likely to be macrophages, since in the typical development of acute inflammatory responses, macrophages become the dominant inflammatory cell type by 48 to 72 hours after traumatic injury, as opposed to the early phase during which neutrophils are dominant [Burkitt et al 1996]. Since the area is generally quite acellular, it seems unlikely for the macrophages to be the original synovial lining cells, although it is theoretically a possibility. There are not many inflammatory cells and this may be explained by a recent suggestion in the literature that pronounced fibrosis may moderate the invasion of both inflammatory cells and mediators of inflammation [Raunest and Derra 1995]. This has also been suggested that it may be a cause for the reduction of arthritic symptoms [Raunest and Derra 1995, Pavelka et al 1975].

On the basis of the above comparison, it was concluded that evidence of necrosis was dramatic at 72 hours. For the entire efficacy study, rabbits were sacrificed and knee joints dissected 72 hours after treatment via BNCS. The observation of necrosis at 3 days after BNCS is consistent with other experimental synovectomy studies [Raunest and Derra 1995].

To determine the time of synovial regeneration, a longer time is required. In experimental surgical and pulsed laser synovectomy, regeneration of neosynovium was observed after 2 months [Raunest and Derra 1995]. Regeneration following experimental photodynamic synovectomy was not observed at 1 month post-treatment [Trauner et al 1998], similar to radiation synovectomy using dysprosium-165 [Zuckerman et al 1989].

(a)

(b)

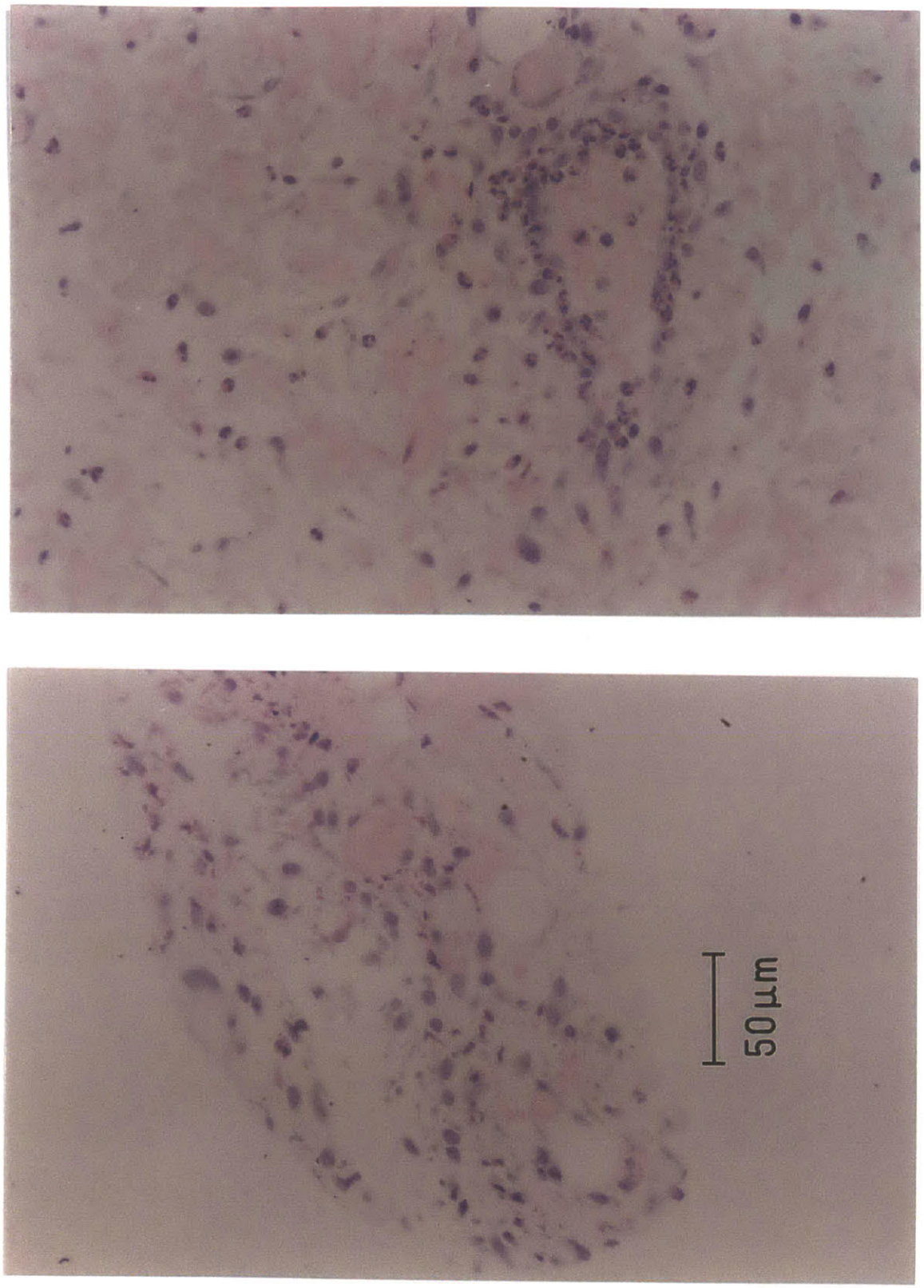

Figure 5.4: Synovial tissue 4 hours after irradiation. H&E 50X.

(a)

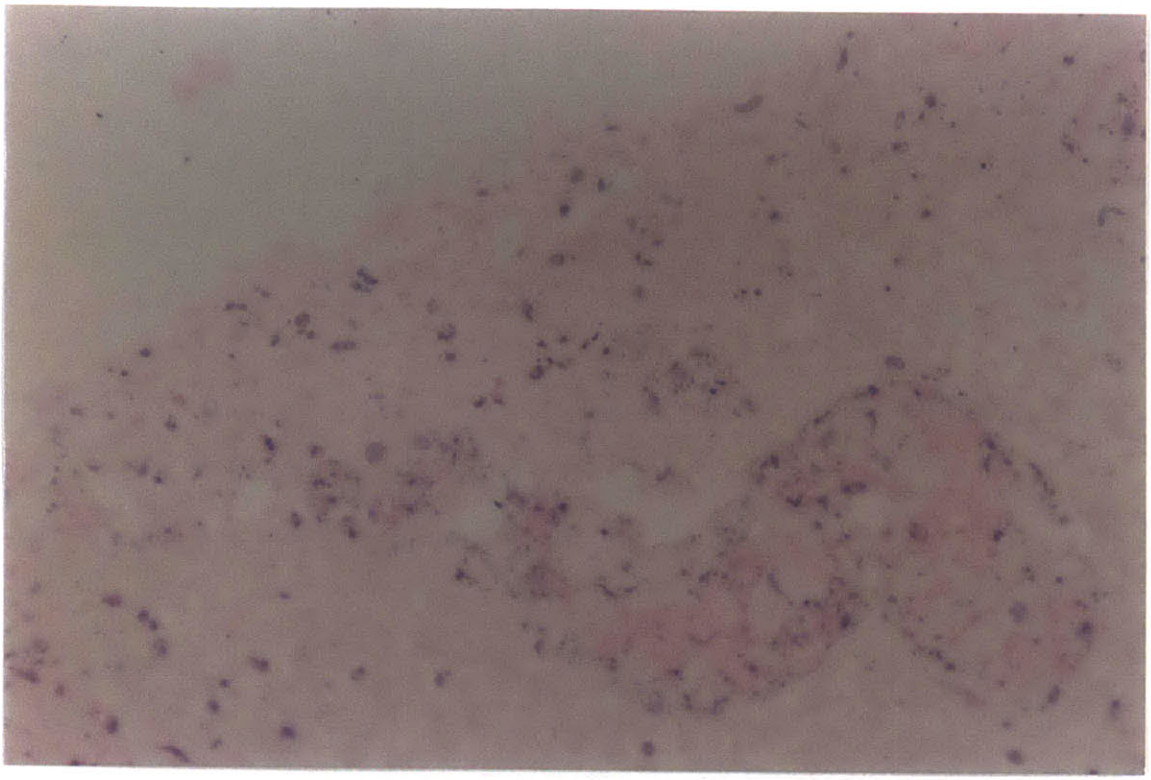

(b)

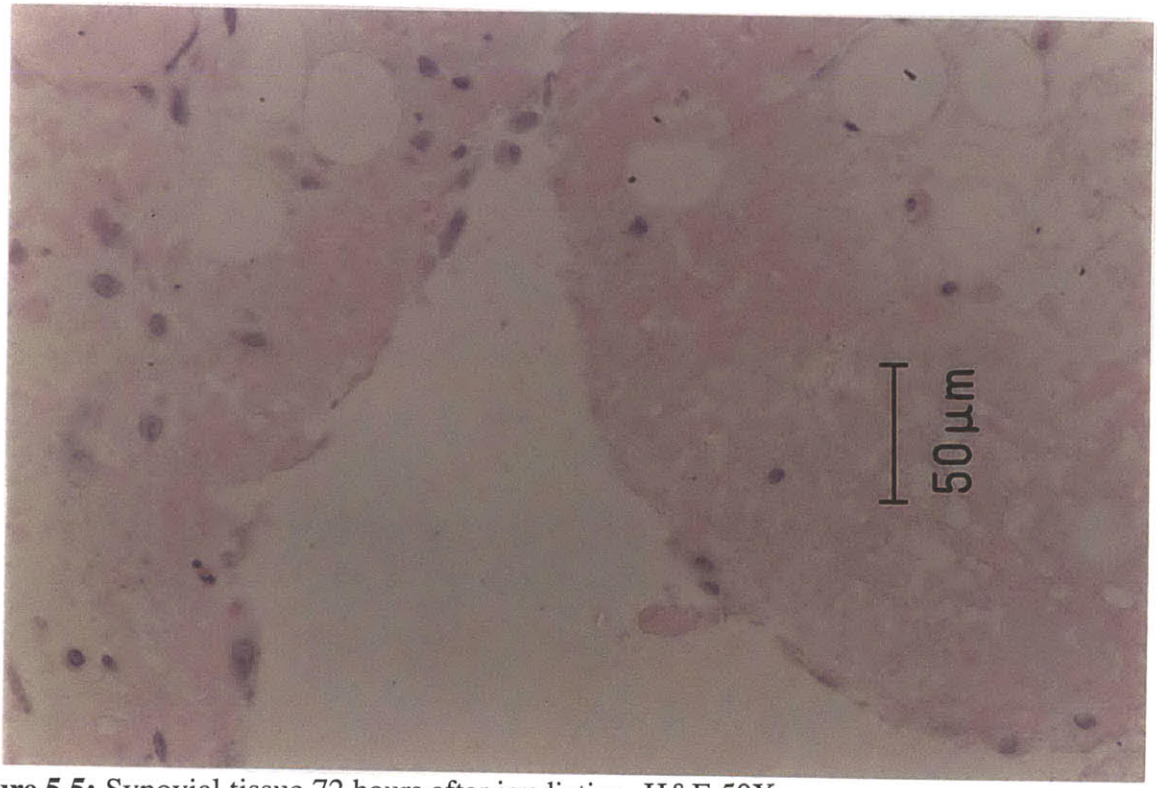

Figure 5.5: Synovial tissue 72 hours after irradiation. H&E 50X.

5.2. Results and discussion

Results are subdivided as follows: controls (5.2.1), doses much greater than 10,000 RBE-cGy (5.2.2), doses around 10,000 RBE-cGy (5.2.3), doses much less than 10,000 RBE-cGy (5.2.4). Since whole joints presented more detailed information than the samples where synovial tissue only was dissected (although they were useful for rapid estimations of results), presentation of results in this section and discussion are limited to whole joints only.

5.2.1 Controls

Three different types of controls were performed. The first control animals (two whole joints) were made arthritic and did not receive any treatment; these were denoted as arthritic only. In the second control, a neutron dose equivalent to that received with the highest synovial target dose, 140,000 RBE-cGy, was delivered to a whole joint; these are denoted as neutron only. The third control entailed intra-articular injection of the boron compound (0.25 ml of 150,000 ppm of boron); these are denoted as compound only.

As discussed in section 2.1, synovium in non-arthritic joints consists of a layer one to three cells thick of synovial cells (or synoviocytes), while in an arthritic condition, synoviocytes increase in both number (hyperplasia) and size (hypertrophy). Although there are two cell types comprising the synovium, type A (macrophage-like) and B (fibroblast-like), it has been shown by various types of methods that recruitment occurs primarily in type A cells [Eulderink 1982].

Figure 5.6 shows two sections of rheumatoid synovium one week after induction (this is the same time at which rabbits undergoing treatment were sacrificed relative to the time of induction). Part (a) of figure 5.6 shows the synovial layer thickened by synoviocyte hypertrophy and hyperplasia. Based on the loosely collagenous tissue beneath the thickened synovial lining, this corresponds to areolar synovium. Figure 5.6(b) shows two small villi, finger-like processes which are formed by hyperplastic synovium. Villi may vary greatly in size and shape within a joint [Freemont 1995]. Several small capillaries are evident in the villi. The overall appearance of the synovium in these arthritic control joints was similar to previous reports in the literature [Dumonde and Glynn 1962, Consden et al 1971]. Caliper readings revealed an increase of 0.3 cm in joint diameter between the time of sacrifice and time of induction, indicating the production of AIA in the rabbit joint.

Sections of articular cartilage from the arthritic (non-treated) rabbit joint are shown in figure 5.7. Femoral cartilage, shown in figure 5.7(a), has healthy-looking clusters of mature cartilage cells (chondrocytes). As expected, the cartilage is completely avascular. The cartilage in figure 5.7(b) corresponds to patellar cartilage and, although it is the same thickness as the femoral cartilage, it appears to be less healthy based on prominence of eosinophilic staining of chondrocytes and the presence of several empty lacunae. This was observed in both of the arthritic control joints and the reason for this occurrence is not clear. One reason could be the juxtaposition of particularly active rheumatoid synovium, a trace of which is seen in the top left corner of the photograph. However, the arthritic has only been present for one week, early for severe cartilage degeneration effects to be manifest.

In the second type of control, the same volume and concentration of boron compound used for the treatment (0.25 ml of 150,000 ppm) was injected intra-articularly without subsequent neutron irradiation. The whole joint was taken for histological staining 72 hours after injection. Figure 5.8 shows sections of the synovium from this compound only whole joint. Part (a) of figure 5.8 is a low-power view showing grossly inflamed and thickened synovium. There is a dense infiltrate of inflammatory cells throughout the synovial lining. No evidence of synovial necrosis is present. The synovium appears arthritic and resembles examples of experimental AIA synovium in the rabbit as previously reported [Consden et al 1971]. Recruitment of inflammatory cells in response to the compound may have occurred; however, they cannot be distinguished from inflammatory cells in response to the arthritis. The difference in caliper readings before induction and injection showed an increase of 0.6 cm in joint diameter, indicating an active arthritis. A close-up view, in figure 5.8(b), shows characteristic synoviocyte hypertrophy and hyperplasia, seen in the arthritic controls. In some areas, microvilli, protruding from the synoviocytes [Freemont 1995], can be seen. There are, as expected, several capillaries throughout the thickened synovial lining. There is no observable difference in the synovium between arthritic and compound only control knees.

Figure 5.9 shows articular cartilage from both the (a) femur and the (b) patella. As in the arthritic control joint, the femoral cartilage appears to be healthy; there are essentially no empty lacunae and the chondrocytes are neither pyknotic nor are associated with eosinophilic debris. However, also as in the arthritic control joint, the patellar cartilage looks less healthy; the lacunae are filled but several chondrocytes are exhibiting pyknotic nuclei and their cytoplasm is very eosinophilic. The cartilage in figure 5.9(a) and (b) closely resembles that in 5.7(a) and (b). It was concluded that there is no observable effect in cartilage with injection of the boron compound alone.

The last control tested the effect of neutron irradiation alone, without the injection of compound. Figure 5.10 shows an example of a synovial villus. Severe hyperplasia has resulted in a greatly thickened synovial lining and hypertrophy is also evident in many of the synoviocytes. The three large holes in the synovium and the dark triangle at the top center of the photographs are cutting artifacts, not physiological manifestations. As expected, there is an infiltration of inflammatory cells and there are several blood vessels. The overall synovial appearance following irradiation with neutrons does not appear to be different from the synovial appearance in the non-treated joints.

Figure 5.11 shows articular cartilage of both patella and femur, on the left and right, respectively. The appearance of the cartilage closely resembles the appearance of the cartilage in the arthritic only joints, as well as the compound only joint. Thus, in this control, no substantial difference was observed. In the Monte Carlo calculations, the cartilage was assumed to contain 1 ppm of boron. Neutron irradiation for a total of 70 minutes at 130 μA resulted in a dose of 2670 RBE-cGy to the articular cartilage; no differences between the articular cartilage of the neutron only control joint and the arthritic only control joint were observed.

In conclusion, the arthritic controls demonstrated the histopathological features of the rabbit AIA model expected based on the literature. Neither injection of KBH alone nor neutron irradiation alone produced effects which were different from the arthritic controls, at least as observable by haematoxylin and eosin staining of several slides from each joint.

(a)

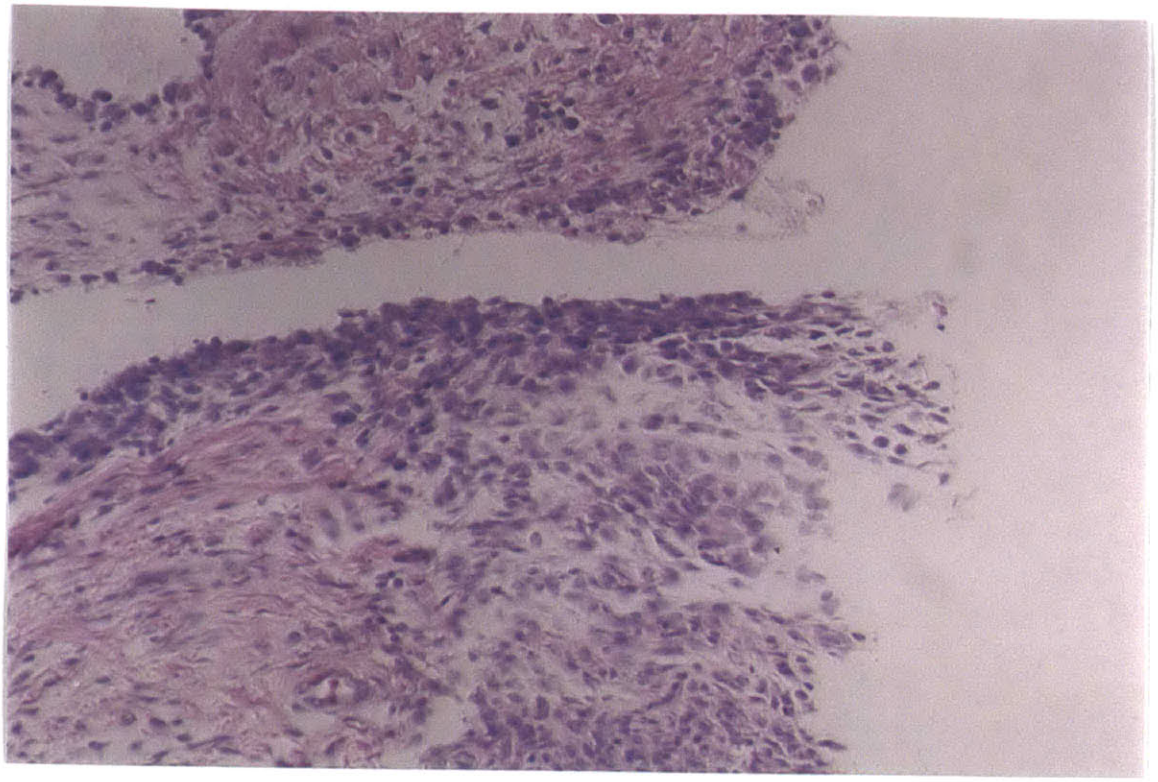

(b)

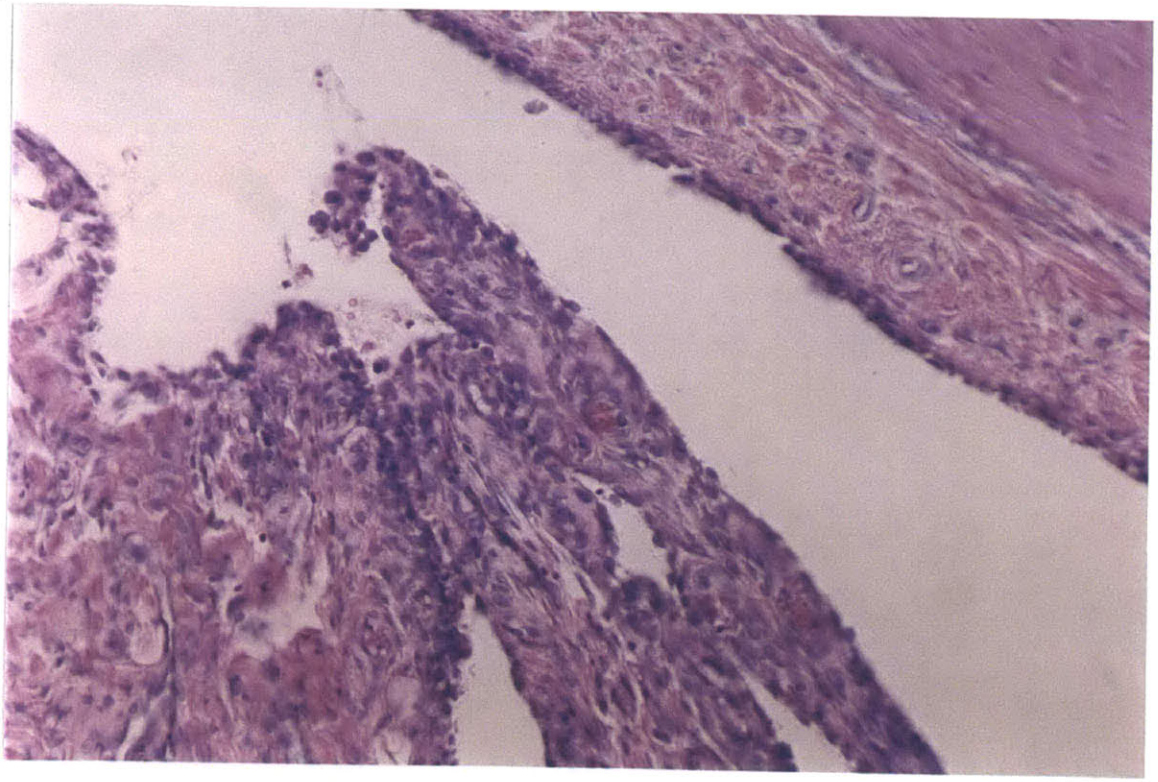

Figure 5.6: Synovium from arthritic control. H&E 50X.

(a)

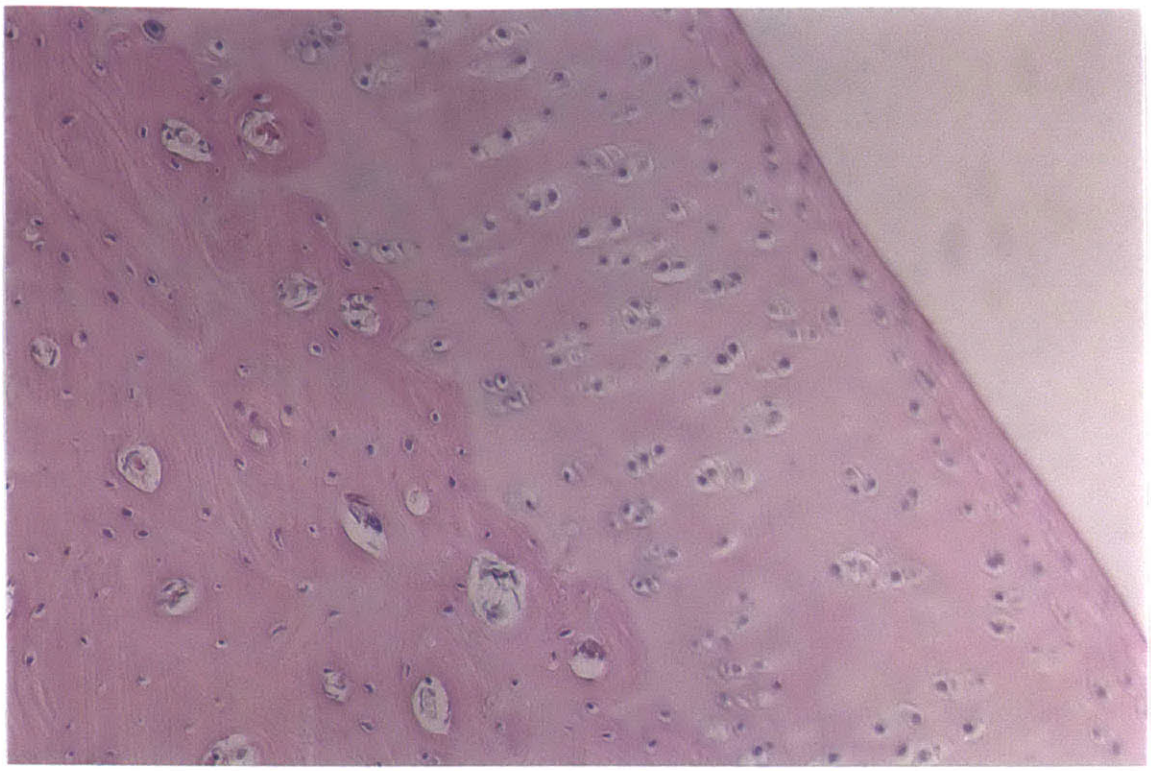

(b)

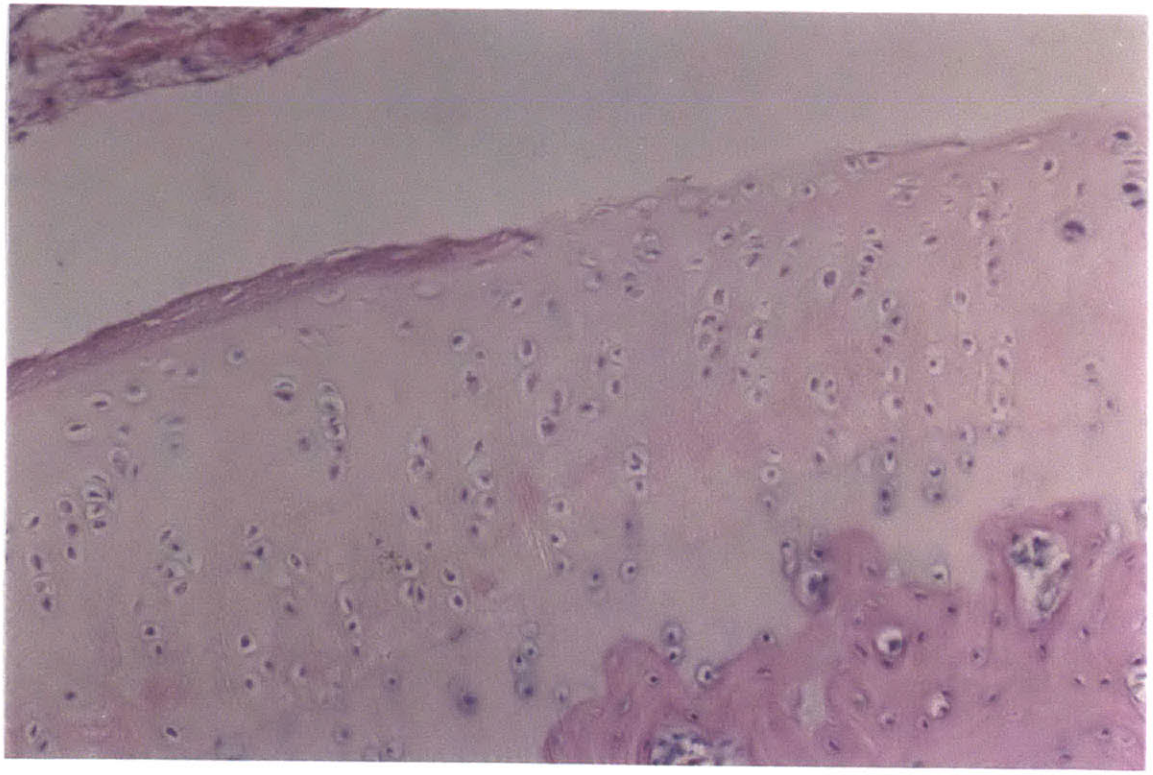

Figure 5.7: Cartilage from arthritic control. H&E 50X.

(a)

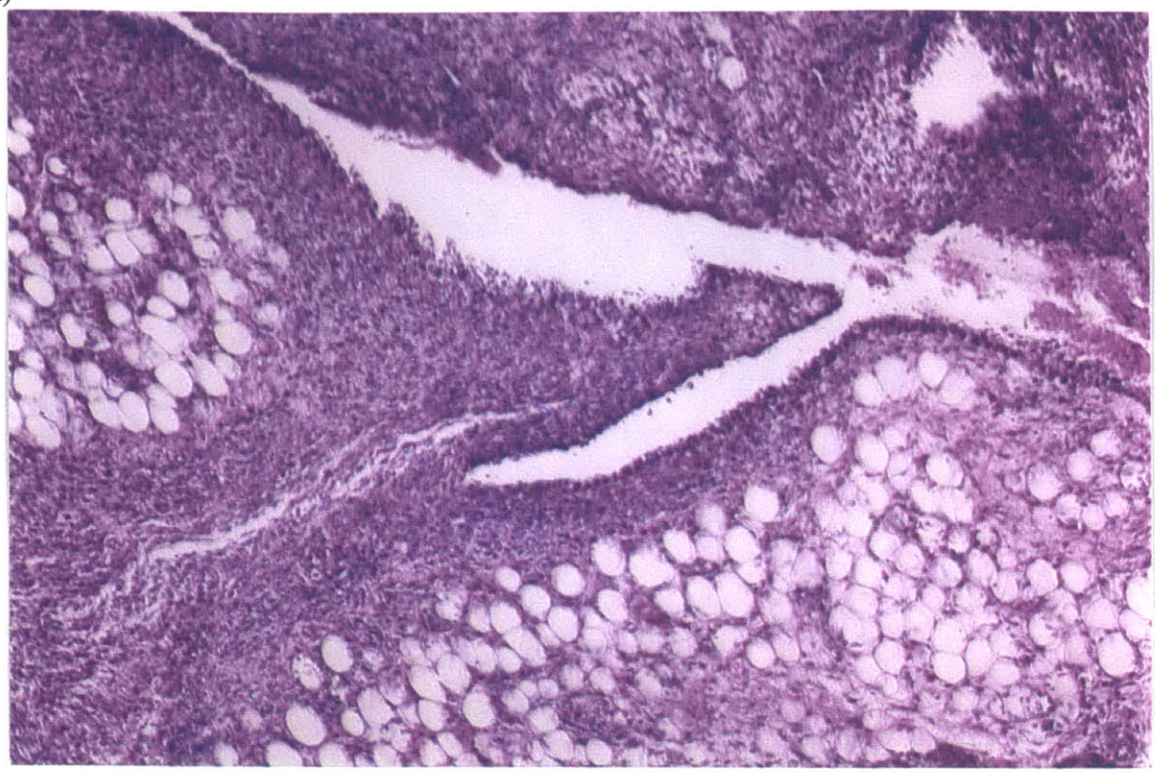

(b)

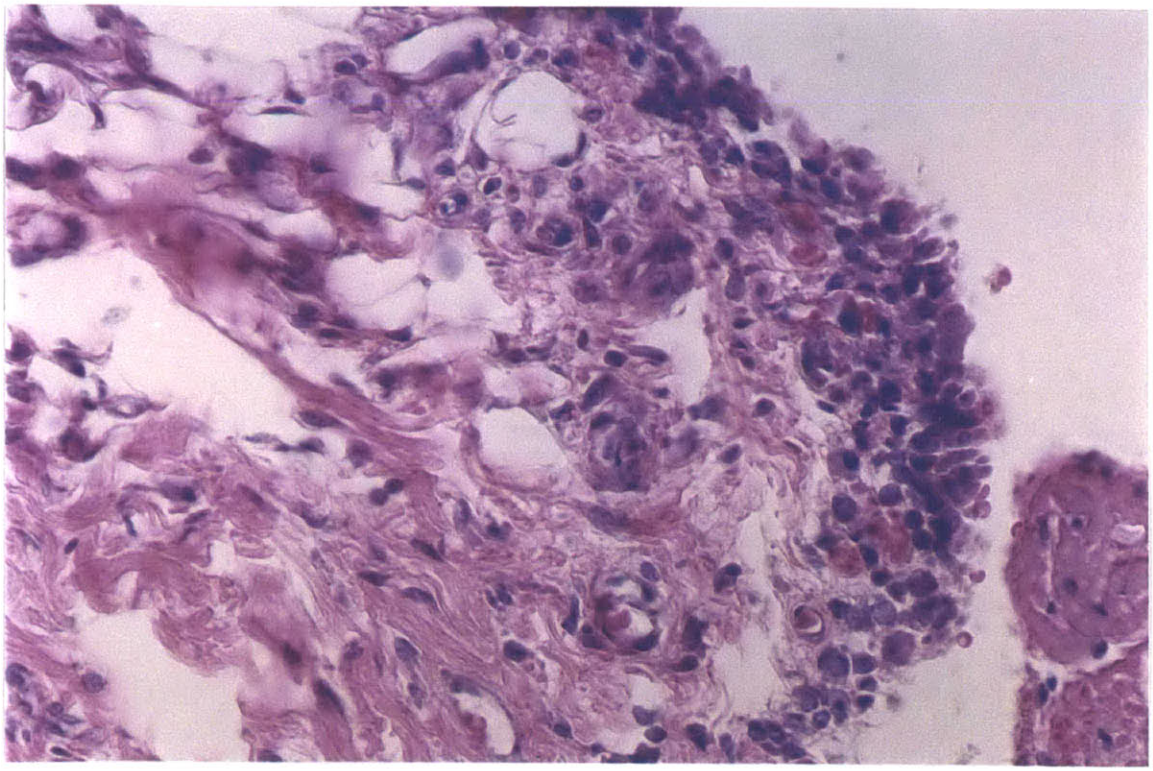

Figure 5.8: Synovium from compound only control. H&E (a) 25X, (b) 100X.

(a)

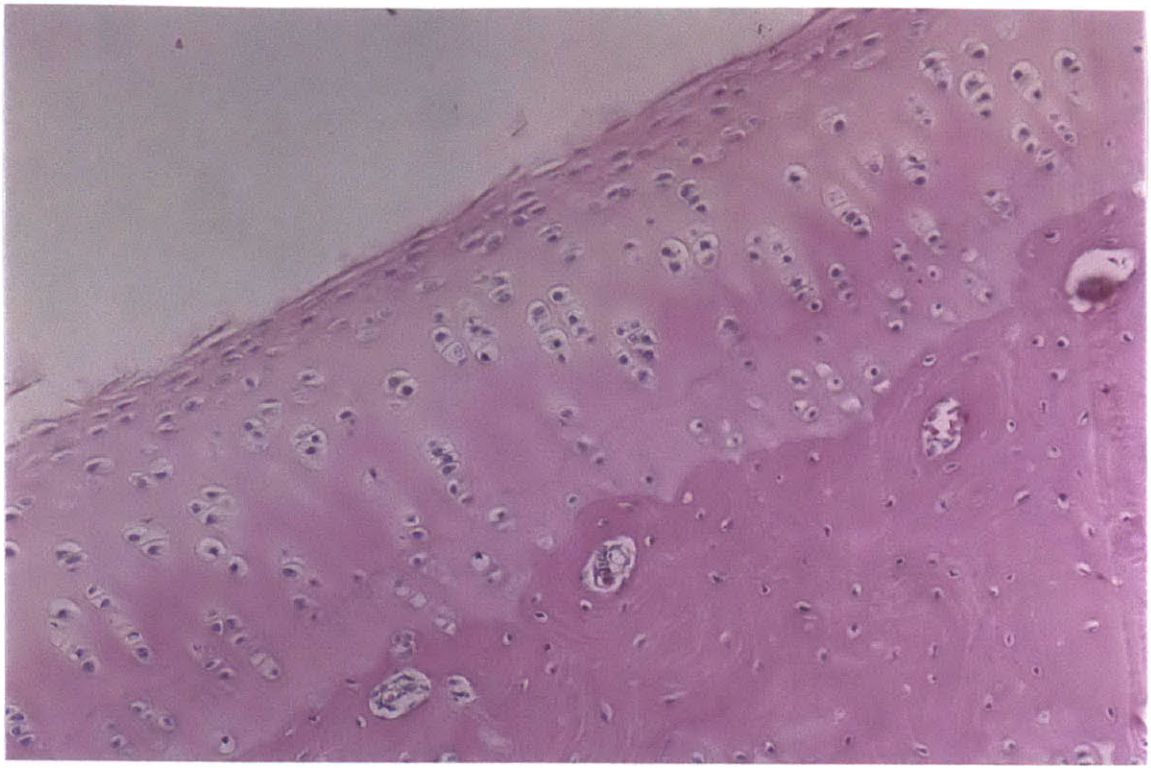

(b)

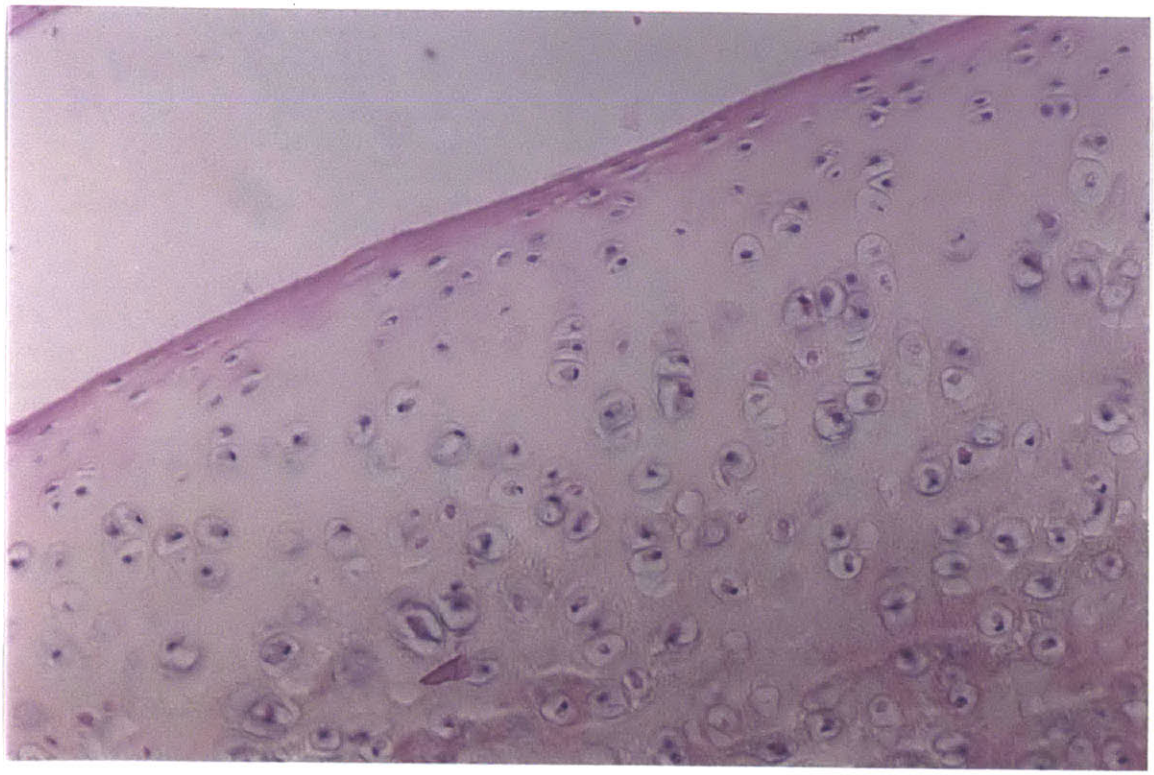

Figure 5.9: Cartilage from compound only control. H&E 50X.

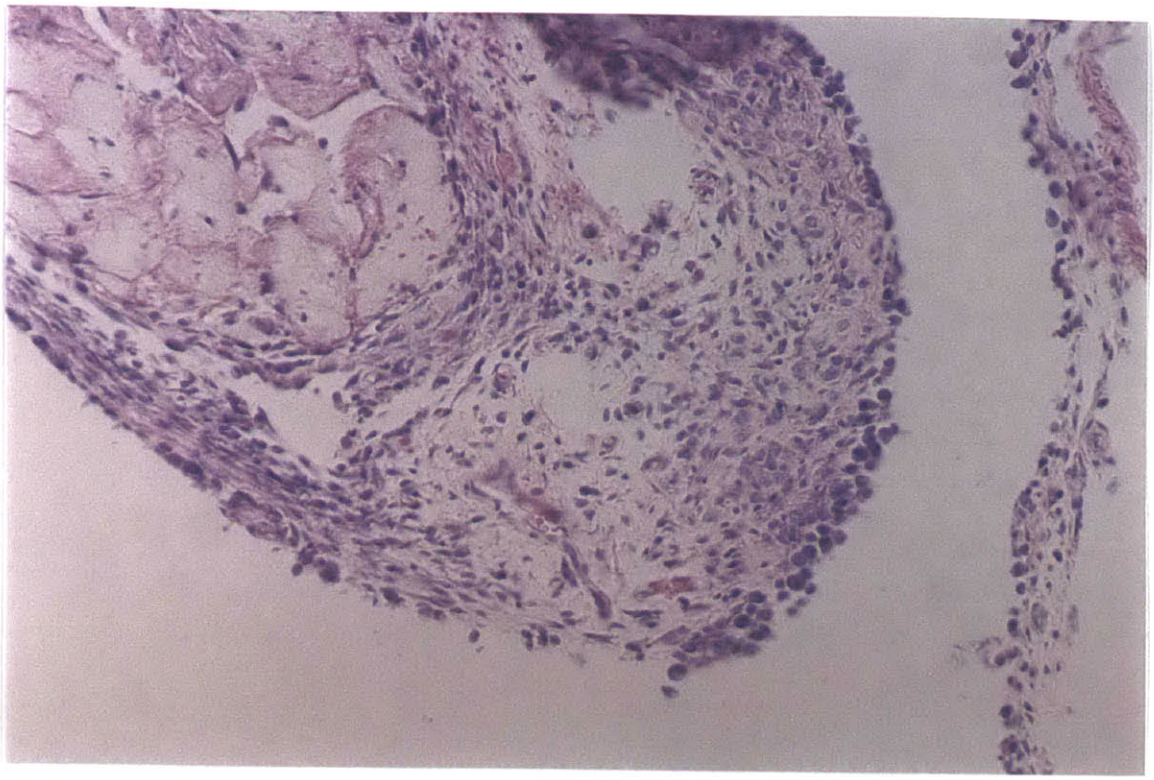

Figure 5.10: Synovium from neutron only control. H&E 50X.

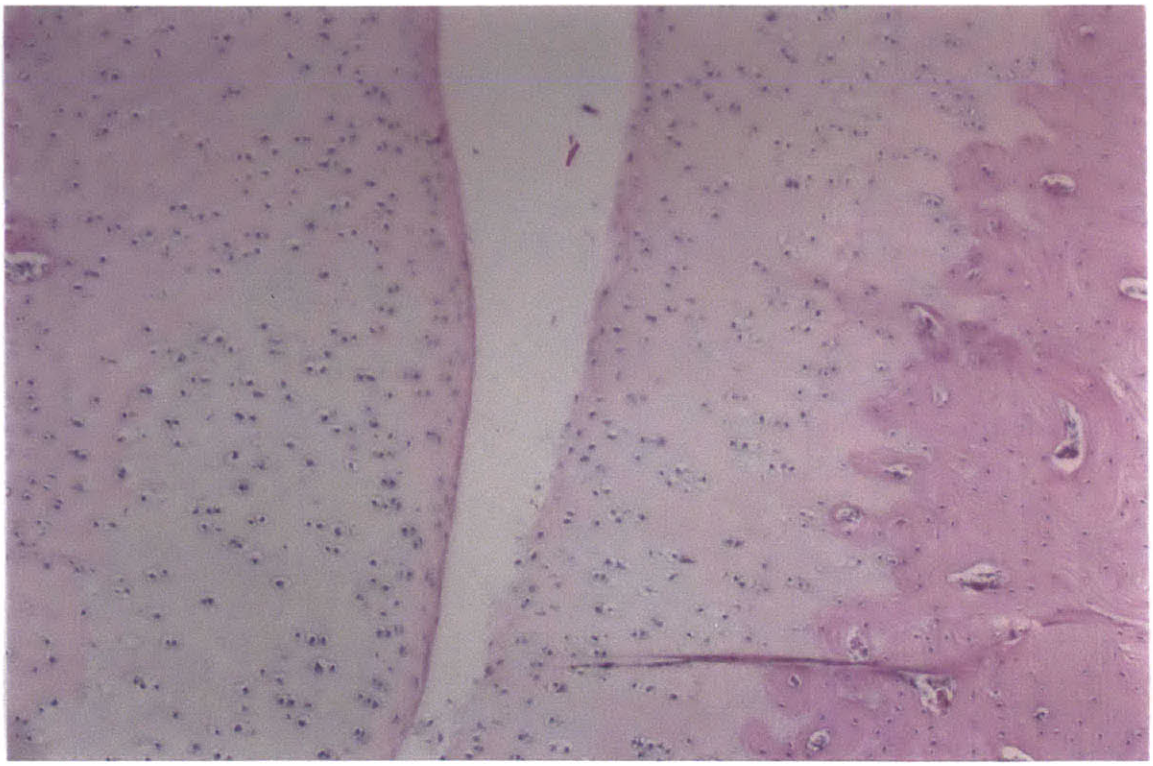

Figure 5.11: Cartilage from neutron only control. H&E 25X.

5.2.2 Doses greater than 10,000 RBE-cGy

The section presents results observed in joints irradiated to target doses of 140,000 and 68,000 RBE-cGy. Figure 5.12 shows synovium and cartilage after delivery of a target dose of 140,000 ppm RBE-cGy. As can be seen in (a), the rheumatoid pannus, has invaded the joint space and is approaching the femoral cartilage. The adipose synovial tissue is highly acellular and is exhibiting coagulative necrosis. A close-up view, (b), shows scattered pyknotic nuclei and eosinophilic debris throughout the acellular synovium. There is clear evidence of synovial ablation.

Average cartilage uptake in vivo over 30 minutes ranges from one half to one third of synovial uptake, as shown in figure 4.24. Choosing a factor of one half as conservative, and based on the result obtained via Monte Carlo simulation [Gierga 1999] that for a rabbit knee, the therapeutic dose ratio (synovium/cartilage) is 1.15 times the uptake ratio (as discussed in 4.2.3), the average dose delivered to cartilage may be 60,000 RBE-cGy. As can be seen in figure 5.12 (a), the surface of the femoral cartilage has a washed out appearance and seems to contain many lacunae filled with eosinophilic debris and pyknotic nuclei. Closer examination of one area of femoral cartilage, figure 5.12 (b), confirms the presence of many lacunae filled with eosinophilic debris and pyknotic nuclei, particularly when compared to control femoral cartilage shown in figures 5.7(a) and 5.9 (a). Irradiation appears to have damaged femoral cartilage.

Figure 5.13 shows (a) synovium and (b) cartilage from two joints treated to a synovial target dose of 68,000 RBE-cGy. In figure 5.13(a) there is a clear example of the tissue coagulative necrosis of several entire villi. In an arthritic rabbit, these would likely be sites for follicular formation of lymphocytes, which, in the original paper establishing the AIA rabbit model, has been termed one of the "most characteristic and striking" features of the histology of rheumatoid synovitis [Dumonde and Glynn 1962]. Underneath the villi, towards the capsule, there is a layer of synovial cells which may have survived due to their depth. These cells are likely the ones involved in the generation of a neosynovium.

Using the scaling method previously described, an estimate of average dose delivered to articular cartilage is about 30,000 RBE-cGy. The cartilage in figure 5.13(b) shows many empty lacunae not in the layer immediately adjacent to the synovial space, but a few cells deeper. There is a band of lacunae which are either empty or filled with eosinophilic debris. Cells toward the bone appear to be relatively healthy (barring a few which seem pyknotic). The appearance of the cartilage is not particularly washed out. Damage is quite variable at this dose. Variability can be influenced by several factors, including boron concentration. Perhaps the boron compound penetrated only a certain distance into the cartilage and accumulated there, creating a region of particularly high boron concentration.

Attention here is focused on the anterior synovium only, particularly when there are significant amounts of synovial tissue adjacent to cartilage surfaces. The following section examines the effect of the delivery of synovial target doses approximately 10,000 RBE-cGy. This is particularly interesting since 10,000 cGy has been used as the clinical target dose in radiation synovectomy currently and widely adopted throughout Europe [Clunie 1995].

(a)

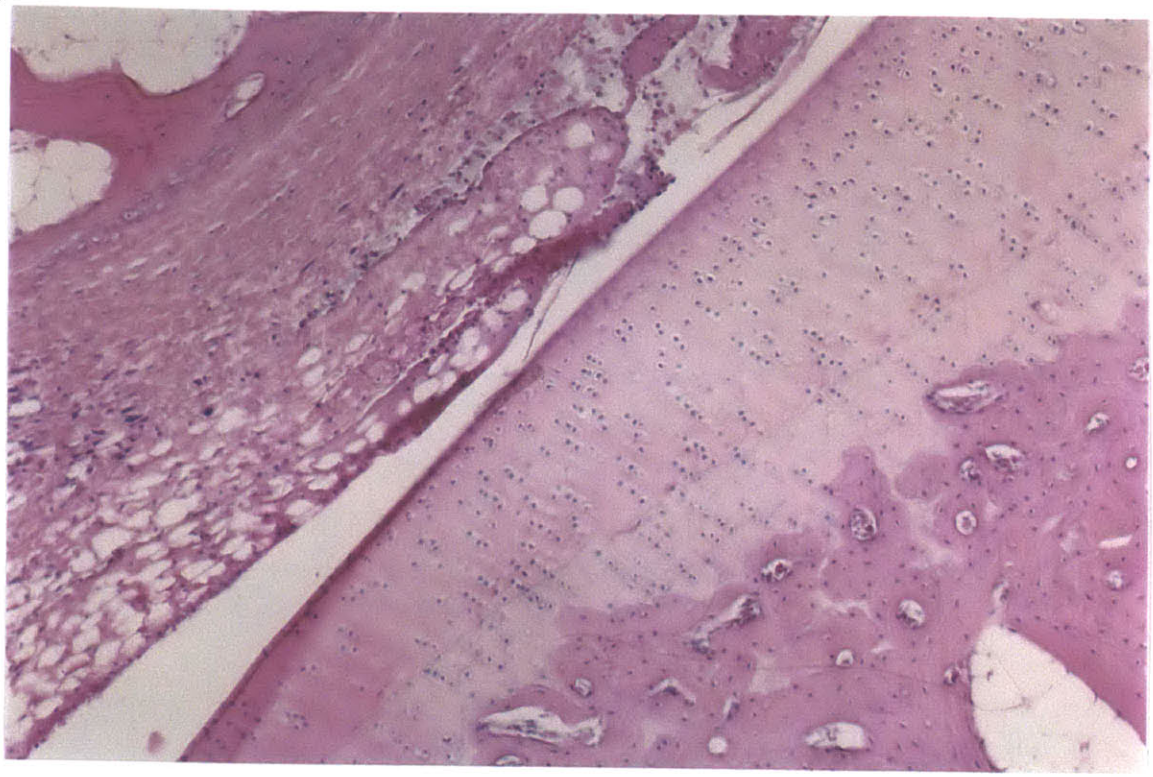

(b)

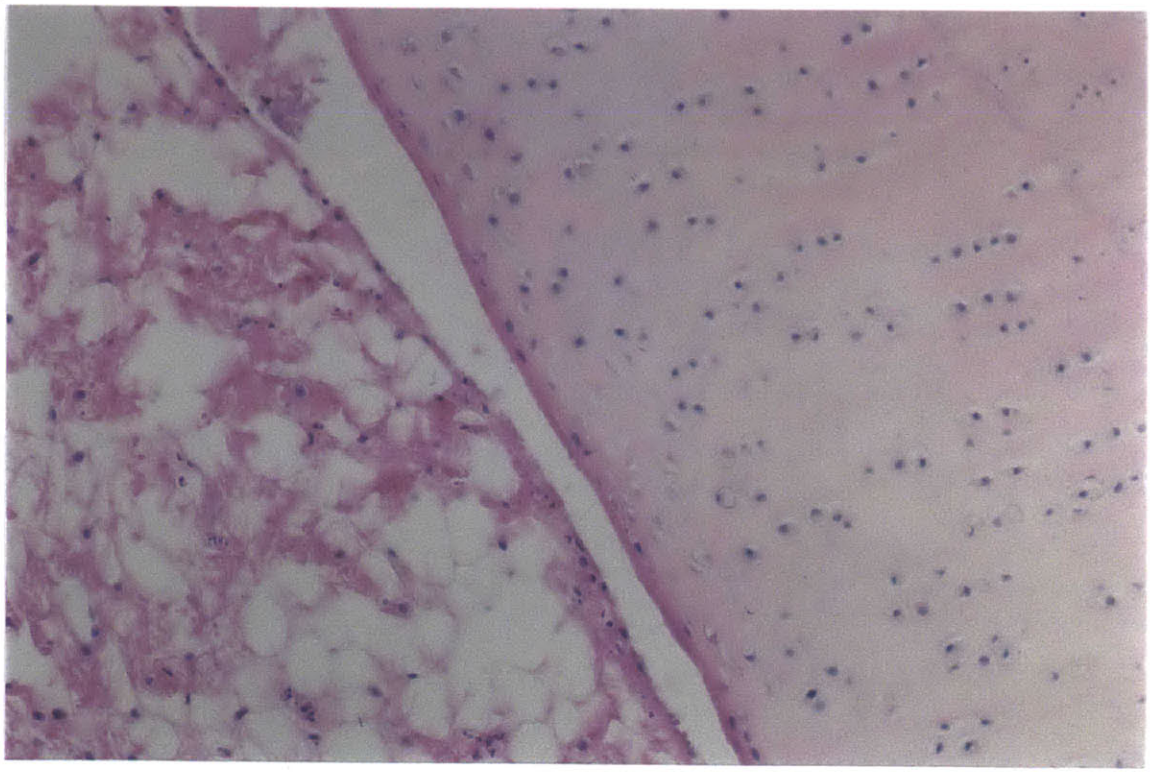

Figure 5.12: Synovium and cartilage ~140,000 RBE-cGy. H&E (a) 25X (b) 50X.

(a)

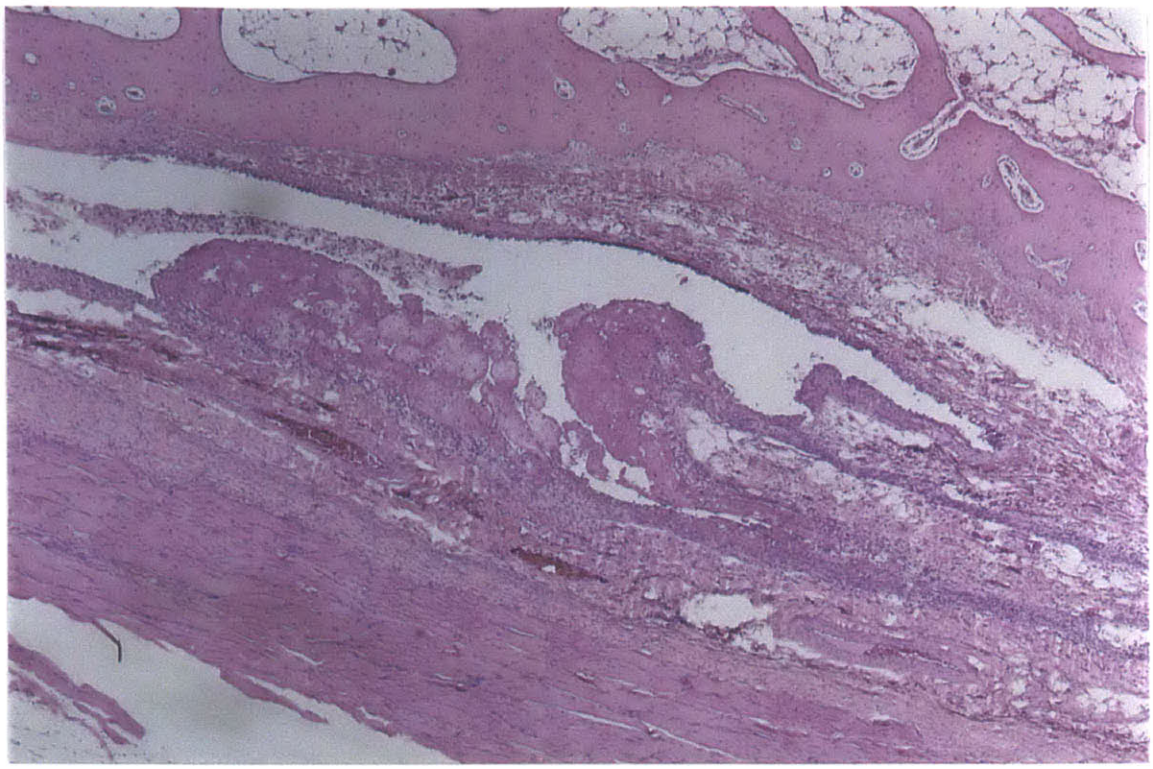

(b)

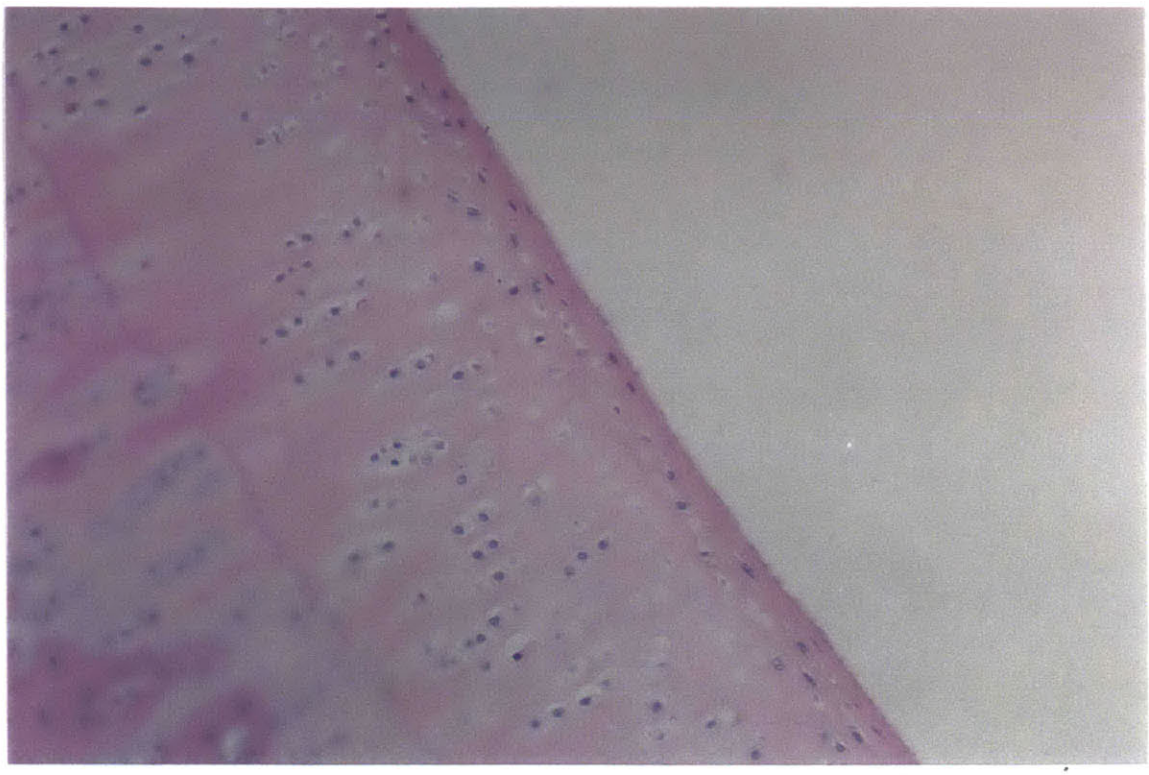

Figure 5.13: H&E of (a) synovium 10X and (b) cartilage 50X ~68,000 RBE-cGy.

5.2.3 Doses around 10,000 RBE-cGy

This section presents results observed in joints irradiated to doses around 10,00 RBE-cGy. The knee joints receiving doses of 13,000 and 12,000 RBE-cGy are shown in figures 5.14 and 5.15, respectively. Figure 5.14(a) shows synovium after delivery of a target dose of 13,000 RBE-cGy. The large oval-shaped fibrin mass emerging from the synovial-bone junction may be a large villus demonstrating coagulative necrosis; there are essentially no living cells in this mass which has a large number of red blood cells, perhaps indicating hemorrhage. The synovium lining the rest of the joint space showed a large increase in fibrin content, perhaps indicative of tissue damage (fibrinogen is exuded by capillaries into the surrounding tissue to be later converted into fibrin as part of acute inflammatory response). There was a marked decrease in both the number and size of the synoviocytes in the synovial tissue. Figure 5.14(b) shows a section of femoral cartilage; there is degradation on the surface and the cells seem to pyknotic. There is no evidence, however, of karyorrhexis. The extent to which degradation is brought about by the irradiation, as opposed to being a result of the arthritic condition alone, is unclear. The light pink piece of tissue which is also amorphous in shape could be fibrin residue from the synovial fluid.

Figure 5.15(a) shows the base of a similar synovial villus that was shown in figure 5.14(a) after delivery of a similar dose, 12,000 RBE-cGy. There is no dense accumulation of inflammatory cells, as could be expected based on literature [Dumonde and Glynn 1962] and morphology of the tissue. However, on the left, synoviocytes appear to be infiltrating the villus. Figure 5.15(b) shows both patellar (left) and femoral (right) cartilage. The patellar cartilage is unhealthy, with a layer several microns thick containing empty lacunae and eosinophilic debris. The patellar cartilage, in both the controls and treated animals, has shown a consistently poorer state, making conclusions difficult. The femoral cartilage has little evidence of necrosis or degradation, especially when viewed at higher magnification.

Thus, delivery of target doses of 12,000 RBE-cGy and 13,000 RBE-cGy resulted in significant ablation of synovial tissue. The level of effect on synovial tissue was similar to that achieved with doses much higher than 10,000 RBE-cGy, while the degree of cartilage damage was less than with the higher dose.

5.2.4 Doses less than 10,000 RBE-cGy

This section examines the results following irradiation to synovial target doses of 6,500 and 6,200 RBE-cGy, as well 3,600 and 1,400 RBE-cGy, completing the range of doses tested in this study. Figure 5.16 shows the space between femur and patella for the rabbit joints treated to a target dose 6,500 RBE-cGy. Synovial folds can be seen in part (a) of figure 516. The folds are less densely populated by inflammatory cells than would be expected from the active nature of the synovium. In part (b) of figure 5.16, the lining of the villus is less dense and in some areas incomplete. It appears that this level of radiation has caused a reduction in the number of synovial inflammatory cells. This does not exclude the possibility that these areas were highly acellular and the cells there represent inflammatory cells recruited as part of the response to the tissue necrosis which is enabled by the presence of capillaries. However, the drastic examples of radiation-induced tissue necrosis achieved with previous doses, are not observed.

(a)

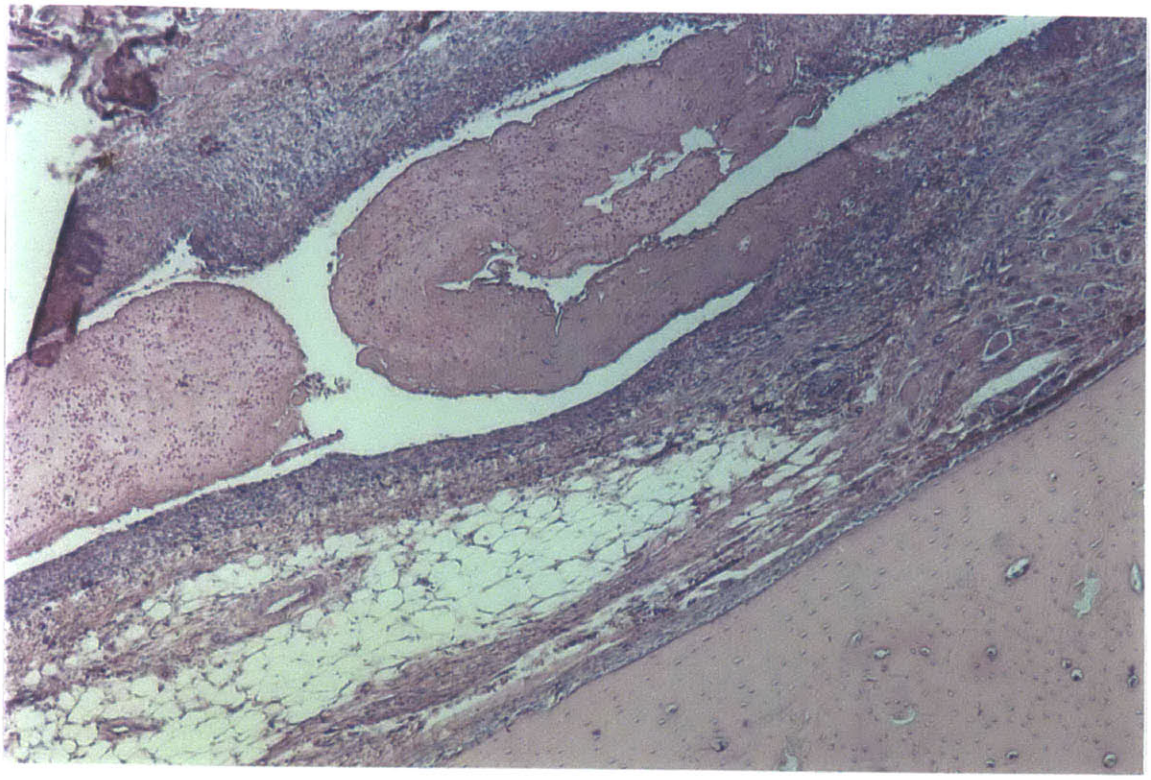

(b)

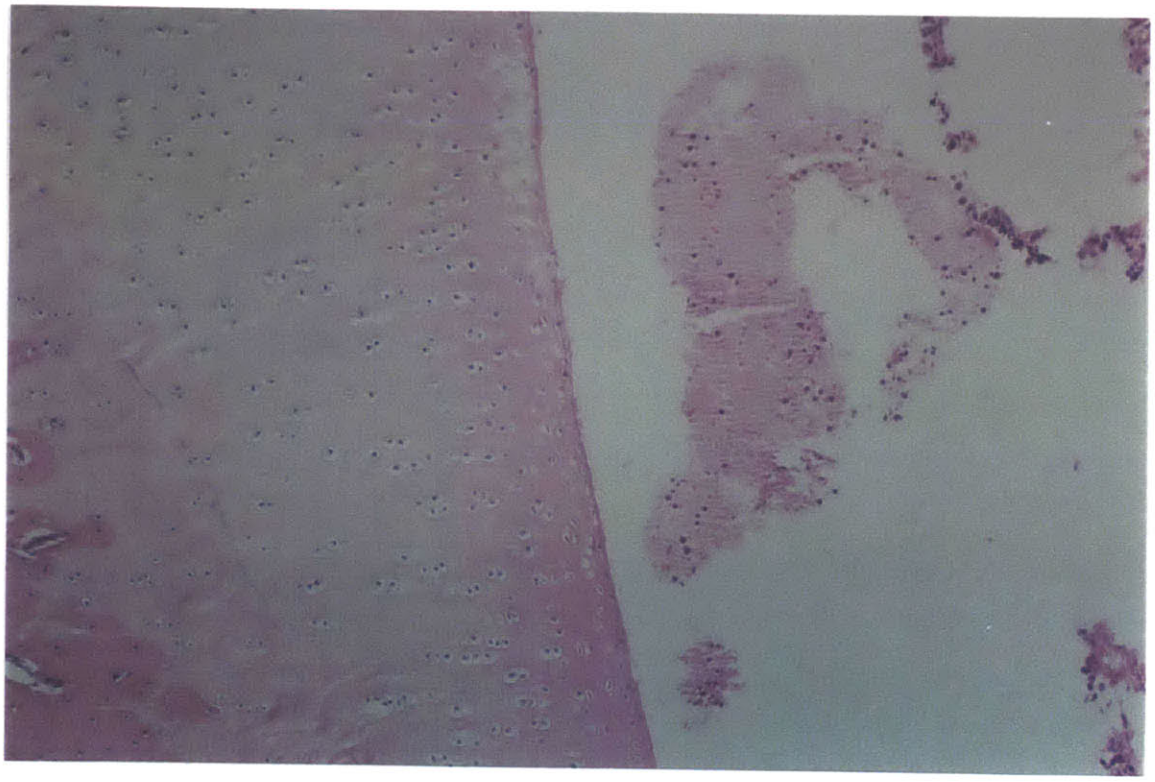

Figure 5.14: H&E of (a) synovium 16X and (b) cartilage 25X ~13,000 RBE-cGy.

(a)

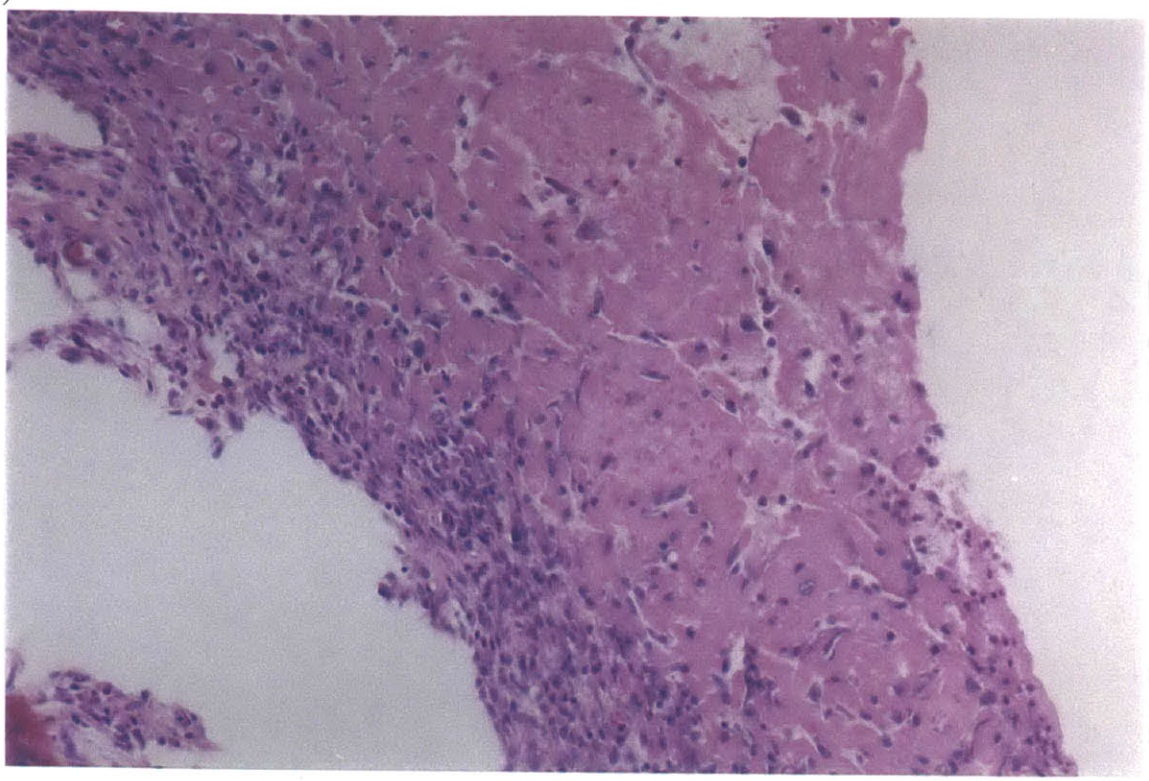

(b)

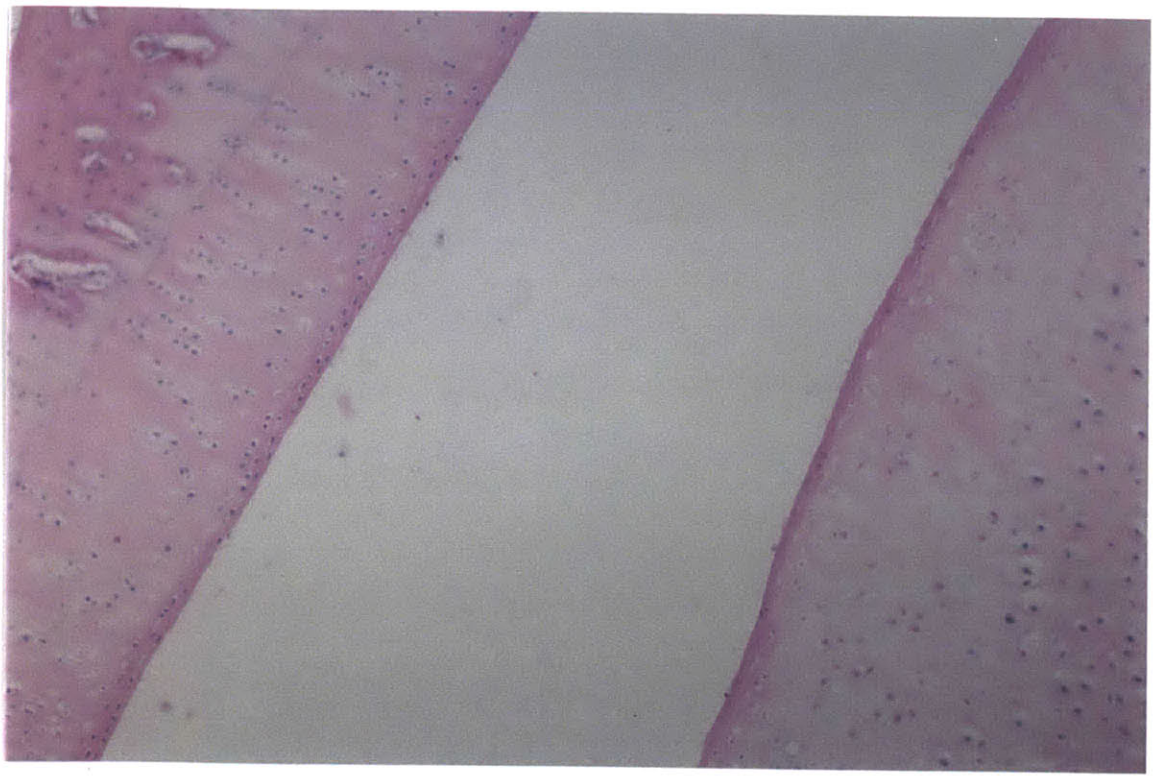

Figure 5.15: H&E of (a) synovium 50X and (b) cartilage 25X ~12,000 RBE-cGy.

The cartilage at the left of figures 5.16(a) and 5.16(b) shows no signs of necrosis. The cartilage which is being encroached upon by synovium can be characterized as degenerate, resulting from the arthritic condition. It is noteworthy that both joint cartilage surfaces on the side not being invaded by synovium do not exhibit necrosis.

A very different scenario emerges in the joint shown in figure 5.17(a) which received a synovial target dose of 6,200 cGy. The large adipose synovial villus has been ablated, as shown by the complete lack of cellularity throughout the tissue.The level of accellularity is the same as after irradiation to 140,000 RBE-cGy and the synovium in figure 5.17(a) closely resembles that shown in figure 5.12(a). On the other hand, the synovium in figure 5.17(b) does not show the same level of acellularity as figure 5.17(a), although they are the same type of synovium in relatively similar orientations. Given that the characteristics of the synovium in figure 5.17(b) are more similar to those seen in figure 5.16 (two joints) which received a similar target dose, it would seem that the gross acellularity shown in figure 5.17(a) is the discrepant joint. Such a discrepancy may have arisen from the mode of injection; perhaps the boron accumulated in this particular area with a greater concentration resulting in increased cell kill. Further experimentation would be required to determine whether doses of about 6,000 RBE-cGy consistently result in synovial ablation.

The cartilage in figure 5.17 shows varying degrees of viability. The articular cartilage, in (a), on the right shows necrosis in the superficial zone, while in (b), the cartilage is healthy. In figure 5.17(b), there may be evidence of subchondral erosion of cartilage, an example of bidirectional cartilage degradation, from "above" and "below"; the bone marrow nearest to the joint loses hematopoietic cells, develops an inflammatory infiltrate and activates two types of multinucleated cells, called osteoclasts and chondroclasts, which erode bone and articular cartilage, respectively [Freemont 1995]. No cause for this type of subchondral lesion was reported.

Synovium and cartilage following the delivery of 3,600 RBE-cGy to the synovium are shown in figure 5.18. The villus shown in figure 5.18(a) has a less thick synovial lining than, for example, the control in figure 5.10. The layer of synovium over the periosteum is only about 1 to 3 cells thick, the same layer as in a non-arthritic rabbit. There are no visible areas of tissue necrosis. This is reminiscent of results obtained upon a single dose of 600 cGy from an external x-ray source; 2 days after treatment, the synovium was reported as smooth and slightly edematous with some immature fibroblasts and "slight focal infiltration of plasma cells, rarely lymphocytes" [Steffen et al 1982]. No necrosis was reported but rather a diminution of inflammatory state of the synovium, as in figure 5.18. Figure 5.18(b) shows articular cartilage which is comparable in state to control cartilage.

Figure 5.19 shows sections of (a) synovium and (b) articular cartilage taken from the joints given a synovial target dose of 1,400 RBE-cGy. The synovium, covering the femoral periosteum, has a moderately dense cellular infiltrate and has the appearance of arthritic synovium. Overall there was a decrease in the density of the inflammatory cell infiltrate and in the thickness of synovial lining when compared to arthritic controls. No signs of necrosis are present, which implies that synovial ablation (as defined by tissue necrosis) was not achieved. Comparison of the periosteal synovium in 5.18(a) and 5.19(a) shows that the synovium is thicker and slightly more infiltrated with inflammatory cells, suggesting a dose-dependent response. The cartilage, shown in figure 5.19(b), has the normal appearance similar to the control cartilage in the arthritic controls.

(a)

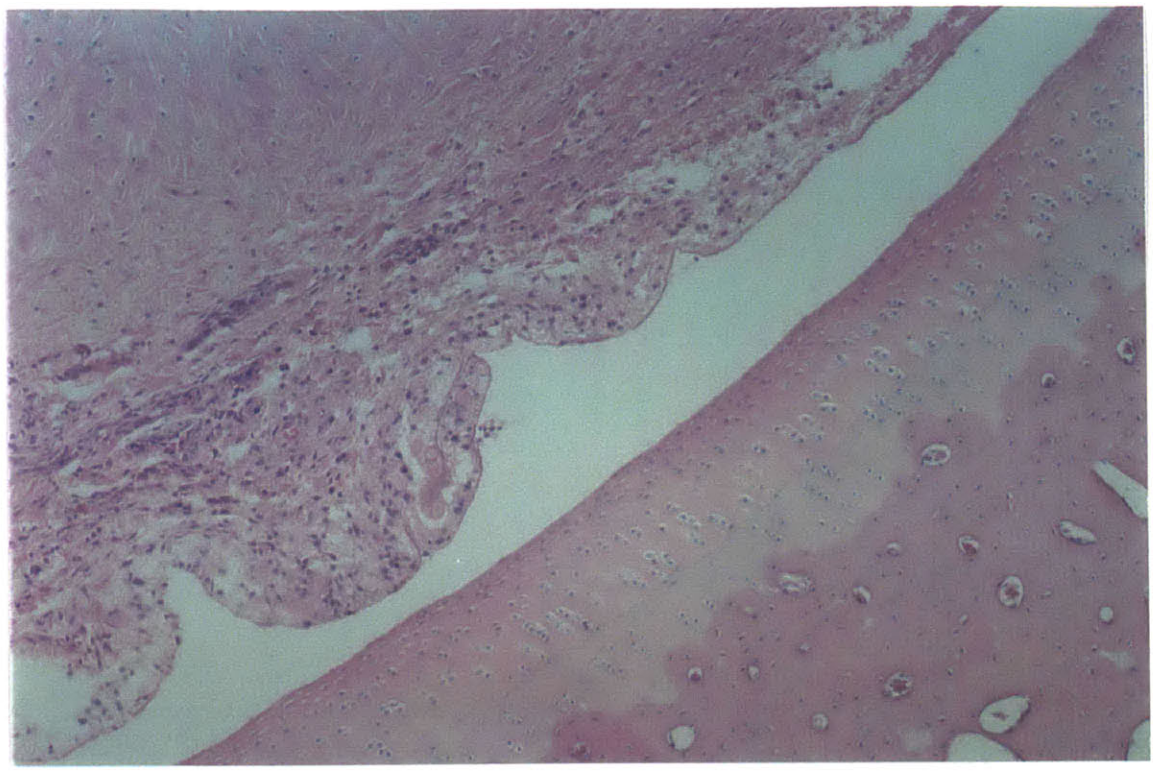

(b)

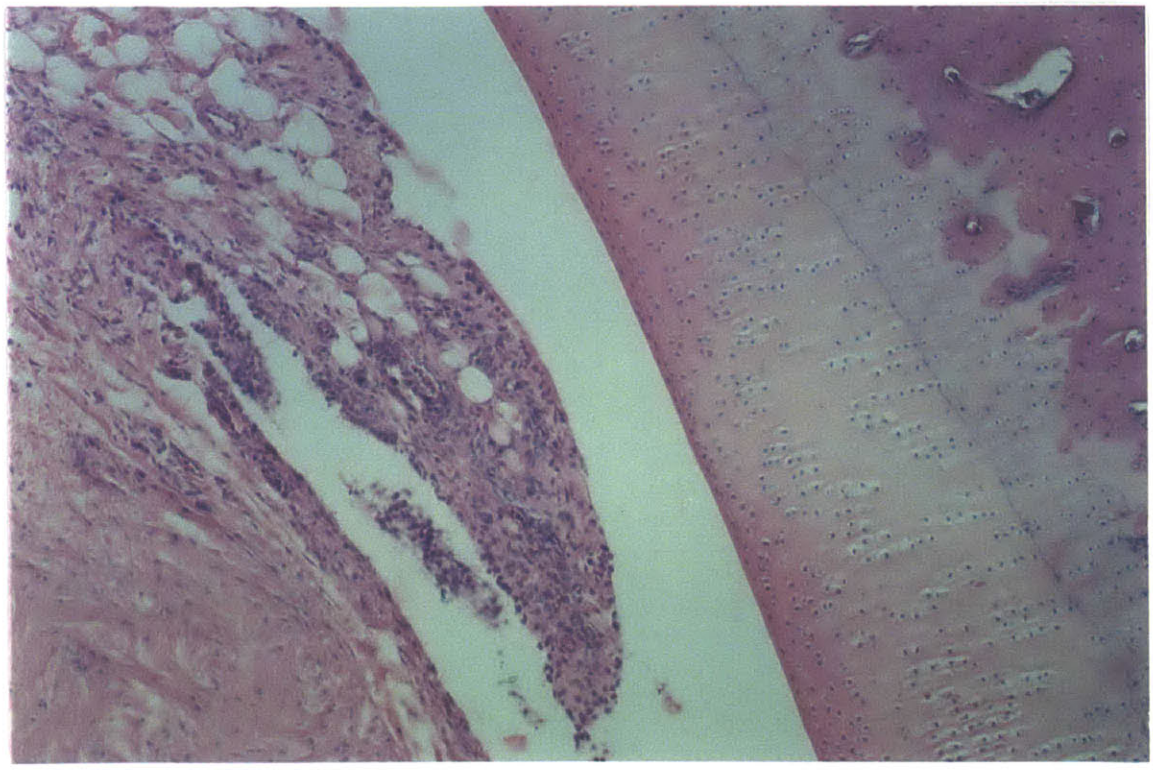

Figure 5.16: Synovium and cartilage ~6,500 RBE-cGy. H&E 25X.

(a)

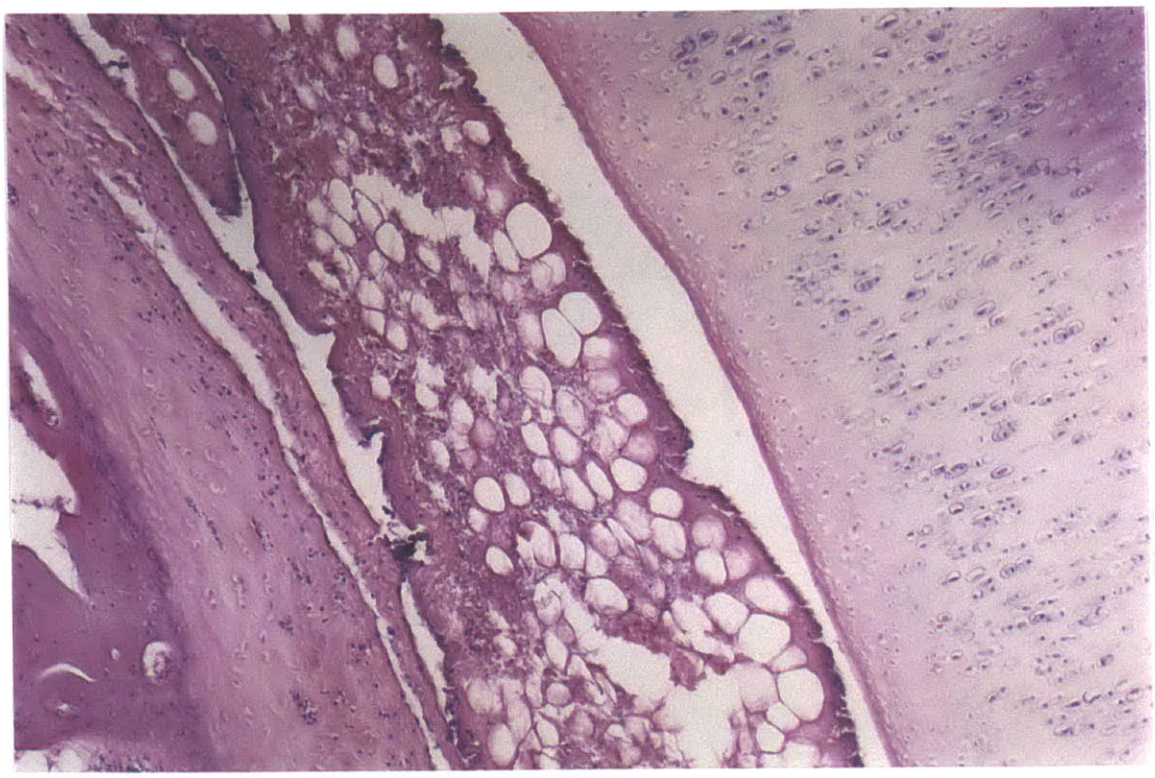

(b)

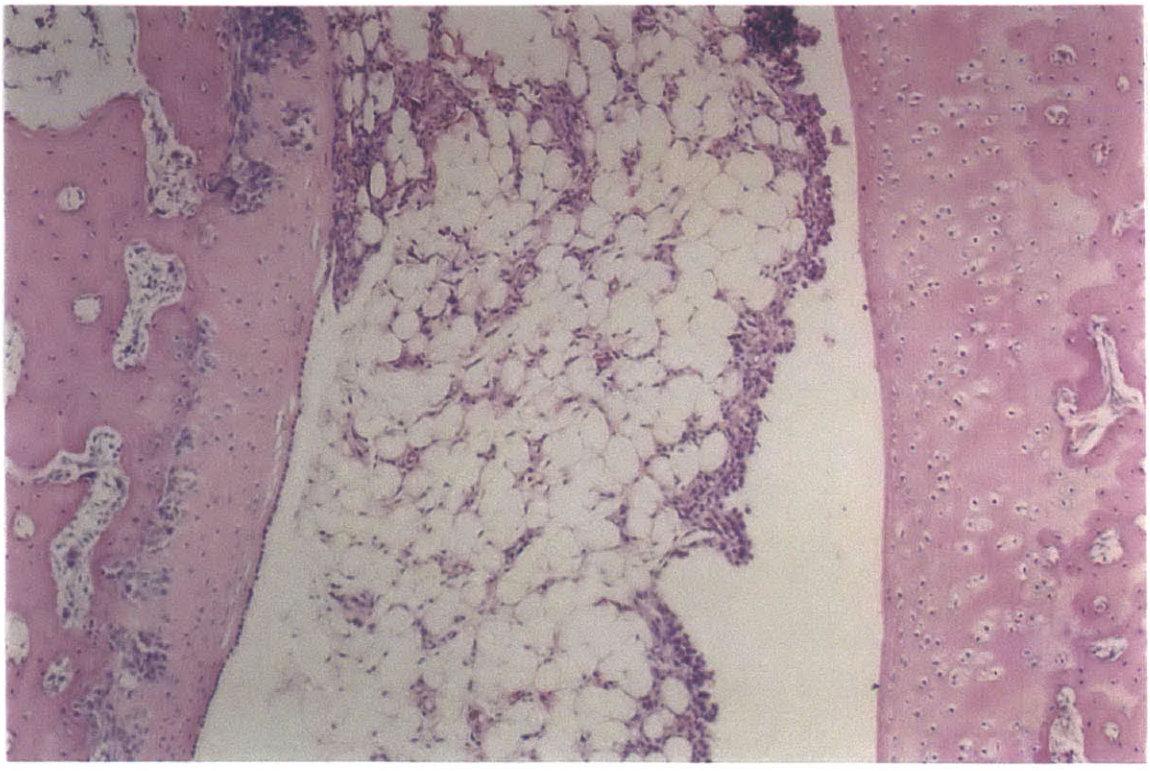

Figure 5.17: Synovium and cartilage ~6,200 RBE-cGy. H&E 25X.

(a)

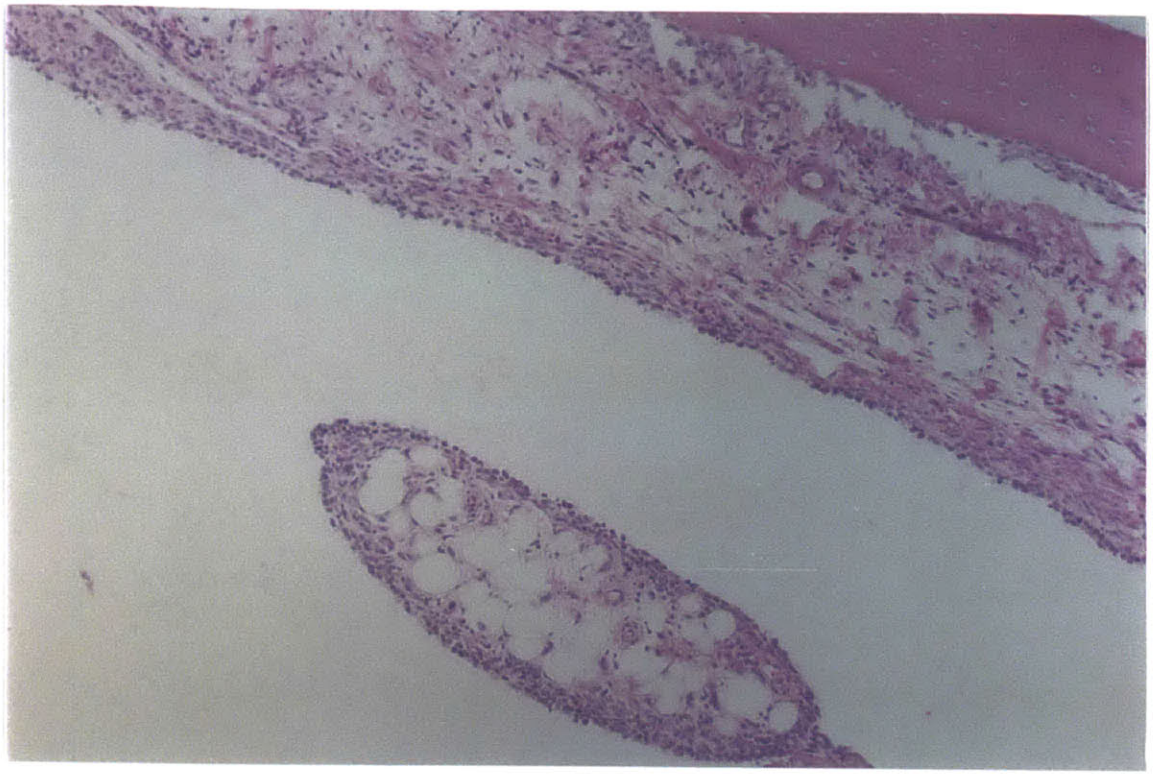

(b)

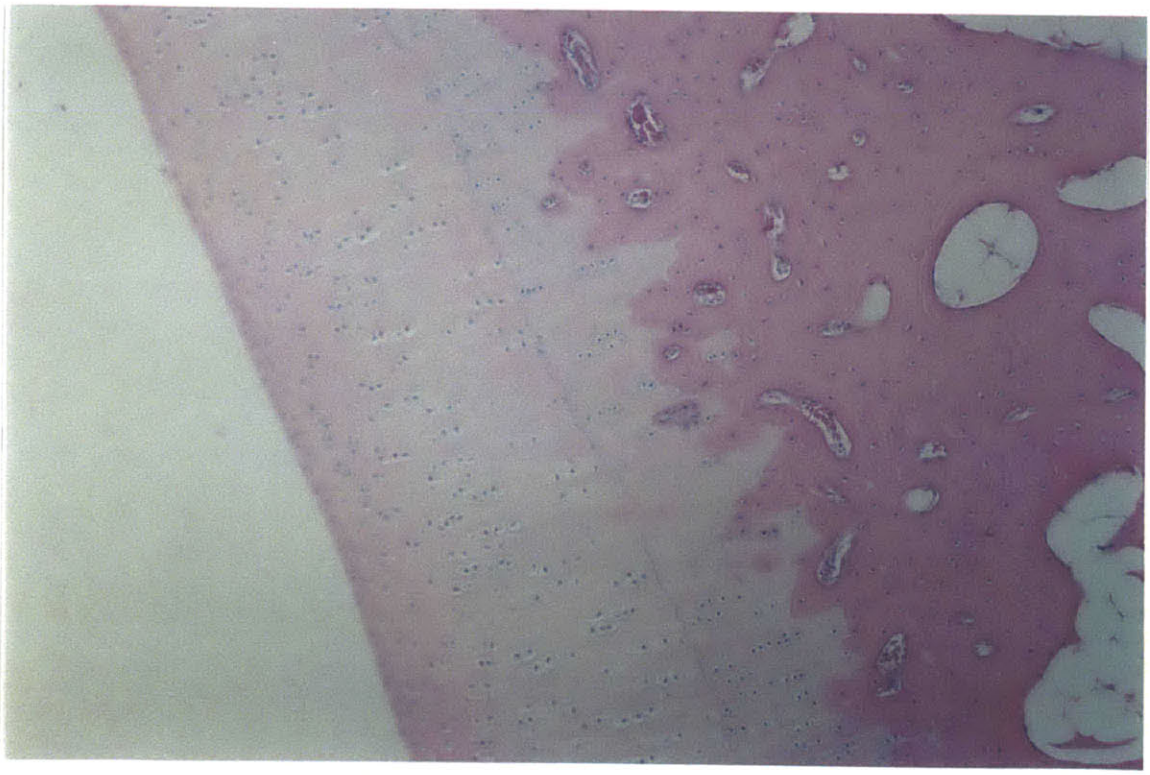

Figure 5.18: H&E of (a) synovium 25X and (b) cartilage 25X ~3,600 RBE-cGy.

(a)

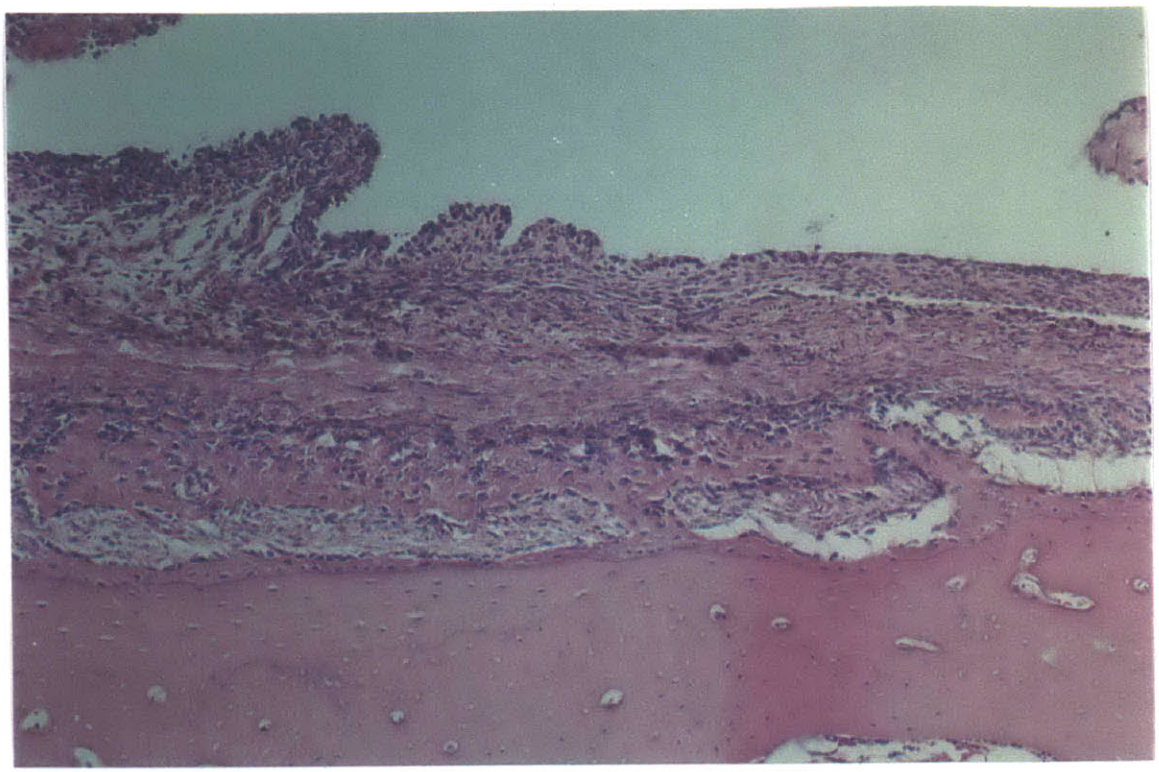

(b)

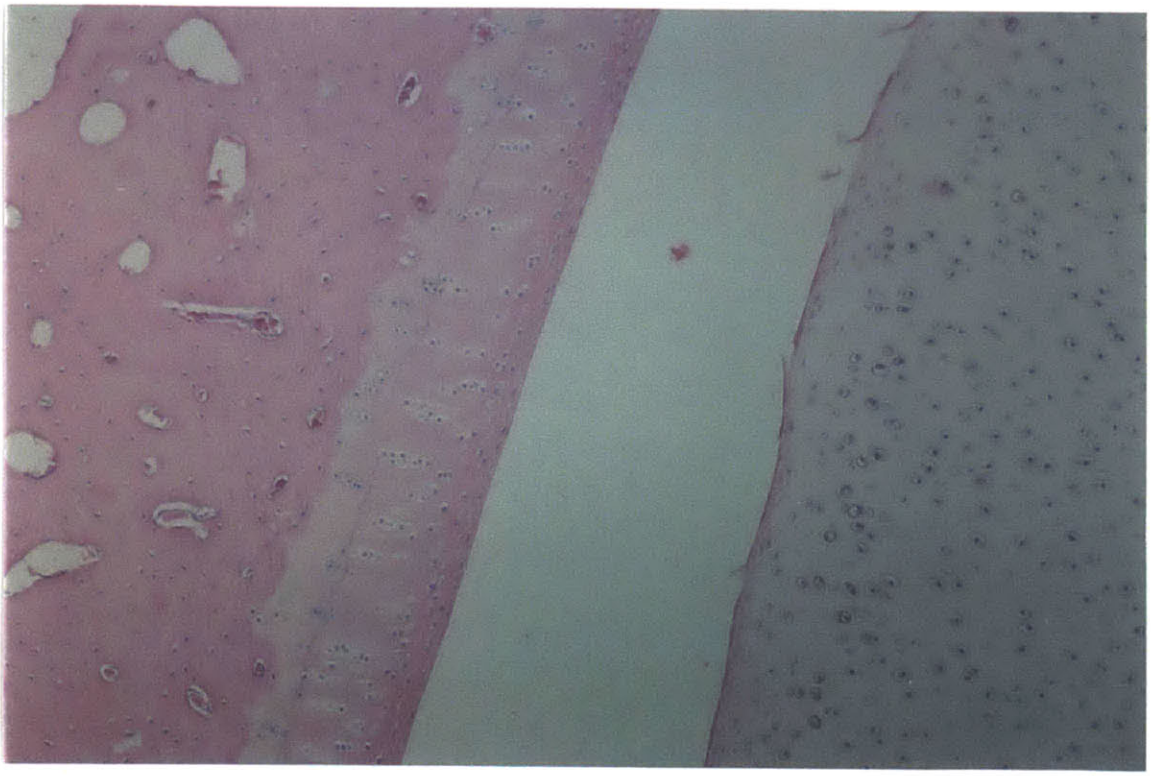

Figure 5.19: H&E of (a) synovium 25X and (b) cartilage 25X ~1,400 RBE-cGy.

Although these last two lower doses did not result in necrosis but rather a decrease in the density of the inflammatory cellular infiltrate, as well as in lining thickness, they may have a beneficial effect in controlling inflammation, particularly the 3,600 RBE-cGy. BNCS at low doses may be able to act as an anti-inflammatory agent rather than as a means of synovectomy. As such, it may have the benefit of avoiding some of the potentially severe side effects associated with many of the strong anti-inflammatory agents. However, the practicality of this would depend on many aspects, including how long the effect lasted, since repeated irradiations, which are not usually recommended for otherwise healthy patients, may be necessary.

5.3 Conclusions

The results of the study described in this chapter show that arthritic synovial tissue can be ablated non-invasively via BNCS. A large range of synovial target doses was tested, from 1,400 RBE-cGy to 140,000 RBE-cGy. Delivery of target doses around 10,000 RBE-cGy, and higher, resulted in synovial necrosis. Doses around 6,000 RBE-cGy caused a large reduction in the inflammatory cell infiltrate in all cases except one where substantial synovial necrosis was also observed. It is unclear whether the existing infiltrate consisted of original lymphocytes, or ones recruited due to tissue damage. Delivery of doses around 3,600 RBE-cGy seemed to have an anti-inflammatory effect, while a dose of 1,400 RBE-cGy only slightly reduced the thickness of the synovial lining. Neither injection of compound alone nor neutron irradiation alone caused necrotic changes to the synovium, thereby allowing the attribution of cellular kill to the boron neutron capture reaction.

It should be noted that doses were based on an average synovial concentration of 19,000 ppm which has been readily achieved in uptake studies in vivo. The range of uptake, however, is quite large and, based on this variation, there could be a 27% to 39% difference between the target dose and actual dose delivered to certain areas of the synovium. The potential error resulting from the neutron yield used for the ^{9}Be(d,n) reaction, in addition to the lack of angular information, may be as high as 24%. The combination of these two sources of error leads to a potential error of up to 46%.

BNCS effects on cartilage were difficult to evaluate, particularly due to the nature of the antigen-induced arthritis. The patella consistently showed increased levels of degradation and necrosis in control and treated joints while femoral cartilage showed signs of damage following irradiation to synovial doses higher than 10,000 RBE-cGy. The degree of damage decreased with decreasing dose; by a dose of 1,400 RBE-cGy, there was no cartilage damage due to irradiation.

KBH has proven to be a useful compound for the experimental testing of synovectomy. However, it is by no means implied that this is an appropriate compound for clinical BNCS. Steps at the determination of the usefulness of KBH for humans should include toxicity testing to determine the maximum concentration and/or amount injectable in humans and biodistribution studies in human joints of, for example, RA patients about to undergo knee replacement.

The search for an ideal compound, one which would selectively accumulate in the synovium alone for long periods of times and in sufficient quantity, should continue. Such a compound would allow a completely selective method of non-invasive destruction in relatively short therapy time. The greater the concentration of boron in the synovium, the less dose to surrounding healthy tissues. The next chapter presents investigations into compound screening via prompt gamma neutron activation analysis.

6. In vivo prompt gamma neutron activation analysis

Several boronated compounds are under development for BCNS. Full in vivo characterization of synovial uptake of a boron compound requires the sacrifice and dissection of several rabbits since various times need to be tested in order to determine the time of optimal synovial uptake. A means of non-invasively evaluating compound residence time in a joint could be an important compound screening tool for BNCS. Performed on a living animal, in vivo prompt gamma neutron activation analysis (IVPGNAA) could be used to yield information about the residence time of a boronated compound in the joint and enable the elimination of some compounds at an early stage, as well as help to narrow down the range of useful time points to test with dissections. There are two approaches to the use of IVPGNAA based on the size of the neutron beam: one is to use a large beam, while the other entails the use of a very narrow beam. Investigations of these two approaches are described in 6.1 and 6.2, respectively.

6.1. Experimental testing of the MITR PGNAA facility

The PGNAA facility described in 3.1.1 was used to experimentally test the potential of a broad beam for IVPGNAA. Experimental testing was performed at the existing PGNAA facility at the MITR [Riley and Harling 1998]. Several issues arise in the evaluation of IVPGNAA for BNCS using a broad beam, including boron movement in the joint during measurement, spatial profile of the beam, as well as detector solid angle. The knee joints of arthritic rabbits range from 2.5 to 2.8 cm in diameter, larger than the beam (2 cm in diameter). The beam has a cosine-shaped profile, rather than a flat one, which will result in varying intensity over the joint. Finally, the detector is close to the rabbit knee which may result in significant difference in signal due to the solid angle subtended by the detector.

Given a reliable measurement of average concentration (relatively uniform $^{10}B/^{1}H$ ratio), it should be noted that this does not distinguish whether the compound is in the synovium, synovial fluid, muscle at any specific site in the joint. Hence, although a high average concentration may be seen, all of the compound could be in the synovial fluid rather than synovium. Conversely, although a low average joint concentration may be seen, the majority of the compound remaining in the joint could be in the synovium.

This section (6.1) will present the experimental work done to address the issues involved in the evaluation of IVPGNAA at the MITR, including the construction of a rabbit stand to fit within the MITR PGNAA facility and a preliminary rabbit trial. An evaluation criterion was developed in

order to try relating IVPGNAA results to results of dissection studies. The construction of several calibration curves and development of a rabbit phantom to test the variation in signal as a function of boron position within a rabbit joint will also be described. After experimental testing of the facility, it became apparent that major modifications to the facility might be necessary for robust IVPGNAA measurements. In order to test the potential benefit of the proposed modifications, MCNP simulations were performed. The following subsections describe in detail the steps involved in evaluation of the potential of broad beam IVPGNAA as a boron compound screening method.

6.1.1 Construction of rabbit stand

Before the experimental testing of the MITR PGNAA facility could begin, a rabbit stand, small enough to fit into the facility's sample cavity but large enough for a rabbit (length: 16" body and 4" head, width: 7-8") had to be constructed. The stand was made of 1" polyethylene sheeting which was already available in the lab. Although polyethylene is hydrogenous, leading to high background (generally not desirable), the hydrogen would be comparable to or less than the amount of hydrogen background resulting from the rabbit body. The part of the stand holding the rabbit knee, i.e. the knee positioner, was made of teflon, since this would be directly in the beam and too much additional hydrogen signal would be generated if the positioner were made of a hydrogenous material such as polyethylene.

Figure 6.1(a) is a view from the top looking down on the neutron beam as it is coming out of the 4DH3 beam port. The area around the neutron beam is enclosed by lead bricks on three sides and a concrete wall of the reactor shielding on the fourth side. The lead bricks are 22" high on the right and bottom of the drawing, and 16" high on the left. A 16" by 8" slab of polyethylene was cut to hold the body of the rabbit, while a thin light piece of aluminum sheeting was taped to the stand and used as a head rest. In this polyethylene slab, a 4" by 4" hole was cut for the rabbit leg as shown in Figure 6.1(a). Figure 6.1(b) shows a side view of the experimental set up and the very simple three slab geometry used to make the rabbit stand. Two polyethylene slabs were cut as legs and placed on the ends of the top slab supporting the body of the rabbit. Tape marks were made on the walls of the sample cavity in order to consistently reposition the stand in the same place each time.

Dimensions for the stand are given in Figure 6.2(a). A set of alternative legs (1" shorter) were made to accommodate smaller rabbits. The knee positioner was built to firmly lodge the knee in front of the detector. It was made from a piece of solid teflon rod 6" tall and 3" in diameter, screwed into a polyethylene slab which extended from one end of the stand to the other and is denoted as the positioner support. As shown in the schematic in Figure 6.2(b), a groove was cut down through the teflon rod and a notch, corresponding to the center of the detector and center of the beam, was made for the knee of the rabbit. The positioner support was screwed in between the two leg slabs. Straps were used to secure the rabbit onto the stand and to secure the knee into the notch (although by design, the knee was firmly wedged into the notch).

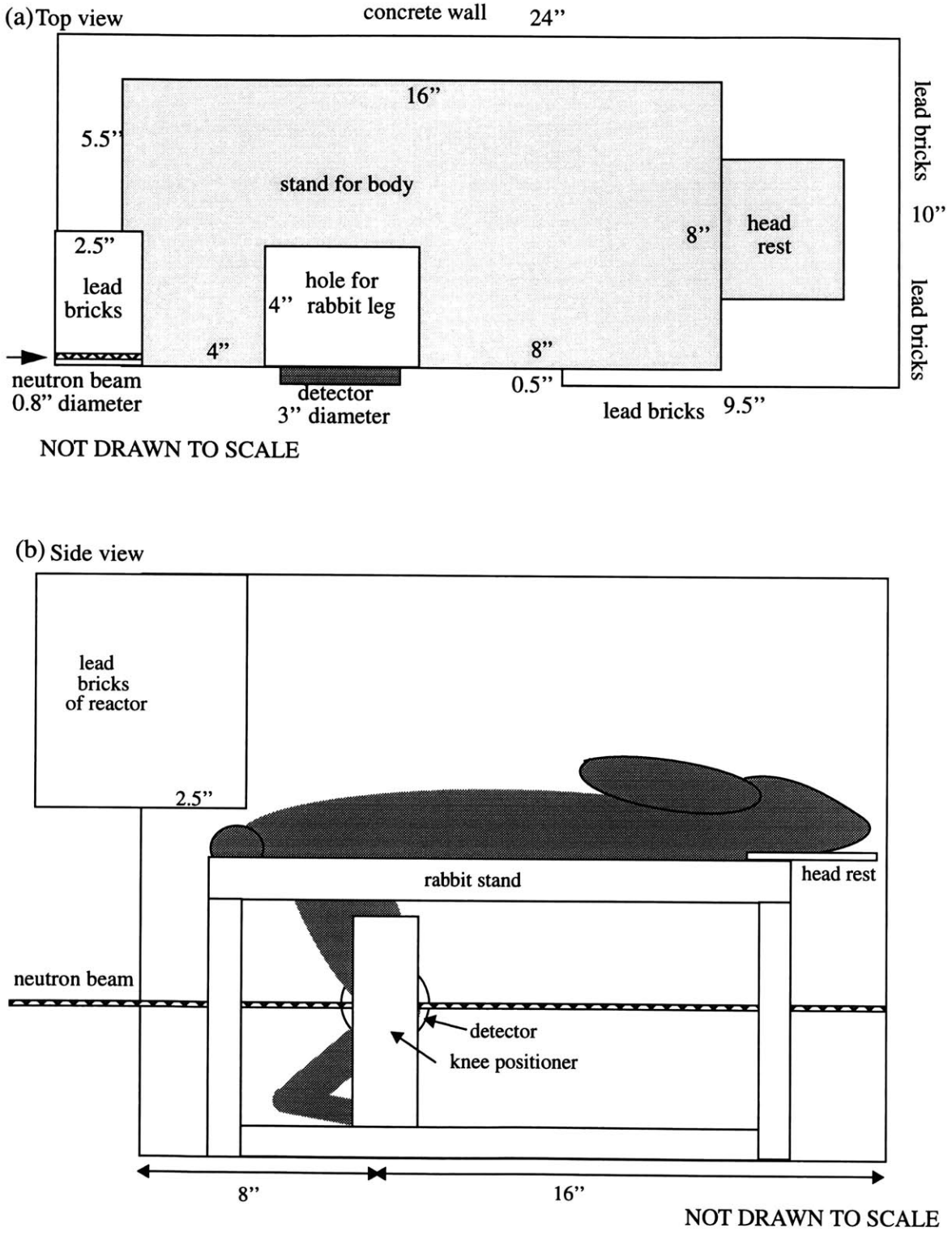

Figure 6.1: Experimental setup: (a) top view of MITR PGNAA facility with proposed rabbit stand in place; (b) side view of the same

(a) rabbit stand

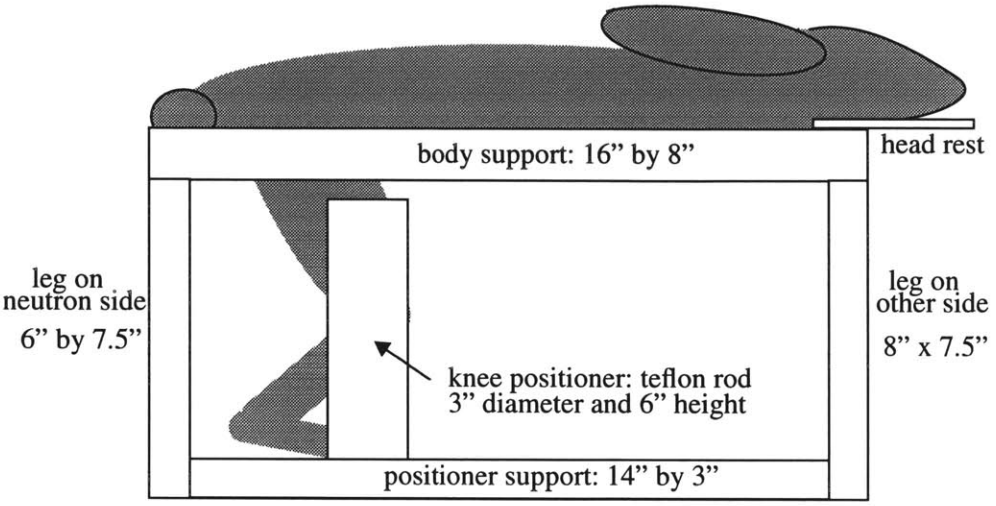

NOT DRAWN TO SCALE

(b) knee positioner

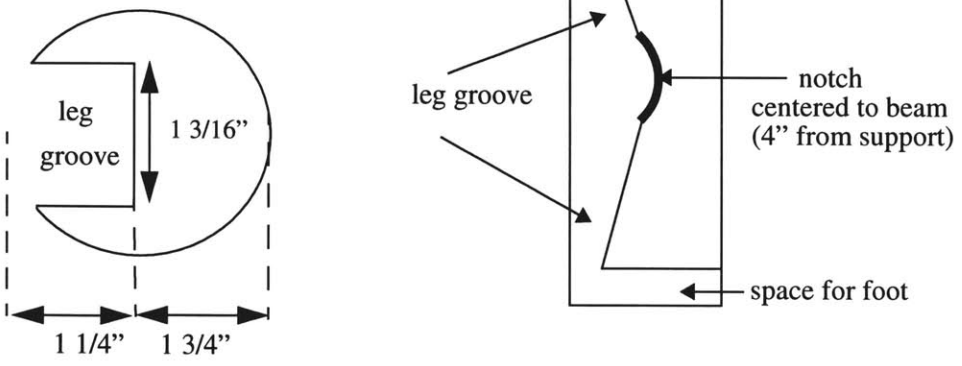

i) top view

ii) cut out from side

NOT DRAWN TO SCALE

Figure 6.2: Rabbit stand: a) side view with dimensions; b) knee positioner.

6.1.2 Determination of incidental dose to rabbit knee

To determine the incidental dose to the rabbit knee joint from an IVPGNAA session, the Monte Carlo for N-particle Transport simulation code [Briesmeister 1986] was used. As a rabbit knee model, the human knee joint model presented in section 2.3.1 was scaled by a factor of 20. A monodirectional and monoenergetic (0.015 eV) neutron source was assumed to be uniformly emitting from a plane with a flux of 5.34×10^7 n/sec (2 cm diameter source with 1.7×10^7 n/cm^2/sec at sample position). The particle flux was determined as a function of depth for all components and then modified by fluence-to-kerma conversion factors, listed in section 2.3.1. Results were obtained in units of cGy/min and then calculated for 10, 30 and 60 min irradiations to yield the total amount of dose potentially received by the rabbit joint from irradiation for the specified times. The length of time that the rabbit joint is irradiated will depend on the length and frequency of the observation period desired, as well as the concentration of boron. If the concentration of boron is low, then longer counting time is required to achieve reasonable statistics, which may limit the frequency of observation or increase the length of the total irradiation time. For example, assuming that the desired observation time is 120 minutes and that the concentration of boron is high, then a counting time of 2 minutes may be enough for reasonable statistics. If one desired to obtain a measurement every 4 minutes, then a total of 20 measurements could be performed with a total irradiation time of 40 minutes. On the other hand, if the concentration were low, then, for example, 6 minutes may be required for reasonable statistics and 20 measurements will imply a total irradiation time of 120 minutes.

In addition to dose, the amount of activity, resulting from sodium activation during irradiations of 10, 30 and 60 minutes, was calculated. Calculations were performed in two ways. In the first way, the following equation for activity was used, i.e.

$$A = N\sigma\phi(1 - e^{-\lambda t})$$

where N is the number of sodium atoms, σ the thermal neutron capture cross-section (cm^2), ϕ the fluence (n/cm^2/sec), λ the decay constant (sec^{-1}) and t the time of irradiation (sec). The value for N was obtained by relying on the MCNP model previously described. In the model, sodium is found in the bone and articular cartilage (although it may be found in other parts of a living joint) which have volumes of 3.76 cm^3 and 0.63 cm^3, respectively. Using the respective densities of 1.92 g/cm^2 and 1.11 g/cm^2, the total weight of bone and articular cartilage was determined to be 7.72 g and 0.69 g. Then, using the mass fractions for sodium in both bone and cartilage (1×10^{-03} and 5×10^{-03}), the total mass of sodium was calculated to be 0.01 g. The final step to obtain the number of sodium atoms involved multiplying the mass, 0.01 g, by the number of grams per mole and multiplying by Avogadro's number. This yielded an N equal to 2.7×10^{20} sodium atoms. The value used for σ was 0.534×10^{-24} cm^2 [Turner 1986] and for ϕ was 1.7×10^7 n/cm^2/sec [Riley and Harling 1998]. In this way, the saturation activity ($N\sigma\phi$) was calculated to be 0.07 μCi. Then, using a λ of 15 hr^{-1} or 1.28×10^{-05} sec^{-1} [Turner 1986], the factor of $(1 - e^{-\lambda t})$ was calculated by varying the time from 10 to 30 to 60 minutes. Therefore, the activity was obtained via an analytical calculation (although the number of atoms was obtained from the MCNP model).

The second type of calculation relied on results of MCNP for the determination of reaction rate and activity. and the following equation was used:

$$A = (\gamma/n)(\phi)(\lambda)(t)$$

where (γ/n) is the number of photons per neutron, ϕ is the flux, 5.34×10^{7} n/sec (again calculated based on a fluence of 1.7×10^{7} n/cm^2/sec from a 2 cm aperture), λ is the same decay constant already described and t is the time of irradiation. The (γ/n) factor was obtained from the summary photon table by nuclide from MCNP which listed 5.83×10^{-05} as the photon weight from neutron captures in sodium. The time was varied from 10 to 30 to 60 minutes and results were compared to the other calculation.

Results of the MCNP simulations to determine the incidental dose to the rabbit knee joint are shown in table 6.1. Results were weighted with the RBE values listed in section 2.3.

Table 6.1: Simulated dose rates assuming 1,000 ppm ^{10}B

	bone (RBE-cGy/min)	cartilage (RBE-cGy/min)	synovium (RBE-cGy/min)	skin (RBE-cGy/min)
neutron	1.7×10^{-3}	1.8×10^{-3}	1.8×10^{-2}	6.4×10^{-2}
gamma	1.2×10^{-2}	1.2×10^{-1}	1.2×10^{-2}	2.5×10^{-2}
boron	1.1×10^{-2}	1.1×10^{-1}	1.2×10^{1}	4.2×10^{-3}
TOTAL	2.5×10^{-2}	2.3×10^{-1}	1.2×10^{1}	8.9×10^{-2}

As can be seen from the above table, the total dose to the synovium, assuming 1000 ppm ^{10}B in the synovium, is 12 RBE-cGy/min. For 10, 30 and 60 minute irradiations, the dose would be 120, 360 and 720 RBE-cGy, respectively. Considering that 10,000 cGy is the target dose delivered in radiation synovectomy using β emitters [Deutsch et al 1993], 720 RBE-cGy represents about 7% of the therapeutic dose. If boron uptake were higher, for example, 20,000 ppm ^{10}B, then, assuming a linear scaling, the boron dose rate could be as high as 240 RBE-cGy/min, implying that for 10, 30 and 60 minutes of irradiation, the dose delivered would be 2400, 7200 and 14400 RBE-cGy, which, in turn, would represent 24%, 72% and 144% of the therapeutic dose. The assumption of a linear scaling is likely to be pessimistic due to flux depression. As shown in section 5.1.1, dose does not scale with synovial boron concentration and the error in scaling linearly from 1,000 ppm to 20,000 ppm may be as large as 60% [Gierga 1999]. Application of this to the percentages of therapeutic dose calculated above results in a change to 14%, 43% and 86% of the therapeutic dose possibly delivered for 10,30 and 60 minute irradiations assuming 20,000 ppm for synovial boron concentration. Counting time may be reduced with a higher boron concentration and this may result in lower dose. However, it should be noted that, as was shown in chapter 5, even low radiation doses have an effect (albeit not necrosis) on the synovium, and hence it is recommended that a rabbit used in IVPGNAA not be used again for any type of irradiation study.

Results of the two types of sodium activity calculations are summarized in table 6.2. As can be seen, there is very little activity even for the longest irradiation time, i.e. less than 0.006 μCi for a 60 minute irradiation. It was therefore determined that the activity would be negligible and not an obstacle to the experiment.

Table 6.2: Calculation of potential ^{24}Na activity

Time of irradiation	Activity equation (μCi)	MCNP calculation (μCi)
10 min	$5.36x10^{-4}$	$6.46x10^{-4}$
30 min	$1.61x10^{-3}$	$1.94x10^{-3}$
60 min	$3.15x10^{-3}$	$3.89x10^{-3}$

6.1.3 Calibration curves with rabbit joint phantoms

This section describes attempts at obtaining calibration curves with standards comparable to a rabbit knee joint in diameter. To simulate an arthritic rabbit joint, a 50 ml Corning polypropylene centrifuge tube, 2.7 cm in diameter, was used. Several tubes were filled to the 15 ml mark with boric acid standards of the following ^{10}B concentrations: 0, 200, 300, 500, 750 and 1500 ppm. Each tube was centered in the knee positioner such that the fluid in the tube was in the knee notch. A calibration curve was constructed. The stand was then tilted in the horizontal plane such that one end of the stand was 1 cm farther from the plane of the detector and the calibration curve was reconstructed in order to quantify the effect of inconsistent stand positioning. This experiment was run at a reactor power level of 250 kW since a previous attempt at a power level of 500 KW resulted in detector deadtimes above the acceptable 20% and caused the boron and annihilation peaks to run into each other, thereby making it hard to get an accurate estimate of the area under the boron peak. Lower reactor power eliminated this problem.

A calibration curve (7 standards) with the stand in both the straight and tilted positions is shown in figure 6.3. Counting errors for both boron and hydrogen peaks were kept below 5% and are not included in the plot. A linefit to the B/H ratio, obtained with the stand in the straight position, yielded the equation $y=0.21 + 0.003x$, while when the stand was tilted the slope increased and the equation was $y=0.16 + 0.004x$. The differences between calibration curves for the straight and tilted stand are beyond counting error and are a result of the different stand geometry.

A notable aspect of both calibration curves is the large y-intercept, around 0.2. This could be a result of flux depression, yielding a lower $^{10}B/^{1}H$ ratio for the highest standard. The calibration curves were refitted in figure 6.4 without including the 1500 ppm ^{10}B standard in the curve. The measured points fit better on the dashed line representing the linefit and the intercept is closer to 0 in both cases. In these curves, the 1500 ppm ^{10}B sample appears to be off the line. It is unlikely that this is due to improper preparation since the calibration standard was remeasured with the regular PGNAA set up and yielded a ^{10}B concentration of 1500 ppm within counting error. Hence, it is more likely an indication of flux depression. The 1500 ppm ^{10}B boric acid standard, contained a total of 15 mg of ^{10}B and could represent the point at which flux depression becomes significant.

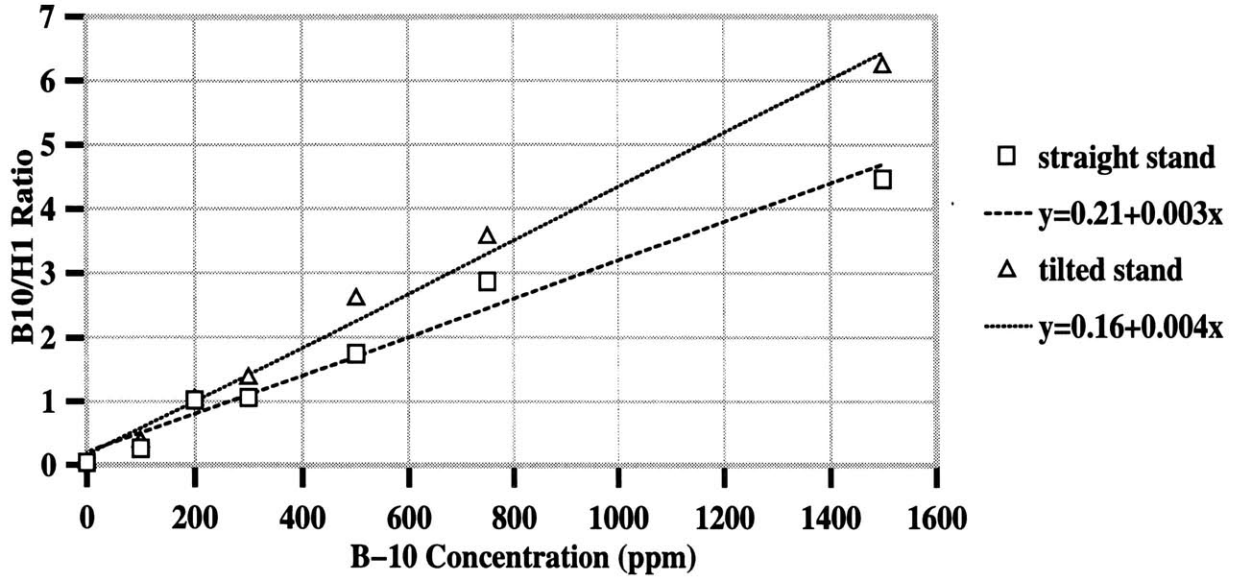

Figure 6.3: Calibration curves using rabbit knee joint phantom and different stand geometries.

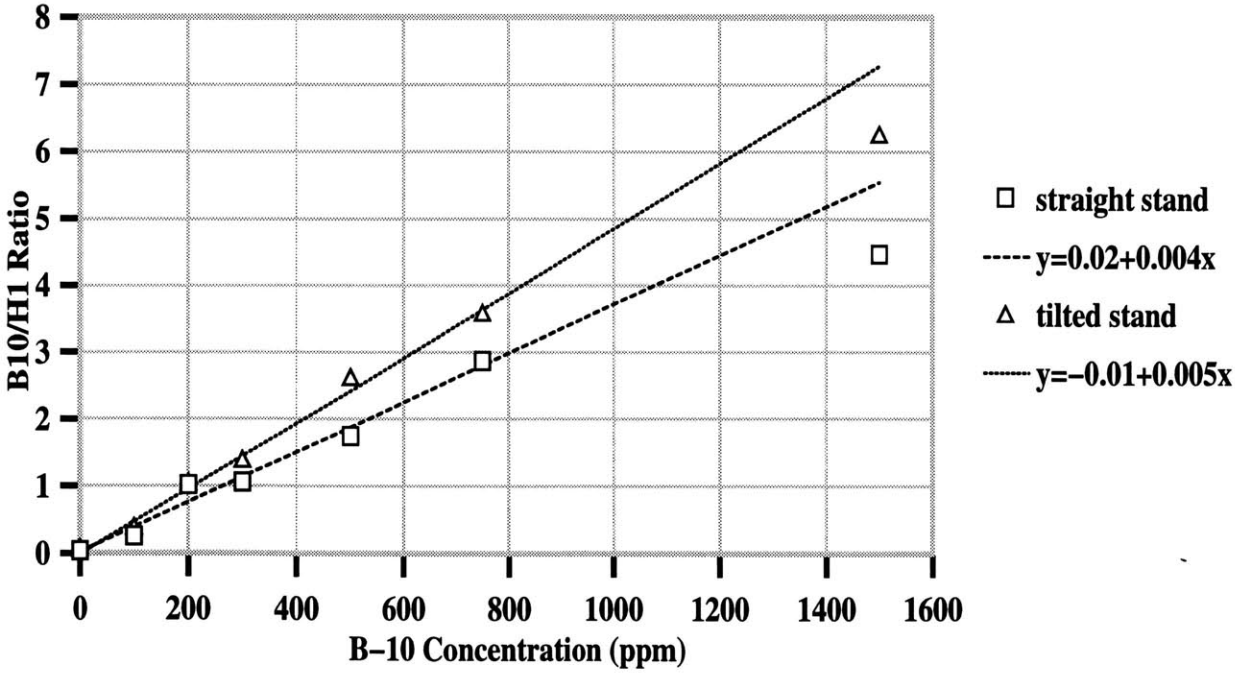

Figure 6.4: Calibration curves from figure 6.3 without the 1500 ppm ^{10}B standard in the curve fit.

The issue of flux depression was addressed by measuring the $^{10}B/^{1}H$ signal from a concentration of 11,500 ppm. An NMR pyrex glass tube (0.7 cm in diameter) was filled with a KBH solution of 150,000 ppm of ^{10}B. Since the beam aperture diameter was 2 cm, the volume of boronated fluid in the beam was 0.77 cm^3, with a total amount of 115,500 μg of ^{10}B. Dividing the total amount of boron by the total amount of fluid in the neutron beam (approximately 10 ml deionized H_2O), 115,500 μg/10 ml of H_2O in beam yielded 11,550 μg/g which is 11,550 ppm. The $^{10}B/^{1}H$ signal was measured and plotted in figure 6.5 with the straight stand calibration curve from figure 6.3. As can be seen from figure 6.5, the measured signal was lower by a factor of 4 from the signal expected from the calibration curve, which is based on a linear relationship between $^{10}B/^{1}H$ signal and ^{10}B concentration. These results suggest that with this particular setup and geometry, the curve is highly nonlinear at total boron amounts of 115 mg and lends support to the hypothesis that flux depression comes into play at approximately 15 mg. It is expected that measurement of additional boron concentrations between 1,500 and 11,500 ppm ^{10}B would confirm this trend.

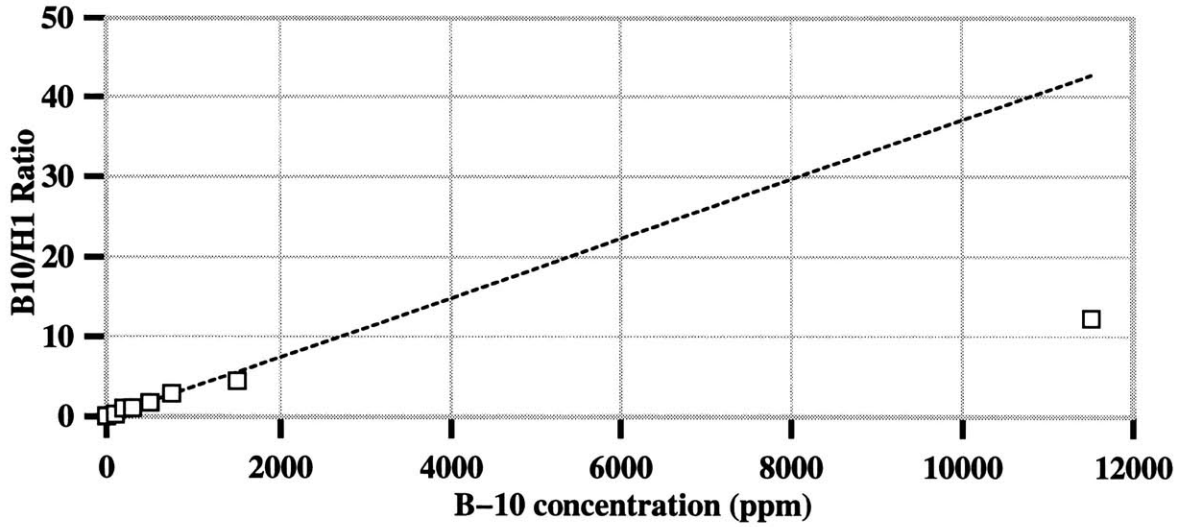

Figure 6.5: Extension of calibration curve showing pronounced effect of flux depression.

6.1.4 $^{10}B/^{1}H$ ratio as a function of position in a rabbit joint phantom

In order to test the variation in the $^{10}B/^{1}H$ ratio as a function of ^{10}B position across the rabbit knee joint phantom, a 50 ml centrifuge tube was filled with 0 ppm standard and positioned in the same manner as described above. A grid was constructed on top of the centrifuge tube and 9 openings were created for a smaller tube to pass through. A 0.7 cm inner diameter NMR glass tube was filled with several milliliters of 150,000 ppm ^{10}B in the form of enriched $K_2B_{12}H_{12}$ (KBH). In order to secure the NMR tube in an upright position in the 50 ml centrifuge tube, a hole (large enough to fit the NMR tube snugly) was made in a styrofoam cube. The 0.7 cm tube was thus placed through the hole in the styrofoam cube which then sat on top of the grid and into one of the 9 positions. This arrangement is shown in figure 6.6. A measurement was made and the $^{10}B/^{1}H$ ratio obtained. This was repeated for all nine positions of the grid.

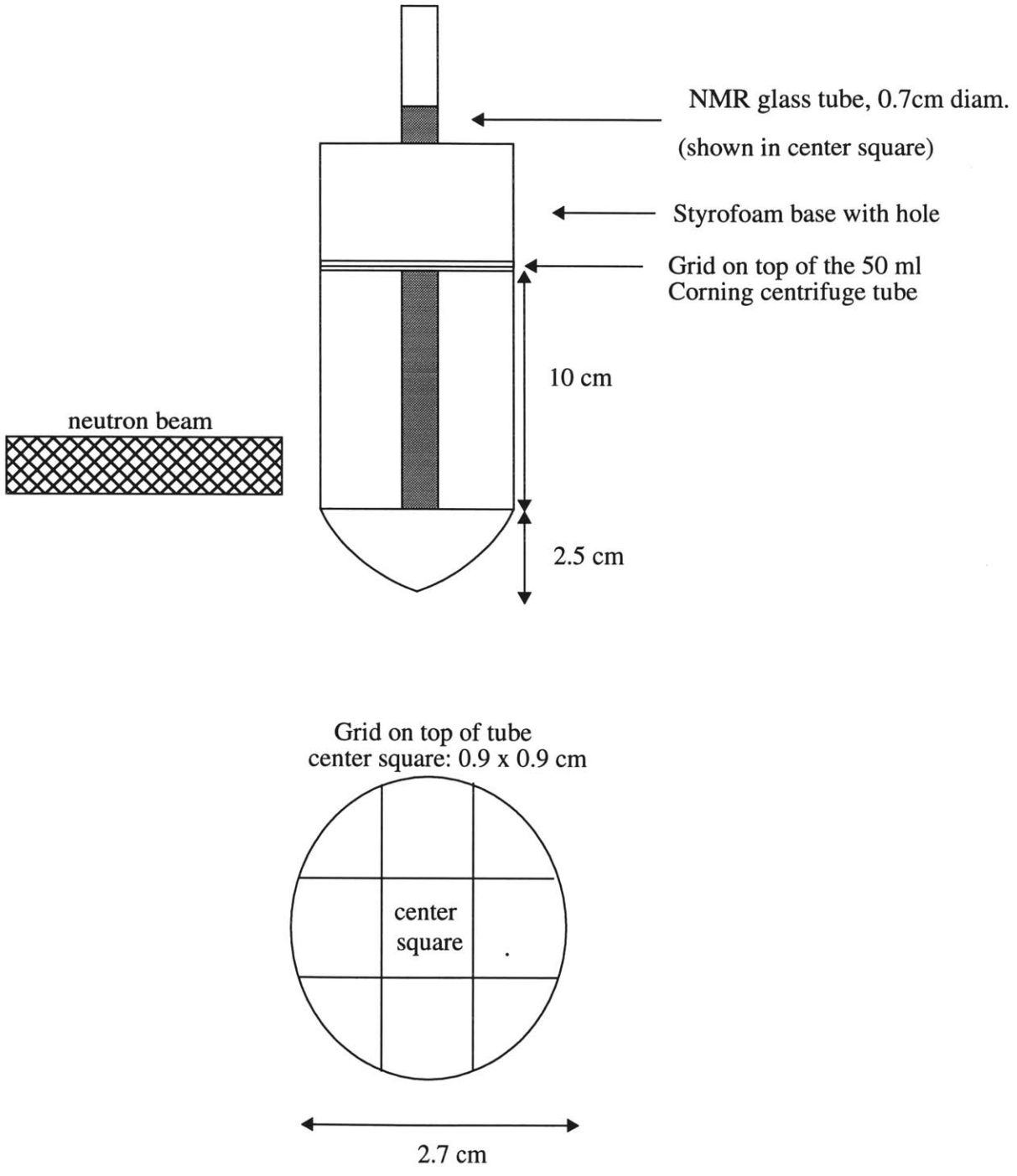

Figure 6.6: Schematic of apparatus for experimental testing of the variation in $^{10}B/^{1}H$ ratio as a function of position within the rabbit knee joint phantom.

The $^{10}B/^{1}H$ ratio was obtained for all 9 positions of the grid on top of the 50 ml centrifuge tube with the stand in both straight and tilted positions, as shown in figure 6.7. Measurement errors for both the boron and hydrogen peaks were maintained below 3% for all positions. The maximum difference in $^{10}B/^{1}H$ ratio in the straight stand geometry was 9.2 (12.2 - 2.98) or a factor of 4.1 (12.2/2.98). In the tilted stand geometry, the maximum difference in the $^{10}B/^{1}H$ ratio was 20.5 (24.2 - 3.75) or a factor of 6.5 (24.2/3.75).

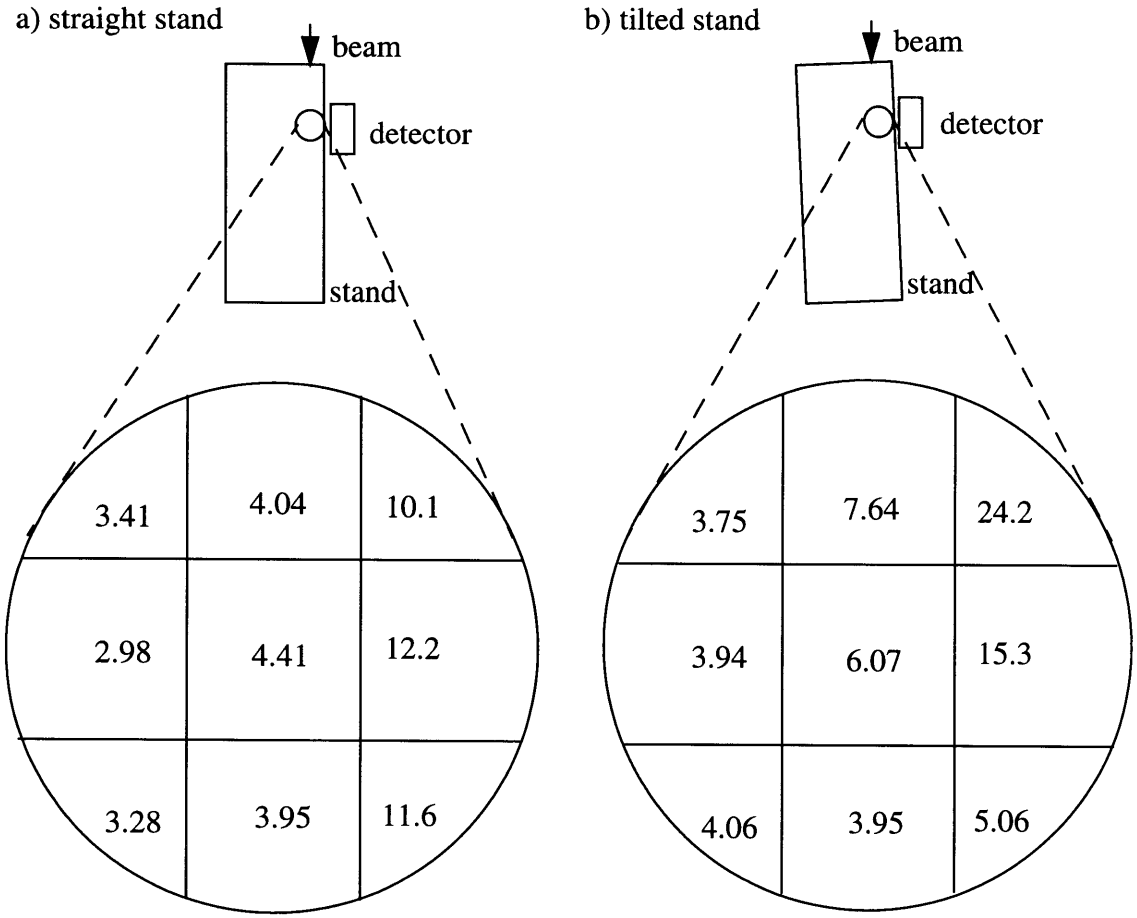

Figure 6.7: Measured $^{10}B/^{1}H$ ratio as a function of position across the rabbit knee joint phantom with (a) a straight stand and (b) a tilted stand.

To give an idea of the magnitude of this variation with respect to concentration, the calibration curve in figure 6.3 was used to plot the concentrations corresponding to the $^{10}B/^{1}H$ ratios and results are shown in figure 6.8. The largest differences in the straight and tilted stand geometries correspond to differences of 3,060 ppm and 5,110 ppm, respectively. Therefore, results indicate that measurement of the $^{10}B/^{1}H$ ratio is sensitive to the position of boron in the rabbit knee joint phantom.

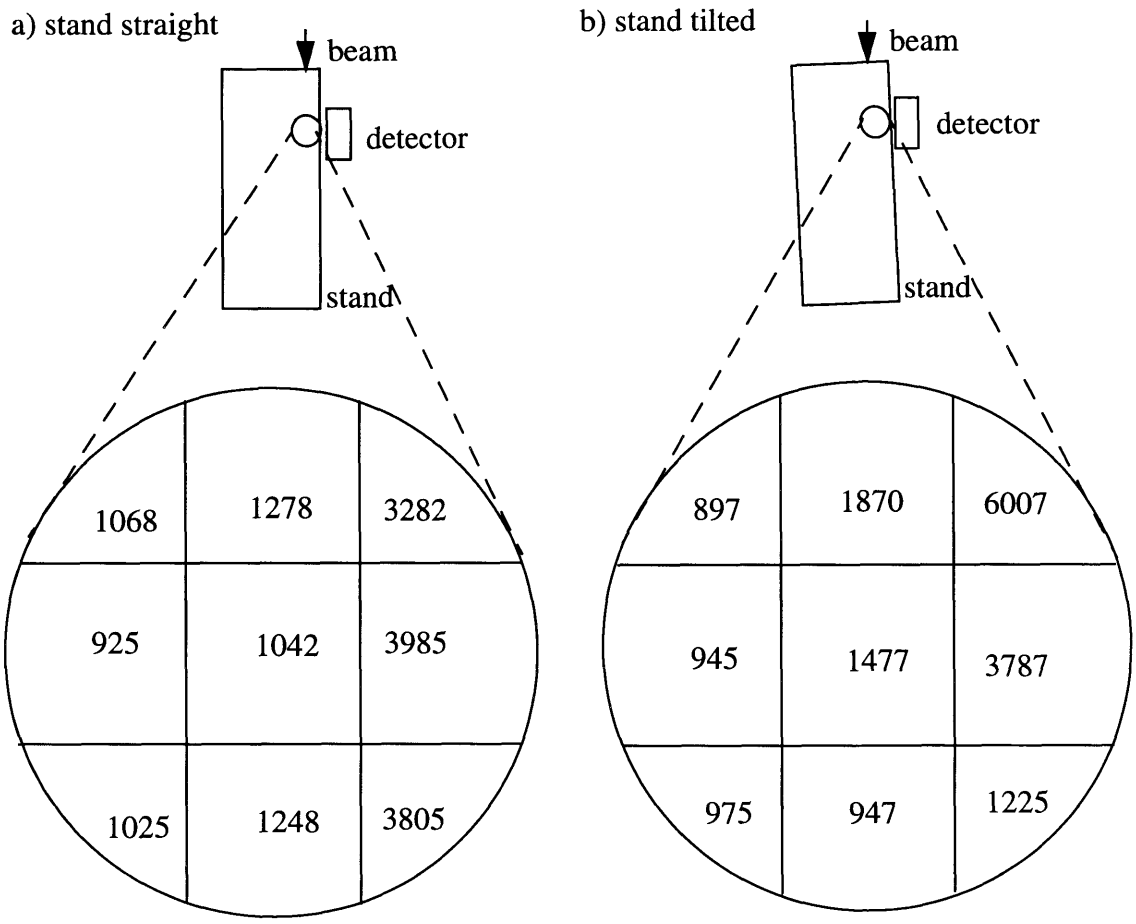

Figure 6.8: Corresponding variation in ^{10}B concentration using the $^{10}B/^{1}H$ ratios shown in figure 6.7 and the calibration curve in 6.3 with (a) a stand straight and (b) tilted stand.

Variation in the $^{10}B/^{1}H$ ratio could be exacerbated by the fact that the beam is smaller than the joint and has a cosine flux distribution. Also, with such large sample volume, differences in the solid angles subtended by the detector so near the joint, may be significant. Therefore, several modifications were proposed. The first was an increase in beam size such that it would be as large as the rabbit joint. At the same time, it was also proposed to shape the neutron flux distribution to be as flat as possible. Finally, it was proposed to move the detector far away from the rabbit joint in order to decrease the effects of the detector's solid angle. However, before a closer and deeper examination of these proposed modifications, a rabbit IVPGNAA trial was performed to obtain an estimate of the current system performance.

6.1.5 Rabbit IVPGNAA trial

Reactor power was lowered to 500 KW to achieve a fluence of $1.7x10^{6}$ n/cm^2/sec from the 2 cm aperture. A non-arthritic New Zealand white rabbit was anesthetized using a standard anesthetic cocktail and placed onto the stand with its leg fitted into the positioner. A background count was performed. The rabbit was then taken out of the stand and 0.25 ml of 150,000 ppm of boron in the

form of unenriched KBH was injected intra-articularly. Since the boron was unenriched, the ^{10}B concentration of the injection was 30,000 ppm and the total amount of ^{10}B injected was 7.5 mg. Considering 8 ml to be the irradiated volume of the non-arthritic rabbit knee joint in beam, then 7.5 mg/8ml corresponds to a maximum ^{10}B concentration of 940 ppm. Both concentration and total amount of boron are within the range of standards tested in section 6.1.3 and lower than the effects of flux depression were observed.

After injection, the knee was subjected to three ranges of motion and the rabbit placed back onto the stand. Total time between injection and final stand positioning was 3 minutes. A one minute count was performed. The shutter was kept open and for the next 30 minutes counts were taken every 2 minutes, while between 30 and 60 minutes, counts were taken every 5 to 10 minutes. After the 1 hour irradiation, the rabbit was taken out and surveyed for surface dose.

Figure 6.9 shows the $^{10}B/^{1}H$ ratio measured in the rabbit joint in vivo after a bolus injection of 0.25 ml of 150,000 ppm boron in the form of unenriched KBH. The $^{10}B/^{1}H$ ratio shows a steady decrease from 0.307 to 0.209 within the first ten minutes. It then fluctuates around 0.2 to 0.25 within counting errors. Counting errors range from 2% to 14%, with an average counting error of 10%.

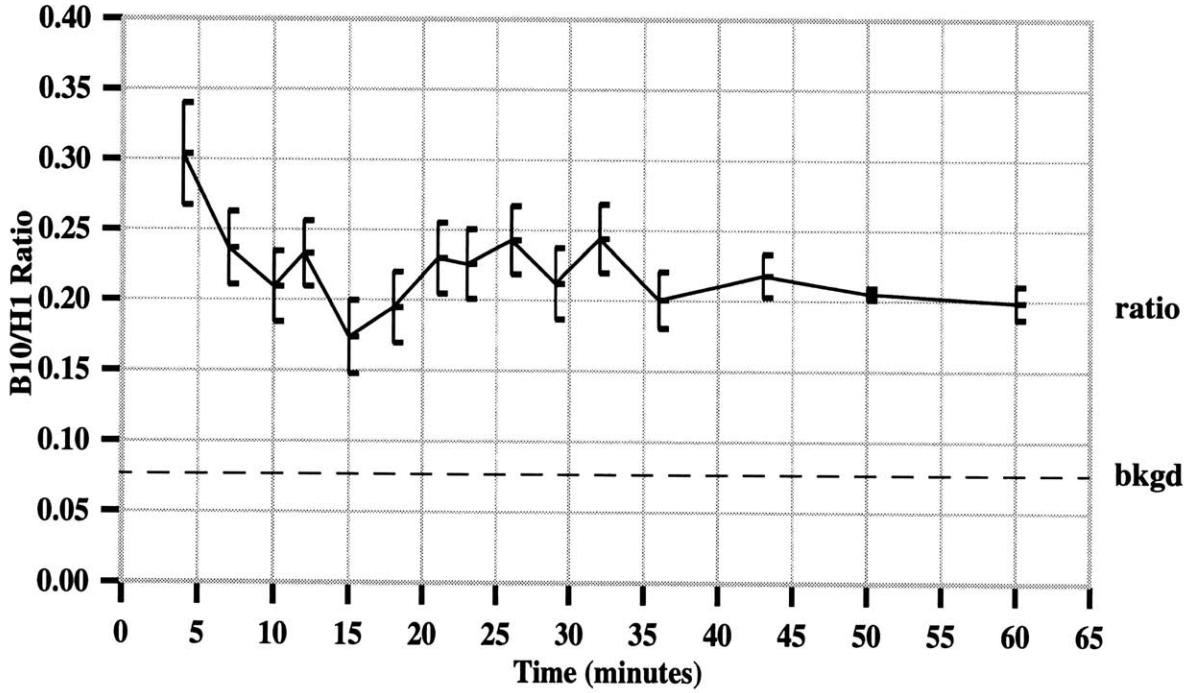

Figure 6.9: $^{10}B/^{1}H$ ratio measured in rabbit joint in vivo after bolus injection of 0.25 ml of 150,000 ppm of boron in the form of unenriched KBH.

Figure 6.10 shows the average boron concentration in the rabbit joint at time intervals ranging from 4 to 60 minutes post-injection. The calibration curve shown in figure 6.4 was used and boron concentrations were scaled to 100% enrichment in ^{10}B. It should be noted that the calibration curve in figure 6.4 is the one where the 1,500 ppm standard was not included in the fit, on the

assumption of flux depression; use of the calibration curve in figure 6.3 leads to several negative values for concentration which is not physically meaningful. As shown in figure 6.10, after a rapid decrease in the first 11 minutes post-injection (from 350 ppm at 4 minutes to 235 ppm) the boron concentration is relatively constant, within statistical fluctuations, and averages 240 ppm.

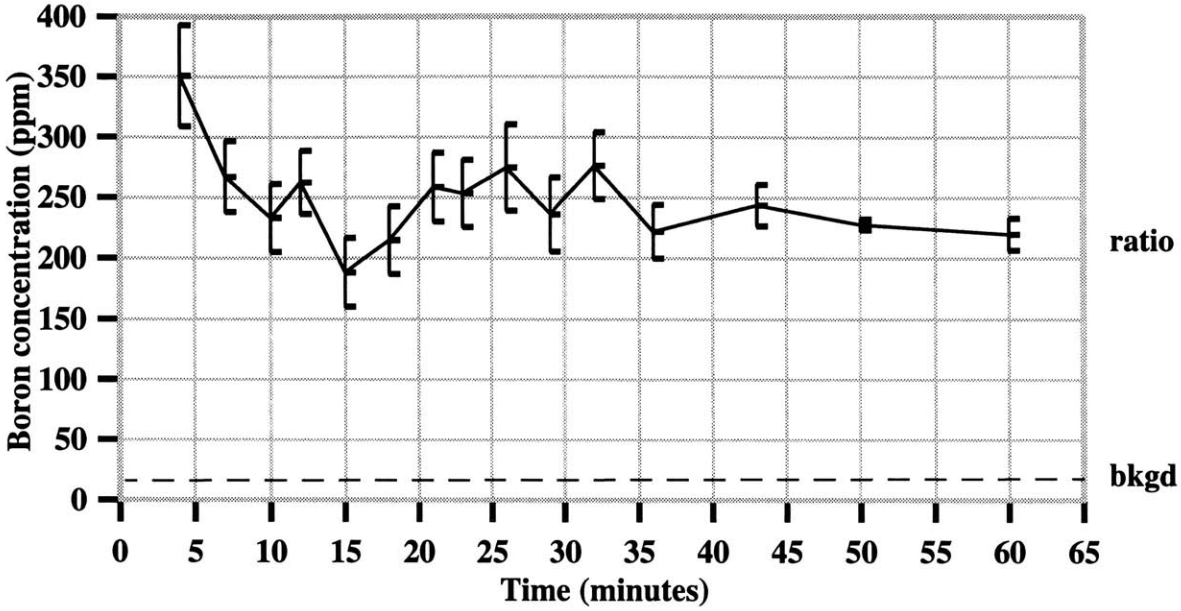

Figure 6.10: Average boron concentration in rabbit joint after bolus injection of 0.25 ml of 150,000 ppm of boron in the form of unenriched KBH.

These numbers are quite low. The total amount of boron injected was 37.5 mg which, divided by the volume of the rabbit joint in the beam (8 ml) yields a maximum boron concentration of 4700 ppm in the joint. Hence, 350 ppm is 7% of the initial (and maximum) boron concentration, while 240 ppm represents 5%. These percentages are the indicators of compound residence (not just the ratio of injected to measured boron concentration).

The time course of the $^{10}B/^{1}H$ ratio obtained in this trial can be compared to that seen in the in vivo uptake data obtained by PGNAA of dissected rabbit synovium and other joint constituents, although it should be noted that the rabbit used for this rabbit trial was non-arthritic whereas the rabbits used in the in vivo uptake studies were arthritic. This affects synovial permeability which, in turn will affect compound residence time. In an arthritic condition, synovial permeability may increase (although one study has claimed a size-dependent effect [Simkin and Pizzorno 1979]), which would result in a decrease in compound joint residence time for arthritic rabbits compared to non-arthritic, i.e. the non-arthritic joints may have a higher boron compound residence time.

Figure 6.11 shows the average uptake from the dissected joint constituents of an AIA rabbit between 5 and 60 minutes after injection of 0.25 ml of 150,000 ppm boron in KBH (with enriched boron). This plot was generated by combining the average values from figures 4.18 through 4.23. Caution must be exercised while making comparisons between the measurement of average joint boron concentration and measurement of dissected samples. If one assumes that the whole rabbit joint (10 ml) is represented by 1000 voxels (0.01 g each in size), then each dissected synovium

sample (0.02-0.03 g) corresponds to 2 to 3 voxels out of the 1000, or 0.2% to 0.3% of the total volume. The sum of the dissected joint constituents is typically not more than 1.5 g, which is 15% of 10 ml. The only way to make a true comparison would be to dissect the entire joint volume in the beam, grind it (without losing any boron) to make a homogeneous solution and take an aliquot for comparison to the in vivo measurement. This is not technically feasible, however, and would require the sacrifice of the rabbit, directly opposed to the goal of keeping the rabbit alive via this technique.

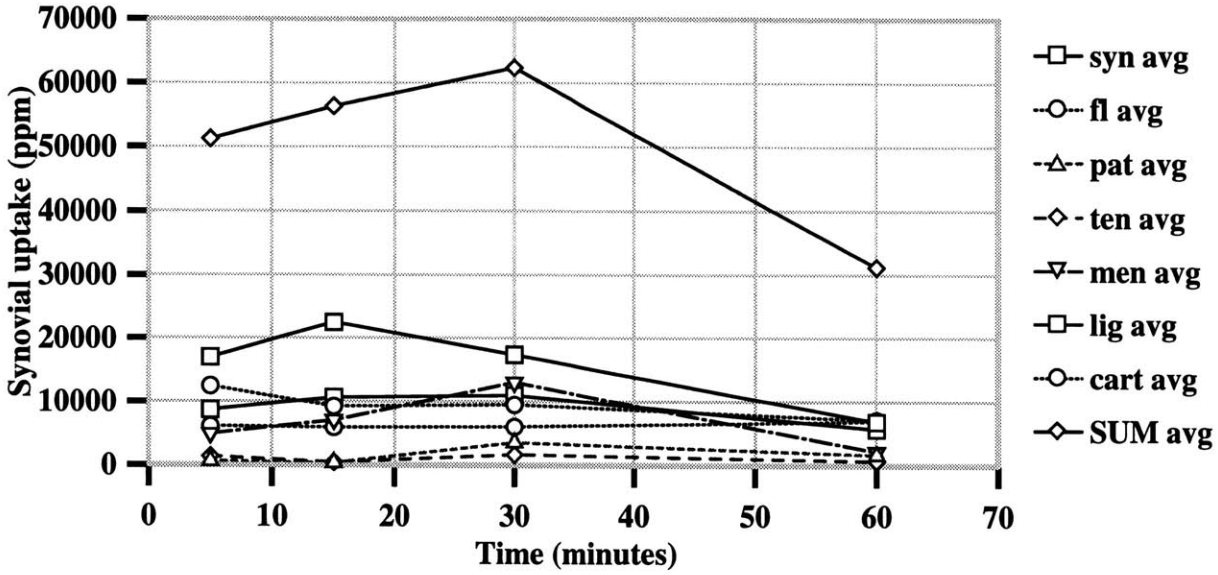

Figure 6.11: Average boron concentration of joint constituents obtained by dissection of AIA joints after a bolus injection of 0.025 ml of 150,000 ppm boron in the form of enriched KBH.

The time courses shown in figures 6.10 and 6.11 indicate different trends; in figure 6.10, the boron concentration decreases after 4 minutes to remain relatively constant throughout the whole hour, while in figure 6.11, the average boron concentration increases around 30 minutes and decreases by 60 minutes. However, the joint constituents listed in figure 6.11 represent only a fraction of the joint volume irradiated by the beam (for example, no muscle or connective tissue was taken) and boron could be in other areas of the joint. The percentage indicating compound residence time was low (7%), although it was notable that the measured signal was clearly above background.

It should be noted that the average joint boron concentration (when above background) does not provide information about synovial uptake. An attempt was made to extract the information about the range of potential synovial uptake. The minimum for the range is zero since there is no way of knowing whether the boronated compound is taken up at all by the synovium. The high end of the range can be obtained by assuming that all the boron signal measured comes from the synovium only and scaling the $^{10}B/^{1}H$ ratio by the ratio of synovial volume to joint volume. Human synovial surface area is approximately 250 cm^2 [Shortkroff 1998]. Assuming a 0.15 cm thickness of arthritic synovium (consistent with the MCNP model in section 2.3) yields an estimate of 37.5 cm^3 for human synovial volume. Calculations in radiation synovectomy with β-emitters have used a scaling factor of 20 between rabbit and human joints [Shortkroff 1998]. Applying this to the estimate of human synovial volume yields an arthritic rabbit synovial volume of 1.875 cm^3. Then,

estimating total joint volume in the beam as 10 ml, the ratio of the synovial to total joint volume is 0.188. In a non-arthritic human, an estimate of synovial thickness is 0.03 cm. Using 100 cm^2 as an estimate of synovial area since the joint is non-arthritic [Shortkroff 1998], the volume would be 3 cm^3. Scaling this by a factor of 20, the estimated rabbit synovial volume would be 0.15cm^3. Then, dividing this by the volume of a non-arthritic rabbit joint in the beam (8 ml), the scaling ratio becomes 0.019.

Table 6.3: Development of $^{10}B/^1H$ scaling ratio

	Synovial thickness	Human volume	Rabbit volume	Scaling ratio
arthritic	0.15 cm	37.5 cm^3	1.875 cm^3	0.188
nonarthritic	0.03 cm	3.0 cm^3	0.15 cm^3	0.019

Applying this to the average joint concentration of 240 ppm shown in Figure 6.10, the maximum synovial uptake would be 1,300 ppm if the rabbit were arthritic and 12,600 ppm if the rabbit were not arthritic (the criterion could be made more precise by measuring the diameter of the specific rabbit joint with calipers; however, the benefit of this correction is dubious, since the range of uptake is already quite large). Thus, the maximum synovial uptake for the rabbit is 12,600 ppm. However, as shown in section 6.1.4, measurement of the $^{10}B/^1H$ ratio is affected by the position of the boron. Taking into account the largest possible variation in the straight stand geometry (which implies that the measured $^{10}B/^1H$ ratio could be a factor of 4 greater), maximum synovial uptake becomes 5,200 ppm if the rabbit were arthritic and 50,400 ppm if the rabbit were non-arthritic. In vivo synovial uptake, with arthritic rabbits, ranged from 3,900 ppm to 37,000 ppm (figure 4.18), which is within the range of synovial concentrations included by the evaluation criterion (although a true comparison can only be made with a dissection study of non-arthritic rabbits). The range of synovial uptake as determined from the evaluation criterion described here is large and may only serve as a very rough estimate.

6.1.6 Simulation study of proposed modifications

In section 6.1.4, several modifications were proposed in order to decrease the amount of variation in $^{10}B/^1H$ signal as a function of boron position within the joint. These modifications included an increase in the diameter of the neutron beam, changing the cosine shaped flux distribution to one uniform across the rabbit joint and an increase in sample-detector distance Since the MITR PGNAA facility is a multi-user facility (it is used for the MIT BNCT clinical trials), further requirements would include the design of a sample holder to accommodate both ex vivo and in vivo samples. To test the potential benefit of the modifications proposed, calculations were done via MCNP.

The overall MCNP geometry, shown in figure 6.12, consisted of a neutron source, a rabbit joint phantom and a collimated detector. The neutron source was a square 3 cm by 3 cm (as large as the rabbit joint) with a flux of $1.8x10^7$ n/cm^2/sec. The phantom was 2.7 cm in diameter and 3 cm in height. It was divided into three layers, each 1 cm in height and each layer was divided into 9

cells. The numbering scheme of the cells in the phantom is shown in figure 6.13; the central cells in the top and bottom layers (i.e. cells #5 and 23) were modeled as bone (and so never contained boron) while the central cell in the middle layer (cell #14) was modeled as fluid (and so could contain boron).

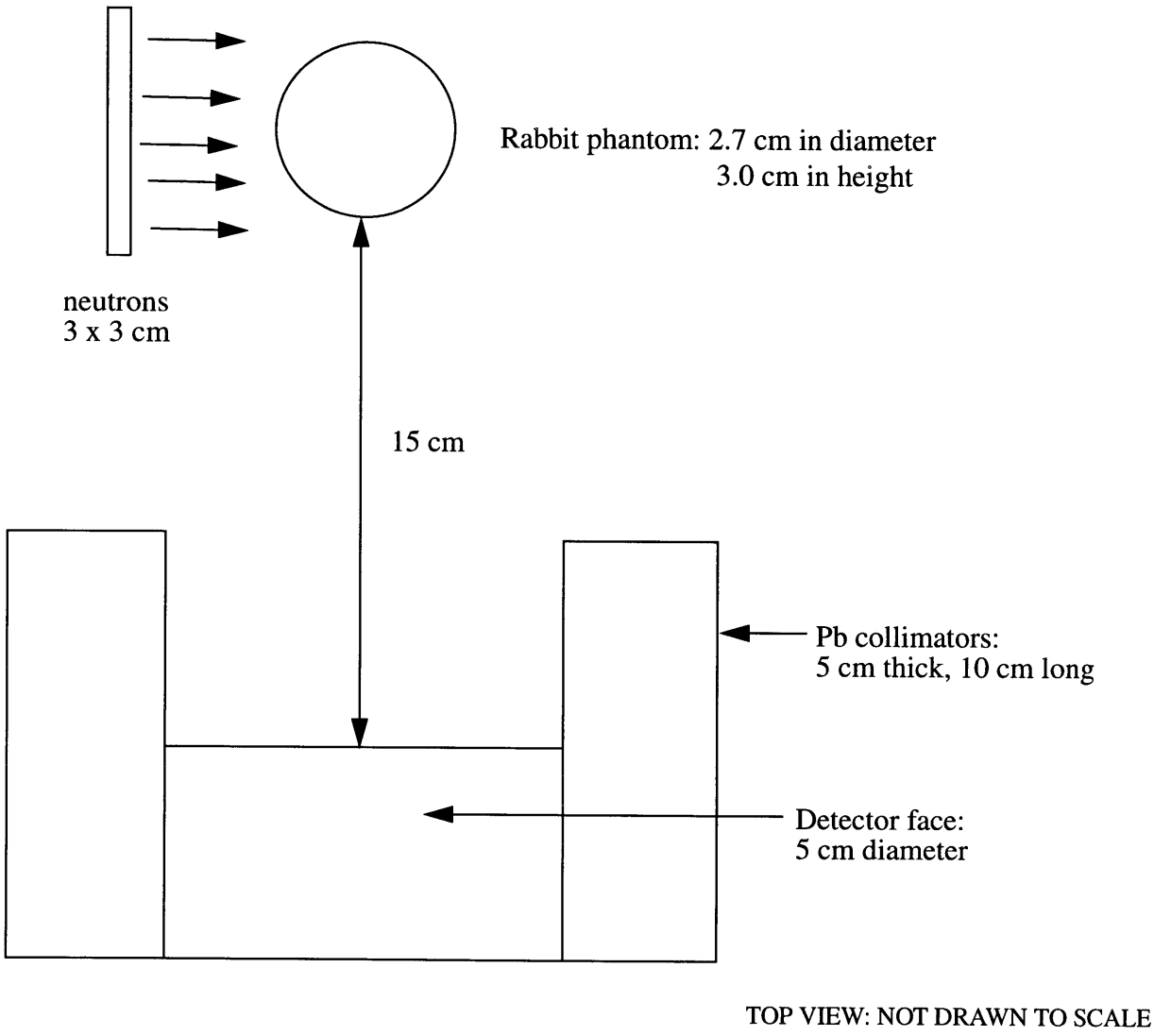

Figure 6.12: Schematic of the MCNP geometry to test the effect of potential modifications.

The detector was modeled as a cylinder in the plane perpendicular to that of the phantom, across from cells #8, 17 and 26. It had a diameter of 5 cm and a length of 5 cm. Lead collimators, 5 cm thick and 10 cm long, were modeled coaxially to the detector. Photons were tallied at the face of detector (15 cm away from the phantom) to give the number of photons in two energy regions: 400-500 keV and 2.1 - 2.3 MeV, which correspond to the energies of the gammas from the boron and hydrogen neutron capture reactions. This photon tally, given in number per starting particle, was multiplied by neutron intensity resulting in the unit of photons/sec. The number of gamma rays from the boron neutron capture reaction was divided by the number of gamma rays from the

hydrogen neutron capture reaction to yield the $^{10}B/^{1}H$ ratio. A boron concentration of 1,000 ppm ^{10}B was placed in each cell, one at a time, for each separate simulation.

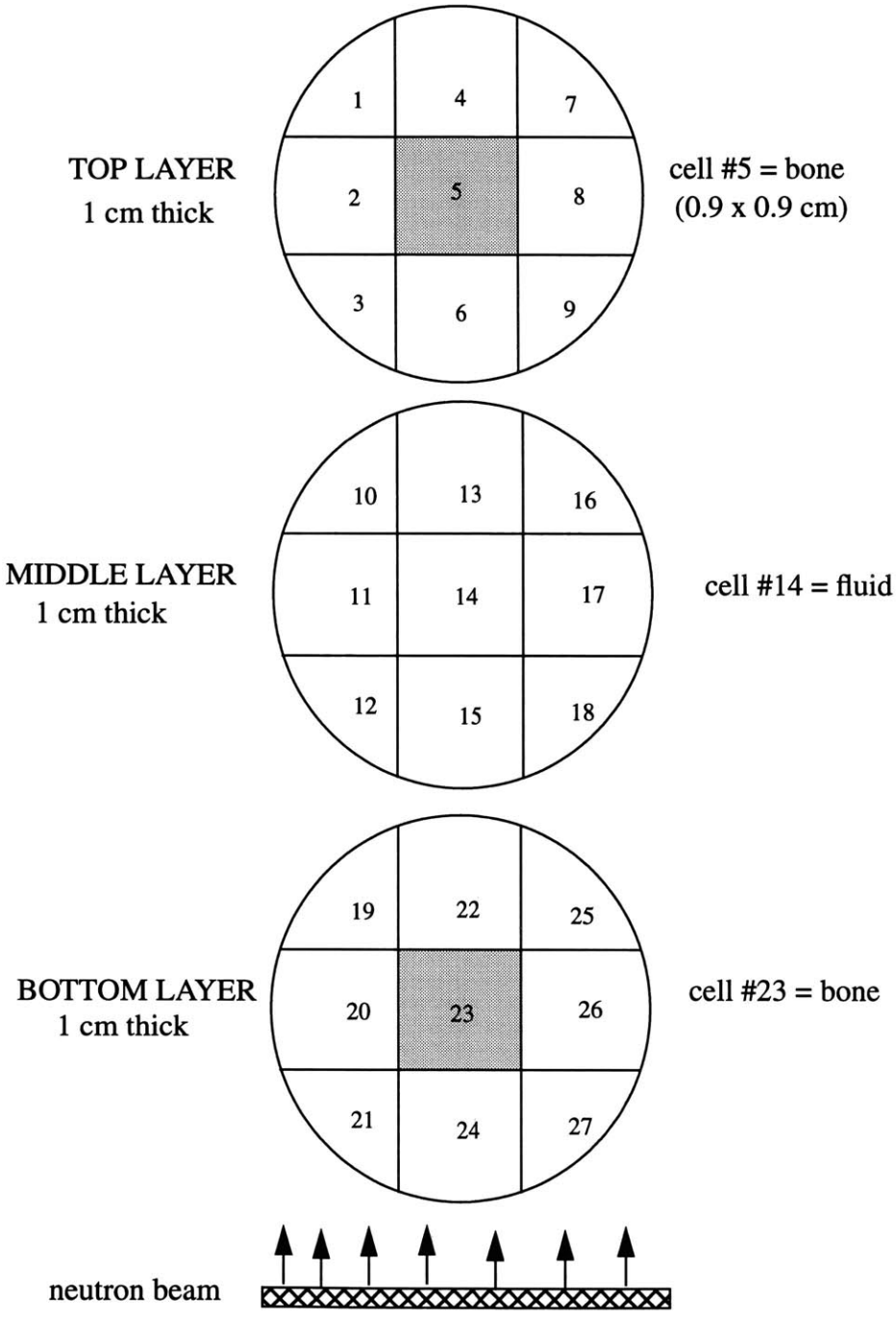

Figure 6.13: Details of cell numbering in the MCNP rabbit joint phantom and relative orientation of the neutron beam. The detector is to the right of the phantom.

Results of the 25 simulations, where boron was moved in each cell of the rabbit joint phantom, are shown in figure 6.14.

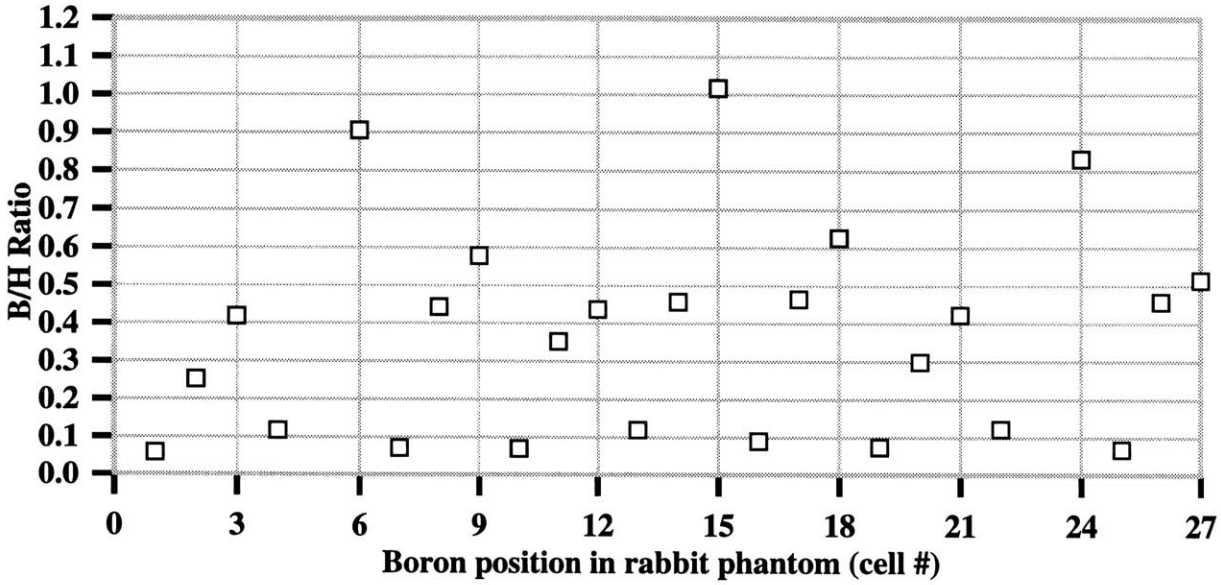

Figure 6.14: Result of MCNP simulation of beam with modified parameters.

As shown in figure 6.14, increasing beam size and homogeneity, as well as moving the detector far from the rabbit joint in order to increase the solid angle, did not result in improvement in the homogeneity of the B/H ratio. This implies that calibration, relating the B/H to concentration, would require knowledge of the boron distribution ahead of time which defeats the purpose of doing IVPGNAA with a broad beam as a means of screening new boron compounds about whose distribution nothing is presumably known.

This type of measurement may be more appropriate for monitoring boron concentrations during treatment, given a boron compound whose behavior has already been well characterized. In fact, a prompt-gamma telescope facility has been constructed at the Petten research reactor to monitor boron levels in patients undergoing BNCT treatment of glioblastomas; results from treatment planning software and biodistribution and phantom studies are used for calibration, and various correction factors are applied [Verbakel and Stecher-Rasmussen 1998].

6.1.7 Conclusions

The main goal of the investigation presented in this section was to experimentally test whether a broad beam IVPGNAA approach, measuring the average concentration of boron in a rabbit joint, would be a reliable means of determining compound residence time in a rabbit joint, which would allow the limitation of the time frame of interest for examination of optimal synovial uptake via dissection studies.

Experimental testing was performed at the MITR PGNAA facility. A stand was constructed to accommodate the rabbits and calibration curves were constructed using a rabbit joint phantom. Testing of the MITR PGNAA beam (2 cm in diameter) using the rabbit knee joint phantom revealed that measurements are highly dependent on the position of the boron within the joint, resulting in a variation in $^{10}B/^{1}H$ ratio as large as a factor of 4 (with a correspondingly large variation in boron concentration). IVPGNAA was tested on a rabbit and the measurement of the $^{10}B/^{1}H$ ratio over 60 minutes after intra-articular injection of 0.25 ml of 150,000 ppm of boron (in the form of unenriched KBH) was clearly above background. Measurement via IVPGNAA can be adequate as a compound screening method in evaluating the compound presence in the joint as a function of time.

Detailed inferences from average joint concentration to synovial uptake are difficult and can be misleading, since the two are not necessarily related, as illustrated in the following example. Assume that there are two boron compounds, A and B. Compound A shows a significant decrease in average joint concentration which occurs at 30 minutes (the maximum measurement will always occur at time 0, since the compound will have just been injected and is all in the joint). However, although there may be less boron in the joint after 30 minutes, there may be more boron in the synovium (it may take the synovium that long to start absorbing the boron compound). Conversely, compound B may not show a significant drop in the average joint concentration until 1 hour but it could be that the maximum synovium concentration was reached within 15 minutes and that by 1 hour, the boron has left the synovium and penetrated into surrounding muscle, which may contribute to the measurement of average joint boron concentration. An evaluation criterion was developed to yield the range of maximum potential synovial boron concentrations from an average joint concentration. This evaluation criterion, based on the relative volumes of synovium to the whole joint, yielded a range which may be too large to be useful.

Possible causes for the large variation in measurement of the $^{10}B/^{1}H$ ratio as a function of position included the diameter of the beam which was 33% smaller than the rabbit knee, its cosine shaped neutron flux distribution, and the nearby placement of the detector. In order to try and decrease the variation in the B/H ratio, it was proposed to increase the beam diameter and flatten the neutron flux distribution, as well as increase the distance between the joint and the detector. This is in addition to the several modifications which would be required since the MITR PGNAA facility is routinely used for the MITR BNCT clinical trials; these included the design and construction of an improved sample holder to accommodate both in vivo and ex vivo samples, as well as the design and installation of a detector positioning system. Since these are major modifications, MCNP simulations were performed to determine that there would be a beneficial effect following the modifications. However, results of the MCNP simulations of an ideal case where the beam, with a flat neutron distribution, was made as large as the rabbit joint and the detector was moved far away still showed large variation in $^{10}B/^{1}H$ signal as a function of boron position within the knee joint.

Attention was then turned to changing the size of the beam in the other direction, i.e. making it much smaller, leading to a different approach in the evaluation of this non-invasive determination of boron compound residence time. In this approach, the average joint boron concentration would not measured but rather the concentration in specific spots of the knee joint would be probed.

6.2 Simulation study of MITR slit beam

This section presents the simulation study designed to assess the potential of using a very narrow thermal neutron beam for the estimation of boron compound residence time in a rabbit joint. Such a beam currently exists at the MITR, although it is used as an experimental facility for a physics laboratory class during the regular semester hours. It could modified and used exclusively for BNCS off-hours and while the class is not in session. MCNP simulations were aimed at testing this specific beam, which shall be called a slit beam, to evaluate its potential for determination of boron residence time in the intact rabbit joint.

6.2.1. Signal as a function of position

The MCNP geometry shown in figures 6.12 and 6.13 was used, except that the neutron source was a thin rectangular slit, 1 mm by 5 mm, with a thermal neutron flux of $2x10^6$ n/cm^2/sec and it was placed parallel to the middle layer of the rabbit joint phantom. The $^{10}B/^{1}H$ ratio was calculated in the same manner as in section 6.1.6. A constant concentration of 1,000 ppm of ^{10}B was modeled separately in each cell of the rabbit phantom (except for the two cells designated as bone) and the B/H ratio was determined. This was done for three beam positions, i.e. with the beam incident on cells #12, 15 and 18.

Figure 6.15 (a) and (c), shows the results of the B/H signal as a function of boron position for beam positions 12 and 18, respectively. There is a marked rise in signal when the boron is in the cell upon which the beam is incident. The boron position of the cell with the second highest signal corresponds to the cell directly behind the cell upon which the beam is incident (i.e. cells #11 and #17 for beam positions 12 and #18). Although signal differentiation is already significant with beam positions 12 and 18, an even clearer distinction in signal, between the cell upon which the beam is incident and the other positions, is seen for beam position 15, shown in figure 6.15 (b). In this case, the signal in cell #15 ranges from 5 to 10 times higher than the signal in other cells of the rabbit phantom. The boron position with the second highest signal is cell #14, directly behind cell#15, although it is still 5 times lower than the signal from cell #15.

This decrease in signal differentiation between the beam positions may be an effect of voxel size. Cells #12 and #18 are about one half the size of cell #15, closer to the mean free path of thermal neutrons (0.3 cm), and therefore making it more likely for neutrons to affect the signal in the cell behind the one facing the beam. However, it is very significant that the cell upon which the beam is incident gave a clearly high and distinguishable signal. A practical implication is that the joint could be rotated around the slit beam and thereby detect areas of tissue containing the boron.

(a)

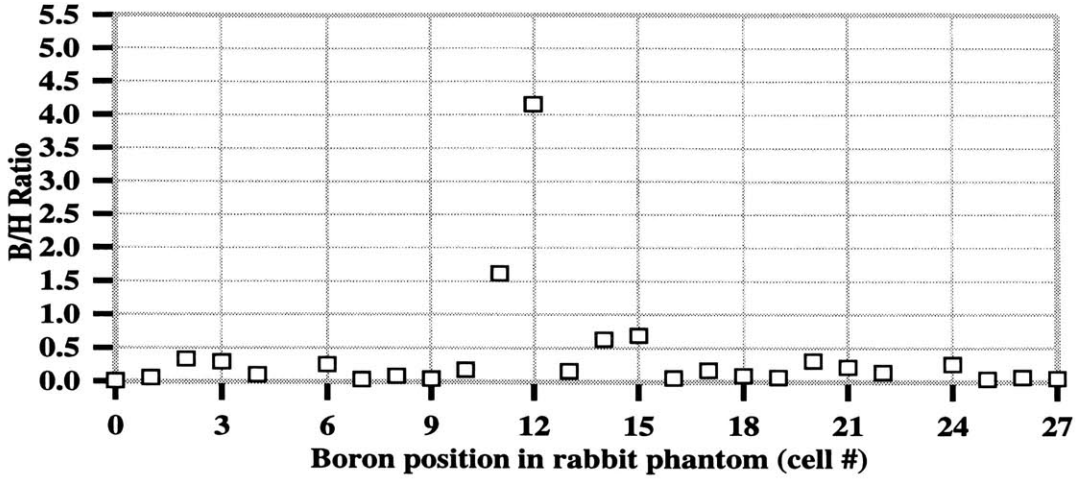

(b)

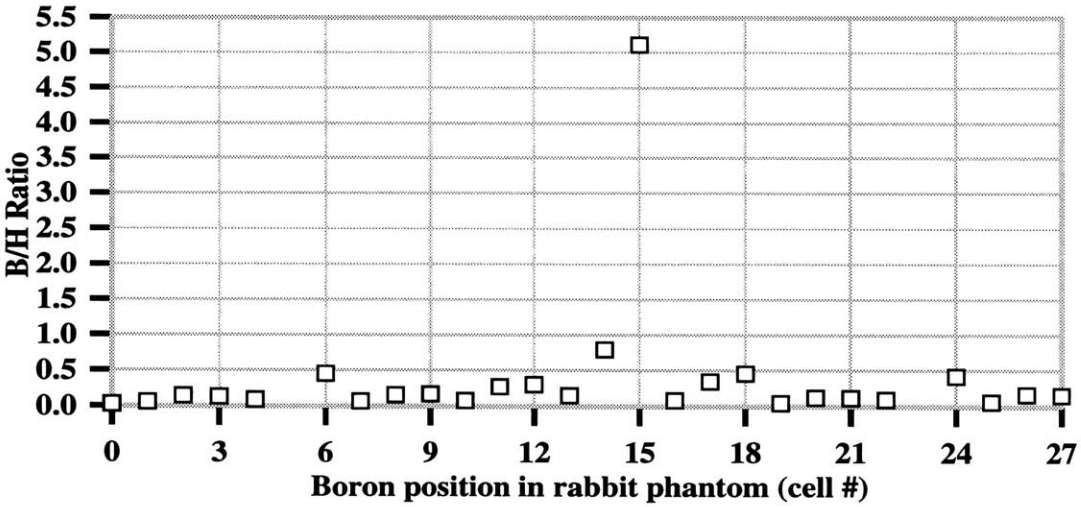

(c)

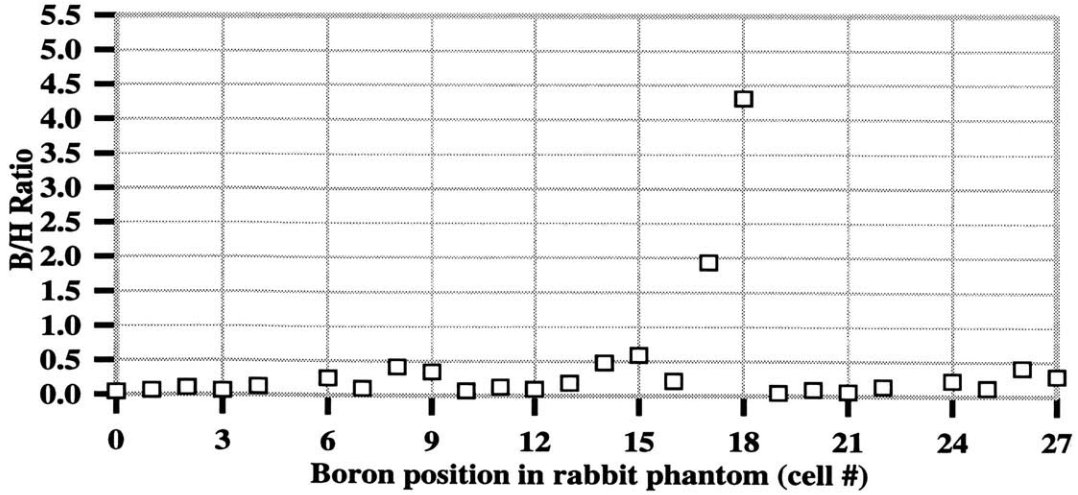

Figure 6.15: Signal as a function of boron position for beam positions (a) 12, (b) 15 and (c) 18.

6.2.2 Signal as a function of boron concentration in one cell at a time

For each beam position, simulations were performed to look at the B/H ratio as a function of boron concentration in one cell at a time. The selection of cells was restricted to those being in the middle layer, adjacent to the cell upon which the neutron beam is incident and the last one in line with the neutron beam (i.e. cells #10,13,16). Boron was modeled in one cell at a time with 5 boron concentrations ranging from 100 ppm to 10,000 ppm. The curves in figure 6.16 and 6.17 show the signal resulting from boron being present in one cell at a time and allow the determination of the contribution of each single cell to overall signal.

Figures 6.16 and 6.17(a) show the increase for each cell at beam positions 12 and 18, while figure 6.17(b) shows the results at beam position 15. As expected from the previous results of signal as a function of position, beam position 15 (part (b) of figure 6.15) gives the highest differentiation between the boron signal upon which the cell is incident (cell #15) and the one directly behind it (cell #14), which is higher than all of the other cells in that plane. The difference increases with concentration (at 100 ppm, cell #15 is 5 times higher than cell #14, while at 10,000 ppm, it is 20 times higher). An implication of these plots is that it will be easier to distinguish between signals at higher boron concentrations, i.e. a measured B/H ratio over 5 primarily indicates the presence of boron in cell #15 (assuming that no more than 10,000 ppm exist in any other part of the joint). Boron in cell #13 gives rise to the smallest signal in comparison to cell #15; 10,000 ppm of boron in cell #13 yields the same signal as 100 ppm in cell #15. This implies that having boron in cell #13 will have little effect on the measurement of boron in cell #15 because the neutron scattering into cell 13 is not significant. Results of other cells (#11,12,17 and 18) lie in between cells #13 and #14.

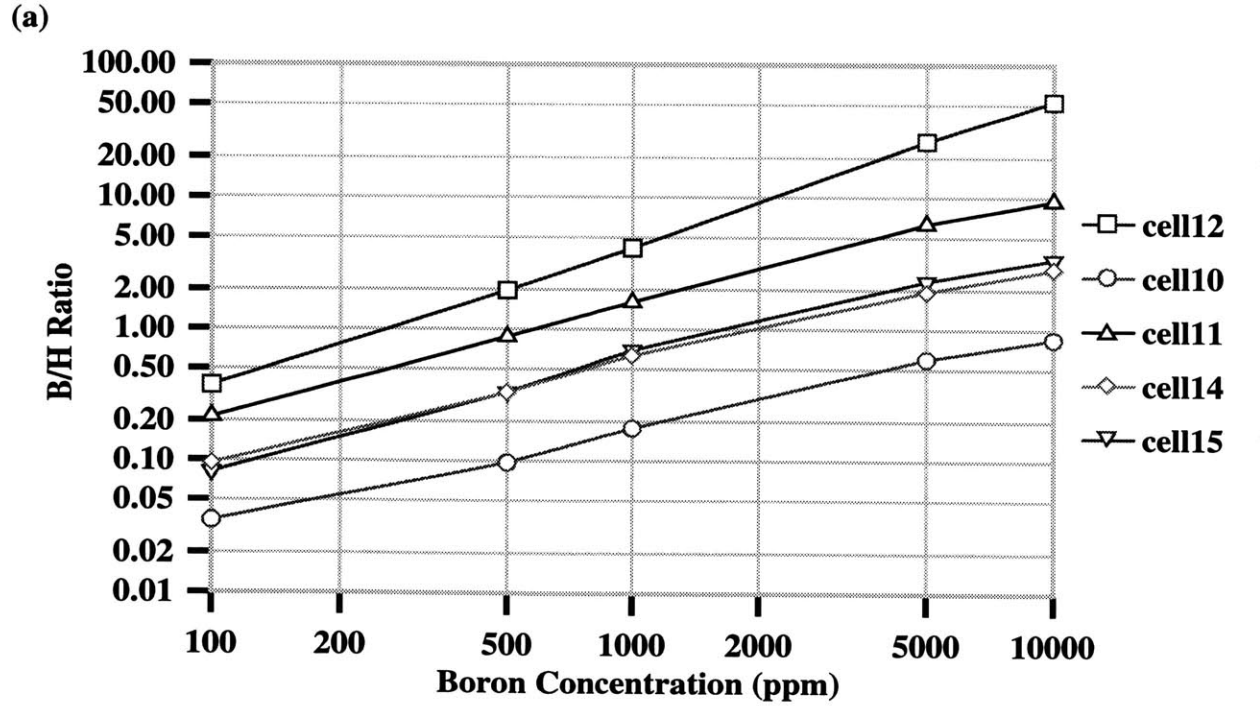

Figure 6.16: Signal as a function of boron concentration in each cell for beam position 12.

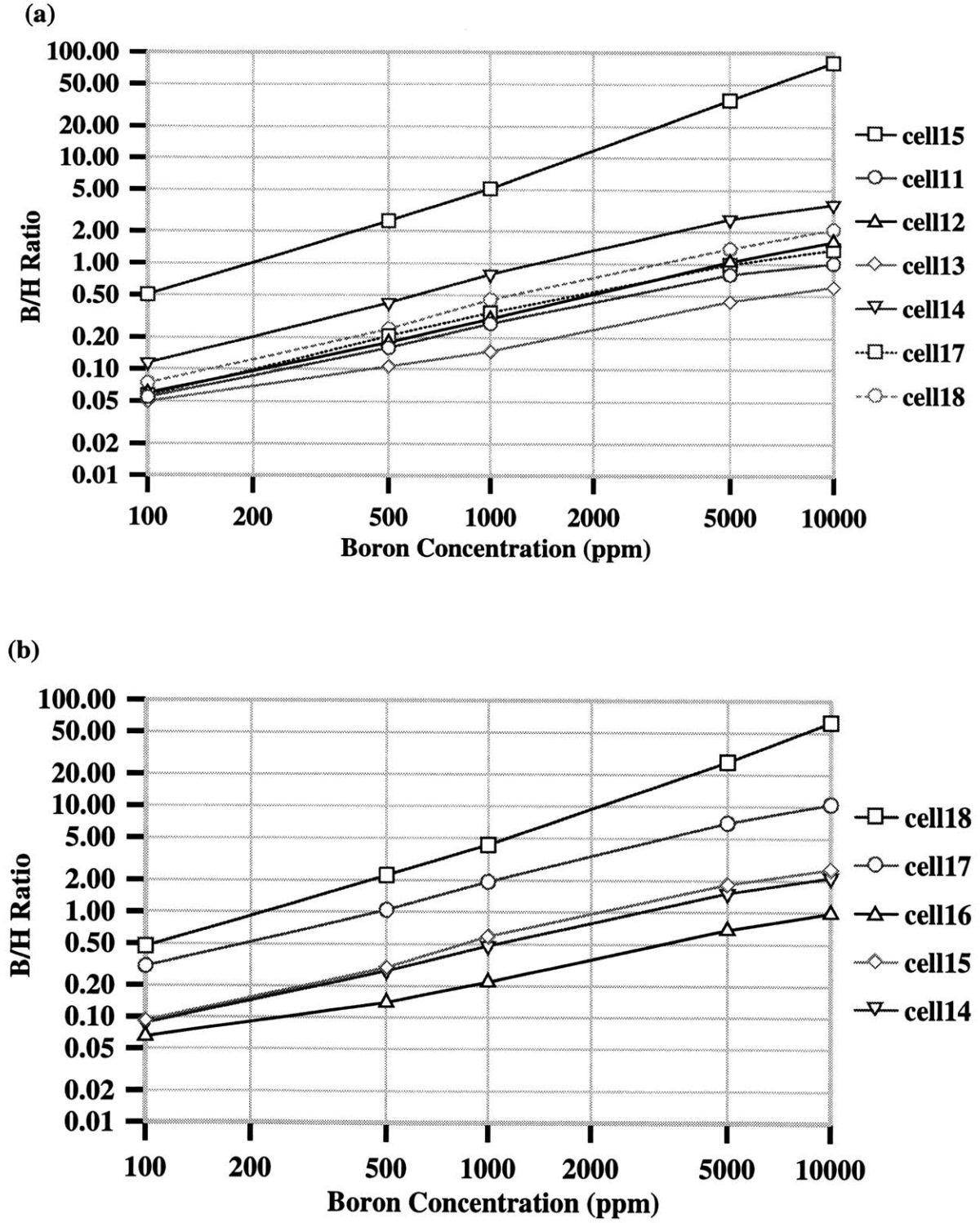

Figure 6.17: Signal as a function of boron concentration in each cell for (a) beam positions 15 and (b) beam position 18.

Beam positions 12 and 18 have essentially the same characteristics in that signal increases with increasing boron concentration. However, the smaller ratio makes it harder to distinguish whether signal is from the cell upon which the beam is incident. For example, looking at beam position 18, if a B/H ratio of 2 is measured, it could mean either that there is 500 ppm in cell #18 or 1,000 ppm in cell #17 or 5,000 ppm in cell #15 or 10,000 ppm in cell #14. Boron in cell #16 gives rise to very little signal (3,000 ppm boron concentration in cell #16 has the same signal as 100 ppm in cell #18).

Since it is unlikely that a boron compound, especially if diffusion-based, remains in only one spot, the B/H ratio with boron in two cells at the same time was investigated. This was done for all three beam positions. However, only the results of beam position 15 will be included in the text here, since as it has been shown, this beam position has the clearest differentiation in signal. The results for signal as a function of boron concentration in two cells simultaneously for beams incident on cell #12 and #18 can be found in Appendix C.

6.2.3 Signal as a function of boron concentration in two cells simultaneously

These runs examined at boron in two cells simultaneously. There were three subsets of studies. The first subset kept the boron concentration in the cell upon which the beam is incident at 100 ppm, while the concentration of neighboring cells was varied from 100 ppm to 10,000 ppm (total of 5 concentrations). In the second subset, the boron concentration of the cell upon which the beam is incident was kept at 500 ppm, while the concentration in the neighboring cells increased from 500 ppm to 10,000 ppm (total of 4 concentrations). Finally, the last subset kept the boron concentration in the cell upon which the beam is incident at 1,000 ppm while varying the boron concentration of neighboring cells from 1,000 ppm to 10,000 ppm (total of 3 concentrations).

Figures 6.18 through 6.20 show the results of simulations in which the boron concentration in the cell, upon which the beam was incident, was kept constant, while the boron concentration of the neighboring cells was increased.

Variation in the boron concentration of cell #14 resulted in the largest effect on the B/H ratio and the effect decreased as the boron concentration in cell #15 was increased. Specifically, when the concentration in cell #15 was kept at 100 ppm, increasing the boron concentration in cell #14 from 1,000 ppm to 10,000 ppm resulted in a signal increase of a factor of 4. When the concentration in cell #15 was kept at 1,000 ppm, then increasing the concentration in cell #14 from 1,000 ppm to 10,000 ppm only increased the signal by a factor of 1.5. At high concentrations of boron in cell #15, the effect of cell #14 is largely diminished.

Variation in the boron concentration of other cells revealed smaller effects on signal. Boron in cell #13 had essentially no effect on the signal, while boron in cells #11 and #17, as well as #12 and #18, exhibited similar trends; when the concentration in cell #15 was kept at 100 ppm, 500 ppm and 100 ppm, the signal from varying the concentration in cells #11,17,12 and 18 from 1,000 ppm to 10,000 ppm rose by 100, 25 and 15%.

(a)

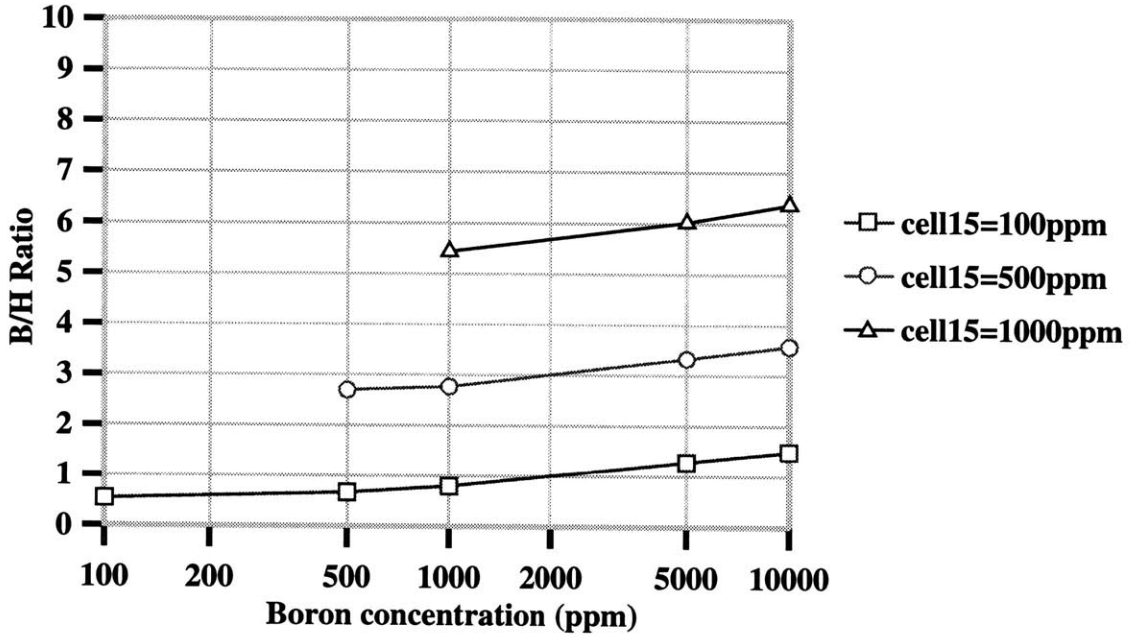

(b)

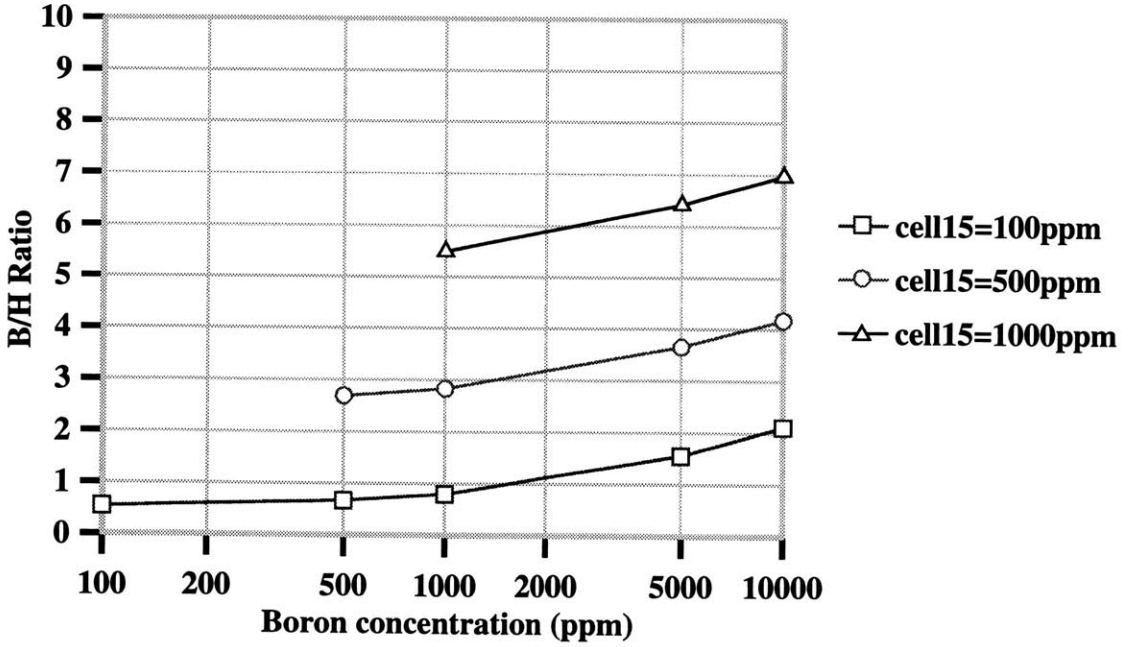

Figure 6.18: Signal as a function of concentration in two cells simultaneously for beam position 15. Boron concentration was kept constant in cell #15 and varied in cell (a) #11 and (b) #12.

(a)

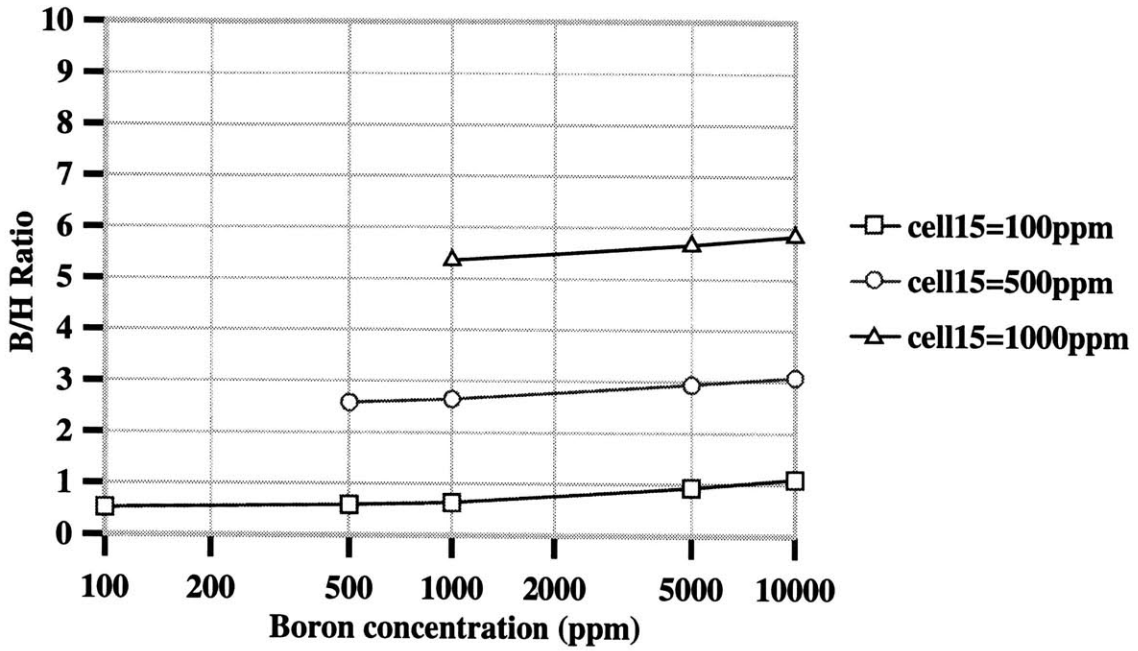

(b)

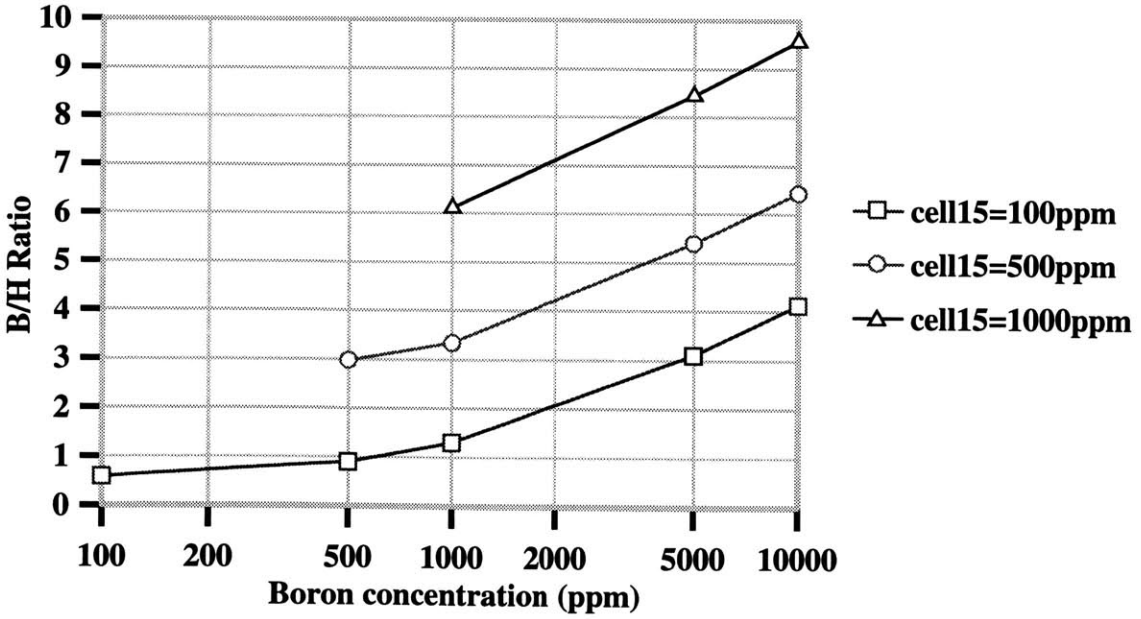

Figure 6.19: Signal as a function of concentration in two cells simultaneously for beam position 15. Boron concentration was kept constant in cell #15 and varied in cell (a) #13 and (b) #14.

(a)

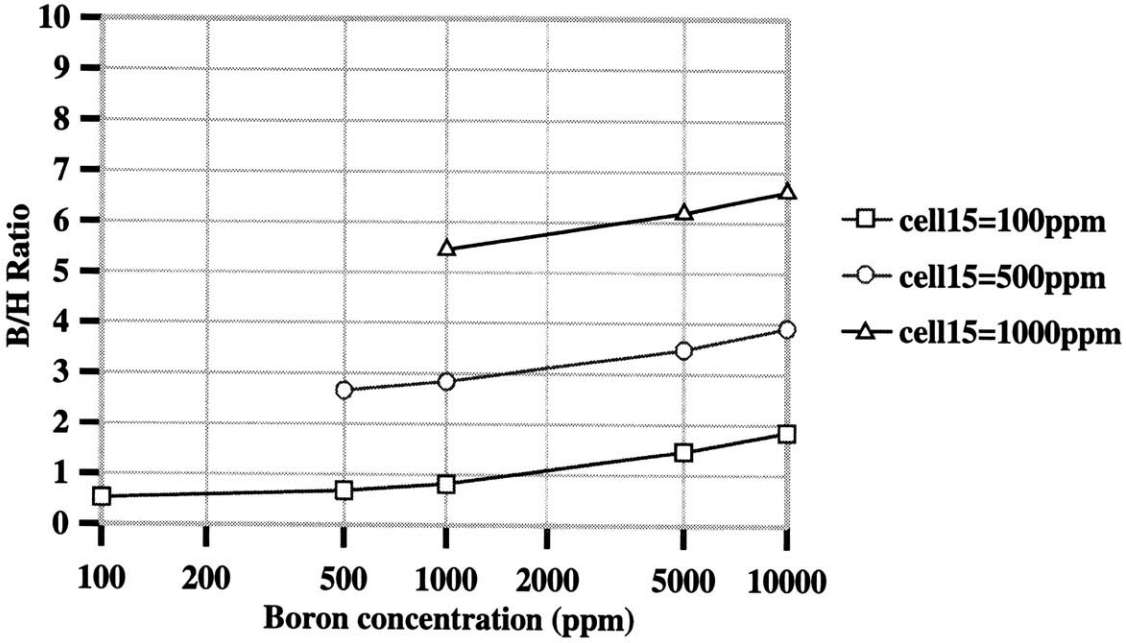

(b)

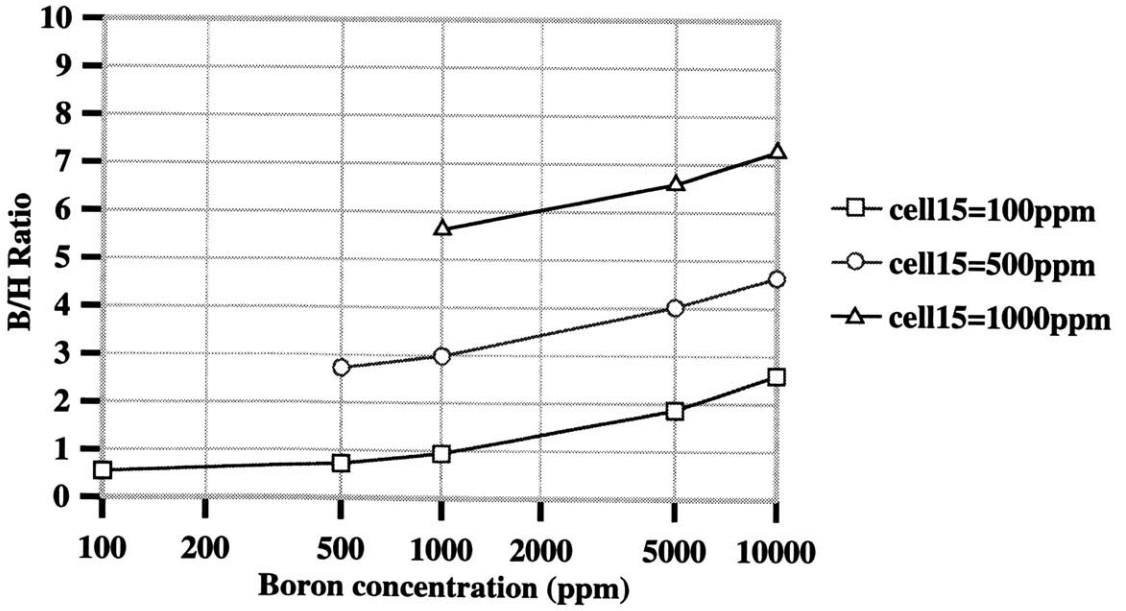

Figure 6.20: Signal as a function of concentration in two cells simultaneously for beam position 15. Boron concentration was kept constant in cell #15 and varied in cell (a) #17 and (b) #18.

6.2.4 Conclusions

In the IVPGNAA approach investigated here (6.2), the average joint boron concentration is not measured but rather the knee joint would be probed in different spots with a highly collimated beam. MCNP simulation studies of the slit beam (1 mm by 5 mm) in a rabbit knee joint phantom examining signal as a function of boron position within the joint showed that signal was a factor of 2 to 5 higher in cells upon which the beam was incident relative to other cells in the phantom. Signal was examined as a function of boron concentration in one cell at a time and it was found that the boron concentration in neighboring cells would need to be 4 to 10 times higher in order to produce the same signal as the cell upon which the beam is incident. Simulations investigating the effects of boron concentration in two cells at a time showed that the largest contribution to signal originated from the cell directly behind the cell upon which the beam is incident; an increase of a factor of 10 in the boron concentration of the cell behind the irradiated cell caused a 50% rise in signal. These simulations provide motivation to pursue the development of what could be, in essence, a crude neutron tomographic system as a means to screen boron compounds for BNCS.

Many monitoring options are available. The rabbit joint could be rotated through many angles and signal measured. Another option is to keep the slit beam fixed at one point and monitor the change in signal over time. Although traditionally applied for nondestructive material testing, slit beam IVPGNAA could be a novel approach for a non-invasive temporal and spatial characterization of boron compounds in a rabbit joint.

Future work should include the consideration of many engineering issues, such as verification of the neutron distribution from the beam port, cost of equipment (related to building an appropriate stand, detector, multichannel analyzer, collimators) and experimental verification of simulation studies. Attempts could be aimed at deconvolving the signal and reconstructing the compound behavior. This could potentially lead to the ability of obtaining both spatial and temporal aspects of the behavior of boronated compounds for BNCS, an immensely useful compound screening method.

7. Summary and recommendations for future work

Boron Neutron Capture Synovectomy (BNCS) proposes to use the $^{10}B(n,\alpha)^{7}Li$ nuclear reaction to destroy the inflamed synovium in patients with Rheumatoid Arthritis. In a treatment, a boronated compound would be injected into the joint space/cavity and be taken up by the synoviocytes. Then, the joint would be irradiated, inducing the boron neutron capture reaction which, in turn, would induce cell death in the boron loaded cells via the dense energy deposition of the products from the boron neutron capture reaction. The overall goal of this thesis was to experimentally determine whether BNCS is an effective means of ablating arthritic synovium.

Several investigations were required before the efficacy of BNCS could be tested in an animal model. Synovectomy literature was extensively reviewed for information on pathology, treatment options and animal models for rheumatoid arthritis. An understanding of the pathologic lesions existing in a rheumatoid joint was important for the assessment of the efficacy of BNCS based on histological evidence. The status of synovectomy in the treatment regime for rheumatoid arthritis was assessed and the alternatives to surgical synovectomy, both clinical and experimental, were examined, aiding in the development of therapy goals, such as therapy time, which would make BNCS a competitive treatment option.

Although based on the same physical principle as BNCT for glioblastomas, the different nature and depth of the target tissue in BNCS led to significant differences in therapy parameters due to the delivery of the boron compound and the design of a neutron source. The synovium typically lies 1.3 to 1.5 cm below the surface of the skin, contrasting with tumors treated via BNCT which may extend up to 7 cm below the surface. In BNCS, the boron compound is delivered by a local intra-articular injection, making the achievement of high boron concentrations in the target tissue more likely, while in BNCT, the boron-labelled pharmaceutical is administered intra-vascularly or orally and must reach the tumor via metabolic pathways. The above differences had a profound effect on the required neutron beam energy range and overall beam design for BNCS.

In neutron beam design for BNCS, therapeutic usefulness is based on examination of overall treatment time and the ratio of synovium dose to each of two healthy tissues: the skin and bone surface. The minimum dose ratio of synovium to skin was set at 12, based on empirical findings that a dose of 10,000 cGy has been required for clinical success in synovectomy using β-emitters [Deutsch et al 1993] and that mild skin reddening is observed at 800 RBE-cGy [Nias 1990]. This limit is very conservative. No limits were set for the ratio of synovium to bone surface dose since potential carcinogenic effects to the bone may be considered stochastic. Based on a conservative estimate of synovial boron concentration in the synovium, therapeutically useful neutron beam energies range from 0.025 eV to 5 keV. As synovial boron concentration increases, therapeutic ratios become more favorable and allow the use of a beam with more contamination.

Neutron beam design was aimed at the development of a suitable moderator/reflector geometry for the tandem electrostatic accelerator currently in operation at MIT LABA. Using either the Li(p,n) reaction with 2.5 MeV protons or the Be(p,n) reaction with 4.0 MeV protons as neutron sources, materials of choice were heavy water for the moderator and graphite for the reflector. MCNP simulations of in-air dosimetry allowed the determination of optimal moderator diameter and reflector dimensions, as well as determination of a preliminary range of moderator lengths. The effect of moderator length was examined in an MCNP human knee joint phantom and was quantified via the calculation of therapy parameters. The most dramatic increase in therapeutic dose ratios was observed when the moderator length was increased from 20 to 35 cm (with much smaller improvements as length was increased to 50 cm). The shortest moderator lengths gave the shortest therapy times with highly acceptable therapeutic dose ratios. The effect of synovial boron concentration on therapy parameters was examined for short moderator lengths and it was found that concentrations of 300 ppm with a lithium target and 500 ppm with a beryllium target yield acceptable therapeutic parameters with therapy times less than 30 minutes, which was considered as the longest acceptable therapy time for BNCS to be competitive. The criteria for minimum acceptable synovial boron concentrations were determined in light of beam design requirements.

Further neutron beam optimization, as well as beamline construction, was carried out by other MIT LABA members. Also, recent improvements in target cooling, also by MIT LABA members, allowed the installation of a beryllium target able to withstand necessary heat loads. The work by these MIT LABA members resulted in a fully operational beamline and target assembly used for the animal irradiations to determine the efficacy of BNCS. Results of the experimental verification of the assembly, as well as an improved simulation model, by MIT LABA members, were used for the calculation of target doses in the animal irradiations.

Several boron compounds were first tested, including boron particulate powder and a boronated ferric hydroxide macroaggregate that required substantial developmental work (e.g. testing boron compounds in varying concentrations, varying iron concentrations, and varying particle sizes). The boron particulate, at a concentration of 1 mg/ml, coagulated in the synovial fluid and the maximum average synovial concentration achieved with particulate concentrations of 0.5 mg/ml and 0.1 mg/ml was 67 ppm. Injection of a ferric hydroxide macroaggregate preparation with 11,600 ppm of boron, resulted in average synovial uptake of 40 and 65 ppm, at 4 and 24 hours, respectively. In light of the requirement of minimum synovial uptake concentrations of 300 to 500 ppm of boron (developed in the neutron beam design), uptake characteristics achieved of these compounds did not yield warrant continuation to animal irradiations.

The uptake of $K_2B_{12}H_{12}$ (KBH) was fully characterized in vitro (monocytic cell line), ex vivo (human excised RA synovium) and in vivo (AIA rabbit model). A method for measurement of boron uptake by cells was developed and results were consistent with tissue uptake studies. Good agreement was found between cell and tissue uptake with respect to the boron concentrations achievable at given incubation concentrations. Results of tissue uptake as a function of time lay within data obtained from cells between 30 and 60 minutes, while at times less than 30 minutes, tissue uptake was lower; it was hypothesized that tissue uptake should be lower than cellular uptake since time is required for KBH, a possibly diffusion-based compound, to diffuse through the entire tissue. Studies of compound washout from cells and tissues indicated this to be a rapid

process, with only a 15% to 25% of the original concentration remaining after 15 to 30 minutes. The level of boron concentration retained in tissue upon washout increased with initial boron incubation concentration; this was attributed to the larger absolute total amount of boron present, taking longer to wash out of the tissue.

Synovial concentrations in vivo, obtained by dissection of arthritic rabbit knee joints following intra-articular injection of 0.25 ml of two boron concentrations (5,000 and 150,000 ppm) in the form of enriched KBH, were roughly consistent with predictions from tissue uptake studies. While the relative synovial boron concentrations after 15 minutes agreed between concentrations (a roughly linear increase in uptake with increasing concentration), the boron concentration in the synovium after 30 minutes differed possibly due to differences in the absolute magnitude of boron injected (1.25 and 37.5 mg with 5,000 and 150,000 ppm of boron respectively). With a boron injection concentration of 5,000 ppm, at 30 minutes average synovial concentration was 27% of the concentration at 15 minutes, whereas with an injection concentration of 150,000 ppm, average synovial concentration at 15 and 30 minutes was approximately the same. It took longer for the boron to be cleared from the synovium when the injection concentration was 150,000 ppm. After a boron injection concentration of 150,000 ppm, the boron concentration in the other tissues of the joint were such that the ratio of uptake between the synovium and other joint tissues ranged from 2 to 30 over 30 minutes. The uptake after intra-articular injection of 0.25 ml of 150,000 ppm resulted in an average synovial boron concentration of 19,000 ppm over 30 minutes. This was more than adequate to warrant continuation to animal irradiations, i.e. where a BNCS treatment would be carried out and effects on both the synovium and other joint tissues could be examined.

Using KBH as the boron compound, the efficacy of BNCS at different radiation doses was tested on the AIA rabbit model with the tandem accelerator in operation at MIT LABA. AIA rabbits received an intra-articular injection of 0.25 ml of 150,00 ppm of boron in the form of enriched KBH and their joints were irradiated using the moderated 1.5 MeV Be(d,n) reaction as neutron source, and thereby effecting a BNCS treatment. It was shown that arthritic synovial tissue can be ablated non-invasively via BNCS. A large range of target doses was tested varying from 1,400 to 140,000 RBE-cGy. Delivery of doses around 10,000 RBE-cGy, and higher, resulted in substantial synovial tissue necrosis, while doses around 6,000 RBE-cGy in all cases caused a reduction in the inflammatory cell infiltrate. In one case, dramatic tissue necrosis was also observed, while in the others it was unclear whether the existing cell infiltrate consisted of original lymphocytes, or ones recruited due to tissue damage. Delivery of a synovial target dose of 3,600 RBE-cGy seemed to have an anti-inflammatory effect, while a target dose of 1,400 RBE-cGy only slightly reduced the thickness of the synovium. Neither injection of the compound alone nor neutron irradiation caused necrotic changes to the synovium, thereby allowing the attribution of cellular kill to the boron neutron capture reaction. It should be noted that doses were based on an average synovial concentration of 19,000 ppm. The range of uptake, however, was large and the potential variation in the dose to anterior synovium could as high as 40%. Also, discrepancies in dosimetry between the MCNP calculations and experimental measurements lead to a scaling of yield of the ^{9}Be(d,n) reaction, as reported in the literature. This, in addition to the lack of angular information, may lead to a further error in target doses to the synovium, of up to 50%. However, a dose-dependent effect of BNCS is suggested and the efficacy of BNCS in causing synovial ablation of arthritic synovium has been demonstrated.

Although KBH has proved to be a useful compound for the experimental testing of synovectomy, it is by no means implied that this is an appropriate compound for clinical BNCS and the search for an ideal compound should continue. The creation and evaluation of many potential BNCS boron compounds would be greatly facilitated by a non-invasive and rapid screening method. One such method could entail in vivo prompt gamma neutron activation analysis (IVPGNAA). Two approaches, based on the size of the beam (broad or narrow) were investigated.

Experimental testing was performed at the MITR PGNAA facility using a broad beam. A stand was constructed to accommodate the rabbits and calibration curves were obtained using a rabbit joint phantom. Testing of the MITR PGNAA beam (2 cm in diameter) using the rabbit knee joint phantom revealed that measurements are highly dependent on the position of the boron within the joint, resulting in a variation in B/H ratio as large as a factor of 4 (with a correspondingly large variation in boron concentrations). IVPGNAA was tested on a rabbit and the measurement of the B/H ratio over 60 minutes after intra-articular injection of 0.25 ml of 150,000 ppm of boron (in unenriched KBH) was clearly above background. Measurement via IVPGNAA can be adequate as a compound screening method in evaluating the compound presence in the joint as a function of time. More detailed inferences about synovial uptake are difficult; an evaluation criterion was developed to yield the range of potential synovial boron concentrations given an average joint concentration, however, the range may be too large to be useful (particularly in light of the finding that the B/H ratio may vary by a factor of 4 depending on the position of boron within the joint).

Possible causes for the large variation included the diameter of the beam which was 33% smaller than the rabbit knee, its cosine shaped neutron flux distribution, and the nearby placement of the detector. In order to decrease the variation in the B/H ratio, it was proposed to increase the beam diameter, flatten the neutron flux distribution and increase the detector to joint distance. MCNP simulations were performed to test the effects of these proposed modifications and results still showed large variation in signal as a function of boron position within the knee joint.

Attention was then turned to changing the size of the beam in the other direction, i.e. making it much smaller, leading to an entirely different approach to the non-invasive determination of boron compound residence time. In this approach, the average joint boron concentration is not measured but rather the knee joint would be probed in different spots with a highly collimated beam. MCNP simulation studies of a slit beam (1 mm by 5 mm) in a rabbit joint phantom examining signal as a function of boron position within the joint showed that signal was a factor of 2 to 5 higher in cells upon which the beam was incident relative to the other cells in the phantom. Signal was also examined as a function of boron concentration in one cell at a time; the boron concentration in neighboring cells would need to be 4 to 10 times higher in order to produce the same signal as the cell upon which the beam is incident. Simulations investigating the effects of boron concentration in two cells at a time showed that the largest contribution to signal originated from the cell directly behind the cell upon which the beam is incident; an increase of a factor of 10 in the boron concentration of the cell behind the irradiated cell caused a 50% rise in signal. These simulations provide a motivation to pursue the development of what could be, in essence, a crude neutron tomographic system as a means to screen boron compounds for BNCS.

Future work in IVPGNAA should include the consideration of many engineering issues, such as the verification of the neutron distribution from the beam port, the cost of equipment (related to building an appropriate stand, detector, multichannel analyzer, collimators) and the experimental verification of simulation studies. In addition, attempts could be aimed at deconvolving the signal and reconstructing compound behavior. This could potentially lead to the ability of determining both spatial and temporal aspects of the behavior of boronated compounds for BNCS, which would be immensely useful for boron compound screening.

Given the demonstration of the ability to effect synovial ablation via BNCS with KBH, the next steps with the continuation of this compound include toxicity testing to determine the maximum concentration and/or amount injectable in humans and biodistribution studies in a human joint, for example, in patients about to undergo total knee joint replacement. Generally, pharmacokinetics are faster in animals than humans, which could imply longer retention times in a human joint. An additional advantage in humans is the wealth of pharmacological information available. However, clinical uptake evaluation will be required to determine whether KBH is a useful compound for clinical BNCS.

The development of new types of boron compounds must continue with the goal of obtaining an ideal BNCS agent, one which would accumulate in the synovium and not in other joint tissues (to an appreciable amount). Boronated compounds to be developed include liposomes, carboranes, and others.

References

AFC (Arthritis Foundation Committee on Evaluation of Synovectomy): Multicenter evaluation of synovectomy in the treatment of rheumatoid arthritis, report of results at the end of three years. Arthritis Rheum 20:765-771, 1976.

Anderson RJ: The orthopedic management of rheumatoid arthritis. Arthritis Care Res 9:223-228, 1996.

Ansell BA, Crook A, Mallard JR, Bywaters EGL: Evaluation of intra-articular colloidal gold-Au in the treatment of persistent knee effusions. Ann Rheum Dis 22:435-439, 1963.

ARC (Arthritis and Rheumatism Council and British Orthopedic Association): Controlled trial of synovectomy of knee and MCP joints in rheumatoid arthritis. Ann Rheum Dis 35:437-442, 1976.

Armin J, Grant RT, Pels H, Reeve EB: The plasma, cell and blood volumes of albino rabbits as estimated by the dye (T 1824) and 32P marked cell methods. J Physiol(London) 116:59-73, 1952.

Arnett FC, Edworthy SM, Bloch DA, McShane DJ, Fries JF, Cooper NS, Healey LA, Kaplan SR, Lian MH, Luthra HS, Medsger Jr TA, Mitchell DM, Neustadt DH, Pinals RS, Schaller JG, Sharp JT, Wilder RL, Hunder GG: The American Rheumatism Association 1987 revised criteria for the classification of rheumatoid arthritis. Arthritis Rheum 31:315-24, 1988.

Arnoczky SP, Warren RF: The microvasculature of the meniscus and its reponse to injury: an experimental study in the dog. Am J. Sports Med. 11:131-141, 1983.

Ball J, Chapman JA, Muirden KD: The uptake of iron in rabbit synovial tissue following intra-articular injection of iron dextran. J Cell Biol 22:351-364, 1964.

Barth RF, Soloway AH, Fairchild RG, Brugger RM: Boron neutron capture therapy for cancer. Cancer 70:2995-3007, 1992.

Beynon TD, Allen DA, Beddoe A, Constantine G, Earwaker LG, James N, Green S, Morgan WN, Weaver DR: Towards the final design of an accelerator-based facility for clinical boron cancer therapy (BCT). In: Advances in Neutron Capture Therapy, Volume 1: Medicine and Physics, edited by B Larsson, J Crawford, R Weinreich. Elsevier, Amsterdam, 1997.

Blackburn BW, Yanch JC, Klinkowstein RE: Development of a high-power water cooled beryllium target for use in accelerator-based boron neutron capture therapy. Med Phys 25:1967-1975, 1998.

Boland AT, Deland JT: Sports Medicine. In: Arthritis Surgery, edited by CB Sledge, S Ruddy, ED Harris, WN Kelley. WB Saunders Co, Philadelphia, 1994.

Bonanomi MH, Velvart M, Stimpel M, Roos KM, Fehr K, Weder HG: Studies of pharmacokinetics and therapeutic effects of glucocorticoids entrapped in liposomes after intraarticular application in healthy rabbits and in rabbits with antigen-induced arthritis. Rheumatol Int 7:203-212, 1987.

Bridgman JF, Bruckner F, Eisen V, Tucker A, Bleehen NN: Irradiation of the synovium in the treatment of rheumatoid arthritis. Q J Med 42:357-367, 1973.

Briesmeister JF: MCNP - A General Monte Carlo Code for N-Particle Transport. Los Alamos National Laboratory LA 7396-M Rev. 2, 1986.

Burkitt HG, Young B, Heath JW, Editors: Wheater's Functional Histology. Churchill Livingstone Incorporated, Edinburgh, 1993.

Burkitt HG, Stevens A, Lowe JS, Young B, Editors: Wheater's Basic Histopathology. Churchill Livingstone, New York. 1996.

Busse PM, Zamenhof RG, Harling OK, Kaplan I, Kaplan J, Chuang C, Goorley J, Kiger III WS, Riley K, Tang L, Solares GR, Palmer MR: Harvard-MIT BNCT program: overview of the clinical trials and translational research. To be published in: Proceedings of the Eighth International Symposium on Neutron Capture Therapy for Cancer, La Jolla, 1998.

Capala J, Makar MS, Coderre JA: Accumulation of boron in malignant and bornal cells incubated in vitro with boronophenylalanine, mercaptoborane or boric acid. Rad Res 146:554-560, 1996.

Caswell RS, Coyne JJ, Randolph ML: Kerma factors for elements and compounds for neutron energies below 30 MeV. Int J Appl Radiat Isot 33:1227-1262, 1982

Chabeuf JN: Design and construction of a prompt gamma activation analysis facility, and improvement of the on-line beam monitor system for the medical beam at the MITR-II. Thesis for Nuclear Engineer degree, Department of Nuclear Engineering, MIT, 1993.

Chan KA, Felson DT, Yood RA, Walker AM: The lag time between onset of symptoms and diagnosis of rheumatoid arthritis. Arthritis Rheum 37:814-820, 1994.

Chu WT, Bleuel DL, Donahue RJ, Grough RA, Hoff MD, Kwan J, Leung KN, Ludewigt BA, Peters C, Phillips TL, Reginato LL, Staples JW, Wells RP, Yu SS: Design of a new BNCT facility based on an ESQ accelerator. In Advances in Neutron Capture Therapy, Volume 1: Medicine and Physics, edited by B Larsson, J Crawford, R Weinreich. Elsevier, Amsterdam, 1997.

Clayton ML: Synovectomy. In: Surgery for Rheumatoid Arthritis. Churchill Livingstone Incorporated, Edinburgh, 1992.

Clement SD, Choi JR, Zamenhof RG, Yanch JC, Harling OK: Monte Carlo methods of neutron beam design for neutron capture therapy at MITR-II. In: Neutron Beam Design, Development, and Performance for Neutron Capture Therapy, edited by OK Harling, JA Bernard, RG Zamenhof. Plenum Press, New York, 1990.

Clunie G, Ell PJ: A survey of radiation synovectomy in Europe, 1991-1993. Eur J Nucl Med 22:970-976, 1995.

Cooke TDV: Antigen-induced arthritis, polyarthritis and tenosynovitis. In: CRC Handbook of Animal Models for the Rheumatic Diseases, Volume 1, edited by RA Greenwald, HS Diamond. CRC Press Incorporated, Boca Raton, 1988.

Consden R, Doble A, Glynn LE, Nind AP: Production of a chronic arthritis with ovalbumin. Ann Rheum Dis 30:307-315, 1971.

Cotton FA, Wilkinson G: Basic Inorganic Chemistry. J Wiley and Sons, Ann Arbor, 1985.

Davis MA, Chinol M: Radiopharmaceuticals for radiation synovectomy: evaluation of two yttrium-90 particulate agents. J Nucl Med 30:1047-1055, 1989.

Deutsch E, Brodack JS, Deutsch KR: Radiation synovectomy revisited. Eur J Nucl Med 20:1113-1127, 1993.

Diaz AZ, Chanana AD, Capala J, Chadha M, Coderre JA, Elowitz EH, Iwai J, Joel DD, Liu HB, Ma R, Shady M, Slatkin DN, Tyson GW, Wielopolski L: Safety and efficacy of BNCT for glioblastoma multiforme: results from the initial dose escalation studies. To be published in: Proceedings of the Eighth International Symposium on Neutron Capture Therapy for Cancer, La Jolla, 1998.

Dolphin GW: Biological hazards of radiation. Ann Rheum Dis 32(Suppl 6):23-28, 1973.

Dumonde DE, Glynn LE: The production of arthritis in rabbits by an immunological reaction to fibrin. Br J Exp Pathol 43:373-383, 1962.

Edmonds J, Smart R, Laurent R, Butler P, Brooks P, Hoschl R, Wiseman J, Goerge S, Lovegrove F, Warwick A, Owen E, Webb J, Booth R, Clemens L, McLaren A, Druce M, Hetherington E, Prosser S, Whitwell J, Lambrecht Rl: A comparative study of the safety and efficacy of dysprosium-165 hydroxide macro-aggregate and yttrium-90 silicate colloid in radiation synovectomy--a multicentre double blind clinical trial. Australian Dysprosium Trial Group. Br J Rheumatol 33:947-953, 1994.

Emami B, Lyman J, Brown A, Coia L, Goitein M, Munzenrider JE, Shank B, Solin LJ, Wesson M: Tolerance of normal tissue to therapeutic irradiation. Int J Radiation Oncology Biol Phys 21:109-122, 1991.

Eulderink F: The synovial biopsy. In: Bone and Joint Disease, edited by CL Berry. Springer-Verlag, New York, 1982.

Fairchild RG, Kahl SB, Laster BH, Kalef-Ezra J, Popenoe EA: In vitro determination of uptake, retention, distribution , biological efficacy and toxicity of boronated compounds for neutron capture therapy: a comparison of porphyrins with sulfhydryl boron hydrides. Cancer Res 50:4860-4865, 1990.

Fernandez-Repollet E, Schwartz A: Microspheres and phagocytosis. In: Microspheres: Medical and Biological Applications, edited by A Rembaum. CRC Press, Boca Raton, 1988.

Firestein, GS: Etiology and pathogenesis of rheumatoid arthritis. In: Textbook of Rheumatology, 5th Edition, edited by WN Kelley, ED Harris Jr, S Ruddy, CB Sledge. W. B. Saunders Company, Philadelphia, 1997.

Fleming A, Crown JM, Corbett M: Incidence of joint involvement in early rheumatoid arthritis. Rheumatol Rehab 15:92-96, 1976.

Foong WC, Green KL: Treatment of antigen-induced arthritis in rabbits with liposome-entrapped methotrexate injected intra-articularly. J Pharm Pharmacol 45:204-209, 1993.

Forbes RM, Cooper AR, Mitchell HH: On the occurrence of beryllium, boron, cobalt, and mercury in human tissues. J Biol Chem 209:857-865, 1954.

Freemont AJ: Histopathology of the rheumatoid joint. In: Mechanisms and Models in Rheumatoid Arthritis. Academic Press, London, 1995.

Geens S: Synovectomy and debridement of the knee in rheumatoid arthritis. Part I. Historical review. J Bone Joint Surg [Am] 51A:617-625, 1969.

Geens S, Clayton ML, Leidholt JD, Smyth CJ, Bartholomew BA: Synovectomy and debridement of the knee in rheumatoid arthritis. J Bone Joint Surg [Am] 51A:62-642, 1969

Gibbons MJ, Butler DL, Grood ES, Byslki-Austrow DI, Levy MS, Noyes FR: Effects of gamma irradiation on the initial mechanical and material properties of goat bone-patellar tendon-bone allografts. J Orthop Res 9:209-218, 1991.

Gierga DP: Personal communication, MIT LABA, 1998,1999.

Gierga DP, Yanch JC, Shefer RE: Development and construction of a neutron beamline for accelerator-based boron neutron capture synovectomy. Submitted to Med Phys, 1999.

Goldberg VM, Lance EM, Davis P: Experimental immune synovitis in the rabbit, relative roles of cell mediated and humoral immunity. Arthritis Rheum 17:993-1005, 1974.

Goldie I: Pathomorphologic features in original and regenerated synovial tissues after synovectomy in rheumatoid arthritis. Clin Orthop 77:295-304, 1971.

Goldlust MB, Rich MS, Brown WR: Immune synovitis in rabbits. Am J Pathol 91:329-344, 1978.

Goodhead DT: The initial physical damage produced by ionizing radiations. Int J Radiat Biol 5:623-634, 1989.

Gordon DA: Gold compounds in the rheumatic diseases. In: Textbook of Rheumatology, edited by WN Kelley, ED Harris JR, S Ruddy, CB Sledge, 4th Edition. W. B. Saunders Company, Philadelphia, 1993.

Gumpel JM, Beer TC, Crawley JCW, Farran HEA: Yttrium 90 in persistent synovitis of the knee - a single centre comparison. The rentention and extra-articular spread of four Y-90 radiocolloids. Brit J Radiol 49:377-381, 1975.

Gumpel GM, Roles NC: A controlled trial of intra-articular radiocolloids versus surgical synovectomy in persistent synovitis. Lancet 1:488-489, 1975.

Harling OK, Rogus R, Choi JR, Moulin DJ, Zamenhof RG, Yanch JC: Dosimetry and dose control for clinical trials of neutron capture therapy at the MITR-II reactor. In: Topics in Dosimetry & Treatment Planning for Neutron Capture Therapy, edited by RG Zamenhof, GR Solares, OK Harling. Advanced Medical Publishing, Madison, 1994.

Harling OK, Roberts KS, Moulin DJ, Rogus RD: Head phantoms for neutron capture therapy. Med Phys 22:579-583, 1995.

Harris, ED Jr: Rheumatoid Arthritis. W. B Saunders Company, Philadelphia, 1997.

Harris WH, Sledge CB: Total hip and total knee replacement. N Engl J Med 323:725-731, 1990.

Hasty KA, Reife RA, Kang AH, Stuart JM: The role of stromelysin in the cartilage destruction that accompanies inflammatory arthritis. Arthritis Rheum 33:388-397, 1990.

Havercroft JM, Ward NI: Boron and other elements in relation to rheumatoid arthritis. In: Trace Elements in Man and Animals, edited by B Momcilovic. IMI, Zagreb, 1991.

Hede A, Larsen E, Sandberg H: Partial versus total meniscectomy. A prospective randomised study with long-term follow-up. J Bone Joint Surg [Br] 74B:118-121, 1992.

Henderson B, Glyn LE, Chayen J: Experimental allergic arthritis in the rabbit: alterations in the cellularity and the rate of cellular proliferation in the synovial linings of the challenged joints of rabbits immunized with antigen in Freund's incomplete adjuvant. Br J Exp Path 63:5-12. 1982.

Hexeberg E, Westby J, Hessevik I, Hexeberg S: Effects of endurance training on left ventricular performance: a study in anaesthetized rabbits. Acta Physiol Scand 154:479-488, 1995.

Hnatowich DJ, Kramer RI, Sledge CB, Noble J, Shortkroff S: Dysprosium-165 ferric hydroxide macroaggregate for radiation synovectomy. J Nucl Med 19:303-308, 1978.

Hou SM, Yu HY: Comparison of systemic absorption of aqueous and liposomal lidocain following intra-articular injection in rabbits. J Formos Med Assoc 96:141-143, 1997.

Howard WB, Yanch JC, Grimes SM, Massey TN, Al-Quaraishi AI, Jacobs DK, Brient CE: Measurement of the $^{9}Be(p,n)$ thick target spectrum for use in accelerator-based boron neutron capture therapy. Submitted for publication in Nuclear Science and Engineering, 1997.

Hunneyball IM: Use of experimental arthritis in the rabbit for the development of antiarthritic drugs. In: Advances in Inflammation Research, Volume 7, edited by I Otterness, R Capetola, S Wong. Raven Press, New York, 1984.

ICRP-30: Reference Manual, International Commmission on Radiation Protection. Elmsford, New York, 1975.

Ishikawa H, Ohno O, Hirohata K: Long-term results of synovectomy in rheumatoid arthritis. J Bone Joint Surg [Am] 68A:198-205, 1986.

Jasin HE, Ziff M: Immunoglobulin and specific antibody synthesis in a chronic inflammatory focus: Antigen-Induced synovitis. J Immunol 102:355-369, 1969.

Jensen CM, Poulsen S, Ostergren M, Hansen KH: Early and late synovectomy of the knee in rheumatoid arthritis. Sand J Rheumatol 20:127-131, 1991.

Johnson LS: Beta-particle dosimetry in radiation synovectomy and the use of the B(n,alpha) nuclear reaction to examine the pathology of rheumatoid arthritis. Thesis for Doctor of Philosophy degree. Massachusetts Institute of Technology, Department of Nuclear Engineering, 1994.

Kanda K: Experience of boron neutron capture therapy in Japan. In: Advances in Neutron Capture Therapy, Volume 1: Medicine and Physics, edited by B Larsson, J Crawford, R Weinreich. Elsevier Press, Amsterdam, 1997.

Kellaway IW, Chawla RS: Factors infllluencing the clearance rates of colloidal particles from the rabbit knee joint. In: Radionuclide Imaging in Drug Research, edited by CG Wilson, JG Hardy, M Frier, SS Davis. Croom Helm, London, 1982.

Klinkowstein RE, Shefer RE, Yanch JC, Howard WB, Song H, Binello E, Blackburn BW, Daigle JL, Sears SM, Goldie CH, Ledoux RJ: Operation of a high current tandem electrostatic accelerator for boron neutron capture therapy. In: Advances in Neutron Capture Therapy, Volume 1: Medicine and Physics, edited by B Larsson, J Crawford, R Weinreich. Elsevier, Amsterdam, 1997.

Knoll GF: Radiation Detection and Measurement. Second edition. J Wiley and Sons, New York, 1989.

Knoth WH, Sauer JC, England DC, Hertler WR, Muetterties EL: Chemistry of boranes. XIX. Derivative chemistry of $B_{10}H_{10}^{-2}$ and $B_{12}H_{12}^{-2}$. J Am Chem 86:3973-3983, 1964.

Kozma C, Macklin W, Cummins LM, Mauer R: Anatomy, physiology and biochemistry of the rabbit. In: Biology of the Laboratory Rabbit, edited by SH Weisbroth, RE Flatt, AL Kraus, Academic Press, New York, 1974.

Laurin CA, Desmarchais J, Daziano L, Gariepy R, Derome A: Long-term results of synovectomy of the knee in rheumatoid patients. J Bone Jont Surg [Am] 56A:521-531, 1974.

Lipscomb WN: Boron Hydrides. WA Benjamin, New York, 1963

Lipsky, PE: Rheumatoid arthritis. In: Harrison's Principles of Internal Medicine, 14th Edition, edited by AS Fauci, E Braunwalk, KJ Isselbacher, JD Wilson, JB Martin, DL Kasper, SL Hauser and DL Longo. McGraw-Hill, New York, 1998.

Liskien H, Paulson A: Neutron production cross sections and energies for the reactions $^{7}Li(p,n)^{7}Be^{*}$. Atomic Data Nuclear Tables 15:57, 1975.

Lorig KL, Mazonson PD, Holman HR: Evidence suggesting that health education for self-management in patients with chronic arthritis has sustained health benefits while reducing health care costs. Arthritis Rheum 36:439-446, 1993.

Marmor L: Surgery of the rheumatoid knee. J Bone Joint Sur [Am] 55A:535-544, 1973.

Matusi N, Taneda Y, Ohta H, Itoh T, Tsuboguchi ST: Arthroscopic versus open synovectomy in the rheumatoid knee. Int Orth 13:17-20, 1989.

McEwen C: Multicenter evaluation of synovectomy in the treatment of rheumatoid arthritis, report of results at the end of five years. J Rheumatol 15:764-769, 1988.

McGinty JB, Geuss LF, Marvin RA: Partial or total meniscectomy: a comparative analysis. J Bone Joint Surg [Am] 59:763-766, 1977.

Meadows JW: The thick target $^{9}Be(d,n)$ neutron spectra for deuteron energies between 2.6 MeV and 7.0 MeV. Argonne National Laboratory ANL/NDM-124, 1991.

Miller HC, Miller NE, Muetterties EL: Chemistry of boranes. XX. Syntheses of polyhedral boranes. Inorg Chem 3:1456-1463, 1964..

Mishima Y: Current clinical paradigms in melanoma BNCT. To be published in: Proceedings of the Eighth International Symposium on Neutron Capture Therapy for Cancer, La Jolla, 1998.

Mott JC: Haemorrhage as a test of the function of the cardiovascular system in rabbits of different ages. J Physiol(London) 181:728-752, 1965.

Muetterties EL, Balthis JH, Chiya YT, Knoth WH, Miller HC: Chemistry of boranes. VIII. Salts and acids of $B_{10}H_{10}^{-2}$ and $B_{12}H_{12}^{-2}$. Inorg Chem 3:444-451, 1964.

Muetterties EL, Knoth WH: Polyhedral Boranes. Marcel Dekker, New York, 1968.

Nakagawa Y and Kageji T: Boron neutron capture therapy - recent aspects and new protocols in Japan. To be published in: Proceedings of the Eighth International Symposium on Neutron Capture Therapy for Cancer, La Jolla, 1998.

Newman AP: Synovectomy. In: Arthritis Surgery, edited by CB Sledge, S Ruddy, ED Harris Jr, WN Kelly. W. B. Saunders Company, Philadelphia, 1994.

Neyeret P, Donell ST, Dejour H: Osteoarthritis of the knee following meniscectomy. Br J Rheumatol 33:267-268, 1994.

Nguyen T, Brownell GL, Holden SA, Teicher BA: Intracellular distribution of various boron compounds for use in boron neutron capture therapy. Biochem Pharmacol 45:147-155, 1993.

Nias AHW: An Introduction to Radiobiology. John Wiley and Sons, New York, 1990.

Nielsen FH: Other Elements: Sb, Ba, B, Br, Cs, Ge, Rb, Ag, Sr, Sn, Ti, Zr, Be, Bi, Ga, Au, In, Nb, Sc, Te, Tl, W. In: Trace Elements in Human and Animal Nutrition, Volume 2, 5th Edition, edited by W Mertz. Academic Press, Orlando, 1986.

Nielsen FH, Mullen LM, Gallagher SK, Hunt JR, Hunt CD, Johnson LK: Effects of dietary boron, aluminum and magnesium on serum alkaline phosphatase, calcium and phosphorous, and plasma cholesterol in postmenopausal women. In: Trace Elements in Man and Animals, edited by LS Hurley, CL Keen, B Lonnerdal, RB Rucker. Plenum Press, New York, 1988.

Nielsen FH, Mullen LM, Gallagher SK: Effect of boron depletion and repletion on blood indicators of calcium status in humans fed a magnesium-low diet. J Trace Element Exp Med 3:45-54, 1990.

Nigg DW, Mitchell HE, Harker YD, Harmon JF: Experimental investigation of filtered epithermal photoneutron beams for BNCT. In: Advances in Neutron Capture Therapy, Volume 1: Medicine and Physics, edited by B Larsson, J Crawford, R Weinreich. Elsevier, Amsterdam, 1997.

Noble J, Jones AG, Davies MA, Sledge CB, Kramer RI, Livni E. Leakage of radioactive particle systems from a synovial joint studies with a gamma camera. J Bone and Joint Surg [Am] 65A: 381-389, 1983.

Ochi T, Iwase R, Kimura T, Hirooka A, Masada K, Owaki H, Wakitani S, Murata N, Ono K: Effect of early synovectomy on the course of rheumatoid arthritis. J Rheumatol 18:1794-1798, 1991.

Ogilvie-Harris DJ, Weisleder L: Arthroscopic synovectomy of the knee: Is it helpful?. Arthroscopy 11:91-95, 1995.

Ogilvie-Harris DJ, Basinski A: Arthroscopic synovectomy for rheumatoid arthritis. Arthroscopy 7:91-97, 1991.

Oka M. Radiation synovectomy of the rheumatoid knee with yttrium 90. Ann Clin Res 7:205-210, 1975.

Patzakis MJ, Mills DM, Clayton ML, Smyth CJ: A visual, histological, and enzymatic study of regenerating rheumatoid synovium in the synovectomized knee. J Bone Joint Surg [Am] 55A:287-300, 1973.

Pavelka K, Meier-Ruge W, Mauller W, Fridrich R: Histological study of effects of colloidal 90 yttrium on knee joint tissues of rabbits. Ann Rheum Dis 34: 64-69, 1975.

Pitochelli AR, Hawthorne MF: Structure of $B_{12}H_{12}^{-2}$ ion. J Am Chem Soc 82:4427-4428, 1960.

Platsoucas CD, Chae FH, Collins N, Kernan N,Laver J, Ellingsen T, Stentstad P, Bjorgum J, Rembaum A, O'Reilly R, Ugelstad J: The use of magnetic monosized polymer particles for the removal of T cells from human bone marrow cell suspensions. In: Microspheres: Medical and Biological Applications, edited by A Rembaum. CRC Press, Boca Raton, 1988.

Raaijmakers CPJ, Konijnenberg MW, Verhagen HW, Miknheer BJ: Determination of dose components in phantoms irradiated with an epithermal neutron beam for boron neutron capture therapy. Med Phys 22:321-329, 1995.

Ranawat CS, Malcolm LE, Straub LR: Synovectomy and debridenment of the knee in rheumatoid arthritis (a study of 60 knees). Arthritis Rheum 15:571-581, 1972.

Rangger C, Klestil TK, Gloetzer W, Kemmler G, Benedetto KP: Osteoarthritis after arthroscopic partial meniscectomy. Am J Sports Med 23K240-244, 1995.

Raunest J, Derra E: Laser synovectomy of the knee joint. Arch Orthop Traum Surg 114:220-225, 1995.

Reichel W, Weber KJ: The stabilizing effect of synovectomy on the synovial membrane in arthritic rabbit knees. Arch Orthop Trauma Surg 105:11-17, 1986.

Riley KR: Improved boron-10 quantification via PGNAA and ICP-AES. Thesis for combined Master of Science and Nuclear Engineer degrees. Massachusetts Institute of Technology, Department of Nuclear Engineering, 1997.

Riley KJ, Harling OK: An improved prompt gamma neutron activation analysis facility using a focused diffracted neutron beam. Nucl Instr Meth Phys Res B143:414-421, 1998.

Rodriguez JA, Saddler S, Edelman S, Ranawat CS: Long-term results of total knee arthroplasty in class 3 and 4 rheumatoid arthritis. J Arthroplasty 11:141-145, 1996.

Rogus RD, Harling OK, Yanch JC: Mixed field dosimetry of epithermal neutron beams for boron neutron capture therapy at the MITR-II research reactor. Med Phys 21:1611-1625, 1994.

Roos H, Lauren M, Adalberth T, Roos E, Jonsson K, Lohmander S: Knee osteoarthritis after meniscectomy. Arth Rheum 4:687-693, 1998.

Rosenberg AE: Skeletal system and soft tissue tumors. In: Robbins Pathologic Basis of Disease, 5th Edition, edited by RS Cotran, V Kumar, SL Robbins. WB Saunders Company, New York, 1994.

Salehpour A, Butler DL, Proch FS, Schwartz HE, Feder SM, Doxey CM, Ratcliffe A: Dose-dependent response of gamma irradiation on mechanical properties and related biochemical composition of goat bone-patellar tendon-bone allografts. J Orthop Res 13:898-906, 1995.

Sauerwein W, Moss R, Hideghety K, Stecher-Rasmussen F, deVries M, Reulen H-J, Gvtz C, Paquis P, Wiestler F, Haselsberger K, Wolbers J, Rassow J, Pignol JP, Watkins P, Vroegindeweij C, Ravensberg K, Garbe S, Wiestler OD, Turowski B, Zanella F, Tuow D, Siefert A, Huiskamp R, Frankhauser H, Gabel D: Status Report on the European Clinical Trial of BNCT at Petten. To be published in: Proceedings of the Eighth International Symposium on Neutron Capture Therapy for Cancer, La Jolla, 1998.

Sculco TP: The knee joint in rheumatoid arthritis. Rheum Dis Clin 24:143-156, 1998.

Shapiro AE: Development of micromagnetic particles as carriers for compounds to be localized in the body. Supervised by Dr. I Olmez, principal research scientist at the MIT Nuclear Reactor Laboratory, and final paper in presentations of the Research Science Institute, Summer, 1997.

Shaw IH, Dingle JT: Liposomes as steroid carriers in the intra-articular therapy of rheumatoid arthritis. In: Liposomes in Biological Systems, ediated by G Gregoriadis and AC Allison. John Wiley and Sons Limited, New York, 1980.

Shefer RE, Klinkowstein RE, Yanch JC, Howard WB: Tandem electrostatic accelerators for BNCT. Proceedings of the First International Workshop for Accelerator-based Neutron Sources for Boron Neutron Capture Therapy. Jackson, Wyoming, September 1994, INEL CONF-940976, 1994.

Shibata T, Shiraoka K, Takubo N: Comparison between arthroscopic and open synovectomy for the knee in rheumatoid arthritis. Arch Orthop Trauma Surg 105:257-262, 1986.

Shortkroff S, Jones AG, Sledge CB: Radiation synovectomy. in: Advances in Metals in Medicine, volulme 1. JAI Press Incorporated, 1993.

Shortkroff S: Personal communication. 1998.

Simkin PA, Pizzorno JE: Synovial permeability in rheumatoid arthritis. Arth Rheum 22:689-696, 1979.

Sledge CB: Introduction to surgical management of the patient with arthritis. In: Textbook of Rheumatology, 5th Edition, edited by WN Kelley, ED Harris Jr, S Ruddy, CB Sledge. W. B. Saunders Company, Philadelphia, 1997.

Sledge CB, Zuckerman JD, Shortkroff S, Zalutsky MR, Venkatesan P, Snyder M, Barrett WP: Synovectomy of the rheumatoid knee using intra-articular injection of Dysprosium-165-ferric hydroxide macroaggregates. J Bone and Joint Surg [Am] 69A: 970-975, 1987.

Sledge CB, Zuckerman JD, Zalutsky MR, Atcher RW, Shortkroff S, Lionberger DR, Rose HA, Hurson BJ, Lankenner Jr. PA, Anderson RA, Bloomer WA: A Treatment of rheumatoid synovitis of the knee with intra-articular injection of Dysprosium-165-ferric hydroxide macroaggregate. Arthritis Rheum 29:153-159, 1986.

Sledge CB, Ewald FC: Total knee arthroplasty experience at the Robert Breck Brigham Hospital. Clin Orthop 145:78-84, 1979.

Small NC, Glogau AI, Berezin MA, Farless BL: Office operative arthroscopy of the knee: technical considerations in the preliminary analysis of the first hundred patients. Arthroscopy 10:534-539, 1994.

Smiley P, Wasilewski SA: Arthroscopic synovectomy. Arthroscopy 6:18-23, 1990.

Sodern: fluxes from the Genie 46 neutron generator. Sodern, 20 avenue Descartes, 94451 Lineil-Brevannes, Cedex, France, 1996.

Sokoloff L. Animal models of rheumatoid arthritis. In: International Review of Experimental Pathology, volume 26. Academic Press Incorporated, New York, 1984.

Song H: Accelerator based neutron brachytherapy. PhD Thesis, Department of Physics, Massachusetts Institute of Technology, 1998.

Steffen C, Muller C, Stellamor K, Zeitlhofer J: Influence of x-ray treatment on antigen-induced experimental arthritis. Ann Rheum Dis 41:532-537, 1982.

Stone, CS: Lifetime economic cost of RA. J. Rheumatol 11:819-827, 1984.

Strand S, Andersson L, Bergqvist L: Applications and characterization of radiolabeled or magnetizable nano-and microparticles for RES, lymph, and blood flow studies. In: Microspheres: Medical and Biological Applications, edited by A Rembaum. CRC Press, Boca Raton, 1988.

Strand V, Scott DL, Simon LS, Editors: Novel Therapeutic Agents for the Treatment of Autoimmune Diseases. Marcel Dekker Incorporated, New York, 1997.

Stuart MJ, Rand JA: Total knee arthroplasty in young adults who have rheumatoid arthritis. J Bone Joint Surg [Am] 70A:84-87, 1988.

Takahashi S, Sugimoto M, Kotoura Y, Masanori O, Sasai K, Abe M, Yamamuro T: Long-lasting tolerance of articular cartilage after experimental intraoperative radiation in rabbits. Clin Orthop 275:300-305, 1992.

Tapper EM, Hoover NW: Late results after meniscectomy. J Bone Joint Surg [Am] 51A:517-526, 1969.

Teichman S, Crawford JF: Theroetical study of a spallation neutron source for BNCT. In: Advances in Neutron Capture Therapy, Volume 1: Medicine and Physics, edited by B Larsson, J Crawford, R Weinreich. Elsevier, Amsterdam, 1997.

Trauner KB, Gandour-Edwards R, Bamberg M, Shortkroff S, Sledge CB, Hasan T: Photodynamic synovectomy using benzoporphyrin derivative in an antigen-induced arthritis model for rheumatoid arthritis. Photochem Photobio 67(1):133-139, 1998.

Travers RL, Rennie GC, Newnham RE: Boron and arthritis: the results of a double-blind pilot sudy. J Nutr Med 1:127-132, 1990.

Tsuchiya S, Yamabe M, Yamaguchi Y, Kobayashi Y, Konno T, Tada K: Establishment and characterization of a human acute monocytic leukemia cell line (THP-1). Int J Cancer 26:171-176, 1980.

Turner JE: Atoms, Radiation, and Radiation Protection. McGraw-Hill, New York, 1986.

Utkhede D, Yeh V, Szucs M, Tilcock C: Uptake of yttrium-90 into lipid vesicles. J Liposome Res 4:1049-1061, 1994.

Valtin H, Schafer JA: Renal Function. Little Brown and Company, Boston, 1995.

Verbakel WFAR, Stecher-Rasmussen F: In-vivo prompt gamma-ray boron determination in patients during BNCT in Petten. To be published in: Proceedings of the Eighth International Symposium on Neutron Capture Therapy for Cancer, La Jolla, 1998.

Verdeck WN, McBeath AA: Knee synovectomy for rheumatoid arthritis. Clin Orth 134:168-172, 1978.

Wallis WJ, Simkin PA, Nelp WB, Foster DM: Intraarticular volume and clearance in human synovial effusions. Arth Rheum 28:441-449, 1985.

Walsh DA, Sledge CB, Blake DR: Biology of the normal joint. In: Textbook of Rheumatology, 5th Edition, edited by WN Kelley, ED Harris Jr, S Ruddy, CB Sledge. W. B. Saunders Company, Philadelphia, 1997.

Watson-Clark RA, Banquerigo ML, Shelly K, Hawthorme MF, Brahn E: Model studies directed toward the application of boron neutron capture therapy to rheumatoid arthritis: Boron delivery by liposomes in rat collagen-induced arthritis. Proc Natl Acad Sci USA 95:2531-2534, 1998.

Weinblatt ME, Kaplan H, Germain BF, Block S, Solomon SD, Merriman RC, Wolfe F, Wall B, Anderson L, Gall E: Methotrexate in rheumatoid arthritis. Arthritis Rheum 37:1492-1498, 1994.

Wheeler FJ, Parsons DK, Bigg DW, Wessol DE, Miller LG, Fairchild RG: Physics design for the Brookhaven Medical Research Reactor epithermal neutron source. In: Neutron Beam Design, Development, and Performance for Neutron Capture Therapy, edited by OK Harling, JA Bernard, RG Zamenhof. Plenum Press, New York, 1990.

Whipple TL, Duval MJ: Arthroscopy and synovectomy. In: Textbook of Rheumatology, 5th Edition, edited by WN Kelley, ED Harris Jr, S Ruddy, CB Sledge. W. B. Saunders Company, Philadelphia, 1997.

White SM: Beam characterization for accelerator-based boron neutron capture therapy using the ^{9}Be(d,n) nuclear reaction. Thesis for Master of Science degree. Massachusetts Institute of Technology, Department of Nuclear Engineering, 1998.

Whittlestone S: Neutron distributions from the deuteron bombardment of a thick beryllium target. J Phys D(Appl. Phys) 10:1715-1723, 1977.

WHO (World Health Organization): Trace Elements in Human Nutrition and Health. World Health Organization, Geneva, 1996.

Widder KJ, Senyei AE, Scarpelli DG: Magnetic microspheres: a model system for site specific drug delivery in vivo. Proc Soc Exp Biol Med 158:141-146, 1978.

Williams ED, Caughey DE, Hurley PJ, John MB: Distribution of yttrium 90 ferric hydroxide colloid and gold-198 colloid after injection into knee. Ann Rheum Dis 35:516-520, 1976.

Wilson MG, Kelley K, Thornhill TS: Infection as a complication of total knee replacement arthroplasty: risk factors and treatment in sixty-seven cases. J Bone Joint Surg [Am] 72A:878-883, 1990.

Windsor RE, Insall JN: The knee. In: Textbook of Rheumatology, 5th Edition, edited by WN Kelley, ED Harris Jr, S Ruddy, CB Sledge. W. B. Saunders Company, Philadelphia, 1997.

Wood GW: An introduction to Boron: history, sources, uses and chemistry. Env Health Persp 102(suppl 7):5-11, 1994.

Wunderlich J, Lipscomb WN: Structure of the $B_{12}H_{12}^{=}$ ion. J Am Chem Soc 82:4427-4428, 1960.

Yanch JC, Zhou XL, Brownell GL: A Monte Carlo investigation of the dosimetric properties of monoenergetic neutron beams for neutron capture therapy. Radiat Res 126: 1-20, 1991.

Yanch JC, Zhou XL, Shefer RE, Klinkowstein RE: Accelerator-based epithermal neutron beam design for neutron capture therapy. Med Phys 19:709-721, 1992.

Zalutsky MR, Noska MA, Gallagher PW, Shortkroff S, Sledge CB: Use of liposomes as carriers for radiation synovectomy. Nucl Med Biol 15:151-156, 1988.

Zamenhof RG, Murray BE, Brownell GL, Wellum GR, Tolpin EI: Boron neutron capture therapy for the treatment of cerebral gliomas. I. Theoretical evaluation of the efficacy of various neutron beams. Med Phys 2:47-60, 1975.

Zhou XL: A design of an accelerator-based epithermal neutron beam for boron neuton capture therapy. Thesis for degrees of Master of Science and Nuclear Engineer. Massachusetts Institute of Technology, Department of Nuclear Engineering, 1990.

Ziegler JF, Biersack JP, Littmark U: The Stopping and Range of Ions in Solids. Pergamon Press, New York, 1996.

Zuckerman JD, Sledge CB, Shortkroff S, Venkatesan P: Treatment of antigen-induced arthritis in rabbits with dysprosium-165-ferric hydroxide macroaggregates. J Orth Res 7:50-60, 1989.

Appendices

A: Dose depth profiles in the MCNP human knee phantom for ideal beams with combinations of boron concentrations in synovium and bone (section 2.3.1)

B: Dose depth profiles in the MCNP human knee phantom for ideal beams with combinations of boron concentrations in synovium, synovial fluid and cartilage (section 4.2.3)

C: Results of the IVPGNAA slit beam simulations which examined signal as a function of boron concentration in two cells simultaneously for beam positions 12 and 18 (section 6.2.2)

A1: Dose per depth in joint phantom
0.025 eV ideal isotropic beam energy
1000 ppm synovium: 1 ppm elsewhere
(boron concentrations of combination #0)

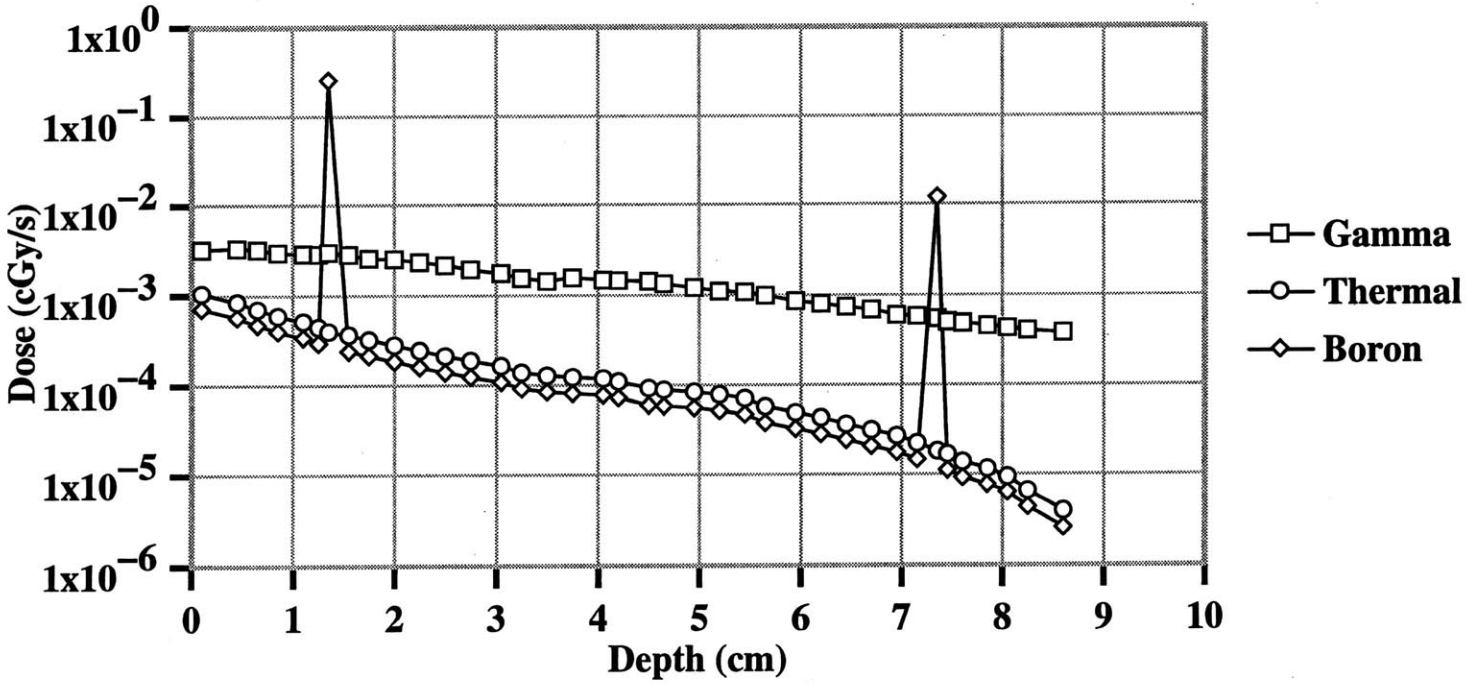

A2: Dose per depth in joint phantom
0.1 eV ideal isotropic beam energy
1000 ppm synovium: 1 ppm elsewhere
(boron concentrations of combination #0)

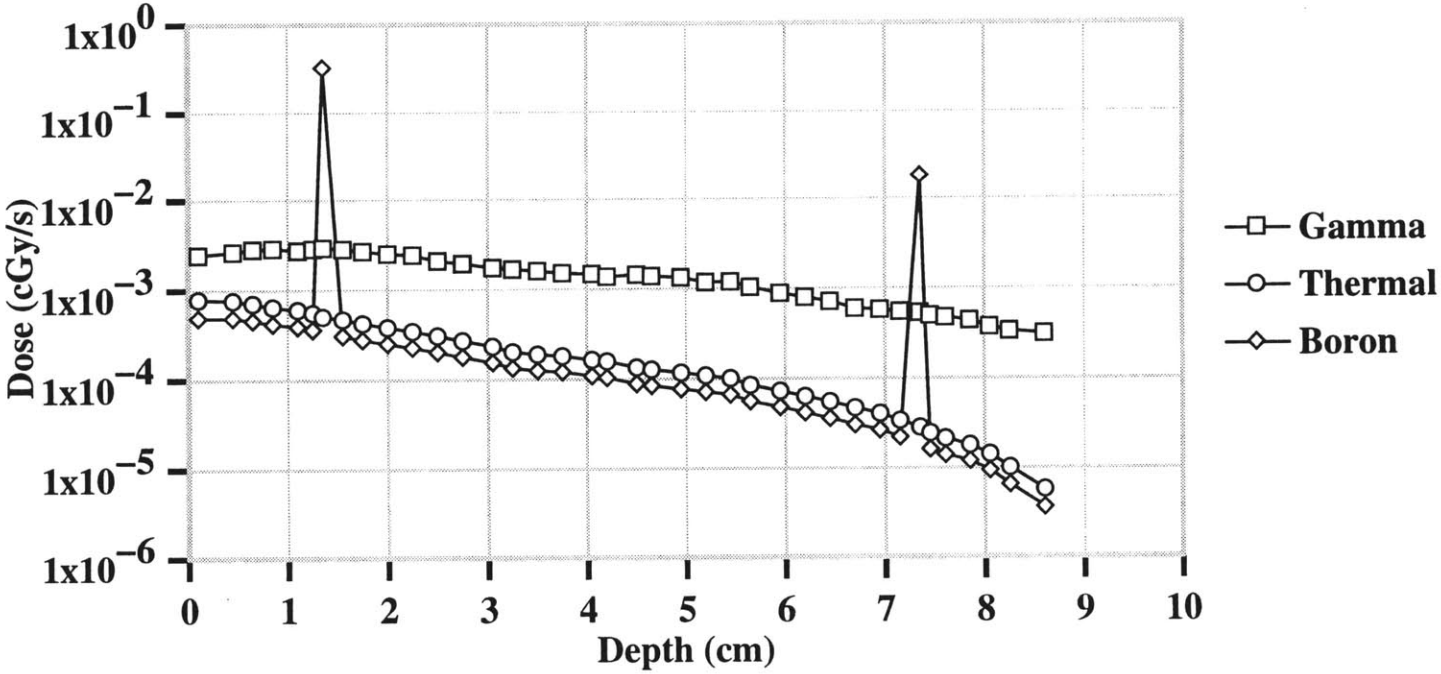

A3: Dose per depth in joint phantom
1 eV ideal isotropic beam energy
1000 ppm synovium: 1 ppm elsewhere
(boron concentrations of combination #0)

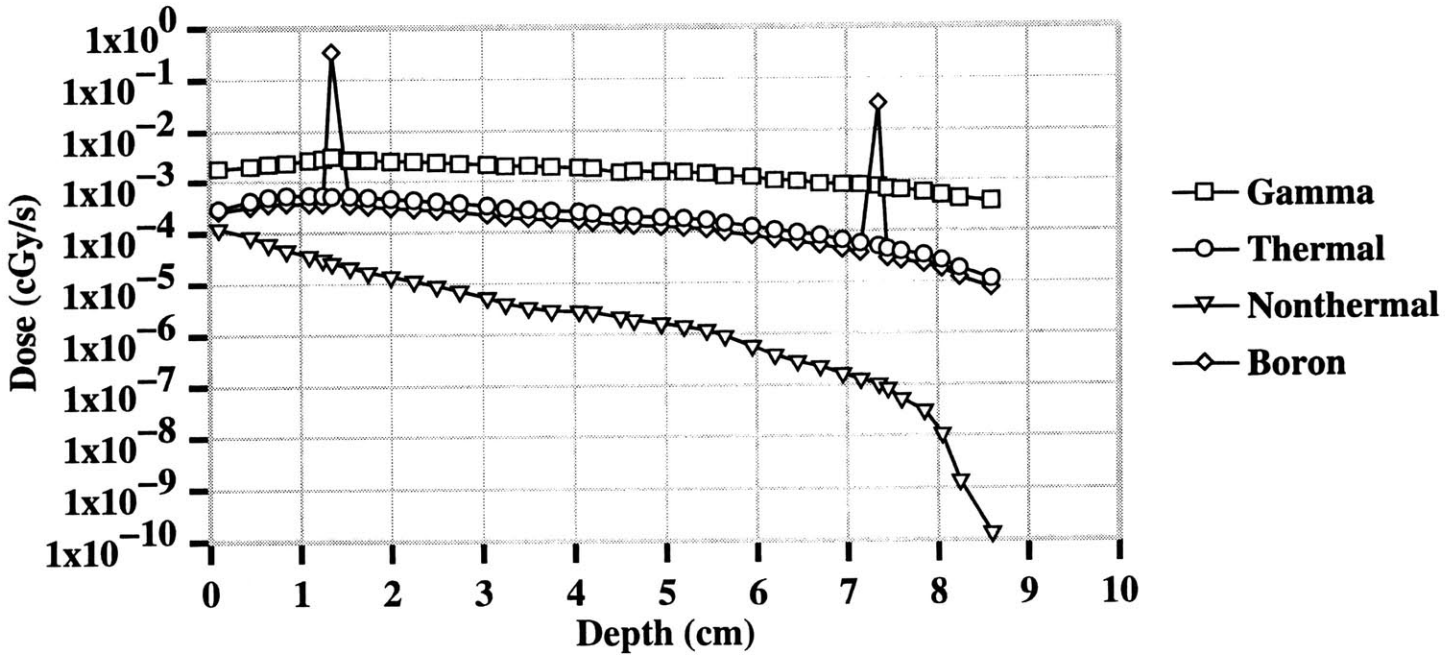

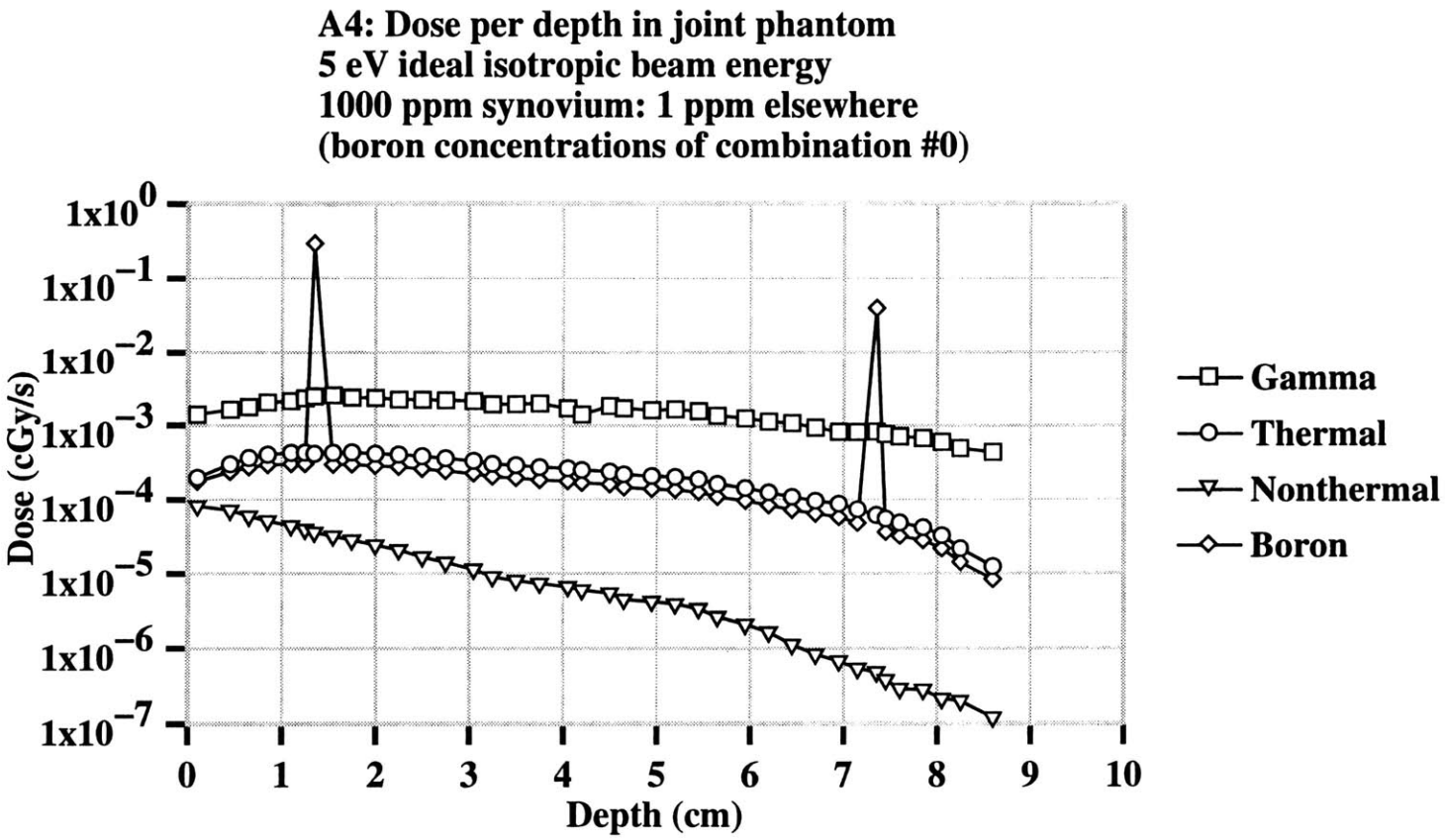
A4: Dose per depth in joint phantom
5 eV ideal isotropic beam energy
1000 ppm synovium: 1 ppm elsewhere
(boron concentrations of combination #0)
Dose (cGy/s)
1x10^0
1x10^-1
1x10^-2
1x10^-3
1x10^-4
1x10^-5
1x10^-6
1x10^-7
0
1
2
3
4
5
6
7
8
9
10
Depth (cm)
Gamma
Thermal
Nonthermal
Boron

A5: Dose per depth in joint phantom
10 eV ideal isotropic beam energy
1000 ppm synovium: 1 ppm elsewhere
(boron concentrations of combination #0)

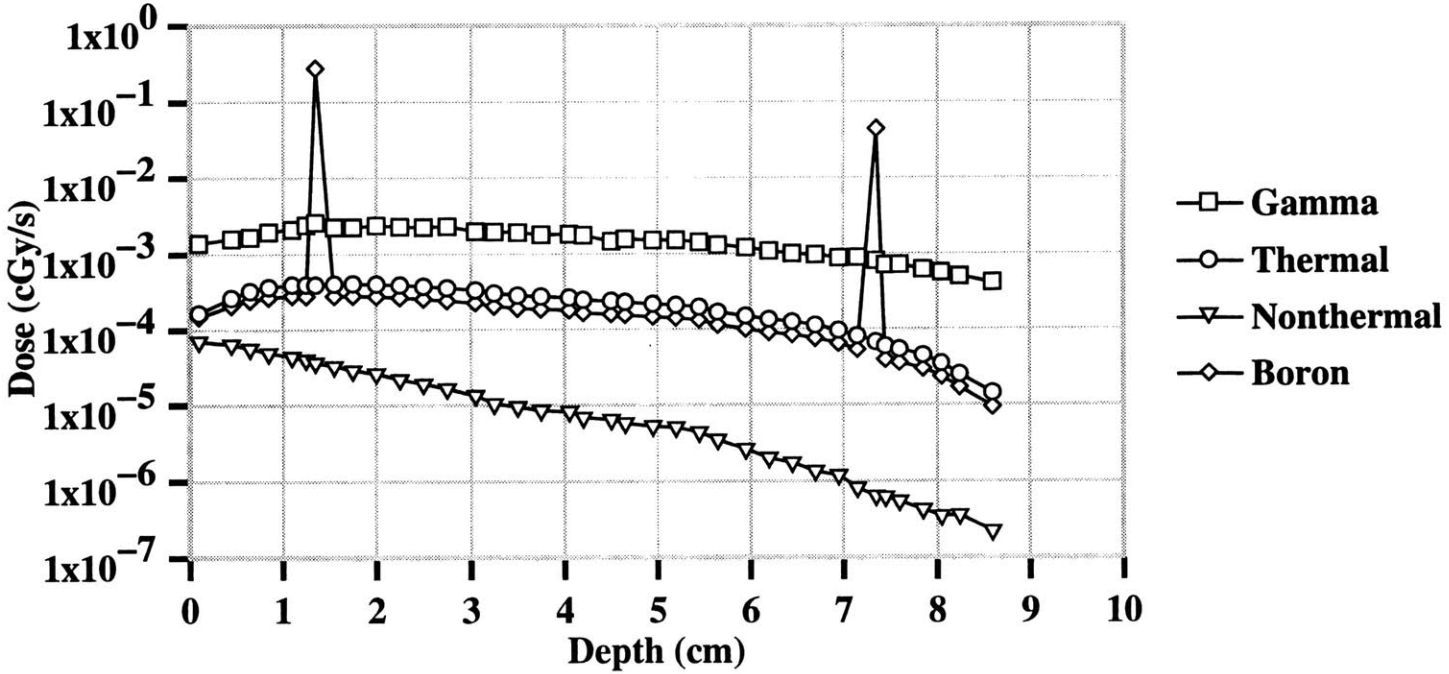

A6: Dose per depth in joint phantom
25 eV ideal isotropic beam energy
1000 ppm synovium: 1 ppm elsewhere
(boron concentrations of combination #0)

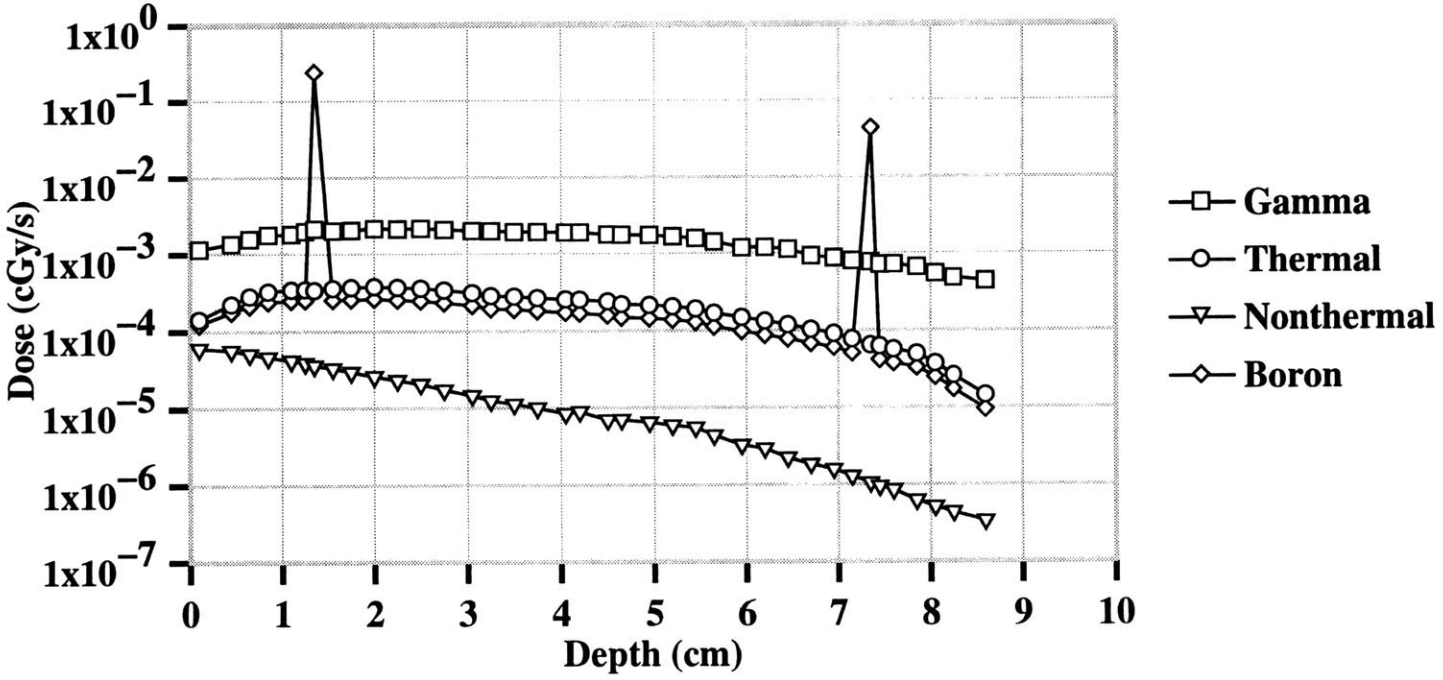

A7: Dose per depth in joint phantom
50 eV ideal isotropic beam energy
1000 ppm synovium: 1 ppm elsewhere
(boron concentrations of combination #0)

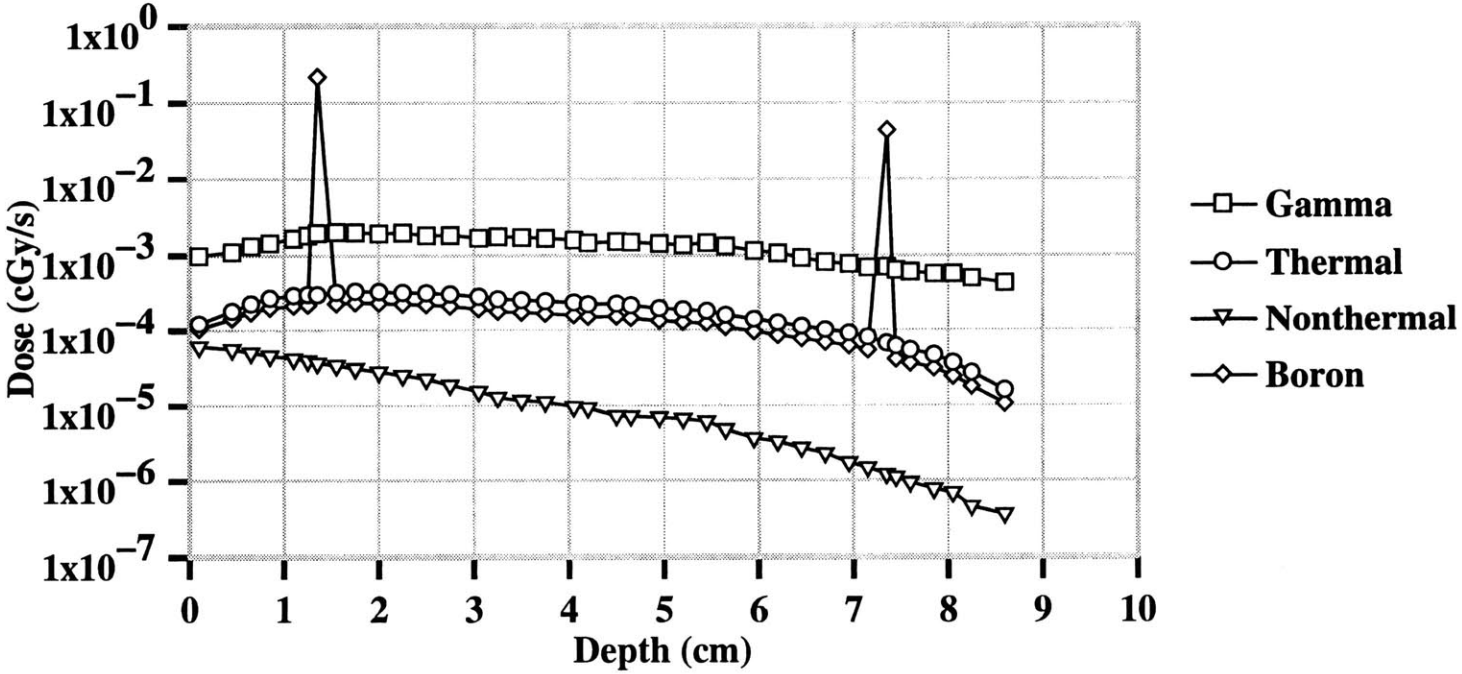

A8: Dose per depth in joint phantom
75 eV ideal isotropic beam energy
1000 ppm synovium: 1 ppm elsewhere
(boron concentrations of combination #0)

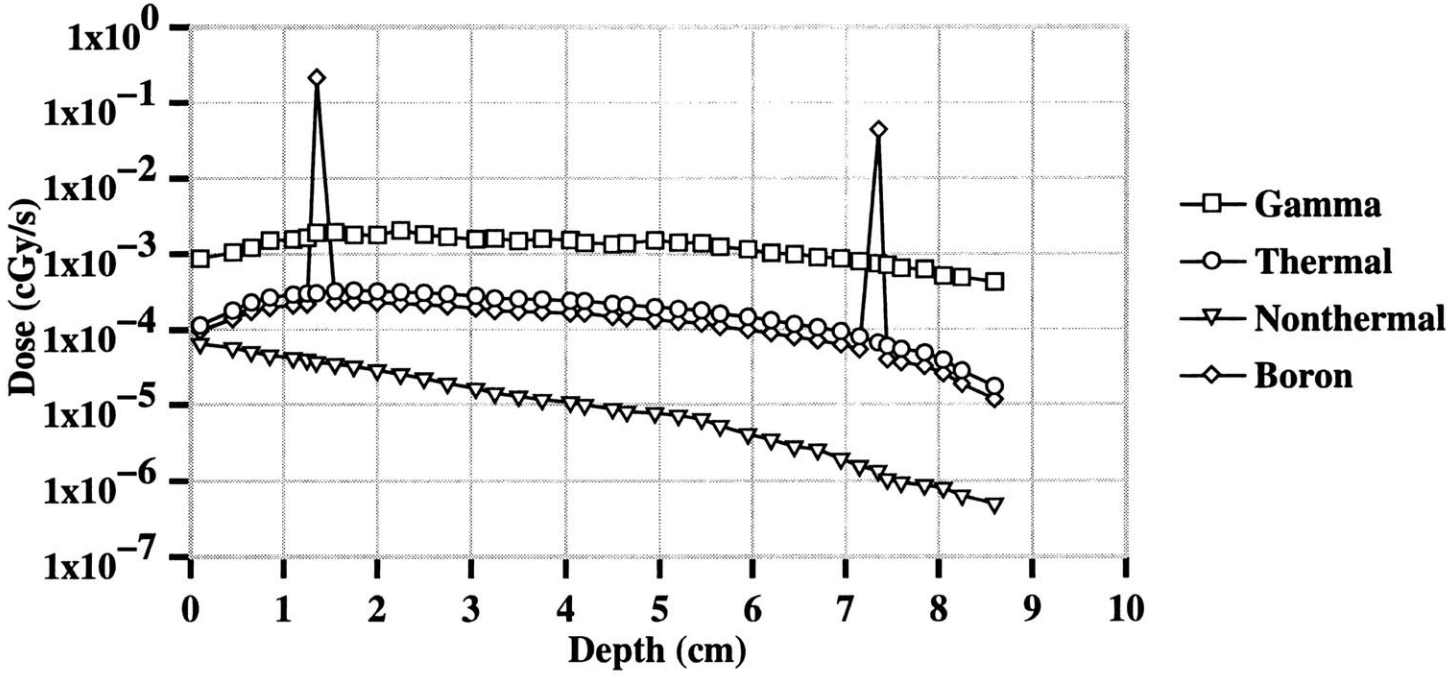

A9: Dose per depth in joint phantom
100 eV ideal isotropic beam energy
1000 ppm synovium: 1 ppm elsewhere
(boron concentrations of combination #0)

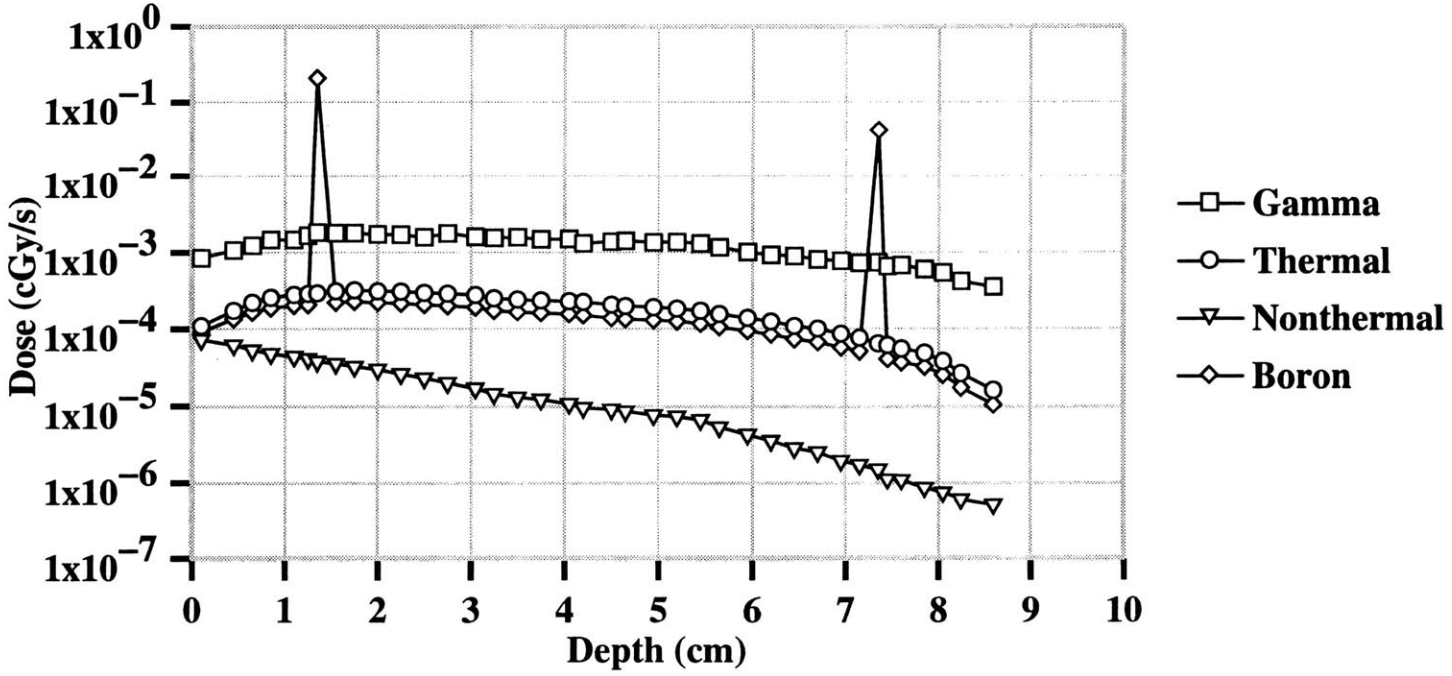

A10: Dose per depth in joint phantom
125 eV ideal isotropic beam energy
1000 ppm synovium: 1 ppm elsewhere
(boron concentrations of combination #0)

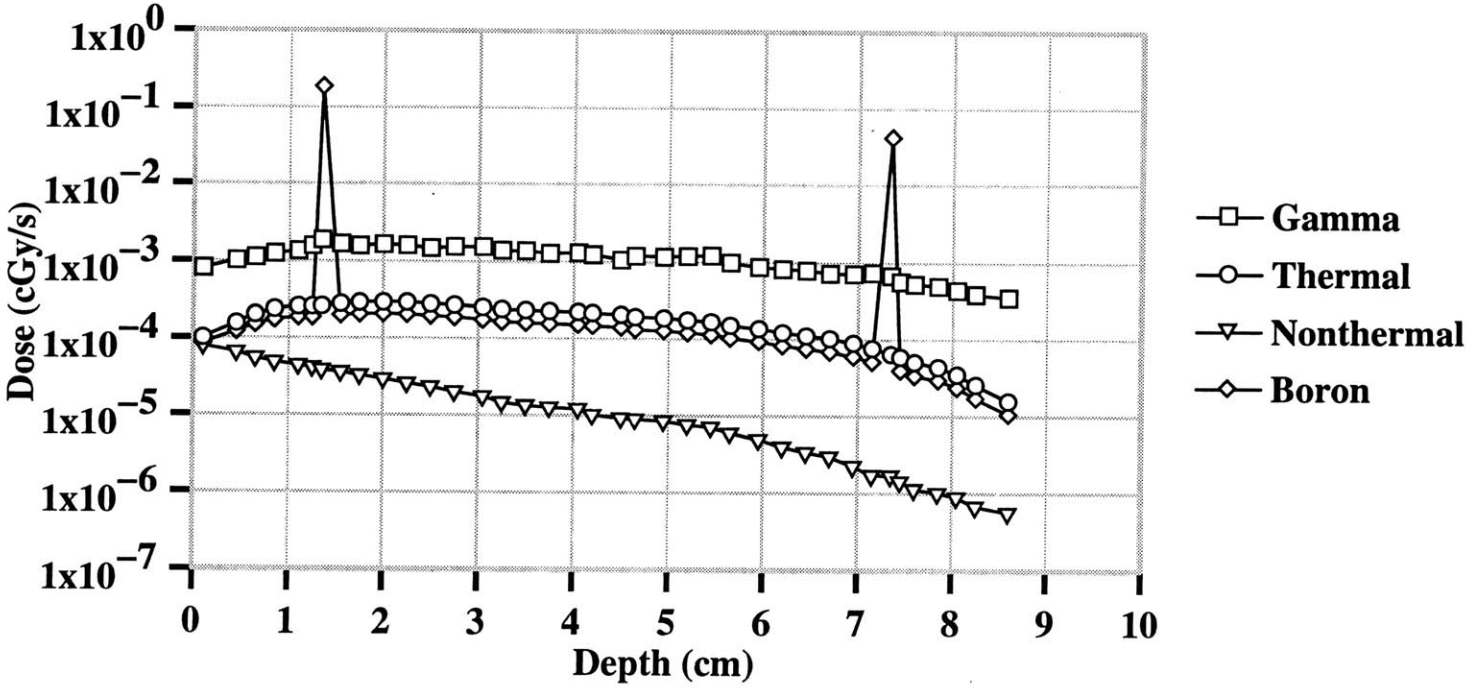

A11: Dose per depth in joint phantom
250 eV ideal isotropic beam energy
1000 ppm synovium: 1 ppm elsewhere
(boron concentrations of combination #0)

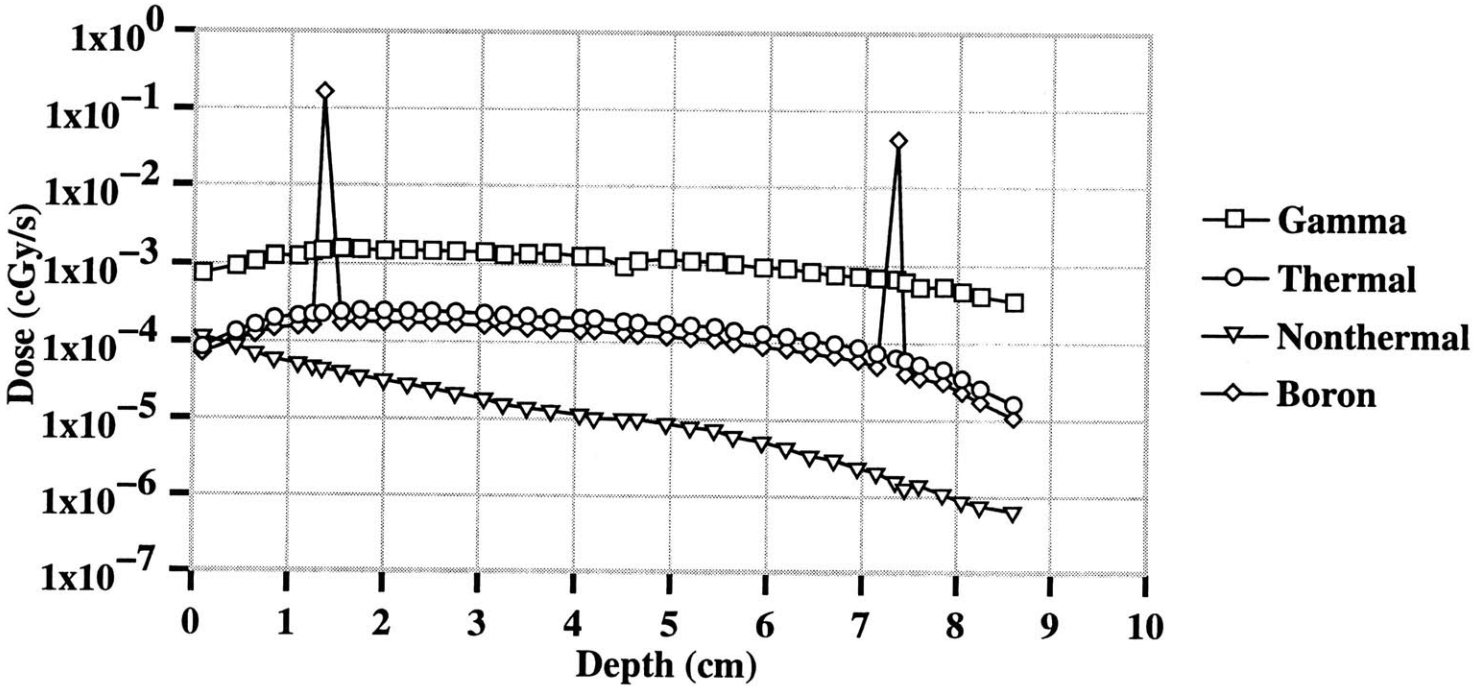

A12: Dose per depth in joint phantom
500 eV ideal isotropic beam energy
1000 ppm synovium: 1 ppm elsewhere
(boron concentrations of combination #0)

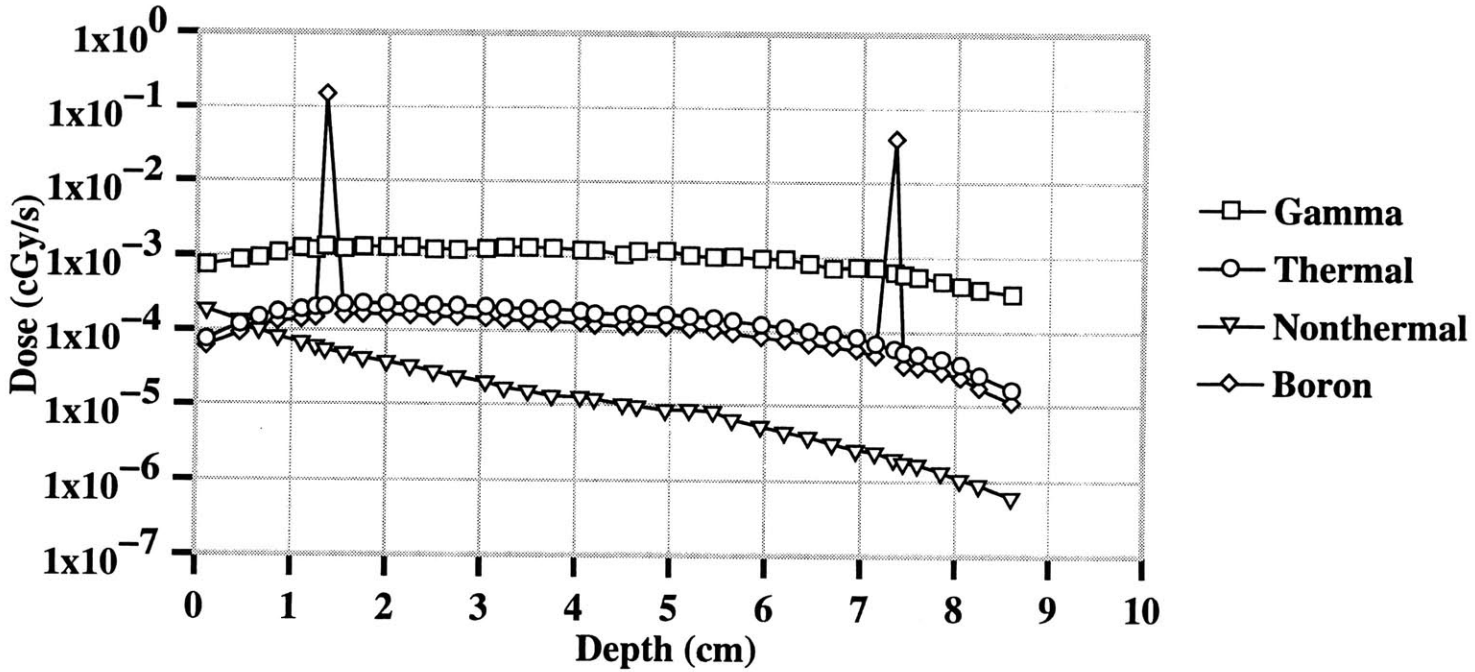

A13: Dose per depth in joint phantom
750 eV ideal isotropic beam energy
1000 ppm synovium: 1 ppm elsewhere
(boron concentrations of combination #0)

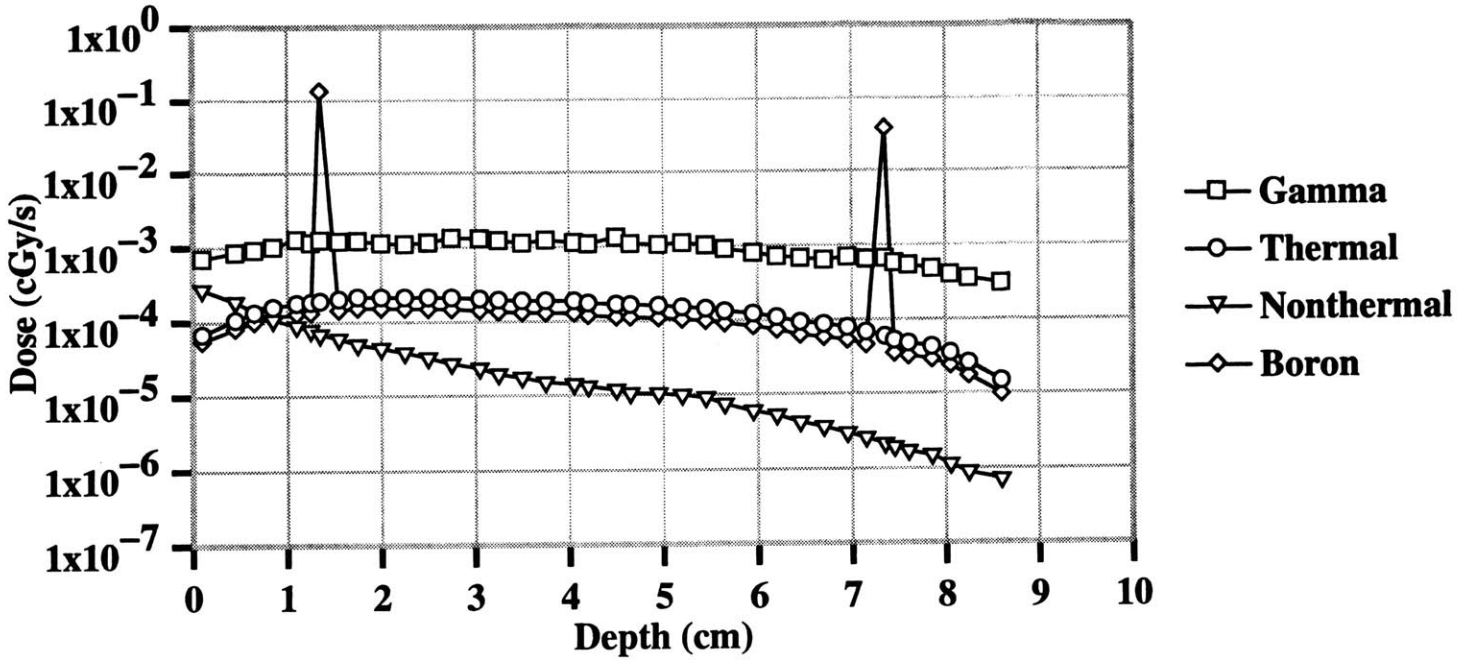

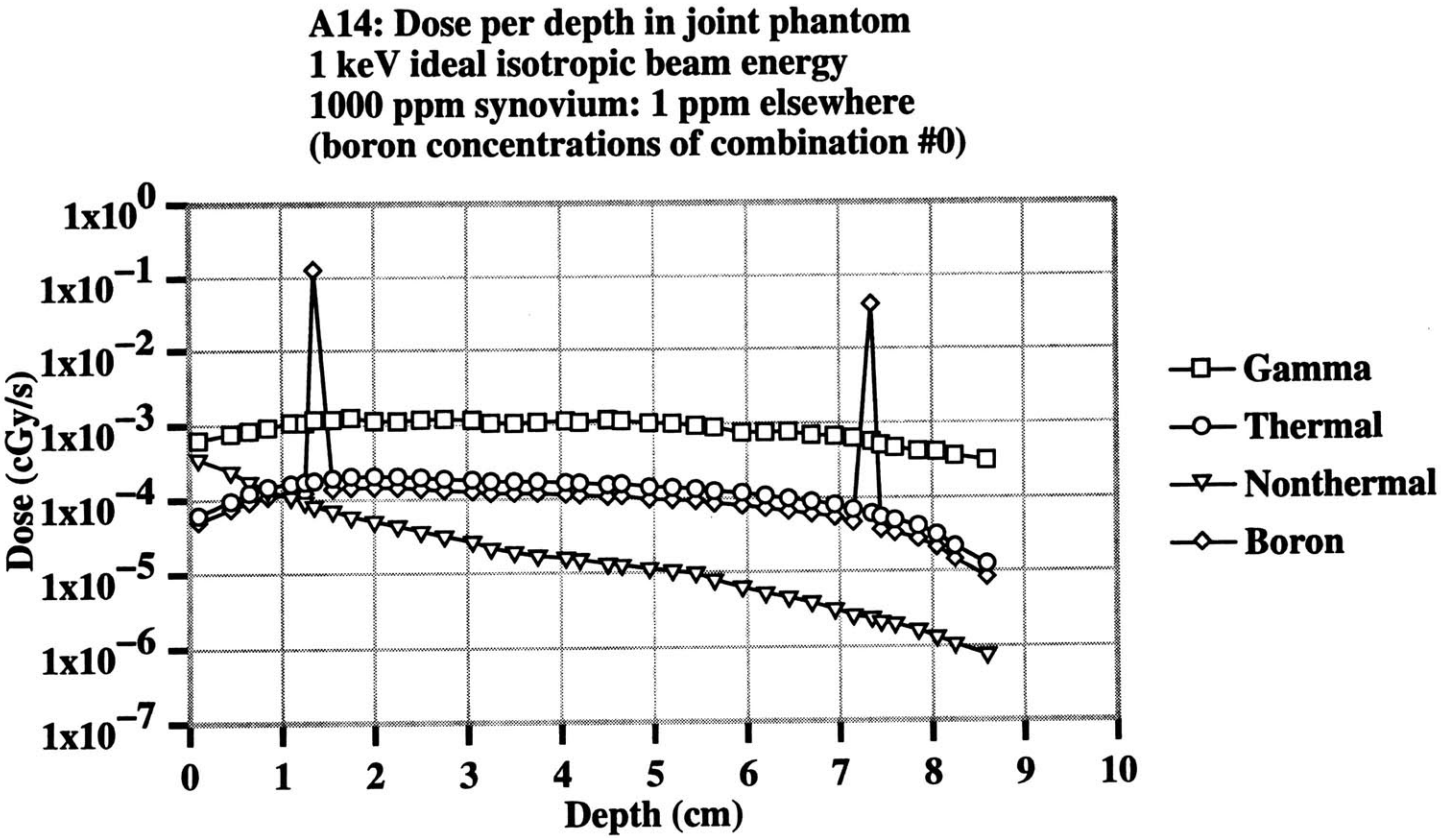
A14: Dose per depth in joint phantom
1 keV ideal isotropic beam energy
1000 ppm synovium: 1 ppm elsewhere
(boron concentrations of combination #0)
Dose (cGy/s)
1x10^0
1x10^-1
1x10^-2
1x10^-3
1x10^-4
1x10^-5
1x10^-6
1x10^-7
0
1
2
3
4
5
6
7
8
9
10
Depth (cm)
Gamma
Thermal
Nonthermal
Boron

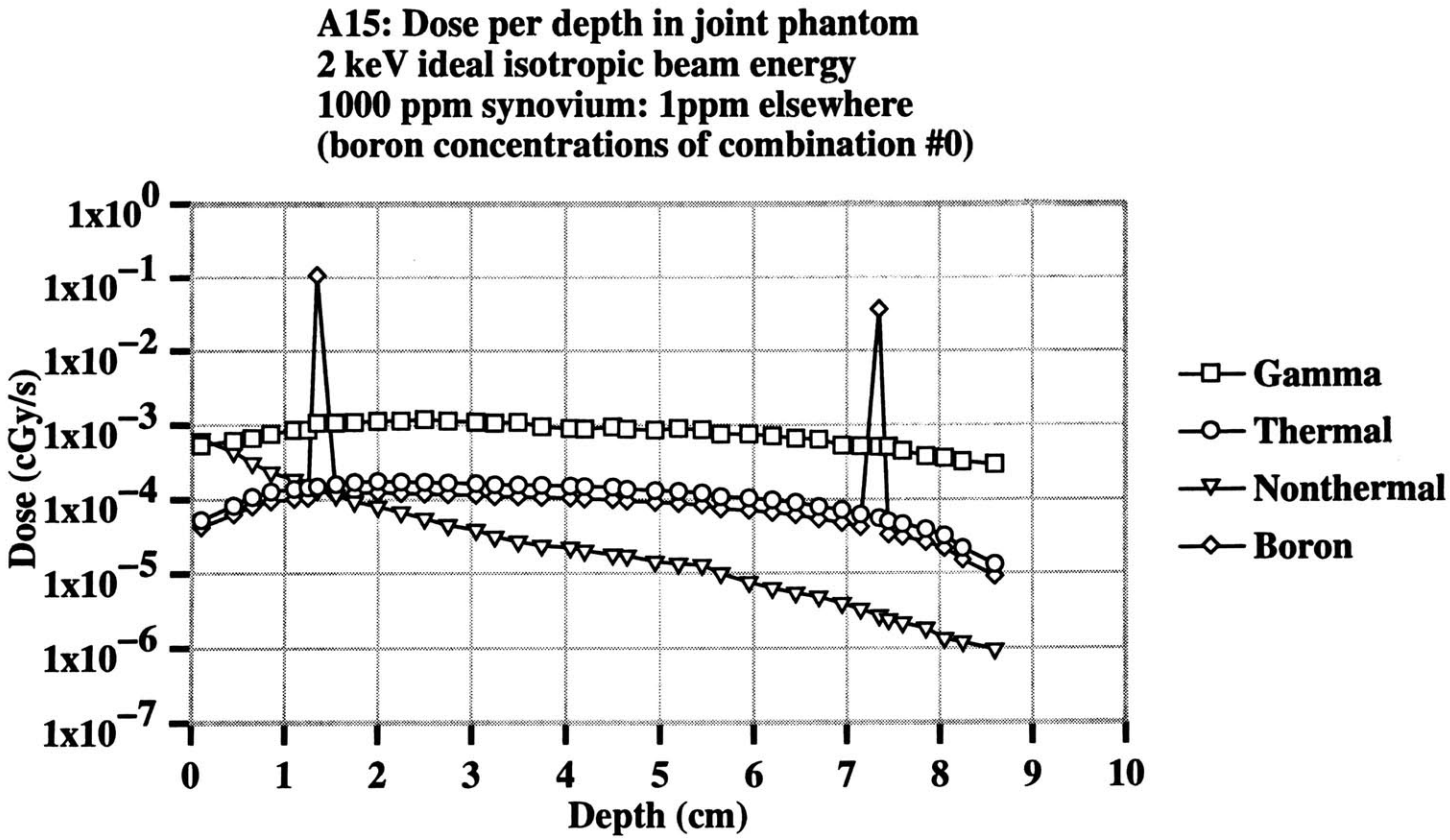
A15: Dose per depth in joint phantom
2 keV ideal isotropic beam energy
1000 ppm synovium: 1ppm elsewhere
(boron concentrations of combination #0)
Dose (cGy/s)
1x10^0
1x10^-1
1x10^-2
1x10^-3
1x10^-4
1x10^-5
1x10^-6
1x10^-7
0
1
2
3
4
5
6
7
8
9
10
Depth (cm)
Gamma
Thermal
Nonthermal
Boron

A16: Dose per depth in joint phantom
3 keV ideal isotropic beam energy
1000 ppm synovium: 1 ppm elsewhere
(boron concentrations of combination #0)

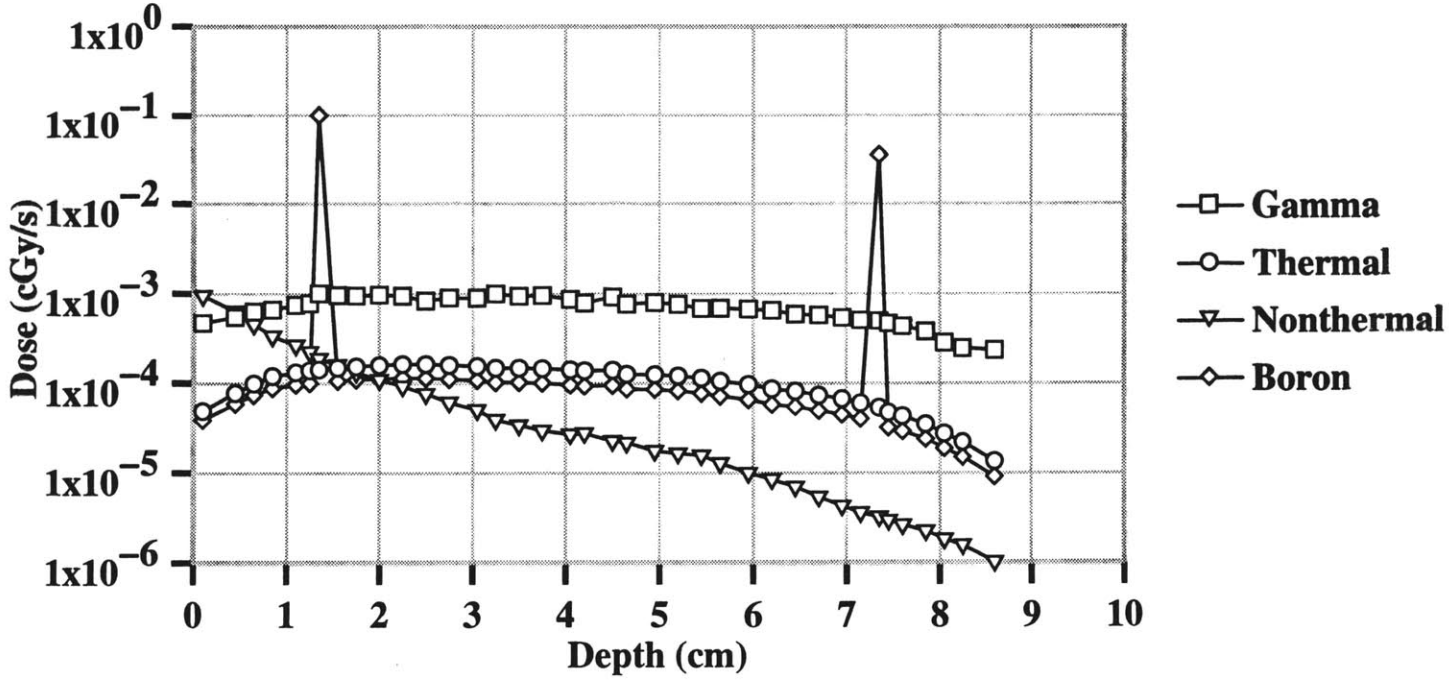

A17: Dose per depth in joint phantom
5 keV ideal isotropic beam energy
1000 ppm synovium: 1 ppm elsewhere
(boron concentrations of combination #0)

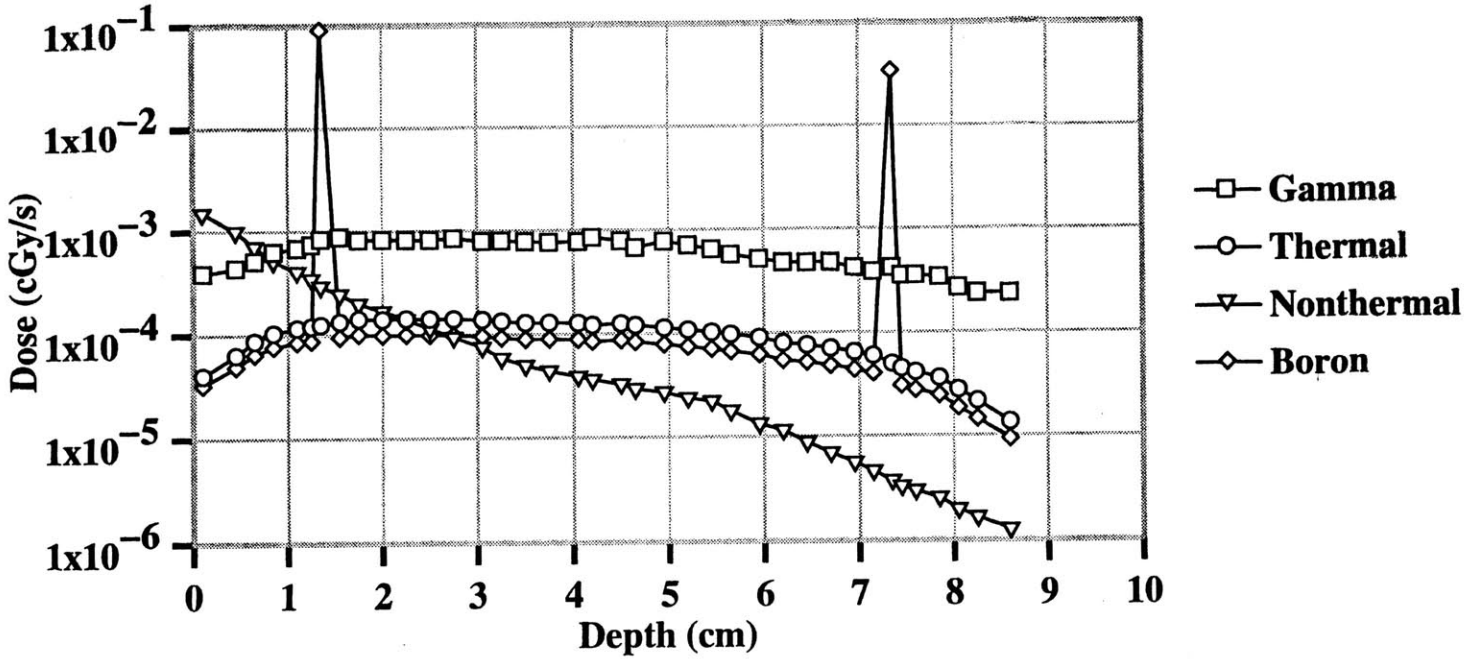

A18: Dose per depth in joint phantom
7 keV ideal isotropic beam energy
1000 ppm synovium: 1 ppm elsewhere
(boron concentrations of combination #0)

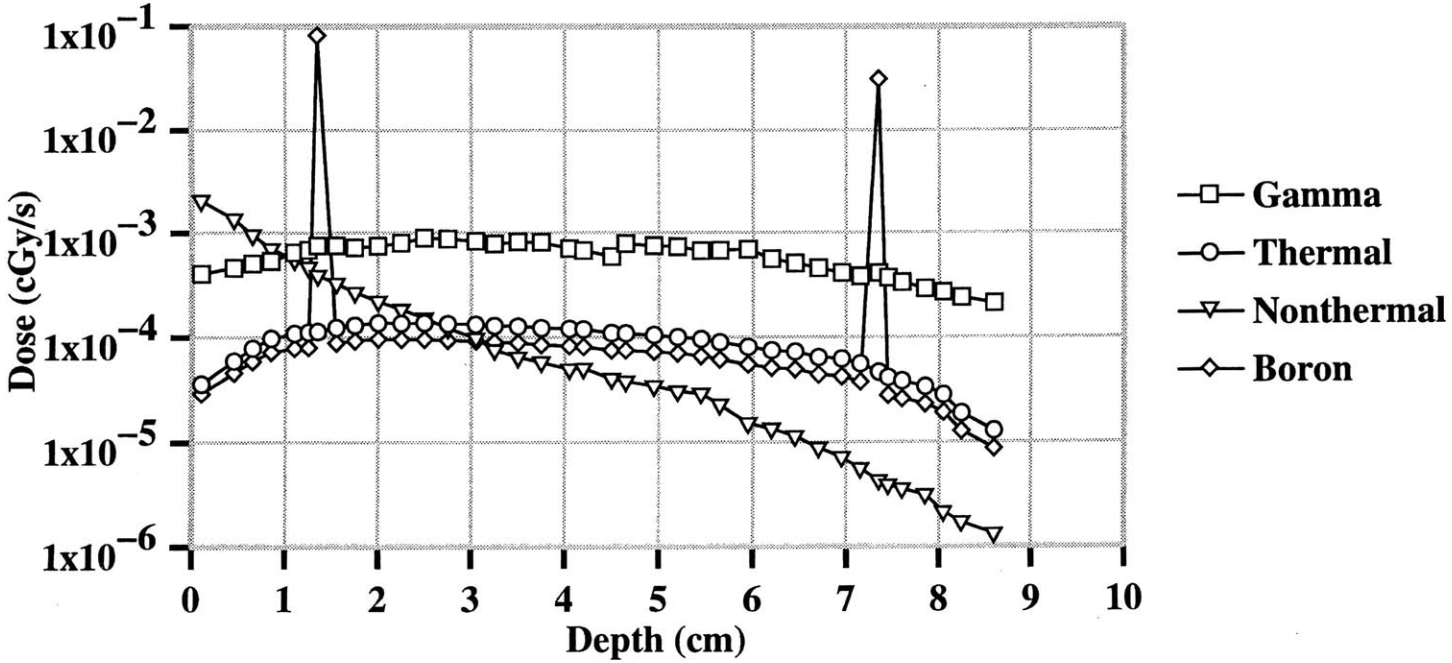

A19: Dose per depth in joint phantom
10 keV ideal isotropic beam energy
1000 ppm synovium: 1 ppm elsewhere
(boron concentrations of combination #0)

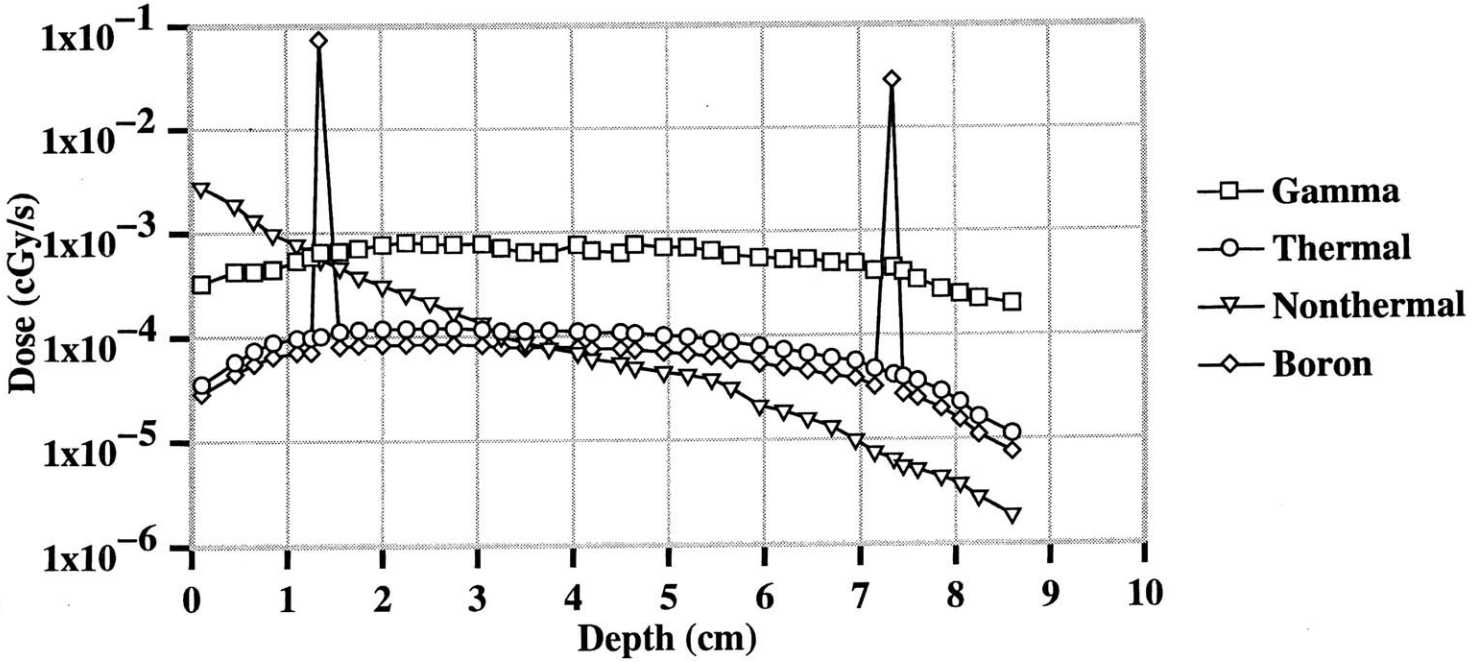

A20: Dose per depth in joint phantom
50 keV ideal isotropic beam energy
1000 ppm synovium: 1 ppm elsewhere
(boron concentrations of combination #0)

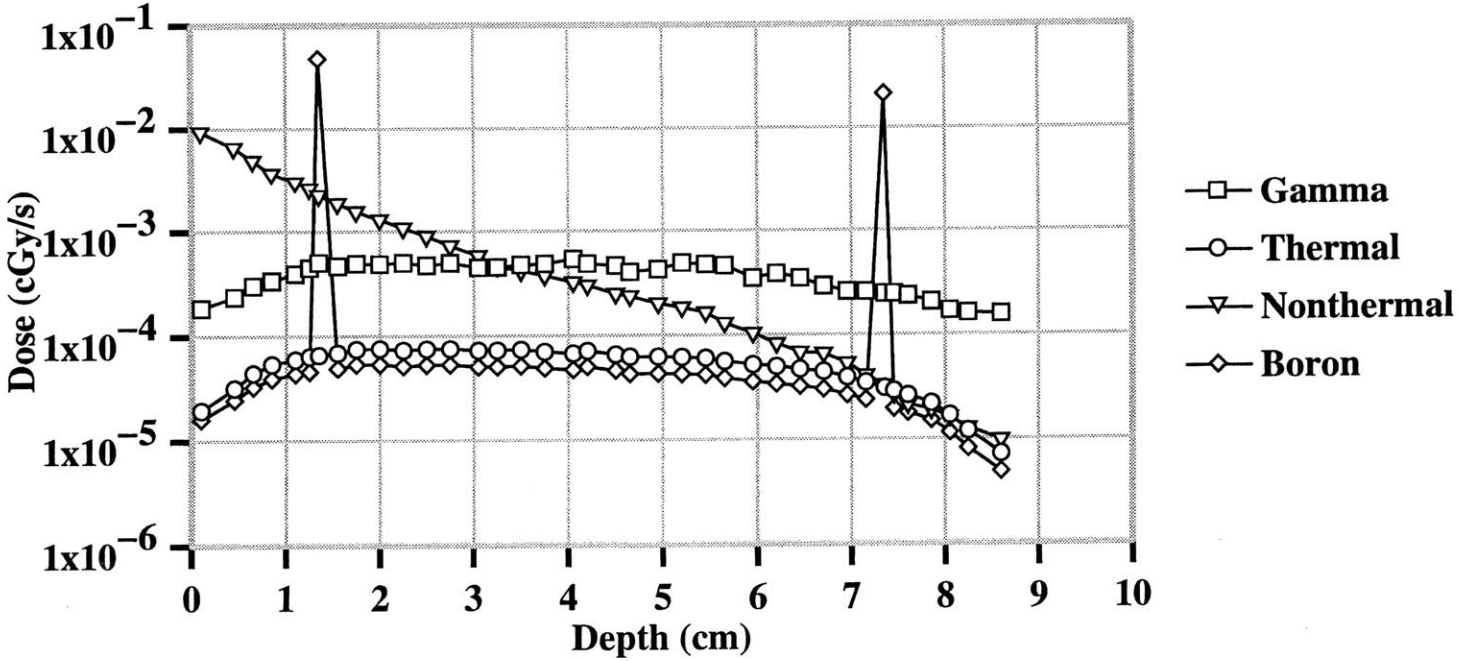

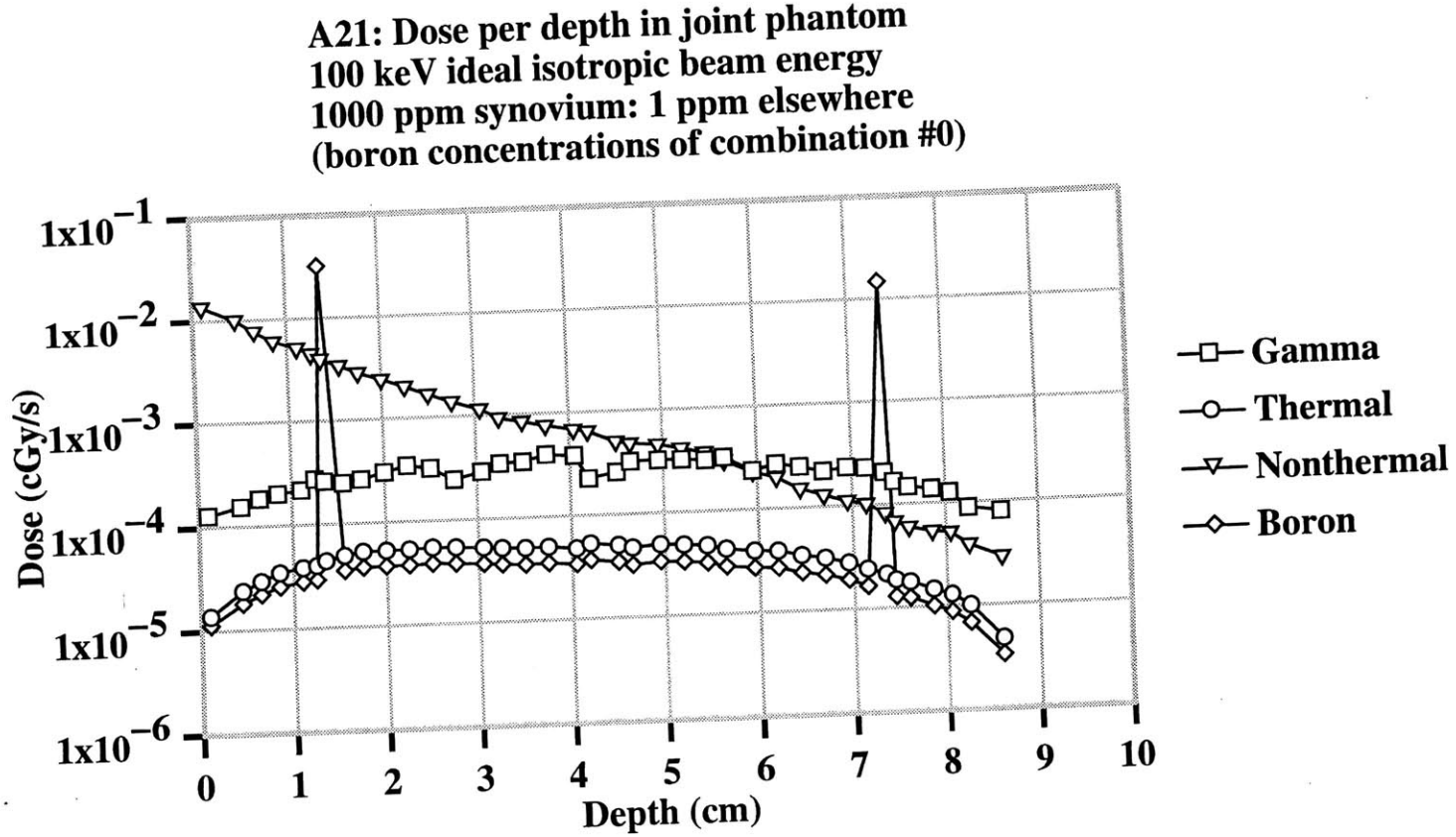
A21: Dose per depth in joint phantom
100 keV ideal isotropic beam energy
1000 ppm synovium: 1 ppm elsewhere
(boron concentrations of combination #0)
Dose (cGy/s)
1x10−1
1x10−2
1x10−3
1x10−4
1x10−5
1x10−6
0
1
2
3
4
5
6
7
8
9
10
Depth (cm)
Gamma
Thermal
Nonthermal
Boron

A22: Dose per depth in joint phantom
0.025 eV ideal isotropic beam energy
1 ppm skin: 100 ppm synovium: 10 ppm bone
(boron concentrations of combination #1)

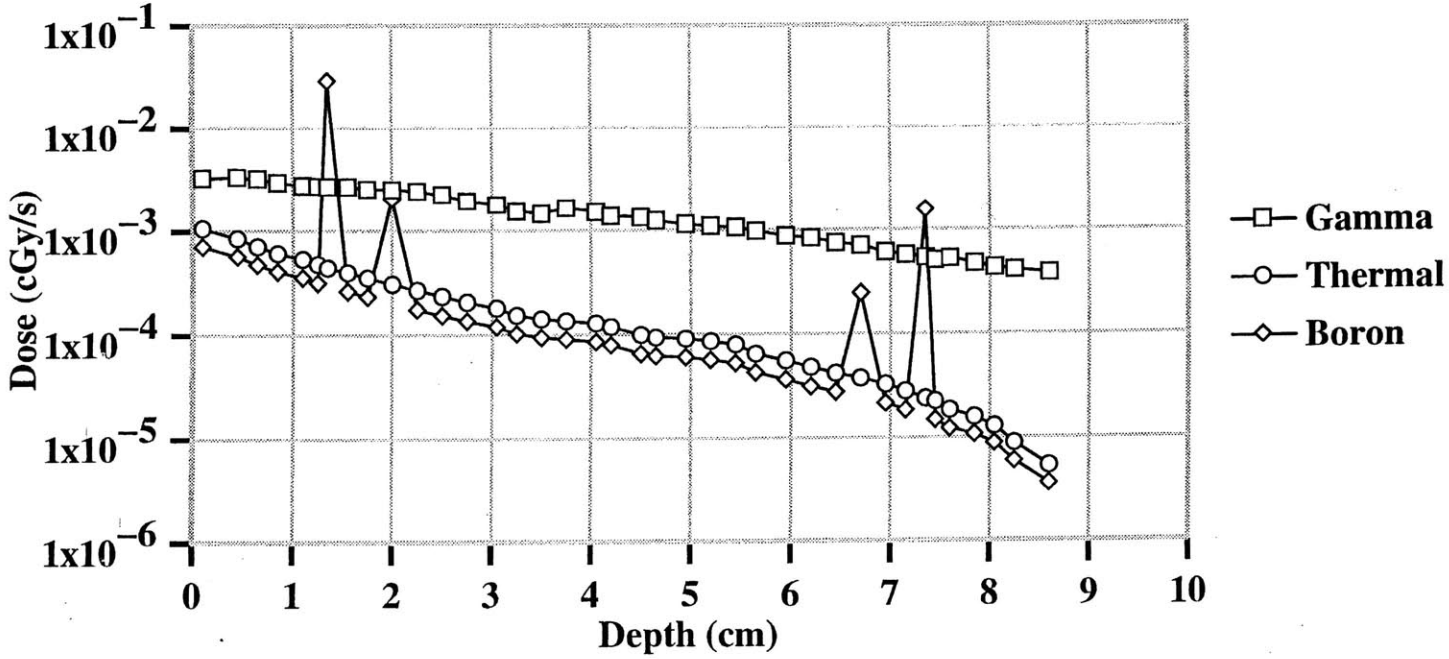

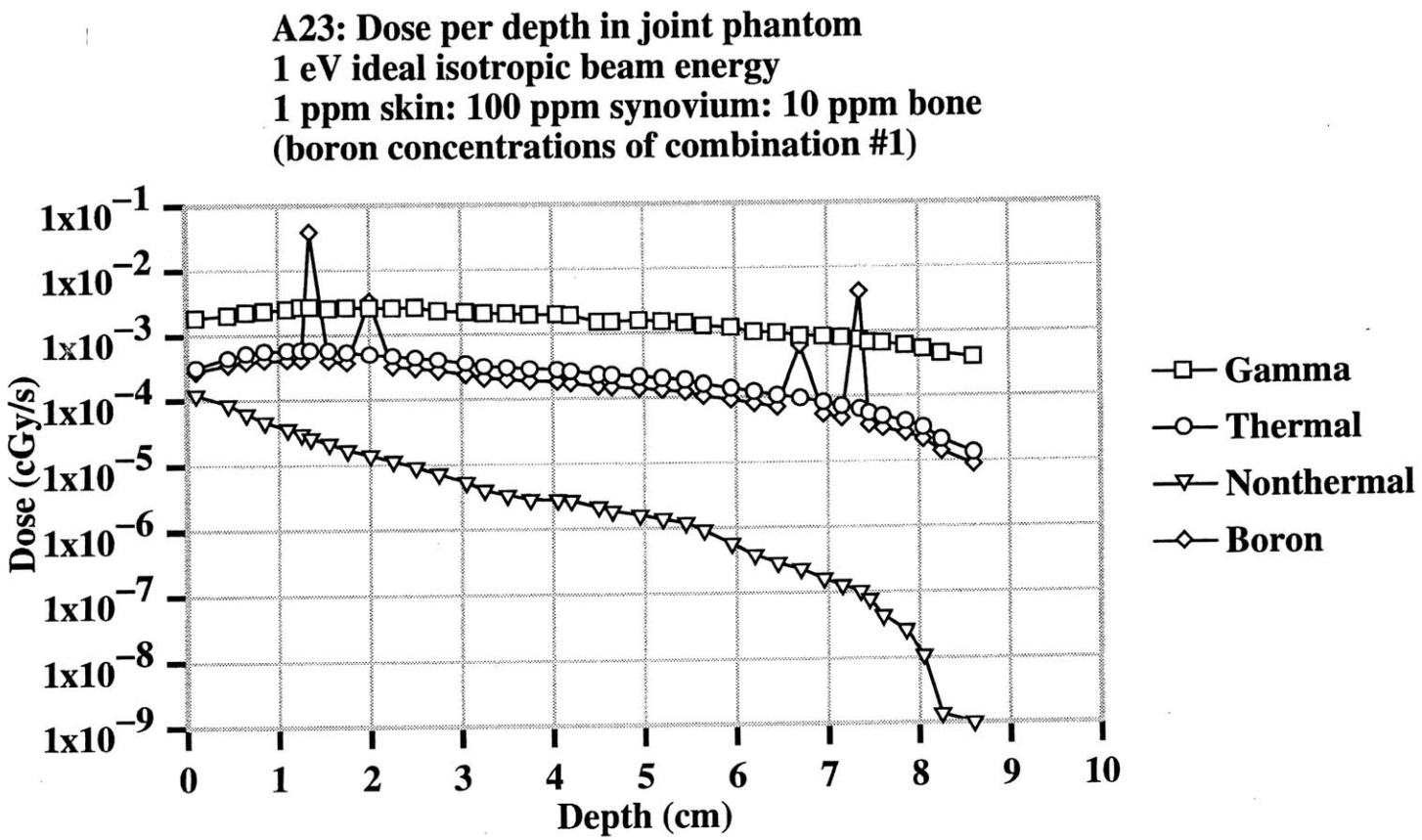
A23: Dose per depth in joint phantom
1 eV ideal isotropic beam energy
1 ppm skin: 100 ppm synovium: 10 ppm bone
(boron concentrations of combination #1)
Dose (cGy/s)
1x10−1
1x10−2
1x10−3
1x10−4
1x10−5
1x10−6
1x10−7
1x10−8
1x10−9
0
1
2
3
4
5
6
7
8
9
10
Depth (cm)
Gamma
Thermal
Nonthermal
Boron

A24: Dose per depth in joint phantom
10 eV ideal isotropic beam energy
1 ppm skin: 100 ppm synovium: 10 ppm bone
(boron concentrations of combination #1)

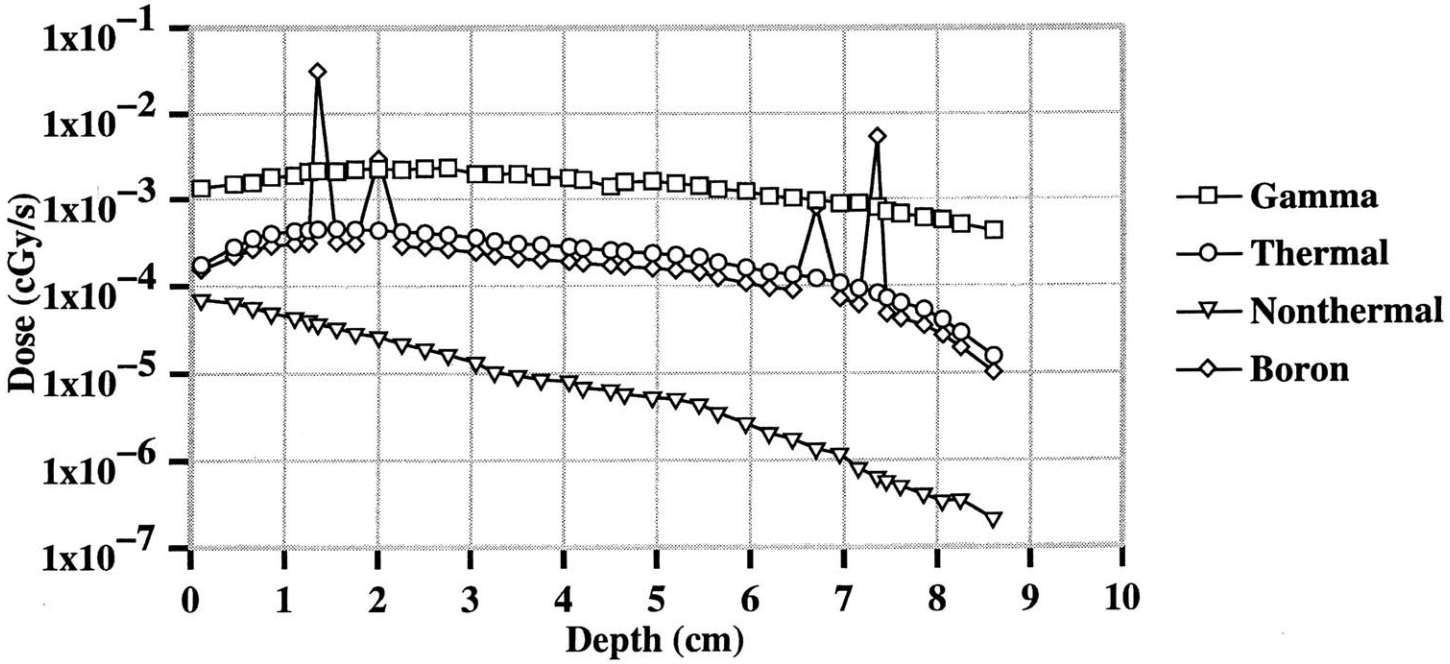

A25: Dose per depth in joint phantom
100 eV ideal isotropic beam energy
1 ppm skin: 100 ppm synovium: 10 ppm bone
(boron concentrations in combination #1)

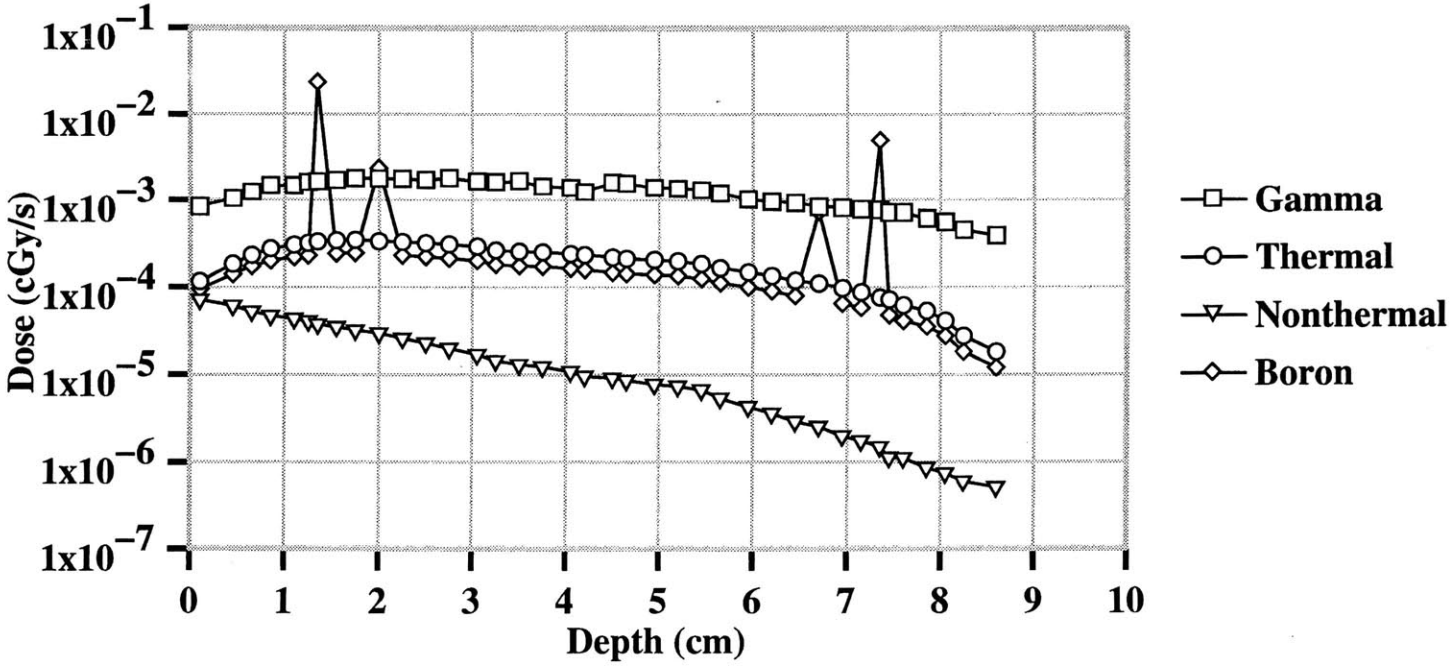

A27: Dose per depth in joint phantom
1 keV ideal isotropic beam energy
1 ppm skin: 100 ppm synovium: 10 ppm bone
(boron concentrations of combination #1)

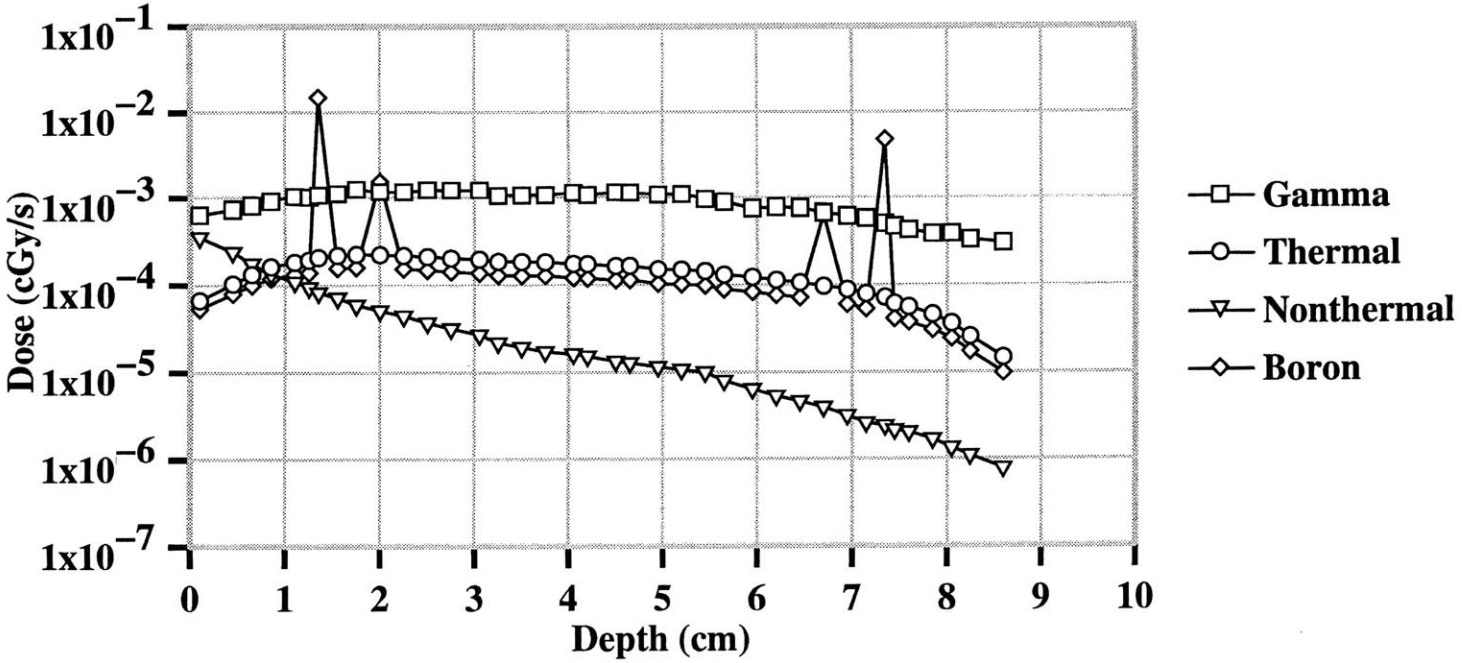

A27: Dose per depth in joint phantom
1 keV ideal isotropic beam energy
1 ppm skin: 100 ppm synovium: 10 ppm bone
(boron concentrations of combination #1)

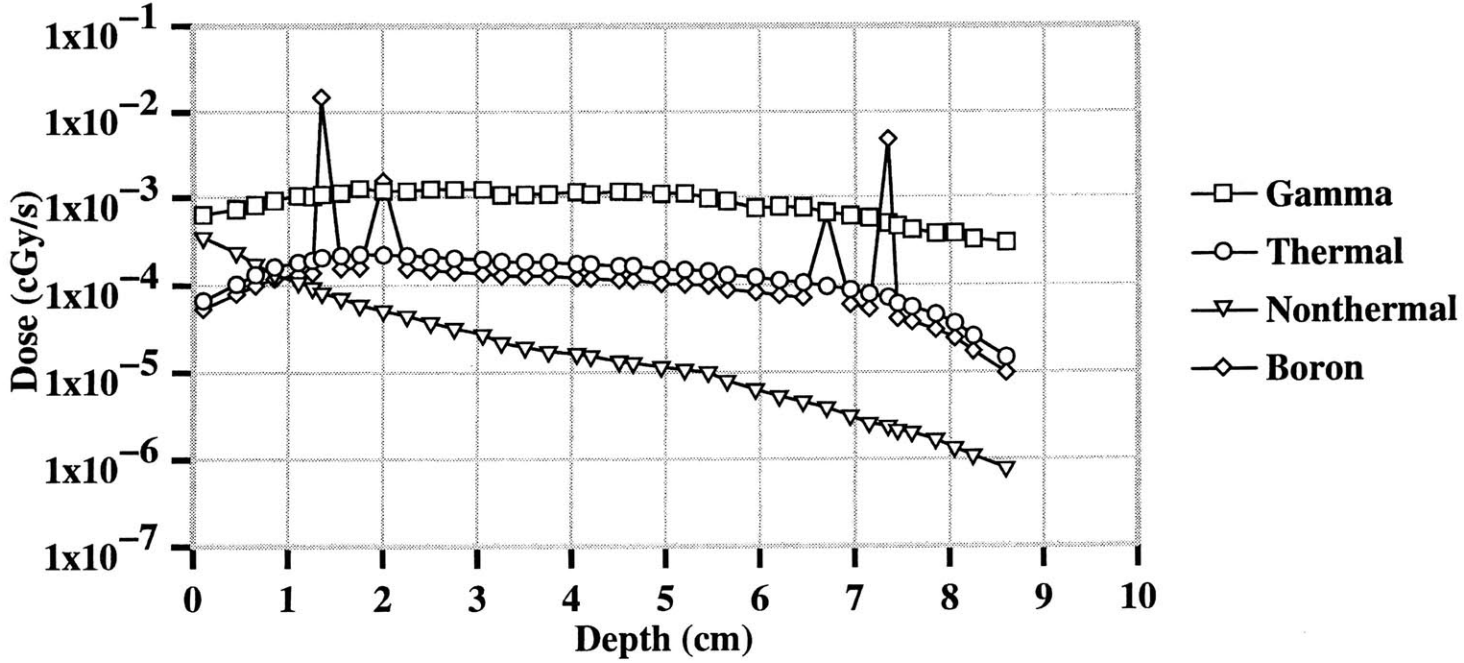

A28: Dose per depth in joint phantom
10 keV ideal isotropic beam energy
1 ppm skin: 100 ppm synovium: 10 ppm bone
(boron concentrations of combination #1)

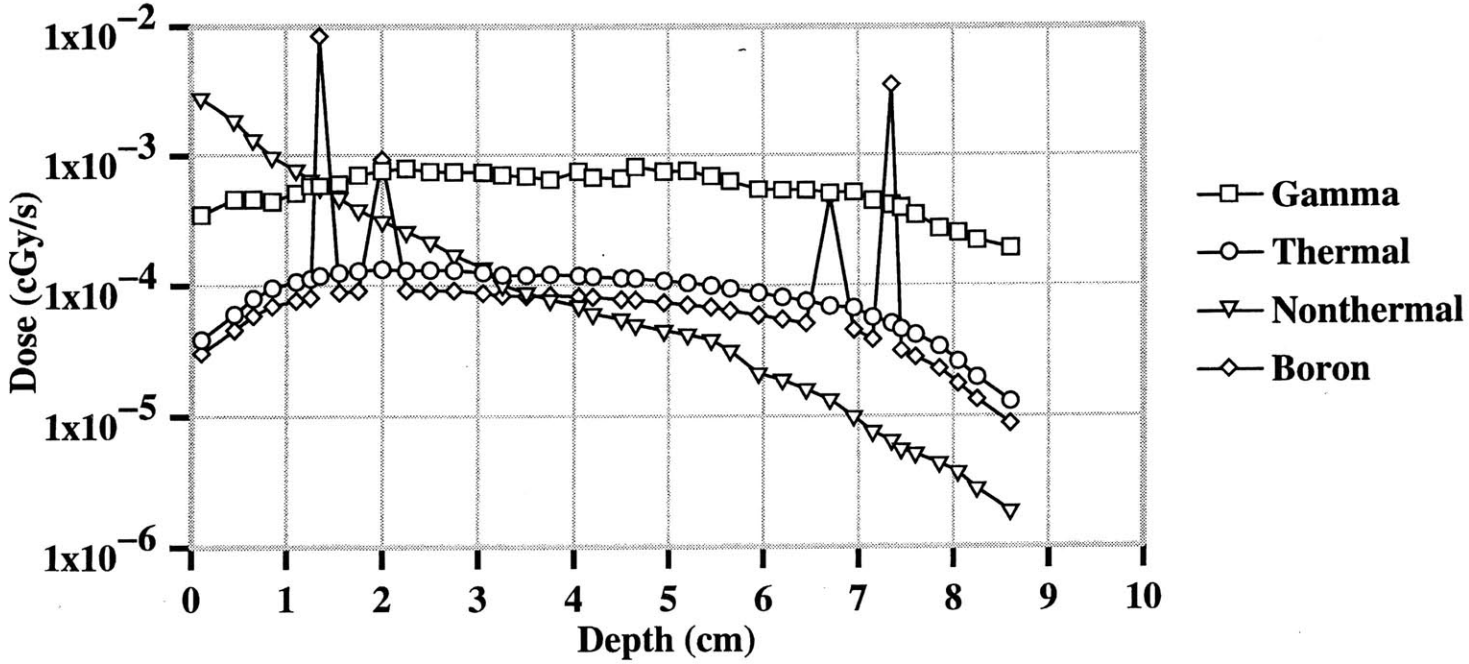

A29: Dose per depth in joint phantom
100 keV ideal isotropic beam energy
1 ppm skin: 100 ppm synovium: 10 ppm bone
(boron concentrations of combination #1)

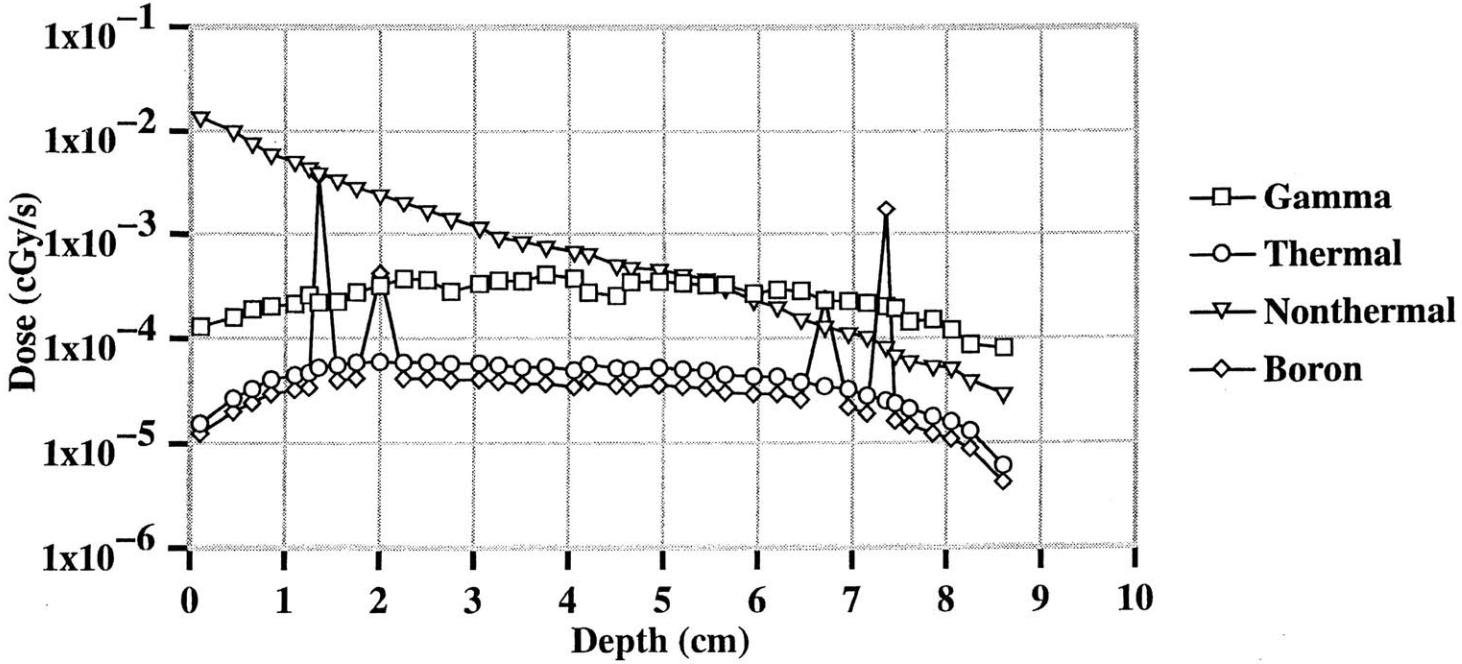

A30: Dose per depth in joint phantom
0.025 eV ideal isotropic beam energy
1 ppm skin: 1000 ppm synovium: 100 ppm bone
(boron concentrations of combination #2)

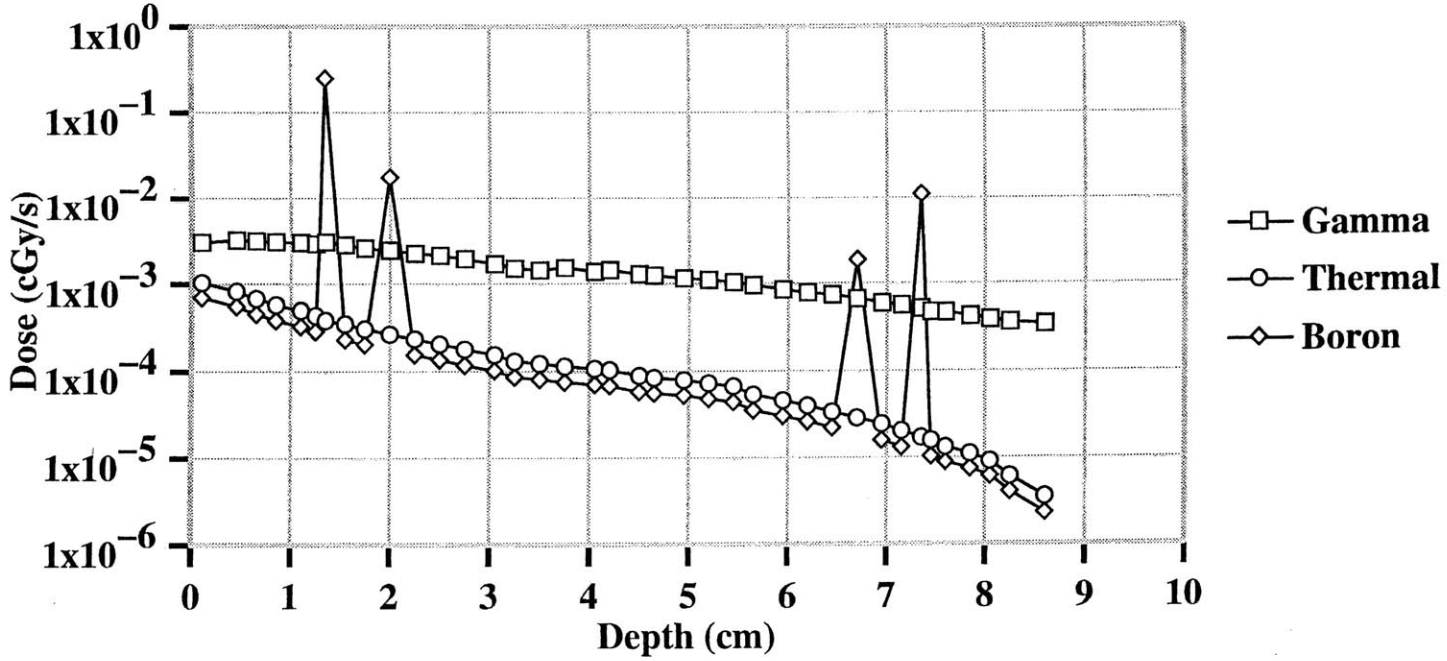

A31: Dose per depth in joint phantom
0.1 eV ideal isotropic beam energy
1 ppm skin: 1000 ppm synovium: 100 ppm bone
(boron concentrations of combination #2)

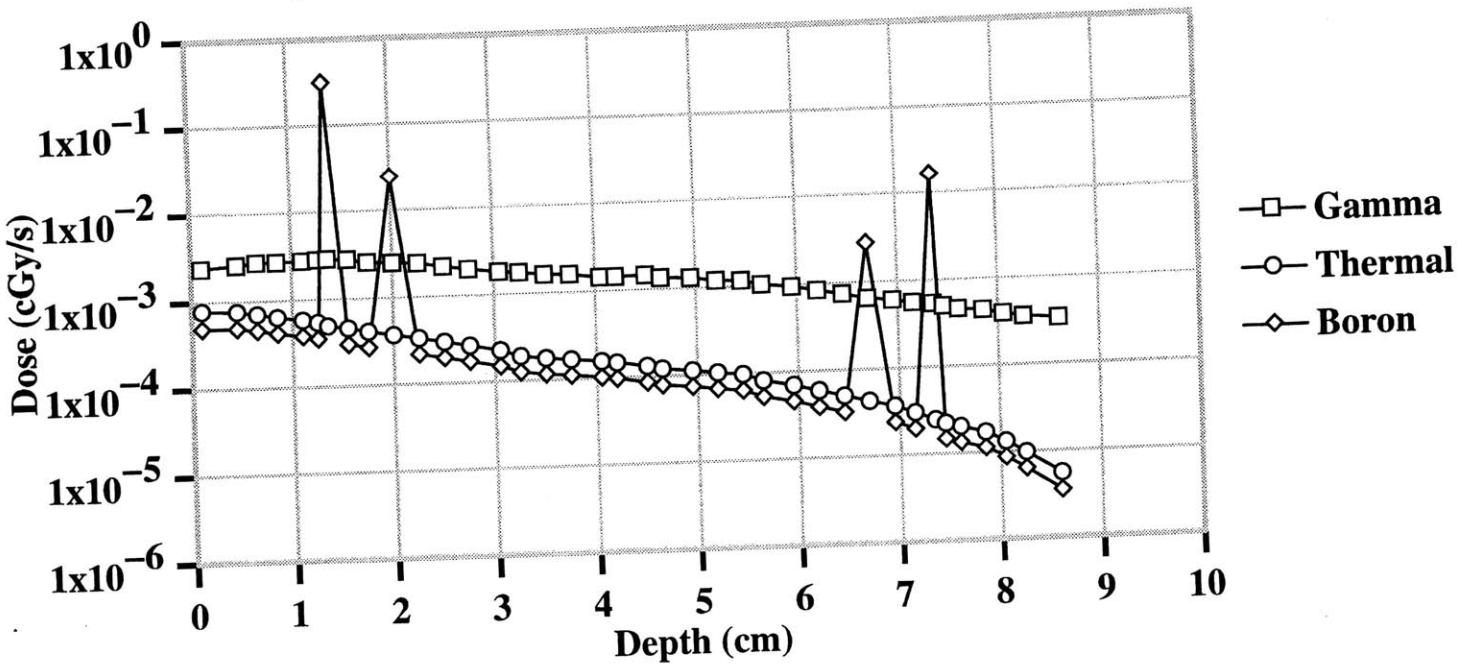

A32: Dose per depth in joint phantom
1 eV ideal isotropic beam energy
1 ppm skin: 1000 ppm synovium: 100 ppm bone
(boron concentrations of combination #2)

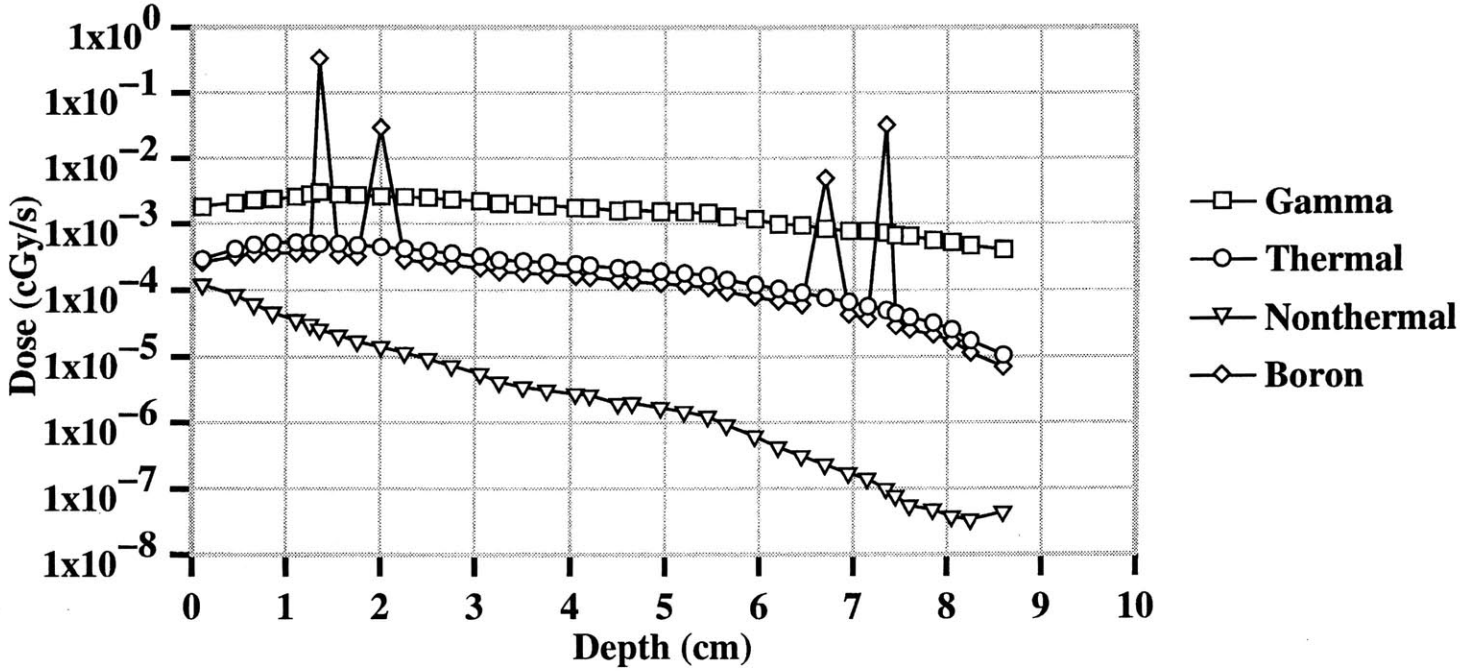

A32: Dose per depth in joint phantom
1 eV ideal isotropic beam energy
1 ppm skin: 1000 ppm synovium: 100 ppm bone
(boron concentrations of combination #2)

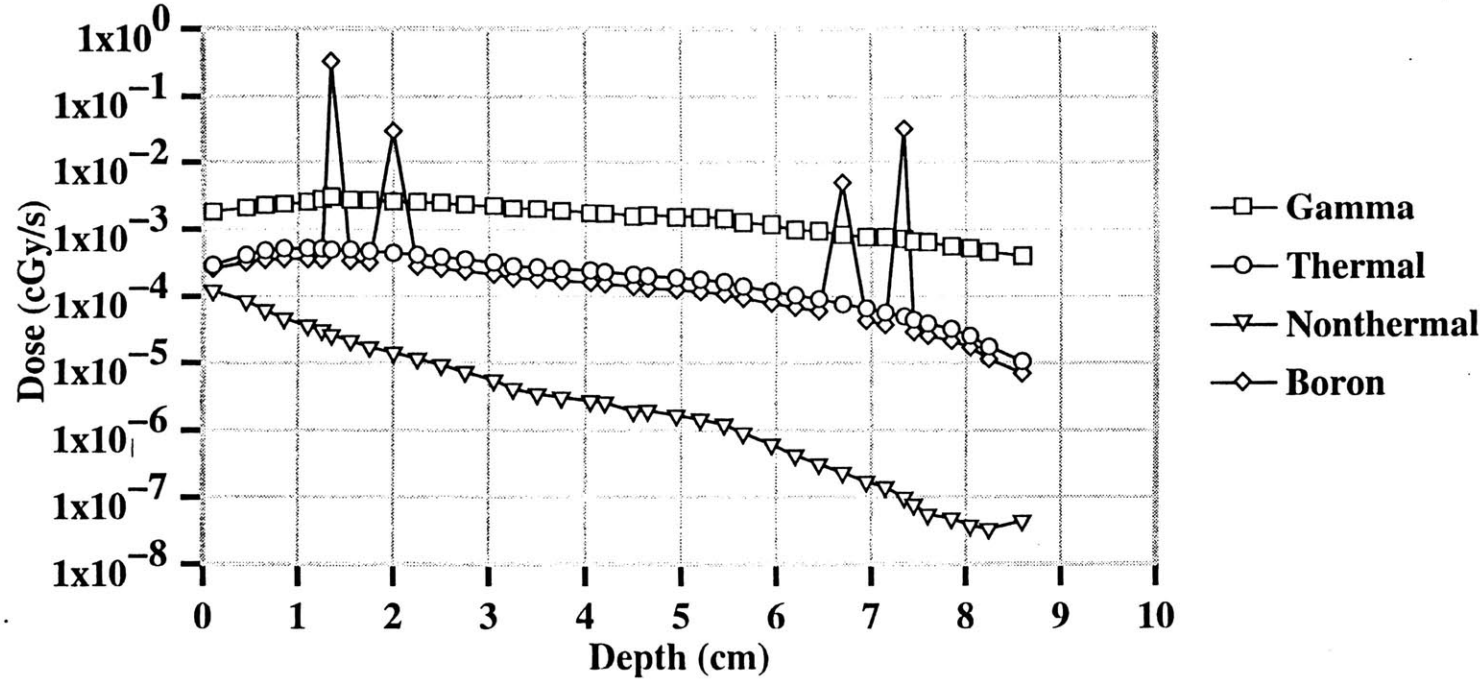

A33: Dose per depth in joint phantom
10 eV ideal isotropic beam energy
1 ppm skin: 1000 ppm synovium: 100 ppm bone
(boron concentrations of combination #2)

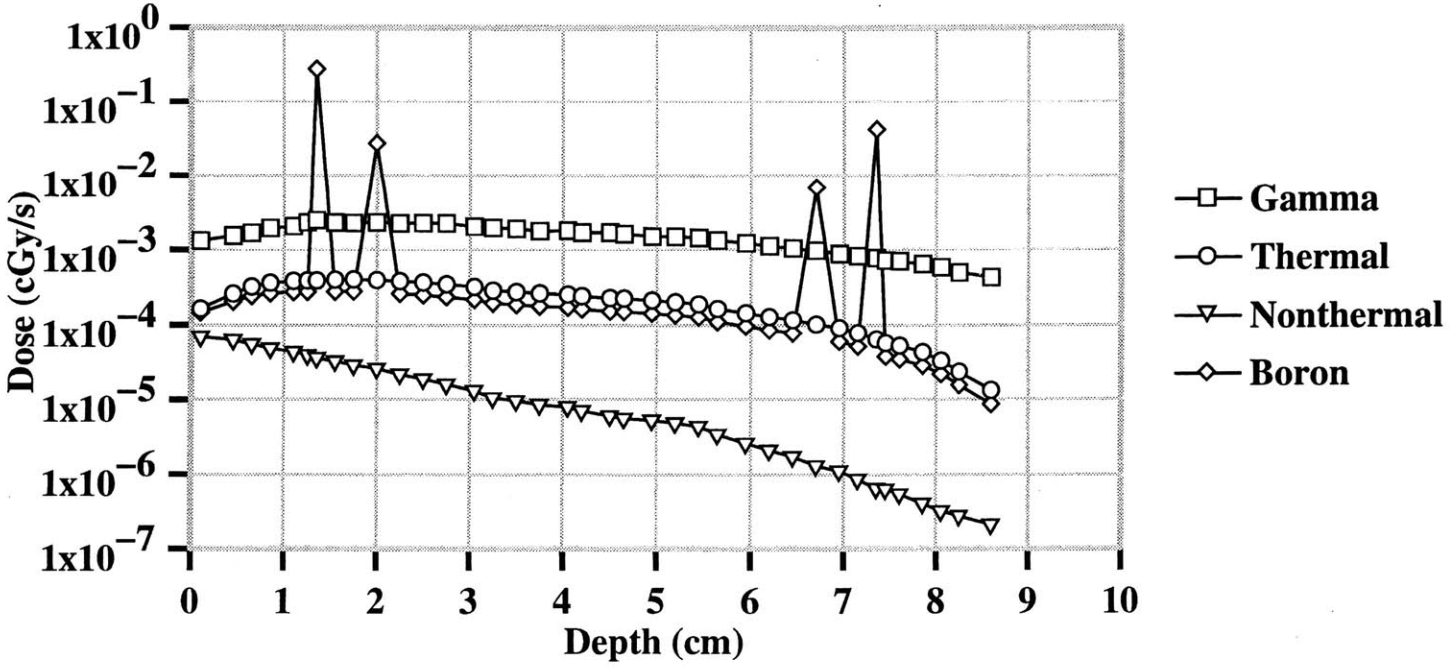

A35: Dose per depth in joint phantom
500 eV ideal isotropic beam energy
1 ppm skin: 1000 ppm synovium: 100 ppm bone
(boron concentrations of combination #2)

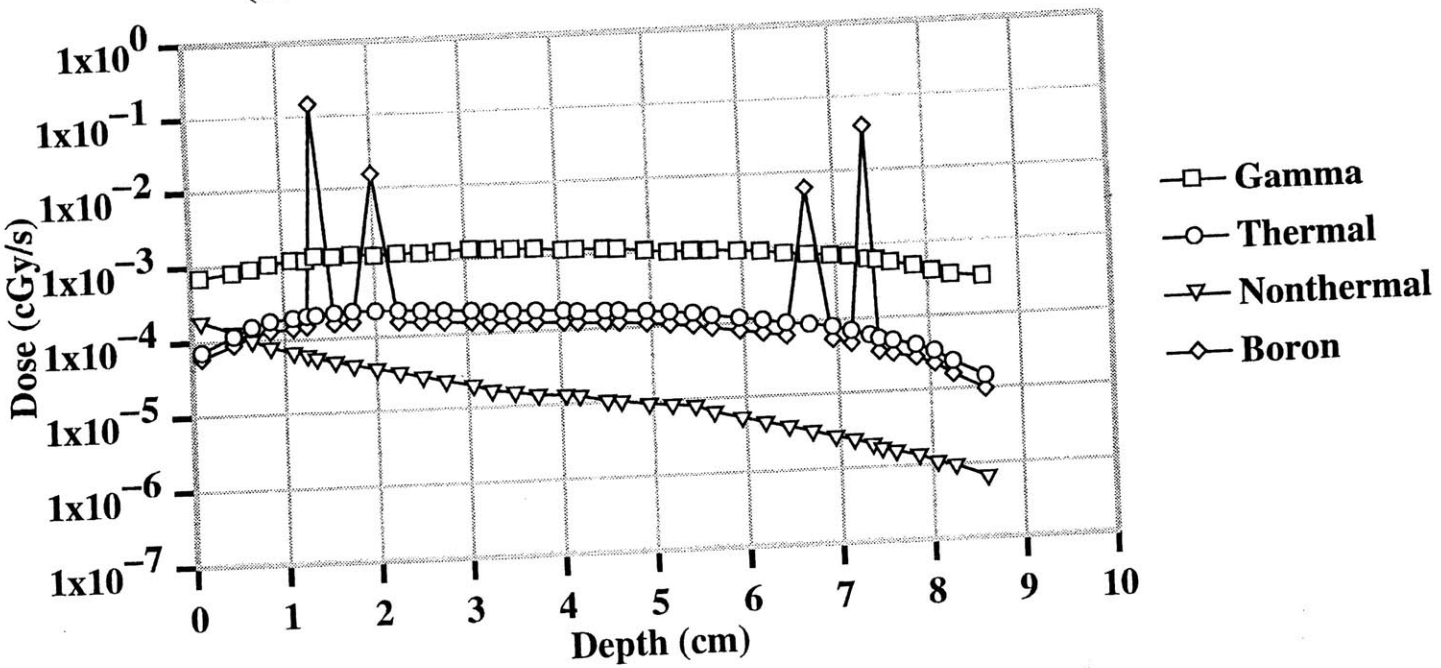

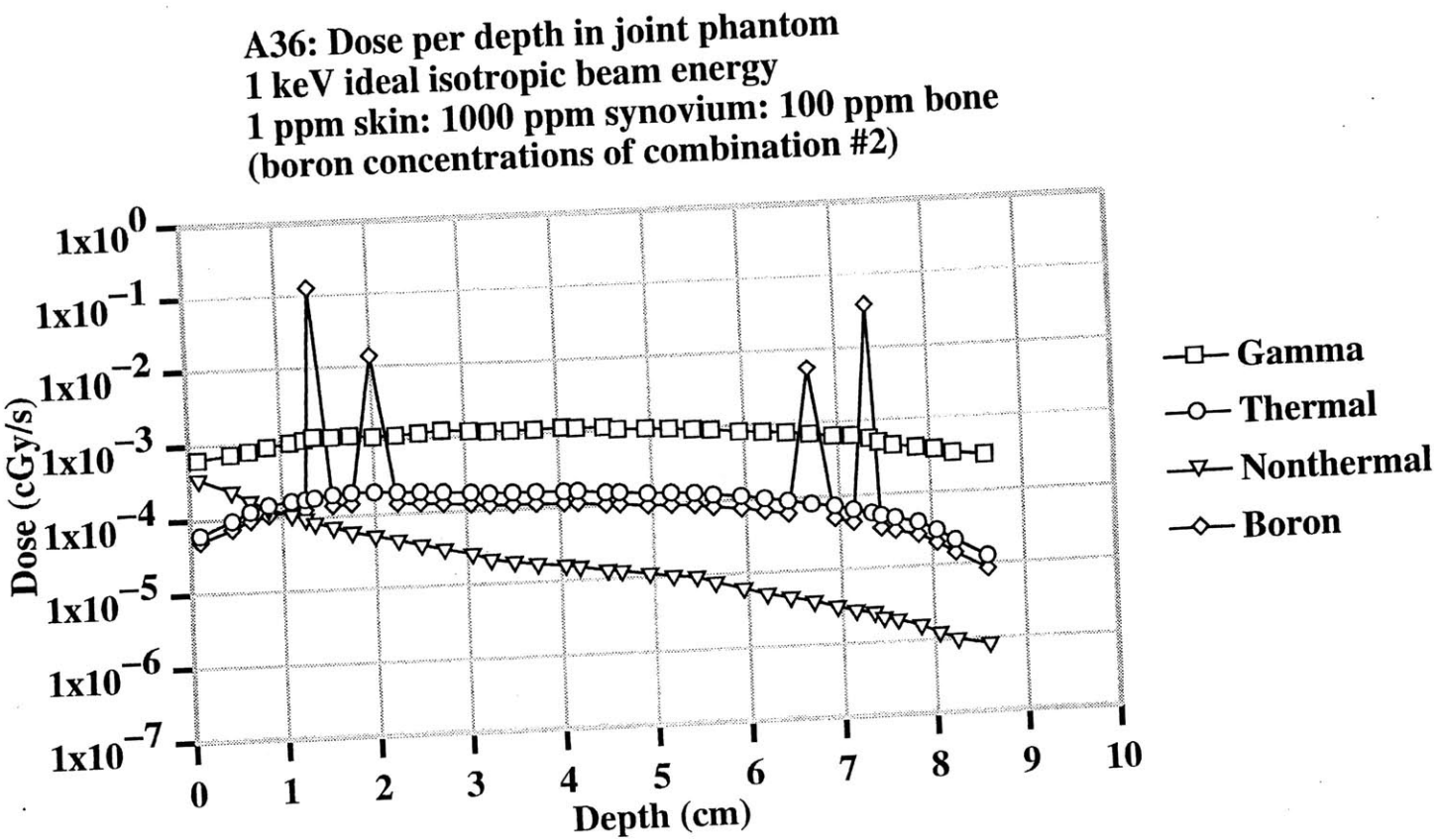
A36: Dose per depth in joint phantom
1 keV ideal isotropic beam energy
1 ppm skin: 1000 ppm synovium: 100 ppm bone
(boron concentrations of combination #2)
Dose (cGy/s)
1x10^0
1x10^-1
1x10^-2
1x10^-3
1x10^-4
1x10^-5
1x10^-6
1x10^-7
0
1
2
3
4
5
6
7
8
9
10
Depth (cm)
Gamma
Thermal
Nonthermal
Boron

A37: Dose per depth in joint phantom
5 keV ideal isotropic beam energy
1 ppm skin: 1000 ppm synovium: 100 ppm bone
(boron concentrations of combination #2)

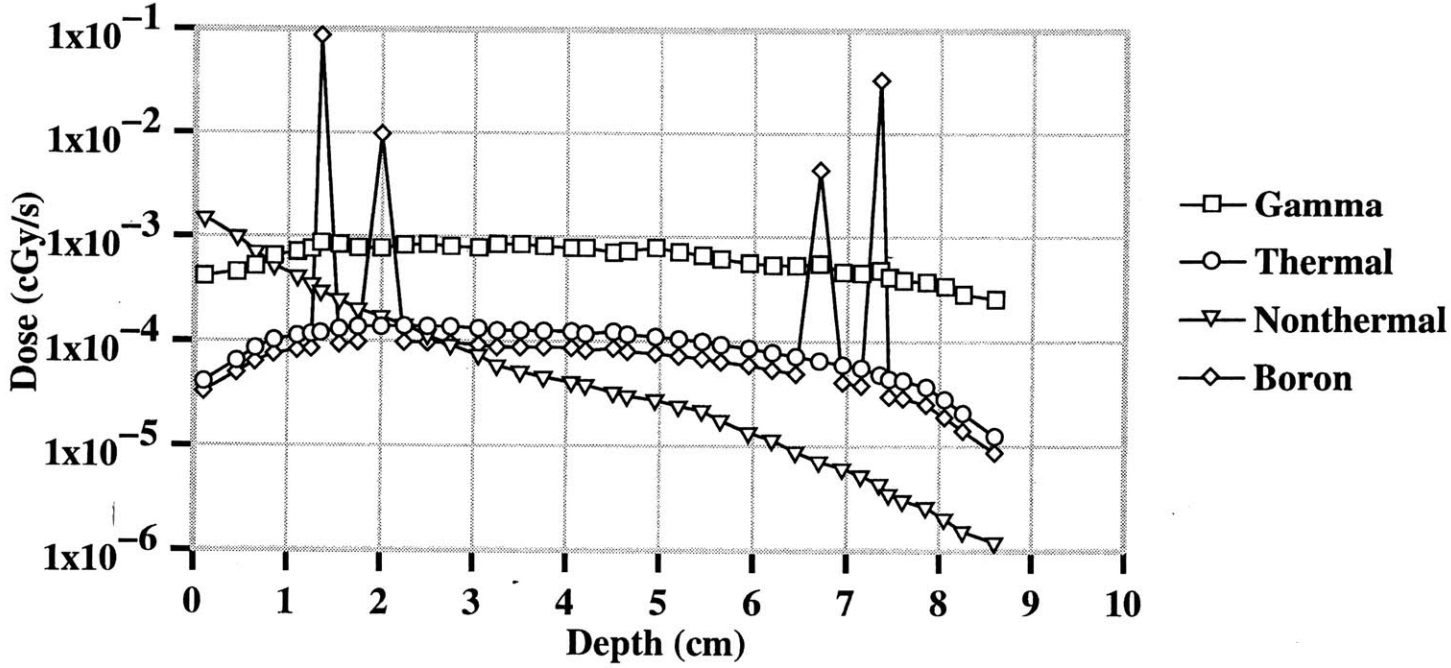

A38: Dose per depth in joint phantom
10 keV ideal isotropic beam energy
1 ppm skin: 1000 ppm synovium: 100 ppm bone
(boron concentrations of combination #2)

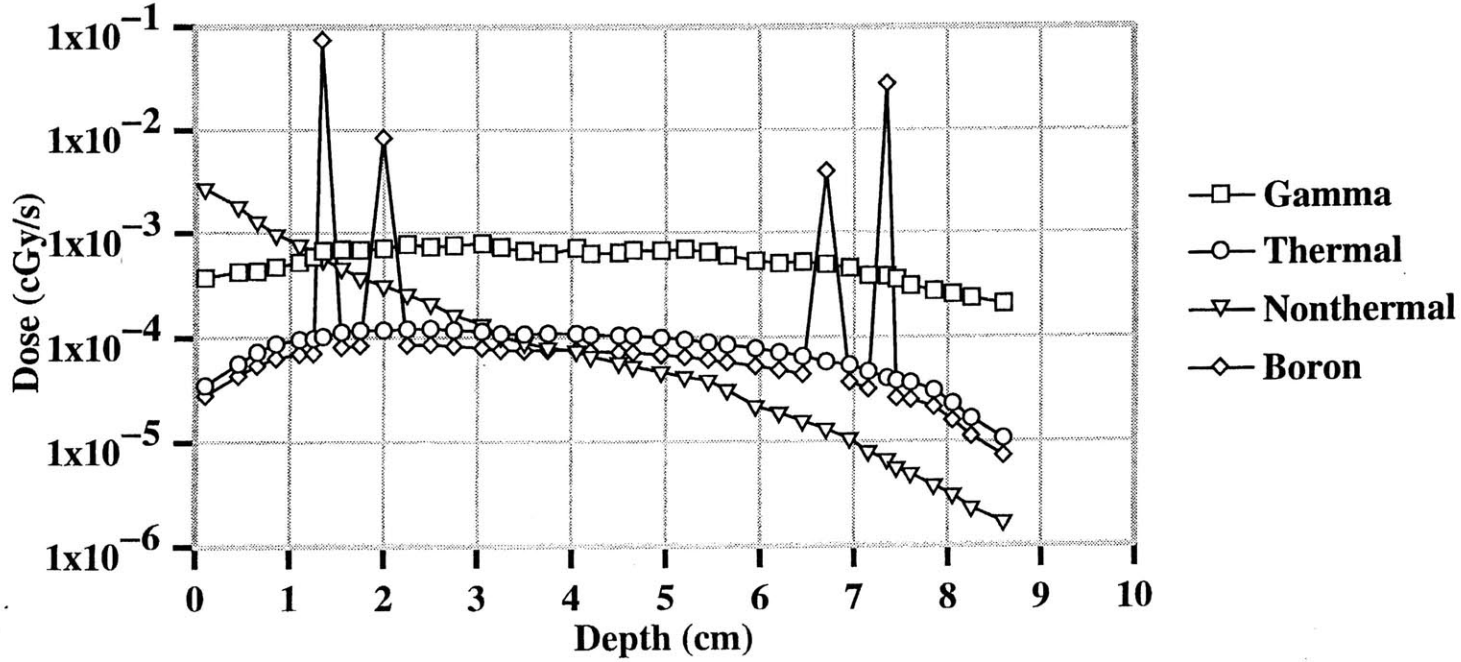

A39: Dose per depth in joint phantom
100 keV ideal isotropic beam energy
1 ppm skin: 1000 ppm synovium: 100 ppm bone
(boron concentrations of combination #2)

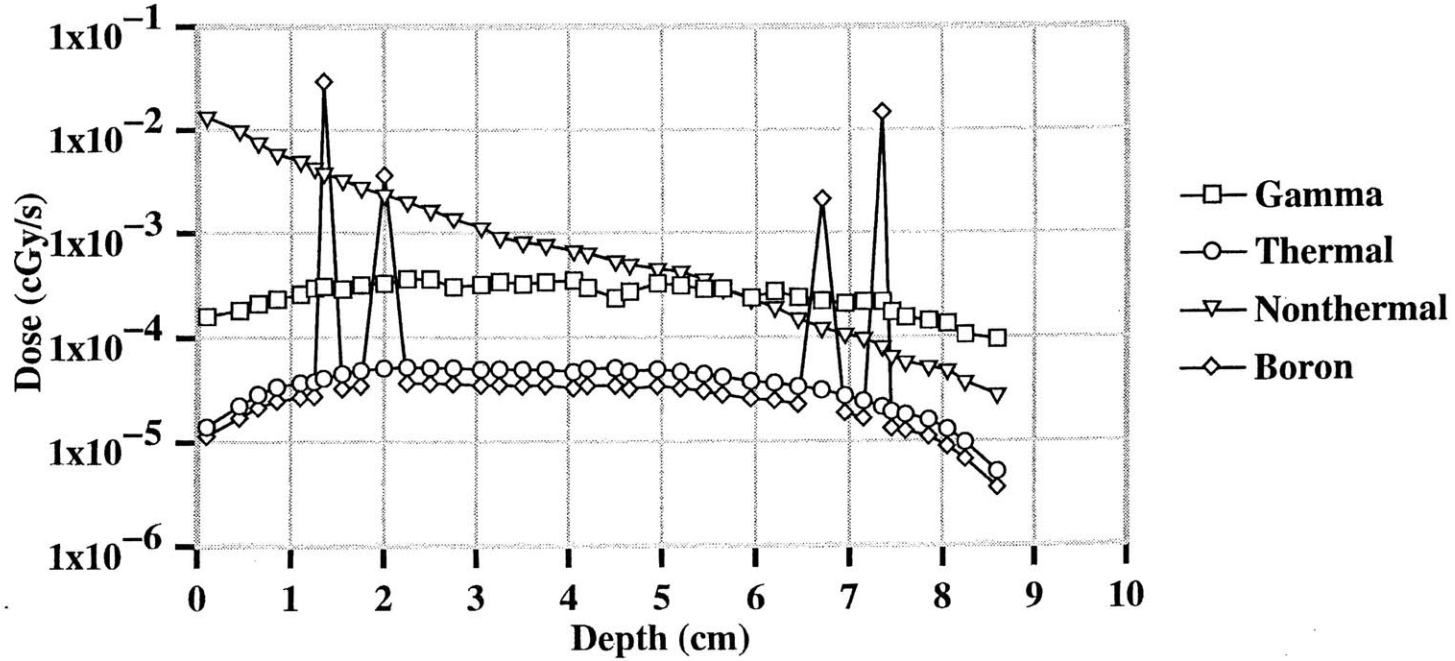

A40: Dose per depth in joint phantom
0.025 eV ideal isotropic beam energy
1 ppm skin: 10,000 ppm synovium: 100 ppm bone
(boron concentrations of combination #3)

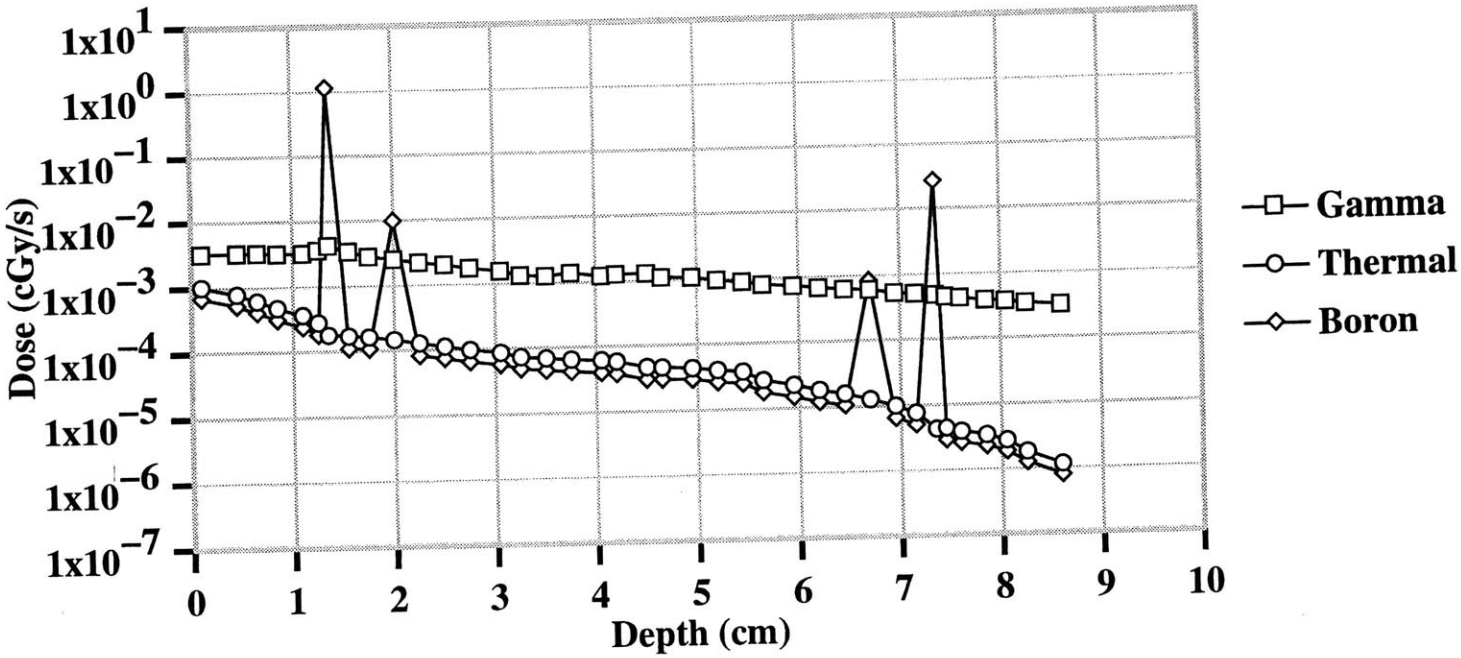

A41: Dose per depth in joint phantom
0.1 eV ideal isotropic beam energy
1 ppm skin: 10,000 ppm synovium: 100 bone
(boron concentrations of combination #3)

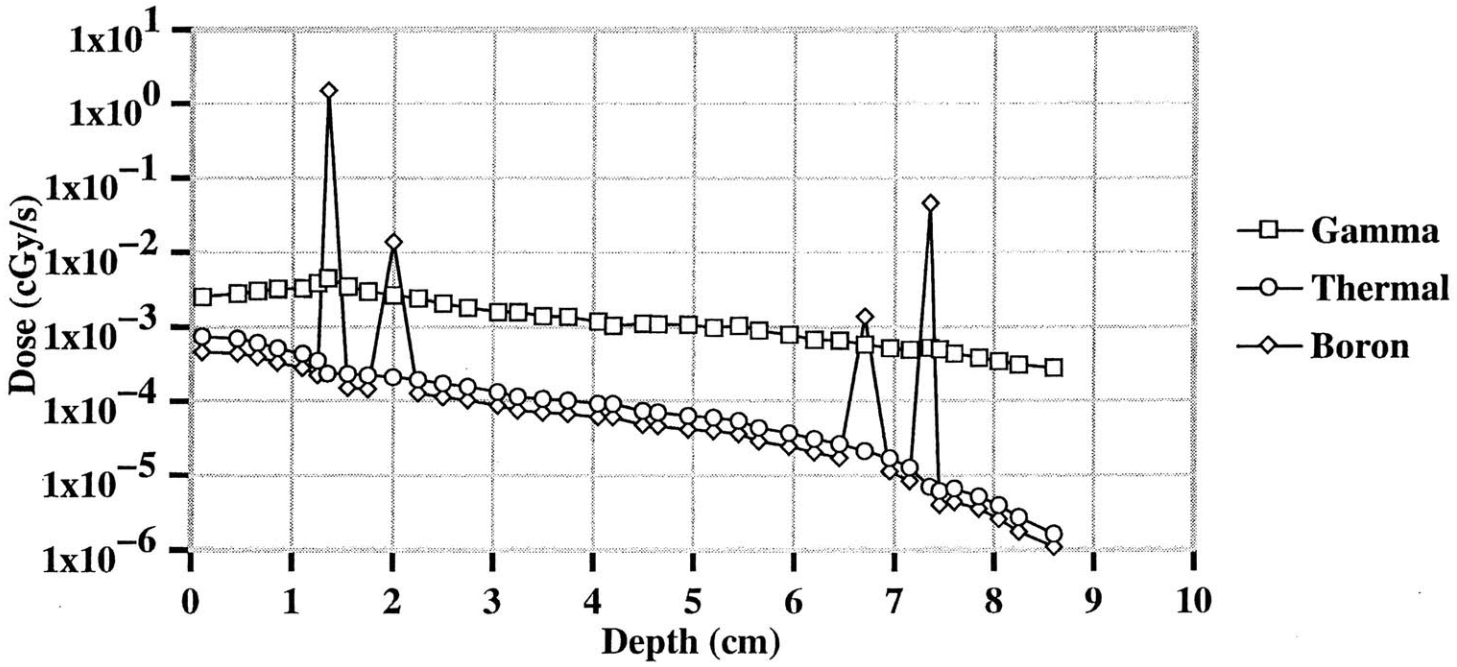

A42: Dose per depth in joint phantom
1 eV ideal isotropic beam energy
1 ppm skin: 10,000 ppm synovium: 100 ppm bone
(boron concentrations of combination #3)

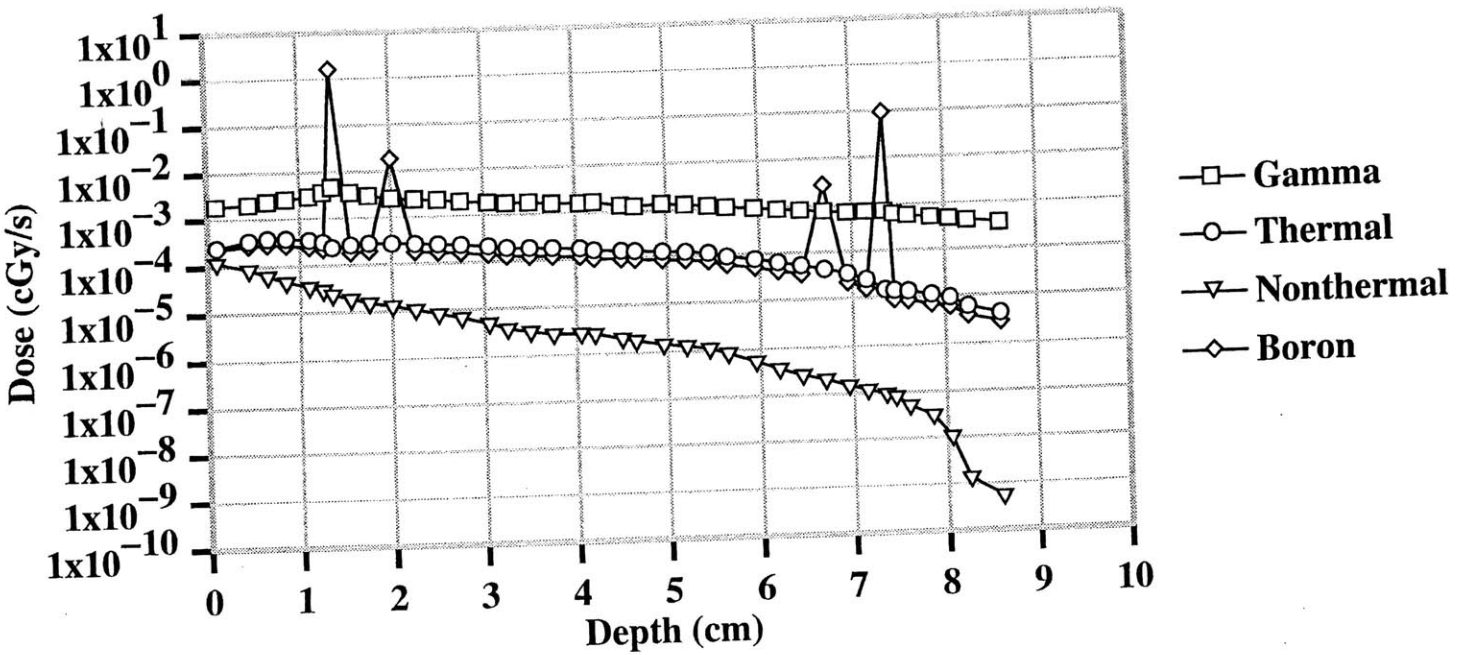

A43: Dose per depth in joint phantom
10 eV ideal isotropic beam energy
1 ppm skin: 10,000 ppm synovium: 100 ppm bone
(boron concentrations of combination #3)

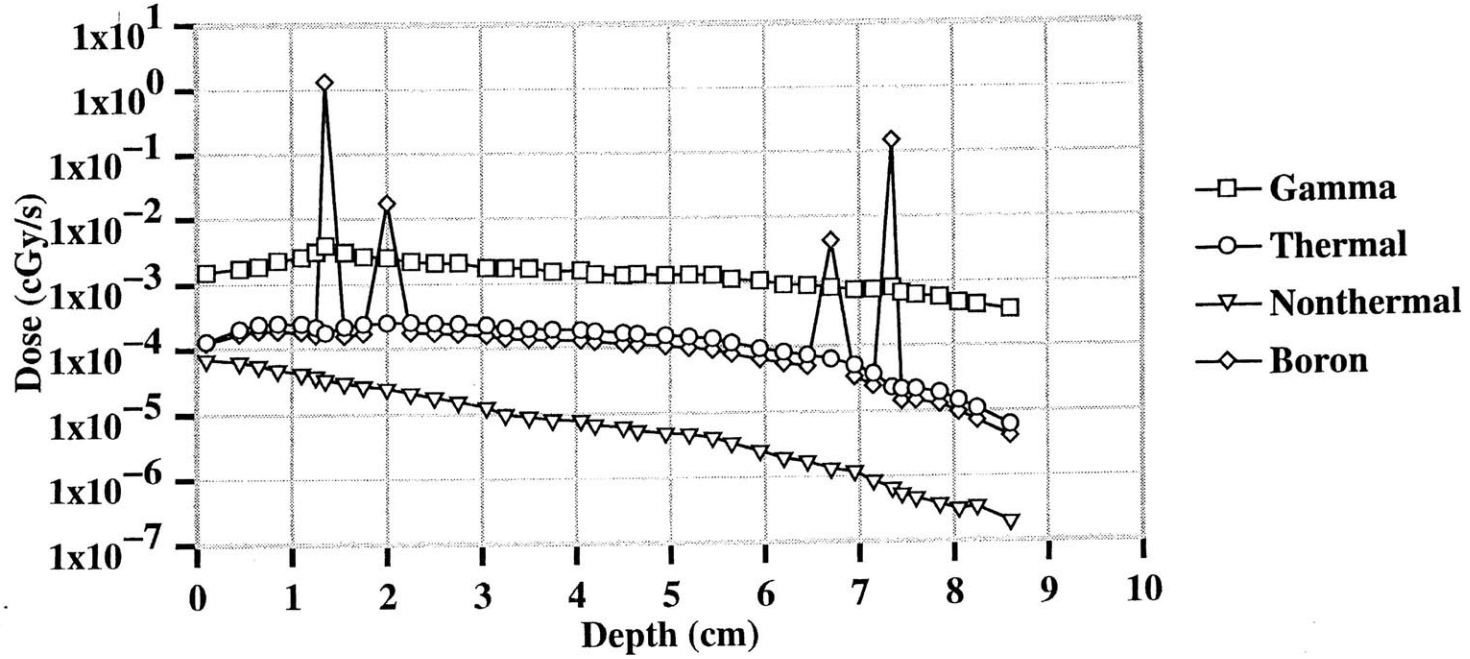

A44: Dose per depth in joint phantom
100 eV ideal isotropic beam energy
1 ppm skin: 10,000 ppm synovium: 100 ppm bone
(boron concentrations of combination #3)

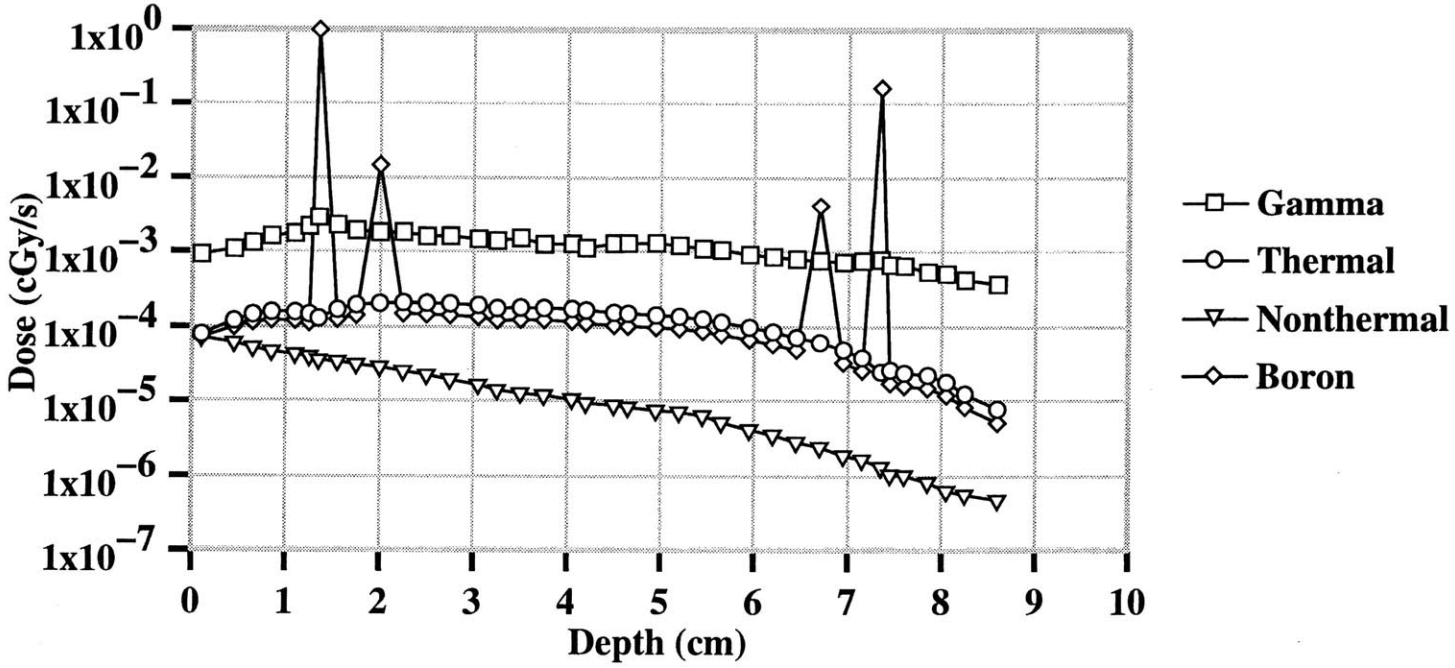

A45: Dose per depth in joint phantom
500 eV ideal isotropic beam energy
1 ppm skin: 10,000 ppm synovium: 100 ppm bone
(boron concentrations of combination #3)

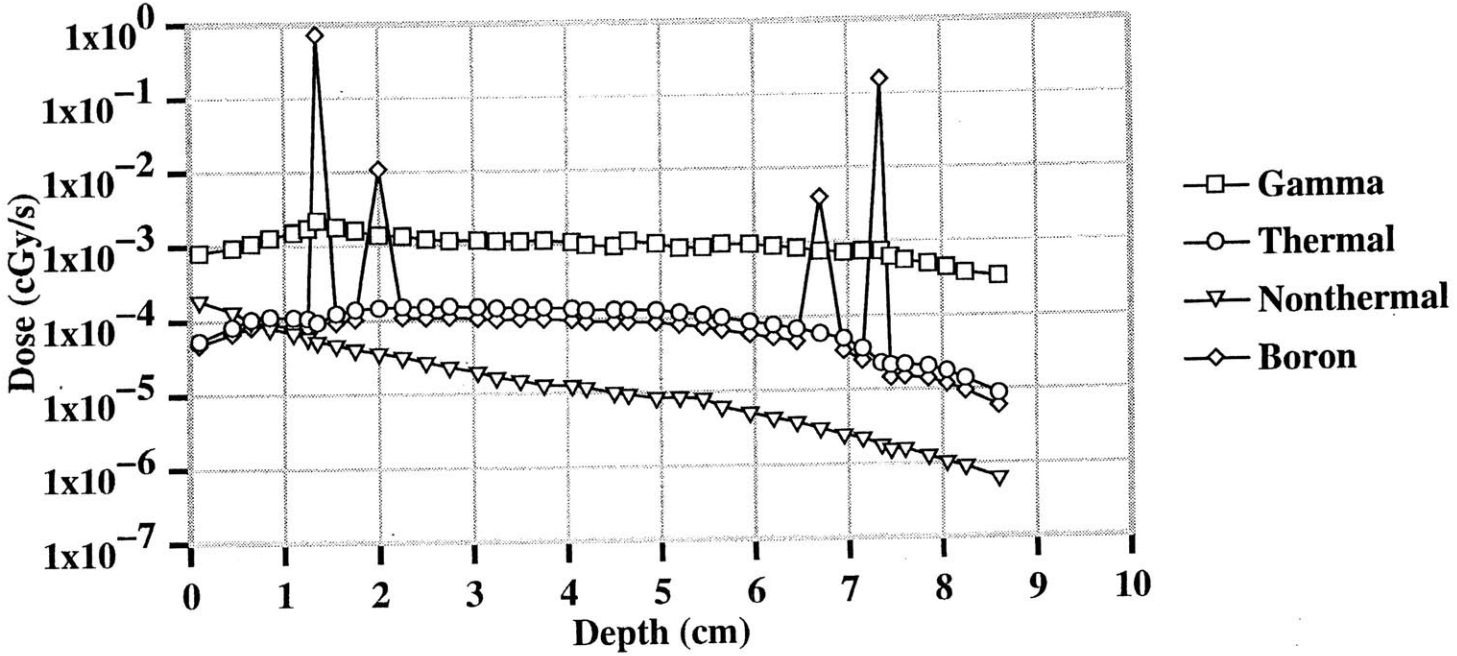

A46: Dose per depth in joint phantom
1 keV ideal isotropic beam energy
1 ppm skin: 10,000 ppm synovium: 100 ppm bone
(boron concentrations of combination #3)

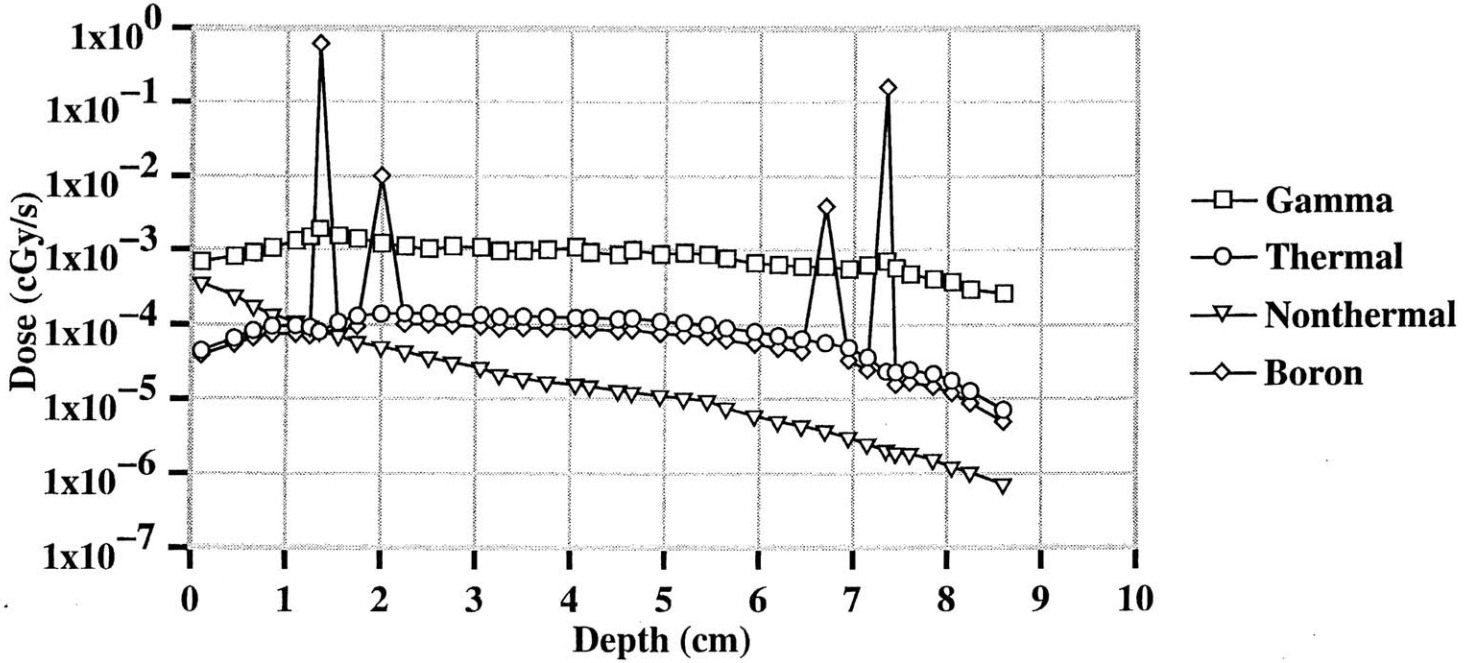

A47: Dose per depth in joint phantom
10 keV ideal isotropic beam energy
1 ppm skin: 10,000 ppm synovium: 100 ppm bone
(boron concentrations of combination #3)

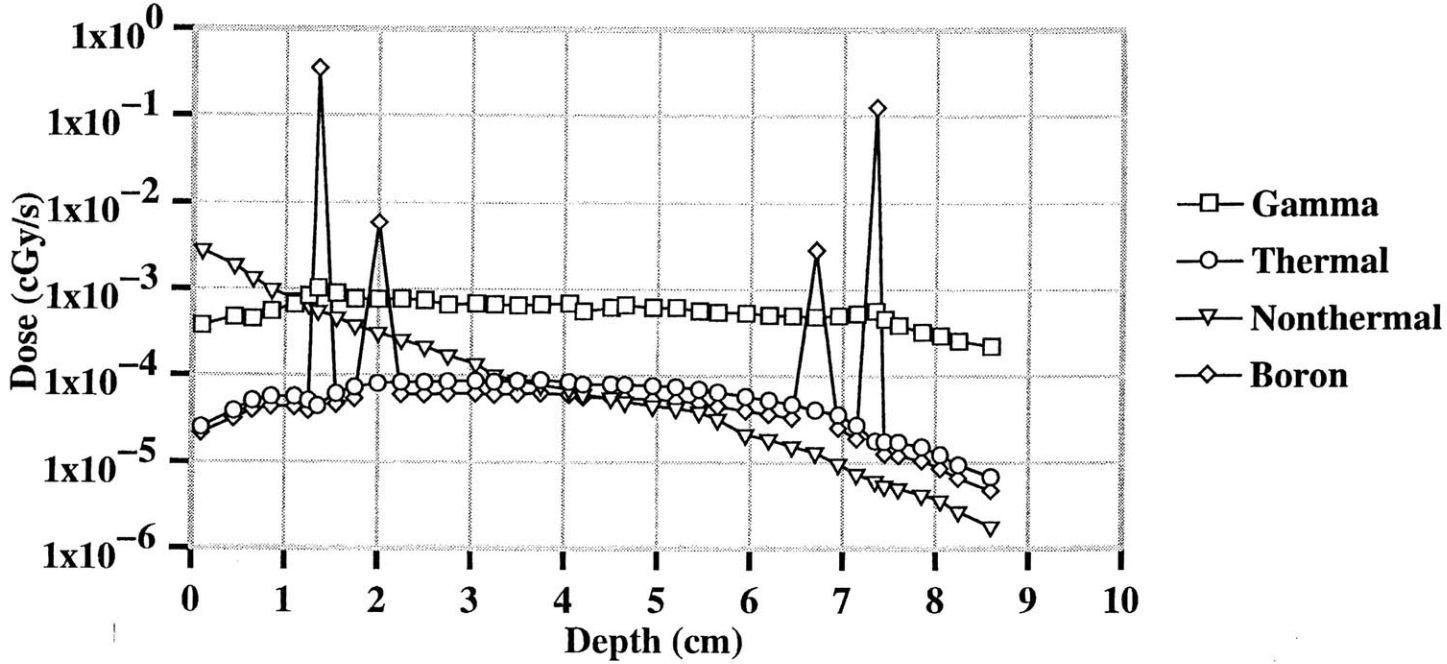

A48: Dose per depth in joint phantom
100 keV ideal isotropic beam energy
1 ppm skin: 10,000 ppm synovium: 100 ppm bone
(boron concentrations of combination #3)

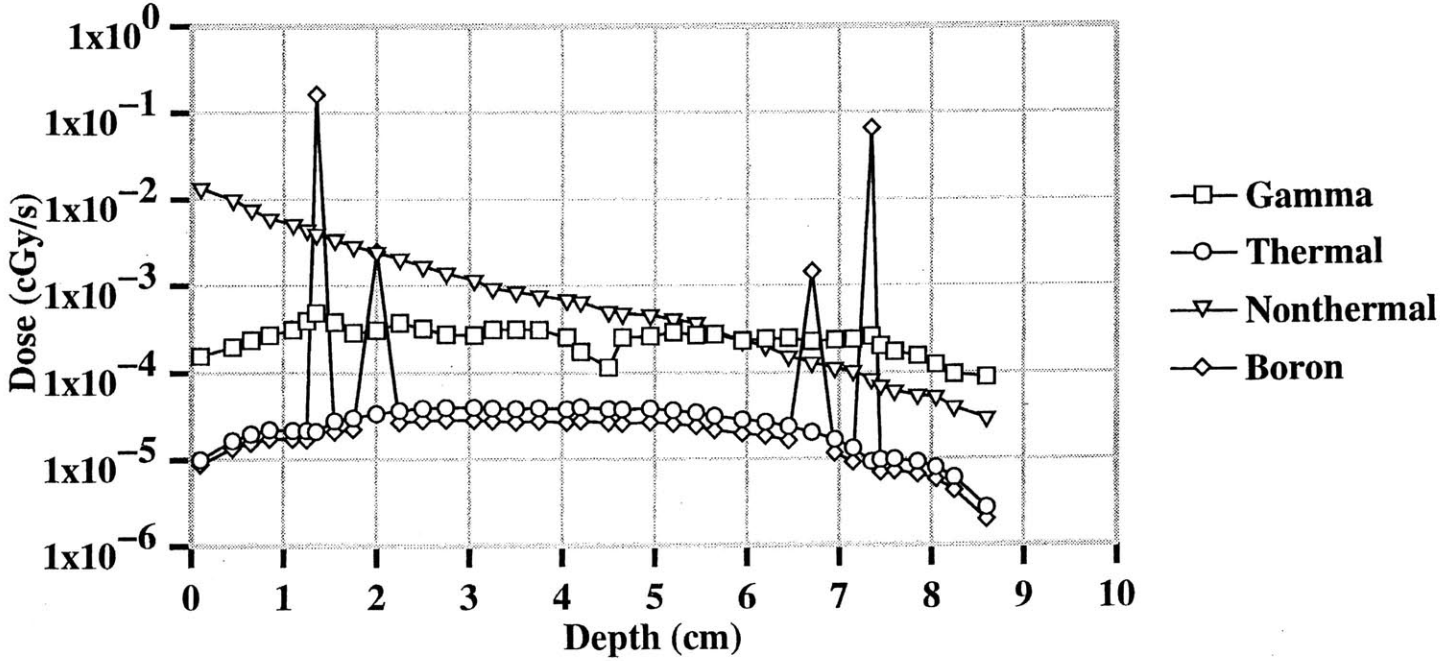

B1: Dose per depth in joint phantom
0.025 eV ideal isotropic beam energy
10,000 ppm synovium: 10,000 ppm fluid: 5,000 ppm cartilage
(boron concentrations of set 2A)

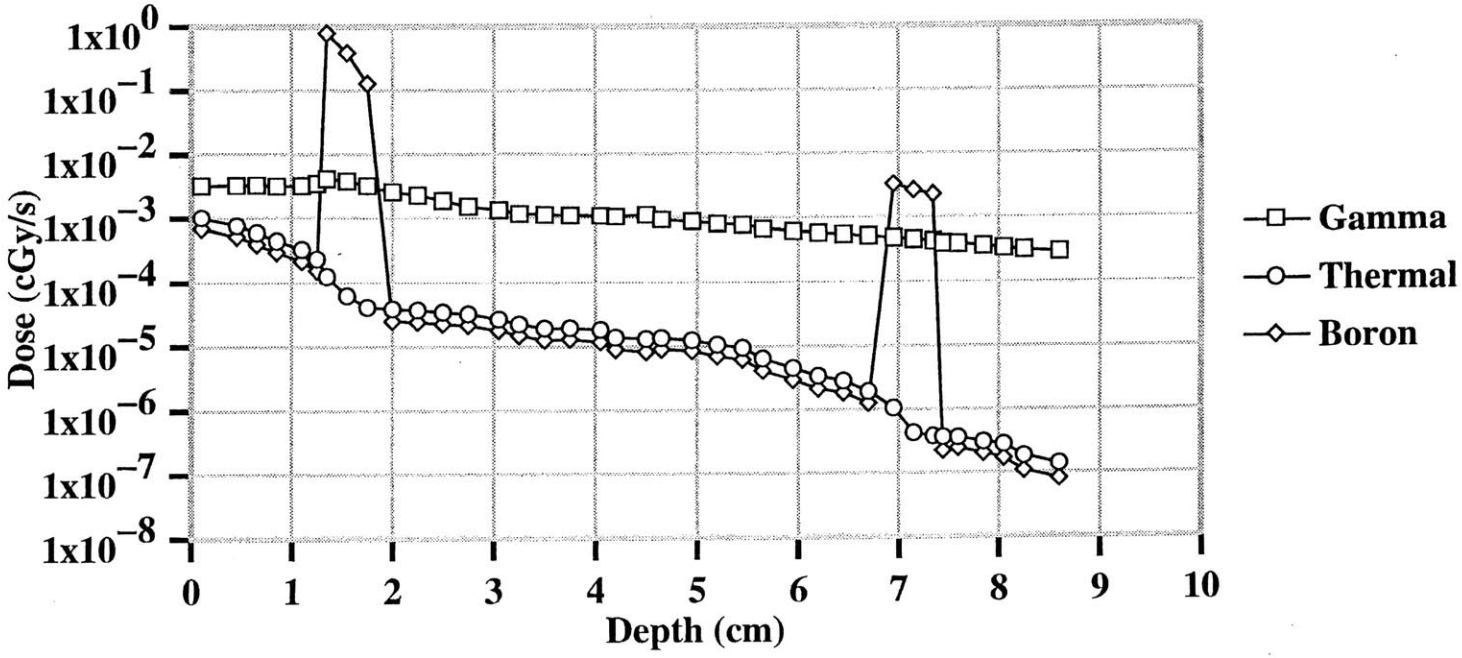

B2: Dose per depth in joint phantom
10 eV ideal isotropic beam energy
10,000 ppm synovium: 10,000 ppm fluid: 5,000 ppm cartilage
(boron concentrations of set 2A)

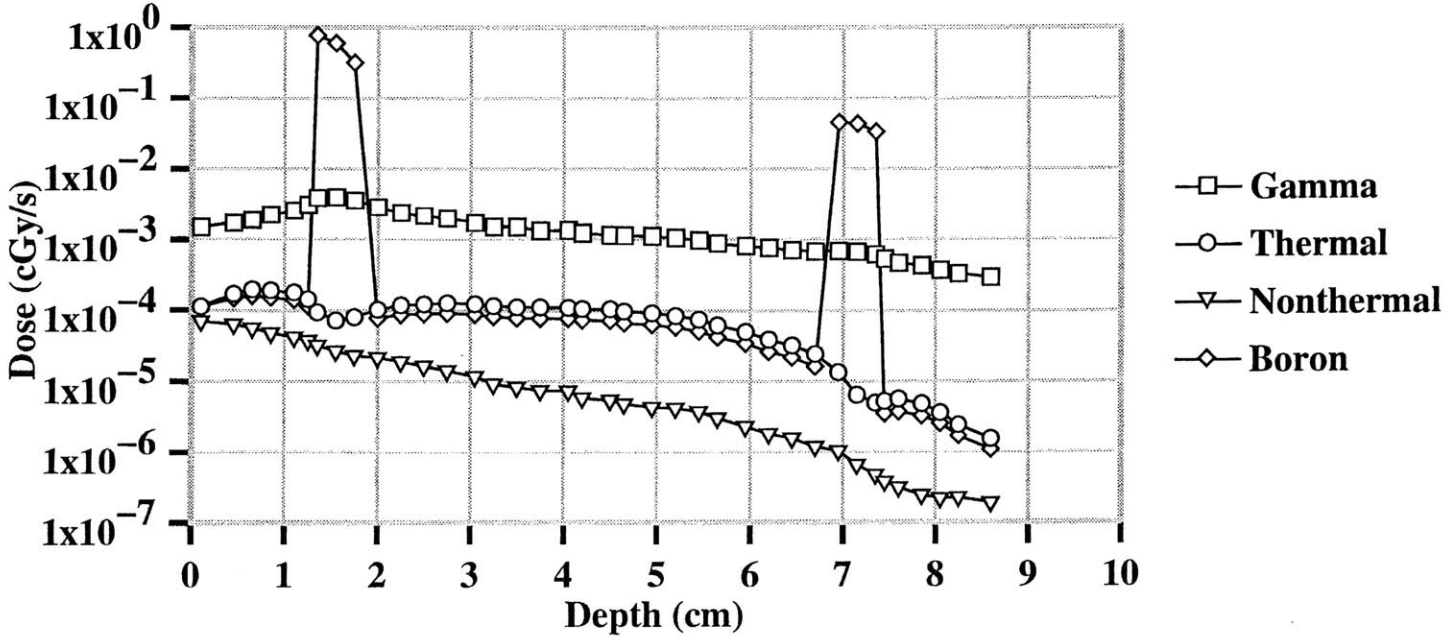

B3: Dose per depth in joint phantom
100 eV ideal isotropic beam energy
10,000 ppm synovium: 10,000 ppm fluid: 5,000 ppm cartilage
(boron concentrations of set 2A)

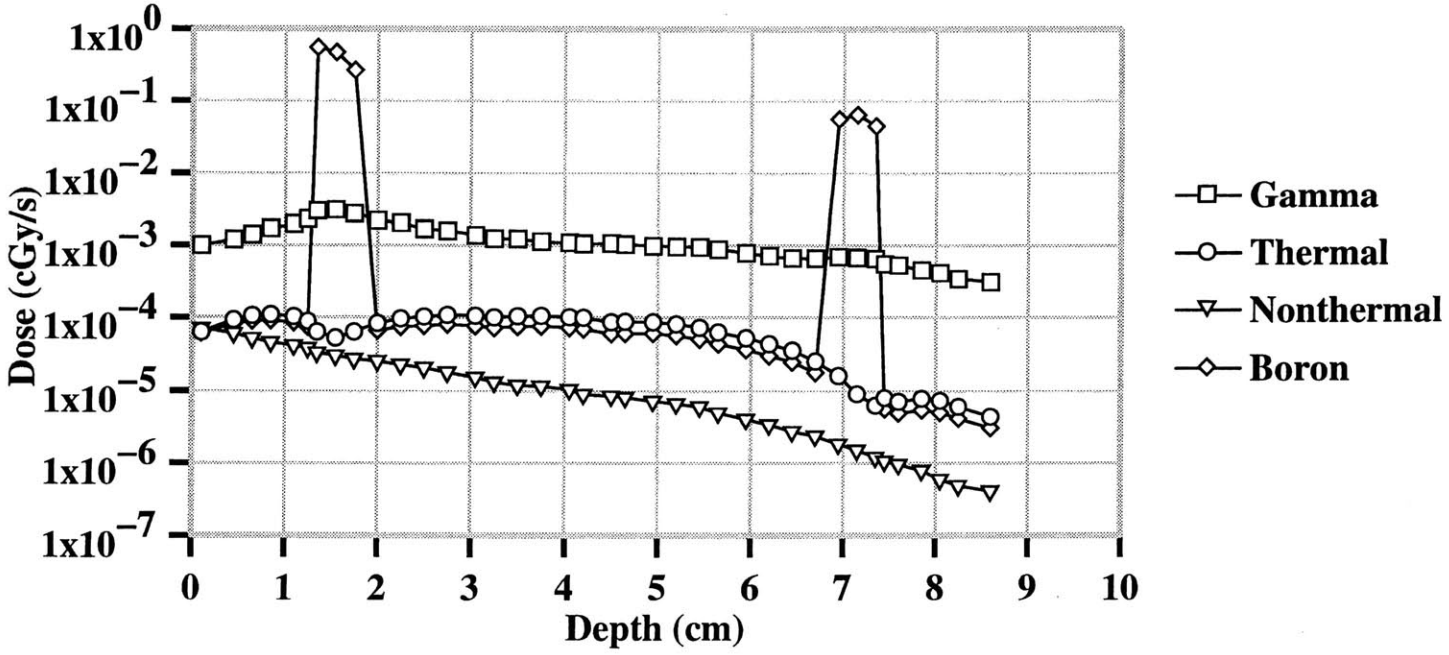

B4: Dose per depth in joint phantom
1 keV ideal isotropic beam energy
10,000 ppm synovium: 10K ppm fluid: 5,000 ppm cartilage
(boron concentrations of set 2A)

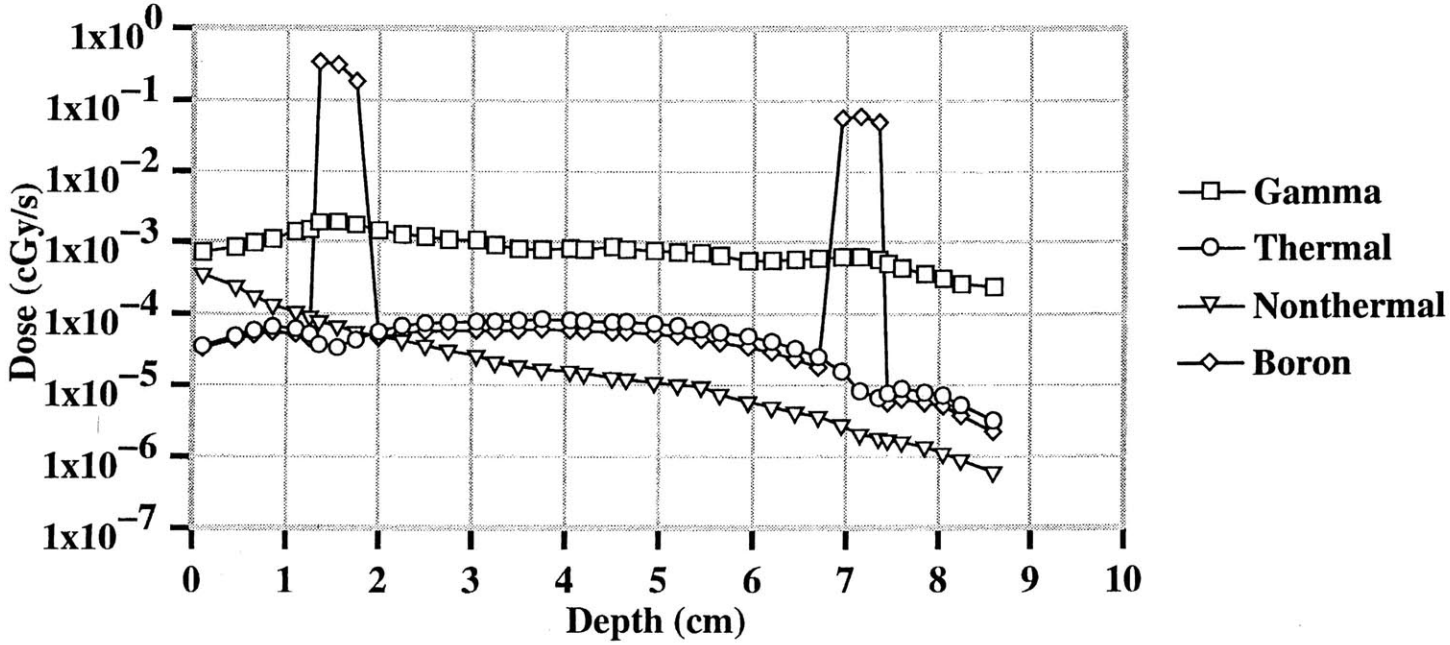

B5: Dose per depth in joint phantom
100 keV ideal isotropic beam energy
10,000 ppm synovium: 10,000 ppm fluid: 5,000 ppm cartilage
(boron concentrations of set 2A)

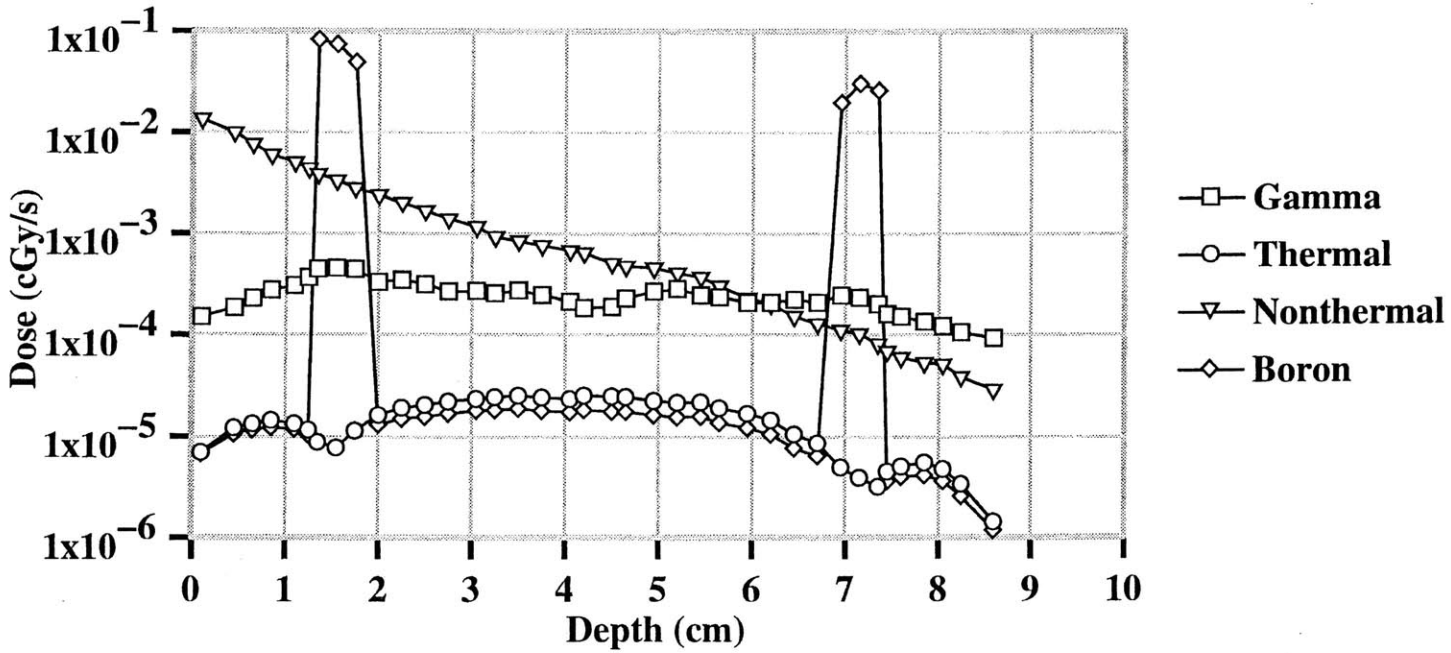

B6: Dose per depth in joint phantom
0.025 eV ideal isotropic beam energy
20,000 ppm synovium: 20,000 ppm fluid: 10,000 ppm cartilage
(boron concentrations of set 2B)

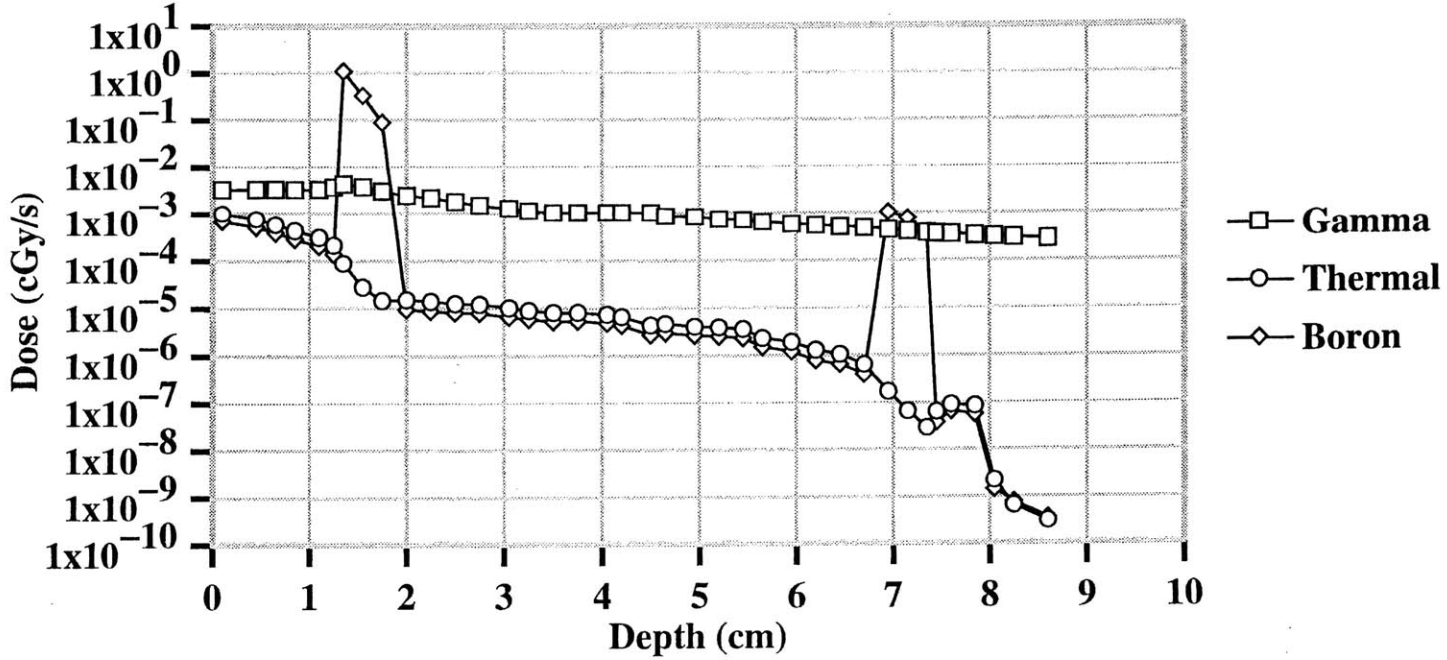

B7: Dose per depth in joint phantom
10 eV ideal isotropic beam energy
20,000 ppm synovium: 20,000 ppm fluid: 10,000 ppm cartilage
(boron concentrations of set 2B)

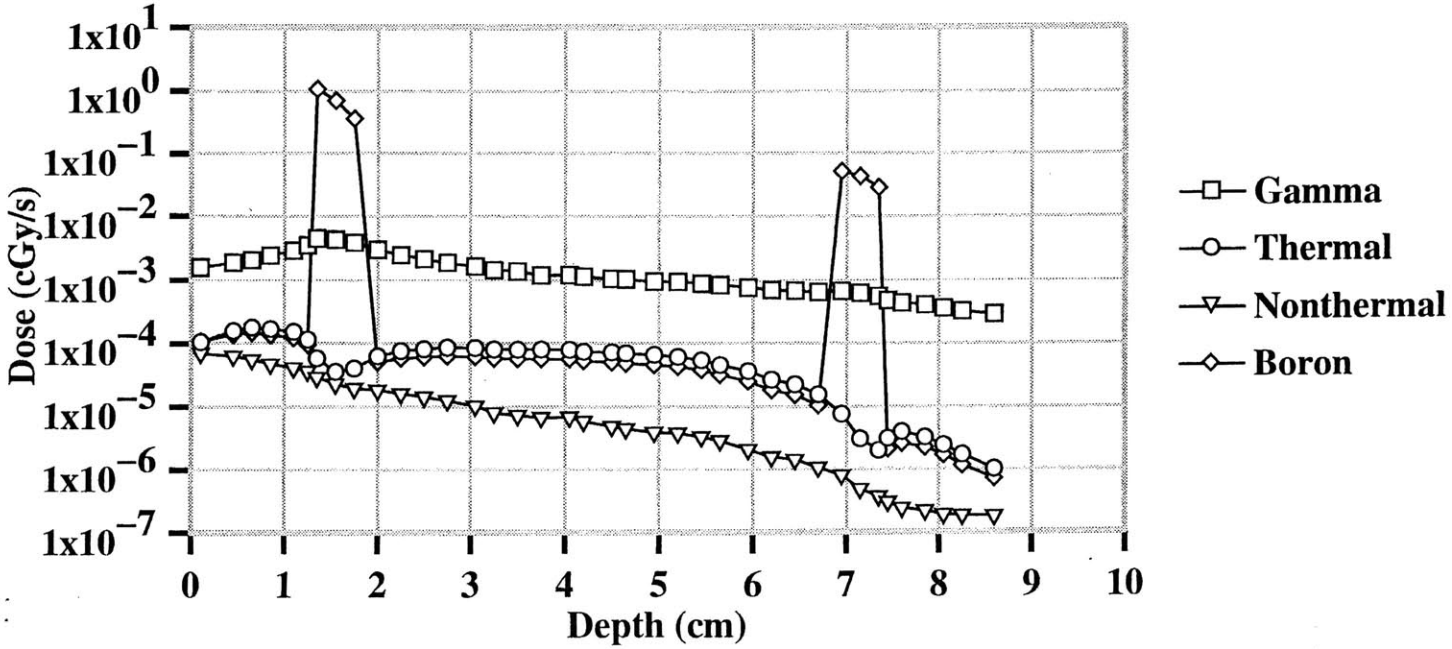

B8: Dose per depth in joint phantom
100 eV ideal isotropic beam energy
20,000 ppm synovium: 20,000 ppm fluid: 10,000 ppm cartilage
(boron concentrations of set 2B)

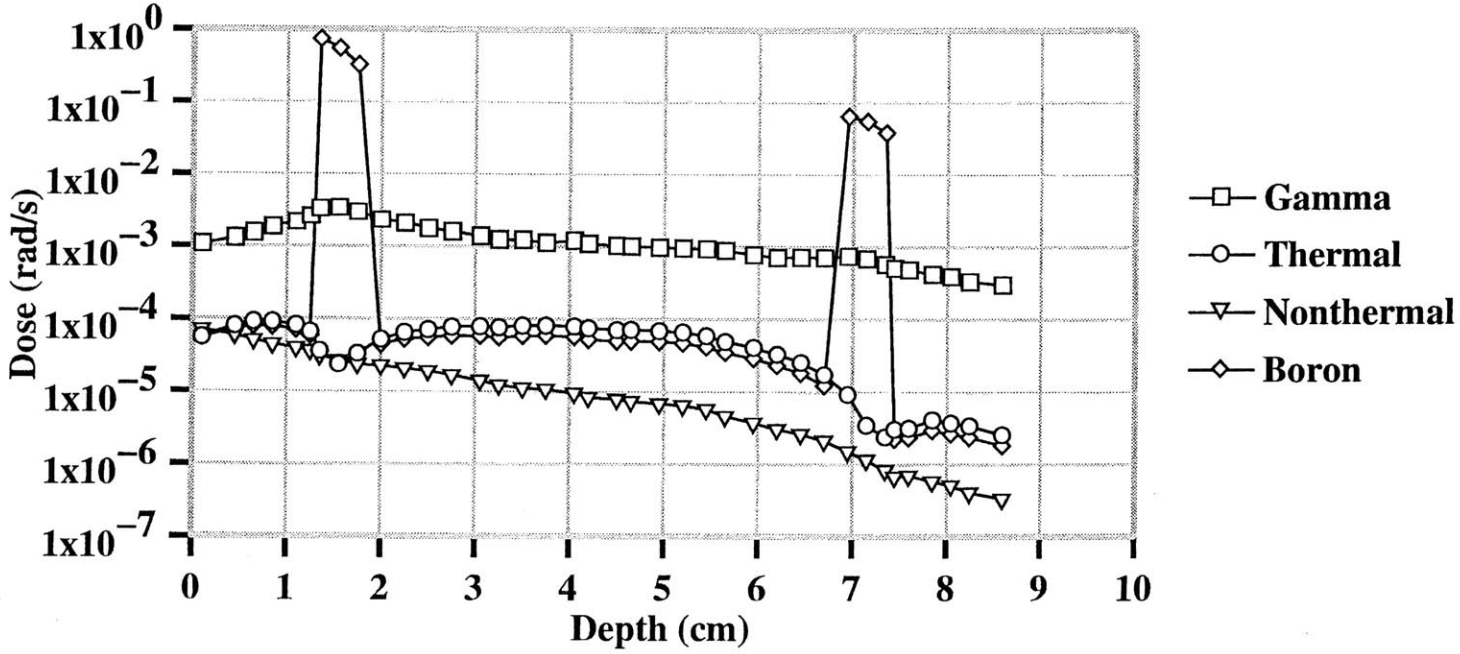

B9: Dose per depth in joint phantom
1 keV ideal isotropic beam energy
20,000 ppm synovium: 20,000 ppm fluid: 10,000 ppm cart
(boron concentrations of set 2B)

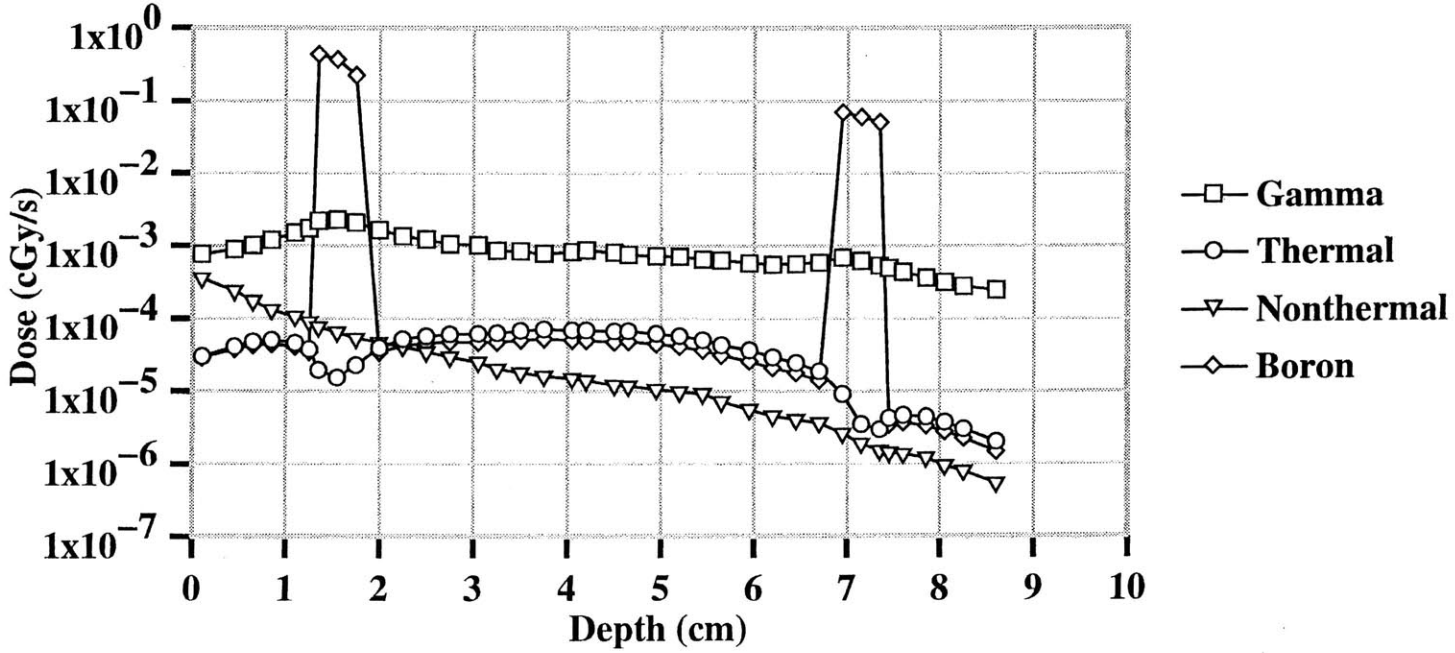

B10: Dose per depth in joint phantom
100 keV ideal isotropic beam energy
20,000 ppm synovium: 20,000 ppm fluid: 10,000 ppm cartilage
(boron concentrations of set 2B)

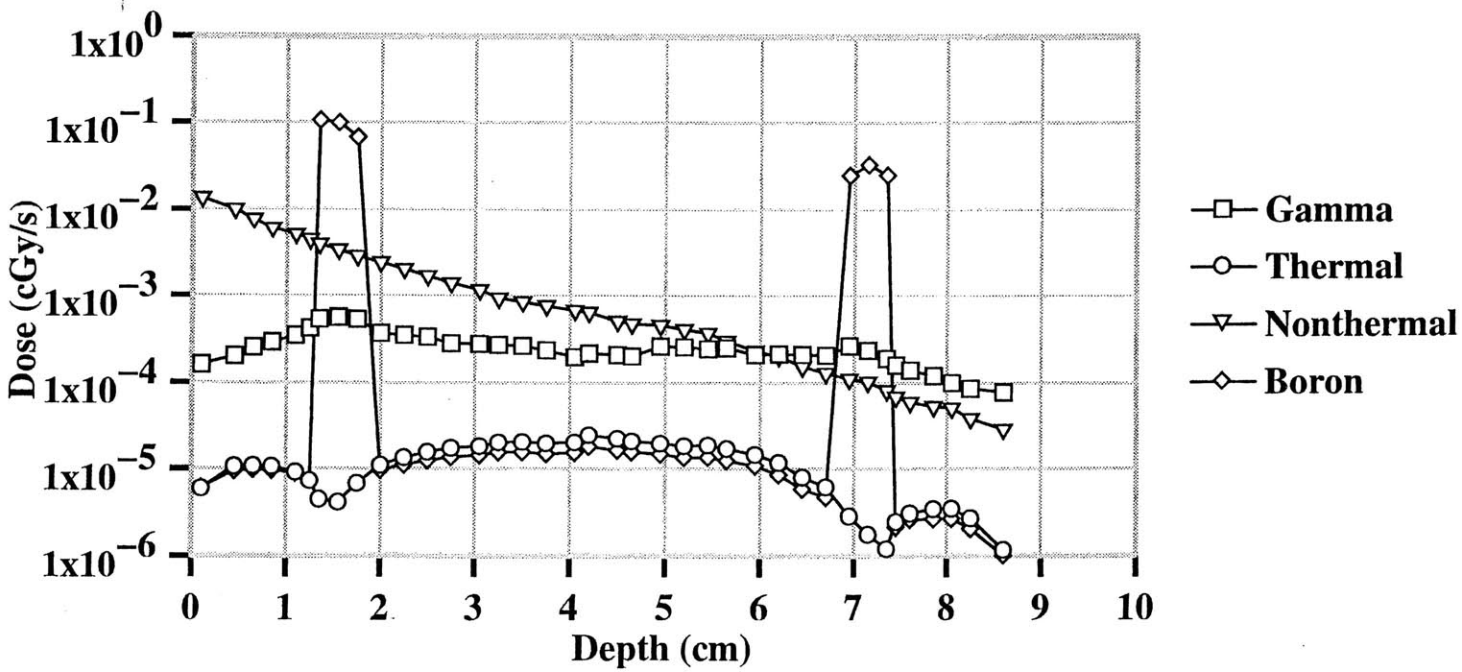

B11: Dose per depth in joint phantom
0.025 eV ideal isotropic beam energy
20,000 ppm synovium: 1 ppm fluid: 10,000 ppm cartilage
(boron concentrations of set 2C)

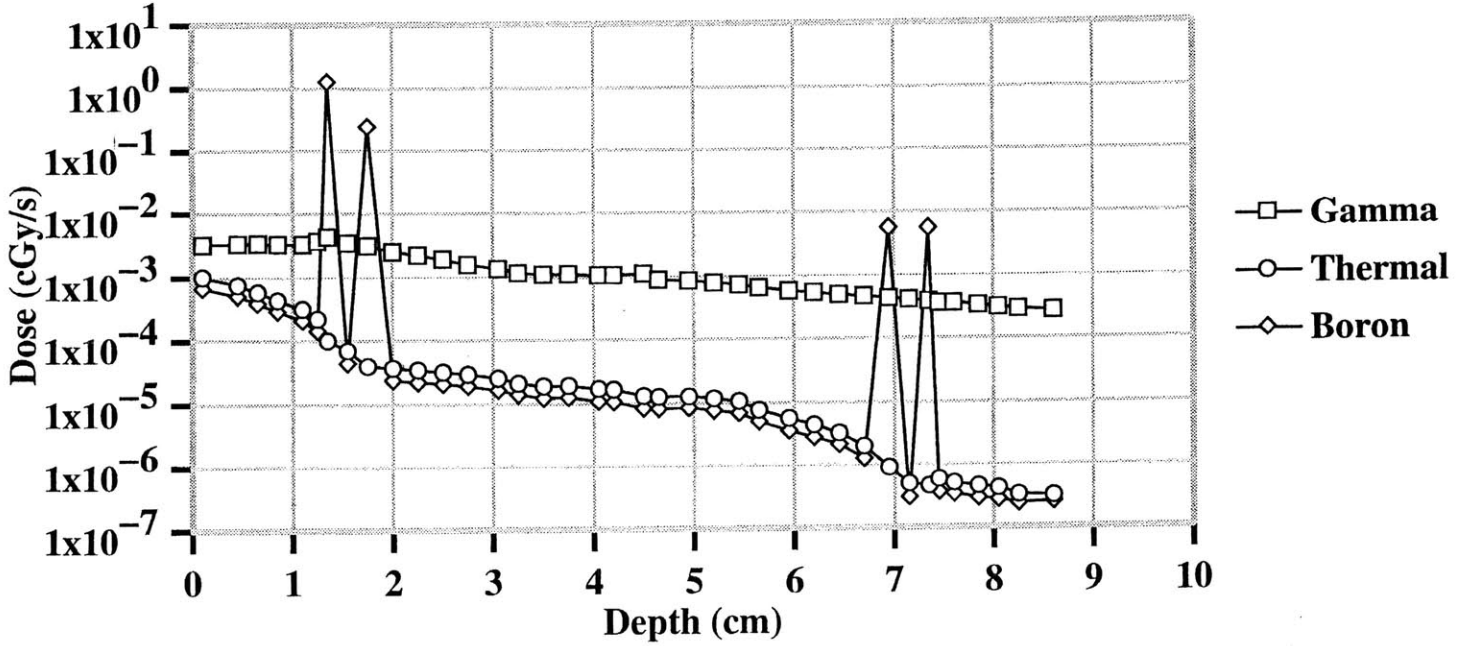

B12: Dose per depth in joint phantom
10 eV ideal isotropic beam energy
20,000 ppm synovium:1 ppm fluid: 10,000 ppm cartilage
(boron concentrations of set 2C)

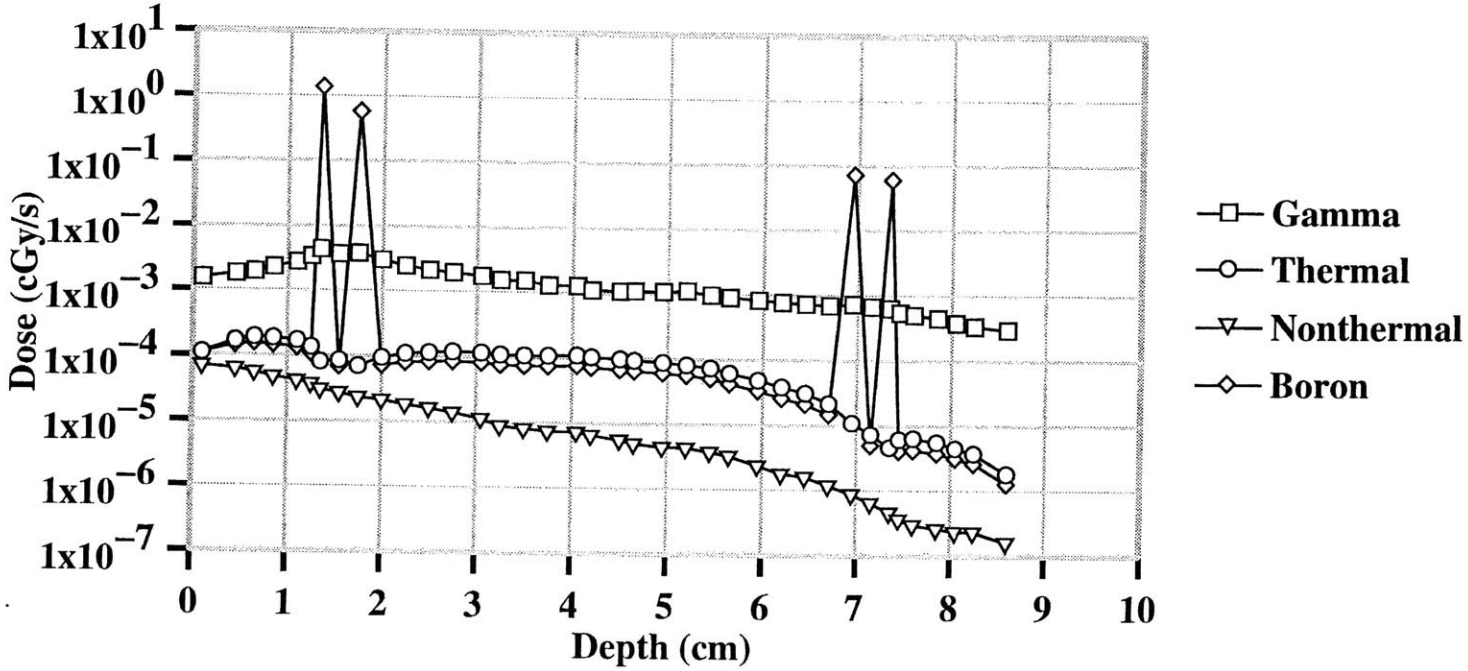

B13: Dose per depth in joint phantom
100 eV ideal isotropic beam energy
20,000 ppm synovium: 1 ppm fluid: 10,000 ppm cartilage
(boron concentrations of set 2C)

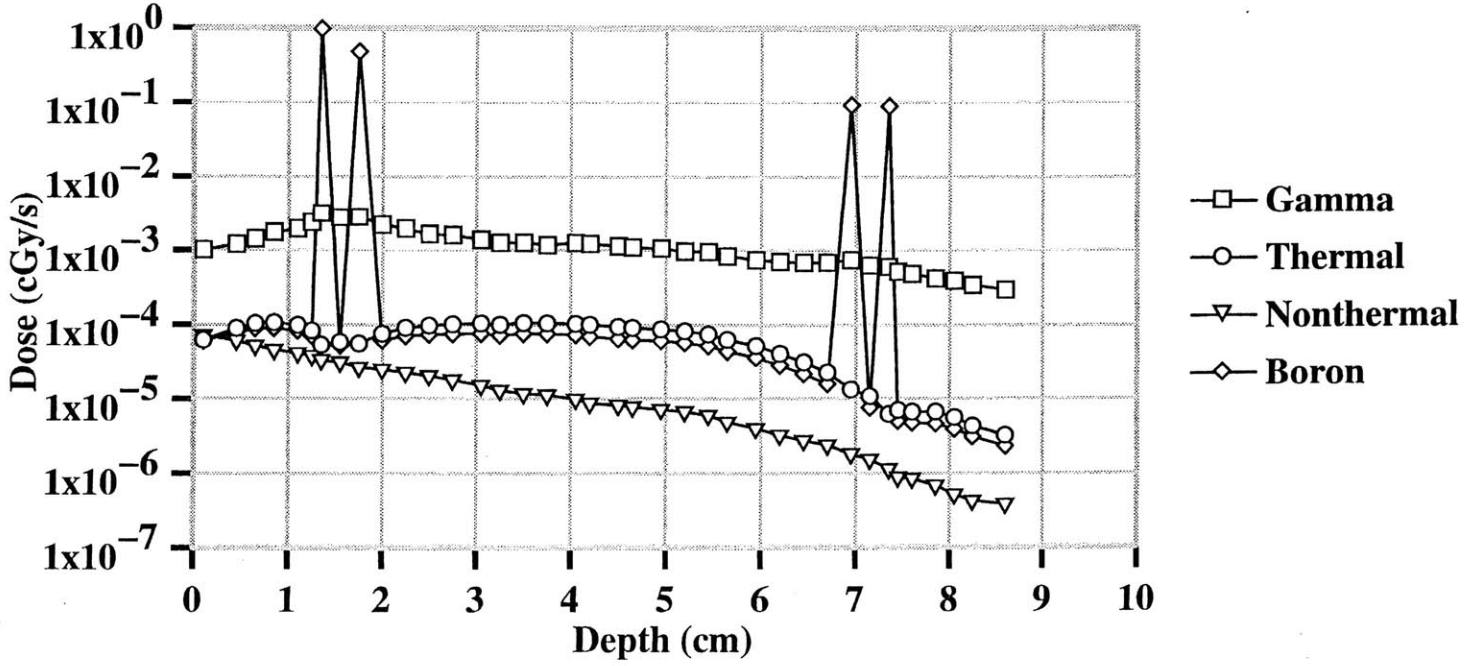

B14: Dose per depth in joint phantom
1 keV ideal isotropic beam energy
20,000 ppm synovium: 1 ppm fluid: 10,000 ppm cartilage
(boron concentrations of set 2C)

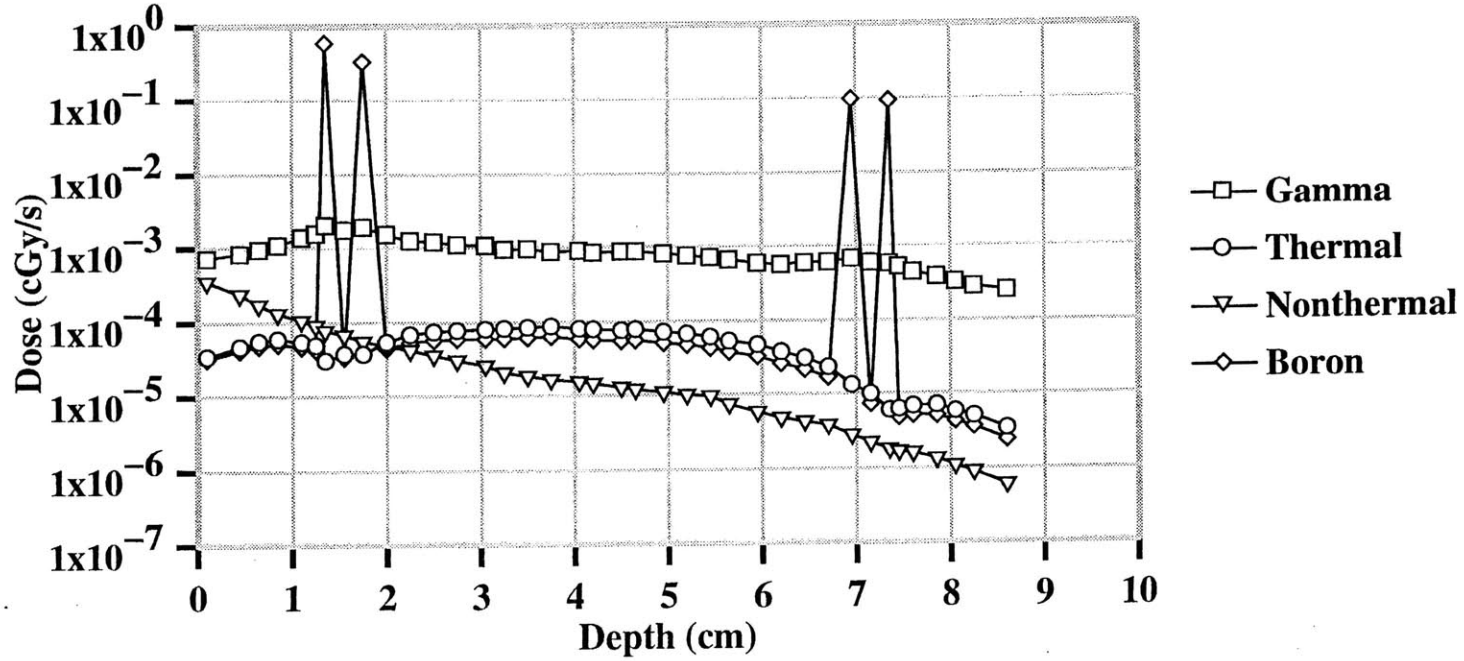

B15: Dose per depth in joint phantom
100 keV ideal isotropic beam energy
20,000 ppm synovium: 1 ppm fluid: 10,000 ppm cartilage
(boron concentrations of set 2C)

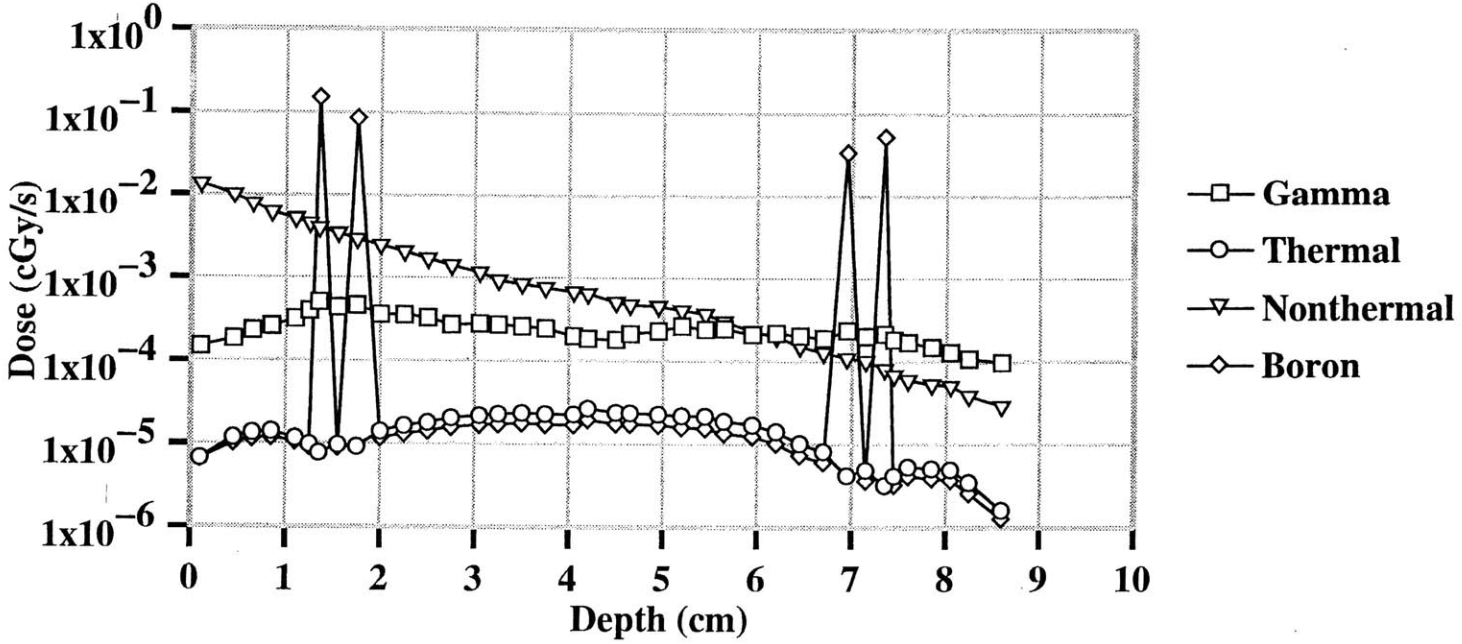

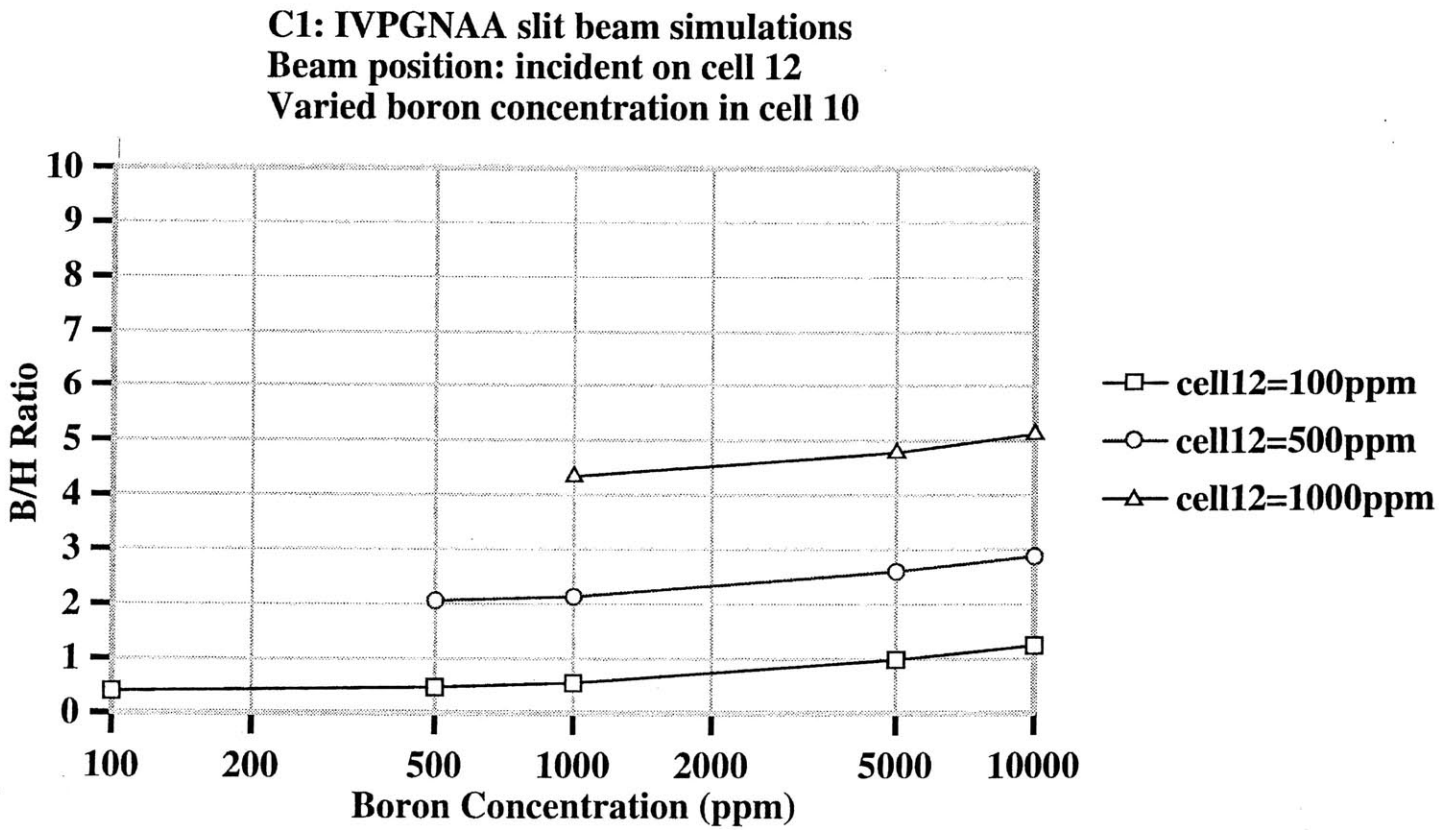
C1: IVPGNAA slit beam simulations
Beam position: incident on cell 12
Varied boron concentration in cell 10
B/H Ratio
10
9
8
7
6
5
4
3
2
1
0
100
200
500
1000
2000
5000
10000
Boron Concentration (ppm)
cell12=100ppm
cell12=500ppm
cell12=1000ppm

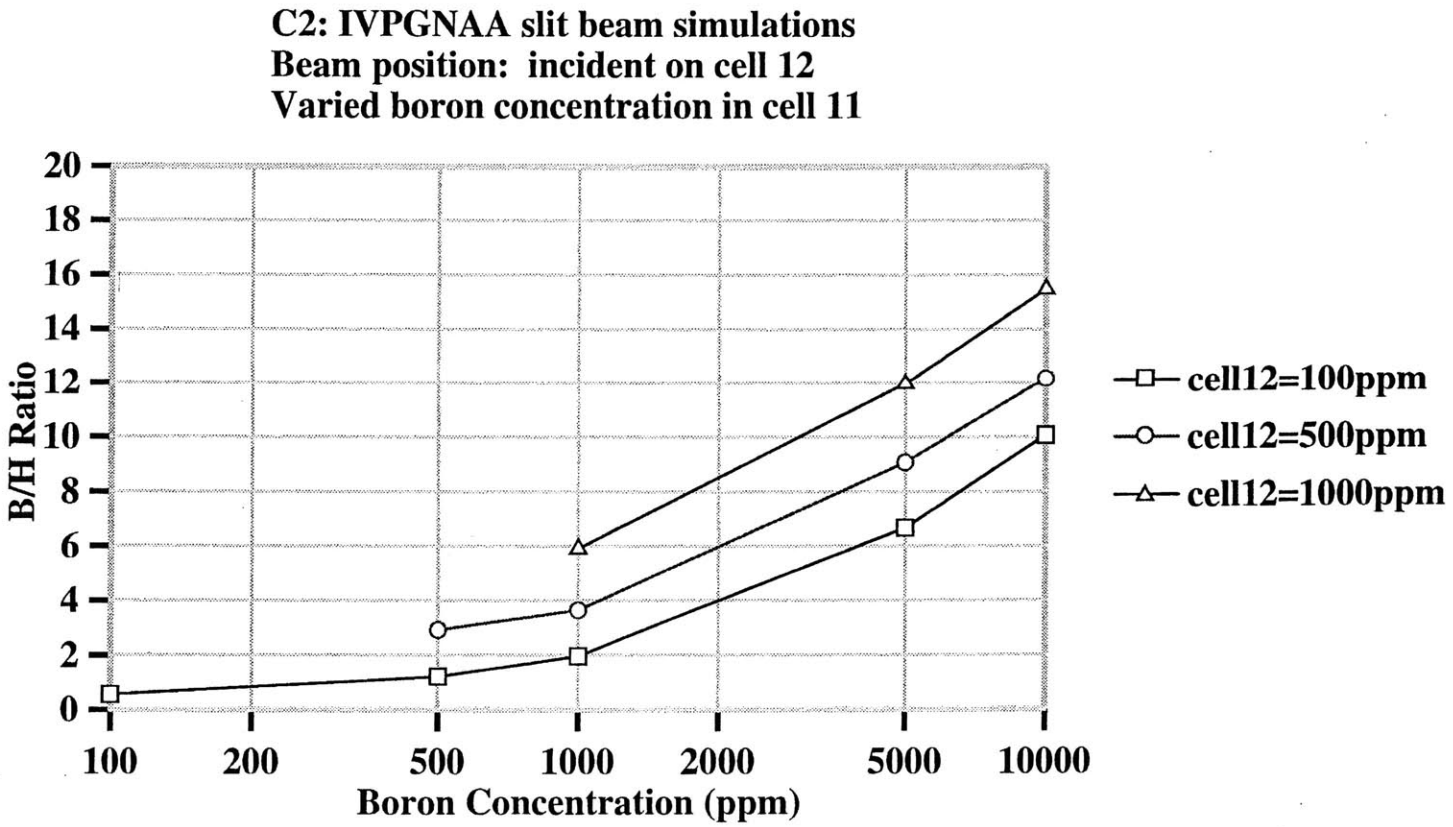
C2: IVPGNAA slit beam simulations
Beam position: incident on cell 12
Varied boron concentration in cell 11
B/H Ratio
20
18
16
14
12
10
8
6
4
2
0
100
200
500
1000
2000
5000
10000
Boron Concentration (ppm)
cell12=100ppm
cell12=500ppm
cell12=1000ppm

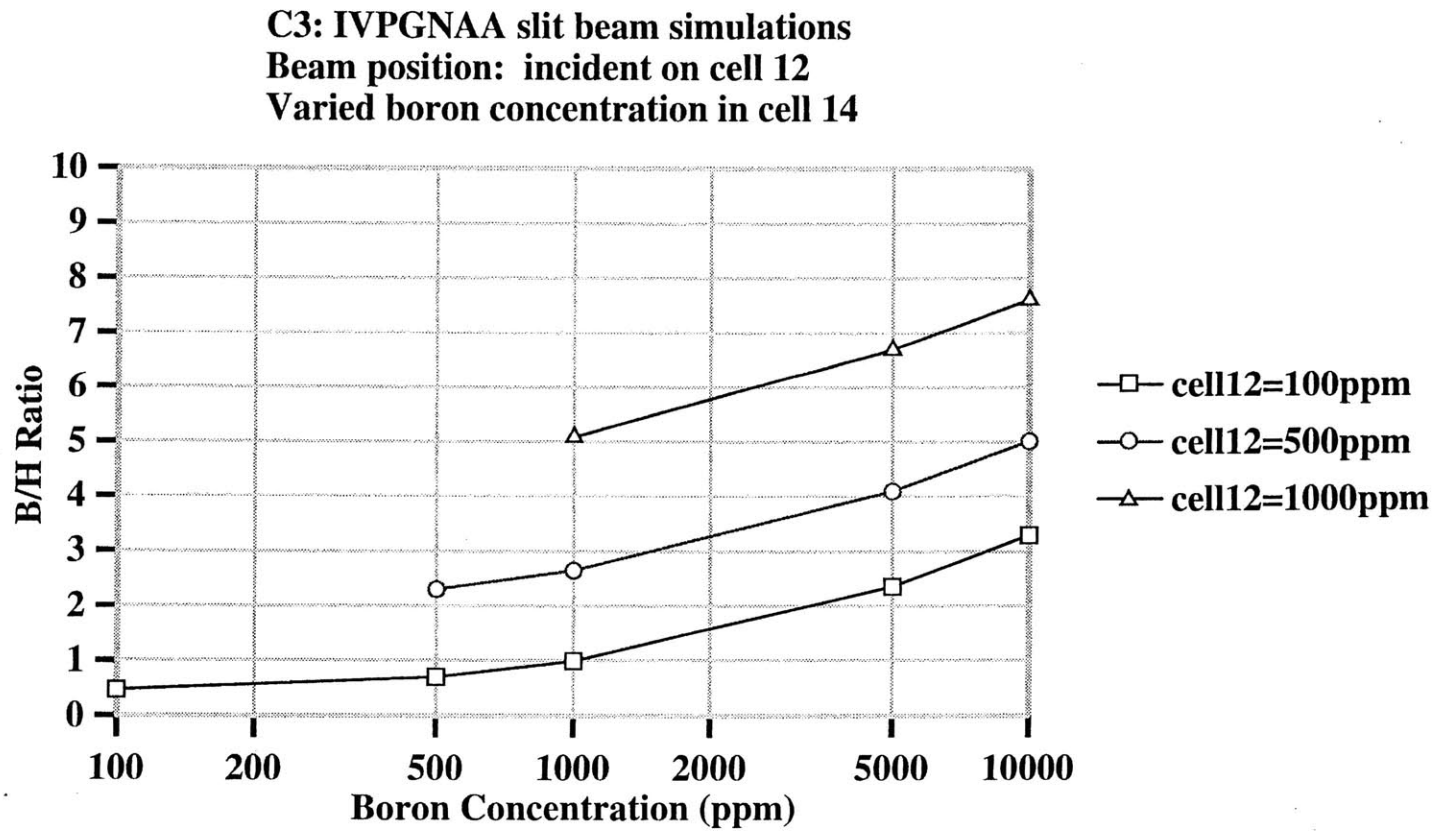
C3: IVPGNAA slit beam simulations
Beam position: incident on cell 12
Varied boron concentration in cell 14
B/H Ratio
10
9
8
7
6
5
4
3
2
1
0
100
200
500
1000
2000
5000
10000
Boron Concentration (ppm)
cell12=100ppm
cell12=500ppm
cell12=1000ppm

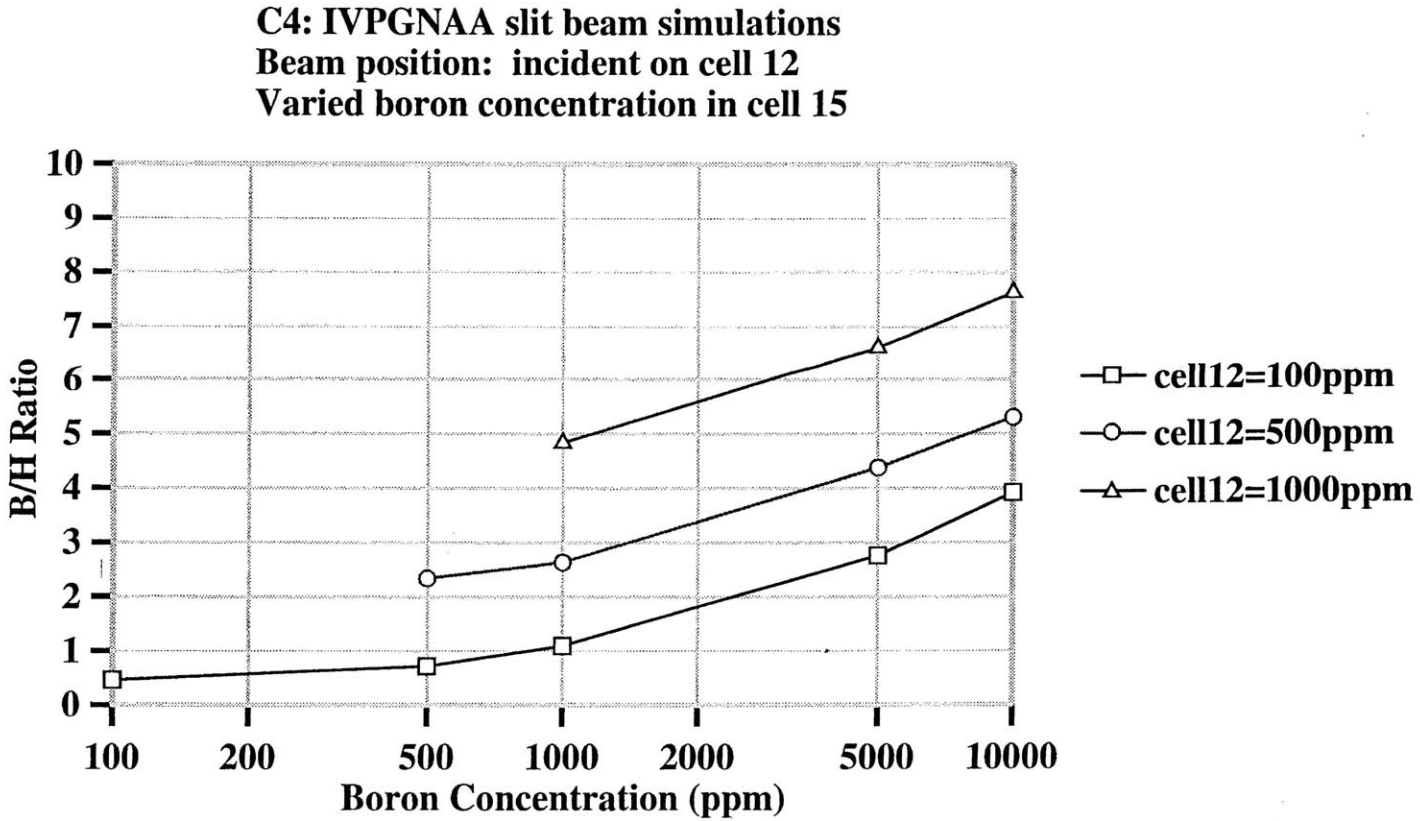
C4: IVPGNAA slit beam simulations
Beam position: incident on cell 12
Varied boron concentration in cell 15
B/H Ratio
10
9
8
7
6
5
4
3
2
1
0
100
200
500
1000
2000
5000
10000
Boron Concentration (ppm)
cell12=100ppm
cell12=500ppm
cell12=1000ppm

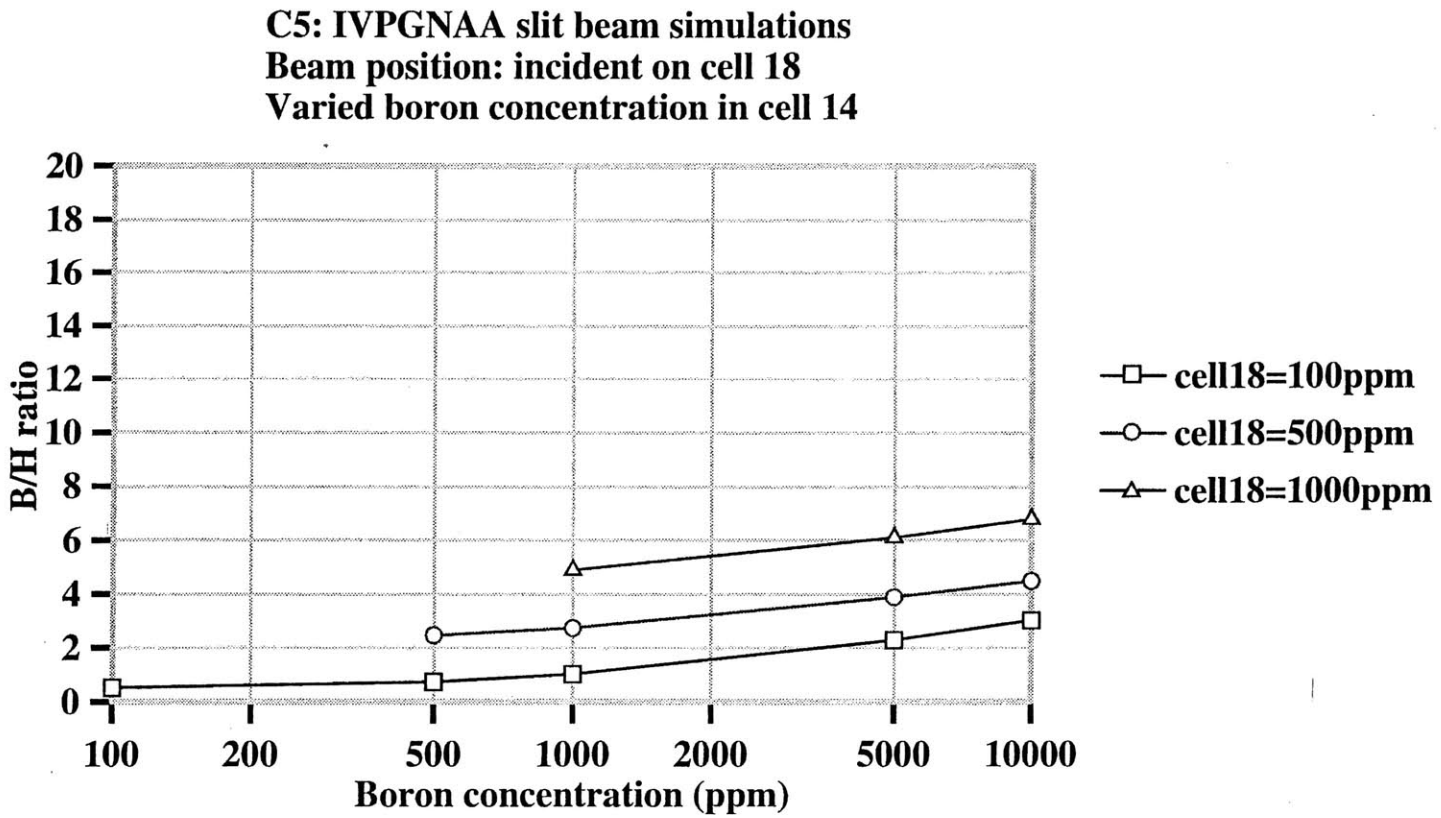
C5: IVPGNAA slit beam simulations
Beam position: incident on cell 18
Varied boron concentration in cell 14
B/H ratio
20
18
16
14
12
10
8
6
4
2
0
100
200
500
1000
2000
5000
10000
Boron concentration (ppm)
cell18=100ppm
cell18=500ppm
cell18=1000ppm

C6: IVPGNAA slit beam simulations
Beam position: incident on cell 18
Varied boron concentration in cell 15

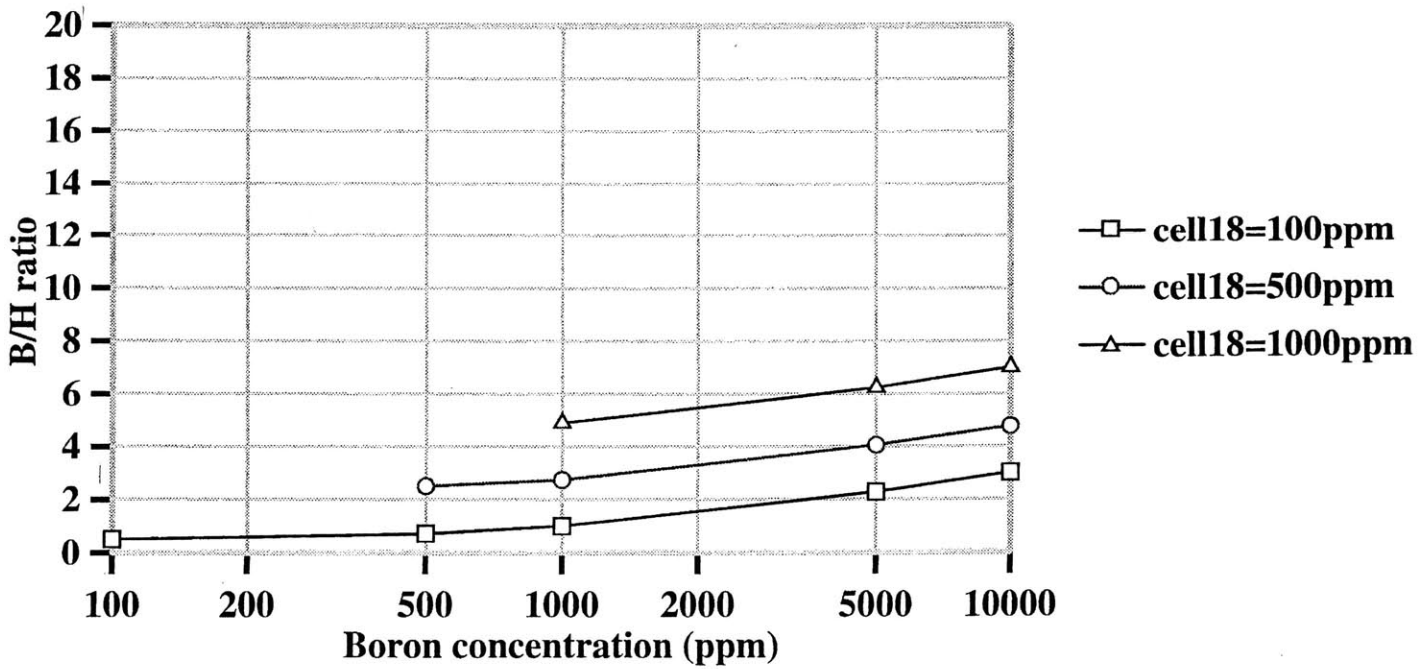

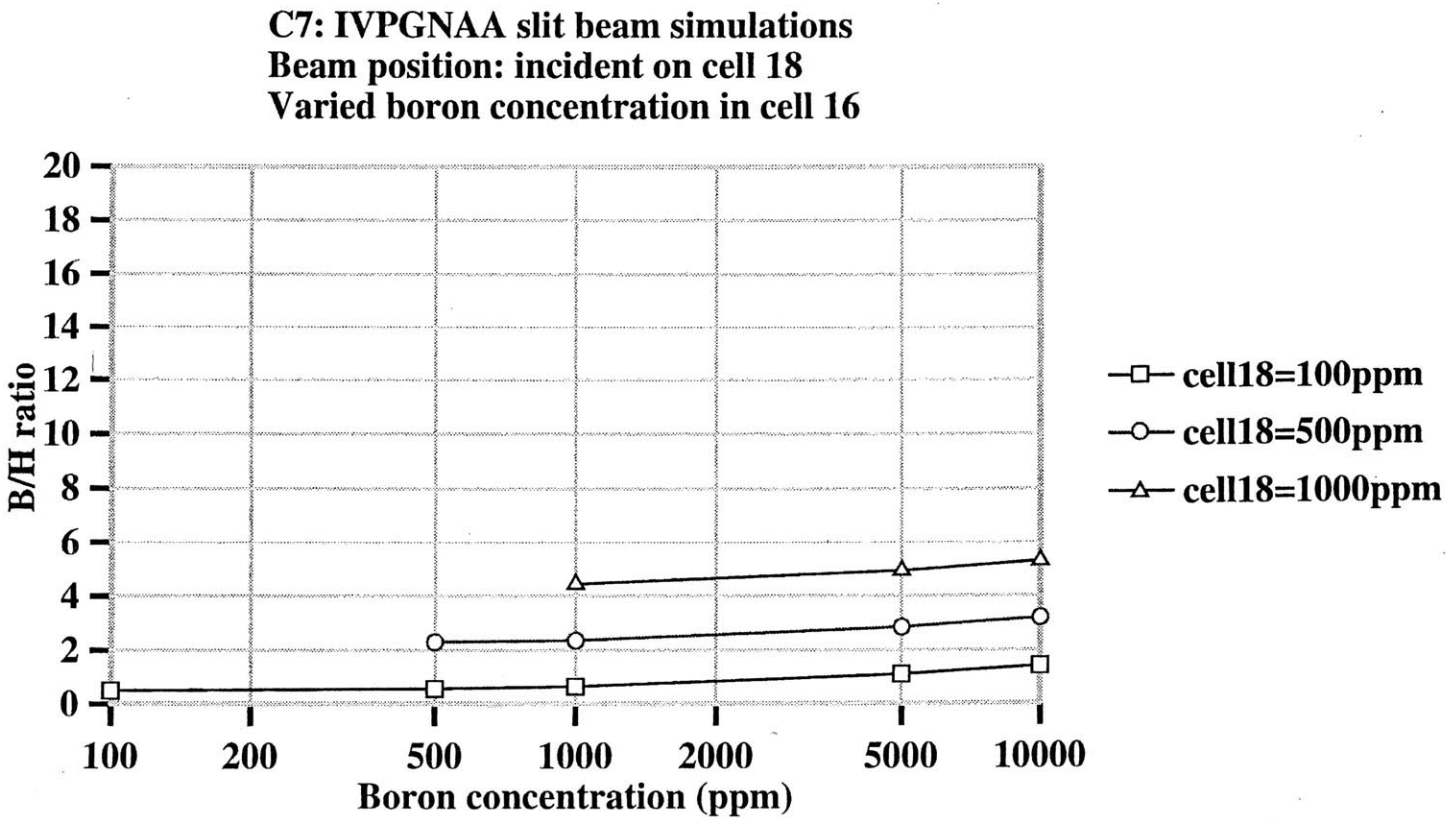
C7: IVPGNAA slit beam simulations
Beam position: incident on cell 18
Varied boron concentration in cell 16
B/H ratio
20
18
16
14
12
10
8
6
4
2
0
100
200
500
1000
2000
5000
10000
Boron concentration (ppm)
cell18=100ppm
cell18=500ppm
cell18=1000ppm

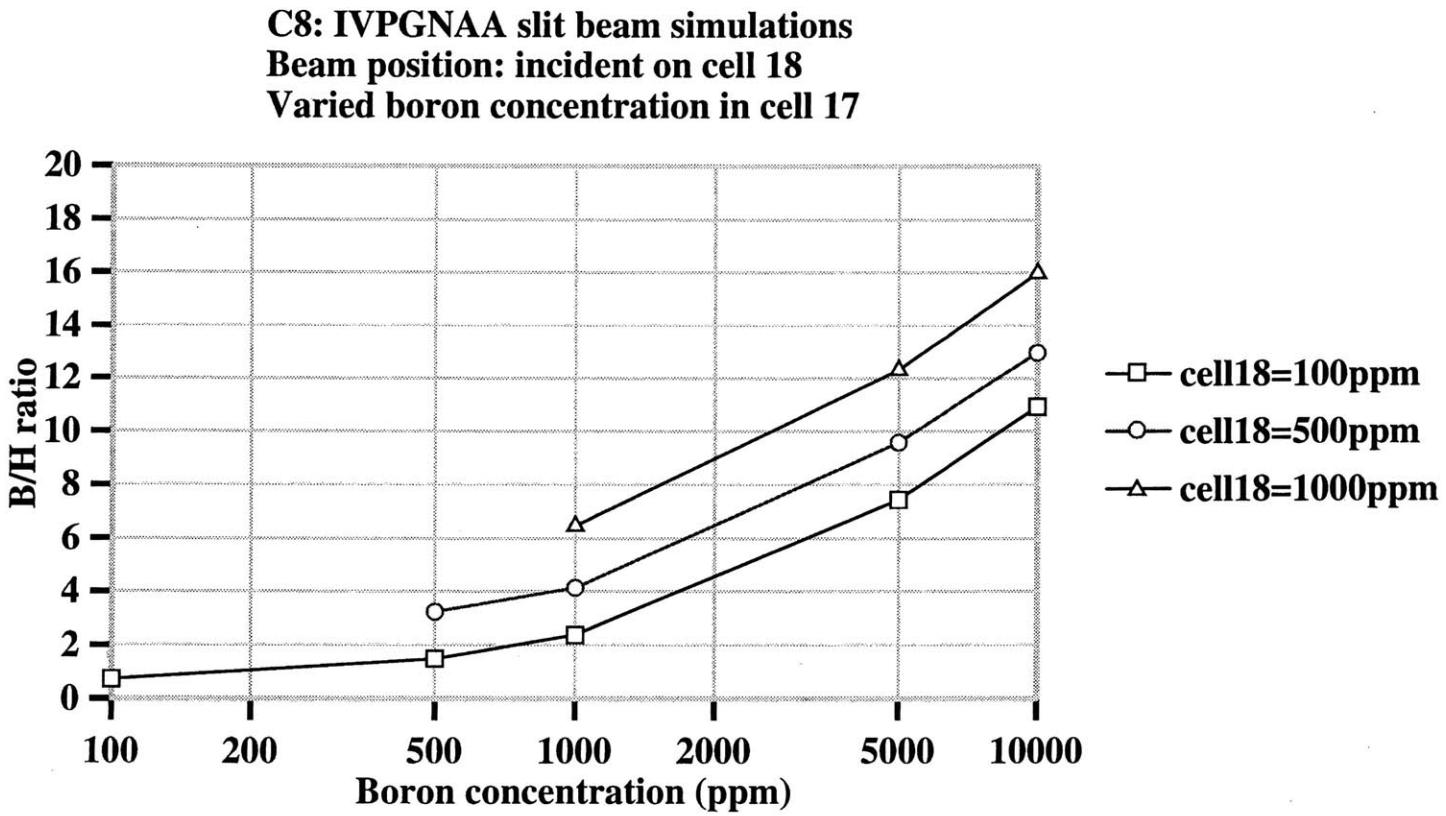
C8: IVPGNAA slit beam simulations
Beam position: incident on cell 18
Varied boron concentration in cell 17
B/H ratio
20
18
16
14
12
10
8
6
4
2
0
100
200
500
1000
2000
5000
10000
Boron concentration (ppm)
cell18=100ppm
cell18=500ppm
cell18=1000ppm